The Dissertation Committee for Zachary Pace Smith Certifies that this is the approved version of the following dissertation:

Fundamentals of Gas Sorption and Transport in Thermally Rearranged Polyimides

Committee:

Benny D. Freeman, Supervisor

Donald R. Paul, Co-Supervisor

C. Grant Willson

Isaac C. Sanchez

Anita J. Hill

Fundamentals of Gas Sorption and Transport in Thermally Rearranged Polyimides

by

Zachary Pace Smith, B.S.; M.S.E.

Dissertation

Presented to the Faculty of the Graduate School of

The University of Texas at Austin

in Partial Fulfillment

of the Requirements

for the Degree of

Doctor of Philosophy

The University of Texas at Austin

May 2014

Dedication

To my family

Acknowledgements

I consider myself beyond fortunate for the friendships I have made, the opportunities I have been given, and the professional growth I have experienced as a graduate student. Looking back at the winding road I have traveled, I see that each meandering curve was there for a reason. As the crow flies, the distance seems small, but it's the journey you remember for a lifetime.

I am greatly indebted to my thesis advisors, Professors Benny Freeman and Don Paul. Their dedication to the field of polymer science and engineering has provided invaluable clarity and guidance to my work, and their approach to graduate mentorship has demonstrated the combined, intangible qualities of leadership and stewardship. I am particularly grateful for their support in allowing me to develop, engage, and work with collaborators, which took me away from Austin for extended periods of time. I look back fondly at the many friends and colleagues I have met because of this freedom.

The work for this dissertation could never have been completed without the generous support from research sponsors. In particular, I would like to thank Dr. Ken McCarley from ConocoPhillips, Dr. Atsushi Morisato from Cameron Oil, Dr. Keith Murphy from Air Products, and Drs. Tim Merkel and Haiqin Lin from Membrane Technology and Research for their many excellent ideas and support.

I have made many lasting friendships with the other graduate students in both Prof. Paul's and Prof. Freeman's research groups. To those who came before me, Dr. Bryan McCloskey, Dr. Allison Sagle, Dr. Brandon Rowe, Dr. Lauren Greenlee, Dr. Victor Kusuma, Dr. 'Richard' Hua Li, Dr. Hao Ju, Dr. Claudio Ribeiro, Dr. Grant Offord, Dr. Norman Horn, Dr. Kevin Tung, Katrina Czenkusch, and Joe Cook, thank you for

setting such an excellent example through your hard work, and for showing me the ropes. To my contemporaries, Dr. David Sanders and Hee Jeung Oh, thank you for joining me in the journey. David, your prowess in research was only matched by your prowess on the b-ball court. I am grateful that I no longer have to guard your shot. Hee Jeung, I aspire to one day tell jokes as proficiently as you. To the younger students, Sirirat 'Peach' Kasemset, Albert Lee, Qiang Liu, Kevin Stevens, Ni Yan, Zhengwang 'Lisa' He, Jovan Kamcev, Amanda Paine, Lu Wang, Jaesung Park, Eui Sung Jang, and Michelle Dose, thank you for your patience as I have feverously worked to complete my dissertation. To our current postdoctoral researchers, Drs. Kris Gleason and Michele Galizia, thank you for your help with my research. Kris, thank you for helping make my dreams of system automation a reality. You have single-handedly ended my three AM trips to the lab. Finally, I would like to acknowledge all of the undergraduate students and the high school student who worked so diligently with me on my projects: Cindy Tran, Gabrielle Gunawan, Ralm Ricarte, Andres Cervantes, and Advaith Anand.

I am grateful for all of the help I received from some outstanding chemists and engineers. In particular, I would like to acknowledge Prof. Jim McGrath, Prof. Angel Lozano, and Prof. Lloyd Robeson. Prof. McGrath gave me countless lessons on condensation polymerization, and my ability to independently synthesize polymers is a result of his teaching. Prof. Lozano allowed me to work in his labs during a two-week trip to Madrid, Spain. In addition to learning condensation polymerization from Prof. McGrath, Prof. Lozano taught me how to synthesis diamine monomers, thus opening my world to some very unique types of chemistry. Prof. Robeson allowed me to work with him on analyzing the contributions of solubility selectivity to the upper bound.

My work also took me to CSIRO in Melbourne, Australia for 2 1/2 months, where I worked with Drs. Anita Hill, Cara Doherty, and Kristina Konstas on positron

annihilation lifetime spectroscopy. Their efforts greatly influenced my understanding of polymer morphology. During this trip, I was fortunate to meet Dr. Tim Bastow, who introduced me to the world of solid-state NMR. Tim was gracious in letting me run many experiments on his equipment, and these tests revealed the possibility of determining the precise chemical structure of polymers I was studying. In addition, these tests lead me to Dr. Sungsool Wi, who helped propel my solid-state NMR work to the forefront of controversy, investigating the structure of thermally rearranged polymers. I am truly grateful for these wonderful interactions and experiences.

In addition to Prof. Freeman, Prof. Paul, and Dr. Anita Hill, I would also like to thank my two other committee members, Profs. Isaac Sanchez and Grant Willson, for their help and guidance. I have been truly fortunate to be surrounded by the best minds in polymer science and engineering at the University of Texas.

To my mother and father, thank you for your life-long encouragement of my educational pursuits. To my brothers, Trey and Ethan, and my sister Alex, thank you for helping me laugh when I should have felt more stressed. To my beautiful wife, Gina, thank you for supporting me during the many sleepless nights I spent writing and working on projects. I am eternally grateful for your life and support.

Finally, I would like to acknowledge Jesus Christ, the author and perfecter of my faith and the source of my endurance. I can do all things through Christ who strengthens me (Philippians 4:13).

Fundamentals of Gas Sorption and Transport in Thermally Rearranged Polyimides

Zachary Pace Smith, Ph.D.

The University of Texas at Austin, 2014

Supervisors: Benny D. Freeman and Donald R. Paul

Thermally rearranged polymers are formed from the solid-state thermal reaction of polyimides and polyamides that contain reactive groups ortho position to their diamine. These polymers have shown outstanding transport properties for gas separation applications. The thrust of this work is to critically examine the chemical and morphological structure of these polymers and to identify the fundamental contributions of gas sorption to permeability. To accomplish this goal, a series of TR polymers and TR polymer precursors have been synthesized and investigated for transport properties. As a function of conversion, diffusivity increases more dramatically than sorption, which explains the outstanding permeabilities observed for these samples. Modifications to the polymer backbone structure, which can be achieved by adding rigid functional groups such as hexafluoroisopropylidene-functional linking groups, can further be used to improve permeabilities. The precursor used to form TR polymers has dramatic effects on the final polymer transport properties. Despite having nearly identical polymer structure, TR polymers formed from polyamide precursors have lower combinations of permeability and selectivity than TR polymers formed from polyimide precursors. In addition to structure-property studies with TR polymers, this thesis also present comparisons of permeability, diffusivity, and sorption of sparingly soluble gases (i.e.,

hydrogen and helium) for hydrocarbon-based polymer, highly fluorinated polymers, perfluoropolymers, and a silicon-based polymer. An explanation for the unique transport properties of perfluoropolymers is presented from the standpoint of the solution-diffusion model, whereby perfluoropolymers have uniquely different solubility selectivities than hydrocarbon-based polymers. Additionally, a large database of sorption, diffusion, and permeability coefficients is used to determine the contributions of free volume on solubility selectivity in polymers.

Table of Contents

List of Tables

List of Figures

Figure 8.5: Upper bound comparison for the H_2/CH_4 gas pair. Polyimide and polyamide precursors are shown as open circles, and TR polymers are shown as open squares. TR polymers formed from polyimide precursors were treated at 450°C for 30 min, and TR polymers formed from polyamide precursors were treated at 350°C for 60 min. Literature data are shown as gray circles from Robeson's database,[44] and additional industrially relevant data points (cellulose acetate (CA), polysulfone (PSF), Matrimid®, and poly(2,6-dimethyl-1,4-phenylene oxide) (PPO)) are highlighted from the review by Sanders *et al.*[1] Data points are plotted for pure gas permeability determined between approximately 1 bar and 50 bar with the exception of the HAB-6FDA and HAB-6FDA-SS polyimides, which are only plotted for pressures below their CO_2 plasticization pressure point. The change of permeability and selectivity with increasing pressure is indicated for the APAF-6FDA TR polymer. This figure includes data for certain samples reported in Chapter 4.253

Chapter 1: Introduction

Within the petrochemical industry, there are many applications involving the separation of gas mixtures. For example, nitrogen generation requires purifying nitrogen from air, natural gas sweetening requires removal of carbon dioxide from natural gas, and the production of feed stocks for polyolefin synthesis requires separating olefins from paraffins.[1-3] Cryogenic distillation is widely used for O_2/N_2 separation from air[2] and for olefin/paraffin separations;[4] amine absorption is often used for removal of CO_2 from natural gas.[5] These separation processes are energy intensive, and, in the case of absorption, potentially chemically hazardous.[5] With proper material synthesis and membrane design, low energy, environmentally benign polymer membrane-based separations could provide a promising alternative to these traditional separation processes.

Some material properties that can limit the utility of polymer membranes include low gas permeability, low selectivity, poor chemical stability, and poor thermal stability.[2,6-8] The challenge of overcoming these materials limitations is addressed in this dissertation, which focuses on investigating of a new class of polymeric materials for potential use in membrane-based separations.

1.1 DISSERTATION GOALS

Gas transport in polymer membranes can be described from kinetic and thermodynamic relationships. From a physical perspective, gases must dissolve into a polymer interface, diffuse across the polymer, and finally desorb from the polymer.[9] The dissolution of gases into a polymer is described thermodynamically by gas sorption coefficients, and gas diffusion across a polymer is described kinetically by gas diffusion coefficients. It is the difference in these sorption and diffusion coefficients that enable

membranes to selectivity separate molecules. The goal of this dissertation is to investigate the contribution of sorption and diffusion to permeation for diverse classes of polymers. In doing so, this work intends to guide materials scientists and polymer chemists with criteria for designing and synthesizing new polymer membranes for applications in gas separations.

To focus the scope of this work, gas transport is broadly investigated for a specific class of high-performing polymers known as thermally rearranged (TR) polymers. First reported by Park *et al.* in 2007,[10] these polymers have shown outstanding properties for a number of gas separations such as CO_2/CH_4, O_2/N_2, and hydrogen separations.[10-24] TR polymers are formed from the solid-state thermal reaction of polyimides and polyamides containing reactive functional groups at the *ortho*-position to their diamine. These TR polymers are, however, frequently insoluble in common solvents, which has precluded detailed solution-state characterization and has lead to wide-spread and disparate conclusions about their chemical structure.[25-27] To address this outstanding composition question in the field of TR polymer research, the work contained in this dissertation describes the use of unique chemical synthesis techniques to synthesize a partially soluble TR polymer. Proton, carbon, and 2-D solution NMR, coupled with cross-polarization magic-angle spinning (CP-MAS) solid-state ^{13}C NMR, suggest that the partially soluble TR polymer and related insoluble TR polymers are composed of polybenzoxazole (PBO) units.

Using a polyimide precursor known as HAB-6FDA, the effect of thermal rearrangement on gas sorption has been investigated for He, H_2, N_2, O_2, CH_4, and CO_2. These gases are frequently used for membrane-based separations and provide a useful comparison of the selective sorption and diffusion expected for this class of polymers.[23] During conversion, sorption increases by a factor of approximately 2 to 2.5 for all gases;

however, diffusion coefficients increase more significantly, which indicates that diffusion (i.e., kinetics) plays a large role in determining the transport properties of these polymers. In addition to analyzing the role of sorption and diffusion in HAB-6FDA polymers, analysis of sorption parameters permits a qualitative determination of equilibrium and non-equilibrium contributions to gas sorption in these materials. As conversion increases, the degree of non-equilibrium free volume increases in these polymers.

In this dissertation, a specific emphasis has been applied to sorption of sparingly soluble gases that are rarely studied in the literature. These gases, specifically H_2 and He, are among the least condensable gases and often have extraordinarily low sorption in polymers,[28,29] which makes the determination of accurate sorption parameters difficult. To address these experimental challenges, this dissertation reports sorption isotherms for H_2 over a range of temperatures for polyimides, TR polymers, and other polymers often considered in the membrane literature. Additionally, this dissertation presents He sorption isotherms at 35°C. Interestingly, the ability to determine H_2 and He isotherms extends the scope of this work to address another outstanding question in the polymer literature. Specifically, this question relates to the unusual separation properties of perfluoropolymers for He/H_2 separations.[30] By determining the contribution of sorption and sorption selectivity to permeability and permselectivity for perfluoropolymers, hydrocarbon-based polymers (e.g., certain polyimides and TR polymers), and a silicon-based polymer (i.e., poly(dimethylsiloxane)), the outstanding properties of perfluoropolymers is shown to be related to their unique He/H_2 sorption selectivity, which is much closer to unity than the He/H_2 sorption selectivity for hydrocarbon-based polymers.

In addition to reporting sorption and diffusion relationships, this dissertation also seeks to elucidate the role of polyimide, polyamide, and TR polymer structure on gas

permeability and plasticization resistance. To accomplish this end, the pure gas permeability coefficients of several poly(*hydroxy*-imide)s, a poly(*hydroxy*-amide), and corresponding TR polymers have been characterized. Incorporation of rigid functional groups, such as hexafluoroisopropylidene groups, into the polymer backbone improves the combination of permeability and selectivity of these polymers. In addition, thermally rearranging polymers inhibits CO_2 plasticization. From an upper bound perspective, two polyimides and one TR polymer from this study have permeabilities and selectivities that are at or above the Robeson upper bound for H_2/CH_4 separation,[30] and one TR polymer has permeabilities and selectivities above the Koros propylene/propane upper bound.[31]

The final goal of this dissertation is to analyze solubility and diffusion relationships as a function of free volume using a large database of parameters collected by Robeson *et al.*[29] From this analysis, solubility selectivity decreases with increasing free volume. These relationships have been observed for a few individual families of polymers, but the work described here extends the scope of this observation to hundreds of polymers. Furthermore, the analysis of diffusion data allows for a more accurate determination of effective gas diameters for polymer membrane-based separations.

1.2 DISSERTATION OUTLINE

A brief introduction to the essential concepts and theory of polymer membrane-based gas separations is included in Chapter 2. Furthermore, an overview of current and emerging membrane-based gas separations is reviewed. Experimental methods for the results presented in this dissertation are provided in Chapter 3.

Chapter 4 and Chapter 5 present characterization work proving that TR polymers are composed of polybenzoxazole repeat units. Chapter 4 focuses on solution-state NMR characterization of a partially soluble TR polymer formed from a polyamide precursor.

Comparisons between the solution-state characterized sample and an insoluble sample of similar structure are made using solid-state NMR. In addition, Chapter 4 and Chapter 5 report characterization of the thermal rearrangement process using thermogravimetric analysis coupled with mass spectrometry, differential scanning calorimetry, and Fourier transform infrared spectroscopy.

Chapter 5 also presents sorption data for H_2, N_2, O_2, CH_4, and CO_2 for an HAB-6FDA polyimide and three partially converted TR polymers. From this work, TR polymers achieve their outstanding separation performance because of increases in diffusivity. Additionally, this work shows the effect of non-equilibrium free volume on gas transport in TR polymers, which is far more significant than that of their precursor polyimides.

Chapter 6 extends the work from Chapter 5 to include more accurate values of H_2 sorption coefficients. The isotherms presented in this chapter were determined gravimetrically using a magnetic suspension balance. In addition to improving the accuracy of these sorption isotherms, the effect of temperature on hydrogen sorption was investigated between -20°C and +70°C, and comparisons are made between polyimides, TR polymers, and other polymers frequently investigated in the literature. As a function of thermal rearrangement, there is no significant change in the hydrogen enthalpy of sorption, which remains between -5.8 and -7.3 kJ/mol for the HAB-6FDA polyimide and corresponding TR polymers.

Chapter 7 investigates the role of diffusivity and sorption of H_2 and He in 12 different polymers, including two polyimides, a TR polymer, several hydrocarbon-based polymers, several highly or completely fluorinated polymers, and PDMS. This work provides detailed He sorption isotherms over a broad range of pressures, and these results

conclude that perfluoropolymers achieve their above upper bound separation performance for He/H_2 separations because of their unique He/H_2 solubility selectivity.

Structure/property results for permeation of light gases and CO_2 are analyzed for polyimides and TR polymers in Chapter 8. These results show an increase in TR polymer reactivity by using more flexible monomers and by using monomers that do not contain strong electron withdrawing groups, such as hexafluoroisopropylidene groups. Additionally, olefin/paraffin results are presented for the best performing TR polymer, and these results show above upper-bound separation characteristics for propylene/propane separation. Finally, hysteresis curves are presented for CO_2 in this chapter. Upon thermal rearrangement, TR polymers show an increased resistance to plasticization.

A detailed study describing the effect of free volume on solubility selectivity is presented in Chapter 9 using a database collected by Robeson.[29] For polymer membrane-based separations, solubility selectivity decreases as free volume increases. Additionally, the effective diameters of gas molecules for polymer membrane-based separations have been calculated from diffusion correlations. Finally, conclusions and recommendations for future research are presented in Chapter 10.

1.3 REFERENCES

1. Baker, R.W., *Future directions of membrane gas separation technology*. Industrial & Engineering Chemistry Research, **2002**. 41(6), 1393-1411.

2. Baker, R.W., *Membrane technology and applications*. **2004**, Chichester, John Wiley & Sons, Ltd.

3. Koros, W. and R. Mahajan, *Pushing the limits on possibilities for large scale gas separation: which strategies?* Journal of Membrane Science, **2000**. 175(2), 181-196.

4. Eldridge, R.B., *Olefin/paraffin separation technology: A review.* Industrial & Engineering Chemistry Research, **1993**. 32(10), 2208-2212.

5. Baker, R.W. and K. Lokhandwala, *Natural gas processing with membranes: An overview.* Industrial & Engineering Chemistry Research, **2008**. 47(7), 2109-2121.

6. Yampolskii, Y., I. Pinnau, and B.D. Freeman, eds. *Materials science of membranes for gas and vapor separation*. **2006**, John Wiley and Sons: Chichester.

7. Paul, D.R. and Y.P. Yampolskii, *Polymeric gas separation membranes*. **1994**, Boca Raton, CRC Press.

8. Drioli, E. and L. Giorno, *Membrane operations: Innovative separations and transformations*. **2009**, Weinheim, Wiley-VCH.

9. Wijmans, J.G. and R.W. Baker, *The solution-diffusion model: A review.* Journal of Membrane Science, **1995**. 107(1-2), 1-21.

10. Park, H.B., C.H. Jung, Y.M. Lee, A.J. Hill, S.J. Pas, S.T. Mudie, E. Van Wagner, B.D. Freeman, and D.J. Cookson, *Polymers with cavities tuned for fast selective transport of small molecules and ions.* Science, **2007**. 318(5848), 254-258.

11. Han, S.H., J.E. Lee, K.-J. Lee, H.B. Park, and Y.M. Lee, *Highly gas permeable and microporous polybenzimidazole membrane by thermal rearrangement.* Journal of Membrane Science, **2010**. 357(1-2), 143-151.

12. Park, H.B., S.H. Han, C.H. Jung, Y.M. Lee, and A.J. Hill, *Thermally rearranged (TR) polymer membranes for CO_2 separation.* Journal of Membrane Science, **2010**. 359(1-2), 11-24.

13. Choi, J.I., C.H. Jung, S.H. Han, H.B. Park, and Y.M. Lee, *Thermally rearranged (TR) poly(benzoxazole-co-pyrrolone) membranes tuned for high gas permeability and selectivity.* Journal of Membrane Science, **2010**. 349(1-2), 358-368.

14. Han, S., H. Kwon, K. Kim, J. Seong, C. Park, S. Kim, C.M. Doherty, A. Thornton, A.J. Hill, A. Lozano, K. Berchtold, and Y. Lee, *Tuning microcavities in thermally rearranged polymer membranes for CO_2 capture.* Physical Chemistry Chemical Physics, **2012**. 14(13), 4365-4373.

15. Park, C.H., E. Tocci, Y.M. Lee, and E. Drioli, *Thermal treatment effect on the structure and property change between hydroxy-containing polyimides (HPIs) and thermally rearranged polybenzoxazole (TR-PBO).* The Journal of Physical Chemistry B, **2012**. 116(42), 12864-12877.

16. Li, S., H.J. Jo, S.H. Han, C.H. Park, S. Kim, P.M. Budd, and Y.M. Lee, *Mechanically robust thermally rearranged (TR) polymer membranes with spirobisindane for gas separation.* Journal of Membrane Science, **2013**. 434, 137-147.

17. Jiang, Y., F.T. Willmore, D. Sanders, Z.P. Smith, C.P. Ribeiro, C.M. Doherty, A. Thornton, A.J. Hill, B.D. Freeman, and I.C. Sanchez, *Cavity size, sorption and transport characteristics of thermally rearranged (TR) polymers.* Polymer, **2011**. 52(10), 2244-2254.

18. Sanders, D.F., Z.P. Smith, C.P. Ribeiro, R.L. Guo, J.E. McGrath, D.R. Paul, and B.D. Freeman, *Gas permeability, diffusivity, and free volume of thermally rearranged polymers based on 3,3 '-dihydroxy-4,4 '-diamino-biphenyl (HAB) and 2,2 '-bis-(3,4-dicarboxyphenyl) hexafluoropropane dianhydride (6FDA).* Journal of Membrane Science, **2012**. 409, 232-241.

19. Smith, Z.P., D.F. Sanders, C.P. Ribeiro Jr, R. Guo, B.D. Freeman, D.R. Paul, J.E. McGrath, and S. Swinnea, *Gas sorption and characterization of thermally rearranged polyimides based on 3,3'-dihydroxy-4,4'-diamino-biphenyl (HAB) and 2,2'-bis-(3,4-dicarboxyphenyl) hexafluoropropane dianhydride (6FDA).* Journal of Membrane Science, **2012**. 416, 558-567.

20. Guo, R., D.F. Sanders, Z.P. Smith, B.D. Freeman, D.R. Paul, and J.E. McGrath, *Synthesis and characterization of thermally rearranged (TR) polymers: Influence of ortho-positioned functional groups of polyimide precursors on TR process and gas transport properties.* Journal of Materials Chemistry A, **2013**. 1(2), 262-272.

21. Kim, S., H.J. Jo, and Y.M. Lee, *Sorption and transport of small gas molecules in thermally rearranged (TR) polybenzoxazole membranes based on 2,2-bis(3-amino-4-hydroxyphenyl)-hexafluoropropane (bisAPAF) and 4,4'-hexafluoroisopropylidene diphthalic anhydride (6FDA).* Journal of Membrane Science, **2013**. 441, 1-8.

22. Guo, R., D.F. Sanders, Z.P. Smith, B.D. Freeman, D.R. Paul, and J.E. McGrath, *Synthesis and characterization of thermally rearranged (TR) polymers: Effect of glass transition temperature of aromatic poly(hydroxyimide) precursors on TR process and gas permeation properties.* Journal of Materials Chemistry A, **2013**. 1(19), 6063-6072.

23. Sanders, D.F., Z.P. Smith, R. Guo, L.M. Robeson, J.E. McGrath, D.R. Paul, and B.D. Freeman, *Energy-efficient polymeric gas separation membranes for a sustainable future: A review.* Polymer, **2013**. 54(18), 4729-4761.

24. Sanders, D.F., R. Guo, Z.P. Smith, Q. Liu, K.A. Stevens, J.E. McGrath, D.R. Paul, and B.D. Freeman, *Influence of polyimide precursor synthesis route and ortho-position functional group on thermally rearranged (TR) polymer properties: conversion and free volume.* Polymer, **2014**. In Press.

25. Hodgkin, J.H. and B.N. Dao, *Thermal conversion of hydroxy-containing polyimides to polybenzoxazoles. Does this reaction really occur?* European Polymer Journal, **2009**. 45(11), 3081-3092.

26. Hodgkin, J.H., M.S. Liu, B.N. Dao, J. Mardel, and A.J. Hill, *Reaction mechanism and products of the thermal conversion of hydroxy-containing polyimides.* European Polymer Journal, **2011**. 47(3), 394-400.

27. Kostina, J., O. Rusakova, G. Bondarenko, A. Alentiev, T. Meleshko, N. Kukarkina, A. Yakimanskii, and Y. Yampolskii, *Thermal rearrangement of functionalized polyimides: IR-spectral, quantum chemical studies, and gas*

permeability of TR polymers. Industrial & Engineering Chemistry Research, **2013**. 52(31), 10476-10483.

28. Smith, Z.P., R.R. Tiwari, T.M. Murphy, D.F. Sanders, K.L. Gleason, D.R. Paul, and B.D. Freeman, *Hydrogen sorption in polymers for membrane applications.* Polymer, **2013**. 54(12), 3026–3037.

29. Robeson, L.M., Z.P. Smith, B.D. Freeman, and D.R. Paul, *Contributions of diffusion and solubility selectivity to the upper bound analysis for glassy gas separation membranes.* Journal of Membrane Science, **2014**. 453, 71-83.

30. Robeson, L.M., *The upper bound revisited.* Journal of Membrane Science, **2008**. 320(1-2), 390-400.

31. Burns, R.L. and W.J. Koros, *Defining the challenges for C_3H_6/C_3H_8 separation using polymeric membranes.* Journal of Membrane Science, **2003**. 211(2), 299-309.

Chapter 2: Background

2.1 THE UPPER BOUND

Separation performance in polymer membranes is often characterized by a material's permeability, P_i, and selectivity, $\alpha_{i/j}$:[1-4]

$$P_i = \frac{N_i l}{\Delta p_i} \tag{2. 1}$$

$$\alpha_{i/j} = \frac{P_i}{P_j} \tag{2. 2}$$

where N_i is the steady-state flux of component i, l is membrane thickness, and Δp_i is the partial pressure difference of component i across the membrane. P_j is the gas permeability of component j and it is defined analogously to P_i.

For a given separation, increasing permeability can improve the efficacy of the separation by, for example, decreasing the membrane surface area required for a given separation. Similarly, increasing selectivity can reduce loss of a desired gas product. However, an increase in permeability is often accompanied by a decrease in selectivity, and *vice versa*.[5,6] This empirical tradeoff was first described for a large database of polymers by Robeson in 1991[5] and redefined in 2008.[6] A fundamental theory describing the basis for this tradeoff was proposed by Freeman.[7] Figure 2.1 shows the Robeson upper bound for CO_2/CH_4 separation, which maps material properties of polymers in terms of CO_2 permeability and CO_2/CH_4 selectivity. Gray circles signify literature data from Robeson's upper bound,[6] green circles signify data for polyimides, and blue/white squares signify data points for thermally rearranged (TR) polymers.[8,9] In general, TR

This chapter has been adapted with permission from sections of: Sanders, D.F., Z.P. Smith, R. Guo, L.M. Robeson, J.E. McGrath, D.R. Paul, and B.D. Freeman, *Energy-efficient polymeric gas separation membranes for a sustainable future: A review.* Polymer, **2013**. 54(18), 4729-4761.

polymers have property sets beyond many other polymers reported in the literature, and several of these polymers have property sets above the 2008 upper bound.

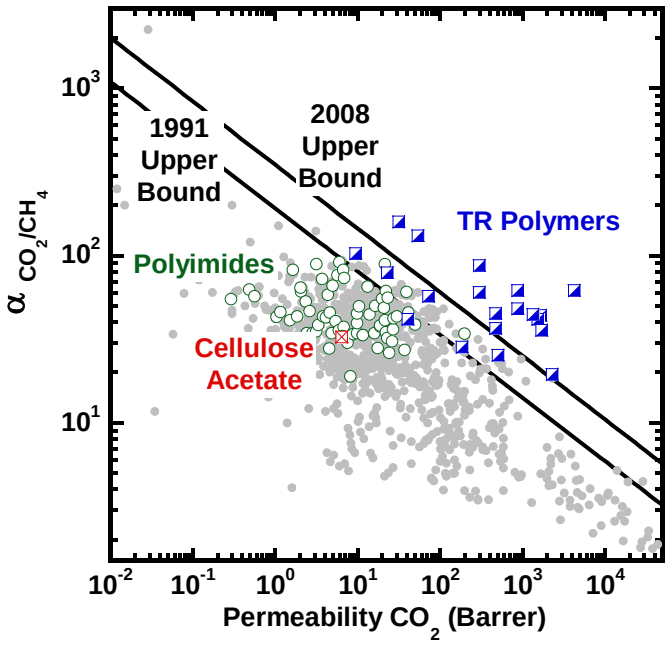

Figure 2.1: The Robeson upper bound for CO_2/CH_4 separation with additional polyimides, TR polymers, and cellulose acetate.[6,8,9] 1 Barrer = 10^{-10} cm^3(STP) cm/(cm^2 s cmHg). α_{CO_2/CH_4} represents pure gas selectivity of carbon dioxide to methane.

2.2 MITIGATING PLASTICIZATION EFFECTS

An industrial application for polymer membrane-based separations that has emerged over the last few decades is the removal of CO_2 from natural gas.[10] This separation is typically accomplished by amine absorption, which requires a large plant footprint and stringent oversight of amine degradation to prevent amine mixtures from corroding the absorption system.[10] Nevertheless, because amine absorption is a more established technology, it still overshadows membranes-based separations. Today, membrane technology only accounts for approximately 5% of the natural gas purification

market.[10] Of the membranes used for natural gas purification, the state-of-the-art material, cellulose acetate (CA), shown in Figure 2.1, operates well below the upper bound and can be plasticized by high partial pressures of CO_2.[11,12] Plasticization is the swelling of a polymer in the presence of highly condensable gases, an effect that increases the permeability of all components and decreases selectivity.[13] Polyimides with hexafluoroisopropylidene (6F) functionality, which have shown separation performance at or near the Robeson upper bound, are extensively reported in the membrane literature.[14-16] But, like cellulose acetate, these materials are often susceptible to plasticization and have not been deployed commercially.[8,10,17]

Park *et al.* have reported permeation data for mixtures of CO_2 and CH_4 in TR polymers, and these results are shown in Figure 2.2.[8] Unlike cellulose acetate and a 6F polyimide, TR polymers resist CO_2 plasticization for CO_2 partial pressures up to approximately 15 atm.[8] Additionally, the reported permeability of CO_2 in this TR polymer is nearly 300 and 500 times more permeable than cellulose acetate and the 6F polyimide, respectively.

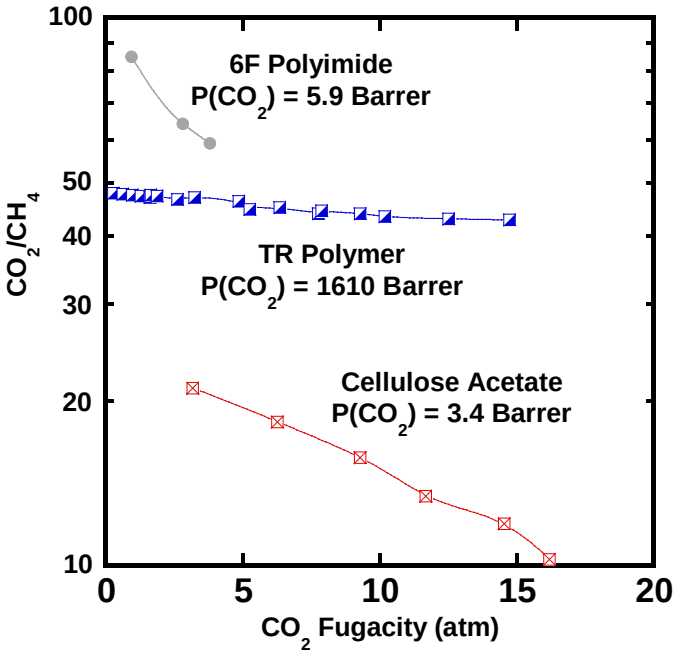

Figure 2.2: Effect of CO_2 feed fugacity on CO_2/CH_4 mixed-gas selectivity for a 6F polyimides, a TR polymer, and cellulose acetate.[8]

2.3 PROCESSING OF GAS SEPARATION MEMBRANES

Solution casting is a standard practice in membrane manufacturing.[2] This technique is conducive for casting thin films (*e.g.*, 100 nm thick films) which, in turn, permits high gas flux.[2,18] Furthermore, polymers can be cast from solution into useful geometries such as hollow fibers or spiral wound membranes.[18] These geometries provide an economic benefit to membrane separations because high surface area to volume ratios reduce the footprint of the membrane module required to treat a given flow rate of gas.[18]

While solution casting is a requirement for polymer membrane fabrication, this process requires polymers that are soluble in organic solvents. Polymers that easily dissolve in organic solvents are often susceptible to swelling in the presence of condensable gases, and this swelling manifests itself in reduced separation efficiency

through plasticization. In a number of applications where polymer membranes could be used to separate condensable gases (*e.g.* propylene/propane separation), membranes plasticize and consequently lose selectivity during operation, thus making these separations inaccessible.[10,19,20] Certain classes of polymers such as polybenzoxazoles have chemical resistance[21,22] that may mitigate plasticization, but these polymers are often insoluble in common solvents[21] and, therefore, cannot be cast into films or membranes by traditional solution casting techniques.

2.4 SYNTHESIS OF TR POLYMERS

TR polymers are a unique class of insoluble polybenzoxazoles (PBOs), polybenzothiazoles (PBTs), and polybenzimidazoles (PBIs). Park *et al.* demonstrated that the processing challenge to forming PBO, PBT, and PBI films could be circumvented through a solid-state synthesis route.[8,23-25] To accomplish this transformation, a soluble polyimide with a reactive group *ortho*-position to the polyimide diamine is cast as a film from a common organic solvents such as N-methyl-2-pyrrolidone (NMP) or dimethylacetamide (DMAc). Next, these films are thermally transformed into TR polymers through a solid-state reaction at elevated temperatures.[8] Polyimide synthesis is well-established,[26,27] and the simplicity of converting *ortho*-functional polyimide precursor into an insoluble, highly chemically resistant TR polymer permits new families of materials to be considered for membrane applications.

2.5 SOLUTION-DIFFUSION MODEL

Molecular transport of gases in dense polymer films is governed by the solution diffusion model:[28]

$$P = \left[\overline{D}\right]\left[\overline{S}\right] \tag{2. 3}$$

$$\alpha_{i/j} = \frac{P_i}{P_j} = \frac{\left[\overline{D}\right]_i}{\left[\overline{D}\right]_j} \frac{\left[\overline{S}\right]_i}{\left[\overline{S}\right]_j} = \alpha_{D_i/D_j} \times \alpha_{S_i/S_j} \tag{2. 4}$$

where $\left[\overline{D}\right]$ is the effective, concentration averaged diffusion coefficient, and $\left[\overline{S}\right]$ is the sorption coefficient, $\frac{P_i}{P_j}$ and $\alpha_{i/j}$ is the permselectivity of gas *i* to gas *j*, $\frac{\left[\overline{D}\right]_i}{\left[\overline{D}\right]_j}$ and α_{D_i/D_j} are the diffusivity selectivities, and $\frac{\left[\overline{S}\right]_i}{\left[\overline{S}\right]_j}$ and α_{S_i/S_j} are the sorption selectivities. Decoupling the contributions of diffusivity and solubility to permeability permits development of fundamental structure/property correlations to guide rational structural modifications for a given family of polymers to achieve optimal separation performance.

2.6 DUAL-MODE SORPTION

Sorption of gases in glassy polymers is often described by the dual-mode sorption model, which partitions gas sorption into equilibrium and non-equilibrium regions in a polymer matrix.[1,3,29,30]:

$$C = k_D p + C_H^{'} \frac{bp}{1+bp} \tag{2. 5}$$

where C is the penetrant concentration in the polymer, k_D is the Henry's law solubility constant, $C_H^{'}$ is the Langmuir capacity constant, b is the affinity constant, and p is pressure. Pressure can be replaced with fugacity for non-ideal gases. The solubility coefficient is the ratio of penetrant concentration in the polymer to the pressure of the gas in the gas phase:

$$S = \frac{C}{p} \tag{2. 6}$$

2.7 CURRENT COMMERCIAL MEMBRANE GAS SEPARATION

Today, separations account for 4,500 trillion Btu of energy per year in the United States, which is approximately 22% of all in-plant energy use.[31] Much of this energy consumption comes from distillation. There are over 40,000 distillation columns used for over 200 different separations in the United States, which accounts for 49% of industrial separation energy consumption.[31] Other separation processes include absorption, crystallization, and membrane separations. Of these processes, membranes are attractive because they do not involve sorbants or a thermal driving force to separate mixtures.

Industrially, membranes are currently used, at least to some capacity, for acid gas removal, nitrogen enrichment, ammonia purge gas recovery, refinery off-gas purification, syngas ratio adjustment, and dehydration, as shown in Table 2.1.

Gas Pair	Application
CO_2/CH_4	Acid Gas Removal
N_2/O_2	Nitrogen Enrichment
H_2/N_2	Ammonia Purge Gas Recovery
H_2/CH_4	Refinery Off-gas Purification
H_2/CO	Syngas Ratio Adjustment
H_2O/Air	Dehydration

Table 2.1: Current industrial gas separations for polymer membranes.

2.7.1 Hydrogen Recovery

Compared to most gases, hydrogen is highly permeable and has low condensability. Thus, separating hydrogen from other gases was an initial target for membrane separations. Currently, hydrogen separation membranes are used for

recovering hydrogen from ammonia purge gas, syngas ratio adjustment for oxo-chemical synthesis, and refinery off-gas purification.

The first large scale commercial membrane application was hydrogen recovery from ammonia purge gas.[2] Ammonia is synthesized by combining nitrogen and hydrogen with a catalyst at high pressures (*e.g.*, >100 atm) and high temperatures (*e.g.*, >400°C).[32] After removal of water and carbon dioxide, the nitrogen feedstock still contains argon, which is a trace component in air.[32] Furthermore, the hydrogen feedstock, which is typically taken from reforming of hydrocarbons, contains methane, carbon dioxide, carbon monoxide, and water. The carbon dioxide, carbon monoxide, and water can poison the ammonia catalyst and are, therefore, largely removed from the feedstock.[32] The methane, however, is inert to the ammonia catalyst and is left in the hydrogen feedstock as an impurity. Therefore, an ammonia plant has impurities of argon and methane in the reaction chamber. Because typical reactor yield is less than 30%, a recycle loop is needed to achieve adequate conversion of reagents.[32] Components that would otherwise build up in the reactor are purged from the recycle loop, meaning a net loss of valuable hydrogen gas from the reaction. Hydrogen is much lighter than other gases purged from an ammonia plant, meaning that it can be recovered using a diffusion selective membrane. Recovery of hydrogen was therefore initially targeted as a membrane application.

Monsanto was the first company in this market, offering a polysulfone hollow fiber system marketed as Prism® membranes around 1979.[18] Because membrane systems were a new unit operation, Monsanto marketed their modules with the slogan "Like operating a piece of pipe", a slogan which emphasized that membranes could perform separations simply through a pressure drop.[33] Today, membranes used for ammonia

purge gas recovery is a proven technology. Prism® membranes can achieve up to a 95% recovery of H_2, and certain systems have been in operation since 1979.[34]

Other hydrogen separations involve adjusting molar ratios of syngas (H_2/CO) and refinery off-gas purification (H_2/CH_4). Syngas is a mixture of H_2 and CO produced from steam reforming of natural gas, oxidation of heavy oils, or gasification of coal or coke.[35] Depending on the method used to produce syngas, H_2:CO ratios will vary between 1 and 5,[36] and this ratio must be adjusted for specific synthesis applications. Several reaction products involving syngas, the reactions by which they are synthesized, and the required syngas ratios are shown in Table 2.2. Because an appropriate H_2:CO ratio is required to satisfy reaction stoichiometry, the synthesis product will dictate how the raw syngas needs to be treated.

Because H_2 can easily be separated from CO with diffusion selective membranes, the first industrial polymer membranes targeted this type of separation. Prism® membranes produced by Monsanto were first installed in 1977 for syngas ratio adjustment,[34] and other companies now offer a range of products for these applications.[37]

Reaction Product	**Reaction**	**Required H_2:CO Ratio**
oxoalcohols	$RCH{=}CH_2 + CO + H_2 \rightarrow RCH_2CH_2CHO$	1.0
methanol	$2H_2 + CO \rightarrow CH_3OH$	2.0
ethanol	$4H_2 + 2CO \rightarrow CH_3CH_2OH + H_2O$	2.0
acetic acid	$2H_2 + 2CO \rightarrow CH_3COOH$	1.0
acetaldehyde	$3H_2 + 2CO \rightarrow CH_3CHO + H_2O$	1.5
ethylene glycol	$3H_2 + 2CO \rightarrow CH_2OH\text{-}CH_2OH$	1.5

Table 2.2: Reaction products involving syngas feedstocks, the reactions by which they are produced, and the syngas ratio needed for these reactions.

Refinery off-gas purification is a focus in the petrochemical industry. Petroleum crude feed stocks contain many different molecular weight products that must be separated before use. The heavier fraction of these products is often cracked, *i.e.*, broken down into smaller components through a catalytic process known as hydrocracking. This process relies on injecting hydrogen into the cracker to improve several aspects of the reactions chemistry. For example, hydrogen often reacts with polycyclic aromatic compounds that are generally inert to other cracking processes. Furthermore, hydrogen helps to eliminate unsaturated hydrocarbons and reduces the formation of tar and coke.[38] Increasing the purity of hydrogen used in a hydrocracker can increase the life of the cracker catalyst and can increase the production of higher paraffinic compounds.[38] Therefore, it is highly desirable to recycle H_2 from the hydrocrackate products to the hydrocracker feed.

To achieve this separation, polymer membranes are used in the recycle loop. Being a high-throughput process, it is best to use membranes with H_2/CH_4 selectivities of approximately 20 – 25 and very high permeabilities.[38] As with many other hydrogen separations, Prism® membranes are often used for refinery off gas purification.[2]

2.7.2 Air Separation

The composition of air and slight differences in O_2 and N_2 molecular size (*i.e.*, 3.46 Å and 3.64 Å kinetic diameters for O_2 and N_2, respectively) promote glassy polymers for air separation. Interestingly, some of the earliest membrane experiments performed by Sir Thomas Graham involved oxygen enrichment using India-rubber.[39]

Today, air separation is accomplished by several industrial processes, including cryogenic distillation, pressure swing adsorption (PSA), and membranes. By far, the largest market penetration for membrane air separations is for nitrogen enrichment

applications. Figure 2.3 shows the approximate economic range for separation processes used to achieve N_2 purities at a specified flowrate. For users who consume small amounts of high purity N_2, gas cylinders or N_2 from a liquid nitrogen supply is often used. However, for users who require N_2 flowrates between approximately 5000 scfd to 1 MMscfd, membranes are often the most economical option, especially if purities are kept between about 95 and 99%.[2] The competing technologies (*i.e.*, cryogenic distillation and PSA), are used to process higher gas flowrates and, for cryogenic distillation, to achieve higher purity N_2.[40] Over the past 25 years, developments of higher performance polymers have helped advance the range of N_2 purity and flux that can be achieved with membrane systems.[2,40-43]

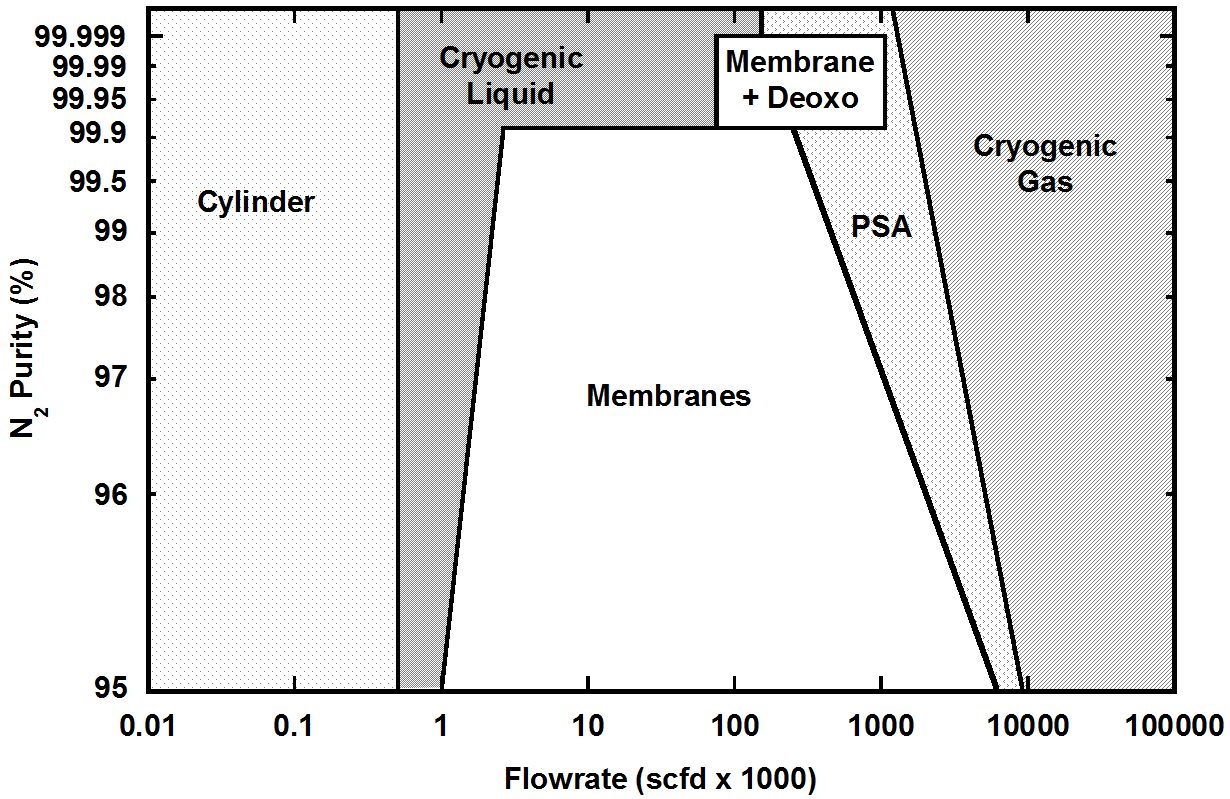

Figure 2.3: Approximate economic range of membranes for air separation.[2,42]

Several N_2 enrichment applications for membranes include combustion/reaction processes, refrigeration, inerting[44], and other niche markets.[45] Many other high-volume, high-purity N_2 applications exist, such as enhanced oil recovery, metallurgical processes, and gas feeds for the electronics industry, but these applications are not typically pursued as membrane-specific separation processes because of the large gas volumes or high gas purity required for these N_2 streams.[42]

Designing a membrane system requires a balance and optimization of many parameters. For example, there are compressor costs, purity requirements, gas flowrates, and gas rejection specifications that are highly process-specific. Membranes with selectivities as low as 2 can be used to produce 99% pure N_2; however, at these

conditions, N_2 recovery is typically too low, and compressor costs too high for N_2 enrichment applications.[2] Therefore, much of the early work in this field focused on improving membrane selectivity.

Some of the earliest air separation membranes were produced by Generon in the mid-1980s.[43] These membranes were made of poly(4-methyl-1-pentene) (TPX) and had selectivities of approximately 4, which limited their use.[43] Research into new membrane materials and design quickly improved air separation performance, and by the early 1990s, several new hollow fiber membranes were brought into the market, including tetrahalogenated bisphenol-based polycarbonates by Generon,[46] polyimides by Praxair,[43] and polyimide and polyaramide membranes by Medal.[43] During this time, the push for nitrogen enrichment applications brought about significant advances in the design and fabrication of many asymmetric membrane systems. Eikner *et al.* summarize 44 patents describing these advances.[47]

The largest cost in a nitrogen enrichment plant comes from the compressor, which can account for nearly two-thirds the total cost.[43] Improvements in membrane materials have helped lower these costs, and innovative system design including one-, two-, and three-stage membrane systems have helped to improve N_2 purity.[40] Still, the sole use of membranes to produce N_2 with purities above 99.9% without disadvantageous product loss is a difficult challenge.[2] Some work has focused on producing higher purity N_2 by addition of a deoxygenation system, which involves reacting excess oxygen from a membrane-purified N_2/O_2 mixture using H_2 gas and a noble metal catalyst, followed by H_2 and H_2O removal from the product stream.[40,48] The approximate range that this technology is economically viable is highlighted in Figure 2.3.

2.7.3 Natural Gas Purification

Natural gas is a complex mixture of methane, carbon dioxide, ethane, higher paraffins, hydrogen sulfide, inert gases, and trace components of many other compounds, including BTEX aromatics (benzene, toluene, ethylbenzene, and xylene).[10] The actual composition of natural gas varies depending on the well, and delivery of gas to the U.S. national pipeline grid requires all natural gas to be treated, at least to some degree. This treatment is designed to prevent pipeline corrosion and adjust the heating value of the fuel. Typical pipeline specifications require natural gas to contain less than 2% CO_2, 4 ppm H_2S, 7 lb/MMscf water, and having a C_3+ heating value between 950 and 1050 Btu/scf.[10,49]

All natural gas must be dehydrated before use.[2] Natural gas is often saturated with water when it is removed from a well, and upon cooling, this water condenses and forms solid hydrates with hydrocarbons in the natural gas stream.[50] These hydrates can potentially deposit on valves, meters, instruments, piping, and other equipment, consequently adding to system maintenance and increasing the likelihood of taking a system off-line.[50] Removal of water from natural gas is typically accomplished using glycol dehydrators, and there are at least 55,000 such units in the US alone.[51] The dehydrators operate by absorbing water and heavier hydrocarbons from natural gas streams using an absorbant such as triethylene glycol, and boiling off the absorbed components in a reboiler.[50] Because water content in natural gas is typically less than 100 lb/MMscf,[41] glycol dehydration units are relatively small compared to other separation units in natural gas systems such as amine absorption units. Furthermore, these dehydrators are highly efficient and inexpensive, requiring a capital cost of approximately $100,000 and an operating cost of a few cents per 1000 scf of treated gas.[10] Therefore, these units are widely used in industry.

Still, opportunities in natural gas dehydration exist for membrane systems. In certain applications, such as offshore drilling, where the weight of glycol units would be disadvantageous to platform costs, membranes may have a niche. Furthermore, BTEX compounds, which are absorbed and released by the glycol dehydration process, have been classified as Hazardous Air Pollutants (HAPs), and are therefore regulated internationally.[52] For certain natural gas streams, controlling the release of BTEX may need to be factored into process design, and membranes can help reduce the release of these HAPs.[51]

Many membranes have very high H_2O/CH_4 selectivities, so, with proper system design, these processes can operate with very high efficiency. Of particular concern, pressure ratio limitations can affect these types of separations. The maximum H_2O/CH_4 selectivity is always less than the ratio of H_2O partial pressure on the feed and permeate side of the membrane. Several patents have focused on addressing this problem by adding a vacuum pump on the permeate side of the membrane[53] or by sweeping dry methane past the permeate[54] to increase the pressure ratio of H_2O removal.

Removal of CO_2 and H_2S (*i.e.*, acid gases) from natural gas is a growing area of membrane technology. In 2008, Baker estimated the worldwide market for natural gas equipment was approximately $5 billion/yr, and membrane technology accounted for less than 5% of this market.[10] Furthermore, the membrane market is estimated to grow by 2020.[43]

Membrane separation competes most directly with amine absorption, which has existed since the 1930s and is a proven technology in industry.[55] Amine absorption processes for natural gas purification generally fit three categories: physical absorbents, chemical reactant absorbents, or a combination of both.[56] Regardless of the mechanism, natural gas sweetening involves introducing amines to a contactor and regenerating the

amines using a thermal process. It is estimated that 3 – 7 scf of acid gas can be treated per gallon of absorbent, and the energy cost to regenerate amines is approximately 1000 to 1200 BTUs/gallon.[56] Therefore, amine plants are sized to treat the amount of acid gas in a natural gas feed, and the larger the amine plant, the more energy intensive the purification. Additionally, about 1% of methane is lost to vent gas with amine absorption, and another 1 – 4% is used as fuel for the reboiler in the stripper, meaning that approximately 2 – 5% hydrocarbon is lost in the process.[10]

Amines are also subject to degradation when in contact with acid gases. These corrosion mechanisms are exacerbated by heating amines during regeneration and by increasing acid gas loading in the absorbents.[49] Amine plants can be fully constructed from carbon steel, but without stringent oversight and proper maintenance, detrimental system corrosion can occur. Consequently, most amine absorption plants contain many expensive stainless steel or alloy components.[49]

The capital costs, energy consumption, plant footprint, and maintenance costs of amine absorption have encouraged the development of membrane systems and membrane/absorption hybrid systems for natural gas purification.[56] The first membranes for natural gas purification were developed in the early to mid-1980s, but many of the seminal advancements needed to develop these membranes began two decades earlier. Reverse osmosis membranes had been developed from cellulose acetate membranes in the 1960s using the Loeb-Sourirajan process. Due to surface tension, pores in these membranes collapse when drying, and this pore collapse results in significant loss of desalination properties.[18,57] In 1969, Vos and Burris developed a drying technique, whereby RO membranes were first soaked in glycerol and ethylene glycol plasticizers.[57] Upon evaporating and re-soaking these membranes, there was no loss in RO properties.[57] Gas separation properties had previously been reported for dry cellulose acetate

membranes,[58] so the ability to produce these membranes on a large scale led to the development of the first CO_2 removal membranes in the early to mid-1980s.[18]

Because of advances in dry cellulose acetate membranes, the first natural gas membranes were developed from these materials. W.R. Grace (now part of UOP) and Separex (now part of UOP) developed spiral-wound membranes, and Cynara (now part of Cameron) developed hollow-fiber membranes.[10] These cellulose acetate membranes are still widely in use today, but polyimides and perfluoropolymers have gained some traction in this field over the past 15 – 20 years.[10]

Table 2.3 highlights several design approaches taken by industry to incorporate membranes into natural gas separation. The simplest approach is to use a one-stage membrane, thereby eliminating the need for a compressor. This approach is simple and straight-forward to install, but it results in a high hydrocarbon/methane product loss, and is therefore only used for low flowrates of gas, typically less than 5MMscfd.[2] Higher flowrates of gas (*i.e.*, 5MMscfd – 30MMscfd) often require the addition of a second membrane, a compressor, and a recycle loop in the process stream, and the added process costs from these additions allow membranes and amine absorption to compete in this range of flowrates.[2] Finally, three-stage membrane systems, which combine three membranes and one compressor, are often used for the highest flowrate of gases.[10,41] These systems require less compressor costs than similar-sized two-stage systems, but also have characteristically lower methane recovery.[41] Therefore, these types of systems are often used to reduce CO_2 content to < 8% in large, off-shore oil platforms.[10] Modest acid gas removal permits piping the natural gas from the off-shore platform to shore for further treatment.

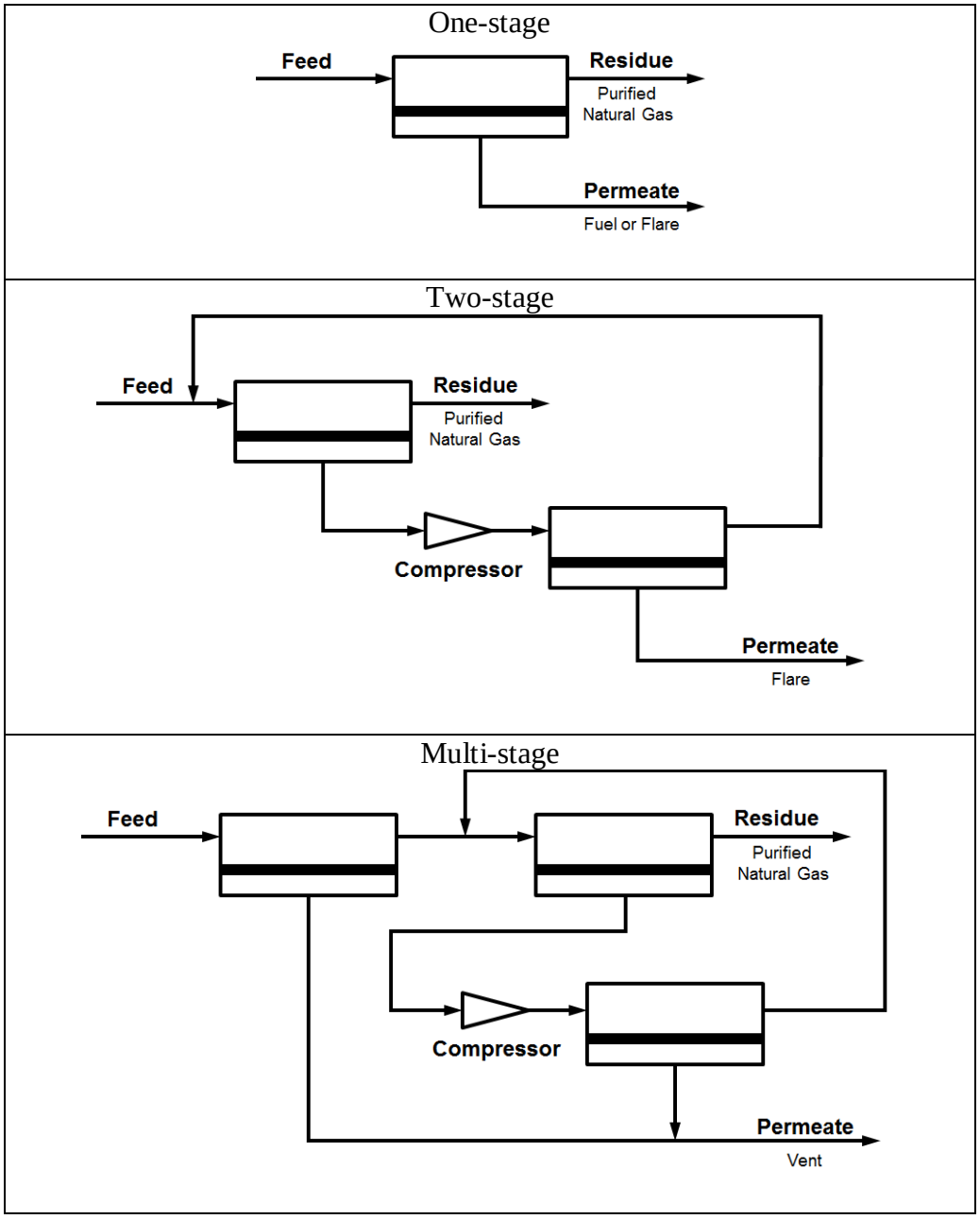

Table 2.3: Process diagrams for one-stage, two-stage, and multi-stage membrane systems for natural gas purification. Figures adapted from reference.[41]

The highest cost for membrane systems is not from the membranes themselves, but from components in the hollow fiber module and the membrane skids.10 High

pressure acid gases, being highly corrosive, require exceptional caution with skid design and therefore many stainless steel components. In fact, the material cost for membranes only accounts for approximately 4% of the total skid cost.10 To reduce costs, manufacturers aim to reduce the size of membrane skids, therefore reducing the number/size of stainless steel components. Several approaches have been taken to accomplish this goal. First, all companies seek to develop membranes with higher permeance and stability to plasticizing gases, which reduces the membrane area used per module, thus reducing the amount of stainless steel components. Alternatively, for a given material, companies have increased the size of membrane modules, which also reduces overall skid cost. For example, Cynara started with a 5" diameter membrane module in 1978, and has increased their membrane module to 30" diameter module in 2003.

2.8 EMERGING COMMERCIAL MEMBRANE GAS SEPARATION

Current trends in research and development show several emerging applications for gas separations with polymer membranes. Several gas pairs of interest and related applications are shown in Table 2.4. Many of these applications require material advancements to increase gas permeance and increase resistance to aggressive feed conditions.

Gas Pair	**Application**
CO_2/N_2	Carbon Capture
C_3H_6/C_3H_8	Propylene/Propane
C_2H_4/C_2H_6	Ethylene/Ethane
$EtOH/H_2O$	Ethanol/Water

Table 2.4: Emerging commercial gas separations.

2.8.1 Olefin/Paraffin

In 2009, over 22 million metric tons of ethylene, and over 13 million metric tons of propylene were produced in the US, making ethylene and propylene the two largest-volume organic chemical feedstocks.[59] The variety of synthetic chemicals derived from these olefins highlights their utility. Ethylene is used in the synthesis of polyethylene, ethylene oxide, ethylene chloride, and ethylbenzene.[60] Propylene is used in the synthesis of polypropylene, acrylonitrile, oxo-alcohols, cumene, and propylene oxide.[60]

Olefin/paraffin separation is accomplished through a distillation process that requires a high capital cost and high energy consumption. A large ethylene unit can cost several billion dollars,[61] and a large portion of the cost is devoted to the olefin/paraffin separation train.[62] Because olefin/paraffin components have very similar condensabilities, ethylene/ethane and propylene/propane splitters are massive pieces of equipment, towering between 200 and 300 feet high, containing over 100 trays, and operating with reflux ratios between 10 and 15.[44,63] The total energy cost for these operations is approximately 0.12 Quads of energy (1 Quad = 1x1015 BTU) per year,[62] which accounts for 6% of the total distillation energy consumption in the US, making olefin/paraffin separation the fourth most energy intensive separation process in the US, behind only petroleum, crude oil, and liquefied petroleum gas.[31]

Worldwide, 99% of ethylene and over 50% of propylene are produced from steam cracking.[64] Alternatively, propylene is also derived from fluid catalytic cracking, propane dehydrogenation, oxygenate conversion, and isomerization.[60,65] These processes produce an assortment of chemicals that require extensive treatment, making separations an important part of olefin production. A simplified process diagram of a steam cracker separation train is shown in Figure 2.4.[62] In this process, a mixture of hydrocarbons is first separated by a deethanizer into two streams: one stream with C2 (i.e., ethylene and

ethane) and lighter compounds, and one stream with C3 (i.e., propylene and propane) and heavier compounds. The light compounds are sent to a C2 splitter where ethylene and ethane are recovered with high purities. The heavier components are sent through a depropanizer to remove C4+ compounds (i.e., compounds with higher molecular weights than C3 compounds) before the C3 compounds are separated in a final splitter to recover propylene and propane in high purities. Despite the high energy and capital cost of this ethylene plant train, polymer grade olefins are recovered economically with this process.[62]

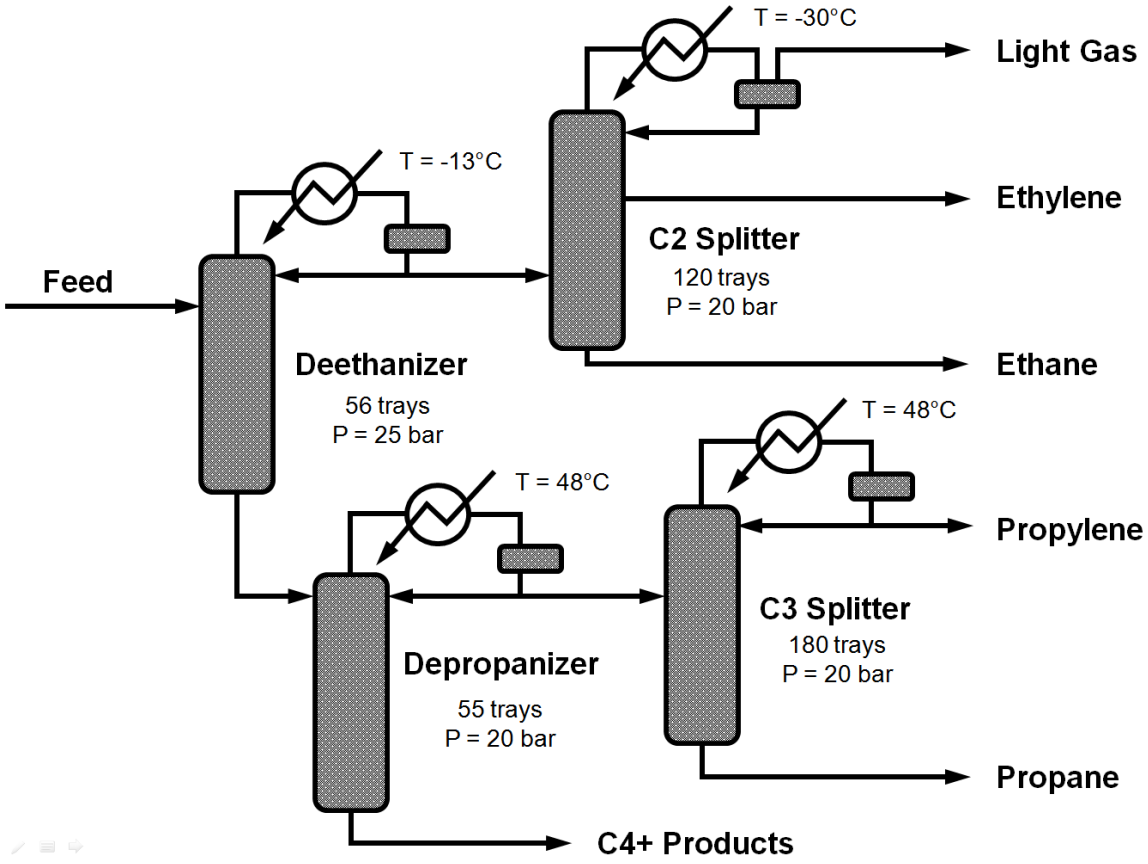

Figure 2.4: Typical olefin/paraffin separation train from a steam cracker feed.[62]

The opportunity for capital and energy savings in olefin/paraffin distillation has spurred several research efforts to explore the feasibility of polymer membranes for these separations.[19,20,65-67] Burns *et al.* have even defined a polymer upper bound for propylene/propane[20] analogous to those originally described by Robeson for other gas pairs[5,6] and fit by the Freeman model.[7] Still, as Table 2.5 demonstrates, ethylene/ethane and propylene/propane separation is inherently difficult because of the relative size and condensability of these gas molecules. Furthermore, it is well known that the best performing polymers for these separations are glassy,[20] and under high gas activities, or in the presence of mixtures, there can be a significant loss in selectivity due to plasticization.[67]

Gas	Lenard Jones Diameter (Å)	Critical Temperature (K)
Ethylene	4.16	282.5
Ethane	4.44	305.3
Propylene	4.68	365.2
Propane	5.12	369.9

Table 2.5: Size and critical temperature of C2 and C3 olefins and paraffins.

The C3 upper bound is shown in Figure 2.5, and several upper bound materials are highlighted. Interestingly, while 6FDA-based polyimides define the C3 polymer upper bound, they are inherently susceptible to plasticization. Figure 2.6 shows pure and mixed gas permeability of C_3H_6 and C_3H_8 for 6FDA-TrMPD at 323K.[67] At these low gas activities, typical dual-mode behavior is observed for both gases.[29] The mixed-gas results in Figure 2.6 demonstrate the effect of plasticization on glassy polymers for propylene and propane. At pressures near 2 atm, propane permeability begins to increase with

increasing pressure, an indication of plasticization.[3,13] Additionally, selectivity is lower for the mixed-gas experiments than in the pure-gas experiments.[67]

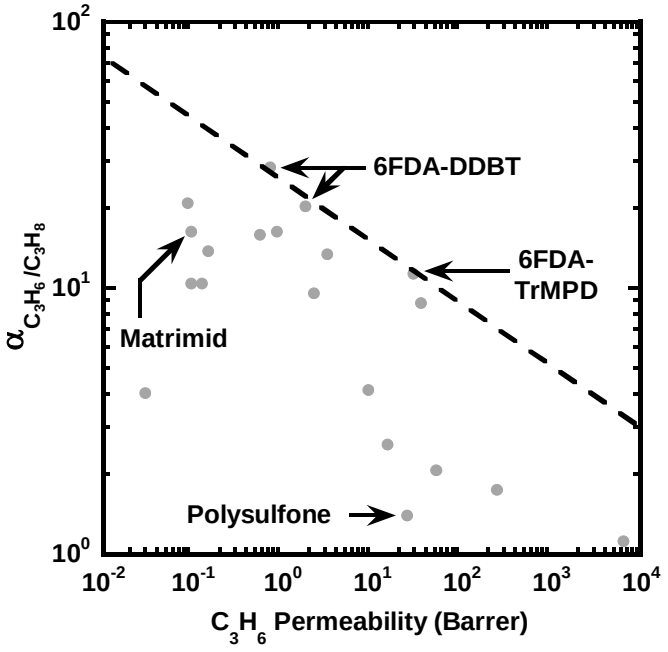

Figure 2.5: Propylene/propane upper bound. Data was taken between 26°C and 50°C, and for feed pressures between 1 and 4 atm. Polysulfone and several polyimides (Matrimid®, 6FDA-DDBT, and 6FDA-TrMPD) are highlighted.[20] The two 6FDA-DDBT points are reported in two independent studies.[20,68]

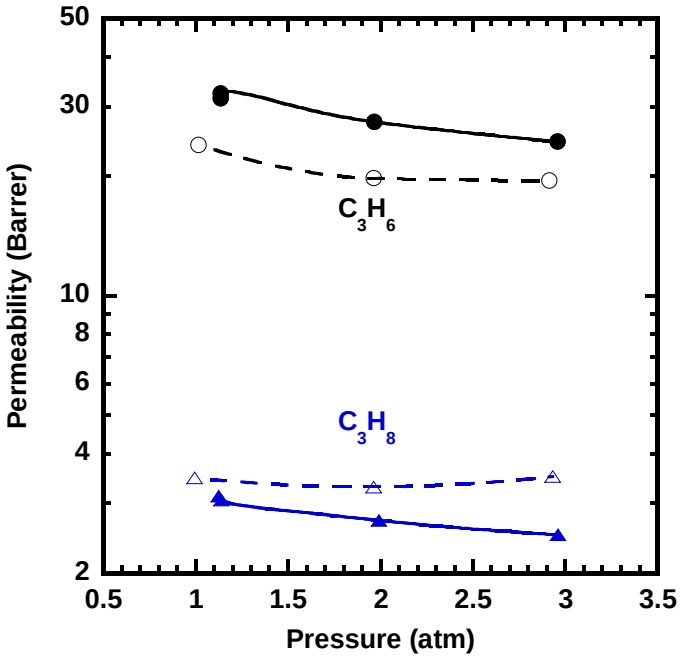

Figure 2.6: 6FDA-TrMPD propylene and propane permeability. Filled symbols are pure gas results, and open symbols are mixed gas results. The data was taken at 323K, and mixed gas data is for a 50:50 mixture.[67]

Finding high performance polymeric materials that operate under realistic feed conditions will be essential for the development of membranes in olefin/paraffin separation. To date, the lack of acceptable materials has prevented industrial development, and advances in the field will be needed to realize the full utility of polymer membranes for these separations.

Three major suggestions exist for incorporation of membranes into olefin/paraffin separations. The first two approaches are the simplest – (1) recover propylene vent gas from a propylene reactor,[43] and (2) incorporate membranes into the separation train with membrane-distillation hybrid systems.[44] The third approach is the most ambitious - (3) replace the olefin/paraffin distillation columns completely. Approach (1) takes place far downstream from the polyolefin process line. To synthesize polypropylene, polymer

grade propylene (approximately 99.5%) is injected into a reactor. Because propylene is a valuable feed, high recovery of propylene is essential, so unreacted propylene monomer at the exit of the reactor is recycled to the reactor feed. Propane, a contaminant in the original propylene feed begins to build up in the reactor because of the recycle loop. Out of necessity, a flare is used to remove the excess propane along with a concomitant loss of propylene. The loss of propylene can be significant, totaling approximately 1 – 2 % of the total propylene feed.[43] Adding a membrane to this vent may only require a selectivity of 3 – 5 and could provide yearly savings of approximately $1 million per plant.[43]

The second approach is more ambitious. Olefin/paraffin separation is a high-flow process run at high gas activities, making membrane stability and performance essential. Because ethylene/ethane distillation is operated under cryogenic conditions, there is a complex system of refrigeration integrated into the entire line. This cryogenic system complicates the energy analysis needed to examine the true cost of a membrane-distillation hybrid and also makes retrofitting existing C2 separation lines more difficult.[44] Therefore, most economic evaluations have focused on propylene/propane separation.[44,63] Referring to Figure 2.4, membranes can be incorporated into the C3 splitter by installation at the top of the column, the bottom of the column, or at the feed of the column. Membranes installed at the feed of the column would have to efficiently separate low-purity propane into high-purity propane, and based on current state-of-the-art membranes, selectivity would be too low, necessitating high recycle rates and expensive equipment.[44] Membranes installed on the downstream side of the column would operate under different requirements. At the top of the column a propylene-rich stream would need to be further purified to produce chemical grade (*i.e.*, 94%) or polymer grade (*i.e.*, 99.5%) product, while at the bottom of the column, a propylene-poor stream would need to be further diluted. Because the membrane area required for a

separation is dictated by the permeate flux, a lower propylene permeate flux at the bottom of the C3 column makes this option the most practical.[44] A schematic of the proposed location of a membrane in a membrane-distillation hybrid is shown in Figure 2.7.

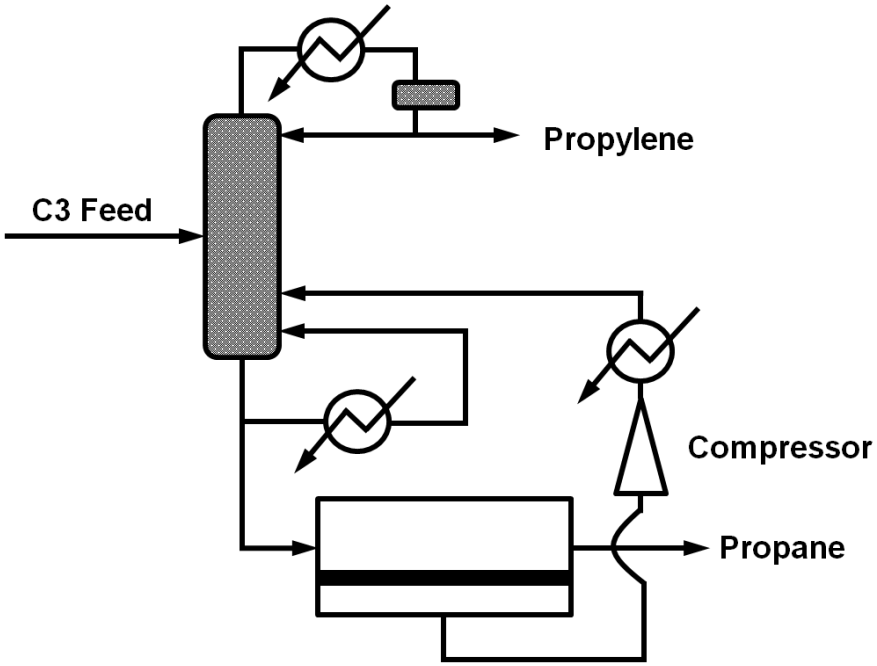

Figure 2.7: Proposed location of membrane in a membrane-distillation hybrid system.[44]

The ultimate goal of using membranes in propylene/propane separation is to replace the entire C3 distillation column. This goal is very ambitious, and several papers describe the need for materials with higher selectivity, adequate flux, and good stability.[2,20,43] Table 2.6 shows a proposed two-stage membrane system to produce chemical grade propylene and a three-stage membrane system to produce polymer grade propylene.[60] Calculations have shown that the two-stage system could operate successfully using membranes with propylene/propane selectivities of 35, and propylene permeabilities of 1 Barrer.[60] The three-stage system could operate with all membranes

having a selectivity of 15 and permeability of 2 Barrer, but far lower energy costs result from adding more selective membranes (*e.g.*, selectivity = 35, permeability = 1 Barrer) to the three-stage membranes module.[60]

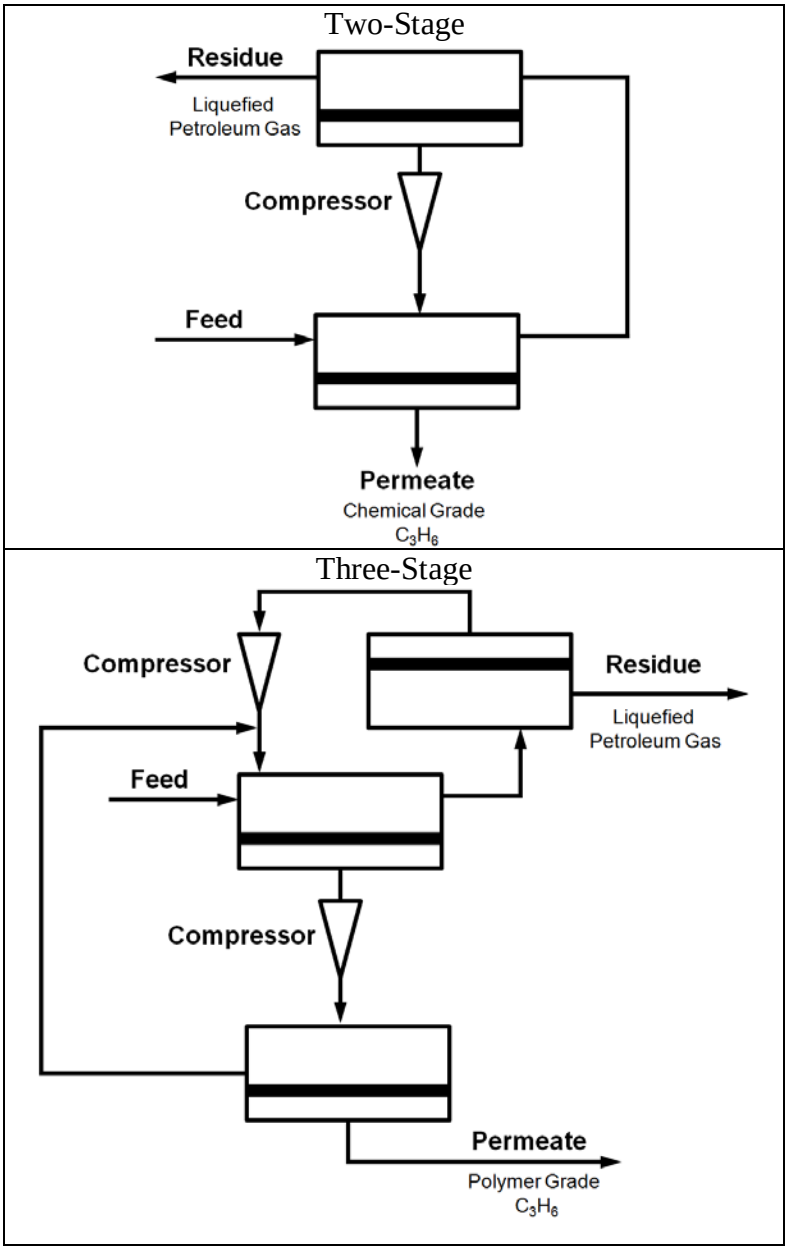

Table 2.6: Proposed process diagrams for membrane replacement of propylene/propane distillation columns. Feed conditions are taken as an industry average (70/30 propylene/propane). The two stage diagram is set up to produce chemical grade (94%) propylene, and the three-stage diagram is set up to produce polymer grade (99.5%) propylene. Liquefied petroleum gas has less than 5% propylene.[60]

2.8.2 Ethanol/Water

In response to limited oil reserves, energy independence, and climate change, significant research and government policy has focused on developing biofuels as an alternative to petroleum.[69] An important subset of biofuels is bioethanol, which is used as an additive to fuel. While a liter of ethanol only contains 66% of the energy as a liter of gasoline, it has a higher octane rating. Additionally, mixing ethanol with petroleum improves exhaust gas emissions by reducing carbon monoxide, hydrocarbons, sulfur content, and carcinogens.[70]

Bioethanol is produced from fermentation of a number of sugar-rich sources, including corn, sugarcane, wheat, and sugar beet.[70] Furthermore, starch and cellulose, which can easily be converted to sugar, are also used to produce bioethanol.[70] Fermented products from these sources are generally dilute, containing only 5 – 12 % ethanol by weight.[71] Therefore, separations are required to reach the fuel-grade ethanol purity levels of greater than 99%.[2]

Because of the relative volatilities of ethanol and water at low concentrations of ethanol, distillation would seem an obvious choice for separating these compounds. However, ethanol/water mixtures form an azeotrope at approximately 95.7 wt.% ethanol,[72] and an alternative process to distillation is therefore needed to reach fuel-grade ethanol purity. Today, most large-scale ethanol/water mixtures are separated with multiple distillation columns followed by molecular sieve adsorption to break the azeotrope.[73] The first step in this distillation process is a beer column, used to capture the ethanol produced from fermentation, followed by a stripper and rectification column.[74] The downstream of these distillation processes typically produces 93% ethanol, which is then fed to molecular sieves to increase ethanol purity to over 99%.[75]

Alternative separation processes, including gas stripping, steam stripping, liquid-liquid extraction, adsorption, pervaporation, and vapor permeation have also been pursued for ethanol/water purification.[73] Of these alternatives, pervaporation and vapor permeation offers the best option for replacing molecular sieves in small scale plants. For plants treating less than 5000 L/h of feed, pervaporation is less expensive than molecular sieves, but as feed rate increases, distillation/adsorption processes, which scale at a rate of 0.6 to 0.7 times that of pervaporation, become more economical.[2]

A basic schematic of a pervaporation and a vapor separation system is shown in Table 2.7. These processes are thermodynamically equivalent; a liquid feed must be vaporized and permeated through a membrane. Therefore, the separation factor associated with pervaporation is equal to the separation factor of evaporation times the separation factor of vapor permeation. The driving force for permeation comes about from the permeate-side condenser, which, upon condensation, creates a vacuum at the downstream-side of the membrane.

Pervaporation	Vapor Permeation
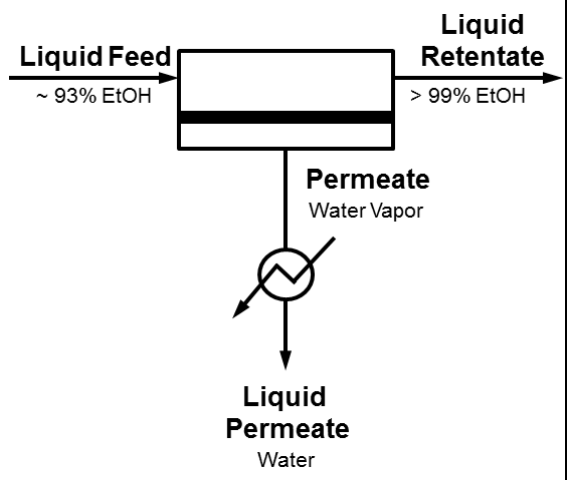	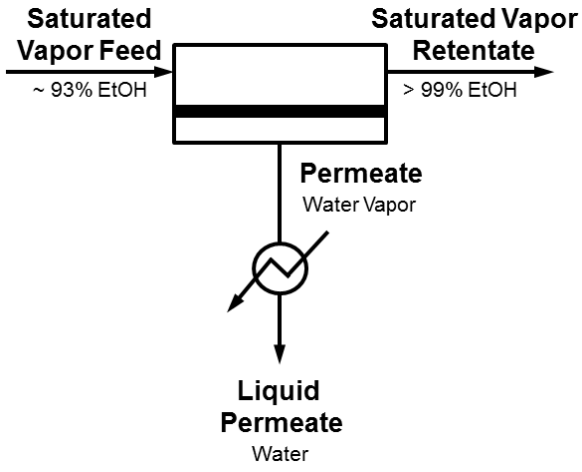

Table 2.7: Comparison of pervaporation and vapor permeation.

There are a number of challenges with using polymer membranes for ethanol/water separation. These challenges can be separated into two categories: membrane performance and process integration. More specifically, higher membrane selectivity, higher membrane flux, improved membrane stability, improved heat/energy integration, and better process design to increase pervaporation temperature are needed.[76]

Interestingly, membrane selectivity is not a major concern, at least in terms of material design, for these separations. The most widespread ethanol-water pervaporation membrane used today is the PERVAP™ membrane produced by Sulzer.[77] These membranes are made crosslinked polyvinyl alcohol,[77] have ethanol/water selectivities of approximately 200,[2] and their performance (*i.e.*, selectivity and flux) at various feed temperatures and compositions have been summarized by Chapman *et al.*[78] Industrially, this high selectivity can only be achieved when the process is designed with a high pressure ratio. Therefore, the condensers shown in Table 2.7 are essential for creating a permeate-side vacuum, thus preventing the pervaporation/vapor permeation system from

operating under a pressure ratio limited regime. Still, most ethanol/water plants are relatively small, and membrane module costs for these small systems can be 15 to 40% of the total plant cost.[2] Therefore, increasing membrane flux can reduce the area of membrane needed to make a separation and can reduce system costs, especially in a pressure ratio limited regime where selectivity can be lowered.

Membrane stability is a critical requirement for separation performance. Hot ethanol/water solutions are aggressive feed streams, and for this reason, most pervaporation tests for polymeric films are run at low temperatures. Chapman *et al.* have reviewed the literature on pervaporation using poly(vinyl alcohol), chitosan, alginate, polysulfone, polyimides, polyamides, polyelectrolytes, and polyaniline, among other polymers.[78] With a few exceptions, most of these experiments were conducted at temperatures at or below 60°C. Many polymers have very limited stability as temperature increases. For example, cellulose esters, poly(vinyl alcohol), chitosan, and fluorinated ion-exchange membranes begin to show signs of degradation after exposure to 100°C water for only 24 hrs.[79,80] Furthermore, polyimides are susceptible to hydrolysis,[81] and condensation on polyimide films can lead to degradation under typical pervaporation conditions.[80]

One approach for advancing market penetration of membranes in ethanol/water separation is to replace both the distillation column and the molecular sieve adsorption unit from the separation process. This approach, which operates with a hybrid stripper column/vapor permeation unit, has been pursued by Membrane Technology and Research (MTR), and a simplified schematic of their system is shown in Figure 2.8[79,80,82]. Because heat/energy integration and process design have prevented wide-spread acceptance of membranes for ethanol/water separation,[76] MTR has addressed these problems by using membrane materials that can operate under very aggressive vapor

permeation conditions. In pervaporation, 3 – 5 membranes are typically used in series, and heat must be applied to each feed to vaporize the liquid permeate.[2] Alternatively, at slightly higher temperatures, vapor permeation can be run isothermally, greatly simplifying the heat integration process for membrane modules.[2] Additionally, higher transmembrane flux is obtained by operating the vapor permeation system at elevated temperatures.

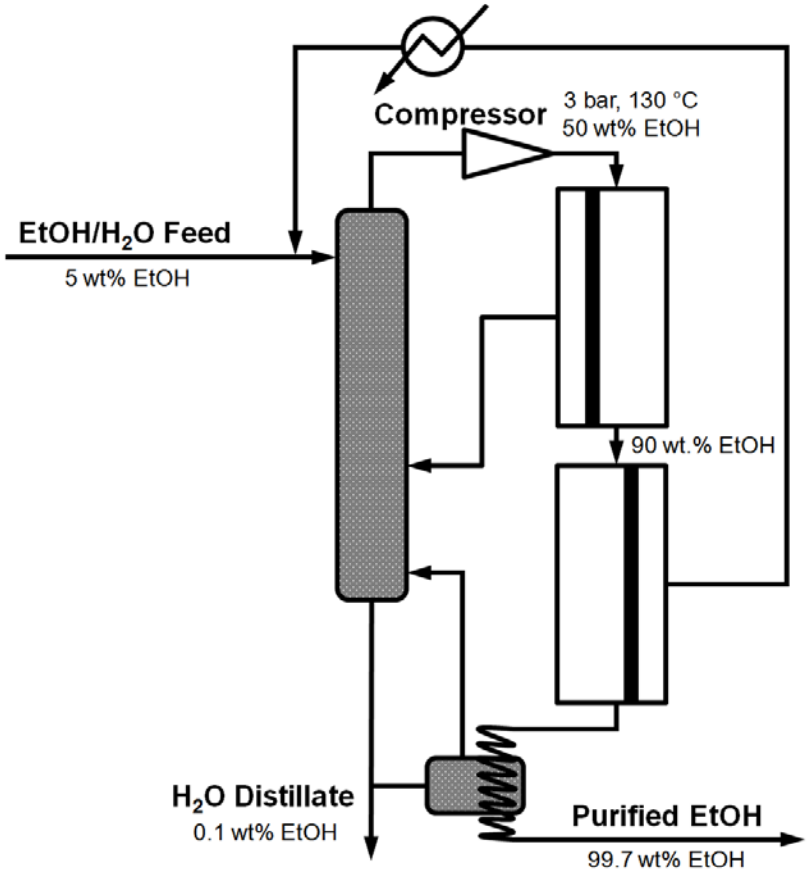

Figure 2.8: Simplified stripper column/vapor permeation system for ethanol/water separation. Basic ethanol/water composition and operating conditions are labeled.[80]

Despite the advantages of running ethanol/water separation with vapor permeation, finding polymer materials that are stable under these conditions is

challenging. MTR has designed their vapor permeation system around perfluoropolymers (*e.g.*, Cytop™, Hyflon® AD, and Teflon® AF),[80] and a patent by Huang *et al.* addresses some of the important criteria for selecting membranes for ethanol/water separation.[79] Research and development of other highly stable polymer materials will be a focus in ethanol/water separations over the coming years.

2.8.3 Carbon Capture

Combustion of fossil fuels (*e.g.*, coal, petroleum, and natural gas) and biofuels is used to produce energy for electricity, industrial processes, and transportation. These processes result in high CO_2 emission to the atmosphere, which has been linked with global warming.[83] In 2007, 37 Gt of CO_2 were released into the atmosphere, and 85% of that CO_2 resulted from global energy use.[84] Furthermore, in the United States, 40% of the CO_2 was due to energy production, 30% resulted from industrial processes, and 30% was from transportation.[84] Research, development, and government policy are being directed at developing methods of capturing and storing or utilizing CO_2 to reduce climate change.[85,86]

The Department of Energy has recently identified membranes as one of three basic research needs for separation processes in carbon capture.[84] For industrial energy production, which appears well-suited for membrane separations, there are three potential locations for membrane integration in the process stream: (1) post-combustion capture, (2) pre-combustion capture, and (3) oxo-combustion. The potential location of membranes is shown in Figure 2.9.[87] For post-combustion capture, membrane units would be installed downstream of the combustion process, and low pressure CO_2 would need to be separated from N_2 before sequestration. For pre-combustion capture, high pressure CO_2 would need to be separated from syngas (CO and H_2) before combustion.

Oxy-combustion would use membranes to produce high-purity oxygen feeds for combustion reactions, therefore creating a CO_2 and H_2O stream that would be dehydrated and compressed.

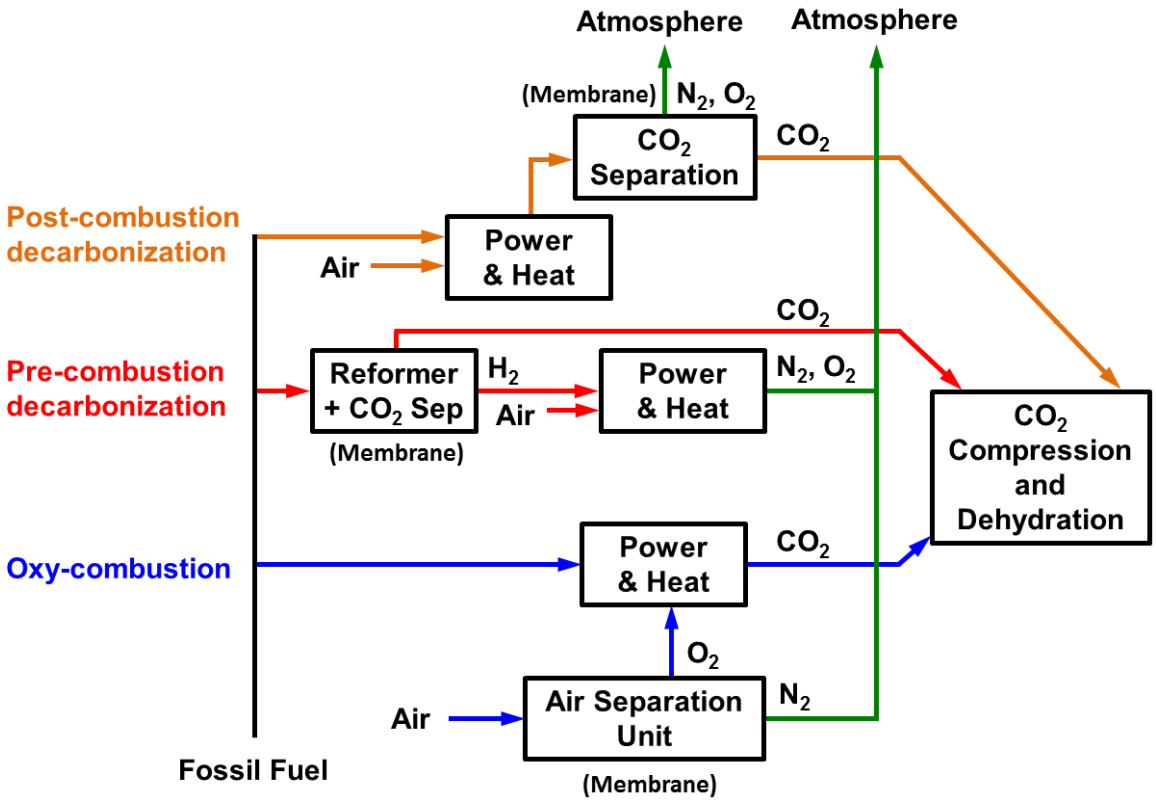

Figure 2.9: Potential process locations for membrane integration in carbon capture applications. Figure adapted from source.[87]

Table 2.8 shows the basic gas pairs that would need to be separated for each carbon capture application. The actual separation processes, however, are much more complex. Post-combustion membranes would be installed downstream of a coal-fired power plant. A typical 550 MW plant produces 2 MMscf of flue gas per minute, and only 12 – 14% of that gas is CO_2.[84] Flue gas also contains water, oxygen, nitrogen, and

trace amounts of sulfur oxides and nitrogen oxides.[84] Because of the low concentration of CO_2 in post-combustion flue gas, a number of studies have estimated that high membrane CO_2/N_2 selectivities (*i.e.*, ~100) would be needed for membranes to compete with other technologies such as amine absorption, but most of these studies model carbon capture with single-stage membrane systems.[88-90] MTR has recently developed their Polaris™ membrane, which has a CO_2/N_2 selectivity of 50 and a permeance of about 1000 gpu, for carbon capture applications.[87,91] With an extensive process optimization analysis, they found that a two-stage membrane system, combining a slight feed compression, partial permeate vacuum, and a sweep operation, could be competitive with other technologies.[87]

Carbon Capture Application	Dominant Gas Separation
Post-combustion	CO_2/N_2
Pre-combustion	CO_2/H_2
Oxy-combustion	O_2/N_2

Table 2.8: List of important gas separations for carbon capture applications with membranes.

Oxy-combustion carbon capture is a very challenging application for polymer membranes. High purity O_2 must be fed to the reactor, and current state-of-the art polymer membranes cannot achieve these separations, as described in the Air Separation section of this review. The most likely integration of membranes in oxy-combustion applications would be for high-temperature ceramic membranes.[84]

Although pre-combustion carbon capture has a much more favorable gas composition of approximately 40% CO_2, 56% hydrogen, and the remaining 4% is carbon monoxide, methane, nitrogen, and argon and hydrogen sulfide,[92] very high temperatures may be required to economically achieve these separations. For example, membrane

operating temperatures of approximately 700°C are preferred membrane reformers, and temperatures between approximately 300°C and 500°C are preferred for water gas shift reactors.[84] At these high temperatures and high concentrations of CO_2, it is difficult to find high performing and stable polymer membranes. Still, some recent research efforts have focused on CO_2 and H_2 selective membranes for these applications. CO_2 selective membranes operate best at low temperatures,[5,6,93] making process integration of these membranes more difficult. Several high temperature, H_2 selective polymer membranes have been investigated for pre-combustion applications. Polybenzimidazole membranes have the highest operating temperature of polymer membranes (*e.g.*, 200°C – 400°C),[94] and MTR has tested membranes at 150°C.[92] More research is needed to develop and investigating polymer membrane stability at high temperatures, and better membrane process integration is needed for pre-combustion applications.

2.9 REFERENCES

1. Yampolskii, Y., I. Pinnau, and B.D. Freeman, eds. *Materials science of membranes for gas and vapor separation*. **2006**, John Wiley and Sons: Chichester.

2. Baker, R.W., *Membrane technology and applications*. **2004**, Chichester, John Wiley & Sons, Ltd.

3. Paul, D.R. and Y.P. Yampolskii, *Polymeric gas separation membranes*. **1994**, Boca Raton, CRC Press.

4. Drioli, E. and L. Giorno, *Membrane operations: Innovative separations and transformations*. **2009**, Weinheim, Wiley-VCH. 551-551.

5. Robeson, L.M., *Correlation of separation factor versus permeability for polymeric membranes.* Journal of Membrane Science, **1991**. 62(2), 165-185.

6. Robeson, L.M., *The upper bound revisited.* Journal of Membrane Science, **2008**. 320(1-2), 390-400.

7. Freeman, B.D., *Basis of permeability/selectivity tradeoff relations in polymeric gas separation membranes.* Macromolecules, **1999**. 32(2), 375-380.

8. Park, H.B., C.H. Jung, Y.M. Lee, A.J. Hill, S.J. Pas, S.T. Mudie, E. Van Wagner, B.D. Freeman, and D.J. Cookson, *Polymers with cavities tuned for fast selective transport of small molecules and ions.* Science, **2007**. 318(5848), 254-258.

9. Sanders, D.F., Z.P. Smith, C.P. Ribeiro, R.L. Guo, J.E. McGrath, D.R. Paul, and B.D. Freeman, *Gas permeability, diffusivity, and free volume of thermally rearranged polymers based on 3,3 '-dihydroxy-4,4 '-diamino-biphenyl (HAB) and 2,2 '-bis-(3,4-dicarboxyphenyl) hexafluoropropane dianhydride (6FDA).* Journal of Membrane Science, **2012**. 409, 232-241.

10. Baker, R.W. and K. Lokhandwala, *Natural gas processing with membranes: An overview.* Industrial & Engineering Chemistry Research, **2008**. 47(7), 2109-2121.

11. Puleo, A.C., D.R. Paul, and S.S. Kelley, *The effect of degree of acetylation on gas sorption and transport behavior in cellulose acetate.* Journal of Membrane Science, **1989**. 47(3), 301-332.

12. Sada, E., H. Kumazawa, P. Xu, and S.T. Wang, *Permeation of pure carbon dioxide and methane and binary mixtures through cellulose acetate membranes.* Journal of Polymer Science Part B: Polymer Physics, **1990**. 28(1), 113-125.

13. Matteucci, S.T., Y.P. Yampolskii, B.D. Freeman, and I. Pinnau, *Transport of gases and vapors in glassy and rubbery polymers*, in *Materials science of membranes for gas and vapor separation*, Y. Yampolskii, I. Pinnau, and B.D. Freeman, Editors. **2006**, John Wiley & Sons: Chichester. 1-47.

14. Hirayama, Y., T. Yoshinaga, Y. Kusuki, K. Ninomiya, T. Sakakibara, and T. Tamari, *Relation of gas permeability with structure of aromatic polyimides I.* Journal of Membrane Science, **1996**. 111(2), 169-182.

15. Hirayama, Y., T. Yoshinaga, Y. Kusuki, K. Ninomiya, T. Sakakibara, and T. Tamari, *Relation of gas permeability with structure of aromatic polyimides II.* Journal of Membrane Science, **1996**. 111(2), 183-192.

16. Wind, J.D., D.R. Paul, and W.J. Koros, *Natural gas permeation in polyimide membranes.* Journal of Membrane Science, **2004**. 228(2), 227-236.

17. Staudt-Bickel, C. and W.J. Koros, *Improvement of CO_2/CH_4 separation characteristics of polyimides by chemical crosslinking.* Journal of Membrane Science, **1999**. 155, 145-154.

18. Lonsdale, H.K., *The growth of membrane technology.* Journal of Membrane Science, **1982**. 10(2-3), 81-181.

19. Staudt-Bickel, C. and W.J. Koros, *Olefin/paraffin gas separations with 6FDA-based polyimide membranes.* Journal of Membrane Science, **2000**. 170(2), 205-214.

20. Burns, R.L. and W.J. Koros, *Defining the challenges for C_3H_6/C_3H_8 separation using polymeric membranes.* Journal of Membrane Science, **2003**. 211(2), 299-309.

21. Vasudevan, V.J. and J.E. McGrath, *Atomistic modeling of amorphous aromatic polybenzoxazoles.* Macromolecules, **1996**. 29(2), 637-645.

22. Wolfe, J.F., *Rigid-rod polymers. 1. Synthesis and thermal properties of para-aromatic polymers with 2,6-benzobisoxazole units in the main chain.* Macromolecules, **1981**. 14(4), 909-915.

23. Tullos, G. and L. Mathias, *Unexpected thermal conversion of hydroxy-containing polyimides to polybenzoxazoles.* Polymer, **1999**. 40(12), 3463-3468.

24. Tullos, G.L., J.M. Powers, S.J. Jeskey, and L.J. Mathias, *Thermal conversion of hydroxy-containing imides to benzoxazoles: Polymer and model compound study*. Macromolecules, **1999**. 32(11), 3598-3612.

25. Kardash, I. and A.N. Pravednikov, *Aromatic polyimides containing hydroxy- and methoxy-groups.* Vysokomol Soyed, **1967**. 9(12), 873-876.

26. Ohya, H., V.V. Kudryavtsev, and S.I. Semenova, *Polyimide membranes: Applications, fabrications, and properties*. **1996**, Amsterdam, Gordon and Breach Publishers.

27. Ghosh, M.K. and K.L. Mital, *Polyimides: Fundamentals and applications*. **1996**, New York, Marcel.

28. Wijmans, J.G. and R.W. Baker, *The solution-diffusion model: A review.* Journal of Membrane Science, **1995**. 107(1-2), 1-21.

29. Koros, W.J., D.R. Paul, and A.A. Rocha, *Carbon dioxide sorption and transport in polycarbonate*. Journal of Polymer Science: Polymer Physics Edition, **1976**. 14(4), 687-702.

30. Frisch, H.L., *Sorption and transport in glassy polymers - A review.* Polymer Engineering and Science, **1980**. 20(1), 2-13.

31. *US Department of Energy Report. Materials for separation technology: Energy and emission reduction opportunities*. **2004**, BCS, Incorportated, Oak Ridge National Laboratory.

32. Perry, E. *Process for the recovery of hydrogen from ammonia purge gases*, **1979**, US Pat. 4172885.

33. *Recovery..., hydrogen... made simple*. Chemical & Engineering News, **1979**. 57(48), 26-27.

34. *Advanced Prism® membrane systems for cost effective gas separations.* Available from: http://www.airproducts.com/products/Gases/supply-options/~/media/Downloads/Brochure/advanced-prism-membrane-system-brochure.ashx.

35. Scott, K., *Handbook of Industrial Membranes*. First Edition ed. **1995**, Oxford, UK, Elsevier Science Publishers Ltd.

36. Lu, K., C. Song, and V. Subramani, eds. *Hydrogen and syngas production and purification technologies*. **2010**, John Wiley & Sons, Inc.: Hoboken, NJ.

37. *Hydrogen Separations in Syngas.* 2009; Available from: http://www.mtrinc.com/pdf_print/refinery_and_syngas/MTR_Brochure_Hydrogen_Separations.pdf.

38. Posey, L.G. *Processes*, **1983**, US Pat. 4367135.

39. Graham, T., *On the absorption and dialytic separation of gases by colloid septa Part I. Action of a septum of caoutchouc.* The London, Edinburgh, and Dublin Philosophical Magazine and Journal of Science, **1866**. 32, 401-420.

40. Prasad, R., F. Notaro, and D.R. Thompson, *Evolution of membranes in commercial air separation.* Journal of Membrane Science, **1994**. 94, 225-248.

41. Spillman, R.W., *Economics of gas separation membranes.* Chemical Engineering Progress, **1989**. 85(1), 41–62.

42. Prasad, R., R.L. Shaner, and K.J. Doshi, *Comparison of membranes with other gas separation technologies*, in *Polymeric gas separation membranes*, D.R. Paul and Y.P. Yampolskii, Editors. **1994**, CRC Press: Boca Raton.

43. Baker, R.W., *Future directions of membrane gas separation technology.* Industrial & Engineering Chemistry Research, **2002**. 41(6), 1393-1411.

44. Gottschlich, D.E. and D.L. Roberts, *Energy Minimization of Separation Processes Using Conventional/Membrane Hybrid Systems*. **1990**, U.S. Department of Energy: Menlo Park.

45. Puri, P.S., *Commercial applications of membranes in gas separations*, in *Membrane engineering for the treatment of gases Vol 1: Gas separation problems with membranes*, E. Drioli and G. Barbieri, Editors. **2011**, Royal Society of Chemistry.

46. Sanders Jr, E.S., D.O. Clark, J.A. Jensvold, H.N. Beck, G.G. Lipscomb, and F.L. Coan. *Process for preparing POWADIR membranes from tetrahalobisphenol A polycarbonates*, **1988**, US Pat. 4772392.

47. Ekiner, O.M., R.A. Hayes, and P. Manos. *Novel multicomponent fluid separation membranes*, **1992**, US Pat. 5085676.

48. Prasad, R. *Process and system for the production of dry, high purity nitrogen*, **1990**, US Pat. 4931070.

49. Kohl, A. and R. Nielsen, *Gas purification: 5th edition*. **1997**, Houston, TX, Gulf Publishing Company.

50. Choi, D.W., *How to buy glycol dehydrators.* Hydrocarbon Processing **2006**. 85(7), 69-76.

51. Wijmans, J.G., A. Ng, and A.P. Mairal. *Natural gas dehydration apparatus*, **2004**, US Pat. 20040206242 A1.

52. *Region VIII pretreatment guidance on the analysis of BTEX*. 1999; Available from: http://www.epa.gov/region8/water/pretreatment/pdf/BTEXGuidance.pdf.

53. Friesen, D.T., R.J. Ray, D.D. Newbold, and S.B. McCray. *Countercurrent dehydration by hollow fibers*, **1992**, US Pat. 5108464.

54. Auvil, S.R., J.S. Choe, and L.J. Kellogg, Jr. *Use of membrane separation to dry gas streams containing water vapor*, **1993**, US Pat. 5259869.

55. Bottoms, R.R. *Process for separating acidic gases*, **1931**, US Pat. 1834016.

56. Cooley, T.E. and A.B. Coady. *Removal of H_2S and/or CO_2 from a light hydrocarbon stream by use of gas permeable membrane*, **1978**, US Pat. 4130403.

57. Vos, K.D. and F.O. Burris, *Drying cellulose acetate reverse osmosis membranes.* Industrial & Engineering Chemistry Product Research and Development, **1969**. 8(1), 84-89.

58. Merten, U., S. Beach, and P.K. Gantzel. *Method and apparatus for gas separation by diffusion*, **1968**, US Pat. 3415038.

59. *Facts & figures: Output declines in U.S., Europe.* Chemical & Engineering News, **2010**. 88(27), 54-62.

60. Colling, C., J. Huff, GA, and J.V. Bartles. *Processes using solid perm-selective membranes in multiple groups for simultaneous recovery of specified products from a fluid mixture*, **2004**, US Pat. 6830691 B2.

61. Carroll, J. *Chevron Phillips studying ethylene cracker amid gas glut*. Bloomberg News 2012; Available from: http://www.bloomberg.com/news/2012-02-23/chevron-phillips-may-build-ethylene-cracker-amid-shale-gas-glut.html.

62. Eldrige, R.B., *Olefin/paraffin separation technology: A review.* Industrial & Engineering Chemistry Research, **1993**. 32(10), 2208-2212.

63. Cougard, N., A. Baudot, and V. Coupard. *Process for separating propane and propylene using a distillation column and a membrane separation column*, **2008**, US Pat. 2011/0049051 A1.

64. Wang, G., Z. Zhang, S. Chen, and L. Zhang. *Process for producing olefins*, **2010**, US Pat. 2010/0274063 A1.

65. Das, M. and W.J. Koros, *Performance of 6FDA–6FpDA polyimide for propylene/propane separations.* Journal of Membrane Science, **2010**. 365(1-2), 399-408.

66. Pinnau, I. and L.G. Toy, *Solid polymer electrolyte composite membranes for olefin/paraffin separation.* Journal of Membrane Science, **2001**. 184(1), 39-48.

67. Tanaka, K., A. Taguchi, J. Hao, H. Kita, and K. Okamoto, *Permeation and separation properties of polyimide membranes to olefins and paraffins.* Journal of Membrane Science, **1996**. 121(2), 197-207.

68. Okamoto, K., K. Noborio, J. Hao, K. Tanaka, and K. Hidetoshi, *Permeation and separation properties of polyimide membranes to 1, 3-butadiene and n-butane.* Journal of Membrane Science, **1997**. 134(2), 171-179.

69. Escobar, J.C., E.S. Lora, O.J. Venturini, E.E. Yáñez, E.F. Castillo, and O. Almazan, *Biofuels: Environment, technology and food security.* Renewable and Sustainable Energy Reviews, **2009**. 13(6-7), 1275-1287.

70. Nigam, P.S. and A. Singh, *Production of liquid biofuels from renewable resources.* Progress in Energy and Combustion Science, **2011**. 37(1), 52-68.

71. Huang, H.-J., S. Ramaswamy, U.W. Tschirner, and B.V. Ramarao, *A review of separation technologies in current and future biorefineries.* Separation and Purification Technology, **2008**. 62(1), 1-21.

72. Gmehling, J., J. Menke, J. Krafczyk, K. Fischer, J.C. Fontaine, and H.V. Kehiaian, *Azeotropic data for binary mixtures*, in *CRC Handbook of Chemistry and Physics, 92nd Edition (Internet Version 2012)*, W.M. Haynes, Editor. **2012**, CRC Press/Taylor and Francis: Boca Raton, FL.

73. Vane, L., *Separation technologies for the recovery and dehydration of alcohols from fermentation broths.* Biofuels, Bioproducts and Biorefining, **2008**. 2(6), 553-588.

74. Kwiatkowski, J.R., A.J. McAloon, F. Taylor, and D.B. Johnston, *Modeling the process and costs of fuel ethanol production by the corn dry-grind process.* Industrial Crops and Products, **2006**. 23(3), 288-296.

75. Huang, Y., R.W. Baker, and L.M. Vane, *Low-energy distillation-membrane separation process.* Industrial & Engineering Chemistry Research, **2010**. 49(8), 3760-3768.

76. Vane, L.M., *A review of pervaporation for product recovery from biomass fermentation processes.* Journal of Chemical Technology & Biotechnology, **2005**. 80(6), 603-629.

77. *Membrane Technology*. 2012; Available from: http://www.sulzerchemtech.com/de/portaldata/11/Resources//brochures/pt/Membrane_Technology.pdf.

78. Chapman, P.D., T. Oliveira, A.G. Livingston, and K. Li, *Membranes for the dehydration of solvents by pervaporation.* Journal of Membrane Science, **2008**. 318(1-2), 5-37.

79. Huang, Y., J. Ly, T. Aldajani, and R.W. Baker. *Liquid-phase and vapor-phase dehydration of organic/water solutions*, **2008**, US Pat. 8000874 B2.

80. Huang, Y., J. Ly, D. Nguyen, and R.W. Baker, *Ethanol dehydration using hydrophobic and hydrophilic polymer membranes.* Industrial & Engineering Chemistry Research, **2010**. 49(23), 12067-12073.

81. Pryde, C.A., *Polyimide hydrolysis measurement by fourier transform — IR spectroscopy*, in *Polymeric Materials for Electronics Packaging and Interconnection*, J.H. Lupinski and R.S. Moore, Editors. **1989**, American Chemical Society: Washington, DC. 57-66.

82. Vane, L., F. Alvarez, L. Rosenblum, and S. Govindaswamy, *Efficient ethanol recovery from yeast fermentation broth with integrated distillation-membrane process.* Industrial & Engineering Chemistry Research, **2012**. 52(3), 1033–1041.

83. Hansen, J., M. Sato, R. Ruedy, K. Lo, D.W. Lea, and M. Medina-Elizade, *Global temperature change.* Proceedings of the National Academy of Sciences of the United States of America, **2006**. 103(39), 14288-14293.

84. *Basic research needs for carbon capture: Beyond 2020, US Department of Energy Basic Energy Sciences Workshop for Carbon Capture*. 2010 March 4-5; Available from: http://science.energy.gov/~/media/bes/pdf/reports/files/CCB2020_rpt.pdf.

85. *The future of coal: An interdisciplinary MIT study*. 2007; Available from: http://web.mit.edu/coal/The_Future_of_Coal.pdf.

86. Moss, R.H., J.A. Edmonds, K.A. Hibbard, M.R. Manning, S.K. Rose, D.P.V. Vuuren, T.R. Carter, S. Emori, M. Kainuma, T. Kram, G.A. Meehl, J.F.B. Mitchell, N. Nakicenovic, K. Riahi, S.J. Smith, R.J. Stouffer, A.M. Thomson, J.P. Weyant, and T.J. Wilbanks, *The next generation of scenarios for climate change research and assessment.* Nature, **2010**. 463(7282), 747-756.

87. Merkel, T.C., H.Q. Lin, X.T. Wei, and R.R. Baker, *Power plant post-combustion carbon dioxide capture: An opportunity for membranes.* Journal of Membrane Science, **2010**. 359(1-2), 126-139.

88. Bounaceur, R., N. Lape, D. Roizard, C. Vallieres, and E. Favre, *Membrane processes for post-combustion carbon dioxide capture: A parametric study.* Energy, **2006**. 31, 2556-2570.

89. Brunetti, A., F. Scura, G. Barbieri, and E. Drioli, *Membrane technologies for CO_2 separation.* Journal of Membrane Science, **2010**. 359(1-2), 115-125.

90. Favre, E., *Carbon dioxide recovery from post-combustion processes: Can gas permeation membranes compete with absorption?* Journal of Membrane Science, **2007**. 294(1-2), 50-59.

91. Merkel, T.C. *NETL Report: Membrane process to capture carbon dioxide from coal-fired power plant flue gas.* Available from: http://www.netl.doe.gov/File%20Library/Research/Coal/ewr/co2/5312-43085-MTR-spiral-wound-polymeric-membrane.pdf.

92. Merkel, T.C., M. Zhou, and R.W. Baker, *Carbon dioxide capture with membranes at an IGCC power plant.* Journal of Membrane Science, **2012**. 389, 441-450.

93. Lin, H., E. Van Wagner, B.D. Freeman, L.G. Toy, and R.P. Gupta, *Plasticization-enhanced hydrogen purification using polymeric membranes.* Science, **2006**. 311(5761), 639-642.

94. Krishnan, G., D. Steele, K. O'Brien, R. Callahan, K. Berchtold, and J. Figueroa, *Simulation of a process to capture CO_2 from IGCC syngas using a high temperature PBI membrane.* Energy Procedia, **2009**. 1(1), 4079-4088.

Chapter 3: Materials and Experimental Methods

This chapter describes the materials and characterization experiments used for this dissertation. The materials section describes the synthesis, casting, and treatment of all samples, and the experimental methods section describes the permeability and sorption experiments, along with additional standard characterization techniques.

3.1 MATERIALS

3.1.1 Polymer Synthesis

3.1.1.1 Synthesis of HAB-6FDA-C

The *acetate*-functional polyimide in this dissertation was prepared from 3,3′-dihydroxy-4,4′-diamino-biphenyl (HAB) ′ and 2,2 -bis-(3,4-dicarboxyphenyl) hexafluoropropane dianhydride (6FDA). HAB-6FDA-C was synthesized via chemical imidization following a procedure that has been previously reported.[1] HAB (CAS # 2373-98-0) was either purchased from Chriskev (Overland Park, KS) or supplied from Wakayama Seiko Kogyo Co., Ltd. and 6FDA (CAS # 1107-00-2) was purchased from Sigma Aldrich. HAB powder was held at 50°C under vacuum for 24 h before use and, to

---

This chapter has been adapted with permission from sections of: **(1)** Smith, Z.P., D.F. Sanders, C.P. Ribeiro Jr, R. Guo, B.D. Freeman, D.R. Paul, J.E. McGrath, and S. Swinnea, *Gas sorption and characterization of thermally rearranged polyimides based on 3,3'-dihydroxy-4,4'-diamino-biphenyl (HAB) and 2,2'-bis-(3,4-dicarboxyphenyl) hexafluoropropane dianhydride (6FDA).* Journal of Membrane Science, **2012**. 416, 558-567.; **(2)** Smith, Z.P., R.R. Tiwari, T.M. Murphy, D.F. Sanders, K.L. Gleason, D.R. Paul, and B.D. Freeman, *Hydrogen sorption in polymers for membrane applications.* Polymer, **2013**. 54(12), 3026–3037.; **(3)** Smith, Z.P., K. Czenkusch, K.L. Gleason, G.H.G.C. Alvarez, A.E. Lozano, D.R. Paul, and B.D. Freeman, *Effect of polymer structure on gas transport properties of polyimides, polyamides and TR polymers (in preparation).*; **(4)** Smith, Z.P., K. Czenkusch, S. Wi, K.L. Gleason, G.H.G.C. Doherty, K. Konstas, T. Bastow, C. Alvarez, A.J. Hill, A.E. Lozano, D.R. Paul, and B.D. Freeman, *Confirmation of polybenzoxazole structure of thermally rearranged polymers (in preparation).*; **(5)** Smith, Z.P., R.R. Tiwari, M.E. Dose, K.L. Gleason, T.M. Murphy, D.F. Sanders, G. Gunawan, L.M. Robeson, D.R. Paul, and B.D. Freeman, *The influence of diffusivity and sorption on helium and hydrogen separations in hydrocarbon, silicon, and fluorocarbon-based polymers (Submitted).*

prevent degradation, was shielded from light by placing aluminum foil over the vacuum oven window.[2] 6FDA was held under vacuum at room temperature for 30 min, after which air was reintroduced to the vacuum oven through a Drierite column (W.A. Hammond Drierite Co., Ltd., Xenia, OH). The 6FDA powder was then heated to 200°C for 6 h at -10 in Hg and then cooled to 120°C and held under full vacuum for at least twelve hours to dehydrate any dianhydride rings that may have hydrolyzed. Ultra-high purity N_2 gas (99.999%) was purchased from Airgas. N-methyl-2-pyrrolidone (NMP, ≥ 99%), N, N-dimethylacetamide (DMAc,≥ 99%), pyridine (99.9%) and acetic anhydride (99.5%) were purchased from Sigma Aldrich. Either anhydrous NMP (Sigma Aldrich, 328634) or distilled NMP was used for synthesis. For distilled NMP, the distillation cut was taken at 203°C.

A general schematic for the synthesis procedure is shown in Figure 3. In a typical synthesis, HAB diamine (20 mmol) was added to a three-neck flask, held under N_2 atmosphere, and dissolved in 44 mL of NMP. The solution was stirred vigorously for approximately 30 minutes until the diamine was fully dissolved. 6FDA (20 mmol) was then added all at once to the reaction flask, and an additional 44 mL of NMP was added to make a 15% (total mass of monomers in g/total volume of NMP in mL) solution. While continually stirring, an ice bath was placed below the reaction flask and the reaction was allowed to proceed for 12 h.

The poly(amic acid) was imidized by standard chemical imidization techniques.[3,4] To the reaction flask, 8 moles of pyridine and 8 moles of acetic anhydride were added per mole of HAB, and additional NMP was added to make an 8% (total mass of monomers in g/total volume of solvent in mL) solution. Imidization was allowed to proceed for 24 h.

The reaction solution was again diluted with NMP to make a 5% (total mass of monomers in g/total volume of solvent in mL) solution. Approximately 5 mL aliquots of

this solution were precipitated into approximately 200 mL aliquots of methanol (99.8%, BDH) while stirring the methanol at high speed in a blender. The polyimide was separated from the reaction solution by vacuum filtration and thorough rinsing of the polyimide with methanol. The polyimide was placed in a 1.5 L solution of methanol and stirred overnight. After 24 h, the polyimide was separated from the methanol and residual reaction solution by vacuum filtration and added to a fresh 1.5 L of methanol and stirred for an additional 24 h. The polyimide was vacuum filtered a final time and placed in a vacuum oven under full vacuum for 24 h at 100°C, 24 h at 120°C, and 48 h at 200°C. The polymer structure was confirmed by ^{1}H NMR, as reported previously.[1]

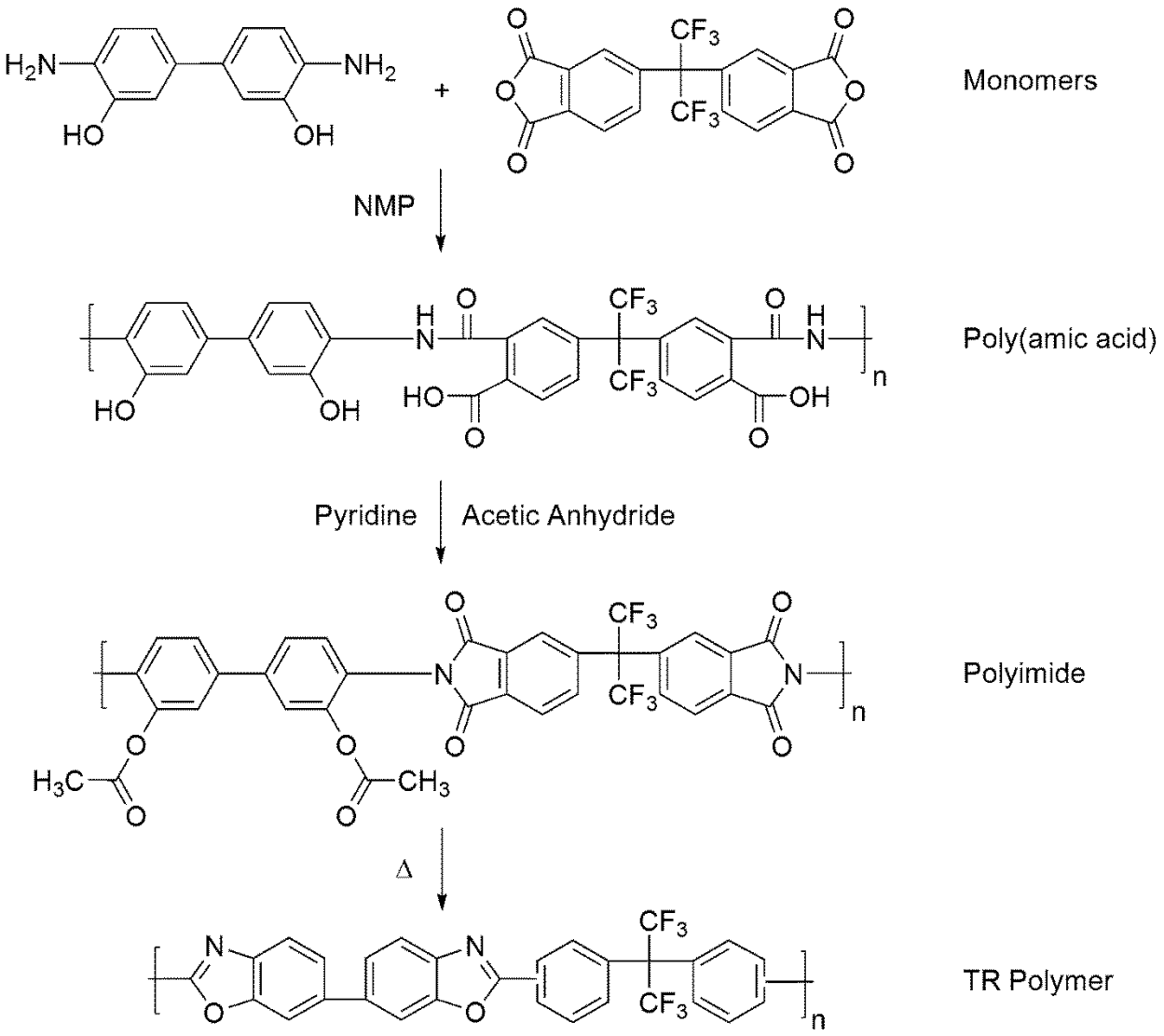

Figure 3.1: Synthesis of HAB-6FDA-C TR polymers through chemical imidization. NMP stands for N-methyl-2-pyrrolidone, and Δ stands for applying heat.

3.1.1.2 Thermal imidization in solution for HAB-6FDA and APAF-ODPA

Standard thermal imidization techniques were used to prepare HAB-6FDA and APAF-ODPA.[3,4] To prepare the monomers for synthesis, HAB and APAF were placed in a vacuum oven, which was shielded from light, and dried under full vacuum for 12 h at

60°C and 120°C, respectively. The dianhydrides were prepared using a two-step process. First, 6FDA and ODPA were held at 200°C under -10 in Hg for 6 h to dry the monomers and to close any hydrolyzed rings in the dianhydrides. Second, the oven temperature was lowered to 120°C and held for 12 h under full vacuum.

All monomers were allowed to cool to room temperature under full vacuum before beginning synthesis. Reactions were performed in a three-neck flask with an overhead mechanical stirrer. Synthesis glassware and Teflon® stirring blades were kept in a drying oven at approximately 115°C for 24 h before use. Ultra-high purity nitrogen gas (Airgas, 99.999%) was flowed through a Drierite column (W.A. Hammond Drierite Co., Ltd., Xenia, OH) to minimize the presence of water vapor in the reaction vessel.

In a typical synthesis batch, 25 mmol of diamine was added to the reaction flask. The diamines were dissolved in anhydrous N-methyl-2-pyrrolidone (NMP, Sigma-Aldrich, P/N 328634). HAB was dissolved in approximately 55 mL of NMP, and APAF was dissolved in approximately 51 mL of NMP. The diamines were allowed to dissolve for approximately 1 h before adding the dianhydrides. To the reaction flask containing HAB, 25 mmol of 6FDA were slowly added before adding an additional 55 mL of NMP. For the reaction flask containing APAF, 25 mmol of ODPA were slowly added before adding an additional 51 mL of NMP. Therefore, the HAB-6FDA solution was 15% and the APAF-ODPA solution was 20%. Each reaction flask was placed in an ice bath, and the reaction proceeded for approximately 18 h.

To begin thermal imidization, additional anhydrous NMP and an azeotropic agent, 1,2-dichlorobenzene (Sigma Aldrich, P/N 240664) were added to the reaction flask. To the HAB-6FDA poly(amic acid), approximately 55 mL of NMP and 41 mL of 1,2-dichlorobenzene were added to make an 8% solution, where a 1:4 volumetric ratio was maintained for 1,2-dichlorobenzene to NMP. A 10% solution was used for APAF-

ODPA. A Dean Stark trap and condenser was attached to the nitrogen outlet of the reaction flasks, and the poly(amic acid)s were imidized at 180°C for 24 h.

Following imidization, the polymer solutions were cooled, further diluted with NMP to decrease the solution viscosity, and precipitated in a non-solvent. HAB-6FDA was diluted to a 5% solution, and APAF-ODPA was diluted to an 8% solution. For HAB-6FDA, the non-solvent was methanol (VWR, P/N BDH-1135), and for APAF-ODPA, the non-solvent was an 85:15 mixture of methanol:deionized water. Approximately 10 mL of polymer solution was precipitated in approximately 400 mL aliquots of non-solvent, which were left stirring on low speeds in a blender. The polymers were filtered from the solvent/non-solvent mixture using a Büchner funnel, and the polymer samples were washed with the non-solvent mixture during this step.

Solvent was initially removed by extraction. HAB-6FDA was left stirring in approximately 1.5 L of methanol, and APAF-ODPA was left stirring in 1.5 L of a 20:80 mixture of methanol:deionized water for approximately 24 h. The polymers were then filtered and rinsed using a Büchner funnel, and the polymers were placed in fresh batches of extraction solvent. After waiting an additional 24 h, the polymers were again filtered and rinsed using a Büchner funnel, and the polymer powders were placed in evaporation dishes and transferred to a vacuum oven. Samples were dried in the vacuum oven at 80°C for 24 h, 120°C for 24 h, and 200°C for 48 h. Complete removal of solvent was confirmed by thermogravimetric analysis (TGA).

3.1.1.3 Thermal imidization in the solid-state for HAB-6FDA

HAB-6FDA was also prepared via solid state imidization. The label, -SS, will be used to designate this type of imidization. For this synthesis method, the HAB-6FDA poly(amic acid) was prepared identically to that described for the thermally imidized

HAB-6FDA sample. However, instead of imidizing the poly(amic acid), the poly(amic acid) solution was diluted with NMP to make a 10% solution, and the solution was poured onto flat glass plates. The glass plates were placed in a vacuum oven and heated under a light vacuum of approximately -10 in Hg at 60°C, 100°C, and 150°C for 1 h, 1.5 h, and 1.5 h, respectively. Next, the temperature was increased to 200°C for 1.5 h and 250°C for 1.5 h while applying full vacuum. Residual solvent was removed from the HAB-6FDA-SS films by heating at approximately 270°C for 12 h under full vacuum. Solvent removal was confirmed by thermogravimetric analysis.

3.1.1.4 Synthesis of APAF-6FDA

In a typical synthesis batch of APAF-6FDA, the monomers were purified using vacuum sublimation. The diamine, 2,2-bis (3-amino-4-hydroxyphenyl)-hexafluoropropane (APAF, Chriskev, CAS # 83558-87-6) was sublimated at approximately 220°C and the dianhydride, 2,2'-bis-(3,4-dicarboxyphenyl) hexafluoropropane dianhydride (6FDA, Sigma Aldrich, CAS # 1107-00-2) was sublimated at approximately 235°C. Sublimated crystals were used immediately for synthesis.

Lozano *et al.* have shown that higher molecular weight polyamides can be achieved by first silylating diamines prior to amidization.[5] Furthermore, this synthesis technique has been used for the synthesis of similar polyimides by several researchers.[6,7] Therefore, in addition to monomer sublimation, silylation was used to produce a polyimide with sufficient molecular weight to cast films.

In a typical synthesis batch, 25 mmol of APAF were added to a three neck flask with nitrogen a purge (Airgas, 99.999%) and an overhead mechanical stirrer. The nitrogen was flushed through a Drierite column (W.A. Hammond Drierite Co., Ltd.,

Xenia, OH) to remove water vapor before reaching the reaction flask. Anhydrous NMP (38 mL, Sigma Aldrich, 328634) was used to dissolve the diamine, and, after the diamine was fully dissolved, an ice bath was used to chill the reaction vessel. Chlorotrimethylsilane (CTMS, 14.4 mL, Sigma-Aldrich, 92361) and pyridine (12 mL, Sigma-Aldrich, 270407) were then added to the reaction flask as the silylating and activating agents, respectively. Approximately 4.4 moles of CTMS and pyridine were used per mole of APAF. Silylation was allowed to proceed for approximately 30 min.

After silylation, 25 mmol of 6FDA were slowly added to the reaction vessel. Because the APAF diamine contains strongly electron withdrawing hexafluoroisopropylidene groups, a small amount of co-base, 4-dimethylaminopyridine (DMAP), was added to the reaction mixture to improve reactivity.[8] The amount of DMAP added to the reaction vessel was 10% of the molar ratio of pyridine used in the reaction. An additional 38 mL of anhydrous NMP was added to the reaction flask to make a 20% solution (total mass of monomers in g/total volume of solvent in mL), and the poly(amic acid) reaction proceeded for 24 h.

To imidize the poly(amic acid), 1,2-dichlorobenzene (27 mL, Sigma-Aldrich, 240664) and additional anhydrous NMP (7 mL) was added to the reaction flask to make a 15% solution (total mass of monomers in g/total volume of solvent in mL). The volume of 1,2-dichlorobenzene to total volume of solvent added was 1:4. The reaction solution was then heated to 180°C for 24 h to imidize the poly(amic acid).

Following imidization, the reaction solution was precipitated as thin, light pink fibers in deionized water. Approximately 10 mL aliquots of polymer solution were precipitated in approximately 400 mL aliquots of deionized water, which were left stirring in a blender. To extract solvent, the polyimide fibers were rinsed with water and then left stirring in a 70:30 mixture of deionized water:methanol for 24 h. The methanol

was purchased from VWR (BDH-1135). The polymer fibers were then filtered and rinsed with water before stirring them in a fresh 70:30 solution of deionized water:methanol for an additional 24 h. The polymer fibers were rinsed a final time and then added to an evaporation dish, placed in a vacuum oven, and heated under full vacuum at 80°C, 120°C, and 200°C for 24 h, 24 h, and 48 h, respectively.

3.1.1.5 Synthesis of APAF-6fCl

In a typical synthesis batch, the 6fCl monomer was prepared by adding approximately 25.5 mmol of 4,4′-(hexafluoroisopropylidene)bis(benzoic acid) (Aldrich, 367672) to a single neck flask. Thionyl chloride ($SOCl_2$, Scharlau, CL0360) was added in 10 times molar excess (20 mL) and a catalytic amount of N,N-dimethylformamide (DMF, 10 drops, Scharlau, DL1062) was also added. The mixture was allowed to stir for approximately 2 hours before increasing the temperature of the reaction to approximately 55°C for 1 h. Following heating, the reaction vessel was cooled and allowed to stir at room temperature overnight for approximately 12 h. The reaction solution was then heated to 65°C for approximately 30 min and then 2 mL of toluene (Merck, 108325) was added to the reaction vessel before heating to 75°C for approximately 1.5 h. The reaction vessel was then allowed to cool for approximately 1 h before adding a distillation column to the single neck flask.

To distill off the $SOCl_2$ and DMF, the reaction vessel was heated to 80°C for approximately 1 h and then 100°C for approximately 30 min. To prevent the distillation column from drying, approximately 5 mL of toluene was added to the solution and the temperature was increased to 105°C for 45 min. To further remove $SOCl_2$ and DMF, a light vacuum was attached to the distillation column and the temperature was held at 80°C for 15 min followed by increasing the temperature to 100°C for 30min. The

viscous reaction solution was dissolved in 20 mL of hexane (Scharlau, HE0222) at 60°C and then allowed to recrystallize in a refrigerator for 12 h.

The recrystallized monomer was rinsed with cold hexane and filtered before drying the monomer in a vacuum oven for 1 h to remove excess hexane. The 6fCl monomer was then sublimed under vacuum at 60°C for approximately 2 h, 80°C for 30 min, 100°C for 1 h, and 120°C until sublimation was complete. Similar to the synthesis of the APAF-6FDA in this study, the APAF monomer was purified by sublimation at approximately 220°C.

Polymer synthesis proceeded as follows. The APAF diamine (18 mmol) was added to a three neck flask and dissolved in anhydrous N, N-dimethylacetamide (DMAc, 18 mL, Sigma-Aldrich, 271012). The diamine was allowed to dissolve for approximately 1 h before silylating the diamine by adding CTMS (10.2 mL) and pyridine (6.4 mL). After approximately 30 min, the 6fCl diacid chloride (18 mmol), DMAP (1.46 g, 15% pyridine by mole), and an additional 18 mL of anhydrous DMAc were added to the reaction flask.

The polymer was allowed to react for approximately 24 h at room temperature. Next, an additional 50 mL of DMAc was added to the reaction flask before slowly precipitating the polymer solution into a beaker of deionized water that was left stirring on a stir plate. The polymer fibers were left to stir in deionized water for approximately 1 h before drying with a Büchner funnel and placing the fibers in a 50:50 mixture of deionized water and ethanol to extract solvent. Solvent was extracted from the polymer solution for approximately 24 h before the sample was again filtered with a Büchner funnel and placed in a drying oven at approximately 100°C for 72 h. The fibers were again added to a 50:50 mixture of deionized water and ethanol, which was heated at

approximately 50°C for 2 h. The fibers were again filtered, dried at 80°C for 12 h without vacuum, and then dried under full vacuum at 75°C for 24 h.

3.1.2 Film Casting

3.1.2.1 Polyimides

Polymers were typically dissolved in DMAc to make 2% by weight solutions. HAB-6FDA, which was more difficult to filter, was prepared in a 1% by weight solution of DMAc. The polymers were filtered through a 5 µm Millex-LS PTFE filter (Millipore, SLLS025NS) before casting the solutions. Solutions were poured into glass rings attached to flat, glass casting plates by silicone caulk. Because the APAF-6FDA and APAF-ODPA samples would stick strongly to untreated glassware, the glassware for these samples was silylated according to the following protocol. A 30:70 solution of CTMS:toluene was poured into the glass casting ring to lightly coat the surface of the plate. The toluene was allowed to evaporate at room temperature leaving a thin layer of CTMS on the glassware, after which the plate was heated to 200°C for 30 min under full vacuum to silylate the glass.

To form films, cast polymer solutions were first held at 80°C for 24 h under approximately -10 in Hg. During this part of the casting procedure, solvent from the headspace of the vacuum ovens was occasionally removed by pulling a light vacuum in the oven while partially opening the vacuum pump vent to maintain a pressure of approximately -10 in Hg. Next, the samples were heated to 100°C and held an additional 24 h while occasionally pulling partial vacuum, as needed. Finally, the samples were treated at 100°C under full vacuum to complete film formation. Films were removed from their glassware by pealing or by submerging the films in warm deionized water.

Final solvent removal was achieved by heating the poly(*hydroxy*-imide) films under full vacuum at approximately 270°C for 12 h. The APAF-6fCl films were treated under full vacuum at 225°C for 12 h, and the HAB-6FDA-C films were treated under full vacuum at 200°C for 24 h. After these heating protocols, solvent was not detectable based on TGA.

3.1.2.2 Fluoropolymers

Teflon® AF, which is available from DuPont, is an amorphous copolymer of tetrafluoroethylene and 2,2-bis(trifluoromethyl)-4,5-difluoro-1,3-dioxole (BDD) and was generously supplied by Membrane Technology and Research (MTR) Inc., CA, USA. Teflon® AF 2400 and Teflon® AF 1600 contain 87 mol % and 65 mol % of BDD, respectively.[9-11] Hyflon® AD, an amorphous copolymer of tetrafluoroethylene and 2,2,4-trifluoro-5-(trifluoromethoxy)-1,3-dioxole (TTD), was purchased from Solvay Solexis Inc., NJ, USA. Hyflon® AD 60 contains about 60 mol % of TTD.[12] Perfluoropolymers were dried in a vacuum oven at 80°C for 8 h to remove moisture. These polymers are soluble in perfluorinated solvents. Performance Fluid PF-5060 (3M, St. Paul, MN, USA) purchased from AMS Materials, LLC, FL, USA was used as a solvent for the amorphous perfluoropolymers. Perfluoropolymers (1.2 – 1.42 wt%) were dissolved in 18 mL of PF-5060 solvent, and solutions were prepared in 20 mL disposable borosilicate scintillation vials (Fisher Scientific) by mixing with a magnetic stirring bar (Fisher Scientific, Pittsburgh, PA, USA) at room temperature for 48 h. Solutions were filtered through a 0.45 µm TITAN2 30 mm regenerated cellulose syringe filter (Thermo Scientific Sun SRI, Wilmington, NC, USA). Owing to the higher solubility of Teflon® AF 1600 and Hyflon® AD 60 in perfluorinated solvent compared to Teflon® AF 2400, their solutions were further filtered using a 0.2 µm Puradisc™ 25 PTFE syringe filter (25 mm) (Whatman®,

NJ, USA). Following filtration, all solutions were sonicated for 30 s using an FS30H sonicator (40 kHz, 100 W) (Fisher Scientific, Pittsburgh, PA, USA) at room temperature and left to stand overnight to remove any traces of air bubbles. Thick films (~ 40 μm) were prepared by solution casting on a leveled glass petri dish (85 mm internal dia.) in a sealed transparent inflatable glove bag (model X-17-17 from I^2R, PA, USA) containing UHP nitrogen. The petri dish was covered with a glass plate to slow evaporation of solvent, which limits non-uniformities in the film caused by high evaporation rates. The solvent evaporated in about 48 h. Films were then lifted from the glass surface using distilled water and air dried for 24 h on Berkshire Durx 670 clean room wipes followed by drying in a vacuum oven at 60°C for 24 h. Films were further dried for 48 h at 110°C for Teflon® AF grade polymers and 85°C for Hyflon® AD 60. The Hyflon® AD 60 sample has an unusual ability to retain perfluorinated solvents;[13,14] therefore, to ensure solvent removal in these films, the Hyflon® AD 60 sample was heated at 0.1°C/min from approximately ambient temperatures to 200°C. Complete solvent removal was determined with thermogravimetric analysis. The thicknesses of the films were measured using a micrometer.

Dupont™ Nafion® N117 was purchased from Ion Power, Inc. (New Castle, DE, USA). Nafion® N117 is a sulfonated perfluoropolymer with an equivalent weight of 1100 and a thickness of 0.007 in. Equivalent weight is defined for the acid form of dry Nafion® as the grams of Nafion® per mole of sulfonic acid groups.[15]

Tecnoflon® PL 455, P 457, and P 459 samples were kindly provided by Solvay. Thick polymer films (~ 250 μm) were prepared by first dissolving each sample in acetone (Sigma Aldrich, 34885) to make 5 wt% solutions. The solutions were filtered through 5.0 μm Millex-LS PTFE filters (Millipore, SLLS025NS) and cast in an acetone saturated glove bag. The casting plate, which consisted of a glass ring sealed to a flat glass plate

by poly(dimethylsiloxane) caulk, was partially covered with a glass dish to allow for slow evaporation of the solvent. After standing for 72 h, the films were covered and chilled to 0°C to allow for easier removal from the plate. The films were then dried at 50°C under vacuum for a minimum of 18 h to remove any remaining solvent. The glass transition temperature (T_g) for the Tecnoflon® samples was determined using a TA Instruments Q 100 differential scanning calorimeter (DSC). Samples were heated at a rate of 20°C/min with a nitrogen flowrate (Airgas, 99.999%) of 50 mL/min.

3.1.2.3 Additional samples

Matrimid® 5218 (based on monomers of 3,3′-4,4′-benzophenone tetracarboxylic dianhydride and diaminophenylindane, BTDA-DAPI) was obtained from Huntsman Advanced Materials. Approximately 1.6 wt. % solutions of Matrimid® were dissolved in 20 mL disposable borosilicate scintillation vials (Fisher Scientific) using methylene chloride (Fisher Scientific, Pittsburgh, PA, USA). The solutions were mixed with a magnetic stirring bar (Fisher Scientific) at room temperature for 48 h. Following mixing, the Matrimid® solution was then triple filtered using a 0.45 µm, 0.20 µm and 0.1 µm Puradisc™ 25 PTFE syringe filter (25 mm) (Whatman®, NJ, USA). Solutions were then sonicated for 30 s using an FS30H sonicator (40 kHz, 100 W) (Fisher Scientific, Pittsburgh, PA, USA) at room temperature and left to stand overnight to remove any traces of air bubbles. Thick films (~ 40 µm) were prepared by solution casting onto polished prime grade 1-0-0 silicon wafers (125 mm dia.) (MEMC Inc., St. Peters, MO, USA) using a metal casting ring (ID = 100 mm and height = 14.5 mm) in a sealed transparent inflatable glove bag (model X-17-17 from I^2R, PA, USA) containing UHP nitrogen. The metal casting ring was covered with a glass plate to allow slow evaporation of solvent, which limits non-uniformities in the film caused by high

evaporation rates. The solvent evaporated in about 48 h. Films were then removed from the silicon wafer using distilled water and dried in air for 24 h followed by drying in a vacuum oven at 60°C for 24 h and 110°C for the following 2 days. Further drying did not show any weight change due to complete removal of solvent. Film thickness was determined by a micrometer.

UDEL P-3700 polysulfone (PSF) was obtained from Solvay Advanced Polymers. Approximately 80 µm thick PSF films were melt extruded at 293°C using an extrusion system from Case Western Reserve University. Additional details of the extrusion procedure are described by Murphy *et al.*[16]

Filler-free Dehesive Silicone 940A (PDMS) and a proprietary crosslinker (V24) and catalyst (OL) system were obtained from Wacker Silicones Corp. (Adrian, MI). PDMS was dissolved in cyclohexane to make 20 mL batches of 12 wt. % solution. One drop of crosslinker and one drop of catalyst were added to each of these batches before casting the films. The casting surface consisted of a polytetrafluoroethylene laminate (BYTAC®) coated onto a flat glass plate. PDMS films of approximately 350 µm were dried for one week under ambient conditions before the films were heated in air at 110°C for 30 min to remove residual solvent and crosslink the polymer. A detailed description on the film formation procedure and material and transport characterization of these films is described elsewhere.[17,18]

3.1.3 Thermal Rearrangement

Thermally rearranged (TR) polymers were formed via a solid-state reaction of the *ortho*-functional polyimide and polyamide films. Polymer films were placed onto a flat ceramic boat and were covered by a flat ceramic plate. To allow for nitrogen to flow across the sample but to prevent the samples from curling during thermal treatment, the

plate was separated from the boat by approximately 1 mm with metal spacers. The sample was placed into a Carbolite three zone hinged tube furnace (Model HZS 12/–/600, Watertown, Wisconsin, USA), and a nitrogen (Airgas, 99.999%) flowrate of 900 mL/min was applied across the furnace tube. All thermally imidized samples (*i.e.*, HAB-6FDA, HAB-6FDA-SS, APAF-6FDA, and APAF-ODPA) were treated according to the following heating protocol. The samples were heated to 300°C at a rate of 5°C/min, held for 1 h, and then heated to 450°C at a rate of 5°C/min and held for 30 min. Next, the samples were cooled at a rate not to exceed 10°C/min. For the TR polymer formed from the polyamide (*i.e.*, APAF-6fCl), this sample was heated at 5°C/min from ambient temperature to 350°C and held for 1 hr, followed by cooling at a rate not to exceed 10°C/min.

The HAB-6FDA-C polyimide was treated for several different conversion conditions. Samples were heated at 5°C/min from ambient temperature to 300°C and then held at 300°C isothermally for 60 min. Next, the samples were heated at 5°C/min to a final dwell temperature of either 350°C for 60 min, 400°C for 60 min, or 450°C for 30 min. Samples were cooled at a rate not to exceed 10°C/min. These samples are labeled by their final dwell temperature and dwell time. For example, the TR polymer heated at 450°C for 30 min is referred to as HAB-6FDA-C TR 450 30min. Conversion was tracked by comparing the actual mass loss to the theoretical mass loss assuming full conversion of the polyimide precursor to the TR polymer as shown in Figure 3.. The percent conversion was defined as shown in Equation (3.1):

$$\%\,\text{Conversion} = \frac{\text{Actual Mass Loss}}{\text{Theoretical Mass Loss}} \times 100 \qquad (3.1)$$

For the HAB-6FDA-C sample considered in this study, the theoretical mass loss for full conversion to a polybenzoxazole structure is 24.3%.[1,19]

3.2 EXPERIMENTAL METHODS

3.2.1 Pure-gas Permeability

Pure gas permeability was determined for all samples using a constant volume-variable pressure permeation apparatus.[20] These systems operate by applying pressure to the upstream face of a polymer film, p_2, and allowing gas to permeate through the film into a calibrated downstream volume, V_D. At pseudo-steady state, the increase in pressure as a function of time, $\left(\frac{dp_1}{dt}\right)_{ss}$, is used to determine gas permeability through the film according to Equation (3.2):

$$P_i = \frac{V_D l}{p_2 ART}\left[\left(\frac{dp_1}{dt}\right)_{ss} - \left(\frac{dp_1}{dt}\right)_{leak}\right] \tag{3.2}$$

where P_i is the permeability of gas i, l is the film thickness, A is the area of film available for permeation, R is the ideal gas constant, T is the absolute temperature of the experiment, and $\left(\frac{dp_1}{dt}\right)_{leak}$ is the increase in pressure as a function of time when the system is sealed (*i.e.*, the leak rate).

Polymer films used for permeation tests were supported by aluminum tape (Devcon, 145250, Danvers, MA, USA) or by brass shim stock disks (McMaster-Carr, 9011K4). For the brass disks, these supports were machined to fit snuggly into a 47 mm diameter filter holder (Millipore, XX4504700). Concentric holes were bored through the disks, and polymer films were attached to the shim stock supports with epoxy

(McMaster-Carr, Devcon 14240). After allowing the epoxy to cure, the area of exposed polymer film was determined by scanning the support with a LiDE 210 scanner from Canon and analyzing the scanned images using ImageJ software provided by the National Institute of Health.[21]

The permeation systems were designed in-house and consisted of a filter holder (Millipore, XX4504700), several downstream volumes, and an upstream ballast volume. Polymer films on supports were placed into the filter holder and sealed. The downstream volume was designed with Swagelok® tubing and was connected to three cylinders, which were separated from the tubing by Swagelok® VCR® sealed valves. Methanol (VWR, BDH1135) was used to calibrate the cylinder volumes by determining the total mass of methanol needed to fill the volume between each cylinder and valve. The tubing volume was determined by volume expansions.[20] In addition to the cylinders, a low pressure transducer (Baratron®, 626A11TBE) and a burst disc (McMaster-Carr, 4412T11), were connected to the downstream tubing. The upstream tubing was connected to a ballast volume of approximately 1 liter to store high-pressure gas and prevent pressure fluctuations over the course of the experiments.

With each new sample added to the permeation system, vacuum was applied on the upstream and downstream faces of the sample for at least 4 h to desorb any atmospheric gases present in the film under ambient conditions. Nafion® N117, which is highly hygroscopic due to its sulfonated nature, can show increased gas permeability if water is not adequately removed.[22] Bunce *et al.* have shown that approximately one water molecule per sulfonate group remains in Nafion® after it is treated under vacuum at ambient conditions, and additional water cannot easily be removed unless the temperature is increased to over 100°C, which is near the onset of degradation for this polymer.[23] Therefore, we used several steps to ensure sorbed water was removed to the largest extent

possible from our Nafion® samples. First, the sample was held under vacuum for 4 hrs. Next, dry helium gas was permeated through the sample for approximately 30 min at pressures up to 15 atm. During this step, helium permeability was determined at 10 atm. The sample was held under vacuum a second time for 12 h, followed by a second dry helium permeation step. Helium permeability was again determined at 10 atm. Finally, the sample was held under vacuum for an additional 4 h before running a final permeation test. Within the uncertainty of the measurements, helium permeation rates did not change between the second and third helium permeation step.

To run permeation experiments, gas was introduced to the ballast volume upstream of the polymer sample by opening a pneumatic valve (Swagelok, SS-HBV51-C) that was connected to a metering valve (Swagelok, SS-MGVR4). A Python™ software program was used to open and close the pneumatic valve and control upstream pressure. In addition, if the pressure in the downstream cylinders exceeded the pressure range of the low-pressure transducer (*i.e.*, 10 Torr), the program would open the vacuum line to the downstream volume for 30 s using a pneumatic valve before again closing the valve and allowing permeation measurements to proceed. All samples were tested with gases of at least ultra-high purity (UHP) for He, H_2, N_2, O_2, CH_4, and CO_2 purchased from Airgas, Inc.

3.2.2 Volumetric Sorption

The sorption of H_2, N_2, O_2, CH_4, and CO_2 described in Chapter 5 was determined at 35°C and pressures up to 28 atm by a pressure decay method with a dual volume, dual transducer sorption apparatus.[20,24] The sorption apparatus has two chambers: the sample volume and the charge volume, and both volumes were calibrated by the Burnett method.[20,25] The two chambers are separated by a valve. Approximately 0.5 to 1.0 g of

polymer was placed in the sample volume, which was then sealed with a VCR gasket. The sorption apparatus was placed in a constant temperature water bath at 35°C. To fully desorb any dissolved gases in the film present due to contact of the sample with air, vacuum was applied to the sorption system containing the sample for at least 12 h. Afterwards, the valve between the sample and charge volumes was closed, and the charge volume was pressurized with a desired amount of gas. From the pressure transducer attached to the charge volume, along with the known charge cell volume and temperature, the Soave-Redlich-Kwong (SRK) equation of state was used to estimate the number of moles of gas in the charge volume, using critical parameters from Smith *et al.*[26] The valve was then opened and closed, releasing gas from the charge volume into the sample volume. Gas in the sample volume sorbed into the polymer film, causing a decrease in pressure in the sample chamber. Using the SRK equation of state, a mole balance was established between the initial and equilibrium conditions of the sample chamber, allowing calculation of the number of moles of gas which sorbed into the polymer film.[20] Following equilibrium, the charge volume was pressurized again, gas was released into the sample volume, and the sorption measurement was repeated. This process was continued until all data points for the sorption isotherm were obtained. For each sample tested, sorption isotherms were determined as a function of increasing pressure and in the following order: CH_4, H_2, N_2, O_2, and CO_2.

The sorption data were fit to the dual-mode sorption model using a least squares non-linear fit with OriginLab® software (OriginLab, Northampton, MA, USA):

$$C = k_D p + C_H^{'} \frac{bp}{1+bp} \tag{3.3}$$

where C is the concentration of penetrant per volume of polymer, p is pressure, k_D is the Henry's Law solubility constant, C_H' is the Langmuir capacity constant, and b is the affinity constant.[24,27-29] For each polymer, the parameters k_D and b were constrained to follow the same slope as total solubility coefficient versus penetrant critical temperature at 10 atm. The apparent solubility coefficient is defined as the concentration term, C, divided by pressure, p, as is shown in Equation (3.4):[29,30]

$$S = \frac{C}{p} \tag{3.4}$$

3.2.3 Gravimetric Sorption

Gravimetric sorption was used for describing H_2 and He sorption isotherms in Chapters 6 and 7. For each polymer, eight H_2 sorption isotherms were determined between −20°C and +70°C using a Rubotherm Magnetic Suspension Balance, MSB (Rubotherm Präzisionsmeßtechnik GmbH, Bochum, Germany). Ultra-high purity (UHP) H_2 and He gas (99.999%) were purchased from Airgas. To remove water and other condensable impurities from the H_2 and He feed to the MSB, a liquid nitrogen trap was installed upstream of the system.[31] Gas flowed through the liquid nitrogen trap and then into the MSB sample chamber at 100 mL/min, except for measurements at 5 bar, where a flowrate of 70 mL/min was used. Lower flowrates were required at lower system pressures to maintain balance stability. The MSB requires this constant flow of gas through the instrument and past the sample. If the liquid nitrogen trap was not used, large, spurious increases in sample mass, far in excess of what could be anticipated based on H_2 sorption alone, were observed at low temperatures. Presumably, these mass increases are due to minute amounts of trace impurities (*e.g.*, pump oil, carbon monoxide, carbon dioxide, methane, etc.) that might be present at very low levels in UHP gases.

Once the liquid nitrogen trap was installed, these unexpected mass increases were no longer observed, and H_2 sorption levels measured gravimetrically in the MSB were coincident with those measured by conventional volumetric sorption methods. Use of similar condensation traps are reported in the H_2 adsorption literature by Furukawa *et al.*[31]

All samples were degassed under full vacuum at 70°C for 1.5 h before each experiment. After degassing, the MSB temperature was adjusted to the desired isotherm temperature, and pressure was increased from vacuum to 60 bar in intervals of 5 bar. The time for diffusion of H_2 and He into the samples was too rapid to accurately measure using the MSB. However, the pressure was held constant for a much longer period of time, 20 minutes at each pressure, to ensure balance and temperature stability. After reaching 60 bar, vacuum was pulled on the sample chamber, and the system temperature was again increased to 70°C for 1.5 h to degas the films. For H_2 sorption, this procedure was repeated for eight isotherms, in order of decreasing temperature, starting at 70°C and finishing at -20°C. Helium isotherms were run at 35°C.

Because helium sorption was lower than hydrogen sorption for all gases, propagation of error techniques from Bevington and Robinson, which were used for determining uncertainty in hydrogen sorption from this work, resulted in sorption isotherms with large uncertainties.[32] Therefore, to more accurately determine helium sorption isotherms, we ran 4 to 8 identical helium sorption experiments for each sample. Between each isotherm, all samples were held under full vacuum at 70°C for 1.5 h and then under full vacuum at 35°C for 3 h. Isotherms are reported as the average concentration of gas at each of these pressures, and error bars are reported as the standard deviation in gas sorption at these pressures. In addition, at the lowest experimental pressures (*i.e.*, between approximately 5 and 15 bar) for HAB-6FDA, Matrimid®,

Nafion®, and Hyflon AD 60, helium sorption data showed significant scatter. Therefore, we have discarded the lowest pressure data points for these samples. Finally, significant scatter was observed using propagation of error techniques for hydrogen sorption in Hyflon® AD 60 and the three Tecnoflon® samples. Therefore, similar to the helium experiments, these samples were tested 4 - 8 times with hydrogen, and the average sorption isotherm and standard deviations from these measurements are reported.

The MSB is a gravimetric sorption apparatus.[33] Unlike other gravimetric systems, such as a Cahn electrobalance, or a quartz crystal microbalance,[20] the MSB measures the mass of the polymer/penetrant system through the use of an electromagnet and a sensitive analytical balance. The operation of this equipment allows the user to decouple the sample chamber from the measuring apparatus, thereby allowing the high-precision balance to operate under ambient conditions outside of the measuring chamber. The balance has a precision of ±0.01 mg, and the measuring chamber can operate between vacuum and 150 bar. The instrument is equipped with low pressure (*i.e.*, < 36.5 bar) and high pressure (*i.e.*, >36.5 bar) transducers having an uncertainty of ±0.25% full-scale at operating conditions. The full-scale rating of the low and high pressure transducers are 40 bar and 150 bar, respectively. Pressure within the sample chamber is maintained using a gas dosing system, which uses mass flow controllers to maintain specified flowrates within ±1 mL/min. Temperature was controlled using a Julabo (Seelbach, Germany) refrigerated/heating circulator (model FP50-ME), which provides heating/cooling oil for the MSB heat exchanger. A Pt100 temperature sensor, located inside the measuring chamber, has an accuracy of ± 0.05 °C.

Gravimetric sorption was determined by Equation (3.5):

$$m_{sorb} = \Delta m - m_{sc} - m_s + (V_{sc} + V_s) \times \rho_{gas} \tag{3.5}$$

where m_{sorb} is the mass of gas sorbed in the polymer film, Δm is the balance reading, m_{sc} is the mass of the sample holder plus internally suspended components, m_s is the sample mass, V_{sc} is the volume of the sample holder plus internally suspended components, V_s is the sample volume, and ρ_{gas} is the density of sorbed gas. The terms m_{sc} and V_{sc} are characteristic values for the MSB, and they are determined by running a blank experiment. These experiments are run without a sample, and pressure is increased slowly while monitoring the change in the balance reading. Because there is no sample present, Equation (3.5) is simplified:

$$\Delta m = m_{sc} - V_{sc} \times \rho_{gas} \tag{3.6}$$

By plotting Δm versus ρ_{gas}, m_{sc} and V_{sc} can be determined.

For these experiments, m_s was determined by weighing the sample in the MSB at various gas pressures and then extrapolating data from the sorption isotherms to zero pressure. When operating under vacuum in the MSB, sample mass cannot be directly determined due to poor heat conduction in the sample chamber, which causes fluctuations in the balance reading. The term V_s was determined from the sample density and m_s. Among the polymers considered in this study, experimental pressure-volume-temperature data have been reported for AF 2400,[34] PSF,[35,36] and PDMS.[37] For AF 2400 and PSF, experimental data are reported from approximately 25°C to temperatures well above the range considered in this study, and for PDMS, experimental data are reported between -

20°C and 50°C. Between room temperature and 70°C, the density of PSF changes approximately 1% and the density of AF 2400 changes approximately 0.7%. For PSF, density changes from 1.215 g/cm^3 at room temperature to approximately 1.203 g/cm^3 at 70°C. This difference is within the experimental uncertainty of the density values reported in Chapter 6. Likewise, for AF 2400, density changes from 1.744 g/cm^3 at room temperature to 1.733 g/cm^3 at 70°C. Therefore, the influence of correcting polymer density for temperature on the sorption isotherms was within the uncertainty of the sorption measurements. Because there is no change in H_2 sorption for AF 2400 or PSF if density is fixed or adjusted for temperature, we computed the sorption isotherms assuming a constant polymer density (*i.e.*, the values presented in Chapter 6). Furthermore, since the temperature dependence of density is not known for Matrimid or HAB-6FDA and its thermally rearranged analog, we assumed that these materials would behave like the other glassy polymers. Consequently, in calculating the sorption isotherms, we did not adjust the polymer density for the influence of temperature.

Conversely, the density of rubbery PDMS changes by approximately 8% between -20°C and 70°C. This change in density influences sorption isotherms and enthalpies of sorption at levels that are beyond the uncertainty in the sorption measurements. Therefore, we included the effect of temperature on the density of PDMS using the data reported by Raharjo *et al.*[37] Because the density data from Raharjo *et al.* only covered temperatures between -20°C and 50°C, we linearly extrapolated this data to 70°C to determine the approximate density of PDMS for our 70°C isotherm. A further discussion on the effect of the temperature dependence of polymer density on sorption isotherms is included later in Chapter 6.

Sample densities were taken from the literature for AF 2400 and PDMS, and they were determined for the other samples at room temperature by Archimedes' Principle

using a Mettler-Toledo density measurement kit (model P706039) and a Mettler-Toledo Balance. *n*-Heptane (Sigma, >99%) was used as the buoyant liquid for the measurements.

As depicted in Figure 3.2, samples of polymer film are placed in a sample basket for measurements. Introducing gas into the sample chamber begins the gas sorption process and creates a buoyancy effect on the sample holder, polymer sample, and suspended balance components. This buoyancy effect is corrected by the gas density term in Equation (3.5), where ρ_{gas} is calculated from the virial equation of state using parameters from Dymond *et al.*[38]

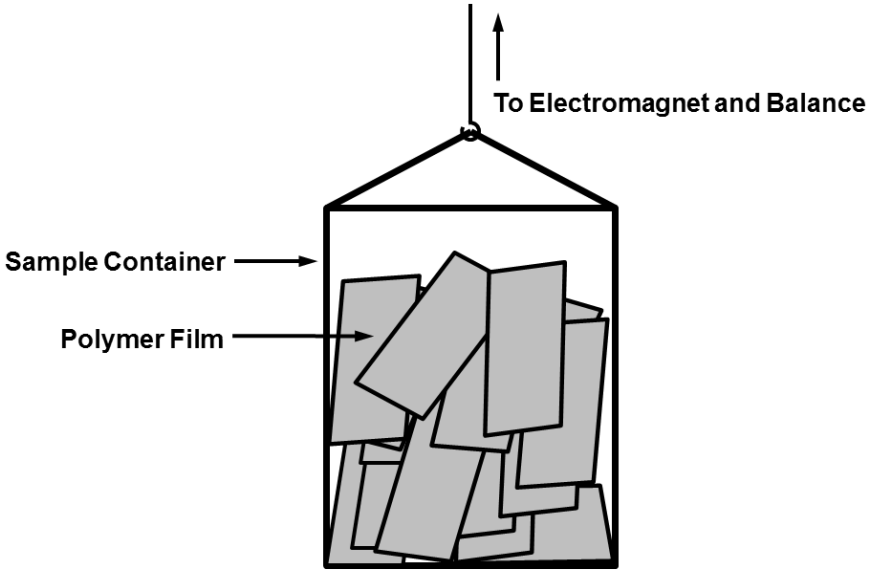

Figure 3.2: Schematic of MSB sample basket loaded with polymer film.

For microporous materials, an additional term, V_{sorb}, is often included in Equation 2 to account for the volume of gas sorbed in a material:[39]

$$m_{sorb} = \Delta m - m_{sc} - m_s + \left(V_{sc} + V_s + V_{sorb}\right) \times \rho_{gas} \tag{3.7}$$

However, this term applies to materials that exhibit volume additivity (*i.e.*, where the volume of the sorbed gas adds to the volume of the material under study to give the total sample volume), and polymer dilation is very small for light gases.[40] For example, Visser *et al.* estimate that the volume of Matrimid® increases (*i.e.*, dilates) by approximately 1.2% when exposed to argon at 60 bar, and less soluble gases, such as H_2, should exhibit substantially less dilation than this.[41] Furthermore, V_{sorb} is not well-defined, and the reason for this ambiguity arises from the difficulty in estimating the sorbed density of a penetrant in a polymer.[42] Therefore, V_{sorb} is excluded from calculations in this report. However, even if V_{sorb} were included in our calculations, the resulting increase in total H_2 sorption would be small. The difference in calculating H_2 sorption by Equation (3.5) and Equation (3.7) are within the uncertainty of the sorption measurement.

3.2.4 Diffusion Coefficient Calculations

Diffusion coefficients were determined from the solution-diffusion model, which is described in Chapter 2. Permeability and sorption were first determined, and then the diffusion coefficient was calculated by dividing the permeability coefficient by a sorption coefficient. For the structure-property study in Chapter 8, diffusion coefficients are estimated by time-lags.[43]

3.2.5 Solution-state nuclear magnetic resonance

Solution-state 1-D NMR results for ^{1}H and ^{13}C spectra were determined using a Varian Inova 500 MHz NMR. Several 2-D experiments, including correlation spectroscopy (COSY), heteronuclear single quantum correlation (HSQC) spectroscopy, and heteronuclear multiple bond correlation (HMBC) spectroscopy were used to assign peaks for these solution spectra. Trace impurities of an aliphatic compound were detected at low ^{1}H and ^{13}C chemical shifts for the APAF-6fCl TR polymer, but these impurities did not show any 2-D correlations with assigned peaks in the polymer.[44]

3.2.6 Solid-state nuclear magnetic resonance

Cross-polarization magic-angle spinning (CP-MAS) was performed at the National High Magnetic Field Laboratory in Tallahassee, FL to determine the solid-state ^{13}C NMR spectra. Polymer samples were packed into 4 mm rotors for ^{1}H-^{13}C CP-MAS experiments using a Bruker Avance 600 wide bore NMR spectrometer (14.1 T) operating at ^{13}C and ^{1}H Larmor frequencies of 150.94 and 600.26 MHz, respectively. After an initial ^{1}H 90 degree pulse, spin-lock pulses of 1 ms duration were applied along both ^{1}H and ^{13}C channels for CP, employing a 50 kHz rf-field at the ^{13}C channel and a ramped rf pulse at the ^{1}H channel whose rf-field strength changes linearly over a 25% range centered at 38 kHz. NMR signal averaging was achieved by co-adding 2048 transients with a 4 s acquisition delay time. ^{1}H and ^{13}C $\pi/2$ pulse lengths were 4 μs and 5 μs, respectively. The small phase incremental alternation with 64 steps (SPINAL-64)[45] decoupling sequence at 63 kHz power was used for proton decoupling during ^{13}C signal detection.

To measure ^{1}H $T_{1\rho}$, ^{1}H magnetizations created by a 90° pulse are spin-locked by a variable rf-pulse block that is 90° out of phase from the initial 90° pulse.[46] A ^{1}H transverse magnetization under the spin-lock pulse undergoes signal decay with a

relaxation parameter $T_{1\rho}$, which is sensitive to molecular motions over time scales of a few microseconds.[46] An indirect CP detection scheme with a short mixing time (<150 μs) was required for the $T_{1\rho}$ experiment. For the ^1H $T_{1\rho}$ measurements, the variable spin-lock pulse duration were extended from 0 to 10 ms in 10 increments of 1 ms each. Relative intensities were found by comparing peak intensities for slices from the different delay times to the intensity of the first slice. For extracting ^1H $T_{1\rho}$ times according to the time frame of the spin-lock period, we have fitted our data to a linear equation, $\ln(M(t)) = \ln(M(0)) - t/T_{1\rho}$, where M(0) is the size of the spin-locked transverse magnetization at the initial point (*i.e.*, immediately after the CP; normalized to 1) and M(t) is the transverse magnetization (either M_x or M_y) monitored after a spin-lock period. The slope of this equation, $1/T_{1\rho}$, was obtained by the least-squares fitting method.

3.2.7 Thermogravimetric Analysis Coupled with Mass Spectrometry

Thermogravimetric analysis (TGA) was performed with a TA instruments Q500 TGA. Ultra-high purity nitrogen (Airgas, 99.999%) was used during these experiments. Nitrogen flowrates were kept at 40 mL/min over the TGA balance and at 60 mL/min in the sample chamber. Two types of TGA experiments were performed. The first experiment was a temperature ramp between room temperature and 800°C at a heating rate of 5°C/min, and the second experiment was used to replicate heating conditions experienced by the films in the tube furnace. The latter experiment was run using the same temperature profile described in Section 0; however, the cooling rate was held to be exactly 10°C/min. Due to the high accuracy of the TGA balance (± 0.1 μg), mass loss during thermal rearrangement was determined with the TGA.

Evolved gas from the TGA experiments was also monitored using a Thermostar GSD 320 mass spectrometer (MS). TGA-MS scans were conducted at 5°C/min between

25°C and 800°C under N_2, and fragmented molecular weights between 10 amu to 90 amu were monitored with the MS.

3.2.8 Fourier Transform Infrared Spectroscopy

Fourier transform infrared spectroscopy (FTIR) was performed with a Thermo Nicolet 6700 spectrometer equipped with a DTGS detector. Samples were tested in attenuated total reflection mode with a resolution of 4 cm^{-1} and 256 scans per sample.

3.2.9 Wide-angle X-Ray Diffraction

A Scintag X1 theta-theta powder diffractometer (XRD) fitted with a solid-state detector using a Cu K-alpha radiation source was used for characterizing the amorphous nature of the polymers in this study and for calculating d-spacing. The diffractometer operated at 40 kV and 30 mA. d-spacing was calculated using Bragg's equation, shown in Equation (3.8), where λ is the wavelength of radiation (1.5405 Å), and 2θ is the scattering angle of maximum intensity.

$$d = \frac{\lambda}{2\sin\theta} \tag{3.8}$$

3.2.10 Differential Scanning Calorimetry

For HAB-6FDA-C, the glass transition temperature (T_g) was estimated from the first, second and third scans from a TA Instruments Q100 differential scanning calorimeter (DSC). The DSC samples were heated at 10°C/min from 25°C to 300°C under N_2 (Airgas 99.999%) with a flowrate of 50 mL/min. The T_g is reported as the midpoint of the step change in heat capacity for each of the scans. DSC experiments for the other samples considered were fun at 20°C/min. For the rubbery Tecnoflon® samples, DSC scans were started from temperatures of -80°C.

3.2.11 Density

Density was determined from Archimedes' Principle using a density measurement kit (Mettler-Toledo GmbH, P706039) and a Mettler-Toledo Balance. The buoyant liquid used for the measurement was *n*-heptane (Sigma, >99%).

3.2.12 Molecular Weight Characterization

Absolute molecular weight measurements were performed on a size exclusion chromatography (SEC) system coupled with a differential refractometer detector (VE 3580 RI detector, Viscotek) and a device containing both differential viscometer (DV) and right angle light scattering (RALS) detectors (Trisec Model 270, Dual Detector, Viscotek). The measurements were performed on three (30 cm x 7.5 mm ID) stainless steel columns packed with 500 Å, 103 Å and 104 Å PLGEL^{TM}, 5µm particle diameter (Polymers Lab). The injector and column compartment were maintained at a constant temperature of 70°C. Each sample was injected at a volume of 100 µL and run in dimethylformamide (DMF) with 0.1 % LiBr (0.870 g/L) at a flow rate of 1 mL/min using an isocratic pump system. The sample was prepared at a concentration of 5 mg/mL and it was filtered through 0.22 µm disposable Teflon filter (Scharlau) before injection. The instruments constants were determined using a narrow range polystyrene standard (Polymer Laboratories, Mp= 66,000).

From IR (concentration), DV (intrinsic viscosity) and RALS (molecular weight) signals, the distribution of intrinsic viscosity and molecular weight of the sample were obtained. The weighted average and number average molecular weight, polydispersity index, and average intrinsic viscosity were determined by using OmniSEC software, version 4.7 from Viscotek. Moreover, Mark-Houwink parameters were calculated from double logarithmic plot of intrinsic viscosity versus molecular weight.

3.2.13 Positron Annihilation Lifetime Spectroscopy

Positron annihilation lifetime spectroscopy (PALS) was performed at ambient temperature under vacuum using an automated EG&G Ortec fast-fast coincidence system. To perform these measurements, a Mylar envelope containing a ^{22}Na radioisotope source was sandwiched between two stacks of polymer films. The stacks of polymer films were at least 1 mm in thickness on each side of the source. The sample bundle was wrapped in aluminum foil to dissipate charge buildup that can occur from ionization of the material.[47] For each sample, at least 5 spectra of over 100,000 integrated counts were collected.

There are typically three lifetimes associated with PALS measurements in polymers. The first and second lifetimes are associated with self-annihilation of *para*-positronium (p-Ps) and free annihilation of positrons, respectively. The third lifetime, τ_3, and its corresponding intensity, I_3, are associated with annihilation of *ortho*-positronium (o-Ps), which correlate with the size and quantity of free volume elements in polymers.[48,49] Data was fit using a computer program, LT9, to determine initial fitting parameters for τ_3 and I_3.[50] These parameters were then used to determine free volume distributions using the computer program PAScual.[51] The values of τ_3 are reported as the peak maximum determined with PAScual.

3.3 REFERENCES

1. Smith, Z.P., D.F. Sanders, C.P. Ribeiro Jr, R. Guo, B.D. Freeman, D.R. Paul, J.E. McGrath, and S. Swinnea, Gas sorption and characterization of thermally rearranged polyimides based on 3,3'-dihydroxy-4,4'-diamino-biphenyl (HAB) and 2,2'-bis-(3,4-dicarboxyphenyl) hexafluoropropane dianhydride (6FDA). Journal of Membrane Science, **2012**. 416, 558-567.

2. Keith, L.H. and D.B. Walters, eds. The national toxicology program's chemical data compendium, volume 7. **1992**, Lewis Publishers, Inc.

3. Ghosh, M.K. and K.L. Mital, Polyimides: Fundamentals and applications. **1996**, New York, Marcel.

4. Ohya, H., V.V. Kudryavtsev, and S.I. Semenova, Polyimide membranes: Applications, fabrications, and properties. **1996**, Amsterdam, Gordon and Breach Publishers.

5. Lozano, A.E., J. de Abajo, and J.G. de la Campa, Synthesis of aromatic polyisophthalamides by in situ silylation of aromatic diamines. Macromolecules, **1997**. 30(8), 2507-2508.

6. Han, S.H., N. Misdan, S. Kim, C.M. Doherty, A.J. Hill, and Y.M. Lee, Thermally rearranged (TR) polybenzoxazole: Effects of diverse imidization routes on physical properties and gas transport behaviors. Macromolecules, **2010**. 43(18), 7657-7667.

7. Calle, M., A.E. Lozano, and Y.M. Lee, Formation of thermally rearranged (TR) polybenzoxazoles: Effect of synthesis routes and polymer form. European Polymer Journal, **2012**. 48(7), 1313-1322.

8. Muñoz, D.M., M. Calle, J.G. de la Campa, J. de Abajo, and A.E. Lozano, An improved method for preparing very high molecular weight polyimides. Macromolecules, **2009**. 42(15), 5892-5894.

9. Han, S.H. and Y.M. Lee, Recent high performance polymer membranes for CO_2 separation, in Membrane engineering for the treatment of gases: Volume 1: Gas-separation problems with membranes. **2011**, The Royal Society of Chemistry. 84-124.

10. Merkel, T., V. Bondar, K. Nagai, B. Freeman, and Y. Yampolskii, Gas sorption, diffusion, and permeation in poly (2,2-bis (trifluoromethyl)-4,5-difluoro-1,3-dioxole-co-tetrafluoroethylene). Macromolecules, **1999**. 32, 8427-8440.

11. Yampolskii, Y., I. Pinnau, and B.D. Freeman, eds. Materials science of membranes for gas and vapor separation. **2006**, John Wiley and Sons: Chichester.

12. Gee, R.H., A. Maiti, S. Bastea, and L.E. Fried, Molecular dynamics investigation of adhesion between TATB surfaces and amorphous fluoropolymers. Macromolecules, **2007**. 40(9), 3422-3428.

13. Jansen, J.C., M. Macchione, and E. Drioli, On the unusual solvent retention and the effect on the gas transport in perfluorinated Hyflon AD® membranes. Journal of Membrane Science, **2007**. 287(1), 132-137.

14. Macchione, M., J.C. Jansen, G. De Luca, E. Tocci, M. Longeri, and E. Drioli, Experimental analysis and simulation of the gas transport in dense Hyflon® AD60X membranes: Influence of residual solvent. Polymer, **2007**. 48(9), 2619-2635.

15. Mauritz, K.A. and R.B. Moore, State of understanding of Nafion. Chemical reviews, **2004**. 104(10), 4535-4585.

16. Murphy, T.M., D.S. Langhe, M. Ponting, E. Baer, B.D. Freeman, and D.R. Paul, Physical aging of layered glassy polymer films via gas permeability tracking. Polymer, **2011**. 52(26), 6117-6125.

17. Rowe, B.W., B.D. Freeman, and D.R. Paul, Physical aging of ultrathin glassy polymer films tracked by gas permeability. Polymer, **2009**. 50(23), 5565-5575.

18. Singh, A., B.D. Freeman, and I. Pinnau, Pure and mixed gas acetone/nitrogen permeation properties of polydimethylsiloxane [PDMS]. Journal of Polymer Science Part B: Polymer Physics, **1998**. 36, 289-301.

19. Sanders, D.F., Z.P. Smith, C.P. Ribeiro, R. Guo, J.E. McGrath, D.R. Paul, and B.D. Freeman, Permeability, diffusivity, and free volume of thermally rearranged polymers based on 3,3'-dihydroxy-4,4'-diamino-biphenyl (HAB) and 2,2'-bis-(3,4-dicarboxyphenyl) hexafluoropropane dianhydride (6FDA). Journal of Membrane Science, **2011**. 409-410, 232-241.

20. Lin, H. and B.D. Freeman, Springer handbook: Permeation and diffusion, H. Czichos, T. Saito, and L. Smith, Editors. **2006**, Springer: New York. 371-387.

21. Rasband, W.S., ImageJ. **1997-2012**, U. S. National Institutes of Health: Bethesda, Maryland, USA.

22. Chiou, J.S. and D.R. Paul, Gas permeation in a dry Nafion membrane. Industrial & Engineering Chemistry Research, **1988**. 27(11), 2161-2164.

23. Bunce, N.J., S.J. Sondheimer, and C.A. Fyfe, Proton NMR method for the quantitative determination of the water content of the polymeric fluorosulfonic acid Nafion-H. Macromolecules, **1986**. 19(2), 333-339.

24. Koros, W.J., D.R. Paul, and A.A. Rocha, Carbon dioxide sorption and transport in polycarbonate. Journal of Polymer Science: Polymer Physics Edition, **1976**. 14(4), 687-702.

25. Burnett, E.S., Compressibility determinations without volume measurements. Journal of Applied Mechanics, **1936**. 3, 136-140.

26. Smith, J.M., H.C. Van Ness, and M.M. Abbott, Introduction to chemical engineering thermodynamics. **2005**, Boston, McGraw-Hill.

27. Paul, D.R., Sorption and transport in glassy polymers. Ber. Bunsenges. Phys. Chern., **1979**. 83(1), 294-302.

28. Koros, W.J., A.H. Chan, and D.R. Paul, Sorption and transport of various gases in polycarbonate. Journal of Membrane Science, **1977**. 2, 165-190.

29. Paul, D.R. and Y.P. Yampolskii, Polymeric gas separation membranes. **1994**, Boca Raton, CRC Press.

30. Matteucci, S.T., Y.P. Yampolskii, B.D. Freeman, and I. Pinnau, Transport of gases and vapors in glassy and rubbery polymers, in Materials science of

membranes for gas and vapor separation, Y. Yampolskii, I. Pinnau, and B.D. Freeman, Editors. **2006**, John Wiley & Sons: Chichester. 1-47.

31. Furukawa, H., M.A. Miller, and O.M. Yaghi, Independent verification of the saturation hydrogen uptake in MOF-177 and establishment of a benchmark for hydrogen adsorption in metal–organic frameworks. Journal of Materials Chemistry, **2007**. 17(30), 3197-3204.

32. Bevington, P.R. and K.D. Robinson, Data reduction and error analysis for the physical sciences: Third edition. **2003**, Boston, McGraw Hill. 320.

33. Dreisbach, F., H.W. Lösch, and P. Harting, Highest pressure adsorption equilibria data: Measurement with magnetic suspension balance and analysis with a new adsorbent/adsorbate-volume. Adsorption, **2002**. 8(2), 95-109.

34. De Angelis, M.G., T.C. Merkel, V.I. Bondar, B.D. Freeman, F. Doghieri, and G.C. Sarti, Gas sorption and dilation in poly(2,2-bistrifluoromethyl-4,5-difluoro-1,3-dioxole-co-tetrafluoroethylene): Comparison of experimental data with predictions of the nonequilibrium lattice fluid model. Macromolecules, **2002**. 35(4), 1276-1288.

35. Zoller, P., Specific volume of polysulfone as a function of temperature and pressure. Journal of Polymer Science: Polymer Physics Edition, **1978**. 16(7), 1261-1275.

36. Zoller, P. and D.J. Walsh, Standard pressure-volume-temperature data for polymers. **1995**, Lancaster, Pennsylvania, Technomic Publishing Company, Inc.

37. Raharjo, R., B. Freeman, and E. Sanders, Pure and mixed gas CH_4 and n-C_4H_{10} sorption and dilation in poly(dimethylsiloxane). Journal of Membrane Science, **2007**. 292(1-2), 45-61.

38. Dymond, J.H., K.N. Marsh, R.C. Wilhoit, and K.C. Wong, eds. The virial coefficients of pure gases and mixtures. ed. M. Frenkel and K.N. Marsh. Vol. Group IV: Physical chemistry vol 21 subvolumes A and B. **2001**, Landolt-Bornstein: Berlin.

39. Staudt, R., G. Saller, M. Tomalla, and J.U. Keller, A note on gravimetric measurements of gas adsorption equilibria. Berichte der Bunsen-Gesellschaft-Physical Chemistry Chemical Physics, **1993**. 97(1), 98-105.

40. Jordan, S. and W. Koros, A free volume distribution model of gas sorption and dilation in glassy polymers. Macromolecules, **1995**. 28(7), 2228-2235.

41. Visser, T. and M. Wessling, When do sorption-induced relaxations in glassy polymers set in? Macromolecules, **2007**. 40(14), 4992-5000.

42. Sircar, S., Gibbsian surface excess for gas adsorption - revisited. Industrial & Engineering Chemistry Research, **1999**. 38, 3670-3682.

43. Lin, H. and B.D. Freeman, Springer handbook of materials measurement methods. Materials Today, **2006**. 9(7-8), 52-52.

44. Gottlieb, H.E., V. Kotlyar, and A. Nudelman, NMR chemical shifts of common laboratory solvents as trace impurities. The Journal of Organic Chemistry, **1997**. 62(21), 7512-7515.

45. Fung, B.M., A.K. Khitrin, and K. Ermolaev, An improved broadband decoupling sequence for liquid crystals and solids. Journal of Magnetic Resonance, **2000**. 142(1), 97-101.

46. Kimmich, R., NMR: tomography, diffusometry, relaxometry. Vol. 432. **1997**, Springer Berlin etc.

47. Xie, W., H. Ju, G.M. Geise, B.D. Freeman, J.I. Mardel, A.J. Hill, and J.E. McGrath, Effect of free volume on water and salt transport properties in directly copolymerized disulfonated poly(arylene ether sulfone) random copolymers. Macromolecules, **2011**. 44(11), 4428-4438.

48. Jean, Y., P. Mallon, and D. Schrader, Principles and applications of positron & positronium chemistry. **2003**, Singapore, World Scientific.

49. Pethrick, R.A., Positron annihilation - A probe for nanoscale voids and free volume? Progress in Polymer Science, **1997**. 22(1), 1-47.

50. Kansy, J., Microcomputer program for analysis of positron annihilation lifetime spectra. Nuclear Instruments and Methods in Physics Research Section A: Accelerators, Spectrometers, Detectors and Associated Equipment, **1996**. 374(2), 235-244.

51. Pascual-Izarra, C., A.W. Dong, S.J. Pas, A.J. Hill, B.J. Boyd, and C.J. Drummond, Advanced fitting algorithms for analysing positron annihilation lifetime spectra. Nuclear Instruments and Methods in Physics Research Section A: Accelerators, Spectrometers, Detectors and Associated Equipment, **2009**. 603(3), 456-466.

Chapter 4: Confirmation of polybenzoxazole structure of thermally rearranged polymers

Reacting ortho-functional poly(hydroxy-imides) via a high-temperature (i.e., 350°C - 450°C) solid-state reaction produces polymers with exceptional gas separation properties for separations such as CO_2/CH_4, CO_2/N_2, and H_2/CH_4. However, these reactions render these so-called thermally rearranged (TR) polymers insoluble in common solvents, which prevents the use of certain experimental characterization techniques such as solution-state nuclear magnetic resonance (NMR) from identifying their chemical structure. In this work, we seek to confirm the chemical structure of TR polymers by synthesizing a partially soluble TR polymer from an ortho-functional poly(hydroxy-amide). The chemical structure of this TR polymer was characterized using 1-D and 2-D NMR. By use of cross-polarization magic-angle spinning ^{13}C NMR, the structure of the polyamide-based TR polymer was compared to that of a polyimide-based TR polymer with a nearly identical proposed structure. The NMR spectra confirm that oxazole functionality is formed for both of these TR polymers. Furthermore, gas permeation results are provided for the precursor polymers and their corresponding TR polymer. The differences in transport properties for these polymers result from differences in the isomeric nature of oxazole-aromatic linkages and the resulting differences in free volume and free volume distribution, polymer rigidity, and crosslinking.

4.1 INTRODUCTION

Thermally rearranged (TR) polymers were first investigated for CO_2/CH_4 separations, and these polymers have shown exceptional permeabilities, selectivities, and a resistance to CO_2 plasticization.[1] These polymers are synthesized via a solid-state reaction of aromatic poly(*hydroxy*-imide)s (PIs), whereby the *hydroxy*-functional group must be *ortho*-positioned to the polyimide diamine. Upon reacting these polyimides to their corresponding TR polymers, the resulting materials become insoluble in all known solvents, and their insolubility prevents the use of traditional characterization techniques, such as solution-state nuclear magnetic resonance (NMR), to confirm their precise chemical structure.

The outstanding transport properties of TR polymers has spurred significant interest in indentifying their chemical structure. Tullos *et al.* drew correlations between the reaction of small molecule *hydroxy*-imides to form oxazoles with the reaction of PIs to form polybenzoxazoles (PBOs).[2,3] Han *et al.* confirmed through mass spectrometry that CO_2 is evolved during thermal rearrangement, also supporting the reaction mechanism of PIs to form PBOs.[4] Lozano *et al.* used Fourier Transform Infrared Spectroscopy (FTIR) to confirm PBO structure of samples synthesized from PIs and poly(*hydroxy*-amide)s (PAs).[5]

Nevertheless, alternative chemical structures have been proposed. Hodgkin *et al.* used FTIR and molecular simulation results to suggest that PI precursors react to form poly(biphenylene bisimide)s instead of PBOs.[6,7] Kostina *et al.* used FTIR and minimization of potential reaction energies to suggest that the predominant chemical structure of TR polymers is an aromatic lactam.[8]

This chapter has been adapted from: Smith, Z.P., K. Czenkusch, S. Wi, K.L. Gleason, G.H.G.C. Doherty, K. Konstas, T. Bastow, C. Alvarez, A.J. Hill, A.E. Lozano, D.R. Paul, and B.D. Freeman, *Confirmation of polybenzoxazole structure of thermally rearranged polymers (in preparation).*

The thrust of this work was to identify the structure of TR polymers through 1-D and 2-D NMR experiments. To accomplish this end, we have employed traditional synthesis techniques to design a partially soluble, fluorinated TR polymer based on 2,2-bis (3-amino-4-hydroxyphenyl)-hexafluoropropane (APAF) and 2,2'-bis(4-carboxy-phenyl)hexafluoropropane diacid chloride (6fCl) (PA-TR). With the exception of a structural isomer, the proposed APAF-6fCl PA-TR is identical in chemical structure to that of a TR polymer prepared from APAF and 2,2'-bis-(3,4-dicarboxyphenyl) hexafluoropropane dianhydride (6FDA) (PI-TR).

Solution-state ^{1}H NMR and ^{13}C NMR coupled with correlation spectroscopy (COSY), heteronuclear single quantum correlation (HSQC) spectroscopy, and heteronuclear multiple bond correlation (HMBC) spectroscopy allows for the confirmation of PBO chemical structure for the soluble fraction of the PA-TR. Moreover, we have employed cross-polarization magic-angle spinning (CP-MAS) ^{13}C NMR to compare the solution and solid-state NMR results for the PA-TR. Within the resolution of the CP-MAS results, several PBO peaks can be clearly identified. By comparing CP-MAS results between the PA-TR and PI-TR, the PA-TR and the PI-TR have nearly the same PBO chemical structure. The only resolved peak that is not clearly the same between the two polymers is explained by an isomeric effect.

We also determined gas permeability for several gas pairs for the PA, PA-TR, PI, and PI-TR polymers. From these results, TR polymers formed from polyimides have higher permeabilities and similar selectivities to TR polymers formed from polyamides. These differences are likely a result of several phenomena. In particular, the PI-TR is more highly crosslinked than the PA-TR, and each TR polymer has morphological differences in its free volume and free volume distribution.

The confirmation that PBOs can be synthesized via PIs has broad implications for designing new polymers for a variety of applications. In addition to gas separation membranes, PBOs and related structures, such as polybenzimidazoles and polybenzothiazoles, are actively being investigated as high-temperature proton exchange membranes in fuel cells,[9-11] nanoporous materials for CO_2 capture and H_2 storage,[12,13] and photoresist polymers in the microelectronics industry.[14-16]

Using this new synthetic approach to make PBOs may facilitate discovery of new adsorbent materials, polymer electrolytes, photosensitive polymers with low dielectric constants, and gas separation membranes.

4.2 RESULTS AND DISCUSSION

The proposed structures considered in this study are presented in Figure 4.1. Figure 4.1(A) shows the solid-state reaction of a poly(*hydroxy*-imide) (PI) to form a TR polymer with the proposed polybenzoxazole (PBO) structure, and Figure 4.1(B) shows the solid-state reaction of a poly(*hydroxy*-amide) (PA) to form a similar proposed PBO structure. The specific polyimide and polyamide were chosen because they contain two hexafluoroisopropylidene functional groups. These functional groups hinder chain packing, resulting in polymers with some of the highest known combinations of permeability and selectivity.[17,18] A notable difference between the two PBO structures in Figure 4.1 is the connection between the oxazole moiety and the neighboring aromatic ring. Reacting the PI to form a PBO could occur with either imide carbonyl, leading to a mixture of *meta*/*para* structural isomers. The PA has only the single amide linkage and, thus, the final PBO would lack the potential for isomerization between the oxazole and aromatic ring. Other than the isomeric nature of the PBO formed from the polyimide and

potential differences in *intra*-molecular cross-linking reactions,[19] both of these structures should be identical.

Figure 4.2 shows thermogravimetric analysis results for heating the polyimide (cf., Figure 4.2(A)) and polyamide (cf., Figure 4.2(B)) at 5°C/min under nitrogen gas from 25°C to 800°C. The two-stage mass loss in these thermograms is characteristic of TR polymers,[1] where the first mass loss is associated with thermal rearrangement, and the second mass loss is associated with thermal degradation. The theoretical mass losses expected from the decarboxylation of the PI and the condensation of the PA are indicated on the thermograms. Moreover, general regions that are characteristic of thermal rearrangement (TR) and thermal degradation are highlighted. Because these two regions are separated at these heating conditions, a processing window is available to produce TR polymers for these samples. The processing window for the PI is between approximately 350°C and 450°C, and the processing window for the PA is between approximately 250°C and 400°C. To achieve near-quantitative conversion and to most closely match work in the literature,[5] we reacted the PI at 450°C for 30min and the PA at 350°C for 60min. (see Appendix A, Section A.1).

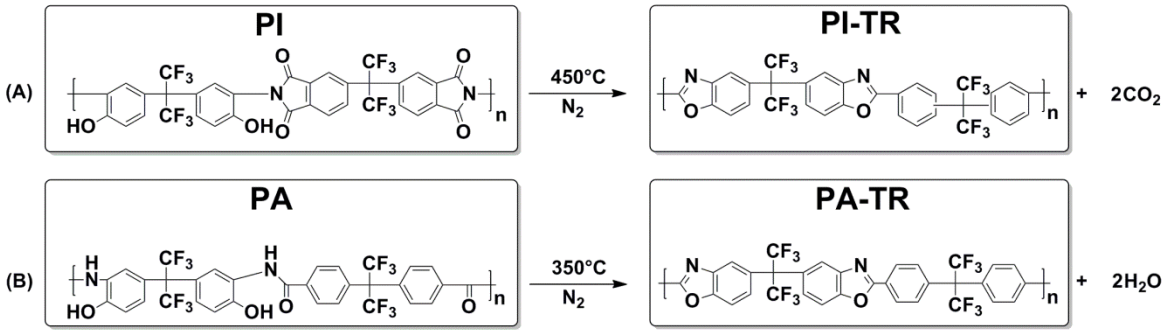

Figure 4.1: Proposed reactions of (A) APAF-6FDA, an ortho-functional poly(hydroxy-imide) (PI), to form a polybenzoxazole (PI-TR) and (B) APAF-6fCl, an ortho-functional poly(hydroxy-amide) (PA), to form a polybenzoxazole (PA-TR).

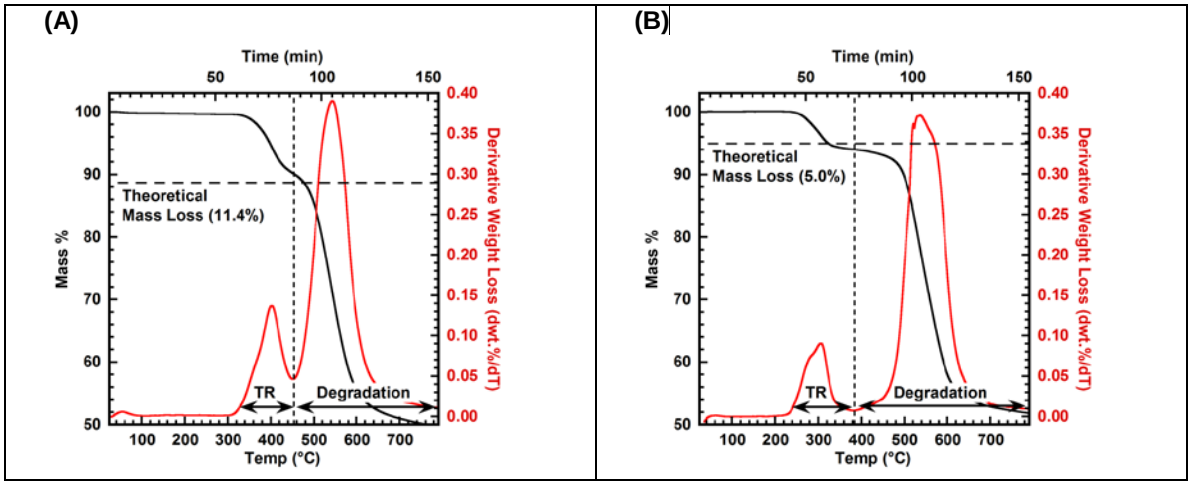

Figure 4.2: Thermogravimetric analysis of (A) APAF-6FDA, an ortho-functional poly(hydroxy-imide) (PI), and (B) APAF-6fCl, an ortho-functional poly(hydroxy-amide) (PA). The mass loss expected stoichiometrically for the thermal rearrangement reaction is highlighted with a long dashed line, and the derivative weight loss is shown on the second y-axis. Regions of mass loss are separated by a short dashed line to highlight regions predominately governed by thermal rearrangement (TR) and regions predominately governed by degradation.

Unlike the PI-TR, the PA-TR polymer is partially soluble in chloroform. The gel fraction, determined from a Soxhlet extractor, was 74.9% (see Appendix A, Section A.2),

so we could run a series of 1-D and 2-D solution nuclear magnetic resonance (NMR) experiments on the soluble fraction of the polymer. Figure 4.3 shows ^{1}H and ^{13}C peak assignments and results from correlation spectroscopy (COSY), heteronuclear single quantum correlation (HSQC) spectroscopy, and heteronuclear multiple bond correlation (HMBC) spectroscopy for the soluble fraction of the PA-TR. For the 2-D correlations, cross correlations between protons and carbons are identified by short, dashed lines. Additionally, traces of the proton and carbon NMR spectra are shown to help guide the eye, and protons and carbons relevant to the particular 2-D analysis are also labeled. The intensity of these correlations ranges from light blue for weak correlations to dark red for strong correlations. Finally, we have color-coded protons and carbons to identify their relative location in the polymer structure. Blue labels identify nuclei originally attached to the diamine functionality of the precursor polymer. Red labels identify nuclei originally attached to the dianhydride or diacid chloride functionality of the precursor polymer. Finally, capital letters indicate protons and lower case letters indicate carbons. Fully assigned ^{1}H and ^{13}C spectra for the PA and PI samples are presented in Appendix A, Section A.3, and the fully assigned ^{1}H and ^{13}C spectra for the PA-TR are presented in Appendix A, Section A.4.

Figure 4.3 (B) shows the COSY spectrum for the PA-TR. The correlation between identical protons is shown as a long, dashed diagonal line on the plot. From this figure, 5 hydrogens are clearly present in the PA-TR, which is consistent with the proposed PBO chemical structure and with solution-state ^{1}H NMR results for APAF-6fCl PBOs synthesized in polyphosphoric acid.[5] Furthermore, peak **K** correlates with peak **L**, and peaks **B**, **E**, and **D** are also correlated. For the PBO structure shown in Figure 4.3 (A), protons **D** and **E** and protons **K** and **L** are separated by three bonds. Therefore, they show a stronger correlation in peak intensity than protons that are separated by 4 bonds,

such as protons **B** and **D**, which only appear as faintly correlated on the COSY spectrum. Protons **B** and **E**, which would be separated by 5 bonds, do not appear on the plot. Moreover, the integration of these proton peaks is consistent with 14 hydrogens in each chemical repeat unit. If a poly(biphenylene bisimide) were formed, which has been proposed for TR polymers formed from polyimides,[6,7] only 10 hydrogens would be present in each repeat unit.

Figure 4.3 (C) shows the HSQC results for the PA-TR. From this experiment, there are clearly five one-bond direct couplings ($^1J_{CH}$) between ^{13}C and ^{1}H nuclei. One proposed chemical structure for TR polymers is an aromatic lactam.[8] However, for the sample considered here, HSQC results indicate that all of the protons are directly coupled with carbons, not other nuclei, such as nitrogen, which would be required in an aromatic lactam. NMR correlated with carbons. The overlapping proton NMR peaks for **L** and **E** can clearly be separated based on the location of the ^{13}C peaks, **l** and **e**. HSQC indicates that peak **E** is shifted slightly upfield of peak **L** for the proton spectra, and peak **k** is shifted slightly upfield of peak **d** for the ^{13}C spectra. A few low intensity (i.e., light blue) peaks that do not correspond with the PBO structure are observed in the HSQC plot. Minor side reactions may contribute to these unassigned correlations.[20]

HMBC was used to determine long-range correlations between carbon nuclei and protons not connected by a single bond. These results are presented in Figure 4.3 (D). For clarity, $^1J_{CH}$ couplings from HSQC are not included in Figure 4.3 (D).

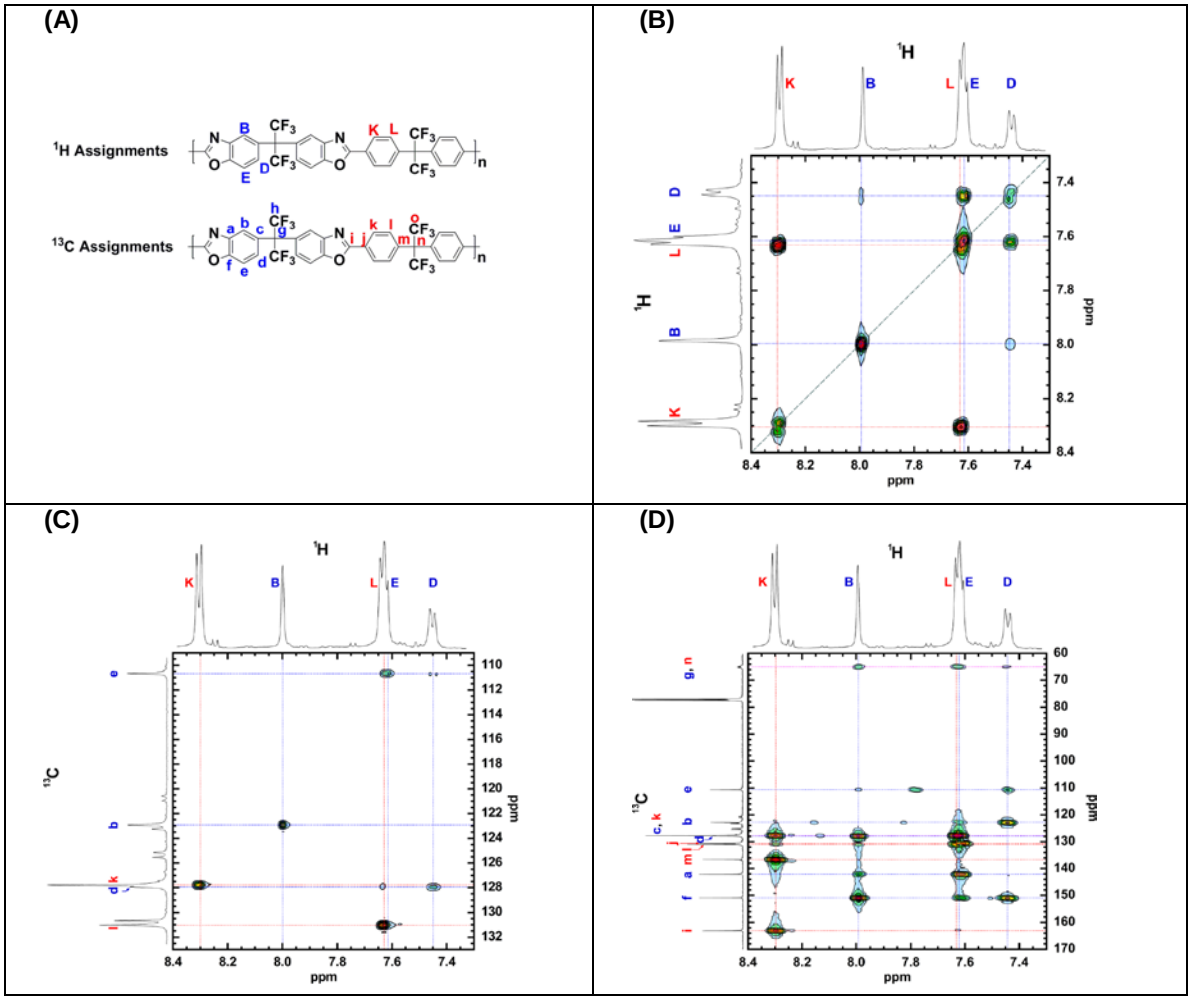

Figure 4.3: ^{1}H and ^{13}C assignment for the PA-TR, and 2-D correlations including (B) COSY, (C) HSQC, and (D) HMBC NMR.

The HMBC spectrum helps identify eight ^{13}C nuclei not directly attached to protons (i.e., carbons **a**, **c**, **f**, **g**, **i**, **j**, **m**, and **n**). To make these identifications, it is important to consider that for HMBC spectra of aromatic systems, three-bond correlations ($^3J_{CH}$) show very strong intensities, and two-bond correlations ($^2J_{CH}$) can be rather weak or sometime missing.[21,22]

For the APAF portion of the PA-TR, carbons, **a** and **c** have strong $^3J_{CH}$ correlation with proton **E** and weak $^2J_{CH}$ correlations with proton **B**. Carbon **f** has a strong $^3J_{CH}$

correlation with protons **B** and **D** and a weak correlation with proton **E**. The quaternary carbon, **g**, is connected to protons **B** and **D** by a $^{3}J_{CH}$ correlation. However, the quaternary carbon is outside the aromaticity of the PBO and therefore only shows a weak correlation. Carbon **c** has a missing $^{2}J_{CH}$ correlation with proton **D**, and therefore, more information was required to identify peaks **a** and **c**. For the small molecule, benzoxazole, peak **a** is shifted further downfield than peak **c**.[23] Therefore, we assume that a similar difference in peak shifts should also apply here.

The same analysis can be applied to the 6fCl portion of the PA-TR. The strong intensity of the correlation between carbon **i** and proton **K** is an indication of $^{3}J_{CH}$ coupling between these nuclei. Furthermore, carbon **i** shows no significant correlation with any other protons, all of which are further than three bonds away. Carbon **j** correlated strongly with proton **L** ($^{3}J_{CH}$) and weakly with proton **K** ($^{2}J_{CH}$), whereas carbon **m** correlates strongly with proton **K** ($^{3}J_{CH}$) and has a missing correlation with proton **L** ($^{2}J_{CH}$). Finally, carbon **n** only shows a correlation with proton **L**, which is the only $^{3}J_{CH}$ interaction for this carbon.

A list of all of the proton-carbon interactions from HSQC and HMBC is recorded in Table 4.1. All observed $^{1}J_{CH}$, $^{2}J_{CH}$ and $^{3}J_{CH}$ correlations are listed. Only two $^{2}J_{CH}$ correlations were not observed (i.e., correlations between peaks **D** and **c** and peaks **L** and **m**). As mentioned previously, $^{2}J_{CH}$ correlations are sometimes weak or missing for HMBC.[23,24] Among all of the carbons in the PBO, only two peaks, **h** and **o**, were not observed with the HMBC experiment. These peaks would only be detected by four-bond correlations ($^{4}J_{CH}$), and HMBC does not typically detect correlations over 3-bonds. We have assigned these peaks based on their characteristic splitting pattern (cf., Appendix A, Section A.4).[24] Finally, peaks **k** and **l** showed coupling for both HSQC and HMBC. Such correlations would typically not be expected because HSQC only detects $^{1}J_{CH}$

coupling, and HMBC does not detect $^{1}J_{CH}$ correlations. However, peaks **k** and **l** have two identical, symmetric carbons within an aromatic ring, so these carbons correlate with $^{1}J_{CH}$ and $^{3}J_{CH}$ coupling while still sharing identical chemical shifts.

	Carbon	a	b	c	d	e	f	g	h	i	j	k	l	m	n	o
Proton	**ppm**	142.0	122.8	127.7	127.8	110.5	150.8	64.9	124.3	163.0	130.5	127.7	130.9	136.5	64.9	123.9
B	7.97	$^2J_{CH}$	$^1J_{CH}$	$^2J_{CH}$	$^3J_{CH}$		$^3J_{CH}$	$^3J_{CH}$								
D	7.43		$^3J_{CH}$	ND	$^1J_{CH}$	$^2J_{CH}$	$^3J_{CH}$	$^3J_{CH}$								
E	7.60	$^3J_{CH}$		$^3J_{CH}$	$^2J_{CH}$	$^1J_{CH}$	$^2J_{CH}$									
K	8.28									$^3J_{CH}$	$^2J_{CH}$	$^1J_{CH}$	$^2J_{CH}$	$^3J_{CH}$		
L	7.62										$^3J_{CH}$	$^2J_{CH}$	$^1J_{CH}$	ND	$^3J_{CH}$	

Table 4.1: Correlations between ^{1}H and ^{13}C peaks for HSQC and HMBC. For HSQC, $^1J_{CH}$, $^2J_{CH}$, and $^3J_{CH}$ stand for 1-bond, 2-bond, and 3-bond correlations, respectively. ND stands for peaks that were not detected.

With the soluble fraction of the PA-TR structure confirmed as a PBO, we then turned to cross-polarization magic-angle spinning (CP-MAS) solid-state NMR experiments. For these experiments, a Total Suppression of Spinning Sidebands (TOSS) pulse sequence was used to eliminate side bands. Figure 4.4 shows the ^{13}C NMR spectra for these samples. The solution NMR results, shown in red, exhibit clear separation between all peaks. The solid-state CP-MAS results were normalized by the intensity of the highest peak (i.e., the peak near 128 ppm). By comparing the solution-state ^{13}C NMR results with the CP-MAS NMR results for the PA-TR, we can confirm that the soluble fraction of the PA-TR has nearly identical chemical structure to that of the insoluble fraction. Moreover, the peaks labeled **i**, **f**, **a**, **m**, **e**, **g**, and **n** can clearly be identified in the CP-MAS NMR spectrum. Four of these peaks (i.e., peaks **i**, **f**, **a**, and **e**) are characteristic of the oxazole moiety in the PA-TR, and the two additional peaks (i.e., peaks **g**, and **n**) are characteristic of the hexafluoroisopropylidene groups between the oxazole and aromatic moieties. Furthermore, peak **m** is characteristic of the aromatic moiety in the PA-TR. Furthermore, the broad peak between approximately 120 ppm and 133 ppm is consistent with overlapping peaks identified with solution NMR. Therefore, CP-MAS results are consistent with the partially soluble fraction of the PA-TR having a nearly identical chemical structure to the insoluble fraction.

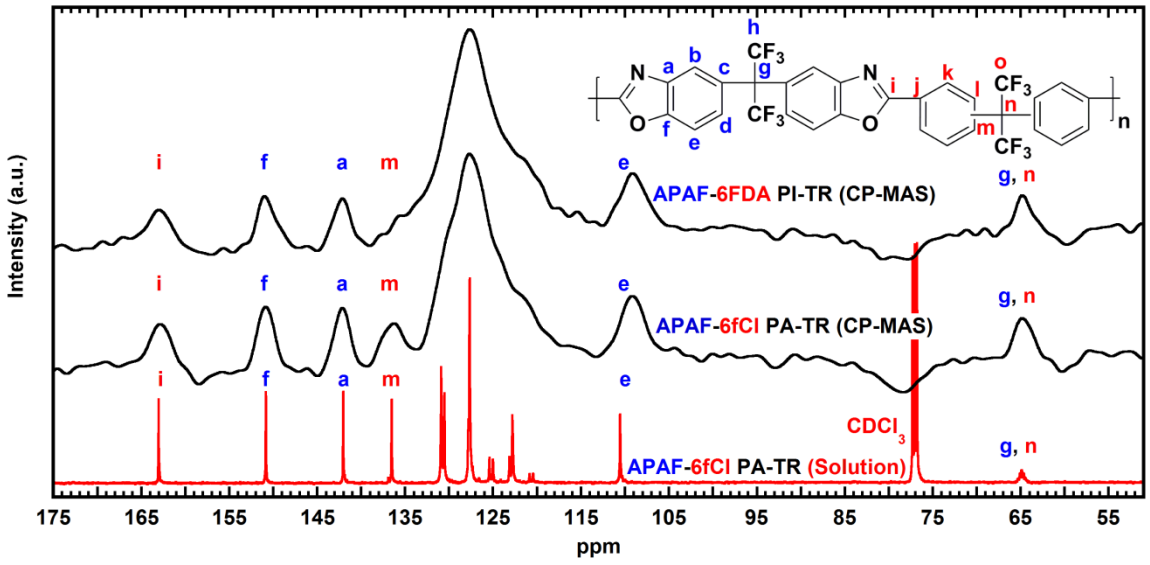

Figure 4.4: Comparison of solution-state ^{13}NMR for the APAF-6fCl TR polymer (PA-TR), solid-state CP-MAS ^{13}C NMR for the APAF-6fCl TR polymer (PA-TR), and solid-state CP-MAS ^{13}C NMR for the APAF-6FDA TR polymer (PI-TR).

CP-MAS NMR was also run on the insoluble PI-TR polymer, and this spectrum is shown in Figure 4.4. Interestingly, nearly identical peak locations and peak intensities between the PA-TR and the PI-TR polymer are observed for the 6 resolved peaks shared among the NMR spectra (i.e., peaks **i**, **f**, **a**, **e**, **g**, and **n**). The only resolved peak for the PA-TR that is not correlated with that of the PI-TR polymer is peak **m**. For the PI-TR polymer, the hexafluoroisopropylidene-functional linkage can be attached to either carbon **m** or **l**, resulting in an isomeric *meta* or *para* linkage (cf., Figure 4.1). This isomeric structure results from the *hydroxyl* group in the precursor PI reacting with either of the two carbonyl groups on the imide in the PI. For the PA-TR, the hexafluoroisopropylidene-functional linkage can only be attached to carbon **m**, which results in a chemical structure with exclusively *para* configuration.

We also performed ^{1}H $T_{1\rho}$ relaxation experiments to compare the motional dynamics of the PA-TR and PI-TR polymers (cf., Appendix A, Section A.5). Since the protons in the solid polymer matrix form a strong ^{1}H-^{1}H homonuclear dipolar coupling network that reaches over several tenths or even hundreds of nanometers via multistep spin diffusions, the measured ^{1}H $T_{1\rho}$ time will reflect structural and motional characteristics of the local domains on the nanoscopic or even mesoscopic level.[25] If an on-resonance spin-lock pulse irradiation whose radio frequency (rf) pulse amplitude is ν_1, the measured relaxation rate, $1/T_{1\rho}$, can be expressed by the following relaxation equation[26,27]

$$\frac{1}{T_{1\rho}} \approx \frac{1}{2}\left(\delta_{H,H}\right)^2 \left[\frac{3\tau_c}{1+4\nu_1^2\tau_c^2}\right] \tag{4.1}$$

where $\delta_{H,H}$ and τ_c are the effective ^1H–^1H dipolar coupling strength experienced by the protons at the measurement site and correlation time of the segmental motions in the polymer chain that are responsible for the $T_{1\rho}$ relaxation, respectively. ^1H $T_{1\rho}$ times were measured indirectly along the directly bonded carbon atoms via ^1H-^{13}C CP, utilizing the pulse sequence shown in Figure 4.5A. The ^{13}C peaks at 127.3 ppm, which is the biggest methine ^{13}C peak, was employed for detecting the ^1H $T_{1\rho}$ time with the best signal-to-noise ratio (Figure 4.5B). We have measured $T_{1\rho}$ values at two different ν1's (ν_1 = 44 and 63 kHz) to simultaneously determine the two unknown parameters τ_c and $\delta_{H,H}$ in Eq. (1). Figure 4.5C shows the $T_{1\rho}$ data measured at ν_1 = 44 and 63 kHz and their least squares best fits. The $T_{1\rho}$ times of the PA-TR and PI-TR polymers are summarized in Table 2. Also summarized in the table are the τ_c and $\delta_{H,H}$ values.

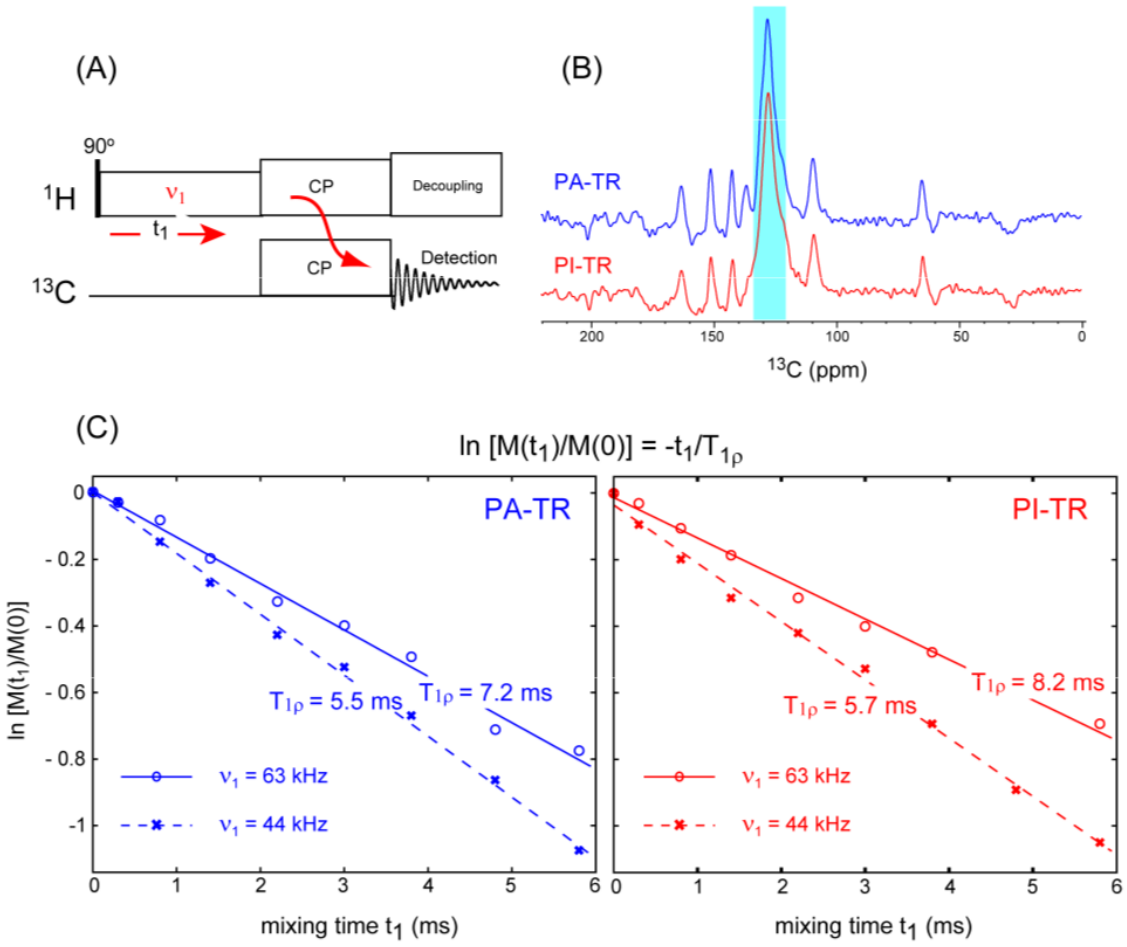

Figure 4.5: (A) ^{1}H $T_{1\rho}$ pulse sequence used, (B) ^{1}H-^{13}C CP-MAS spectra measured on PA-TR and PI-TR by the ^{1}H $T_{1\rho}$ pulse sequence, and (C) the least-square best-fit plots for the data obtained by two different 1H spin-lock rf pulse powers at ν1 = 63 and 44 kHz. The ^{13}C peak position utilized for the ^{1}H $T_{1\rho}$ measurements is colored by sky blue in (B).

Sample	$T1_\rho$ [1]	$T1_\rho$ [2]	$\delta_{H,H}$	τ_c
PA-TR	7.2 ms	5.5 ms	4.82 kHz	7.7 μs
PI-TR	8.2 ms	5.7 ms	4.56 kHz	10. μs

1 ν_1 = 63 kHz; 2 ν_1 = 44 kHz

Table 4.2: $T_{1\rho}$, $\delta_{H,H}$, and τ_c values.

In addition to structural confirmation by CP-MAS NMR, polybenzoxazole bands for both the PA-TR and PI-TR polymer are observed through Fourier transform infrared spectroscopy (FTIR) at 1058 cm^{-1} and 1480 cm^{-1} (cf., Appendix A, Section A.6). Additionally, molecular weight characterization for the PA and PI is included in Appendix A, Section A.7. The PA-TR sample was insoluble in the size exclusion chromatography solvent and, thus, could not be tested for molecular weight.

The effect of synthesis route (i.e., PA versus PI) on the transport properties of the final TR polymer structure was evaluated for several light gases. Gas transport is highly sensitive to morphological differences that could arise from solid-state reactions of different starting materials. For TR polymers, Han *et al.* have even noted differences in transport properties from TR polymers synthesized from identical polyimide structures.[4] Figure 4.6 and Figure 4.7 present Robeson upper bound plots for H_2/CH_4 and CO_2/CH_4 separation. In addition to data points reported in the literature,[28] these plots also include data points from this study for the PA, PA-TR, PI, and PI-TR. Furthermore, data points for commercially relevant polymers[29] are highlighted on these plots. Data for these figures are reported at approximately 10 atm and 35°C, and the effect of pressure on gas transport properties is reported in Appendix A, Section A.8.

The PI has higher permeability and selectivity than the PA for both H_2/CH_4 and CO_2/CH_4 separation. These factors likely relate to a combination of morphological and chain rigidity effects. The T_g of the PI is 301°C,[4] and the T_g of the PA is 258°C.[5] Higher glass transition temperatures often correlate with stronger size sieving capabilities for polymers,[30,31] which would result in a higher selectivity for the PI compared to the PA. Additionally, the PI has a larger average free volume element size than the PA. Using positron annihilation lifetime spectroscopy (cf., Appendix A, Section A.9), the PI had an average free volume diameter of 7.3 Å compared to 7.1 Å for the PA. The larger free

volume element size would likely contribute to the higher permeability for the PI, and the higher glass transition temperature would likely contribute to the higher selectivity for the PI.[31]

The PI-TR polymer had higher permeabilities and slightly lower selectivities than the PA-TR polymer for the CO_2/CH_4 and H_2/CH_4 gas pairs. Due to their rigid nature, the glass transition of these materials could not be determined using DSC, so the effect of chain rigidity on gas selectivity is not clear. However, the higher permeabilities for these materials is consistent with their larger average free volume sizes. The PI-TR polymer has an average free volume element size of 8 Å, and the PA-TR PBO has an average free volume element size of 7.7 Å (cf., Appendix A, Section A.9).

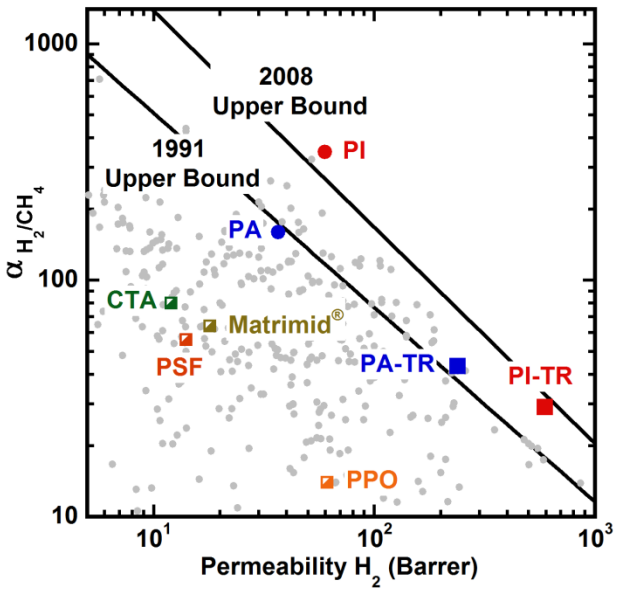

Figure 4.6: H_2/CH_4 trade-off plot for APAF-6FDA PI (PI), APAF-6FDA TR polymer (PI-TR), APAF-6fCl PA (PA), and APAF-6fCl TR polymer (PA-TR). Selectivity of H_2 to CH_4 is labeled as α_{H_2/CH_4}. Literature data is highlighted in light gray,[28] and industrially relevant polymers (i.e., cellulose triacetate (CTA), polysulfone (PSF), Matrimid®, and poly(phenylene oxide) (PPO))[29] are shown for comparison.

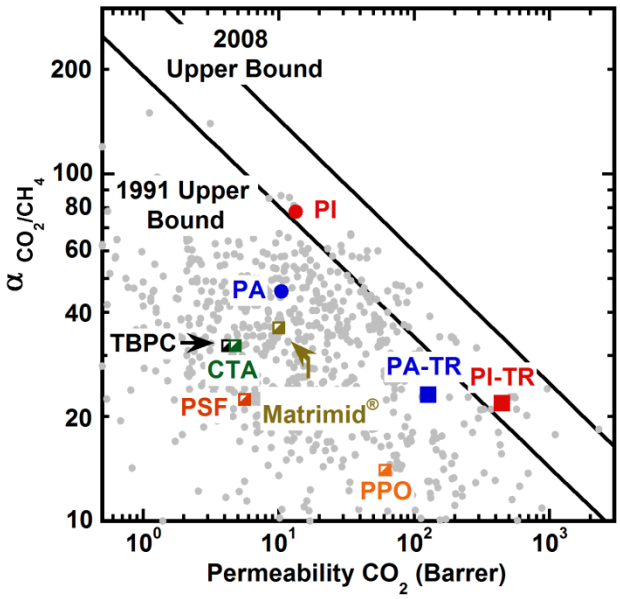

Figure 4.7: CO_2/CH_4 trade-off plot for APAF-6FDA PI (PI), APAF-6FDA TR polymer (PI-TR), APAF-6fCl PA (PA), and APAF-6fCl TR polymer (PA-TR). Selectivity of CO_2 to CH_4 is labeled as α_{CO_2/CH_4}. Literature data is highlighted in light gray,[28] and industrially relevant polymers (i.e., tetrabromo polycarbonate (TBPC), cellulose triacetate (CTA), polysulfone (PSF), Matrimid®, and poly(phenylene oxide) (PPO))[29] are highlighted for comparison.

4.3 CONCLUSIONS

A poly(*hydroxy*-amide) (PA) was synthesized and converted to a TR polymer (PA-TR) that was partially soluble in chloroform. The chemical structure of the soluble fraction of the PA-TR polymer was confirmed to be a polybenzoxazole (PBO) by solution ^1H nuclear magnetic resonance (NMR), ^{13}C NMR, and several 2-D NMR experiments, including correlation spectroscopy (COSY), heteronuclear single quantum correlation (HSQC) spectroscopy, and heteronuclear multiple bond correlation (HMBC) spectroscopy. The chemical structure of the solid-state PA-TR polymer was characterized using cross-polarization magic-angle spinning (CP-MAS) NMR, and the

solution NMR results aligned with the CP-MAS NMR results, indicating that the soluble and insoluble portion of the PA-TR polymer contained comparable PBO chemical structure. Furthermore, a TR polymer with nearly identical structure to the PA-TR sample was synthesized from a poly(*hydroxy*-imide) (PI). CP-MAS NMR confirmed that the PI-TR polymer had a comparable PBO chemical structure to that of the PA-TR polymer, with the only difference in spectra resulting from an inherent *para*/*meta* structural isomer. Compared to PA-TR polymer, the polymer matrix of PI-TR is more rigid due to cross-linking and is less densely packed due to the presence of the *meta* configuration identified by ^{1}H $T_{1\rho}$ relaxation data. The PA-TR and PI-TR polymers had different transport properties for CO_2/CH_4 and H_2/CH_4 separation. These differences were ascribed to differences in chain rigidity and crosslinking, average free volume, and free volume distribution. For H_2/CH_4 separation, the PI sample had transport properties that exceeded the 2008 Robeson upper bound.

4.4 REFERENCES

1. Park, H.B., C.H. Jung, Y.M. Lee, A.J. Hill, S.J. Pas, S.T. Mudie, E. Van Wagner, B.D. Freeman, and D.J. Cookson, *Polymers with cavities tuned for fast selective transport of small molecules and ions.* Science, **2007**. 318(5848), 254-258.

2. Tullos, G. and L. Mathias, *Unexpected thermal conversion of hydroxy-containing polyimides to polybenzoxazoles.* Polymer, **1999**. 40(12), 3463-3468.

3. Tullos, G.L., J.M. Powers, S.J. Jeskey, and L.J. Mathias, *Thermal conversion of hydroxy-containing imides to benzoxazoles: Polymer and model compound study.* Macromolecules, **1999**. 32(11), 3598-3612.

4. Han, S.H., N. Misdan, S. Kim, C.M. Doherty, A.J. Hill, and Y.M. Lee, *Thermally rearranged (TR) polybenzoxazole: Effects of diverse imidization routes on physical properties and gas transport behaviors.* Macromolecules, **2010**. 43(18), 7657-7667.

5. Calle, M., A.E. Lozano, and Y.M. Lee, *Formation of thermally rearranged (TR) polybenzoxazoles: Effect of synthesis routes and polymer form.* European Polymer Journal, **2012**. 48(7), 1313-1322.

6. Hodgkin, J.H. and B.N. Dao, *Thermal conversion of hydroxy-containing polyimides to polybenzoxazoles. Does this reaction really occur?* European Polymer Journal, **2009**. 45(11), 3081-3092.

7. Hodgkin, J.H., M.S. Liu, B.N. Dao, J. Mardel, and A.J. Hill, *Reaction mechanism and products of the thermal conversion of hydroxy-containing polyimides.* European Polymer Journal, **2011**. 47(3), 394-400.

8. Kostina, J., O. Rusakova, G. Bondarenko, A. Alentiev, T. Meleshko, N. Kukarkina, A. Yakimanskii, and Y. Yampolskii, *Thermal rearrangement of functionalized polyimides: IR-spectral, quantum chemical studies, and gas permeability of TR polymers.* Industrial & Engineering Chemistry Research, **2013**. 52(31), 10476-10483.

9. Asensio, J.A., E.M. Sánchez, and P. Gómez-Romero, *Proton-conducting membranes based on benzimidazole polymers for high-temperature PEM fuel cells. A chemical quest.* Chemical Society Reviews, **2010**. 39(8), 3210-3239.

10. Hickner, M.A., H. Ghassemi, Y.S. Kim, B.R. Einsla, and J.E. McGrath, *Alternative Polymer Systems for Proton Exchange Membranes (PEMs).* Chemical Reviews, **2004**. 104(10), 4587-4612.

11. Li, Q., J.O. Jensen, R.F. Savinell, and N.J. Bjerrum, *High temperature proton exchange membranes based on polybenzimidazoles for fuel cells.* Progress in Polymer Science, **2009**. 34(5), 449-477.

12. Rabbani, M.G. and H.M. El-Kaderi, *Template-Free Synthesis of a Highly Porous Benzimidazole-Linked Polymer for CO2 Capture and H2 Storage.* Chemistry of Materials, **2011**. 23(7), 1650-1653.

13. Dawson, R., A.I. Cooper, and D.J. Adams, *Nanoporous organic polymer networks.* Progress in Polymer Science, **2012**. 37(4), 530-563.

14. Fukukawa, K.-i., Y. Shibasaki, and M. Ueda, *A Photosensitive Semi-Alicyclic Poly(benzoxazole) with High Transparency and Low Dielectric Constant.* Macromolecules, **2004**. 37(22), 8256-8261.

15. Fukukawa, K.-i. and M. Ueda, *Recent Development of Photosensitive Polybenzoxazoles.* Polym. J, **2006**. 38(5), 405-418.

16. Ogura, T., T. Higashihara, and M. Ueda, *Pattern formation of polyimide by using photosensitive polybenzoxazole as a top layer.* European Polymer Journal, **2010**. 46(7), 1576-1581.

17. Coleman, M.R. and W.J. Koros, *The transport properties of polyimide isomers containing hexafluoroisopropylidene in the diamine residue.* Journal of Polymer Science Part B: Polymer Physics, **1994**. 32(11), 1915-1926.

18. Morisato, A., K. Ghosal, B.D. Freeman, R.T. Chern, J.C. Alvarez, J.G. de la Campa, A.E. Lozano, and J. de Abajo, *Gas separation properties of aromatic polyamides containing hexafluoroisopropylidene groups.* Journal of Membrane Science, **1995**. 104(3), 231-241.

19. Smith, Z.P., D.F. Sanders, C.P. Ribeiro Jr, R. Guo, B.D. Freeman, D.R. Paul, J.E. McGrath, and S. Swinnea, *Gas sorption and characterization of thermally rearranged polyimides based on 3,3'-dihydroxy-4,4'-diamino-biphenyl (HAB) and 2,2'-bis-(3,4-dicarboxyphenyl) hexafluoropropane dianhydride (6FDA).* Journal of Membrane Science, **2012**. 416, 558-567.

20. Likhatchev, D., C. Gutierrez-Wing, I. Kardash, and R. Vera-Graziano, *Soluble aromatic polyimides based on*

2,2-bis(3-amino-4-hydroxyphenyl)hexafluoropropane: Synthesis and properties. Journal of Applied Polymer Science, **1996**. 59(4), 725-735.

21. Bax, A. and M.F. Summers, *Proton and carbon-13 assignments from sensitivity-enhanced detection of heteronuclear multiple-bond connectivity by 2D multiple quantum NMR.* Journal of the American Chemical Society, **1986**. 108(8), 2093-2094.

22. Jacobsen, N.E., *NMR spectroscopy explained: simplified theory, applications and examples for organic chemistry and structural biology*. **2007**, Wiley.

23. September 23, 2013]; Available from: http://sdbs.riodb.aist.go.jp/sdbs/cgi-bin/direct_frame_top.cgi.

24. Matsuura, T., M. Ishizawa, Y. Hasuda, and S. Nishi, *Polyimides derived from 2, 2'-bis (trifluoromethyl)-4, 4'-diaminobiphenyl. 2. Synthesis and characterization of polyimides prepared from fluorinated benzenetetracarboxylic dianhydrides.* Macromolecules, **1992**. 25(13), 3540-3545.

25. Schmidt-Rohr, K. and H.W. Spiess, *Multidimensional solid-state NMR and polymers*. **1994**, Elsevier.

26. Kimmich, R., *NMR: tomography, diffusometry, relaxometry*. Vol. 432. **1997**, Springer Berlin etc.

27. Look, D.C., I.J. Lowe, and J.A. Northby, *Nuclear magnetic resonance study of molecular motions in solid hydrogen sulfide.* The Journal of Chemical Physics, **1966**. 44(9), 3441-3452.

28. Robeson, L.M., *The upper bound revisited.* Journal of Membrane Science, **2008**. 320(1-2), 390-400.

29. Sanders, D.F., Z.P. Smith, R. Guo, L.M. Robeson, J.E. McGrath, D.R. Paul, and B.D. Freeman, *Energy-efficient polymeric gas separation membranes for a sustainable future: A review.* Polymer, **2013**. 54(18), 4729-4761.

30. Robeson, L.M., *Correlation of separation factor versus permeability for polymeric membranes.* Journal of Membrane Science, **1991**. 62(2), 165-185.

31. Freeman, B.D., *Basis of permeability/selectivity tradeoff relations in polymeric gas separation membranes.* Macromolecules, **1999**. 32(2), 375-380.

Chapter 5: Gas Sorption and Characterization of Thermally Rearranged Polyimides based on 3,3'-dihydroxy-4,4'-diamino-biphenyl (HAB) and 2,2'-bis-(3,4-dicarboxyphenyl) Hexafluoropropane Dianhydride (6FDA)

This chapter focuses on the characterization and sorption properties for an *ortho*-functional polyimide prepared from 3,3'-dihydroxy-4,4'-diamino-biphenyl (HAB) and 2,2'-bis-(3,4-dicarboxyphenyl) hexafluoropropane dianhydride (6FDA). The HAB-6FDA polyimide was partially converted to its corresponding thermally rearranged (TR) polymer by thermal treatments at different times and temperatures. The solubilities of H_2, N_2, O_2, CH_4, and CO_2 were determined over a range of pressures at 35°C. At 10 atm, solubility coefficients of H_2, N_2, O_2, CH_4, and CO_2 increased by a factor of approximately two between the polyimide and the most highly converted TR polymer. Correlations between solubility and penetrant condensability were in good agreement with such correlations in other fluorinated polyimides. Dual-mode sorption model parameters were determined from the sorption isotherms. The affinity constant, Henry's law solubility, and Langmuir capacity constant increased with gas condensability, and increases in the Langmuir capacity constant were observed as TR polymer conversion increased. Comparisons were made between the solubility selectivity of CO_2/CH_4, O_2/N_2, CH_4/N_2, and CO_2/N_2 in HAB-6FDA, its corresponding TR polymers, and in other polymers in the literature. Qualitatively, a decrease in solubility selectivity for gas pairs including CO_2 correlates with imide and acetate loss during conversion.

5.1 INTRODUCTION

To prepare very thin (e.g., 0.1 micrometer thick) polymer membranes for gas separation applications, current membrane fabrication processes invariably involve dissolving the polymer of interest in an organic solvent or solvent mixture and preparing the membrane via a coating or phase inversion process.[1] However, the use of membranes in chemically challenging environments often requires that they be highly resistant to organic compounds in, for example, processing of natural gas, where higher hydrocarbons are often found as contaminants.[2-4] This conundrum, whereby soluble polymers are required to make thin membranes and, as a result of being soluble, the polymers are subject to attack by organic compounds found in the stream to be separated, limits the use of many polymers for applications such as natural gas processing and olefin/paraffin separation. Additionally, many interesting polymers, such as some polybenzoxazoles (PBO), which have excellent chemical and thermal stability,[5,6] are insoluble in common solvents, so they have not been studied significantly or developed for gas separation applications because there are few routes to convert them to thin membranes.[7]

Recently, Park et al.[8] circumvented this limitation by preparing polyimides that were readily soluble in common organic solvents and could then be converted, via a solid-state, thermal rearrangement process, to insoluble PBOs and related materials. Surprisingly, the gas separation properties improved remarkably as a result of this thermal rearrangement process, leading to materials whose properties were often above the upper bound.[8,9] This synthetic approach builds upon work, originally pursued for

---

This chapter has been adapted with permission from: Smith, Z.P., D.F. Sanders, C.P. Ribeiro Jr, R. Guo, B.D. Freeman, D.R. Paul, J.E. McGrath, and S. Swinnea, *Gas sorption and characterization of thermally rearranged polyimides based on 3,3'-dihydroxy-4,4'-diamino-biphenyl (HAB) and 2,2'-bis-(3,4-dicarboxyphenyl) hexafluoropropane dianhydride (6FDA).* Journal of Membrane Science, **2012**. 416, 558-567.

applications other than gas separations, described by Kardash and Pravednikov in 1967[10] and by Tullos et al. in 1999.[11] It permits the use of established synthetic approaches[12,13] to fabricate soluble polyimide precursors which can be thermally rearranged into insoluble PBO, polybenzothiazole, or polybenzimidazole films.

More recently, this approach has been used to prepare benzoxazole-pyrrolone[14] and benzoxazole-polyimide[15] copolymers. Furthermore, gas separation structure-property data[9] and the effect of imidization routes on TR polymer properties[16] have been reported. These initial findings have focused largely on CO_2/CH_4 and O_2/N_2 separations, and permeability and selectivity of the reported materials are often near or above the upper bound.[17,18] Molecular dynamics and Monte Carlo methods have been used[19] to characterize free volume distribution, permeability, solubility, and diffusivity in a series of TR polymers studied by Park et al.[8] and for polymers considered in this study. Additionally, the permeability, diffusivity, and free volume of the materials in this study have been determined experimentally.[20]

This study presents gas sorption and basic characterization data for a TR polymer prepared from the polyimide based on 3,3'-dihydroxy-4,4'-diamino-biphenyl and 2,2'-bis-(3,4-dicarboxyphenyl) hexafluoropropane dianhydride. Sorption isotherms of H_2, N_2, O_2, CH_4, and CO_2 are reported as a function of extent of thermal rearrangement. The resulting polymers were characterized using ^1H nuclear magnetic resonance (for materials that were soluble), Fourier transform infrared spectroscopy, differential scanning calorimetry, X-ray diffraction, and thermogravimetric analysis coupled with mass spectrometry.

5.2 RESULTS AND DISCUSSION

5.2.1 Thermal Conversion of chemically imidized HAB-6FDA

The thermal rearrangement process of an *acetate*-functionalized polyimide prepared from 3,3'-dihydroxy-4,4'-diamino-biphenyl (HAB) and 2,2'-bis-(3,4-dicarboxyphenyl) hexafluoropropane dianhydride (6FDA) is believed to occur in two steps as shown in Figure 4.1.[21] The first step, which occurs near the T_g of the polymer, involves the loss of acetic acid via the presence of catalytic amounts of adventitious water in the sample. The acetate group is replaced by a hydroxyl group that then undergoes a decarboxylation reaction at temperatures between approximately 350°C to 450°C to form the polybenzoxazole structure shown in Figure 4.1.

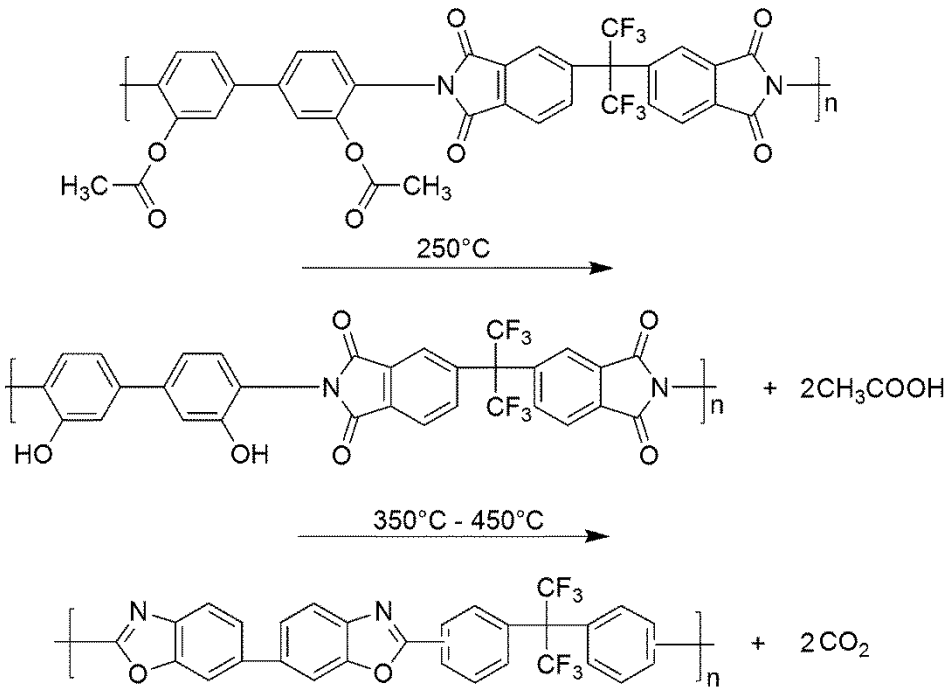

Figure 5.1: Proposed reaction of an acetate-functional HAB-6FDA sample to form a polybenzoxazole.

The HAB-6FDA sample described in this chapter was formed via chemical imidization, and its properties, along with the properties of three partially converted TR polymers are presented in Table 5.1. The percent conversion of these samples is defined by Equation (5.1). The theoretical mass loss required to fully convert the chemically imidized polyimide into a polybenzoxazole according to the reaction described in Figure 4.1 is 24.3%.

$$\%\,\text{Conversion} = \frac{\text{Actual Mass Loss}}{\text{Theoretical Mass Loss}} \times 100 \tag{5.1}$$

Sample	Conversion Temperature (°C)	Dwell Time (min)	Conversion (%)	Density (g/cm^3)	d-spacing (Å)
HAB-6FDA	NA	NA	0	1.407	6.2
TR 350 60min	350	60	39	1.398	5.9
TR 400 60min	400	60	60	1.400	6.2
TR 450 30min	450	30	76	1.34	6.2

Table 5.1: List of samples considered, conversion temperature, dwell time, % conversion, density, and d-spacing.

5.2.2 ^{1}H NMR Characterization of Polyimide Structure

^{1}H nuclear magnetic resonance (NMR) was used to confirm the structure of the HAB-6FDA polyimide. Peak assignments are given in Figure 5.2, where the NMR solvent, chloroform-d, appears at 7.26 ppm, and trace amounts of water in the sample container appear at 1.56 ppm. The aromatic region of the ^{1}H NMR is between 7.4 ppm to 8.2 ppm, with the dianhydride hydrogens (labeled a, b, and c in Figure 5.2) shifted downfield relative to the hydrogen peaks attributed to the diamine (labeled d, e, and f in Figure 5.2). The acetate peak is observed at 2.23 ppm. An enlarged view of the aromatic region is provided for clarity.

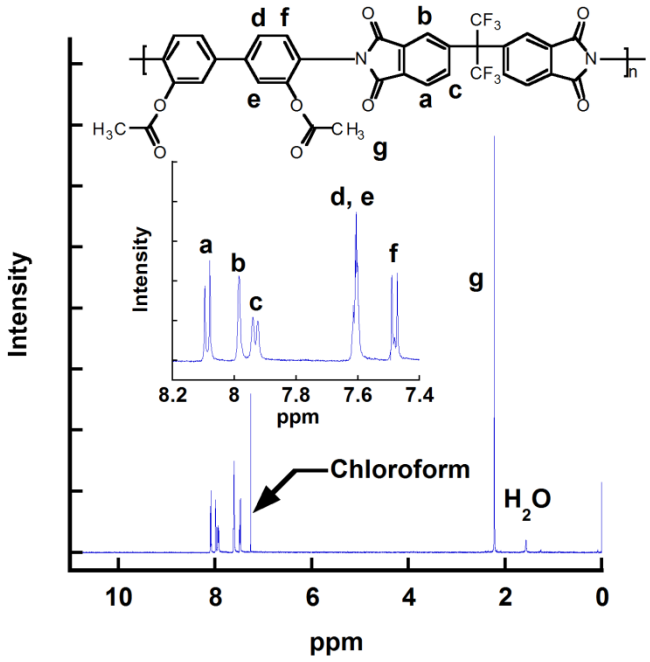

Figure 5.2: ^{1}H NMR spectra with peak assignments for HAB-6FDA.

5.2.3 TGA-MS Characterization

Thermogravimetric analysis coupled with mass spectrometry (TGA-MS) was used to characterize the thermal rearrangement of HAB-6FDA under a N_2 atmosphere. From the TGA scan presented in Figure 5.3, approximately 2% mass loss was observed at 300°C, 5% mass loss at 350°C, 11% mass loss at 400°C, 16% mass loss at 450°C, and 22% mass loss at 500°C. No mass loss was observed below 250°C, indicating removal of solvent to levels undetectable by TGA. As indicated earlier, the theoretical mass loss to fully convert the *acetate*-functional HAB-6FDA to its polybenzoxazole analog is 24.3%. Therefore, at a constant heating rate of 5°C/min, this level of mass loss is not observed until the sample has been heated to more than 500°C, at which point thermal degradation is likely occurring along with thermal rearrangement. Mass spectrometry results, presented below, confirm this interpretation. To avoid widespread thermal degradation,

samples were heated to temperatures of only 350°C, 400°C, and 450°C and held at these temperatures for the times set forth in Table 5.1 to partially rearrange the *ortho*-functional polyimide films. Because a tube furnace was used to thermally rearrange large batches of polyimides for characterization and solubility tests, mass loss comparisons for films were made between the TGA and the tube furnace, which agreed within ±2% in the percent conversion.

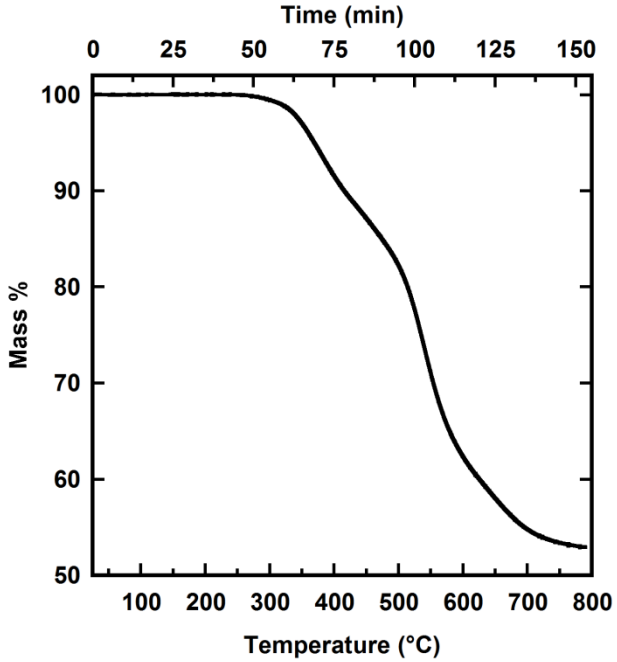

Figure 5.3: TGA scan of HAB-6FDA. The sample was heated at 5°C/min from 25°C to 800°C under N_2 atmosphere.

TGA-MS was used to characterize the composition of material lost from the polymer sample during the TGA scan. Using the same experimental conditions for the TGA experiment presented in Figure 5.3, Figure 5.4A and Figure 5.4B shows the molecular weights of evolved products between 10 and 100 amu. Components having molecular weights of 17, 18, 19, 20, 41, 42, 44, 51, 69, and 85 amu were evolved during the experiment. Figure 5.4A shows the molecular weights of products from the thermal

rearrangement region, and Figure 5.4B shows the molecular weights of products only associated with polymer degradation. At approximately 400°C, an increase in peak intensity is observed for molecular weights of 17, 18, 41, 42, and 44. These peaks are the only observed peaks associated with mass loss below 450°C. A molecular weight of 44 is attributed to decarboxylation of the polyimide during thermal rearrangement. This result is consistent with other mass spectrometry studies on thermally rearranged polymers.[9,15,16] Mass loss associated with molecular weights 41 and 42 is ascribed to loss of the pendant acetate groups in the form of ketene.[22] A weak change in intensity was observed for molecular weights corresponding to that of H_2O (i.e., 17, 18) in the thermal rearrangement region. H_2O evolution in this region indicates that the polyimide synthesis via chemical imidization may be incomplete and, therefore, undergo further thermal imidization at elevated temperatures.[23,24]

As shown in Figure 5.4B, above 450°C, ion current peaks (i.e., intensities) different from those observed in the thermal rearrangement region indicate losses of molecular weights of 19, 20, 51, 69, and 85. These species are associated with polymer degradation. Furthermore, peak intensities of 17, 18, and 44 from Figure 5.4A, which were originally observed during thermal rearrangement, are again observed; this time they are associated with polymer degradation. Molecular weights of 17 and 18 reflect a loss of water due to the presence of oxygen in the aromatic polymer structure;[25] 19, 20, and 69 indicate cleaving of the fluorine moiety on the HAB-6FDA polymer backbone, where these molecular weights correspond to evolution of F, HF, and CF_3, respectively.[26] Similar to other thermal stability studies on polybenzoxazoles,[25] cleavage of the polymer backbone is observed above 450°C, where molecular weights of 44, 51, and 85 could occur because of either aromatic degradation[25] and, for 51 and 85, loss of HCF_2 and COF_3.[26]

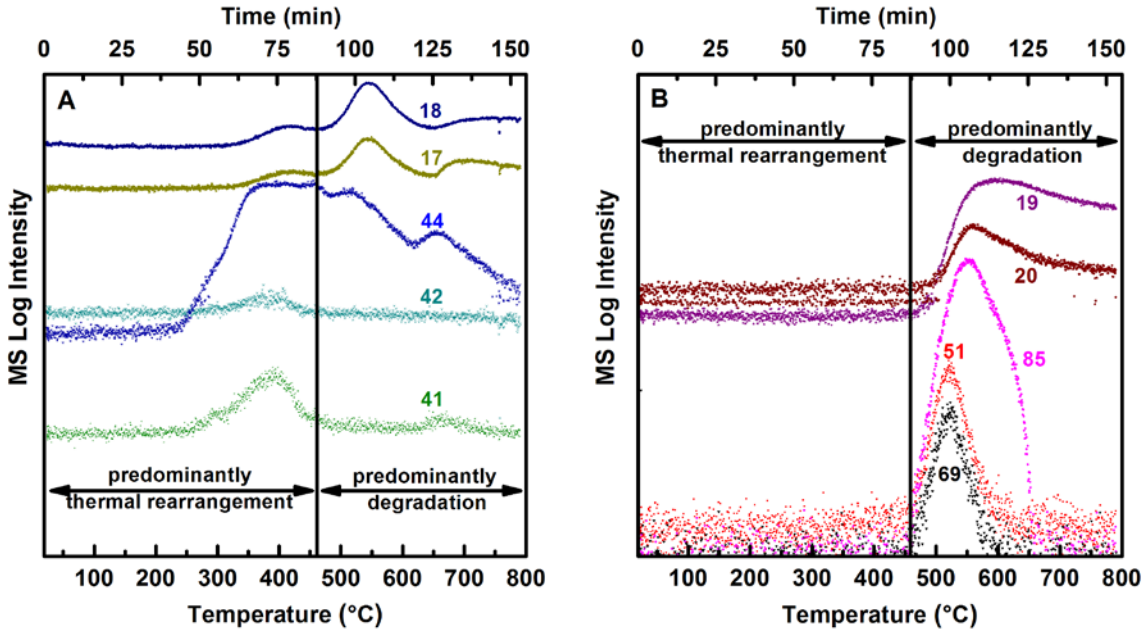

Figure 5.4: TGA-MS of the HAB-6FDA polyimide. The sample was heated at 5°C/min from room temperature to 800°C and the mass loss of molecular weights with observable changes in spectrometer intensity were tracked with conversion. Molecular weights of fragments are written on the plot and are coordinated with spectra by color. (A) shows the molecular weight products associated primarily with thermal rearrangement, and (B) shows the molecular weight products associated mainly with degradation. Some products associated with thermal rearrangement in (A) also appear as polymer degradation products at elevated temperatures.

5.2.4 Infrared Characterization

Polyimide conversion to its corresponding TR polymer is often monitored using Fourier transform infrared spectroscopy (FT-IR).[8,9,14-16] Figure 5.5 presents transmission IR spectra of HAB-6FDA polyimide and partially converted TR polymers. The intensity readings of the FT-IR spectra were normalized using a characteristic C-F stretch at 1255 cm^{-1} as a reference.[11] However, due to some peak overlap near the C-F stretch, this normalization was only used for a qualitative comparison of peak intensities. Symmetric

and asymmetric imide carbonyl stretching is observed at 1780 cm^{-1} (peak b) and 1720 cm^{-1} (peak c), respectively; and C-N imide stretching is observed at 1380 cm^{-1} (peak e).[13] These imide peaks decrease in intensity during thermal rearrangement. Due to the loss of acetate functionality in these films and the resulting formation of a hydroxyl group in its place, a weak OH peak, previously unobserved in the polyimide, appears in the partially converted TR films at approximately 3400 cm^{-1} (peak a). The appearance of this hydroxyl peak indicates that at least some of the acetate functionality may convert to hydroxyl functionality before thermal rearrangement occurs. Conversion to PBO is more subtle; however, weak peaks attributed to PBO ring stretching can be observed at 1060 cm^{-1} (peak f) and 1480 cm^{-1} (peak d).[9,27,28]

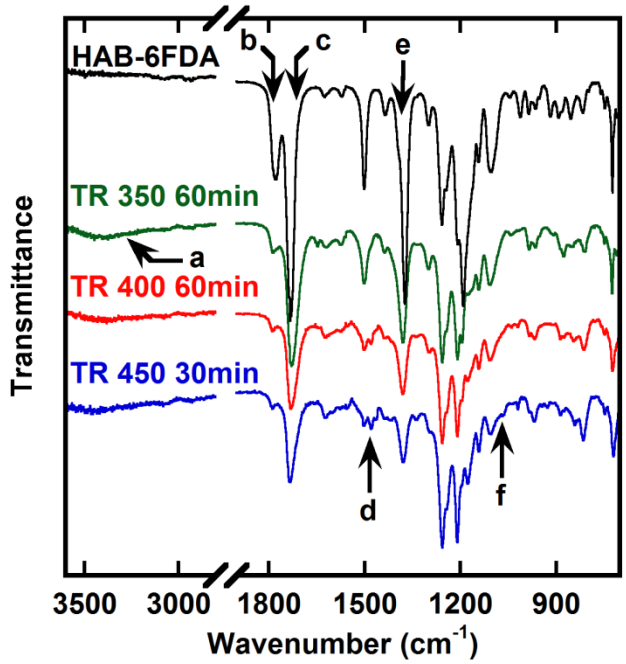

Figure 5.5: Transmission FT-IR of the polyimide precursor (HAB-6FDA) and TR analogs. The spectra have been displaced vertically for easier viewing. Peak a (3400 cm^{-1}) corresponds to hydroxyl functionality, peaks at b (1780 cm^{-1}) and c (1720 cm^{-1}) correspond to imide stretching, peak e (1380 cm^{-1}) corresponds with C-N imide stretching, peaks d (1480 cm^{-1}) and f (1060 cm^{-1}) correspond to benzoxazole ring stretching.

5.2.5 XRD Characterization

X-ray diffraction (XRD) was used to determine d-spacing values for polyimide and TR polymers and to determine if any regions of crystallinity existed. As shown in Figure 5.6, the broad, amorphous halos observed in all samples confirm that the polymers were completely amorphous. d-spacing values were calculated according to Bragg's equation (i.e., $d = \lambda/(2\sin\theta)$) as described in the Materials and Experimental Methods section, and these values are recorded in Table 5.1. Interestingly, d-spacing did not show

a strong correlation with thermal conversion, as has been reported for other TR polymers.[9]

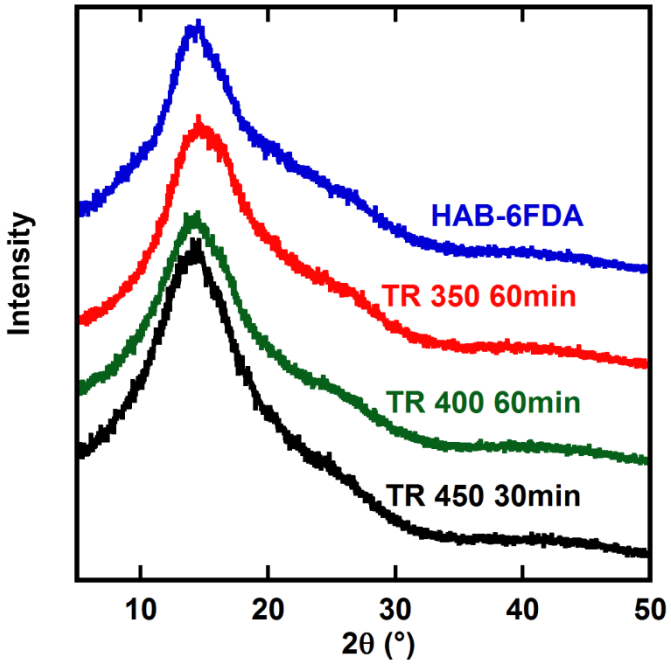

Figure 5.6: XRD of the polyimide and corresponding TR polymers.

5.2.6 DSC Characterization

For HAB-6FDA polyimides, which are converted to PBO materials during thermal treatment, a shift in thermal transitions, such as T_g, to higher values is expected as the polymer undergoes chemical transformation towards a more rigid chemical structure. The T_g of the HAB-6FDA polyimide, as shown in Figure 5.7A and Figure 5.7B, was 255°C during the first DSC scan. However, the T_g increased to 267°C during the second scan, and it increased further to 271°C during the third scan. The most likely explanation for this increase is the conversion of the acetate functionality in the

polyimide to hydroxyl groups during the DSC scan. However, when held at sufficiently high temperatures for sufficiently long periods of time, other effects, such as conversion of the polyimide to more rigid PBO, crosslinking, etc. may occur and would also favor increased T_g values. Also observed in Figure 5.7A is a strong endotherm centered at approximately 100°C for the first DSC scan, indicating the presence of water, which was sorbed into the polyimide during sample preparation under atmospheric exposure. The disappearance of this endotherm during the second and third DSC scan supports this hypothesis. After treating HAB-6FDA at the thermal rearrangement conditions set forth in Table 5.1, no detectable T_g was observed up to 450°C, as is shown for the third scan of the TR 450 30min sample in Figure 5.7C.

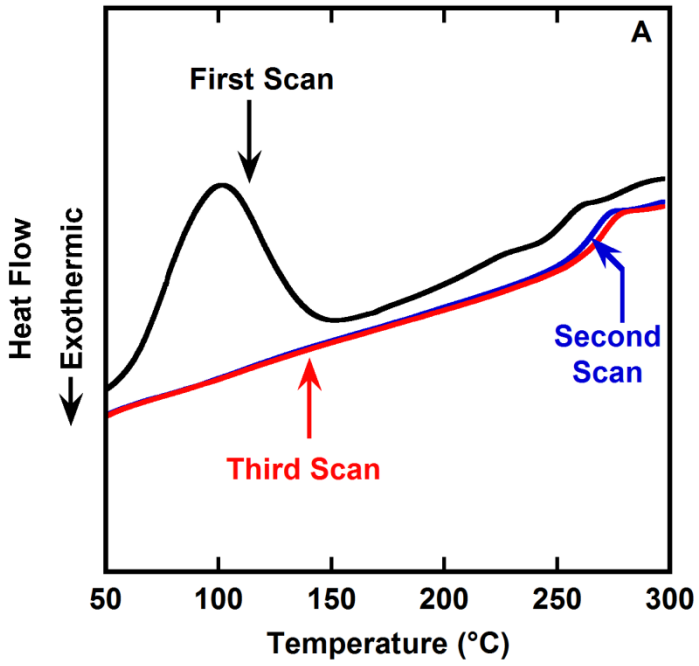

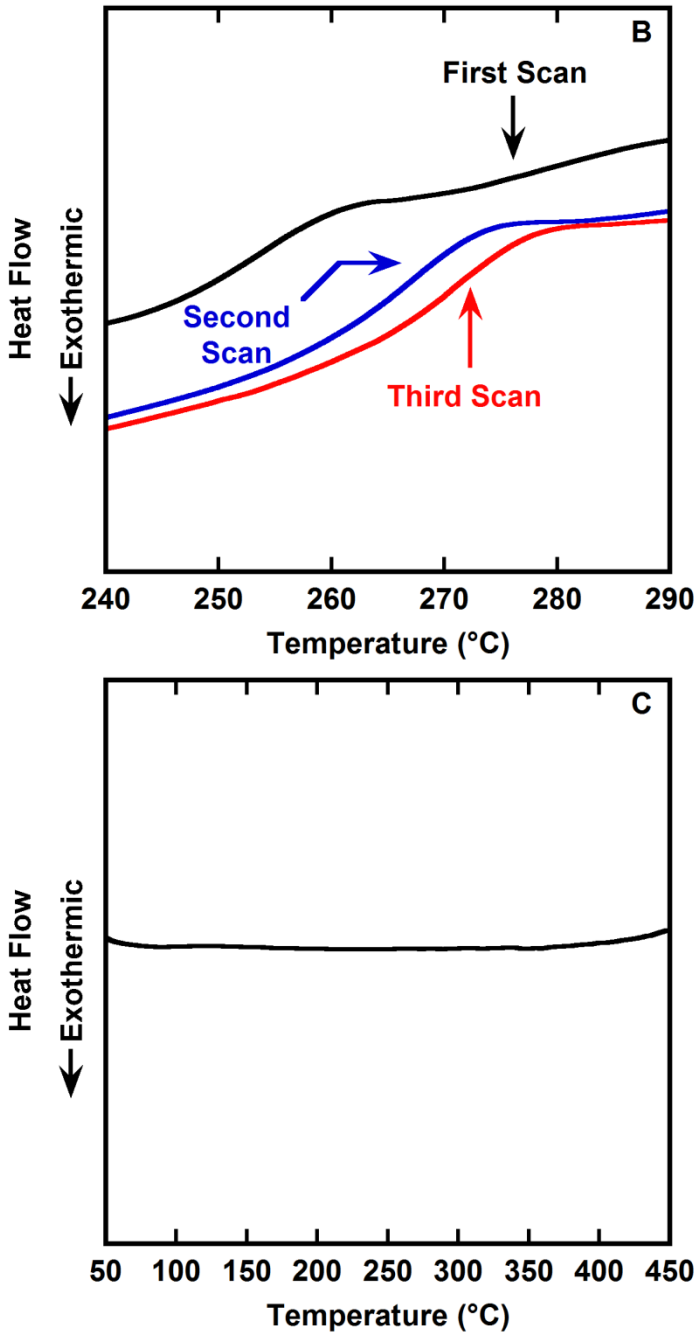

Figure 5.7: DSC scans of HAB-6FDA polyimide and TR 450 30min. (A) Full temperature range for HAB-6FDA polyimide for 3 temperature cycles, (B) enlarged view of T_g from (A), and (C) DSC scan for the TR 450 30min sample.

5.2.7 Sorption Isotherm Characterization

Sorption isotherms for HAB-6FDA polyimide and the corresponding TR polymers are presented in Figure 5.8. Solubility coefficients were calculated using the dual-mode model, which is shown in Equation (5.2), and constraining parameters k_D and b according to the method described in the Materials and Experimental Methods section.

$$C = k_D p + C_H^{'} \frac{bp}{1+bp} \tag{5.2}$$

For N_2, O_2, CH_4, and CO_2, the sorption isotherms are concave to the pressure axis, consistent with dual mode sorption in glassy polymers.[29-31] Gas solubility coefficients in all cases increased as follows: $S_{H_2} < S_{N_2} < S_{O_2} < S_{CH_4} < S_{CO_2}$, so the gas solubility increased in order of increasing gas critical temperature, which is often used as a measure of the tendency of a gas to condense.[30] This trend in gas solubility coefficients is typically observed in polymers.[29-31]

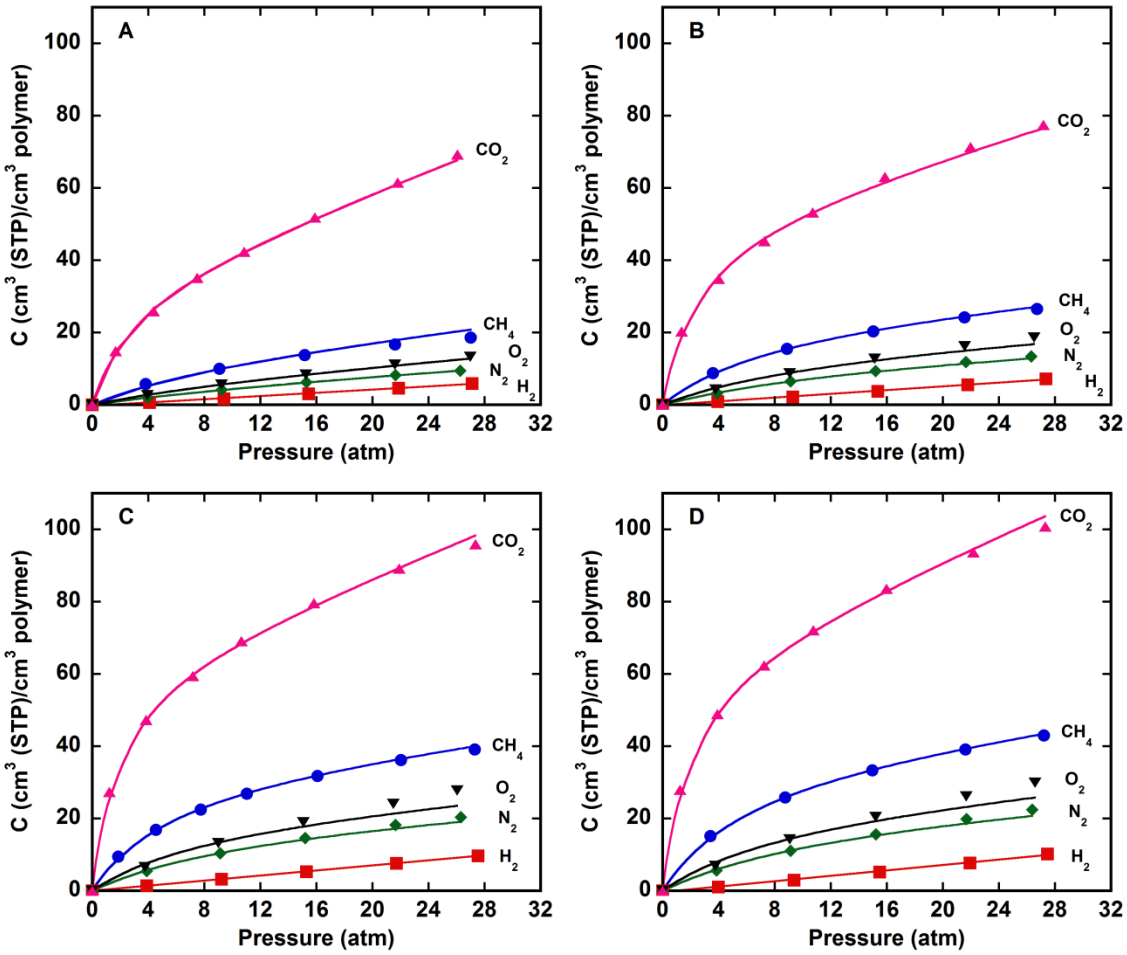

Figure 5.8: Sorption isotherms at 35°C for (a) HAB-6FDA polyimide, (b) TR 350 60min (39% conversion), (c) TR 400 60min (60% conversion), and (d) TR 450 30min (76% conversion).

Interestingly, the sorption of all gases increases as a result of the thermal treatment protocols. For example, the gas solubility coefficients are approximately two times higher at 10 atm in the TR 450 30min sample (converted 76%) than in the polyimide. To put these solubility coefficients in perspective, Table 5.2 presents apparent solubility coefficients in common glassy polymers, HAB-6FDA polyimide, and HAB-6FDA TR polymers. Gas solubility in HAB-6FDA polyimide is higher than that of other materials shown in Table 5.2, but it is closest to that of Matrimid® polyimide,

which is a relatively high free volume polymer. Thermal treatment of HAB-6FDA polyimide to prepare partially converted TR polymers increases gas sorption. For example, at 10 atm the polyimide has an apparent CO_2 solubility coefficient of 4.0 cm^3(STP)/(cm^3 polymer atm) compared to the TR 450 30min sample that has an apparent CO_2 solubility coefficient of 7.0 cm^3(STP)/(cm^3 polymer atm). Similarly, the apparent CH_4 solubility coefficient at 10 atm increases from 1.07 cm^3(STP)/(cm^3 polymer atm) for the polyimide to 2.8 cm^3(STP)/(cm^3 polymer atm) for the 76% converted TR polymer. These increases in sorption are due, at least in part, to increases in non-equilibrium free volume, as will be discussed.

Polymer	Sorption (cm^3(STP)/(cm^3 polymer atm))					Ref.
	H_2	CO_2	O_2	N_2	CH_4	
Polysulfone 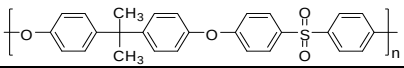		2.08	0.29	0.19	0.67	[24]
Matrimid® Polyimide 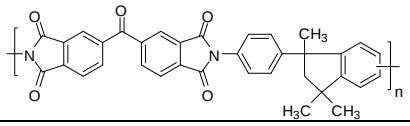		3.4	0.43	0.30	0.87	[32]
Tetrabromobisphenol-A Polycarbonate 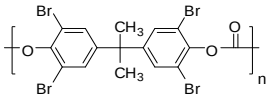		2.6			0.93	[26]
poly(2,6-dimethyl-1,4-phenylene oxide) (PPO) 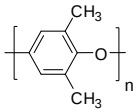		2.65			1.24	[33]
Bisphenol-A Polycarbonate 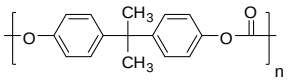		1.6[a]	0.21[a*]	0.17[b]	0.4[a]	a [26], b [34]
HAB-6FDA	0.21±0.07	4.0±0.1	0.60±0.07	0.44±0.07	1.07±0.08	
TR 350 60min	0.25±0.07	5.2±0.2	0.94±0.08	0.69±0.07	1.65±0.09	
TR 400 60min	0.35±0.09	6.7±0.2	1.42±0.09	1.11±0.09	2.6±0.1	
TR 450 30min	0.35±0.08	7.0±0.2	1.52±0.09	1.18±0.09	2.8±0.1	

Data are reported for 35°C and 10 atm except for data labeled *, which represents solubility at 35°C and 2 atm.

Table 5.2: Comparison of sorption of penetrant gases in standard polymeric materials, HAB-6FDA polyimide, and corresponding HAB-6FDA TR polymers.

Propagation of error analysis[35] was used to determine the uncertainty in the sorption measurements. The largest error in the sorption measurements comes from the volume calibration of the sorption cell, which has the greatest effect on low sorbing gases in the polyimide. For example, at 10 atm and 35°C, H_2 sorption has an error of

approximately 30%, whereas CO_2 has an error of less than 3%. The errors in sorption at 10 atm and 35°C are reported in Table 5.2 for HAB-6FDA and its TR analogs.

Sorption of small molecules in polymers typically increases with increasing penetrant condensability, as measured by properties such as critical temperature, normal boiling point, enthalpy of vaporization, etc. Figure 5.9 presents the gas sorption coefficient at 10 atm for HAB-6FDA polyimide and its corresponding TR materials as a function of gas critical temperature. Data for Figure 5.9 was interpolated at 10 atm from the sorption isotherms in Figure 5.8.

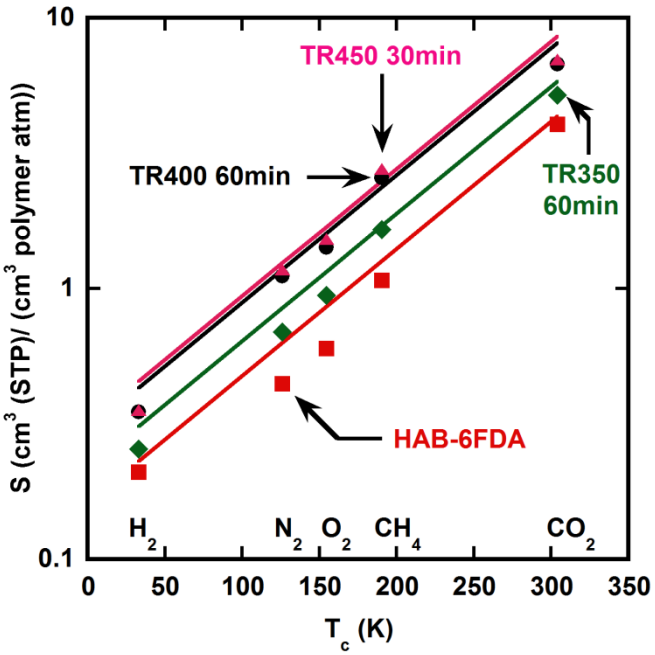

Figure 5.9: Scaling of solubility coefficients with gas critical temperature. The points represent gas sorption values at 35°C and 10 atm. ■ is HAB-6FDA, ◆ is TR 350 60min, ● is TR 400 60min, and ▲ is TR 450 30min.

For polymer films, the logarithm of penetrant solubility coefficients as a function of gas critical temperature often yields a straight line with slope, β, and intercept, α, as indicated in Equation (5.3:

$$\ln S = \alpha + \beta \times T_c \tag{5.3}$$

Generally, for hydrocarbon-based liquids as well as many glassy and rubbery polymers, β is approximately 0.016 - 0.019 K^{-1} at 35°C.[30,31] However, in highly fluorinated polymers, β values are between 0.007 K^{-1} and 0.011 K^{-1}.[36] The actual value of these slopes depends on the pressure of the sorption measurement.[37] Similarly, some 6FDA-based (i.e., fluorinated) polyimides have values of β between 0.011 K^{-1} and 0.012 K^{-1}.[36] As shown in Table 5.3, HAB-6FDA, as well as its TR analogs in this study, have β values similar to 6FDA-based polyimides.

Classification	Medium	$\beta \times 10^3$ (K^{-1})	Reference
Hydrocarbons	benzene	17	[38]
	n-heptane	18	[39]
	amorphous polyethylene	16	[39]
	poly(dimethylsiloxane)	17	[39]
	polysulfone	17	[39]
	poly(phenylene oxide)	16	[39]
	poly(ethylene terepthalate)	19	[39]
Fluorocarbons	*n*-C_7F_{16}	10.5	[39]
	AF1600	11	[39]
	Hyflon AD 80	7	[39]
6FDA-Based Polyimides	6FDA-ODA	12	[39]
	6FDA-MDA	11	[38]
	6FDA-IPDA	11	[38]
Polymers in this Study	HAB-6FDA	10	
	TR 350 60min	10	
	TR 400 60min	10	
	TR 450 30min	10	

Table 5.3: Comparison of hydrocarbon and fluorocarbon relationship to sorption.

Dual-mode parameters for HAB-6FDA polyimide and corresponding TR polymers, listed in Table 5.4, were calculated by fitting experimental data to the dual-mode model using a least squares method. Isotherms were well described by the dual mode model when there were no constraints on the values of k_D, b, and C_H', but these variables did not exhibit highly systematic trends with penetrant condensability or extent of conversion, a problem which is well documented in the literature.[40-42] Therefore, k_D and b were constrained to increase exponentially with critical temperature with the same slope as the total penetrant solubility versus penetrant critical temperature at 10 atm. Similar correlations have been noted for other amorphous polymers.[38]

Gas	Samples	Dual-Mode Sorption Parameters		
		k_D (cm^3(STP)/(cm^3 polymer atm))	C_H' cm^3(STP)/(cm^3 polymer)	b (atm^{-1})
*H_2	HAB-6FDA	0.21		
	TR 350 60min	0.25		
	TR 400 60min	0.35		
	TR 450 30min	0.35		
N_2	HAB-6FDA	0.23	5.9	0.054
	TR 350 60min	0.17	13	0.066
	TR 400 60min	0.24	19	0.091
	TR 450 30min	0.25	21	0.084
O_2	HAB-6FDA	0.30	7.4	0.072
	TR 350 60min	0.23	16	0.089
	TR 400 60min	0.32	23	0.12
	TR 450 30min	0.34	25	0.11
CH_4	HAB-6FDA	0.44	11	0.11
	TR 350 60min	0.34	23	0.13
	TR 400 60min	0.46	32	0.18
	TR 450 30min	0.49	36	0.16
CO_2	HAB-6FDA	1.4	35	0.34
	TR 350 60min	1.1	51	0.42
	TR 400 60min	1.5	60	0.58
	TR 450 30min	1.6	62	0.53

*For H_2, k_D is the effective solubility parameter because dual-mode behavior is not readily observed for H_2.

Table 5.4: Dual-mode parameters for H_2, N_2, O_2, CH_4 and CO_2 for HAB-6FDA polyimide and corresponding TR polymers.

Figure 5.10 and Figure 5.11 present correlations between b and k_D as a function of T_c, respectively. The standard deviation in the data was calculated by adjusting either b or k_D for each polymer and observing variations of chi square near its minimum value.[35] Error is smaller than the size of the data points shown in Figure 5.10 and Figure 5.11. For each gas and for each polymer, values of b increase in the following order:

HAB-6FDA < TR 350 60min < TR 450 30min < TR 400 60min. For HAB-6FDA, TR 400 60min, and TR 450 30min, values of k_D are similar for each gas and for each polymer. Surprisingly, values of k_D as a function of T_c are consistently lower for TR 350 60min. The reason for these trends is not completely clear; however, one possible explanation for the shift in parameters may come from differences in the polymer structure. The subtle formation of hydroxyl functionality in TR 350 60min, which is observed from FT-IR (cf., Figure 5.5), may contribute to the increased density and reduced d-spacing when comparing TR 350 60min with other samples tested in this study. These chemical modifications, along with the onset of thermal rearrangement, may account for changes in the accessibility of equilibrium sorption sites, and for the binding affinity of the Langmuir sites.

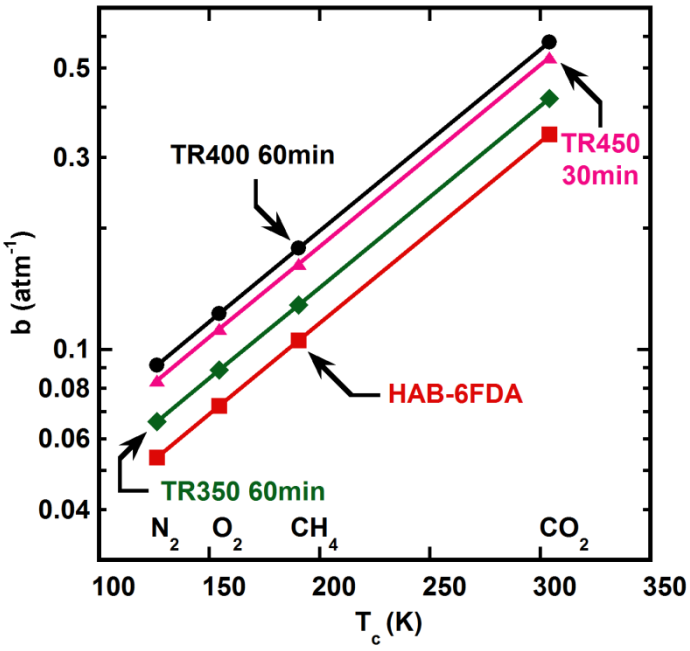

Figure 5.10: Correlation between the Langmuir affinity constant, b, and gas critical temperature. ■ is HAB-6FDA, ◆ is TR 350 60min, ● is TR 400 60min, and ▲ is TR 450 30min. Uncertainty is less than the size of the data points in the fitted parameters.

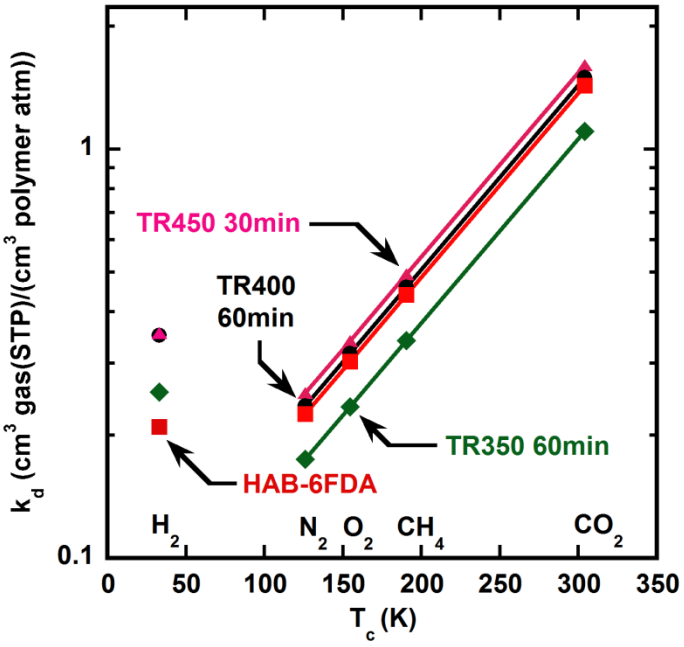

Figure 5.11: Correlation between Henry's Law solubility constant, k_D, and gas critical temperature. An effective Henry's Law solubility coefficient is plotted for H_2. ■ is HAB-6FDA, ◆ is TR 350 60min, ● is TR 400 60min, and ▲ is TR 450 30min. Uncertainty is less than the size of the data points in the fitted parameters.

Because H_2 is much further above its critical temperature than N_2, O_2, CH_4, and CO_2, its sorption levels are low, and the sorption isotherms are linear. Therefore, an independent assessment of k_D, b, and C_H' was not possible. Consequently, the value reported for k_D in Figure 5.11 is the effective solubility coefficient (i.e., C/p), and not the k_D from Equation (5.2.

Figure 5.12 presents the change in Langmuir sorption capacity parameter, C_H', with increasing conversion for N_2, O_2, CH_4, and CO_2. For CH_4, C_H' increases by over 350% between the polyimide and the TR 450 30min sample. For CO_2, C_H' increases by over 75% between the polyimide and the TR 450 30min sample. The Langmuir sorption capacity parameter is often associated with the amount of non-equilibrium excess volume

in a glassy polymer.[43-45] Therefore, increases in C_H' suggest increases in non-equilibrium free volume during thermal rearrangement, which accounts for the majority of the overall solubility increase that occurs during thermal rearrangement.

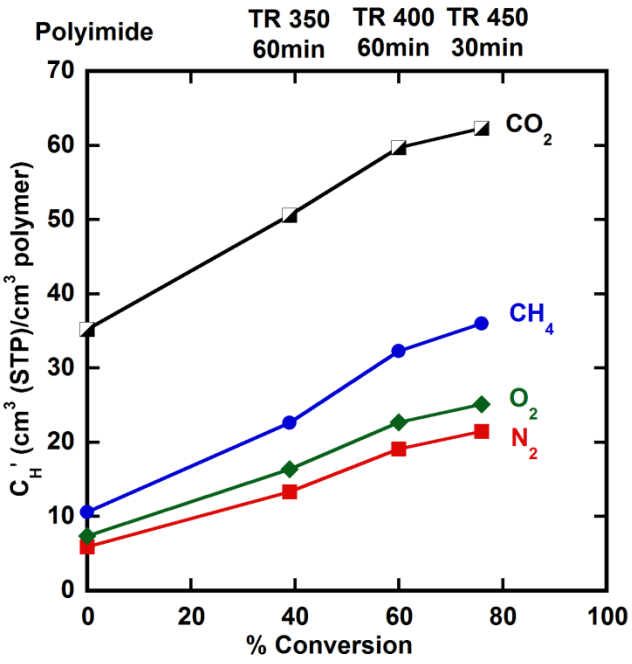

Figure 5.12: Correlation between Langmuir capacity, C_H', and percent conversion.

Figure 5.13 presents the ratio of sorption coefficients for N_2, O_2, CH_4, and CO_2 in partially converted TR polymers to that of their corresponding polyimide, and Table 5.5 presents the solubility selectivity of various gas pairs. For all gases tested, sorption increases during conversion. However, the sorption of N_2, O_2, and CH_4 increases more than that for CO_2. Consequently, for CO_2/CH_4 and CO_2/N_2, solubility selectivity decreases with increasing conversion. The reduced sorption of CO_2 compared to CH_4 and N_2 is consistent with the loss of polar moieties from the HAB-6FDA backbone during rearrangement. Decarboxylation of the HAB-6FDA polyimide results in loss of

carbonyl and acetate functionality, as shown in Figure 4.1. Several studies have shown that CO_2 sorption increases in polymers containing polar functional groups such as styrene methyl/methacrylate copolymers,[46] polysulfone,[36] and cellulose acetate.[47] CO_2, being polarizable, has dipole-quadrupole interactions with polar pendant groups such as carbonyl and acetate functionality, thus increasing CO_2 sorption.[47] Because HAB-6FDA polyimide has acetate and carbonyl functionality, higher CO_2/CH_4 and CO_2/N_2 solubility selectivity is observed for the polyimide than for the analogous thermally rearranged polybenzoxazole, which has neither acetate nor carbonyl functionality. For HAB-6FDA, solubility selectivity of CO_2/CH_4 decreases from 3.8 to 2.5 between the polyimide and 76% converted TR polymer. Similarly, CO_2/N_2 solubility selectivity decreases from 9.2 to 6.0 between the polyimide and 76% converted TR polymer.

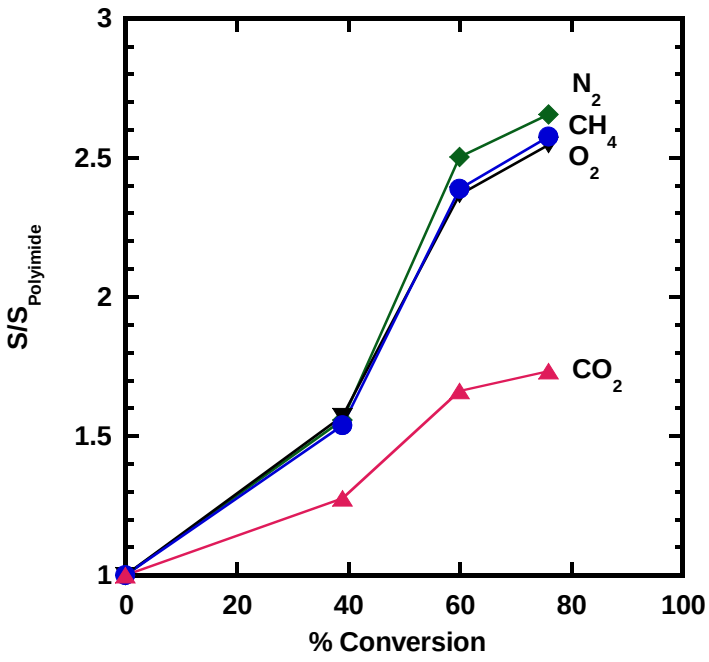

Figure 5.13: Sorption coefficients of N_2, O_2, CH_4, and CO_2 in partially converted TR materials normalized by the sorption coefficients of the gases in the polyimide. The data represent points at 10 atm and 35°C.

Gas Pair	HAB-6FDA	TR 350 60min	TR 400 60min	TR 450 30min
CO_2/CH_4	3.8	3.1	2.6	2.5
O_2/N_2	1.4	1.4	1.3	1.3
CH_4/N_2	2.4	2.4	2.3	2.4
CO_2/N_2	9.2	7.5	6.1	6.0

Table 5.5: Solubility selectivity for HAB-6FDA polyimide and analogous TR polymers at 10 atm and 35°C.

5.3 CONCLUSIONS

Sorption coefficients of H_2, N_2, O_2, CH_4, and CO_2 increased as a function of thermal rearrangement for a polyimide derived from 3,3'-dihydroxy-4,4'-diamino-biphenyl diamine and 2,2'-bis-(3,4-dicarboxyphenyl) hexafluoropropane dianhydride (HAB-6FDA). Sorption coefficients scaled with critical temperature in a manner consistent with trends observed in other fluorinated polymers. Dual-mode parameters were calculated from a least squares fit of the sorption isotherms to the dual-mode sorption model. The Langmuir capacity constant increased as a function of conversion. The overall increase in solubility during conversion is largely explained by increases in the Langmuir capacity constant, $C_H^{'}$, indicating that non-equilibrium free volume becomes more prevalent in thermally rearranged polymers compared with that of their analogous polyimides. Solubility selectivity remained constant during conversion except for gas pairs involving CO_2, where solubility selectivity decreased with loss of acetate and carbonyl functionality on the polyimide.

5.4 REFERENCES

1. Pandey, P., *Membranes for gas separation.* Progress in Polymer Science, **2001**. 26(6), 853-893.

2. Baker, R.W. and K. Lokhandwala, *Natural gas processing with membranes: An overview.* Industrial & Engineering Chemistry Research, **2008**. 47(7), 2109-2121.

3. Lee, J.S., W. Madden, and W.J. Koros, *Antiplasticization and plasticization of Matrimid® asymmetric hollow fiber membranes - Part A. Experimental.* Journal of Membrane Science, **2010**. 350(1-2), 232-241.

4. Lee, J.S., W. Madden, and W.J. Koros, *Antiplasticization and plasticization of Matrimid® asymmetric hollow fiber membranes. Part B. Modeling.* Journal of Membrane Science, **2010**. 350(1-2), 242-251.

5. Wolfe, J.F., *Rigid-rod polymers. 1. Synthesis and thermal properties of para-aromatic polymers with 2,6-benzobisoxazole units in the main chain.* Macromolecules, **1981**. 14(4), 909-915.

6. Choe, E.W. and S.N. Kim, *Synthesis, spinning, and fiber mechanical properties of poly (p-phenylenebenzobisoxazole).* Macromolecules, **1981**. 14(4), 920-924.

7. Moy, T.M. and J.E. McGrath, *Synthesis of hydroxyl-containing polyimides derived from 4,6-diamino-resorcinol dihydrochloride and aromatic tetracarboxylic dianhydrides.* Journal of Polymer Science Part A: Polymer Chemistry, **1994**. 32(10), 1903-1908.

8. Park, H.B., C.H. Jung, Y.M. Lee, A.J. Hill, S.J. Pas, S.T. Mudie, E. Van Wagner, B.D. Freeman, and D.J. Cookson, *Polymers with cavities tuned for fast selective transport of small molecules and ions.* Science, **2007**. 318(5848), 254-258.

9. Park, H.B., S.H. Han, C.H. Jung, Y.M. Lee, and A.J. Hill, *Thermally rearranged (TR) polymer membranes for CO_2 separation.* Journal of Membrane Science, **2010**. 359(1-2), 11-24.

10. Kardash, I. and A.N. Pravednikov, *Aromatic polyimides containing hydroxy- and methoxy-groups.* Vysokomol Soyed, **1967**. 9(12), 873-876.

11. Tullos, G.L., J.M. Powers, S.J. Jeskey, and L.J. Mathias, *Thermal conversion of hydroxy-containing imides to benzoxazoles: Polymer and model compound study.* Macromolecules, **1999**. 32, 3598-3612.

12. Ohya, H., V.V. Kudryavtsev, and S.I. Semenova, *Polyimide membranes: Applications, fabrications, and properties.* **1996**, Amsterdam, Gordon and Breach Publishers.

13. Ghosh, M.K. and K.L. Mital, *Polyimides: Fundamentals and applications.* **1996**, New York, Marcel.

14. Choi, J.I., C.H. Jung, S.H. Han, H.B. Park, and Y.M. Lee, *Thermally rearranged (TR) poly(benzoxazole-co-pyrrolone) membranes tuned for high gas permeability and selectivity.* Journal of Membrane Science, **2010**. 349(1-2), 358-368.

15. Jung, C.H., J.E. Lee, S.H. Han, H.B. Park, and Y.M. Lee, *Highly permeable and selective poly(benzoxazole-co-imide) membranes for gas separation.* Journal of Membrane Science, **2010**. 350(1-2), 301-309.

16. Han, S.H., N. Misdan, S. Kim, C.M. Doherty, A.J. Hill, and Y.M. Lee, *Thermally rearranged (TR) polybenzoxazole: Effects of diverse imidization routes on physical properties and gas transport behaviors.* Macromolecules, **2010**. 43(18), 7657-7667.

17. Robeson, L.M., *Correlation of separation factor versus permeability for polymeric membranes.* Journal of Membrane Science, **1991**. 62(2), 165-185.

18. Robeson, L.M., *The upper bound revisited.* Journal of Membrane Science, **2008**. 320(1-2), 390-400.

19. Jiang, Y., F.T. Willmore, D. Sanders, Z.P. Smith, C.P. Ribeiro, C.M. Doherty, A. Thornton, A.J. Hill, B.D. Freeman, and I.C. Sanchez, *Cavity size, sorption and transport characteristics of thermally rearranged (TR) polymers.* Polymer, **2011**. 52(10), 2244-2254.

20. Sanders, D.F., Z.P. Smith, C.P. Ribeiro, R.L. Guo, J.E. McGrath, D.R. Paul, and B.D. Freeman, *Gas permeability, diffusivity, and free volume of thermally rearranged polymers based on 3,3 '-dihydroxy-4,4 '-diamino-biphenyl (HAB) and 2,2 '-bis-(3,4-dicarboxyphenyl) hexafluoropropane dianhydride (6FDA).* Journal of Membrane Science, **2012**. 409, 232-241.

21. Sanders, D.F., R. Guo, Z.P. Smith, Q. Liu, K.A. Stevens, J.E. McGrath, D.R. Paul, and B.D. Freeman, *Influence of polyimide precursor synthesis route and ortho-position functional group on thermally rearranged (TR) polymer properties: conversion and free volume.* Polymer, **2014**. In Press.

22. Waters, T., R.A.J. O'Hair, and A.G. Wedd, *Catalytic gas phase dehydration of acetic acid to ketene.* International Journal of Mass Spectrometry, **2003**. 228(2-3), 599-611.

23. Farr, I.V., *Synthesis and characterization of novel polyimide gas separation membrane material systems*, Ph.D. **1999**, Virginia Polytechnic Institute and State University: Blacksburg, VA, USA.

24. Farr, I.V., D. Kratzner, T.E. Glass, D. Dunson, Q. Ji, and J.E. McGrath, *The synthesis and characterization of polyimide homopolymers based on 5(6)-amino-1-(4-aminophenyl)1,3,3-trimethylindane.* Journal of Polymer Science Part A: Polymer Chemistry, **2000**. 38(15), 2840-2854.

25. Ehlers, G.F.L., K.R. Fisch, and W.R. Powell, *The thermal breakdown mechanism of polybenzoxazoles and polybenzothiazoles.* Journal of Polymer Science: Polymer Symposia, **1973**. 43(1), 55-75.

26. Wieneke, J.U. and C. Staudt, *Thermal stability of 6FDA-(co-)polyimides containing carboxylic acid groups.* Polymer Degradation and Stability, **2010**. 95(4), 684-693.

27. Tullos, G.L. and L.J. Mathias, *Unexpected thermal conversion of hydroxy-containing polyimides to polybenzoxazoles.* Polymer, **1999**. 40, 3463-3468.

28. Kim, T.K., K.Y. Choi, K.S. Lee, D.W. Park, and M.Y. Jin, *Thermal conversion of t-butyloxycarbonyloxy attached polyamides to polybenzoxazoles.* Polymer Bulletin, **2000**. 44, 55-62.

29. Drioli, E. and L. Giorno, *Membrane operations: Innovative separations and transformations*. **2009**, Weinheim, Wiley-VCH. 551-551.

30. Matteucci, S.T., Y.P. Yampolskii, B.D. Freeman, and I. Pinnau, *Transport of gases and vapors in glassy and rubbery polymers*, in *Materials science of membranes for gas and vapor separation*, Y. Yampolskii, I. Pinnau, and B.D. Freeman, Editors. **2006**, John Wiley & Sons: Chichester. 1-47.

31. Paul, D.R. and Y.P. Yampolskii, *Polymeric gas separation membranes*. **1994**, Boca Raton, CRC Press.

32. Moore, T.T. and W.J. Koros, *Gas sorption in polymers, molecular sieves, and mixed matrix membranes.* Journal of Applied Polymer Science, **2007**. 104(6), 4053-4059.

33. Story, B.J. and W.J. Koros, *Sorption and transport of CO_2 and CH_4 in chemically modified poly (phenylene oxide).* Journal of Membrane Science, **1992**. 67(2-3), 191-210.

34. Koros, W.J., A.H. Chan, and D.R. Paul, *Sorption and transport of various gases in polycarbonate.* Journal of Membrane Science, **1977**. 2, 165-190.

35. Bevington, P.R. and K.D. Robinson, *Data reduction and error analysis for the physical sciences: Third edition*. **2003**, Boston, McGraw Hill.

36. Ghosal, K., R.T. Chern, and B.D. Freeman, *Effect of basic substituents on gas sorption and permeation in polysulfone.* Macromolecules, **1996**. 29(12), 4360-4369.

37. Robeson, L.M., Z.P. Smith, B.D. Freeman, and D.R. Paul, *Contributions of diffusion and solubility selectivity to the upper bound analysis for glassy gas separation membranes.* Journal of Membrane Science, **2014**. 453, 71-83.

38. Ghosal, K. and B.D. Freeman, *Gas separation using polymer membranes: An overview.* Polymers for Advanced Technologies, **1994**. 5(11), 673-697.

39. Prabhakar, R.S., B.D. Freeman, and I. Roman, *Gas and vapor sorption and permeation in poly(2,2,4-trifluoro-5-trifluoromethoxy-1,3-dioxole-co-tetrafluoroethylene).* Macromolecules, **2004**. 37(20), 7688-7697.

40. Morisato, A., B.D. Freeman, I. Pinnau, and C.G. Casillas, *Pure hydrocarbon sorption properties of poly(1-trimethylsilyl-1-propyne) (PTMSP), poly(1-phenyl-1-propyne) (PPP), and PTMSP/PPP blends.* Journal of Polymer Science Part B: Polymer Physics, **1996**. 34(11), 1925-1934.

41. Sanders, E.S., *High-pressure sorption of pure and mixed gases in glassy polymers*, Ph.D. Dissertation in Chemical Engineering. **1983**, North Carolina State University: Raleigh, NC, USA.

42. Koros, W.J., *Sorption and transport of gases in glassy polymers*, Ph.D. Dissertation in Chemical Engineering. **1977**, The University of Texas at Austin: Austin, TX, USA. 254.

43. Koros, W.J. and D.R. Paul, *Sorption and transport of CO_2 above and below the glass transition of poly (ethylene terephthalate).* Polymer Engineering and Science, **1980**. 20(1), 14-19.

44. Tsujita, Y., *Gas sorption and permeation of glassy polymers with microvoids.* Progress in Polymer Science, **2003**. 28(9), 1377-1401.

45. Tokarev, A., K. Friess, J. Machkova, M. Šipek, and Y.P. Yampolskii, *Sorption and diffusion of organic vapors in amorphous Teflon AF2400.* Journal of Polymer Science Part B: Polymer Physics, **2006**. 44(5), 832-844.

46. Raymond, P.C. and D.R. Paul, *Sorption and transport of pure gases in random styrene/methyl methacrylate copolymers.* Journal of Polymer Science Part B: Polymer Physics, **1990**. 28(11), 2079-2102.

47. Koros, W.J., *Simplified analysis of gas/polymer selective solubility behavior.* Journal of Polymer Science: Polymer Physics Edition, **1985**. 23(8), 1611-1628.

Chapter 6: Hydrogen Sorption in Polymers for Membrane Applications

This chapter reports hydrogen sorption properties of a series of polymers. Due to its low condensability, direct measurement of hydrogen sorption is often very difficult in polymers using traditional sorption measurement techniques. In this study, hydrogen sorption isotherms between -20°C and 70°C and at pressures up to 60 bara were determined for a polyimide and its corresponding thermally rearranged (TR) polymers prepared from 3,3′-dihydroxy-4,4′-diamino-biphenyl (HAB) and 2,2-bis-(3,4-dicarboxyphenyl) hexafluoropropane dianhydride (6FDA). Hydrogen sorption increased by a factor of approximately 2.6 between the polyimide precursor and the most highly converted TR polymer. This relative increase in sorption was similar to that observed for other non-polar light gases such as N_2, O_2, and CH_4, but less than that observed for CO_2. Additionally, H_2 sorption was measured for other common polymers, including AF 2400, Matrimid®, polysulfone (PSF), and poly(dimethylsiloxane) (PDMS). Among the glassy polymers tested, polysulfone had the lowest H_2 sorption, and the HAB-6FDA TR polymer had the highest H_2 sorption. A slight dual-mode curvature was observed for H_2 sorption in several of the glassy materials, and it was most pronounced at low temperatures and for the TR polymers. Enthalpies of sorption were also determined. The most exothermic enthalpy of sorption occurred in Matrimid®, and a slightly endothermic enthalpy of sorption was observed in rubbery poly(dimethylsiloxane). Comparisons between gravimetric and volumetric sorption methods showed similar results.

6.1 INTRODUCTION

H_2 is an important component in a number of separations such as ammonia purge gas recovery, refinery off-gas purification, and syngas ratio adjustment.[1-3] These applications are among the oldest commercial applications in industrial membrane separations and are typically accomplished using diffusion-selective glassy polymers to take advantage of the relatively small size of H_2. Monsanto first introduced their Prism® separators, which use polysulfone-based hollow fibers,[4] as early as 1977 for syngas ratio adjustment.[5] Membranes remain an important unit operation for H_2 separations today.

Despite the widespread industrial use of membranes for H_2 separation, little is known today about H_2 sorption in many polymers. Few H_2 sorption results exist in the literature, and the published results are often determined using time-lag measurements.[6-8] Because H_2 has high diffusion coefficients and very low solubility in polymers, especially at ambient temperatures, uncertainty in sorption levels from time-lag or volumetric sorption measurements can be large. Therefore, having H_2 sorption data for several polymers commonly found in the literature could be useful to further extend existing structure-property relationships in gas separation polymers. In nonporous polymers, such as those used for gas separation membranes, gas permeability can be factored into gas solubility and diffusivity.[9-12] Comparisons of permeability, solubility, and diffusion coefficients among different materials are useful to guide new polymer design, which can lead to better performing polymer membranes for a given application.

There has recently been interest in new types of polymers, such as so-called "polymers of intrinsic microporosity", for use as gas separation membrane materials and H_2 storage materials.[13] Another new class of polymers being explored for gas separation

---

This chapter has been adapted with permission from: Smith, Z.P., R.R. Tiwari, T.M. Murphy, D.F. Sanders, K.L. Gleason, D.R. Paul, and B.D. Freeman, *Hydrogen sorption in polymers for membrane applications.* Polymer, **2013**. 54(12), 3026–3037.

applications is so-called thermally rearranged (TR) polymers.[14-17] TR polymers are formed via a solid-state reaction of polyimides. These polyimides contain reactive functional groups in the *ortho*-position relative to the diamine used in the synthesis of the polyimide. This reaction converts a soluble, processable polyimide precursor to an insoluble and possibly crosslinked polybenzoxazole (PBO), polybenzothiazole (PBT), or polybenzimidazole (PBI) polymer.[18,19] Membrane precursors can be spun into hollow fibers or solution cast through traditional solution processing techniques[1] and then thermally treated to form stable TR polymer membranes. In this way, insoluble membranes with high levels of thermal and chemical stability may be prepared from soluble precursors using existing membrane fabrication technologies.

For certain separations, the transport properties of some TR polymers are near or above the Robeson upper bound.[14,15,20-22] These high combinations of permeability and selectivity have been attributed to changes in free volume and free volume distribution that occur during thermal rearrangement.[14,23] Additionally, the *ortho*-position functional groups can be modified to improve transport properties.[24,25] Han *et al.* have explored TR polymers derived from poly(*o*-hydroxylamide), which have shown promising transport properties for H_2/CO_2 separation.[26] Developing a library of sorption data for TR polymers, in addition to drawing comparisons with other commonly studied materials, could be useful in the design of these materials for H_2 separation applications.

6.2 RESULTS AND DISCUSSION

6.2.1 Basic characterization and polymer structures

A brief summary of material and transport properties for the samples considered in this study is shown in Table 6.1, and molecular structures are shown in Table 6.2. A more detailed description of the sample preparation, casting conditions, and experimental

methods for determining these properties is available in the Materials and Experimental Methods section.

Sample	Density (g/cm^3)	Percent Conversion	T_g (°C)	P_{H_2} (Barrer)	P_{N_2} (Barrer)	α_{H_2/N_2}	Reference(s)
HAB-6FDA	1.407 ± 0.009	0	255	37.8 ± 0.9	0.56 ± 0.01	68 ± 2	[17]
TR 350 60min	1.398 ± 0.009	39	*	95 ± 2	1.62 ± 0.03	58 ± 2	[17]
TR 400 60min	1.400 ± 0.009	60	*	290 ± 20	8.7 ± 0.6	33 ± 3	[17]
TR 450 30min	1.344 ± 0.011	76	*	530 ± 10	25.3 ± 0.6	21.0 ± 0.6	[17]
Matrimid®	1.231 ± 0.006	NA	305[27]	17.5[28]	0.22[28]	80[28]	This work, [27], [28]
PSF	1.215 ± 0.017	NA	186[29]	14 ± 1	0.21 ± 0.01	64 ± 8	This work, [29]
AF 2400	1.744	NA	240	3400**	780**	4.3**	[30]
PDMS	0.98[31]	NA	-123[32]	890 ± 30[33,γ]	400 ± 10[33,γ]	2.2 ± 0.1[33,γ]	[31], [32], [33]

NOTES:
Transport properties were measured at 35°C and 10 atm unless otherwise noted. Density values are reported at approximately 23°C to 25°C.
* T_g could not be determined because no DSC peak was observed.
** 50 psig upstream, atmospheric downstream, and 25°C.
γ infinite dilution.
Alphabetic superscripts correspond to data taken from references shown in the reference column. In rows without alphabetic superscripts, all data is taken from the reference shown in the corresponding reference column. Uncertainties represent one standard deviation.

Table 6.1: Basic characterization information for samples tested in this study.

HAB-6FDA Polyimide	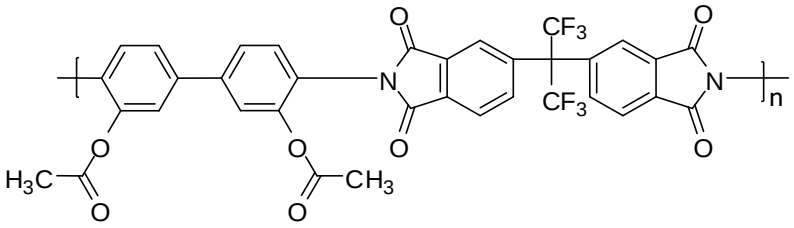
HAB-6FDA TR Polymer	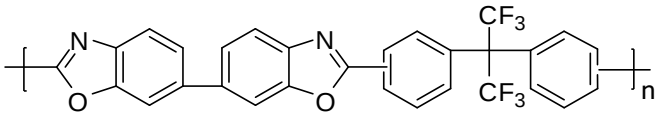
Matrimid®	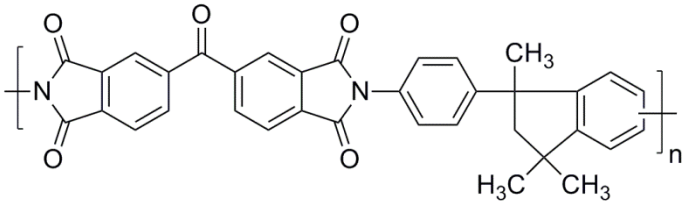
PSF	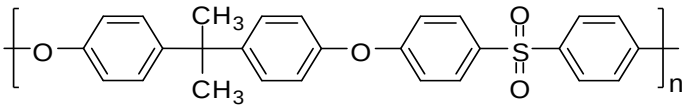
AF 2400	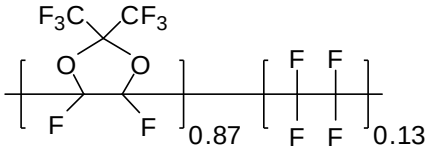
PDMS	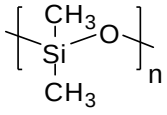

Table 6.2: Sample names and polymer structures considered in this study.

6.2.2 Sorption in thermally rearranged HAB-6FDA

Hydrogen sorption was determined for chemically imidized HAB-6FDA as a function of extent of thermal rearrangement. Figure 6.1 presents sorption isotherms for HAB-6FDA polyimide and partially converted TR polymers. As conversion proceeds from the polyimide to the TR 450 30min sample, sorption increases by a factor of approximately 2.6 for all temperatures. At -20°C and 60 bar, H_2 sorption in the polyimide is approximately 11 cm^3(STP)/cm^3(polymer). For the TR 450 30min sample, H_2 sorption is approximately 26 cm^3(STP)/cm^3(polymer). Put another way, mass uptake of H_2 in these polymers increases over the same thermal conversion from approximately 0.07 wt. % to nearly 0.18 wt. %. Furthermore, sorption increases with decreasing temperature, which is consistent with the temperature dependence of light gas sorption in many polymers.[9,10]

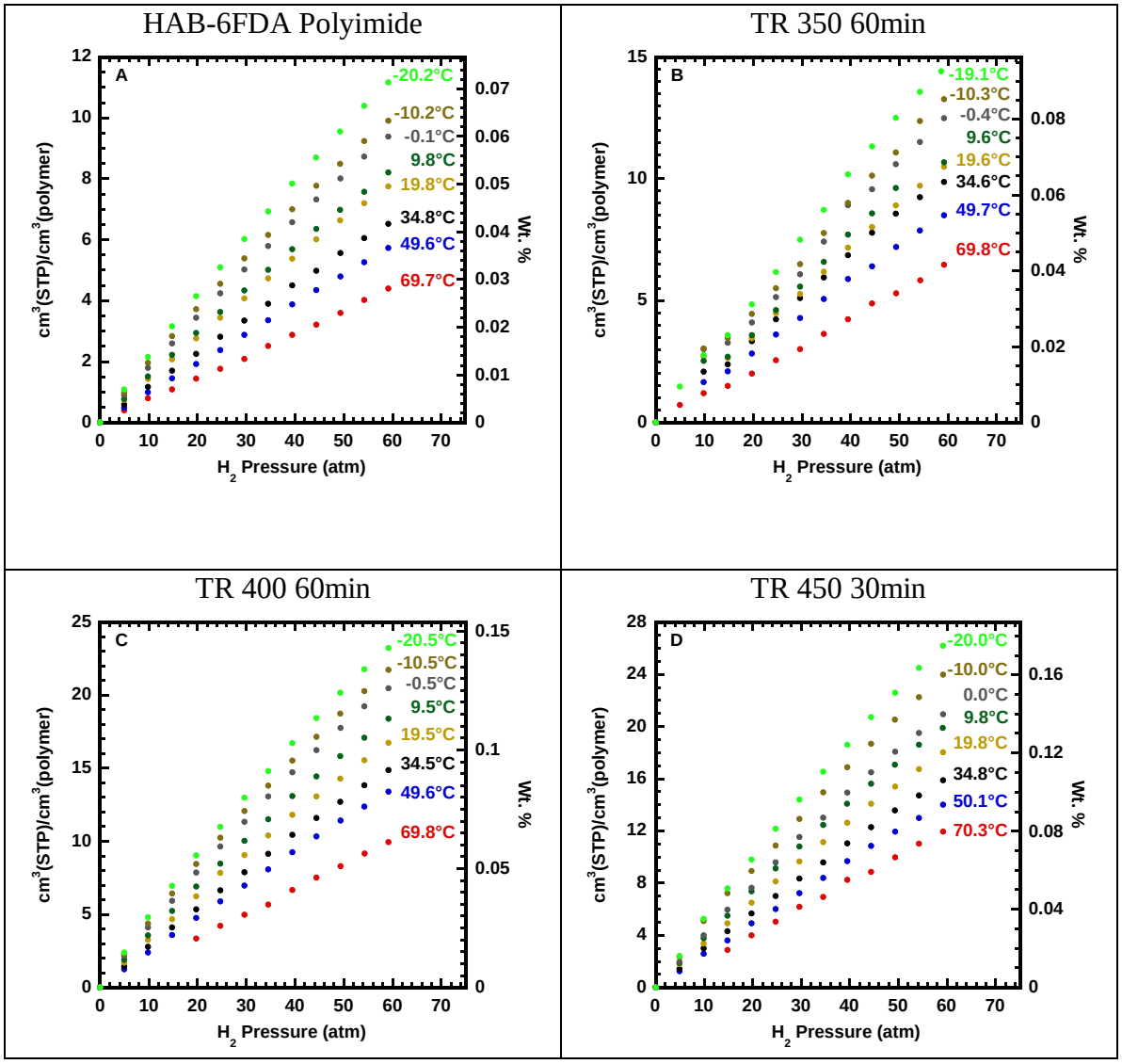

Figure 6.1: H_2 sorption isotherms for: (A) HAB-6FDA polyimide, (B) TR 350 60min, (C) TR 400 60min, and (D) TR 450 30min.

Sorption in glassy polymers is often described by the dual-mode model, which is often characterized by a signature curvature of the sorption isotherms towards the pressure axis at elevated pressure.[34-36] In the data presented in Figure 6.1, for higher temperatures and lower degrees of conversion, sorption isotherms are essentially linear,

which is typical for H_2 sorption isotherms.[16] Such linearity is typically interpreted as being in the low-pressure limit of the dual-mode model.[16] As conversion increases and as temperature decreases, the isotherms become concave towards the pressure axis, which is often taken as an indication of dual-mode sorption behavior.[34-36] An example of these changes in isotherm concavity is demonstrated in Figure 6.2. At approximately 70°C, linear isotherms are observed for the HAB-6FDA polyimide and TR 450 30min sample. However, at approximately -20°C, slight isotherm concavity is observed for the HAB-6FDA polyimide, and even stronger deviations are observed for the TR 450 30min sample.

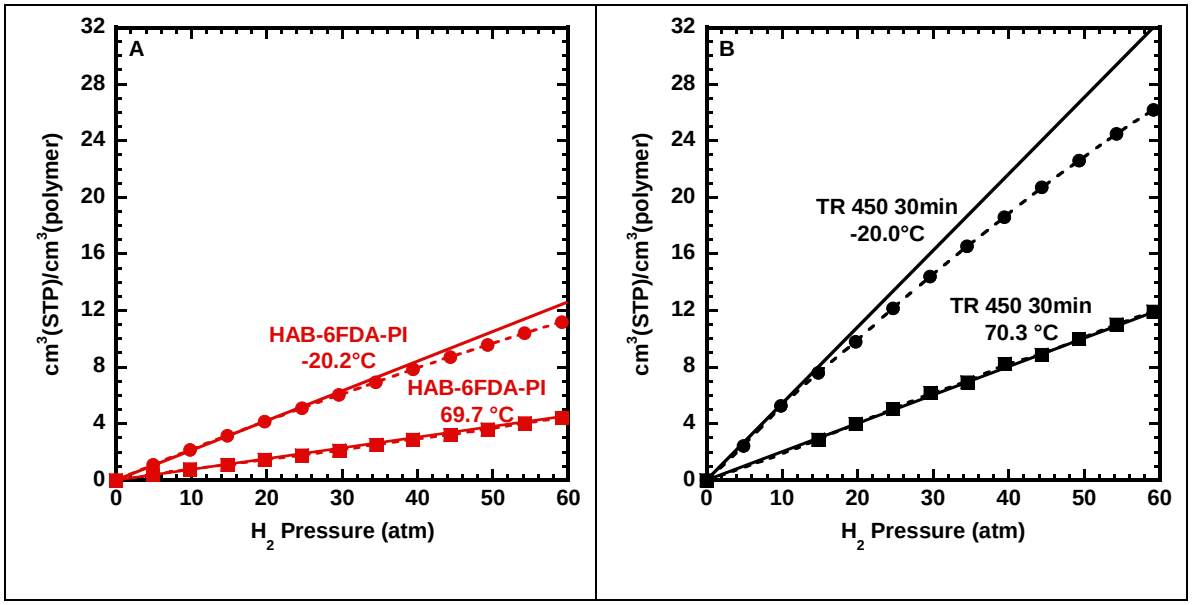

Figure 6.2: Comparison of sorption isotherm concavity between (A) HAB-6FDA polyimide and (B) TR 450 30min at temperatures of approximately 70°C and -20°C. Straight, solid lines indicate infinite dilution solubility, and curved, dashed lines are smooth fits to the data.

Within the framework of the dual-mode model, this change in isotherm curvature indicates an increased presence of non-equilibrium free volume in more highly converted TR polymers.[16] Therefore, the increase in gas sorption that accompanies thermal rearrangement, whether it be for H_2 or other gases, likely arises from increases in non-equilibrium free volume.

In the dual-mode model, the concentration of gas sorbed in a polymer, C, as a function of pressure, p, is described as the sum of two terms: an equilibrium term, which contains Henry's Law partition coefficient, k_D, and a non-equilibrium term, which contains a Langmuir capacity constant, C_H', and an affinity constant, b:[34-36]

$$C = k_D p + C_H' \frac{bp}{1+bp} \tag{6.1}$$

This equation can be written in terms of solubility, S, where $S = C/p$:

$$S = k_D + C_H' \frac{b}{1+bp} \tag{6.2}$$

Sorption in glassy polymers is often viewed as being partitioned between equilibrium and non-equilibrium sorption sites.[34-36] For the TR polymers considered in this study, Henry's Law equilibrium sorption and Langmuir non-equilibrium sorption increase with conversion for N_2, O_2, CH_4, and CO_2.[16] However, non-equilibrium Langmuir sorption increases more with conversion than increases in Henry's Law sorption. One way to analyze the contribution of non-equilibrium and equilibrium sorption in polymers is to compare the ratio of Langmuir sorption to Henry's Law sorption at infinite dilution, which is given by $C_H' b / k_D$.[37] Table 6.3 presents a

comparison of this ratio for the HAB-6FDA polyimide and partially converted TR polymers.[16] In general, conversion of the HAB-6FDA precursor polyimide to its corresponding TR polymer increases the ratio of non-equilibrium sorption for N_2, O_2, CH_4, and CO_2. Therefore, the contribution of non-equilibrium free volume, which results from the solid-state thermal rearrangement process, likely contributes substantially to the increase in total available sorption in these materials.

Sample	$C_H' b / k_D$			
	N_2	O_2	CH_4	CO_2
HAB-6FDA PI	1.4 ± 0.6	1.8 ± 0.3	2.8 ± 1.0	8.5 ± 0.8
TR 350 60min	5.0 ± 0.8	6.2 ± 0.5	8.8 ± 0.7	20 ± 3
TR 400 60min	7.2 ± 0.6	9 ± 2	13 ± 2	23 ± 3
TR 450 30min	7.1 ± 0.9	8.1 ± 0.9	12 ± 1	21 ± 2

Table 6.3: Ratio of non-equilibrium to equilibrium sorption in the HAB-6FDA series polyimide (PI) and TR polymers for N_2, O_2, CH_4, and CO_2.

As shown in Figure 6.3, sorption results for the TR 450 30min sample from this study at 34.8°C ± 0.2°C were compared to those measured in our previous study[16] at 35.0°C ± 0.05°C. The previous results were determined by a pressure decay method (PDM), which is a volumetric sorption technique.[34,38] Error bars represent one standard deviation in the data and were determined using propagation of error analysis as described by Bevington and Robinson.[39] For the MSB sorption isotherm, the increase in the size of the error bars above 35 bar arises from the use of two pressure transducers in the MSB. Below 36.5 bar, pressure is more accurately determined with the low-pressure transducer. Above 36.5 bar, the high-pressure transducer is needed to determine gas pressure, which increases the uncertainty in the buoyancy correction term described in the Materials and Experimental Methods section. However, over the range of pressures where we can use both techniques to measure H_2 sorption, they give results that are in

reasonable agreement, despite the techniques being based on fundamentally different physical principles.

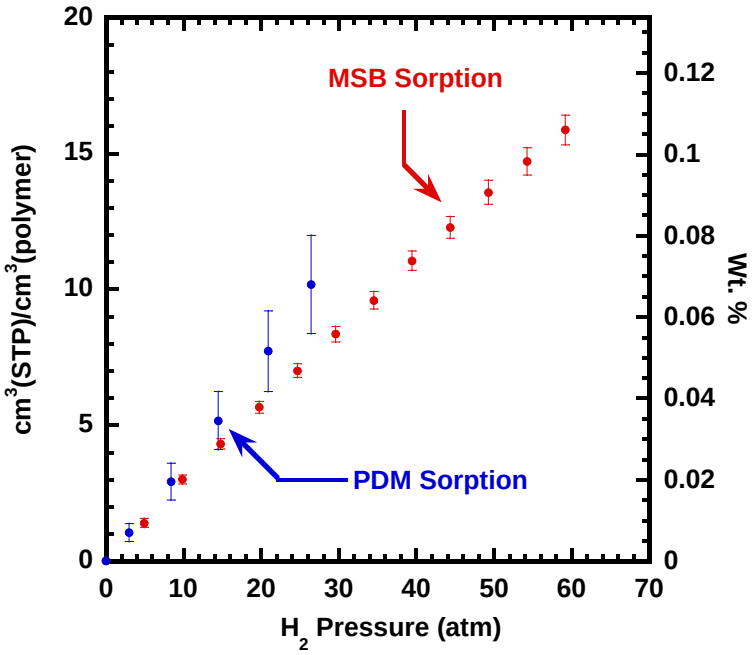

Figure 6.3: Comparison of H_2 sorption isotherms for the TR 450 30min sample as measured by the pressure decay method (PDM)[16] and by the MSB in this study. Sorption was determined at approximately 35°C. Error bars represent one standard deviation.

6.2.3 Sorption in conventional glassy and rubbery polymers

To provide a broader framework for interpreting H_2 sorption in the HAB-6FDA polyimide and corresponding TR polymers, H_2 sorption was also determined for three glassy polymers (i.e., AF 2400, Matrimid®, PSF) and one rubbery polymer (i.e., PDMS).

Matrimid® was chosen because it is widely studied in the polymer membrane literature, and it is currently used in gas separation membranes.[1] Matrimid® is a polyimide derived from 3,3'-4,4'-benzophenone tetracarboxylic dianhydride (BTDA) and diaminophenylindane (DAPI).[40] Compared to most polyimides, incorporation of DAPI

improves selectivity while still maintaining adequate permeability.[41] These improvements in transport characteristics, along with its high T_g (i.e., 305°C) and ability to be processed into hollow fibers, have made Matrimid® of interest for a number of industrial separations, including solvent separations, N_2 enrichment, CO_2 separation (e.g., natural gas sweetening and enhanced oil recovery), and H_2 purification.[1,2,41-44]

Teflon AF 2400 is a member of a class of wholly amorphous, commercially available perfluoropolymers, which includes other materials such as Teflon® AF 1600 (DuPont™), Hyflon® AD (Solvay Solexis), and Cytop™ (Asahi Glass Company).[3,45] AF 2400 is a glassy copolymer with a fractional free volume of 0.327, making it the most permeable polymer in the commercially available Teflon AF family of polymers and one of the most permeable polymers currently known.[30] The high free volume, good thermal stability (T_g = 240°C), and strong resistance to plasticization has made AF 2400 an interesting material for separations where chemical stability and plasticization resistance are important.[45] There has been discussion of its use for H_2 separation from hydrocarbons in refinery applications.[46] Interestingly, AF 2400 has very high sorption coefficients relative to most glassy and rubbery polymers, but the magnitude of these values are mainly attributed to Henry's Law solubility.[37] Conversely, TR polymers have high gas sorption, but their high levels of gas solubility are mainly attributed to high levels of non-equilibrium (i.e., Langmuir) sorption.[16] For example, the ratio of non-equilibrium to equilibrium sorption (i.e., $C_H' b / k_D$) for the TR 450 30min sample is 7.1 $\pm$ 0.9 for N_2 and 21 $\pm$ 2 for CO_2, whereas it is 3.8 for N_2 and 1.1 for CO_2 in AF 2400.[37] Therefore, it is interesting to compare a polymer with inherently high total gas sorption but low non-equilibrium sorption (i.e., AF 2400) to a polymer with high total gas sorption and high non-equilibrium sorption (i.e., TR polymers).

Polysulfone (PSF) is used commercially for H_2 separations.[1] Monsanto first developed these materials as asymmetric hollow fiber membranes in 1977[47,48] and marketed them in Prism™ Separators.[49,50] PSF has been a workhorse material for these separations, although other materials are also used in these applications.[2,51]

Finally, we consider poly(dimethylsiloxane) (PDMS) for H_2 sorption. Unlike Matrimid®, AF 2400, and PSF, PDMS is a rubbery polymer, and therefore has no non-equilibrium free volume contribution to sorption.[52,53] The absence of non-equilibrium free volume in this polymer eliminates the Langmuir capacity constant and affinity constant from Equation (6.1). PDMS is the most permeable rubbery polymer and is used commercially in vapor separations.[33,54]

Figure 6.4 presents the H_2 sorption isotherms for Matrimid®, AF 2400, PSF, and PDMS. Comparisons are made on a volumetric basis using cm^3(STP)/cm^3(polymer) and on a mass basis using weight percent. Somewhat different information can be gleaned from the data depending on which basis is used. The differences between the sorption results on a volumetric and a mass basis are due to the difference in densities of the samples. A volumetric basis is useful for comparing data in the polymer membrane literature, while a mass basis is useful for comparing to data in other fields, such as H_2 storage.[55] For clarity, error bars are not included in these plots. However, the largest contribution to uncertainty in these calculations comes from the buoyancy correction discussed in the Materials and Experimental Methods section. Uncertainties associated with the pressure transducers in the MSB and with the virial coefficients taken from Dymond *et al.*[56] account for the majority of this uncertainty. For the lowest sorbing conditions, namely PSF at 70.4°C, the uncertainty at 60 bar was ± 0.3 cm^3(STP)/cm^3(polymer). Moreover, sorption isotherms are plotted in this work as a function of pressure and not as a function of fugacity. Under the most non-ideal

conditions (i.e., -20°C and 60 bar), the fugacity of H_2 is 62.3 bar, which differs from pressure by approximately 4%.

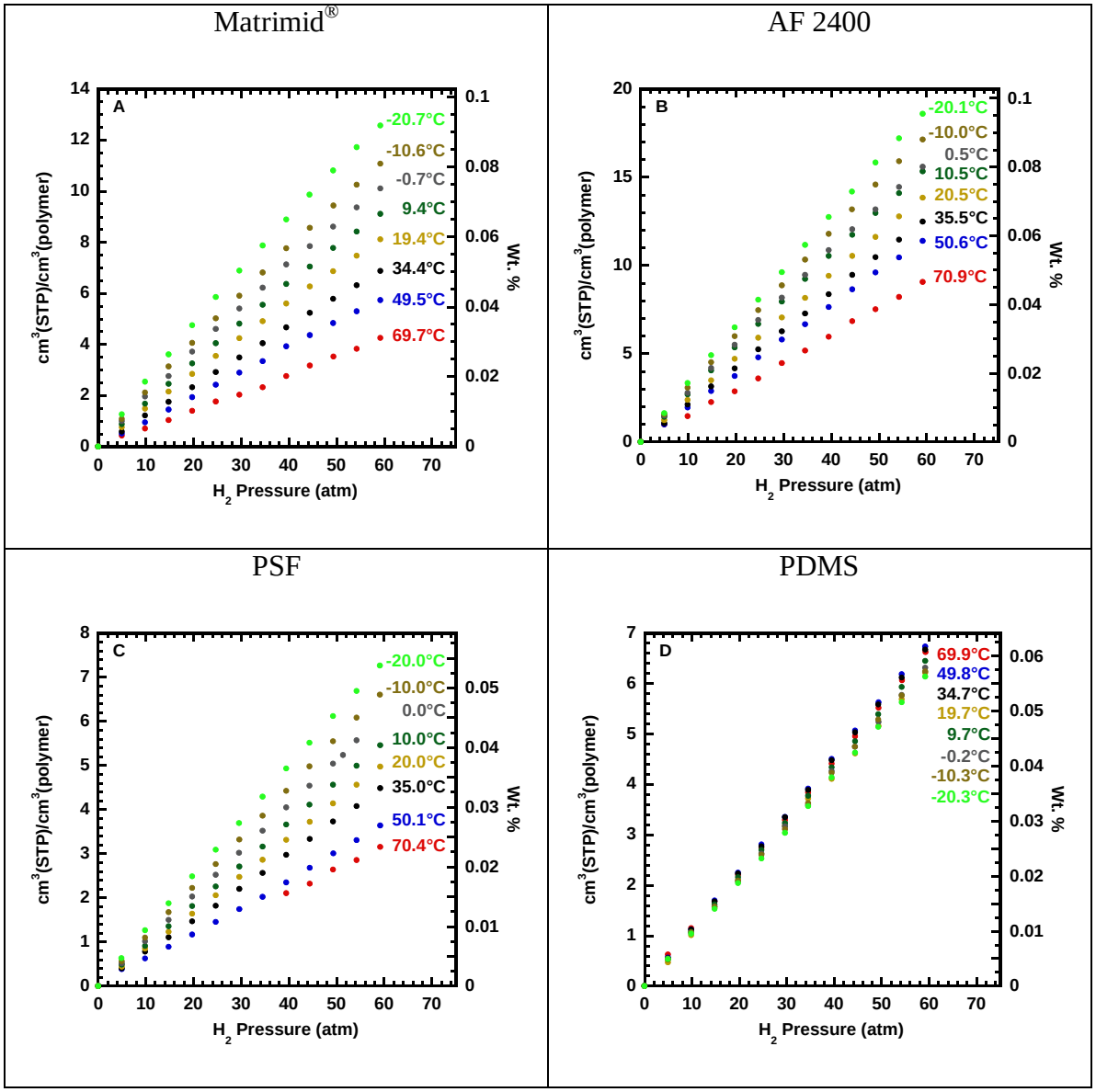

Figure 6.4: H_2 sorption isotherms for (A) Matrimid®, (B) AF 2400, (C) PSF, and (D) PDMS.

Among the polymers studied, Matrimid® had, perhaps not surprisingly, the most similar sorption characteristics to those of HAB-6FDA polyimide. At approximately 35°C, H_2 solubility was approximately 0.12 cm^3(STP)/(cm^3(polymer) atm) for the HAB-6FDA polyimide and approximately 0.11 cm^3(STP)/(cm^3(polymer) atm) for Matrimid®. Both materials are amorphous, glassy aromatic polyimides. The free volume of Matrimid® is 0.170,[57] and the free volume of HAB-6FDA polyimide is 0.150.[17] These similarities in structure, physical properties and free volume may be responsible for the similar H_2 solubilities. AF 2400, which is the highest free volume polymer included in this study (i.e., fractional free volume = 0.327)[30], had volumetric H_2 sorption levels slightly lower than that of the TR 400 60min sample. However, due to the much higher density of AF 2400 compared to the other materials in this study, on a mass basis, AF 2400 had sorption characteristics similar to that of the TR 350 60min sample. PSF had the lowest H_2 sorption of all glassy materials considered, and PDMS had the smallest change in sorption over the temperature range considered.

Interestingly, at the lowest temperatures in this study, all of the glassy polymers had H_2 sorption isotherms that were slightly concave to the pressure axis, similar to those observed in Figure 6.2 for the HAB-6FDA polyimide and TR polymer. The only sample that did not show these effects was rubbery PDMS. Figure 6.5 presents a comparison between the TR 450 30min sample and PDMS at approximately -20°C. A line is drawn next to each sorption isotherm indicating the H_2 sorption isotherm based on the infinite dilution solubility. The dual-mode curvature is readily observed for the TR 450 30min sample, and the PDMS isotherm is essentially linear. The uncertainty in these calculations is too high and the pressure range too narrow to determine the value of dual-mode parameters for the glassy polymers.

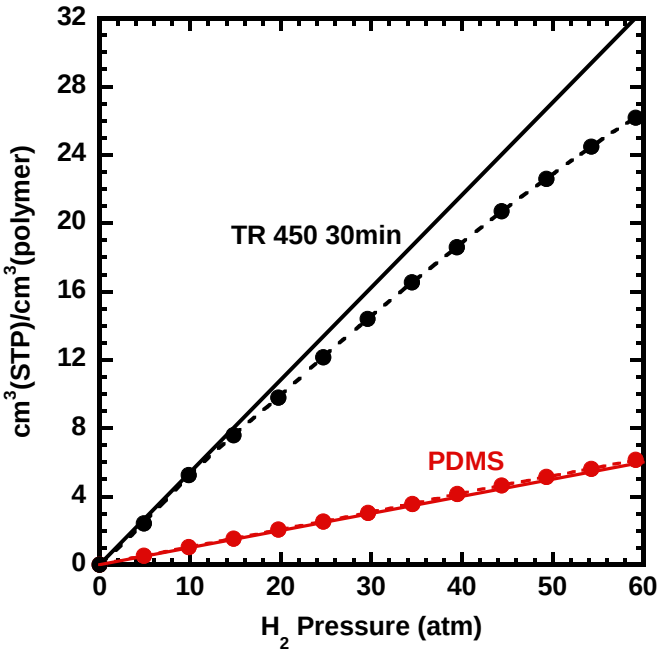

Figure 6.5: Comparison of H_2 sorption in a glassy TR 450 30min sample to that of a rubbery PDMS sample at approximately -20°C. Straight, solid lines indicating the infinite dilution solubility are drawn to demonstrate dual-mode curvature for the TR 450 30min sample and to show the linearity of the H_2 sorption isotherm for PDMS. Dashed lines are a smooth fit to the sorption data.

6.2.4 Enthalpy of Sorption

The critical temperature, T_c, of H_2 is approximately 33K,[58] so the reduced temperature range explored in this study spans 7.6 to 10.3, where the reduced temperature is defined as T/T_c. Over this range of temperatures, sorption increases by a factor of 2.8 for the HAB-6FDA polyimide and a factor of 2.4 for the TR 450 30min sample. This overall change in sorption as a function of temperature can be quantified by the enthalpy of sorption in these polymers, which is described by the Van't Hoff equation for gas dissolution:[9]

$$S = S_0 e^{-\Delta H_S / RT} \tag{6.3}$$

where S_0 is a pre-exponential factor, ΔH_s is the enthalpy of sorption, R is the ideal gas constant, and T is absolute temperature.

Average solubility coefficients were calculated from Figure 6.1 and Figure 6.4, assuming linear sorption isotherms. Therefore, any slight curvature to the isotherms, which is observed for dual-mode behavior, was not considered in this analysis. Within experimental error, this simplification had no effect on fitting data to Equation (6.3). To illustrate this point, we can consider the effect of pressure at approximately -20°C on the TR 450 30min sample, which showed the most significant dual-mode behavior. At infinite dilution, this sample had a sorption coefficient of 0.53 cm^3(STP)/(cm^3(polymer) atm), and at approximately 60 atm, the sample had a sorption coefficient of 0.44 cm^3(STP)/(cm^3(polymer) atm). Over the range of temperatures considered in this study, parameters fit from Equation (6.3) showed no significant dependence on pressure, and regardless of which pressure was used to calculate solubility coefficients, S_0 and ΔH_s were always within experimental error of each other.

A Van't Hoff sorption plot for HAB-6FDA and the corresponding TR polymers is shown in Figure 6.6. The correlation between conversion and total gas sorption is clearly evident from this plot. The most highly converted sample has the highest H_2 sorption. Additionally, the data were fit to the Van't Hoff relationship shown in Equation (6.3). From this fit, the enthalpy of sorption and pre-exponential factor in Equation (6.3) were calculated and are recorded in Table 6.4. Similar analysis for AF 2400, PDMS, Matrimid®, and PSF are shown in

Figure 6.7, and calculated parameters are recorded in Table 6.4. Error bars have been excluded from Figure 6.6 and

Figure 6.7 for clarity. However, the standard error for the parameters fitted from Equation (6.3) is included in Table 6.4.

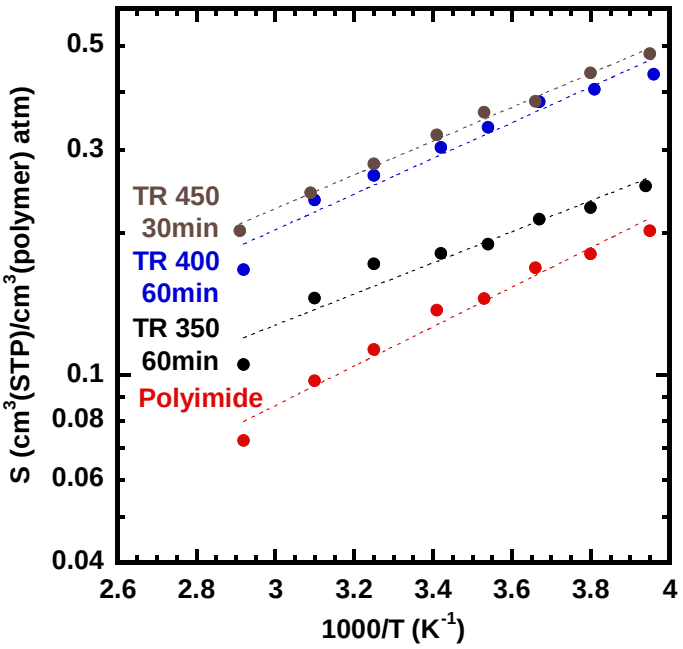

Figure 6.6: Van't Hoff plot for H_2 sorption in the HAB-6FDA polyimide and partially converted TR polymers.

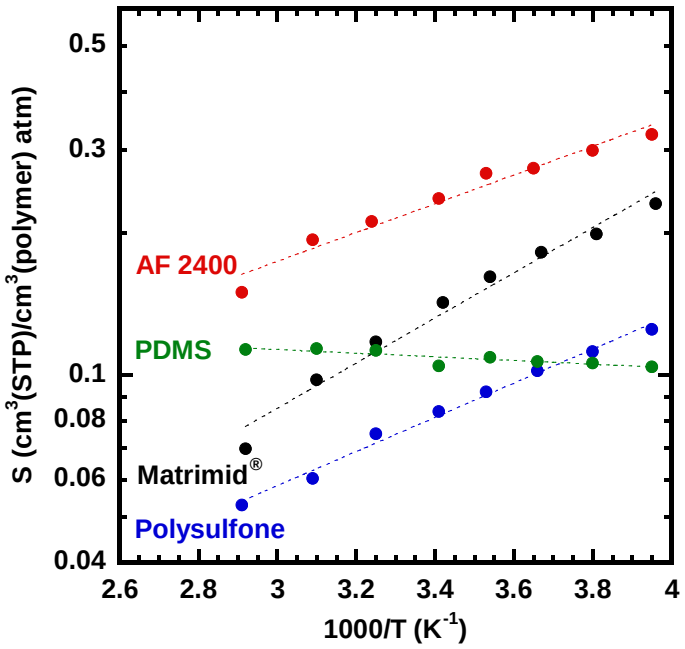

Figure 6.7: Van't Hoff plot for H_2 sorption in AF 2400, PDMS, Matrimid®, and PSF.

The pre-exponential factor in Equation (6.3) is related to the change in entropy that occurs during gas dissolution into a polymer.[37,59] Gas sorption in a polymer can be viewed in terms of Gibbs free energy as follows:[59]

$$S = e^{-\frac{\Delta G_S}{RT}} \tag{6.4}$$

where S is solubility and ΔG_S is the Gibbs free energy. The term ΔG_S can be written in terms of enthalpy and entropy of dissolution, which are defined as ΔH_S and ΔS_S, respectively:

$$S = e^{-\frac{\Delta H_S - T\Delta S_S}{RT}} \tag{6.5}$$

$$S = e^{\frac{\Delta S_S}{R}} e^{-\frac{\Delta H_S}{RT}} \quad (6.6)$$

The first exponential term in Equation (6.6), $e^{\frac{\Delta S_S}{R}}$, is S_0 in Equation (6.3). In general, S_0 increases with increasing thermal rearrangement, and it is particularly high for the most highly converted TR polymers, AF 2400 and rubbery PDMS. The polymers with the lowest values of S_0 are the HAB-6FDA polyimide, Matrimid®, and PSF.

The enthalpy of sorption is the difference in enthalpy between the sorbed state and the gaseous state. Therefore, a large negative value of ΔH_s can be interpreted as a strong interaction between H_2 and the polymer matrix. Conversely, a small negative value of ΔH_s can be interpreted as a weak interaction between H_2 and the polymer matrix. It is also possible to have positive values of ΔH_s. From a molecular perspective, an endothermic/exothermic tradeoff exists for gas dissolution into a polymer.[60] First, an endothermic event must occur, whereby a molecular-sized gap is created in the polymer matrix. Hydrogen enters this gap and then forms favorable (i.e., exothermic) binding interactions with the polymer. The difference in enthalpy between these events contributes to the magnitude and endothermic/exothermic nature of ΔH_s. For rubbery polymers and liquids, the creation of molecular-sized gaps for penetrant dissolution can sometimes dominate sorption, especially for small molecules such as He, H_2 and Ne.[7,8,60-63] Under these conditions, the weak exothermic polymer/liquid-penetrant interactions are dominated by the endothermic dissolution of molecules into the polymer/liquid matrix, thereby creating positive values of ΔH_s. For glassy polymers, which can have large non-equilibrium contributions to their total free volume, the energy required to form

molecular-sized gaps in the polymer for penetrant dissolution is reduced, thereby reducing ΔH_s, often resulting in negative values of ΔH_s.[60,61]

Table 6.4 lists the enthalpies of sorption for samples considered in this study. The propagation of errors method was used to determine uncertainties in the sorption data in Figure 6.6 and

Figure 6.7, and the standard error for data fitted from these plots is shown in Table 6.4.[39] The standard error of these measurements is rather large compared to the enthalpy of sorption values, making it difficult to identify, with certainty, trends in the data. Nevertheless, some general comparisons can be made. Among these samples, Matrimid® had the most negative ΔH_s and PDMS had the only positive ΔH_s. Within experimental uncertainty, there was no trend observed for changes in ΔH_s with thermal rearrangement. Because non-equilibrium free volume increases during thermal rearrangement,[16] the endothermic cost for dissolution should decrease with conversion. However, intermolecular crosslinking reactions, which may occur in these materials,[16] can restrict gas dissolution,[7] potentially increasing the endothermic component of ΔH_s. Furthermore, H_2 sorption increases with rearrangement, which is an indication of stronger binding interaction between H_2 and the TR polymer. A dual-mode interpretation of sorption further helps to explain these binding interactions. For non-polar gases other than H_2, such as N_2, O_2, and CH_4, the dual-mode affinity constant, b, increases with increasing extent of thermal rearrangement.[16] Because b is an indicator of polymer-penetrant binding interactions, the process of H_2 sorption may become more exothermic during rearrangement. These three effects (i.e., increasing non-equilibrium free volume, crosslinking effects, and increasing binding interactions) likely counteract each other, therefore decreasing the endothermic energy barrier to gas dissolution and increasing the exothermic penetrant-polymer interactions, resulting in relatively unchanged enthalpies

of sorption. Among the glassy polymers studied, AF 2400 had the least negative ΔH_s. AF 2400 is a perfluoropolymer, and deviations in the gas sorption properties of perfluoropolymers, relative to those of hydrocarbon-based polymers, are well known.[45]

PDMS had the only positive ΔH_s of all materials considered. However, the value of ΔH_s was only slightly greater than zero. A visual consequence of this result is that sorption increases very slightly with increasing temperature, as shown in Figure 6.4D. Being a rubbery polymer, there is an expected enthalpy barrier to forming molecular sized gaps in the polymer matrix to permit sorption of molecules. The contribution of this positive enthalpy term to H_2 sorption accounts for PDMS having a slightly positive ΔH_s. Interestingly, it has previously been reported that PDMS has an ΔH_s value of +4.4 kJ/mole for H_2.[7] However, this value was determined for PDMS with 0.0554 volume fraction Santocel CS filler. Furthermore, in the same study, it was shown that PDMS with 0.182 volume fraction Aerosil K3 silica filler has an ΔH_s of +10.3 kJ/mole. The study concluded that fillers could act as crosslinking agents, tightening the polymer chain network. Crosslinking-type effects would increase the endothermic barrier to penetrant dissolution, thereby increasing ΔH_s. Furthermore, the fillers may act as adsorption sites that increase the level of sorption and, thus, introduce another temperature dependence. Additionally, no crosslinking density is listed in this study,[7] whereas the crosslinking density for our samples is approximately 7.8×10^{-5} mol/cm^3.[31] Moreover, our study focused on sorption measurements for a filler-free PDMS sample, therefore eliminating any extraneous effects from fillers.

The density of PDMS changes by approximately 8% between -20°C and 70°C.[54] This change in density measurably influences the calculated sorption isotherms, especially for the highest and lowest temperatures considered. To illustrate the influence of the temperature dependence of density on PDMS sorption isotherms, Figure 6.8A

shows PDMS sorption isotherms calculated assuming that the density of PDMS is 0.98 g/cm^3 (i.e., its value at ambient temperature) at all temperatures. Conversely, Figure 6.8B accounts for changes in PDMS density with temperature. At 70°C, the density of PDMS is approximately 0.94 g/cm^3, and at -20°C, the density of PDMS is approximately 1.02 g/cm^3.[54] For PDMS, when the temperature dependence of the polymer density is ignored, the enthalpy of sorption appears to be exothermic; however, when this effect is included in these calculations, the enthalpy of sorption is slightly endothermic. Notably, the relative order of sorption isotherms switch when this assumption is taken into account, and sorption increases slightly with increasing temperature.

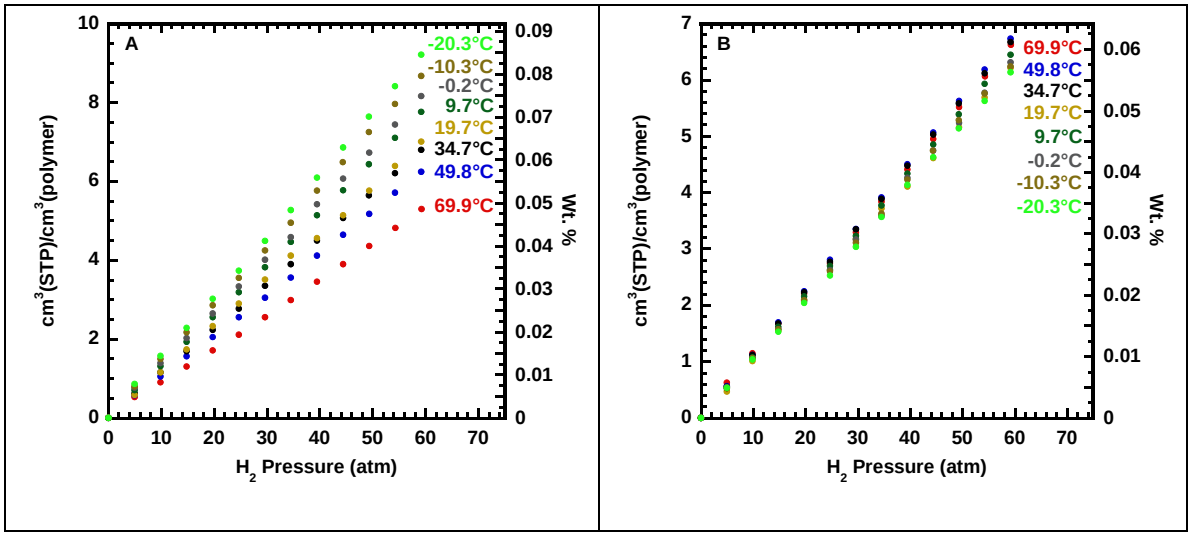

Figure 6.8: Comparison of PDMS isotherms when the density is (A) held constant at 0.98 g/cm^3 or (B) allowed to vary according to temperature as reported by Raharjo et al.[54]

Sample	ΔH_S (kJ/mol)	S_0 (cm^3 (STP)/cm^3 atm)
Polyimide	-7.3 ± 0.5	0.006 ± 0.001
TR 350 60min	-5.8 ± 0.6	0.016 ± 0.004
TR 400 60min	-6.6 ± 0.8	0.020 ± 0.003
TR 450 30min	-6.7 ± 0.2	0.021 ± 0.002
AF 2400	-5.4 ± 0.3	0.025 ± 0.003
Matrimid®	-8.4 ± 0.5	0.004 ± 0.001
PSF	-6.7 ± 0.2	0.005 ± 0.001
PDMS	0.7 ± 0.1	0.015 ± 0.005

Table 6.4: Comparison of ΔH_S and S_0 calculated from the Van't Hoff plots for H_2 sorption shown in Figure 6.6 and Figure 6.7. Uncertainties represent one standard deviation.

6.2.5 Comparison of H_2 sorption with sorption of other gases in TR polymers

The solubilities of N_2, O_2, CH_4, and CO_2 increase with increasing extent of rearrangement for HAB-6FDA.[16] Interestingly, CO_2 sorption relative to that of the polyimide increases less than that of other gases, presumably due to the loss of CO_2-philic acetate and carbonyl functionality during the thermal rearrangement process.[16] The ratio of H_2 sorption in the HAB-6FDA TR polymers to that of the HAB-6FDA polyimide was determined at 10 atm, and the results are shown in Figure 6.9. The relative change in H_2 sorption is nearly identical to that of N_2, CH_4, and O_2, but higher than that of CO_2. Unlike CO_2, which is a quadrupolar gas and, therefore, interacts favorably with polar functional groups, H_2 is a non-polar gas.[64] Therefore, H_2 should follow changes in solubility similar to that of other non-polar gases, which is indeed the case.

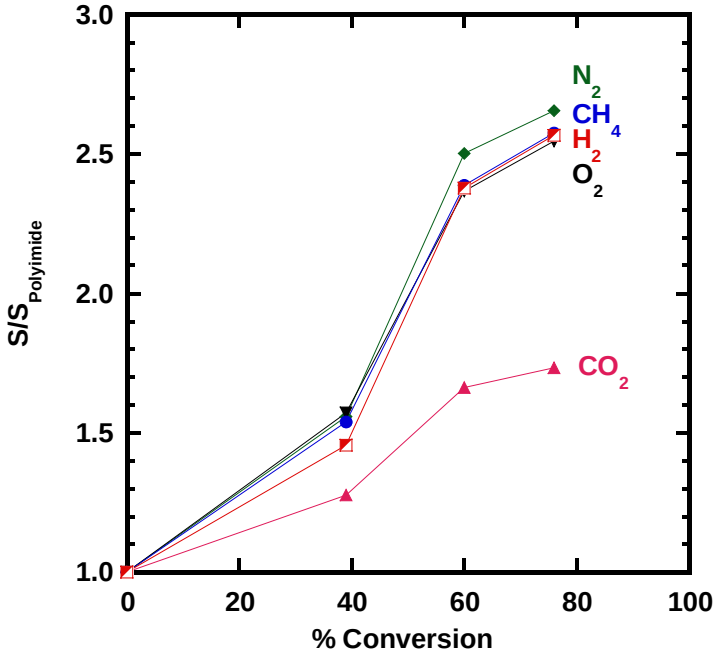

Figure 6.9: H_2, N_2, O_2, CH_4, and CO_2 gas solubility for HAB-6FDA TR polymers relative to that in HAB-6FDA polyimide. These data were determined from sorption isotherms at pressures of 10 atm and temperatures of approximately 35°C.

6.3 CONCLUSIONS

Hydrogen sorption was measured in a polyimide and a series of TR polymers derived from HAB-6FDA, as well as in several conventional polymers, including AF 2400, Matrimid®, PSF, and PDMS. Sorption was measured for temperatures between approximately -20°C and 70°C and for pressures up to 60 bara using a Rubotherm Magnetic Suspension Balance. Sorption increased as a function of thermal rearrangement. The most highly converted TR polymer had sorption levels approximately 2.6 times higher than that of its corresponding polyimide. Furthermore, the most highly converted TR polymer had the highest H_2 sorption among all of the samples tested. Comparisons between volumetric and gravimetric measurements confirmed the accuracy of these experiments. Additionally, gravimetric measurements

showed dual-mode behavior for H_2 sorption in glassy polymers at low temperatures. In comparison with other gases, H_2 sorption increased similarly to that of other non-polar gases such as N_2, O_2, and CH_4 during thermal rearrangement. Conversely, H_2 sorption did not track with changes in sorption observed for CO_2. Additionally, enthalpies of sorption were determined for all of the samples tested in this study. Enthalpy of sorption did not change significantly with thermal rearrangement. PDMS, the only rubbery polymer tested in this study, had a slightly positive enthalpy of sorption. Sorption in rubbery polymers is often more endothermic than sorption in glassy polymers, and our results confirm this result.

6.4 REFERENCES

1. Baker, R.W., *Membrane technology and applications*. **2004**, Chichester, John Wiley & Sons, Ltd.

2. Baker, R.W., *Future directions of membrane gas separation technology*. Industrial & Engineering Chemistry Research, **2002**. 41(6), 1393-1411.

3. Bernardo, P., E. Drioli, and G. Golemme, *Membrane gas separation: A review/state of the art*. Industrial & Engineering Chemistry Research, **2009**. 48, 4638-4663.

4. Lonsdale, H.K., *The growth of membrane technology*. Journal of Membrane Science, **1982**. 10(2-3), 81-181.

5. *Advanced Prism® membrane systems for cost effective gas separations*. Available from: http://www.airproducts.com/products/Gases/supply-options/~/media/Downloads/Brochure/advanced-prism-membrane-system-brochure.ashx.

6. Hosseini, S.S., M.M. Teoh, and T.S. Chung, *Hydrogen separation and purification in membranes of miscible polymer blends with interpenetration networks.* Polymer, **2008**. 49(6), 1594-1603.

7. Barrer, R. and H. Chio, *Solution and diffusion of gases and vapors in silicone rubber membranes.* Journal of Polymer Science: Part C, **1965**. 138(10), 111-138.

8. Michaels, A.S. and H.J. Bixler, *Solubility of gases in polyethylene.* Journal of Polymer Science, **1961**. 50(154), 393-412.

9. Matteucci, S.T., Y.P. Yampolskii, B.D. Freeman, and I. Pinnau, *Transport of gases and vapors in glassy and rubbery polymers*, in *Materials science of membranes for gas and vapor separation*, Y. Yampolskii, I. Pinnau, and B.D. Freeman, Editors. **2006**, John Wiley & Sons: Chichester. 1-47.

10. Paul, D.R. and Y.P. Yampolskii, *Polymeric gas separation membranes*. **1994**, Boca Raton, CRC Press.

11. Drioli, E. and L. Giorno, *Membrane operations: Innovative separations and transformations*. **2009**, Weinheim, Wiley-VCH.

12. Wijmans, J.G. and R.W. Baker, *The solution-diffusion model: A review.* Journal of Membrane Science, **1995**. 107(1-2), 1-21.

13. McKeown, N.B., B. Gahnem, K.J. Msayib, P.M. Budd, C.E. Tattershall, K. Mahmood, S. Tan, D. Book, H.W. Langmi, and A. Walton, *Towards polymer-based hydrogen storage materials: engineering ultramicroporous cavities within polymers of intrinsic microporosity.* Angewandte Chemie, **2006**. 45(11), 1804-1807.

14. Park, H.B., C.H. Jung, Y.M. Lee, A.J. Hill, S.J. Pas, S.T. Mudie, E. Van Wagner, B.D. Freeman, and D.J. Cookson, *Polymers with cavities tuned for fast selective transport of small molecules and ions.* Science, **2007**. 318(5848), 254-258.

15. Han, S.H., J.E. Lee, K.-J. Lee, H.B. Park, and Y.M. Lee, *Highly gas permeable and microporous polybenzimidazole membrane by thermal rearrangement.* Journal of Membrane Science, **2010**. 357(1-2), 143-151.

16. Smith, Z.P., D.F. Sanders, C.P. Ribeiro Jr, R. Guo, B.D. Freeman, D.R. Paul, J.E. McGrath, and S. Swinnea, *Gas sorption and characterization of thermally rearranged polyimides based on 3,3'-dihydroxy-4,4'-diamino-biphenyl (HAB) and 2,2'-bis-(3,4-dicarboxyphenyl) hexafluoropropane dianhydride (6FDA).* Journal of Membrane Science, **2012**. 416, 558-567.

17. Sanders, D.F., Z.P. Smith, C.P. Ribeiro, R. Guo, J.E. McGrath, D.R. Paul, and B.D. Freeman, *Permeability, diffusivity, and free volume of thermally rearranged polymers based on 3,3'-dihydroxy-4,4'-diamino-biphenyl (HAB) and 2,2'-bis-(3,4-dicarboxyphenyl) hexafluoropropane dianhydride (6FDA).* Journal of Membrane Science, **2011**. 409-410, 232-241.

18. Tullos, G. and L. Mathias, *Unexpected thermal conversion of hydroxy-containing polyimides to polybenzoxazoles.* Polymer, **1999**. 40(12), 3463-3468.

19. Tullos, G.L., J.M. Powers, S.J. Jeskey, and L.J. Mathias, *Thermal conversion of hydroxy-containing imides to benzoxazoles: Polymer and model compound study.* Macromolecules, **1999**. 32(11), 3598-3612.

20. Robeson, L.M., *Correlation of separation factor versus permeability for polymeric membranes.* Journal of Membrane Science, **1991**. 62(2), 165-185.

21. Robeson, L.M., *The upper bound revisited.* Journal of Membrane Science, **2008**. 320(1-2), 390-400.

22. Park, H.B., S.H. Han, C.H. Jung, Y.M. Lee, and A.J. Hill, *Thermally rearranged (TR) polymer membranes for CO_2 separation.* Journal of Membrane Science, **2010**. 359(1-2), 11-24.

23. Jiang, Y., F.T. Willmore, D. Sanders, Z.P. Smith, C.P. Ribeiro, C.M. Doherty, A. Thornton, A.J. Hill, B.D. Freeman, and I.C. Sanchez, *Cavity size, sorption and*

transport characteristics of thermally rearranged (TR) polymers. Polymer, **2011**. 52(10), 2244-2254.

24. Han, S.H., N. Misdan, S. Kim, C.M. Doherty, A.J. Hill, and Y.M. Lee, *Thermally rearranged (TR) polybenzoxazole: Effects of diverse imidization routes on physical properties and gas transport behaviors.* Macromolecules, **2010**. 43(18), 7657-7667.

25. Guo, R., D.F. Sanders, Z.P. Smith, B.D. Freeman, D.R. Paul, and J.E. McGrath, *Synthesis and characterization of thermally rearranged (TR) polymers: Influence of ortho-positioned functional groups of polyimide precursors on TR process and gas transport properties.* Journal of Materials Chemistry A, **2013**. 1(2), 262-272.

26. Han, S., H. Kwon, K. Kim, J. Seong, C. Park, S. Kim, C.M. Doherty, A. Thornton, A.J. Hill, A. Lozano, K. Berchtold, and Y. Lee, *Tuning microcavities in thermally rearranged polymer membranes for CO_2 capture.* Physical Chemistry Chemical Physics, **2012**. 14(13), 4365-4373.

27. Lee, J.S., W. Madden, and W.J. Koros, *Antiplasticization and plasticization of Matrimid® asymmetric hollow fiber membranes - Part A. Experimental.* Journal of Membrane Science, **2010**. 350(1-2), 232-241.

28. Zhang, Y., I.H. Musselman, J.P. Ferraris, and K.J. Balkus, *Gas permeability properties of Matrimid® membranes containing the metal-organic framework Cu–BPY–HFS.* Journal of Membrane Science, **2008**. 313(1-2), 170-181.

29. McHattie, J.S., W.J. Koros, and D.R. Paul, *Gas transport properties of polysulphones: 1. Role of symmetry of methyl group placement on bisphenol rings.* Polymer, **1991**. 32(5), 840-850.

30. Pinnau, I. and L.G. Toy, *Gas and vapor transport properties of amorphous perfluorinated copolymer membranes based on 2, 2-bistrifluoromethyl-4, 5-difluoro-1,3-dioxole/tetrafluoroethylene.* Journal of Membrane Science, **1996**. 109, 125-133.

31. Singh, A., B.D. Freeman, and I. Pinnau, *Pure and mixed gas acetone/nitrogen permeation properties of polydimethylsiloxane [PDMS]*. Journal of Polymer Science Part B: Polymer Physics, **1998**. 36, 289-301.

32. Rowe, B.W., B.D. Freeman, and D.R. Paul, *Physical aging of ultrathin glassy polymer films tracked by gas permeability.* Polymer, **2009**. 50(23), 5565-5575.

33. Merkel, T.C., V.I. Bondar, K. Nagai, B.D. Freeman, and I. Pinnau, *Gas sorption, diffusion, and permeation in poly(dimethylsiloxane).* Journal of Polymer Science Part B: Polymer Physics, **2000**. 38(3), 415-434.

34. Koros, W.J., D.R. Paul, and A.A. Rocha, *Carbon dioxide sorption and transport in polycarbonate.* Journal of Polymer Science: Polymer Physics Edition, **1976**. 14(4), 687-702.

35. Paul, D.R. and W.J. Koros, *Effect of partially immobilizing sorption on permeability and the diffusion time lag.* Journal of Polymer Science: Polymer Physics Edition, **1976**. 14(4), 675-685.

36. Koros, W.J. and D.R. Paul, *Sorption and transport of CO_2 above and below the glass transition of poly (ethylene terephthalate).* Polymer Engineering and Science, **1980**. 20(1), 14-19.

37. Bondar, V., B. Freeman, and Y. Yampolskii, *Sorption of gases and vapors in an amorphous glassy perfluorodioxole copolymer.* Macromolecules, **1999**. 32, 6163-6171.

38. Lin, H. and B.D. Freeman, *Springer handbook: Permeation and diffusion*, H. Czichos, T. Saito, and L. Smith, Editors. **2006**, Springer: New York. 371-387.

39. Bevington, P.R. and K.D. Robinson, *Data reduction and error analysis for the physical sciences: Third edition*. **2003**, Boston, McGraw Hill.

40. Huang, Y. and D.R. Paul, *Physical aging of thin glassy polymer films monitored by gas permeability.* Polymer, **2004**. 45(25), 8377-8393.

41. Ekiner, O.M. and R.A. Hayes. *Phenylindane-containing polyimide gas separation membranes*, **1991**, US 5015270.

42. LePree, J., *Membranes for gas separation.* Chemical Engineering Magazine, **2012**. 119(2), 17 - 20.

43. White, L.S., I.-f. Wang, and B.S. Minhas. *Polyimide membranes for separation of solvents from lube oil*, **1993**, US 5264166.

44. Ekiner, O.M., R.A. Hayes, and P. Manos. *Novel multicomponent fluid separation membranes*, **1992**, US Pat. 5085676.

45. Merkel, T.C., I. Pinnau, R. Prabhakar, and B.D. Freeman, *Gas and vapor transport properties of perfluoropolymers*, in *Materials science of membranes for gas and vapor separations*, Y. Yampolskii, P., I. Pinnau, and B.D. Freeman, Editors. **2006**, John Wiley & Sons, Ltd: Chichester. 251 - 270.

46. Baker, R.W., I. Pinnau, Z. He, K.D. Amo, A.R. Da Costa, and R. Daniels. *Hydrogen gas separation using organic-vapor-resistant membranes*, **2003**, US 6544316 B2.

47. Henis, J.M.S. and M.K. Tripodi, *Composite hollow fiber membranes for gas separation: the resistance model approach.* Journal of Membrane Science, **1981**. 8, 233-246.

48. Henis, J.M.S. and M.K. Tripodi. *Multicomponent membranes for gas separations*, **1980**, US 4230463.

49. Henis, J.M.S. and M.K. Tripodi, *A novel approach to gas separations using composite hollow fiber membranes.* Separation Science and Technology, **1980**. 15(4), 1059-1068.

50. *Recovery..., hydrogen... made simple*. Chemical & Engineering News, **1979**. 57(48), 26-27.

51. Aitken, C.L., W.J. Koros, and D.R. Paul, *Effect of structural symmetry on gas transport properties of polysulfones.* Macromolecules, **1992**. 25(13), 3424-3434.

52. Koros, W.J. and D.R. Paul, *CO_2 sorption in poly (ethylene terephthalate) above and below the glass transition.* Journal of Polymer Science: Polymer Physics Edition, **1978**. 16(11), 1947-1963.

53. Paul, D.R., *Sorption and transport in glassy polymers.* Berichte der Bunsengesellschaft für Physikalische, **1979**. 83(1), 294-302.

54. Raharjo, R., B. Freeman, and E. Sanders, *Pure and mixed gas CH_4 and n-C_4H_{10} sorption and dilation in poly(dimethylsiloxane).* Journal of Membrane Science, **2007**. 292(1-2), 45-61.

55. Broom, D.P., *Hydrogen storage materials*. **2011**, London, Springer.

56. Dymond, J.H., K.N. Marsh, R.C. Wilhoit, and K.C. Wong, eds. *The virial coefficients of pure gases and mixtures*. ed. M. Frenkel and K.N. Marsh. Vol. Group IV: Physical chemistry vol 21 subvolumes A and B. **2001**, Landolt-Bornstein: Berlin.

57. Huang, Y., X. Wang, and D. Paul, *Physical aging of thin glassy polymer films: Free volume interpretation.* Journal of Membrane Science, **2006**. 277(1-2), 219-229.

58. Smith, J.M., H.C. Van Ness, and M.M. Abbott, *Introduction to chemical engineering thermodynamics*. **2005**, Boston, McGraw-Hill.

59. Barrer, R., J. Barrie, and N. Raman, *Solution and diffusion in silicone rubber I—A comparison with natural rubber.* Polymer, **1962**. 3(3), 595-603.

60. van der Vegt, N., *A molecular dynamics simulation study of solvation thermodynamical quantities of gases in polymeric solvents.* Journal of Membrane Science, **2002**. 205(1-2), 125-139.

61. Merkel, T., V. Bondar, K. Nagai, B. Freeman, and Y. Yampolskii, *Gas sorption, diffusion, and permeation in poly (2,2-bis (trifluoromethyl)-4,5-difluoro-1,3-dioxole-co-tetrafluoroethylene).* Macromolecules, **1999**. 32, 8427-8440.

62. Ghosal, K. and B.D. Freeman, *Gas separation using polymer membranes: An overview.* Polymers for Advanced Technologies, **1994**. 5(11), 673-697.

63. Fogg, P.G.T. and W. Gerrard, *Solubility of Gases in Liquids*. **1991**, Chichester, John Wiley & Sons.

64. Lin, H. and B. Freeman, *Materials selection guidelines for membranes that remove CO_2 from gas mixtures.* Journal of Molecular Structure, **2005**. 739(1-3), 57-74.

Chapter 7: The Influence of Diffusivity and Sorption on Helium and Hydrogen Separations in Hydrocarbon, Silicon, and Fluorocarbon-Based Polymers

This chapter describes results of a study to determine the permeability, sorption, and diffusion coefficients for helium and hydrogen in a series of polymers. Several highly fluorinated and perfluorinated polymers were chosen to investigate the unusual upper bound behavior of perfluoropolymers for helium/hydrogen separations.

The permeability-selectivity upper bounds show that perfluoropolymers have uniquely different separation characteristics than hydrocarbon-based polymers. For separating helium from hydrogen, these differences are particularly dramatic. At a given helium permeability, the upper bound defined by perfluoropolymers has helium/hydrogen selectivities that are 2.5 times higher than that of the upper bound defined by hydrocarbon-based polymers. Robeson hypothesized that these differences in transport properties resulted from the unusual sorption relationships of gases in perfluoropolymers compared to hydrocarbon-based polymers, and this chapter seeks to test this hypothesis experimentally. To do so, the gas permeability, sorption, and diffusion coefficients were determined at 35°C for hydrogen and helium in a series of hydrocarbon-, silicon-, and fluorocarbon-based polymers. Highly or completely fluorinated polymers have separation characteristics above the upper-bound for helium/hydrogen separation because they maintain good diffusivity selectivities for helium over hydrogen and they have helium/hydrogen sorption selectivities much closer to unity than those of hydrocarbon-based samples. The silicon-based polymer had intermediate sorption selectivities between those of hydrocarbon-based polymers and perfluoropolymers. Comparisons of hydrogen and helium sorption data in the literature more broadly extend the conclusion

that helium/hydrogen sorption selectivity is rather different in hydrocarbon and fluorocarbon-based materials.

7.1 INTRODUCTION

In 1991, when Robeson first reported the He/H_2 upper bound, only one polymer surpassed the upper bound.[1] This polymer, Nafion® N117, which was originally reported by Chiou and Paul,[2] had a He/H_2 permselectivity that was more than double the value expected based on the He/H_2 upper bound for other polymers having similar helium permeability. Over the next 17 years, additional research on hydrogen and helium permeability revealed additional polymers that surpassed the 1991 upper bound.[3-10] A common feature of these polymers was their perfluorinated chemical structure. These results led Robeson to redefine the He/H_2 upper bound to include perfluoropolymers in 2008.[11] In addition to He/H_2, perfluoropolymers also helped re-define, at least in part, the upper bound for H_2/CH_4, He/CH_4, He/N_2, and He/CO_2. In regards to He/H_2, Robeson speculated that the reason for these unusual upper bound properties likely related to perfluoropolymers having "a unique He/H_2 solubility relationship relative to hydrocarbon polymers",[11] and an experimental test of this hypothesis is a key component of this work. In addition to the polymers reported by Robeson in 2008,[11] Belov *et al.* have reported additional perfluoropolymers whose permeability/selectivity combinations lie above the 1991 upper bound.[12]

According to Hildebrand's regular solution theory, the interactions between two species can be described by the differences in their solubility parameters when only dispersive interactions are involved.[13] Materials with similar solubility parameters tend

---

This chapter has been adapted from: Smith, Z.P., R.R. Tiwari, M.E. Dose, K.L. Gleason, T.M. Murphy, D.F. Sanders, G. Gunawan, L.M. Robeson, D.R. Paul, and B.D. Freeman, *The influence of diffusivity and sorption on helium and hydrogen separations in hydrocarbon, silicon, and fluorocarbon-based polymers (Submitted).*

to be miscible. However, as differences in solubility parameters increase, the interactions become more unfavorable, and eventually, at very large differences, the molecules phase separate. For this reasons, it is remarkable that many fluorocarbon liquids and their hydrocarbon analogs, such as *n*-C_7H_{16} and *n*-C_7F_{16}, which have solubility parameters suggesting miscibility, are almost exclusively immiscible with one another.[4,14,15] Scott has reported that these deviations from ideality result from a failure of the geometric mean assumption in regular solution theory,[15] and this observation has prompted significant research to determine the molecular basis for this theoretical anomaly.[4,16-24] Despite efforts by many researchers investigating this anomalous behavior for over 60 years, Song, Rossky, and Maroncelli concluded in their 2003 modeling work on all-atom potentials that "the origins of the weaker-than-expected interactions between perfluoroalkanes and alkanes remain a mystery".[25] Our present work extends the current study of this phenomenon to helium and hydrogen sorption in perfluoropolymers.

Table 7.1 presents the critical temperatures and gas diameters of helium and hydrogen. In polymers, gas sorption often scales with critical temperature[26-28] while gas diffusion scales inversely with molecular size.[29] Therefore, a tradeoff exists for He/H_2 separation; due to the lower critical temperature of helium, helium is expected to be less soluble than hydrogen, and due to its smaller size, helium diffusivity is expected to be higher than that of hydrogen.

Gas	Critical Temperature (K)[a]	Diameter (Å)[b]
Helium	5.2	2.55 ± 0.10
Hydrogen	33.2	2.77 ± 0.08

a. Ref. [29]
b. Ref. [30]

Table 7.1: Comparison of critical temperatures and gas diameters for helium and hydrogen.

Among the gases frequently investigated for polymer membrane applications, hydrogen and helium are among the least condensable and smallest in size.[29-31] These two factors (i.e., condensability and molecular size) often make the determination of accurate sorption and diffusion coefficients for these gases inaccessible, which precludes development of complete structure-property relationships. Researchers often rely on the pressure-decay method to determine gas sorption in polymers,[32,33] but this technique has an inherent drawback in that it relies heavily on the accuracy of a Burnett method volume calibration, which, in turn, relies on the accuracy of pressure transducers used in the sorption cell.[33,34] For gases with higher sorption, the pressure-decay method has provided a wealth of data on gas sorption,[35-37] but for gases with low sorption, such as hydrogen and helium, the reported data is much more limited because of this experimental limitation. Some researchers have determined hydrogen and helium sorption from transient time-lag experiments,[12] but these experiments require very thick polymer films, especially for polymers with high fractional free volume, such as some glassy perfluoropolymers.

Despite these difficulties in determining fundamental transport properties, hydrogen separation (e.g., H_2/N_2, H_2/CH_4, and H_2/CO) and helium separation (e.g., He/CH_4) were among the first industrial applications for polymer membranes.[38-41] This development of industrial membranes persisted without complete knowledge of the underlying, fundamental transport properties of the gases being separated. Therefore, we seek to develop basic structure/property relationships for hydrogen and helium transport in polymers that may be useful in the design of new polymers with more beneficial transport properties for separations involving hydrogen or helium.

Helium is used for a number of applications, including arc welding, silicon wafer manufacturing, inerting of hydrogen fuel lines for rockets, and cooling of magnets

in hospital MRIs, nuclear magnetic resonance machines, and accelerators.[42] Helium is typically recovered from natural gas wells that contain high concentrations of helium, but these wells are being depleted, and alternative processes are needed to recover earth's diminishing supply of helium.[43] One approach to recovering helium is using helium-selective membranes on hydrogen-rich purge gas streams in syngas and ammonia production.[44] The hydrogen feed streams for these processes typically come from natural gas, and residual helium in these streams can accumulate to over 2% by volume in the recycle and purge gas streams.[44] These concentrations of helium have potential to be recovered economically; therefore, membrane-based systems are being explored for these helium/hydrogen separation processes.[44]

Herein, we compare the differences in helium and hydrogen permeation, diffusion, and sorption for hydrocarbon-based polymers, a silicon-based polymer, and fluoropolymers by comparing gas sorption properties of polymers commonly used in commercial applications and commonly reported in the membrane literature. To this end, we considered 12 polymers, both rubbery and glassy, that span hundreds of degrees in glass transition temperature (i.e., -123 °C for poly(dimethylsiloxane) to 305°C for Matrimid®), contain complex morphology (i.e., Nafion® N117), and range from 14.4% fractional free volume (polysulfone) to 33% fractional free volume (Teflon® AF 2400). Studying a wide variety of polymers that differ morphologically, structurally, and chemically permits development of broader, more robust correlations concerning transport and sorption characteristics for different classes of polymers.

The predominantly hydrocarbon-based polymers include polysulfone (PSF), Matrimid® polyimide, HAB-6FDA polyimide, and a thermally rearranged (TR) polymer formed from HAB-6FDA. PSF was first introduced by Monsanto in the late 1970's for applications in hydrogen separations and has been widely used since its introduction.[38,45-

[47] Matrimid®, which is a polymer formed from the monomers 3,3'-4,4'-benzophenone tetracarboxylic dianhydride (BTDA) and diaminophenylindane (DAPI), has shown promising separation results for a number of applications including natural gas sweetening, nitrogen enrichment, solvent separation, and hydrogen recovery.[48] HAB-6FDA is a polyimide, like Matrimid®, but it contains a reactive acetate group in the *ortho*-position to the HAB diamine. This reactive functional group allows thermal conversion of HAB-6FDA to its corresponding TR polymer at elevated temperatures. The TR polymer considered here was converted at 450°C for 30min to achieve approximately 76% conversion from its polyimide to its TR polymer and will be referred to as 'TR 450 30min'. TR polymers have shown high permeabilities and high selectivities for a number of separations, such as CO_2/CH_4, O_2/N_2, and hydrogen separations, and these transport characteristics have spurred significant research.[26,46,49-61]

In addition to the predominantly hydrocarbon-based polymers, we also investigated poly(dimethylsiloxane) (PDMS), which is the most permeable rubbery polymer known, and it has been thoroughly investigated for gas and vapor permeability, sorption, and diffusion.[48,62-65]

Finally, we included several highly or completely fluorinated polymers, three of which were included in Robeson's 2008 paper on the upper bound (i.e., Teflon® AF 2400, Hyflon® AD 60, and Nafion® N117).[11] In addition, we also consider the perfluoropolymer Teflon® AF 1600, and three grades of rubbery Tecnoflon® fluoropolymers: PL 455, P 457, and P 459. The Tecnoflon® samples are terpolymers that contain some vinylidene fluoride, so they are not wholly perfluorinated in structure; however, their sorption characteristics match most closely with the perfluoropolymers considered in this study, and they will be classified with the perfluoropolymers for simplicity.

7.2 RESULTS AND DISCUSSION

7.2.1 Chemical structure and properties of polymers considered in this study

The known chemical structures of samples used in this study are presented in Table 7.2 and Table 7.3. The three Tecnoflon® samples (i.e., PL 455, P 457, and P 459) are proprietary polymers from Solvay, and their exact chemical structure is not currently reported in the open literature. However, Ameduri has reported that the PL family of Tecnoflon® polymers are copolymers of vinylidene fluoride, tetrafluoroethylene, and perfluoromethyl vinyl ether, and the P family of Tecnoflon® polymers are copolymers of vinylidene fluoride, tetrafluoroethylene, and hexafluoropropene.[66] Some basic properties of the glassy, perfluoropolymers are shown in Table 7.4.

HAB-6FDA Polyimide	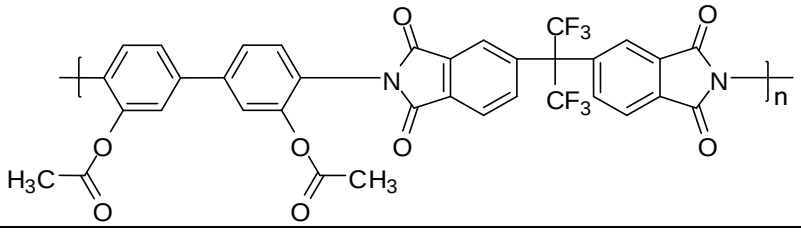
HAB-6FDA TR Polymer	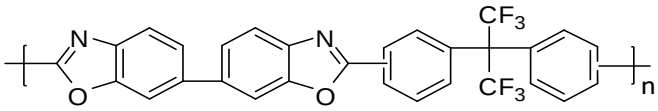
Matrimid®	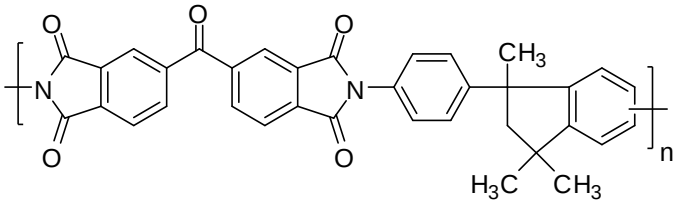
PSF	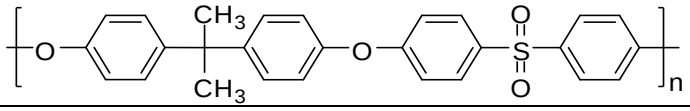
PDMS	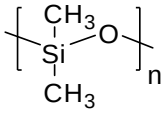

Table 7.2: Chemical structures of predominantly hydrocarbon-based and PDMS polymers considered in this study.

Nafion® N117	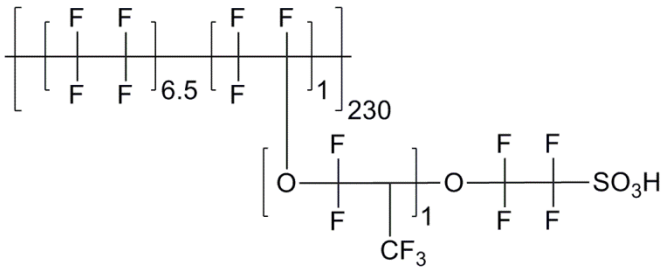
Hyflon® AD 60	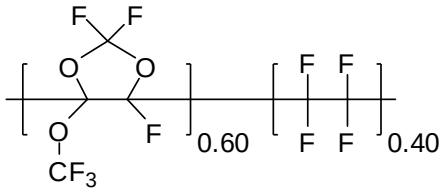
Teflon® AF 1600	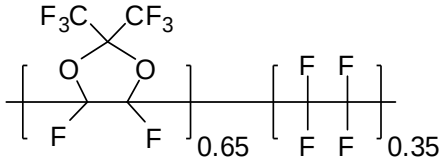
Teflon® AF 2400	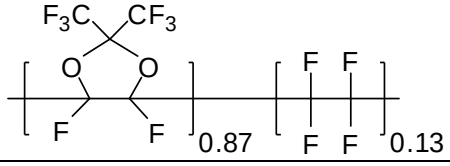
Tecnoflon® PL 455	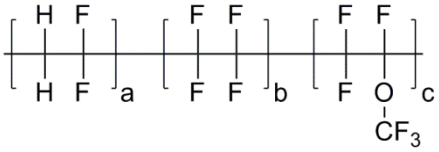
Tecnoflon® P 457	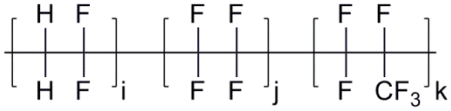
Tecnoflon® P 459	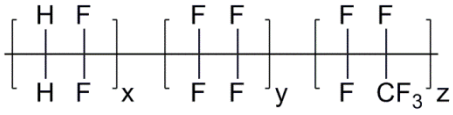

Table 7.3: Chemical structures of perfluorinated and highly fluorinated polymers considered in this study.

Perfluoropolymer	Copolymer (mol %)	ρ (g/cm^3)	T_g (ºC)	FFV
Teflon® AF 2400	87	1.744	240	0.33
Teflon® AF 1600	65	1.836	160	0.31
Hyflon® AD 60	60	1.93	130	0.23

Table 7.4: Properties of glassy, amorphous perfluoropolymers used in this study.[5,20,36,67-69] FFV stands for fractional free volume.

7.2.2 Polymer characterization

Permeation, sorption, and diffusion properties were determined at 35 ± 1°C for hydrogen and helium in a series of polymers. For comparison, 8 glassy polymers and 4 rubbery polymers were considered. Among the 8 glassy polymers, 4 were perfluoropolymers. A list of the samples used for these experiments, along with glass transition temperatures, densities, crystallinity values, and fractional free volume values are recorded in Table 7.5. These data were gathered from literature reports on these samples except for the glass transition temperatures and densities of the Tecnoflon® and AF 1600 samples. The reported values for fractional free volume were estimated from a group contribution method, which relies on density measurements and knowledge of the polymer structure.[70,71] Unless otherwise noted, the T_g values of the polymers listed in Table 7.5 were determined from differential scanning calorimetry. All samples were completely amorphous except for Nafion® N117, which contained approximately 12 wt. % crystallinity.[72]

Sample	T_g (°C)	Density (g/cm^3)	Fractional Free Volume	Crystallinity	Reference
HAB-6FDA Polyimide	255 °C[26]	1.407 ± 0.009[57]	15 %[57]	--	[26, 57]
HAB-6FDA TR 450 30min	*	1.344 ± 0.011	19.6 %	--	[57]
Matrimid®	305 °C[73]	1.231 ± 0.006[48]	17.0 %[74]	--	[73, 48, 74]
PSF	186 °C[75]	1.215 ± 0.017[48]	14.4 %[74]	--	[75, 48, 74]
PDMS	-123 °C[76]	0.98[77]	18 %[78]	--	[76, 77, 78]
Hyflon® AD 60	130 °C[5]	1.93[5]	23 %[4]	--	[5, 4]
Teflon® AF 1600	160 °C[67]	1.836 ± 0.015	31 %[4]	--	[67, 4]
Teflon® AF 2400	240 °C[4]	1.744[3]	33 %[3]	--	[4, 3]
Nafion® N117	110 °C[72,**]	1.98†	NA	12 wt. %[72]	[72]
Tecnoflon® PL 455	-33 °C	1.690 ± 0.045	NA	--	
Tecnoflon® P 457	-18 °C	1.721 ± 0.005	NA	--	
Tecnoflon® P 459	-9 °C	1.855 ± 0.021	NA	--	

* T_g was not observed before polymer degradation.
** T_g determined from tan δ peak. There is some debate in the literature as to the exact location of the glass transition temperature in this material.[72]
† Data provided by the supplier.

Table 7.5: Basic characterization information for samples considered in this study.

7.2.3 Permeation results

Figure 7.1 presents a permeability-selectivity upper bound plot for He/H_2 separation. Gray data points, which were taken from the Robeson's 2008 paper,[11] have been separated by shape to indicate their composition: hydrocarbon-based polymers are presented as circles, and perfluoropolymers are presented as squares. Hydrocarbon-based polymers define the 1991 empirical upper bound, and perfluoropolymers define the 2008 upper bound. This shift in upper-bound data is attributed to increasing availability of permeation results for perfluoropolymers.[1,11] The only He/H_2 perfluoropolymer data point recorded before 1991 was determined by Chiou and Paul in 1988;[2] however, this data point was included but not considered in Robeson's 1991 upper bound correlation

because it had properties so far beyond those observed for the other hydrocarbon-based polymers.[1]

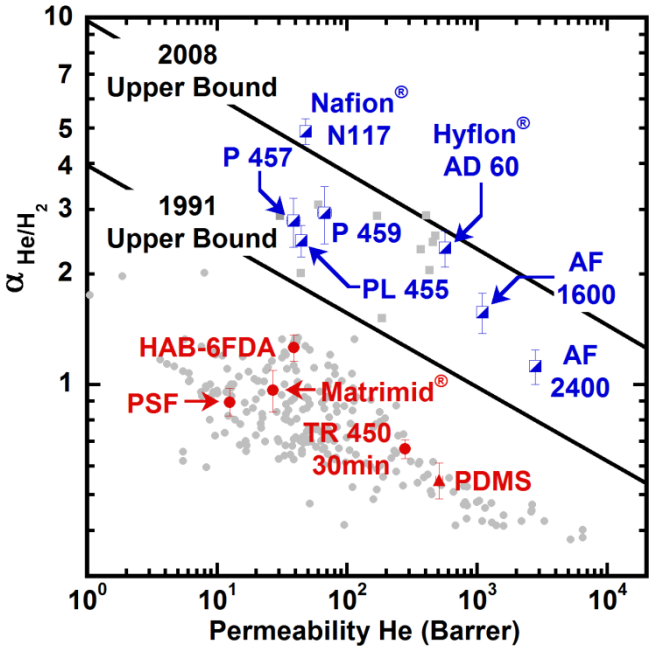

Figure 7.1: Upper bound comparison of hydrocarbon, fluorocarbon, and silicon-based polymers. Red circles indicate predominately hydrocarbon-based polymers, the red triangle represents PDMS, and the blue/white squares represent perlfuorinated or highly fluorinated polymers. Uncertainty is represented as one standard deviation based on propagation of error techniques.[79]

To establish a consistent set of permeation, sorption, and diffusion data between multiple samples, all of the red and blue data points presented in Figure 7.1 were determined independently for this study with the exception of hydrogen permeability of PDMS, which was taken from our previous study.[48] The polymer samples used for permeation were taken from the same batch of samples used for sorption experiments, thus eliminating potential differences in transport results, which may occur due to sample-to-sample variability, differing casting procedures, extrusion conditions, etc.

Red circles in Figure 7.1 represent permeation results for the predominantly hydrocarbon-based samples tested in this study. These results are consistent with other hydrocarbon-based polymers and all fall below the 1991 upper bound. Conversion of the HAB-6FDA polyimide to the TR 450 30min sample results in increased helium permeability but a decrease in permselectivity. The polyimide is slightly helium-selective, and the TR polymer is slightly hydrogen-selective. HAB-6FDA and Matrimid® have similar hydrogen and helium permeabilities, which likely results from their similar morphological and chemical composition, as noted by their similar glass transition temperatures and fractional free volume values in Table 7.5. PDMS, which is a rubbery polymer, has the lowest He/H_2 selectivity but the highest helium permeability of all non-fluorinated samples considered.

The blue/white squares in Figure 7.1 represent permeation results for highly and completely fluorinated polymers tested in this study. All of the fluoropolymers in Figure 7.1 fall above the 1991 upper bound. For the glassy perfluoropolymers, He/H_2 selectivity decreases with increasing He permeability, higher fractional free volume, and higher T_g. Nafion® N117, which lies on the 2008 upper bound, has a helium permeability of 48 ± 3 Barrer and a He/H_2 selectivity of 4.9 ± 0.4. Chiou and Paul have reported very similar transport properties (i.e., He permeability = 40.9 Barrer, He/H_2 selectivity = 4.4) for a Nafion® sample obtained directly from DuPont.[2] The rubbery Tecnoflon® fluoropolymers have permeabilities similar to those of Nafion®; however, they all have lower He/H_2 selectivities.

The PDMS sample tested in this study, which has an Si-O backbone, is presented as a red triangle. PDMS has hydrogen and helium permselectivity most similar to the other hydrocarbon-based samples.

7.2.4 Sorption results

Figure 7.2 presents hydrogen and helium sorption isotherms for the glassy, predominantly hydrocarbon-based samples tested in this study. The hydrogen sorption data in Figure 7.2 was taken from our previous study.[48] Figure 7.2A and Figure 7.2B present sorption for the HAB-6FDA polyimide and the corresponding TR 450 30min polymer, respectively, and, to broaden the scope of our analysis, Figure 7.3 presents the relative change in gas sorption between the HAB-6FDA polyimide and the HAB-6FDA TR polymer as a function of conversion for several gases. Conversion is defined as the actual mass loss for each sample divided by the stoichiometric mass loss needed to fully convert the HAB-6FDA polyimide to its corresponding polybenzoxazole.[26] Conversion of the polyimide to its TR polymer increases helium gas sorption by a factor of approximately 2.5, which is nearly identical to the increase in gas sorption that occurs for H_2, O_2, N_2, and CH_4 in these same polymers.[26,48] For the most highly converted sample in Figure 7.3 (i.e., HAB-6FDA TR 450 30min), the relative increase in helium sorption compared to that of the polyimide for other light, nonpolar gases is similar. Therefore, helium does not have enhanced sorption because of polar groups, which are present as carbonyl groups in the HAB-6FDA polyimide, but absent from the TR 450 30min sample. Enhanced gas sorption in HAB-6FDA because of carbonyl groups has been observed for the quadrupolar gas CO_2.[26] Furthermore, within the uncertainty of the measurements, no detectable change in H_2/He sorption selectivity occurs during conversion of HAB-6FDA; the H_2/He sorption selectivity of the polyimide is approximately 3.7, and the H_2/He sorption selectivity of the TR polymer is approximately 3.6. Nearly identical sorption selectivities have been reported for the HAB-6FDA polyimide and HAB-6FDA TR 450 30min sample for other nonpolar gas pairs such as

O_2/N_2, and CH_4/N_2.[26] Before and after conversion, the O_2/N_2 and CH_4/N_2 sorption selectivities remain approximately 1.4 and 2.4, respectively.[26]

Matrimid® and HAB-6FDA are both polyimides with similar chemical structure, fractional free volume, and glass transition temperature,[48] which likely contributes to the nearly identical sorption isotherms for HAB-6FDA in Figure 7.2A and Matrimid® in Figure 7.2C. The H_2/He sorption selectivity is also nearly identical for these two polymers.

Compared to all of the samples considered in this study, helium sorption was lowest in polysulfone (cf., Figure 7.2D). Moreover, compared to the other hydrocarbon-based polymers, polysulfone also exhibited the lowest hydrogen uptake. The H_2/He sorption selectivity was approximately 3.1, which is similar to the sorption selectivity of the other hydrocarbon-based polymers considered.

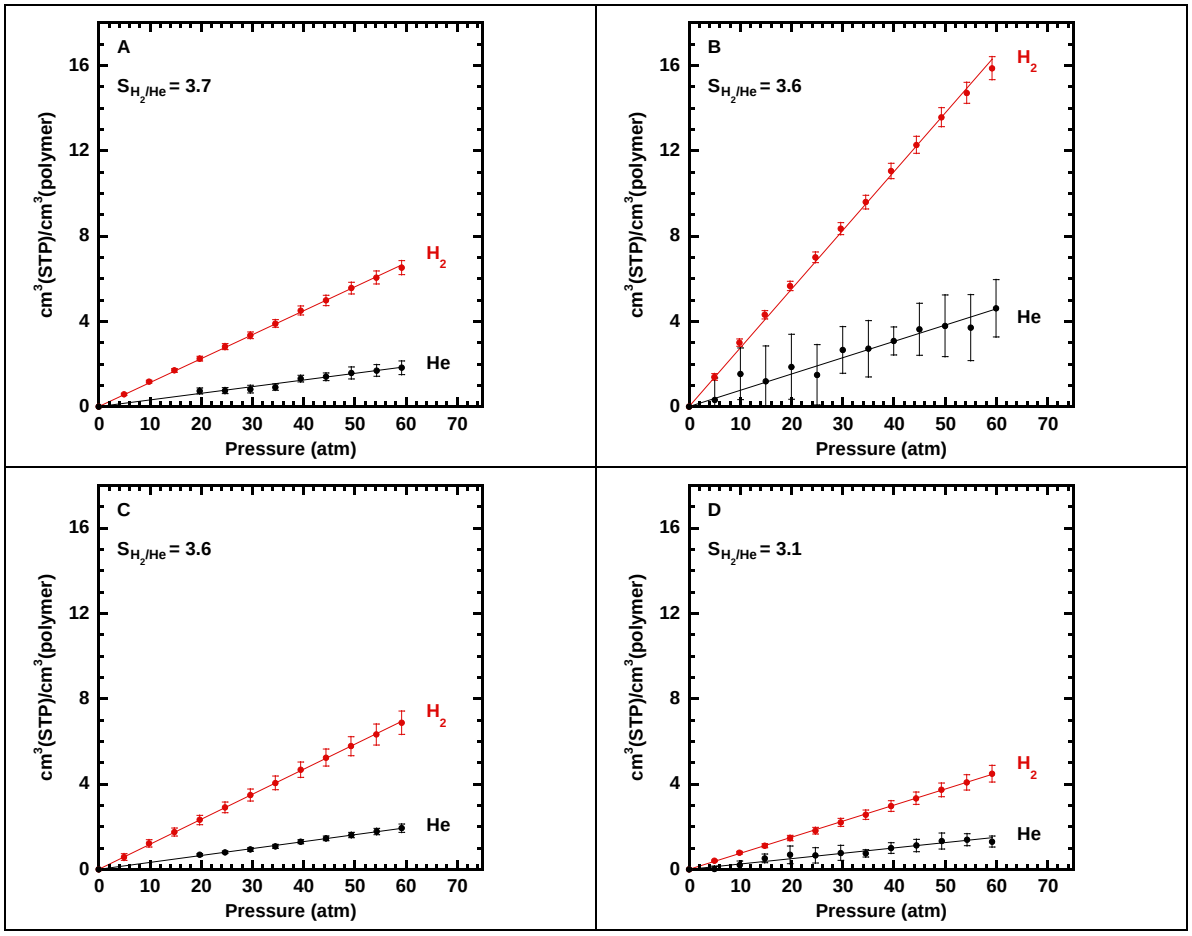

Figure 7.2: Comparison of hydrogen and helium sorption isotherms for glassy, hydrocarbon-based polymers. (A) HAB-6FDA polyimide, (B) HAB-6FDA TR 450 30min, (C) Matrimid®, and (D) PSF. Hydrogen sorption isotherms taken from Ref. 48. For H_2 sorption, uncertainty was calculated from propagation of error techniques,[79] and for He sorption, uncertainty is represented as one standard deviation based on multiple measurements at the same pressure.

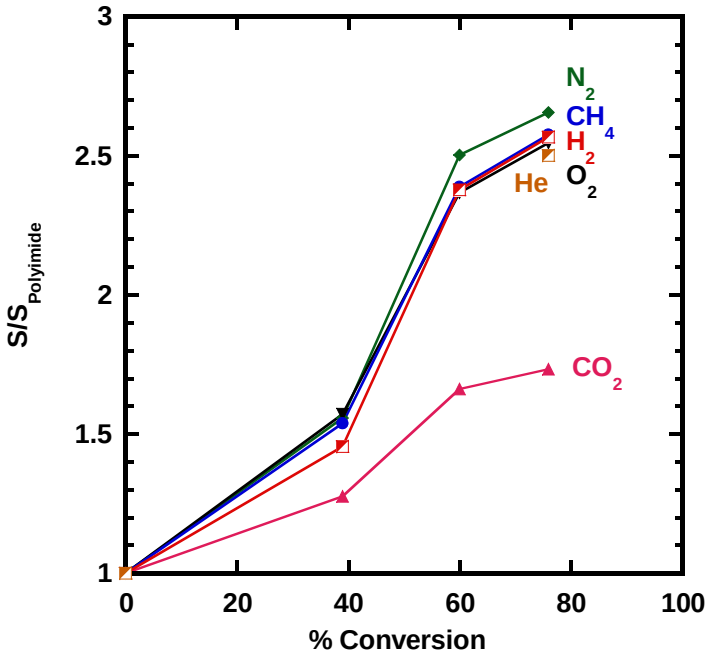

Figure 7.3: Influence of extent of thermal rearrangement (i.e., conversion) of HAB-6FDA polyimide on the relative solubility of He, H_2, N_2, O_2, CH_4, and CO_2. Sorption data were recorded at 10 atm and 35°C. Conversion is defined as the sample mass loss divided by the stoichiometric mass loss needed to fully convert the HAB-6FDA polyimide to its corresponding polybenzoxazole. Figure adapted with permission from Ref. 48.

The sorption of helium and hydrogen in the rubbery samples is presented in Figure 7.4. For PDMS, which is shown in Figure 7.4A, the H_2/He sorption selectivity was approximately 1.7, which was significantly lower than the sorption selectivity for the hydrocarbon-based glassy polymers. From a molecular perspective, the reason for these differences in sorption selectivity for PDMS compared to hydrocarbon-based polymers is currently unknown. However, PDMS has a backbone composed of Si-O repeat units, which differs from the predominantly C-C backbones for the hydrocarbon-based samples. As will be shown later for perfluoropolymers, differences in polymer composition often results in sorption selectivity differences, and these differences in polymer structure may be related to the sorption selectivity differences observed in this case as well.

Figure 7.4B through Figure 7.4D show the helium and hydrogen isotherms for the rubbery fluoropolymers. For all of these samples, the H_2/He sorption selectivity is between 1.1 and 1.3, which is similar to the sorption selectivity of the perfluoropolymers and much lower than the sorption selectivities for the hydrocarbon-based polymers. While sorption may show a dependence on glass transition temperature, it is not likely that sorption selectivities show a strong dependence. Meares has shown that the hydrogen and helium sorption selectivity for polyvinyl acetate changes very little between the rubbery and glassy states.[80] Therefore, the rubbery and glassy fluoropolymers likely have similar sorption selectivities in both their rubbery and glassy states because of their chemical structure, and these properties are likely not influenced strongly by the glass transition temperature.

The Tecnoflon® samples have varying fluorine content as reported by the suppliers: PL 455 has 64%, P 457 has 67%, and P 459 has 70% fluorine by weight. Therefore, we attempted to draw correlations between fluorine content and transport properties. Hydrogen sorption decreased slightly with increasing fluorine content. For example, compared to the PL 455 sample (64% fluorine content), the P 457 sample had 4% lower H_2 sorption and the P 459 sample (70% fluorine content) had 12% lower H_2 sorption. However, there was no systematic trend between fluorine content and helium sorption. Because the exact structure of these samples is not reported, we cannot definitively ascribe the decreasing H_2 sorption to a change in fluorine content or other factors (e.g., polymer structure or fractional free volume). Within the uncertainty of the measurements, there was no trend between fluorine content and permeability or permselectivity.

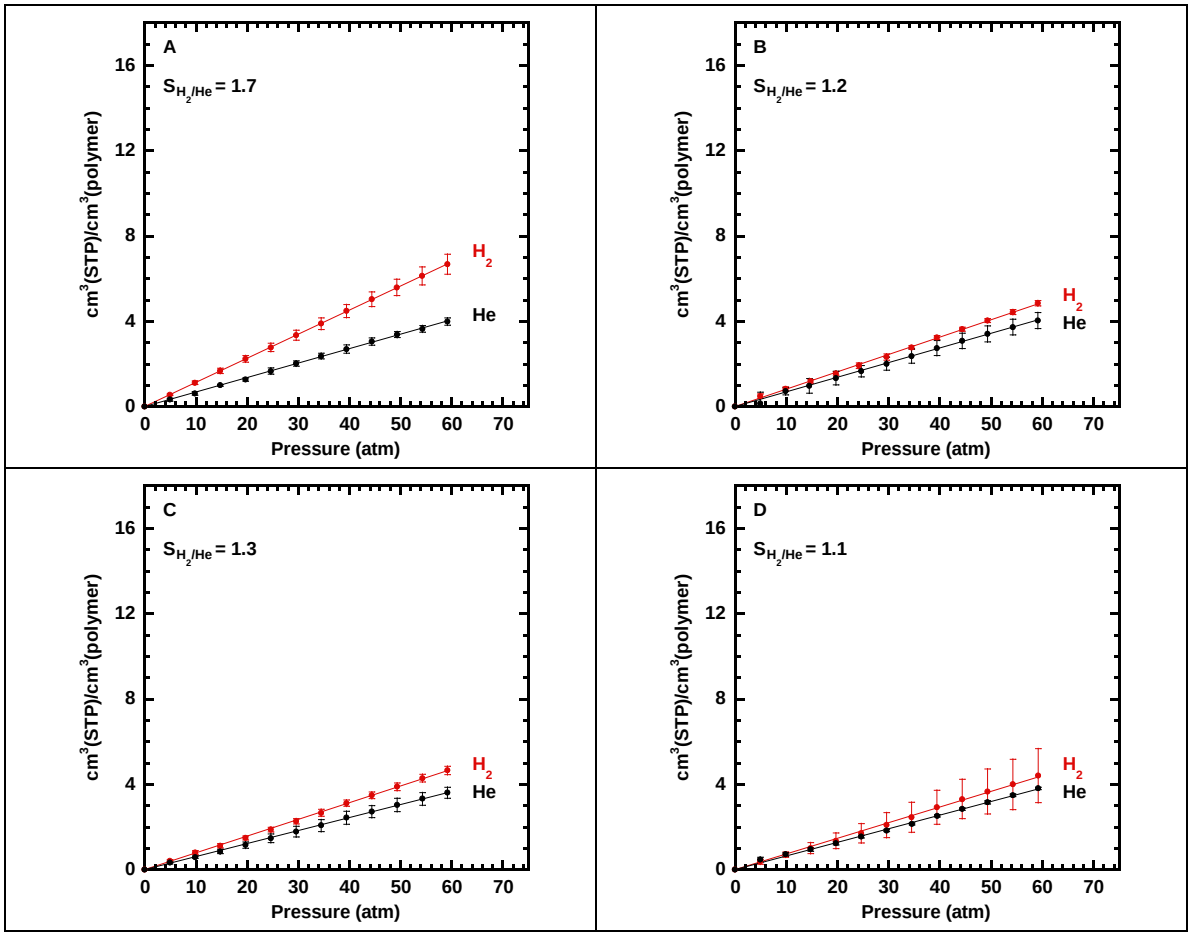

Figure 7.4: (A) Poly(dimethylsiloxane), (B) Tecnoflon® PL 455, (C) Tecnoflon® P 457, and (D) Tecnoflon® P 459 hydrogen and helium sorption isotherms at 35°C. Hydrogen sorption data for PDMS is taken from Ref. 48. Uncertainty is represented as one standard deviation. For H_2 sorption in PDMS, uncertainty was calculated from propagation of error techniques,[79] and for all other isotherms, uncertainty is represented as one standard deviation based on multiple measurements at the same pressure.

Figure 7.5 shows the hydrogen and helium sorption isotherms for the glassy perfluorinated polymers considered in this study. Sorption increases in the following order: Nafion® N117 < Hyflon® AD 60 < Teflon® AF 1600 < Teflon® AF 2400, but there is no significant change in sorption selectivity. Similar to the rubbery fluoropolymers, the H_2/He sorption selectivity was much lower for the glassy

perfluoropolymers than for the hydrocarbon-based polymers. AF 2400 had the highest helium sorption among all samples considered; compared to HAB-6FDA TR 450, which had the highest helium sorption for hydrocarbon-based polymers, AF 2400 had a helium sorption that was twice as high. Helium sorption also increased with increasing glass transition temperature and increasing permeability, which may indicate that there is a correlation between sorption and fractional free volume for these samples, also suggested by Robeson *et al.*[30]

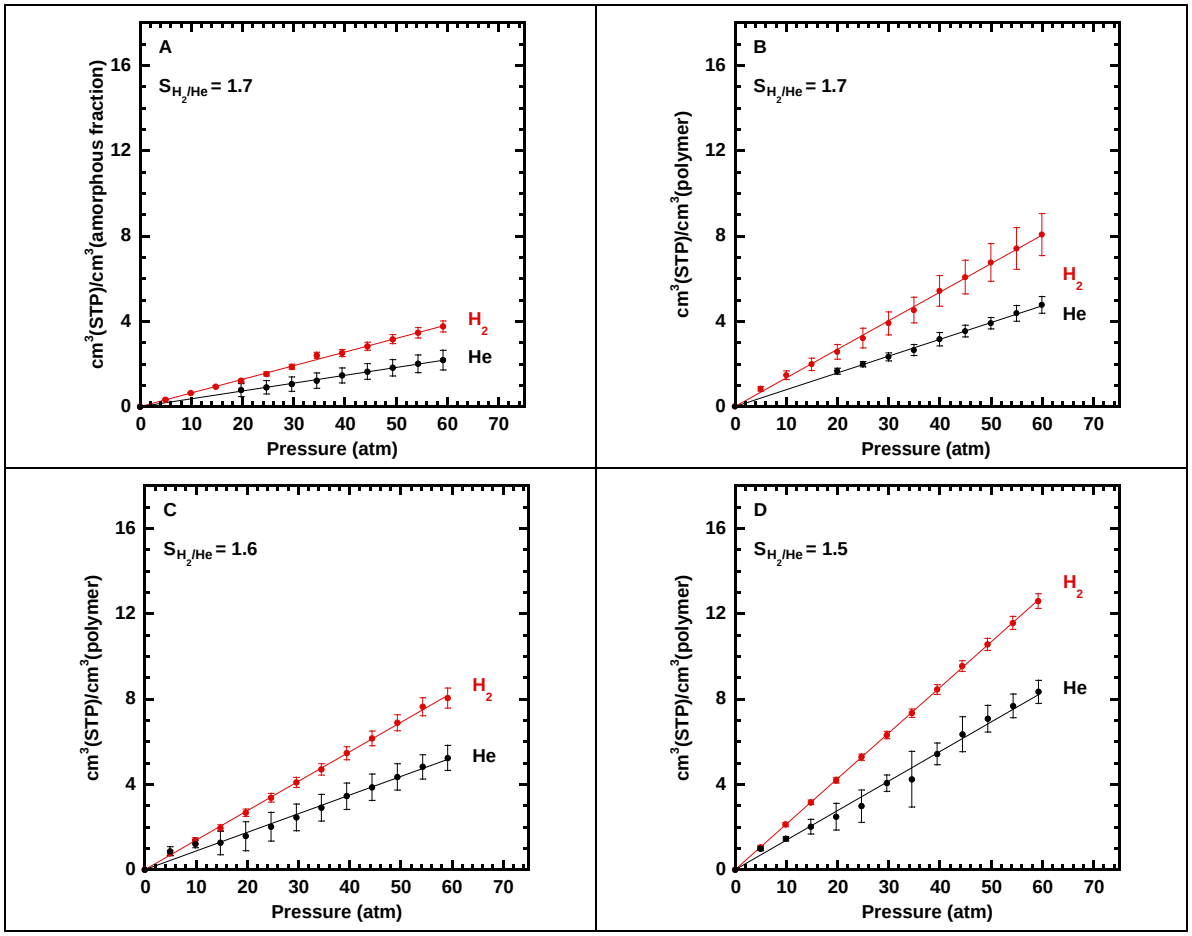

Figure 7.5: Comparison of hydrogen and helium sorption isotherms for glassy perfluoropolymers. (A) Nafion® N117, (B) Hyflon® AD 60, (C) AF 1600, and (D) AF 2400. Hydrogen sorption data for AF 2400 is taken from Ref. 48. For H_2 sorption in AF 2400, uncertainty was calculated from propagation of error techniques,[79] and for all other isotherms, uncertainty is represented as one standard deviation based on multiple measurements at the same pressure.

7.2.5 Interpretation of data with the solution-diffusion model

Gas transport in dense polymers is described using the solution-diffusion model, which is described in Chapter 2. To compare gas diffusion and sorption selectivity in hydrocarbon-based polymers, perfluoropolymers, and PDMS, Figure 7.6A presents the helium/hydrogen diffusion selectivity as a function of helium diffusivity, and Figure 7.6B presents the helium/hydrogen sorption selectivity as a function of helium sorption. Additionally, the tabulated sorption and diffusivity values for hydrogen and helium are included in Appendix B.

As shown in Figure 7.6A, helium/hydrogen diffusivity selectivity decreases with increasing helium diffusivity. The glassy perfluoropolymers have slightly higher helium diffusion coefficients than hydrocarbon-based polymers with similar He/H_2 diffusivity selectivity. Interestingly, the Nafion® N117 sample has the highest diffusivity selectivity, and the reason for this result is not currently known. The rubbery fluoropolymers have diffusivity selectivities that are very similar to those of the hydrocarbon-based polymers. PDMS has a diffusivity selectivity of approximately unity, which means it has the poorest size sieving ability of all samples considered. PDMS is a rubbery polymer with the lowest T_g and most flexible chains among all known polymers, and rubbery polymers often exhibit lower diffusion selectivities than glassy polymers.[29,64,81] Figure 7.6B presents the He/H_2 sorption selectivity as a function of helium sorption. Hydrocarbon-based polymers have very similar He/H_2 sorption selectivities, with all values lying between approximately 0.27 and 0.32 for samples considered in this study. Conversely, fluoropolymers have He/H_2 sorption selectivities between 0.58 and 0.89. PDMS has a sorption selectivity of approximately 0.60, which is similar to that of Nafion® and Hyflon® AD 60 but slightly less than the other fluoropolymers. The similarity of the gas sorption properties of PDMS and perfluoropolymers has been previously noted.[4,21-24,64]

The combination of He/H_2 sorption selectivities that are near unity and He/H_2 diffusivity selectivities that are slightly higher than those of hydrocarbon-based polymers of similar permeability contributes to the perfluoropolymers surpassing the 1991 upper bound. PDMS, which also has a He/H_2 sorption selectivity close to that of the fluoropolymers, has the lowest He/H_2 diffusivity selectivity of all the samples considered. Therefore, its He/H_2 properties are below the 1991 upper bound.

In addition to the sorption and diffusivity data collected for this study, Figure 7.6A and Figure 7.6B also include gray data points for additional polymers reported in the literature. These data were compiled by Robeson to include only glassy, non-perfluorinated polymers.[30] These data contain some scatter, which presumably relates, in part, to differences in free volume distribution or chain rigidity among many different classes of polymers,[82] but also to the experimental difficulty in determining helium and hydrogen diffusivity and sorption coefficients. Nevertheless, the limited data in the literature supports the trend observed for samples in this study: fluoropolymers often have sorption selectivities much closer to unity and similar or higher diffusivity selectivities than hydrocarbon-based polymers.

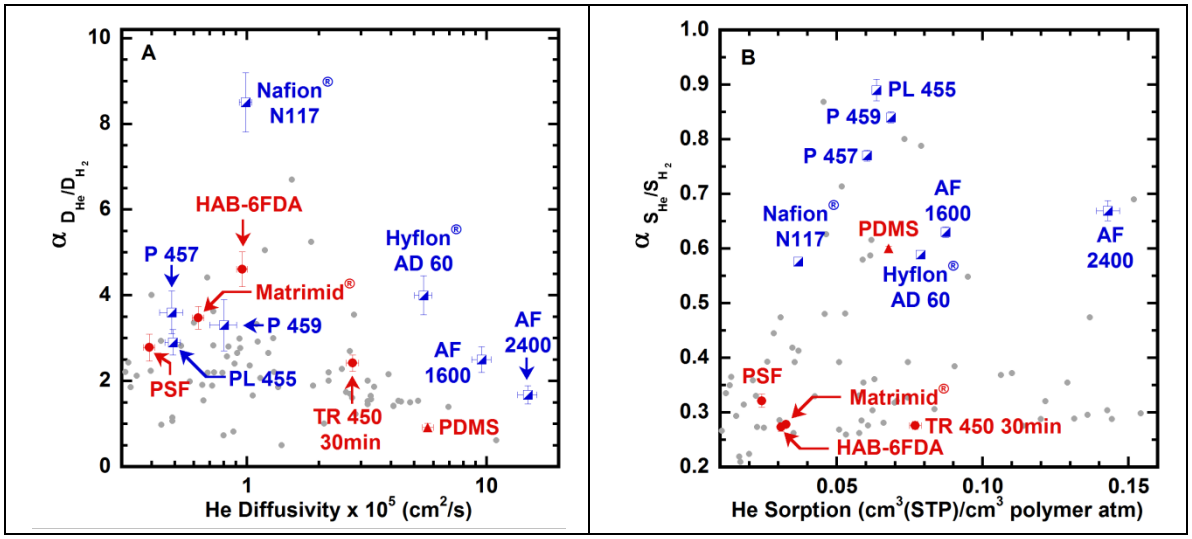

Figure 7.6: Comparison of (A) diffusion selectivity and (B) sorption selectivity for fluoropolymers (blue/white squares), predominantly hydrocarbon-based polymers (red circles), and PDMS (red triangle). Gray circles indicate literature points for glassy, non-perfluorinated polymers from a database collected by Robeson.[30]

7.2.6 Correlations of diffusion and sorption with fractional free volume

Diffusivity of gases in polymers is typically strongly correlated with fractional free volume,[29,35,70,83] and the simplest method to estimate fractional free volume in polymers is the group contribution method:[70,84,85]

$$FFV = \frac{V - V_o}{V} \tag{7.1}$$

where FFV is the fractional free volume, V is the polymer specific volume (i.e., the inverse of the polymer density), and V_o is volume occupied by polymer chains, which is calculated using correlations based on van der Waals volumes of the polymer repeat unit.[70]

Using Equation (7.1), we can compare the effect of fractional free volume on diffusivity using the fractional free volume values reported in Table 7.5. Nafion® N117, which has a complex morphological structure, including crystalline regions and perhaps other types of microscale ordering, was not considered in this analysis due to its structural complexity. The Tecnoflon® samples were also not considered because their exact chemical structure has not been reported in the open literature.

Figure 7.7A presents the correlation between fractional free volume and hydrogen and helium diffusion coefficients. The three perfluoropolymers have FFV values greater than those of the hydrocarbon-based polymers. According to the Freeman theory,[82] the upper-bound trade-off relationship between gas selectivity and gas permeability that was described by Robeson[1,11] results from decreasing diffusion selectivity with increasing FFV. However, for the limited number of samples considered here, there was no evidence for systematically lower diffusivity selectivity with increasing diffusion coefficients between the hydrocarbon-based polymers and the perfluoropolymers. The lowest He/H_2 diffusion selectivity is for PDMS at 0.9 ± 0.1. Interestingly, Nafion® N117, which is not included in Figure 7.7A, had the highest He/H_2 diffusivity selectivity of all samples, 8.5 ± 0.7. Tabulated diffusivity selectivity values are included in Appendix B.

To visually guide the correlation between diffusion coefficients with FFV for polymers of different structure, lines of best fit for each gas are included in Figure 7.7A for the perfluoropolymers and hydrocarbon-based polymers. PDMS, which has a diffusivity selectivity of approximately unity, has relatively high hydrogen and helium diffusion for its modest FFV of approximately 18%; however, diffusion selectivity for gases in rubbery polymers is often lower than in glassy polymers.[29,64,81]

There are relatively few correlations between sorption coefficients and FFV in the literature; however, several such correlations have been noted for specific families of polymers. Aitken *et al.* showed that CO_2 sorption in a series of structurally modified polysulfones changed by a factor of approximately 4 when fractional free volumes increased from 14% to 20%.[86] Pixton and Paul observed similar correlations for O_2 and CO_2 in polyarylates.[87] Miyata *et al.* reported similar correlations between sorption and fractional free volume for 6FDA-based polyimides for CO_2, CH_4, N_2, and O_2.[88] More recently, Robeson *et al.* showed that sorption selectivity varies with permeability, and hence fractional free volume, for a large dataset of polymers and for 15 different gas pairs.[30]

Figure 7.7B presents the correlation between helium and hydrogen sorption and FFV for the samples considered in this study. Helium sorption changes by a factor of approximately 6 between the sample with the lowest FFV (i.e., PSF) and the sample with the highest FFV (i.e., AF 2400). Increases in helium sorption with increasing FFV track closely for all of the classes of polymers considered in this work (i.e., hydrocarbon-based polymers, perfluoropolymers, and PDMS). For helium, the correlation lines for the hydrocarbon-based samples and perfluoropolymers in Figure 7.7B have similar slopes and nearly intersect each other at a value of 1/FFV between approximately 4.5 to 5. However, increases in hydrogen sorption with increasing FFV do not track closely between hydrocarbon-based polymers and perfluoropolymers. For example, the TR 450 30min sample, which had the highest H_2 sorption coefficient of 0.279 ± 0.002 cm^3(STP)/(cm^3(polymer) atm), has a FFV of 19.6%. At 23%, Hyflon AD has a higher FFV than the TR 450 30min sample, but its H_2 sorption is approximately one-half that of the TR polymer.

Because permeability is the product of diffusion and sorption coefficients, Figure 7.7A and Figure 7.7B clearly show that, at the same permeability, perfluoropolymers have greater He/H_2 permselectivity values than hydrocarbon-based polymers and PDMS because of their unique hydrogen and helium sorption characteristics. As a function of FFV, hydrogen sorption is consistently closer to that of helium in perfluoropolymers than in hydrocarbon-based polymers.

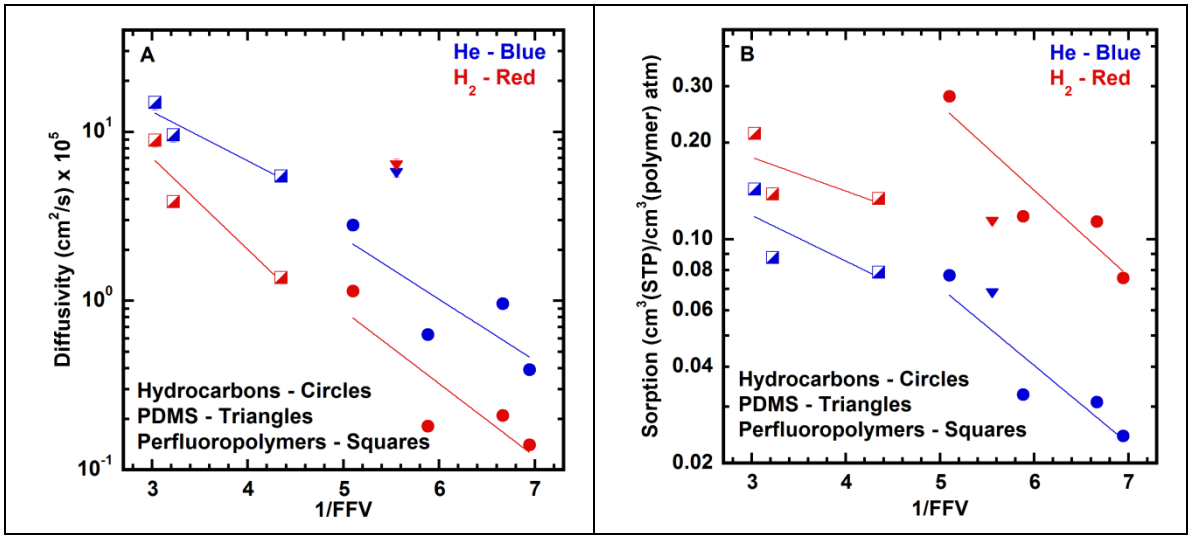

Figure 7.7: Comparison of diffusion coefficients and sorption coefficients with fractional free volume (FFV). FFV was determined by the group contribution method for these polymers. The FFV of Nafion®, which has complex polymer structure, is not easily determined using this method. The FFV of the Tecnoflon® samples could not be determined because the structure is proprietary.

7.2.7 Comparison of gas sorption by critical constants

For polymers and liquids, the logarithm of the infinite dilution gas solubility scales linearly with correlations of penetrant condensability, such as critical temperature (T_c):[26-28]

$$\ln S = \alpha + \beta \times T_c \tag{7.2}$$

where α is the intercept and β is the slope. The term β manifests itself most clearly in explaining solubility selectivities between gas molecules. Larger values of β would indicate larger solubility selectivities between gases, and smaller values of β would indicate smaller solubility selectivities between gases. For hydrocarbon-based polymers and liquids, β is typically between 0.016 and 0.019 K^{-1}.[29,35] However, for perfluorinated liquids and polymers, the values of β are typically smaller than those of hydrocarbons. For example, the value of β is 0.0105 K^{-1} for *n*-C_7F_{16} and 0.011 K^{-1} for AF 1600.[28]

To explore this point, we first examine the HAB-6FDA polyimide and TR 450 30min sample. The gas sorption and transport properties of these polymers have been previously reported.[26,46,48,57,58] The dual-mode model for gas sorption in glassy polymers describes gas sorption into equilibrium and non-equilibrium sorption modes:

$$C = k_D p + C_H^{'} \frac{bp}{1+bp} \tag{7.3}$$

where C is gas concentration, k_D is the Henry's law partition coefficient, $C_H^{'}$ is the Langmuir capacity constant, b is the Langmuir affinity constant, and p is the pressure of gas in contact with the sample. The concentration term in Equation (7.3) can be replaced with gas sorption, S, as follows:

$$S = \frac{C}{p} = k_D + C_H^{'} \frac{b}{1+bp} \tag{7.4}$$

At infinite dilution (i.e., as pressure approaches zero), Equation (7.4) reduces to the sum of two terms: one arising from equilibrium sorption in the Henry's law mode and one from non-equilibrium sorption in the Langmuir mode:

$$\lim_{p\to 0} S = k_D + C_H^{'} b \tag{7.5}$$

For highly non-condensable gases such as hydrogen and helium, sorption isotherms are essentially linear at the experimental conditions considered in this study. Therefore, although glassy polymers contain equilibrium and non-equilibrium contributions to sorption for hydrogen and helium, it is practically impossible to quantify the extent of gas sorption into these modes using dual-mode parameters.

Figure 7.8 presents gas sorption in the HAB-6FDA polyimide and HAB-6FDA TR 450 30min samples as a function of penetrant critical temperature at 10 atm and at infinite dilution. For more condensable gases (i.e., N_2, O_2, CH_4, and CO_2), infinite dilution sorption coefficients were determined by fitting the dual-mode model to the sorption isotherms for each gas and using the dual-mode parameters to estimate the infinite dilution sorption according to Equation (7.5). Hydrogen showed slight dual-mode curvature up to 60 atm for these samples, so a similar approach was taken to determine the sorption at 10 atm and at infinite dilution; however, the limited curvature of these isotherms made it impossible, within experimental uncertainties, to obtain accurate dual-mode parameters.[48] At the conditions of the experiments considered in this study, helium sorption isotherms are within their infinite dilution regime, so sorption coefficients were taken as the slope of the sorption isotherm for these gases. The line of best fit at 10 atm results in a value of β of approximately 0.014 K^{-1} and 0.015 K^{-1}, and the line of best fit at infinite dilution results in a value of β of approximately 0.020 K^{-1},

which is similar that of other hydrocarbon-based polymers. Based upon these results alone, the sorption selectivity of the HAB-6FDA polyimide and the HAB-6FDA TR 450 30min samples should be similar to that of other hydrocarbon-based polymers and liquids, and this is indeed the case. Table 7.6 shows that the sorption selectivity of hydrocarbon-based liquids and polymers, including the samples considered here, have H_2/He sorption selectivities between 2.5 and 3.9. The relatively high value of β for the HAB-6FDA polyimide and HAB-6FDA TR 450 30min sample relates to the high gas sorption selectivity in these materials, even compared to other hydrocarbon-based polymers and liquids. Furthermore, the slopes of the dashed lines in Figure 7.8 are slightly steeper than those reported in our previous work.[26] These differences can be attributed to two factors. First, more accurate hydrogen sorption values determined from the gravimetric instead of volumetric measurements are reported here, and second, the addition of helium sorption values changes the slope of these lines.

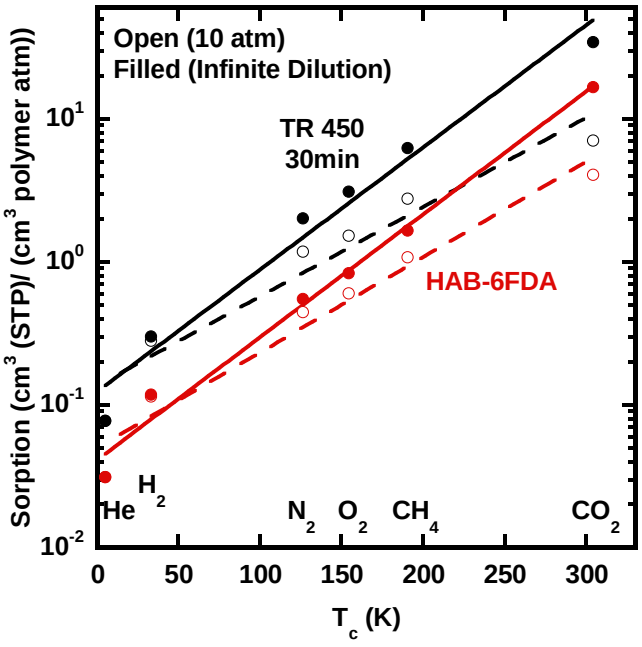

Figure 7.8: Comparison between gas sorption and critical temperature at 10 atm and at infinite dilution for the HAB-6FDA polyimide and the HAB-6FDA TR 450 30min sample.

Classification	Medium	H_2/He Selectivity	Temp (°C)	Refs
Hydrocarbon-based liquids	Benzene	3.3	25	[89,90]
	n-hexane	2.6	25	[90,91]
	n-heptane	2.8	25	[90,91]
	n-octane	2.9	25	[90,91]
	n-nonane	3.0	25	[90,91]
	n-decane	2.7	25	[90,91]
	n-dodecane	2.9	25	[90,91]
	n-tetradecane	2.5	25	[90,91]
Fluorocarbon-based liquids	Perfluoro-*n*-heptane	1.6	25	[92]
Silicon-based polymers	PDMS	1.7	35	This work
	PDMS SiR-1 (0.0554 filler)	1.7	0	[63]
	PDMS SiR-M (0.182 filler)	3.1	0	[63]
Hydrocarbon-based polymers	HAB-6FDA Polyimide	3.7	35	This work
	HAB-6FDA TR 450 30min	3.6	35	This work
	Matrimid®	3.6	35	This work
	PSF	3.1	35	This work
	Nylon 11	3.2	30	[93]
	Nylon 11 (amorphous)	3.4	30	[93]
	PC	3.5	35	[94]
	SBIPC	2.6	35	[94]
	Polyethylene (rubbery)	3.0	30	[93]
	Polyethylene (amorphous, rubbery)	3.9	25	[93]
Fluorocarbon-based polymers	Nafion®	1.7	35	This work
	Hyflon® AD 60	1.7	35	This work
	Teflon® AF 1600	1.6	35	This work
	Teflon® AF 2400	1.5	35	This work
	Teflon® AF 2400	1.4	25	[22]
	Tecnoflon® PL 455 (rubbery)	1.2	35	This work
	Tecnoflon® P 457 (rubbery)	1.3	35	This work
	Tecnoflon® P 459 (rubbery)	1.1	35	This work
	Poly(vinylidene fluoride)	1.7	35	[95]
	Poly(hexafluoropropylene)	1.5	22	[12]
	Poly(hexafluoropropylene-*co*-perfluoromethylvinyl ether)	1.6	22	[12]

Table 7.6: Comparison of H_2/He solubility selectivity in various hydrocarbon-based polymers and liquids, silicon-based polymers, fluoropolymers, and perfluorinated liquids.

Perfluoropolymers typically show different values of β than hydrocarbon-based samples,[28] and this difference ultimately leads to the unique sorption selectivities for these polymers. Figure 7.9 presents the sorption of several gases as a function of critical temperature in the HAB-6FDA polyimide and the HAB-6FDA TR 450 30min sample from Figure 7.8 and also includes the sorption of several gases as a function of critical temperature for three perfluorinated polymers: AF 1600, AF 2400 and Hyflon® AD 60. Infinite dilution solubilities are shown for the HAB-6FDA polyimide, HAB-6FDA TR 450 30min sample, AF 1600, and AF 2400. The conditions at which sorption was determined for Hyflon® AD 60 were not reported.[4] The sorption data for N_2, O_2, CH_4, C_2H_6, CO_2, and C_3H_6 for AF 1600 and AF 2400 were taken from references,[20,96] and sorption data for N_2, CH_4, C_2H_6, and C_3H_8 for Hyflon AD 60 were taken from reference.[4] Data for hydrogen and helium are taken from reference[48] and from the experiments in this study.

For the perfluoropolymers, the term β for the slopes in Figure 7.9 is between approximately 0.009 K^{-1} and 0.012 K^{-1}, which is approximately 50% of the value of β for the hydrocarbon-based samples. The values of β are not significantly affected by the inclusion of helium and hydrogen sorption.

PDMS showed an intermediate H_2/He sorption selectivity, which was between that of hydrocarbon-based polymers and fluoropolymers. Specifically, PDMS had a H_2/He sorption selectivity of 1.7, the hydrocarbon-based samples had H_2/He sorption selectivities between 3.1 and 3.7, and the fluoropolymers had sorption selectivities between 1.1 and 1.7. The term β for PDMS is approximately 0.014 K^{-1},[64] which brackets the values of β for the hydrocarbon-based polymers and liquids and the fluoropolymers and perfluorinated liquids. Therefore, the interaction between hydrocarbon penetrants and the polymer matrix is likely strongly dependent on the

backbone chemistry of PDMS, whereby the differences in sorption are related to the silicon, fluorocarbon, or hydrocarbon-based backbone structure.

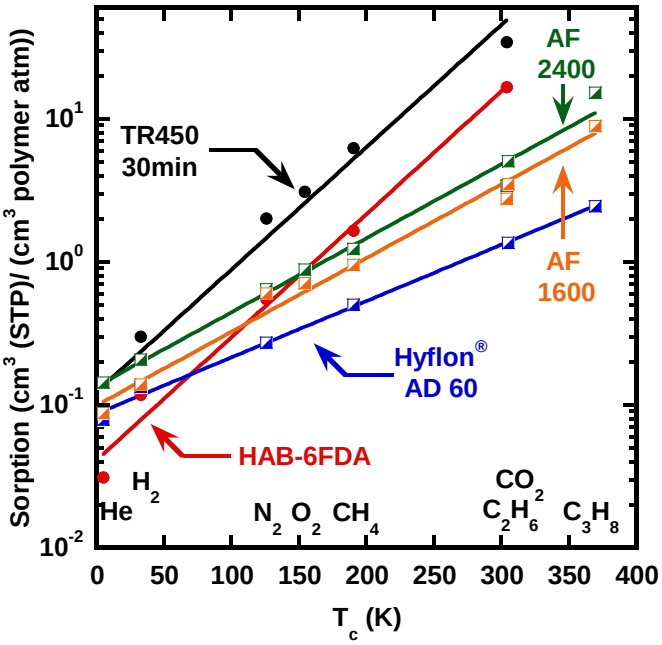

Figure 7.9: Comparison of sorption coefficients as a function of critical temperature for the HAB-6FDA polyimide, HAB-6FDA TR 450 30min, AF 1600, AF 2400, and Hyflon® AD 60. Data for the HAB-6FDA polyimide, HAB-6FDA TR polymer,[26] AF 1600,[20] and AF 2400[96] are reported at infinite dilution, and the pressure for Hyflon AD 60 was not reported.[4]

7.3 CONCLUSIONS

Hydrogen and helium permeability, sorption, and diffusion were determined at 35 °C for polysulfone, an HAB-6FDA polyimide, an HAB-6FDA TR polymer, Matrimid®, poly(dimethylsiloxane), Nafion® N117, Teflon® AF 1600, Teflon® AF 2400, Hyflon® AD 60, Tecnoflon® PL 455, Tecnoflon® P 457, and Tecnoflon® P 459. The glassy perfluoropolymers showed slightly higher He/H_2 diffusivity selectivity as a function of helium diffusion coefficients than the hydrocarbon-based polymers, and

poly(dimethylsiloxane) had the lowest diffusion selectivity of all samples. However, the He/H_2 sorption selectivity was much closer to unity for the fluoropolymers than for the hydrocarbon-based polymers. Therefore, the relatively high H_2/He permselectivities for fluoropolymers is largely a result of sorption selectivities. Poly(dimethylsiloxane), which falls in line with hydrocarbon-based samples on a permeability-selectivity upper bound plot, had He/H_2 sorption selectivity near that of the fluoropolymers but He/H_2 diffusion selectivity that was the lowest of all samples considered. Diffusion coefficients of hydrogen and helium increased with increasing polymer FFV. For helium and hydrogen, correlations of increasing sorption with increasing FFV were also observed for the perfluoropolymers and hydrocarbon-based polymers. Hydrogen/helium sorption selectivities for the samples in this study were compared to the solubility selectivities of other hydrocarbon and fluorocarbon-based polymers and liquids. Within each family of materials, solubility selectivities were similar. Specifically, hydrocarbon-based polymers had H_2/He sorption selectivities between approximately 2.5 and 3.9, and fluoropolymers and fluorinated liquids had solubility selectivities between 1.1 and 1.7. These differences in solubility selectivities are attributed to the relationship between gas solubility and gas condensability. For the AF-series Teflon® samples and Hyflon® AD 60, the linear slope of the logarithm of infinite dilution sorption as a function of critical temperature was between approximately 0.009 K^{-1} and 0.012 K^{-1}; however, for the HAB-6FDA polyimide and corresponding TR polymer, the slope was approximately 0.020 K^{-1}. The difference in these slopes correlates with the lower sorption selectivities of fluoropolymers and fluorinated liquids. PDMS, which has a reported slope of 0.014 K^{-1}, had an intermediate sorption selectivity to that of the hydrocarbon-based samples and the perfluorinated samples.

7.4 REFERENCES

1. Robeson, L.M., Correlation of separation factor versus permeability for polymeric membranes. Journal of Membrane Science, **1991**. 62(2), 165-185.

2. Chiou, J.S. and D.R. Paul, Gas permeation in a dry Nafion membrane. Industrial & Engineering Chemistry Research, **1988**. 27(11), 2161-2164.

3. Pinnau, I. and L.G. Toy, Gas and vapor transport properties of amorphous perfluorinated copolymer membranes based on 2, 2-bistrifluoromethyl-4, 5-difluoro-1,3-dioxole/tetrafluoroethylene. Journal of Membrane Science, **1996**. 109, 125-133.

4. Merkel, T.C., I. Pinnau, R. Prabhakar, and B.D. Freeman, Gas and vapor transport properties of perfluoropolymers, in Materials science of membranes for gas and vapor separations, Y. Yampolskii, P., I. Pinnau, and B.D. Freeman, Editors. **2006**, John Wiley & Sons, Ltd: Chichester. 251 - 270.

5. Macchione, M., J.C. Jansen, G. De Luca, E. Tocci, M. Longeri, and E. Drioli, Experimental analysis and simulation of the gas transport in dense Hyflon® AD60X membranes: Influence of residual solvent. Polymer, **2007**. 48(9), 2619-2635.

6. Jansen, J.C., M. Macchione, and E. Drioli, On the unusual solvent retention and the effect on the gas transport in perfluorinated Hyflon AD® membranes. Journal of Membrane Science, **2007**. 287(1), 132-137.

7. Fitch, M.W., W.J. Koros, R.L. Nolen, and J.R. Carnes, Permeation of several gases through elastomers, with emphasis on the deuterium/hydrogen pair. Journal of Applied Polymer Science, **1993**. 47(6), 1033-1046.

8. Teplyakov, V.V., D.R. Paul, N.B. Bespalova, and E.S. Finkel'shtein, Gas permeation in a fluorine-containing polynorbornene. Macromolecules, **1992**. 25(16), 4218-4219.

9. Alentiev, A.Y., Y.P. Yampolskii, V.P. Shantarovich, S.M. Nemser, and N.A. Platé, High transport parameters and free volume of perfluorodioxole copolymers. Journal of Membrane Science, **1997**. 126(1), 123-132.

10. Park, H. and B. Freeman, Gas separationp properties and their applications of high permeable amorphous perfluoropolymer membranes. Membrane Journal, **2007**. 17(2), 81.

11. Robeson, L.M., The upper bound revisited. Journal of Membrane Science, **2008**. 320(1-2), 390-400.

12. Belov, N.A., A.A. Zharov, A.V. Shashkin, M.Q. Shaikh, K. Raetzke, and Y.P. Yampolskii, Gas transport and free volume in hexafluoropropylene polymers. Journal of Membrane Science, **2011**. 383(1–2), 70-77.

13. Hildebrand, J.H., J.M. Prausnitz, and R.L. Scott, Regular and related solutions: The solubility of gases, liquids, and solids. **1970**, New York, Van Nostrand Reinhold.

14. Hildebrand, J.H., B.B. Fisher, and H.A. Benesi, Solubility of perfluoro-n-heptane with benzene, carbon tetrachloride, chloroform, n-heptane and 2,2,4-trimethylpentane. Journal of the American Chemical Society, **1950**. 72(10), 4348-4351.

15. Scott, R.L., The anomalous behavior of fluorocarbon solutions. The Journal of Physical Chemistry, **1958**. 62(2), 136-145.

16. Siebert, E.D. and C. Knobler, Interaction virial coefficients in hydrocarbon-fluorocarbon mixtures. The Journal of Physical Chemistry, **1971**. 75(25), 3863-3870.

17. Dantzler, E.M. and C.M. Knobler, Interaction virial coefficients in fluorocarbon mixtures. The Journal of Physical Chemistry, **1969**. 73(5), 1335-1341.

18. Dantzler, E.M., C.M. Knobler, and M.L. Windsor, Interaction virial coefficients in hydrocarbon mixtures. The Journal of Physical Chemistry, **1968**. 72(2), 676-684.

19. Lo Nostro, P., Phase separation properties of fluorocarbons, hydrocarbons and their copolymers. Advances in Colloid and Interface Science, **1995**. 56(0), 245-287.

20. Alentiev, A.Y., V.P. Shantarovich, T.C. Merkel, V.I. Bondar, B.D. Freeman, and Y.P. Yampolskii, Gas and vapor sorption, permeation, and diffusion in glassy amorphous Teflon AF1600. Macromolecules, **2002**. 35(25), 9513-9522.

21. De Angelis, M.G., T.C. Merkel, V.I. Bondar, B.D. Freeman, F. Doghieri, and G.C. Sarti, Gas sorption and dilation in poly(2,2-bistrifluoromethyl-4,5-difluoro-1,3-dioxole-co-tetrafluoroethylene): Comparison of experimental data with predictions of the nonequilibrium lattice fluid model. Macromolecules, **2002**. 35(4), 1276-1288.

22. Merkel, T., V. Bondar, K. Nagai, B. Freeman, and Y. Yampolskii, Gas sorption, diffusion, and permeation in poly (2,2-bis (trifluoromethyl)-4,5-difluoro-1,3-dioxole-co-tetrafluoroethylene). Macromolecules, **1999**. 32, 8427-8440.

23. Merkel, T.C., V. Bondar, K. Nagai, and B.D. Freeman, Sorption and transport of hydrocarbon and perfluorocarbon gases in poly(1-trimethylsilyl-1-propyne). Journal of Polymer Science Part B: Polymer Physics, **2000**. 38(2), 273-296.

24. Merkel, T.C., V. Bondar, K. Nagai, and B.D. Freeman, Hydrocarbon and perfluorocarbon gas sorption in poly(dimethylsiloxane), poly(1-trimethylsilyl-1-propyne), and copolymers of tetrafluoroethylene and 2,2-bis(trifluoromethyl)-4,5-difluoro-1,3-dioxole. Macromolecules, **1999**. 32(2), 370-374.

25. Song, W., P.J. Rossky, and M. Maroncelli, Modeling alkane + perfluoroalkane interactions using all-atom potentials: Failure of the usual combining rules. The Journal of Chemical Physics, **2003**. 119(17), 9145-9162.

26. Smith, Z.P., D.F. Sanders, C.P. Ribeiro Jr, R. Guo, B.D. Freeman, D.R. Paul, J.E. McGrath, and S. Swinnea, Gas sorption and characterization of thermally rearranged polyimides based on 3,3'-dihydroxy-4,4'-diamino-biphenyl (HAB) and 2,2'-bis-(3,4-dicarboxyphenyl) hexafluoropropane dianhydride (6FDA). Journal of Membrane Science, **2012**. 416, 558-567.

27. Ghosal, K. and B.D. Freeman, Gas separation using polymer membranes: An overview. Polymers for Advanced Technologies, **1994**. 5(11), 673-697.

28. Prabhakar, R.S., B.D. Freeman, and I. Roman, Gas and vapor sorption and permeation in poly(2,2,4-trifluoro-5-trifluoromethoxy-1,3-dioxole-co-tetrafluoroethylene). Macromolecules, **2004**. 37(20), 7688-7697.

29. Matteucci, S.T., Y.P. Yampolskii, B.D. Freeman, and I. Pinnau, Transport of gases and vapors in glassy and rubbery polymers, in Materials science of membranes for gas and vapor separation, Y. Yampolskii, I. Pinnau, and B.D. Freeman, Editors. **2006**, John Wiley & Sons: Chichester. 1-47.

30. Robeson, L.M., Z.P. Smith, B.D. Freeman, and D.R. Paul, Contributions of diffusion and solubility selectivity to the upper bound analysis for glassy gas separation membranes. Journal of Membrane Science, **2014**. 453, 71-83.

31. Robeson, L.M., B.D. Freeman, D.R. Paul, and B.W. Rowe, An empirical correlation of gas permeability and permselectivity in polymers and its theoretical basis. Journal of Membrane Science, **2009**. 341(1-2), 178-178.

32. Koros, W.J. and D.R. Paul, Design considerations for measurement of gas sorption in polymers by pressure decay. Journal of Polymer Science: Polymer Physics Edition, **1976**. 14(10), 1903-1907.

33. Lin, H. and B.D. Freeman, Springer handbook: Permeation and diffusion, H. Czichos, T. Saito, and L. Smith, Editors. **2006**, Springer: New York. 371-387.

34. Burnett, E.S., Compressibility determinations without volume measurements. Journal of Applied Mechanics, **1936**. 3, 136-140.

35. Paul, D.R. and Y.P. Yampolskii, Polymeric gas separation membranes. **1994**, Boca Raton, CRC Press.

36. Yampolskii, Y., I. Pinnau, and B.D. Freeman, eds. Materials science of membranes for gas and vapor separation. **2006**, John Wiley and Sons: Chichester.

37. Stern, S.A., Polymers for gas separations: the next decade. Journal of Membrane Science, **1994**. 94(1), 1-65.

38. Baker, R.W., Future directions of membrane gas separation technology. Industrial & Engineering Chemistry Research, **2002**. 41(6), 1393-1411.

39. Baker, R.W., Membrane Technology and Applications. 2 ed. **2004**, West Sussex, John Wiley & Sons, Ltd.

40. Stern, S.A., T.F. Sinclair, P.J. Gareis, N.P. Vahldieck, and P.H. Mohr, Helium recovery by permeation. Industrial & Engineering Chemistry, **1965**. 57(2), 49-60.

41. Yampolskii, Y., Polymeric gas separation membranes. Macromolecules, **2012**. 45(8), 3298-3311.

42. Cai, Z., R.H. Clarke, and W.J. Nuttall, Helium demand, in The Future of Helium As a Natural Resource, W.J. Nuttall, R.H. Clarke, and B.A. Glowacki, Editors. **2012**, Routledge: New York. 134-156.

43. Nuttall, W.J., R.H. Clarke, and B.A. Glowacki, Resources: Stop squandering helium. Nature, **2012**. 485(7400), 573-575.

44. Prasad, R., C.J. Heim, and J.J. Maloney. Helium recovery process, **2012**, US 8,152,898 B2.

45. Henis, J.M.S. and M.K. Tripodi. Multicomponent membranes for gas separations, **1980**, US 4230463.

46. Sanders, D.F., Z.P. Smith, R. Guo, L.M. Robeson, J.E. McGrath, D.R. Paul, and B.D. Freeman, Energy-efficient polymeric gas separation membranes for a sustainable future: A review. Polymer, **2013**. 54(18), 4729-4761.

47. Koros, W.J. and G.K. Fleming, Membrane-based gas separation. Journal of Membrane Science, **1993**. 83(1), 1-80.

48. Smith, Z.P., R.R. Tiwari, T.M. Murphy, D.F. Sanders, K.L. Gleason, D.R. Paul, and B.D. Freeman, Hydrogen sorption in polymers for membrane applications. Polymer, **2013**. 54(12), 3026–3037.

49. Park, H.B., C.H. Jung, Y.M. Lee, A.J. Hill, S.J. Pas, S.T. Mudie, E. Van Wagner, B.D. Freeman, and D.J. Cookson, Polymers with cavities tuned for fast selective transport of small molecules and ions. Science, **2007**. 318(5848), 254-258.

50. Han, S.H., J.E. Lee, K.-J. Lee, H.B. Park, and Y.M. Lee, Highly gas permeable and microporous polybenzimidazole membrane by thermal rearrangement. Journal of Membrane Science, **2010**. 357(1-2), 143-151.

51. Park, H.B., S.H. Han, C.H. Jung, Y.M. Lee, and A.J. Hill, Thermally rearranged (TR) polymer membranes for CO_2 separation. Journal of Membrane Science, **2010**. 359(1-2), 11-24.

52. Choi, J.I., C.H. Jung, S.H. Han, H.B. Park, and Y.M. Lee, Thermally rearranged (TR) poly(benzoxazole-co-pyrrolone) membranes tuned for high gas permeability and selectivity. Journal of Membrane Science, **2010**. 349(1-2), 358-368.

53. Han, S., H. Kwon, K. Kim, J. Seong, C. Park, S. Kim, C.M. Doherty, A. Thornton, A.J. Hill, A. Lozano, K. Berchtold, and Y. Lee, Tuning microcavities in thermally rearranged polymer membranes for CO_2 capture. Physical Chemistry Chemical Physics, **2012**. 14(13), 4365-4373.

54. Park, C.H., E. Tocci, Y.M. Lee, and E. Drioli, Thermal treatment effect on the structure and property change between hydroxy-containing polyimides (HPIs) and thermally rearranged polybenzoxazole (TR-PBO). The Journal of Physical Chemistry B, **2012**. 116(42), 12864-12877.

55. Li, S., H.J. Jo, S.H. Han, C.H. Park, S. Kim, P.M. Budd, and Y.M. Lee, Mechanically robust thermally rearranged (TR) polymer membranes with spirobisindane for gas separation. Journal of Membrane Science, **2013**. 434, 137-147.

56. Jiang, Y., F.T. Willmore, D. Sanders, Z.P. Smith, C.P. Ribeiro, C.M. Doherty, A. Thornton, A.J. Hill, B.D. Freeman, and I.C. Sanchez, Cavity size, sorption and transport characteristics of thermally rearranged (TR) polymers. Polymer, **2011**. 52(10), 2244-2254.

57. Sanders, D.F., Z.P. Smith, C.P. Ribeiro, R.L. Guo, J.E. McGrath, D.R. Paul, and B.D. Freeman, Gas permeability, diffusivity, and free volume of thermally rearranged polymers based on 3,3 '-dihydroxy-4,4 '-diamino-biphenyl (HAB) and 2,2 '-bis-(3,4-dicarboxyphenyl) hexafluoropropane dianhydride (6FDA). Journal of Membrane Science, **2012**. 409, 232-241.

58. Guo, R., D.F. Sanders, Z.P. Smith, B.D. Freeman, D.R. Paul, and J.E. McGrath, Synthesis and characterization of thermally rearranged (TR) polymers: Influence of ortho-positioned functional groups of polyimide precursors on TR process and gas transport properties. Journal of Materials Chemistry A, **2013**. 1(2), 262-272.

59. Kim, S., H.J. Jo, and Y.M. Lee, Sorption and transport of small gas molecules in thermally rearranged (TR) polybenzoxazole membranes based on 2,2-bis(3-amino-4-hydroxyphenyl)-hexafluoropropane (bisAPAF) ′ and 4,4 -hexafluoroisopropylidene diphthalic anhydride (6FDA). Journal of Membrane Science, **2013**. 441, 1-8.

60. Guo, R., D.F. Sanders, Z.P. Smith, B.D. Freeman, D.R. Paul, and J.E. McGrath, Synthesis and characterization of thermally rearranged (TR) polymers: Effect of glass transition temperature of aromatic poly(hydroxyimide) precursors on TR process and gas permeation properties. Journal of Materials Chemistry A, **2013**. 1(19), 6063-6072.

61. Sanders, D.F., R. Guo, Z.P. Smith, Q. Liu, K.A. Stevens, J.E. McGrath, D.R. Paul, and B.D. Freeman, Influence of polyimide precursor synthesis route and

ortho-position functional group on thermally rearranged (TR) polymer properties: conversion and free volume. Polymer, **2014**. In Press.

62. Stern, S.A., V.M. Shah, and B.J. Hardy, Structure-permeability relationships in silicone polymers. Journal of Polymer Science Part B: Polymer Physics, **1987**. 25(6), 1263-1298.

63. Barrer, R. and H. Chio, Solution and diffusion of gases and vapors in silicone rubber membranes. Journal of Polymer Science: Part C, **1965**. 138(10), 111-138.

64. Merkel, T.C., V.I. Bondar, K. Nagai, B.D. Freeman, and I. Pinnau, Gas sorption, diffusion, and permeation in poly(dimethylsiloxane). Journal of Polymer Science Part B: Polymer Physics, **2000**. 38(3), 415-434.

65. Raharjo, R., B. Freeman, and E. Sanders, Pure and mixed gas CH_4 and n-C_4H_{10} sorption and dilation in poly(dimethylsiloxane). Journal of Membrane Science, **2007**. 292(1-2), 45-61.

66. Ameduri, B., From vinylidene fluoride (VDF) to the applications of VDF-containing polymers and copolymers: recent developments and future trends. Chem. Rev, **2009**. 109(12), 6632-6686.

67. Gee, R.H., A. Maiti, S. Bastea, and L.E. Fried, Molecular dynamics investigation of adhesion between TATB surfaces and amorphous fluoropolymers. Macromolecules, **2007**. 40(9), 3422-3428.

68. Han, S.H. and Y.M. Lee, Recent High Performance Polymer Membranes for CO_2 Separation, in Membrane Engineering for the Treatment of Gases: Volume 1: Gas-separation Problems with Membranes, E. Drioli and G. Barbieri, Editors. **2011**, Royal Society of Chemistry: Cambridge. 84-124.

69. Merkel, T.C., V. Bondar, K. Nagai, B.D. Freeman, and Y.P. Yampolskii, Gas Sorption, Diffusion, and Permeation in Poly(2,2-bis(trifluoromethyl)-4,5-difluoro-1,3-dioxole-co-tetrafluoroethylene). Macromolecules, **1999**. 32(25), 8427-8440.

70. Park, J.Y. and D.R. Paul, Correlation and prediction of gas permeability in glassy polymer membrane materials via a modified free volume based group contribution method. Journal of Membrane Science, **1997**. 125(1), 23-39.

71. Van Krevelen, D.W., Properties of Polymers: Their Correlation with Chemical Structure, Third Edition. **1997**, Elsevier. 875-875.

72. Mauritz, K.A. and R.B. Moore, State of understanding of Nafion. Chemical reviews, **2004**. 104(10), 4535-4585.

73. Lee, J.S., W. Madden, and W.J. Koros, Antiplasticization and plasticization of Matrimid® asymmetric hollow fiber membranes - Part A. Experimental. Journal of Membrane Science, **2010**. 350(1-2), 232-241.

74. Huang, Y., X. Wang, and D. Paul, Physical aging of thin glassy polymer films: Free volume interpretation. Journal of Membrane Science, **2006**. 277(1-2), 219-229.

75. McHattie, J.S., W.J. Koros, and D.R. Paul, Gas transport properties of polysulphones: 1. Role of symmetry of methyl group placement on bisphenol rings. Polymer, **1991**. 32(5), 840-850.

76. Rowe, B.W., B.D. Freeman, and D.R. Paul, Physical aging of ultrathin glassy polymer films tracked by gas permeability. Polymer, **2009**. 50(23), 5565-5575.

77. Singh, A., B.D. Freeman, and I. Pinnau, Pure and mixed gas acetone/nitrogen permeation properties of polydimethylsiloxane [PDMS]. Journal of Polymer Science Part B: Polymer Physics, **1998**. 36, 289-301.

78. Senthilkumar, U. and B.S.R. Reddy, Polysiloxanes with pendent bulky groups having amino-hydroxy functionality: Structure–permeability correlation. Journal of Membrane Science, **2007**. 292(1–2), 72-79.

79. Bevington, P.R. and K.D. Robinson, Data reduction and error analysis for the physical sciences: Third edition. **2003**, Boston, McGraw Hill.

80. Meares, P., The diffusion of gases through polyvinyl acetate. Journal of the American Chemical Society, **1954**. 76, 3415-3422.

81. Berens, A.R. and H.B. Hopfenberg, Diffusion of organic vapors at low concentrations in glassy PVC, polystyrene, and PMMA. Journal of Membrane Science, **1982**. 10(2–3), 283-303.

82. Freeman, B.D., Basis of permeability/selectivity tradeoff relations in polymeric gas separation membranes. Macromolecules, **1999**. 32(2), 375-380.

83. Cohen, M.H. and D. Turnbull, Molecular transport in liquids and glasses. The Journal of Chemical Physics, **1959**. 31(5), 1164-1169.

84. Bondi, A., van der Waals volumes and radii. The Journal of Physical Chemistry, **1964**. 68(3), 441-451.

85. Bondi, A., Physical Properties of Molecular Crystals, Liquids and Glasses. **1968**, John Wiley & Sons, Inc.

86. Aitken, C.L., W.J. Koros, and D.R. Paul, Effect of structural symmetry on gas transport properties of polysulfones. Macromolecules, **1992**. 25(13), 3424-3434.

87. Pixton, M.R. and D.R. Paul, Gas transport properties of adamantane-based polysulfones. Polymer, **1995**. 36(16), 3165-3172.

88. Miyata, S., S. Sato, K. Nagai, T. Nakagawa, and K. Kudo, Relationship between gas transport properties and fractional free volume determined from dielectric constant in polyimide films containing the hexafluoroisopropylidene group. Journal of Applied Polymer Science, **2008**. 107(6), 3933-3944.

89. Clever, H.L., R. Battino, J.H. Saylor, and P.M. Gross, The solubility of helium, neon, argon and krypton in some hydrocarbon solvents. Journal of Physical Chemistry, **1957**. 61(8), 1078-1082.

90. Fogg, P.G.T. and W. Gerrard, Solubility of Gases in Liquids. **1991**, Chichester, John Wiley & Sons.

91. Hesse, P.J., R. Battino, P. Scharlin, and E. Wilhelm, Solubility of gases in liquids. 20. Solubility of He, Ne, Ar, Kr, N_2 , O_2 , CH_4 , CF_4 , and SF_6 in n-alkanes n-C_lH_{2l+2} ($6 \leq l \leq 16$) at 298.15 K. Journal of Chemical & Engineering Data, **1996**. 41(2), 195-201.

92. Wilhelm, E. and R. Battino, Thermodynamic functions of the solubilities of gases in liquids at 25.deg. Chemical Reviews, **1973**. 73(1), 1-9.

93. Ash, R., R. Barrer, and D. Palmer, Solubility and transport of gases in nylon and polyethylene. Polymer, **1970**. 11(8), 421-435.

94. Hellums, M.W., W.J. Koros, and J.C. Schmidhauser, Gas separation properties of spirobiindane polycarbonate. Journal of Membrane Science, **1992**. 67(1), 75-81.

95. El-Hibri, M.J. and D.R. Paul, Gas transport in poly(vinylidene fluoride): Effects of uniaxial drawing and processing temperature. Journal of Applied Polymer Science, **1986**. 31(8), 2533-2560.

96. Bondar, V., B. Freeman, and Y. Yampolskii, Sorption of gases and vapors in an amorphous glassy perfluorodioxole copolymer. Macromolecules, **1999**. 32, 6163-6171.

97. Zhang, Y., I.H. Musselman, J.P. Ferraris, and K.J. Balkus, Gas permeability properties of Matrimid® membranes containing the metal-organic framework Cu–BPY–HFS. Journal of Membrane Science, **2008**. 313(1-2), 170-181.

Chapter 8: Effect of Polymer Structure on Gas Transport Properties of Polyimides, Polyamides and TR Polymers

Thermally rearranged (TR) polymers have recently gained attention for applications in membrane-based separations. To investigate the effect of structure on the formation and transport properties of these materials, we report characterization and transport properties for 3 poly(*hydroxy*-imide) precursors prepared via thermal imidization in solution and for their corresponding TR polymers. Structural modifications to the polymer backbone can be used to control thermal rearrangement reaction kinetics. In regards to TR polymer formation, samples prepared from diamines with biphenyl functionality reacted more readily than similar samples prepared with hexafluoroisopropylidene-linked aromatic units. Furthermore, incorporation of *ether*-linked aromatic dianhydrides into the polymer backbone increased thermal rearrangement reactivity over hexafluoroisopropylidene-linked aromatic dianhydrides. Nevertheless, for these series of polymers, hexafluoroisopropylidene functional units provided the highest combinations of permeability and selectivity for separations involving H_2, N_2, O_2, CH_4, and CO_2. The effect of synthesis route has also been investigated for a specific TR polymer (i.e., HAB-6FDA) synthesized from polyimide precursors prepared via solution and solid-state thermal imidization. Almost no difference in transport properties was observed between precursor polyimides, regardless of synthesis route. However, upon conversion, the TR polymers prepared from polyimides synthesized via solid-state imidization have higher gas permeabilities than their solution imidized analogs. With the exception of HAB-6FDA polyimides, pure gas CO_2 feed pressures up to approximately 50 bar do not reveal a plasticization pressure point. Conditioning effects are observed for most samples. Pure gas permeability coefficients for olefin/paraffin separations have been determined for an APAF-6FDA TR polymer, and APAF-6FDA TR polymers have

pure-gas permeabilities and selectivities beyond that of other polymers for propylene/propane separation.

8.1 INTRODUCTION

Polymer membranes are currently deployed for applications such as natural gas sweetening, nitrogen enrichment, and syngas ratio adjustment.[1] To improve separation performance, new materials are sought with higher gas throughput, improved selectivity, and chemical/thermal resistance to aggressive feed conditions. Polybenzoxazoles (PBOs) and related structures have recently attracted significant interest from the membrane community, and these polymers are of interest to this work.

In 2007, Park *et al.* reported a method for synthesizing polymer films of PBO, polybenzothiazole, and polybenzimidazole structures.[2] These polymer films were formed from a solid-state reaction of polyimide precursors containing reactive functional groups *ortho*-position to their diamine monomer. Although the technical nomenclature for this type of reaction is a 'condensation reaction', whereby 2 molecules of CO_2 are evolved per repeat unit,[3] due to the thermal processing of these polymers, they are referred to as so-called 'thermally rearranged', or TR polymers.

Several synthetic design parameters can be used to modify the transport properties of these polymers. Han *et al.* investigated differences in the transport properties of TR polymers based on the synthesis route of their polyimide precursors.[4] Calle *et al.* and Guo *et al.* demonstrated that the onset temperature for thermal rearrangement can be affected by the glass transition temperature of the polyimide.[5-7] Work by Guo *et al.* and

---

This chapter has been adapted from: Smith, Z.P., K. Czenkusch, K.L. Gleason, G.H.G.C. Alvarez, A.E. Lozano, D.R. Paul, and B.D. Freeman, *Effect of polymer structure on gas transport properties of polyimides, polyamides and TR polymers (in preparation).*

Sanders *et al.* demonstrated a strong influence of the size of the reactive leaving group attached to the polyimide precursor on transport properties.[8-10]

The thrust of this paper is to extend the current understanding of gas separations with TR polymers by investigating several polymer backbone chemistries. In this regard, we have investigated three poly(*hydroxy*-imide) precursors synthesized via thermal imidization in solution and their corresponding TR polymers. These polymers were selected due to their relevance in the field of polymer membrane research. 6FDA-based polyimides have been of interest for gas separations for years,[11-13] and analogous structures have been pursued for TR polymers.[2,3,14-16] *Ether*-linkages, such as those found in polysulfones and polyamides, show a higher degree of rotational freedom,[17,18] so the effect of these linkages on the thermal rearrangement reaction and transport properties were also investigated. In addition to light gas and CO_2 permeability measurements,[2] *ether* functionalities have also been investigated in TR polymers with dynamic mechanical analysis[19] and for aromatic/aliphatic separations.[20] HAB and APAF-based TR polymers have shown interesting transport properties for separating light gases and CO_2.[2,3,15,16,21] Related structures have been fabricated into hollow-fibers and have been tested as thin films in physical aging studies.[22-24]

For separations involving CO_2 and other condensable penetrants, such as propylene and propane, plasticization can affect membrane performance.[25,26] Polyimides are often susceptible to plasticization effects, and crosslinking strategies have been suggested to increase plasticization resistance.[27-29] These strategies often result in polymers with higher selectivities but lower permeabilities.[30,31] Conversely, for TR polymers, thermal treatment of polyimides result in higher permeabilities and lower selectivities.[2] Similar to crosslinking, however, TR polymers show improved plasticization resistance.[2] This study investigates resistance to CO_2 plasticization through

hysteresis pressurization-depressurization loops for a series of polyimide, polyamide, and TR polymer samples.

Olefin/paraffin separations have been identified as an emerging application for membrane-based separations,[1] and some of the best performing polymers are 6FDA-based polyimides.[26,32,33] To investigate the performance of TR polymers with related structures, this study evaluates pure-gas permeability of C_2H_4, C_2H_6, C_3H_6, and C_3H_8 for one TR polymer, based on APAF-6FDA, and it shows C_3H_6/C_3H_8 performance that is beyond the polymer upper bound.

8.2 RESULTS AND DISCUSSION

8.2.1 Polyimides, polyamide, and TR polymers considered for this study

Chemical structures of the polyimides, polyamide, and TR polymers considered in this work are shown in Table 8.1. Basic transport properties for several of these polymers and related materials have been reported in the literature. Sanders *et al.* and Smith *et al.* have studied the permeability, diffusivity, and solubility of the HAB-6FDA-C polyimide and its corresponding TR polymers.[15,16,34] Guo *et al.* have studied the difference between *acetate* and *hydroxyl* functional HAB-6FDA polyimides and TR polymers.[8] Park *et al.* have reported H_2, N_2, O_2, CH_4 and CO_2 permeabilities for a number of solid-state imidized polyimides and their corresponding TR polymers.[2,3] These samples include an APAF-6FDA-SS polyimide, several APAF-6FDA-SS TR polymers treated for 1 hr at temperatures between 350°C and 450°C, and an APAF-ODPA-SS TR polymer treated for 1 hr at 450°C.[2,3] Han *et al.* extended this work to show the effects of synthesis routes on transport properties for APAF-6FDA polyimides and their corresponding TR polymers.[4] These experiments were performed for polyimides synthesized from solid-state imidization, thermal imidization in solution, and

two forms of chemical imidization: chemical imidization with silylation and chemical imidization without silylation.[4] Additional work by Han *et al.* has shown H_2 and CO_2 permeation results over a range of temperatures for the APAF-6fCl polyamide and corresponding TR polymer.[21]

Permeation and characterization data for the HAB-6FDA-C polyimide and TR polymers converted at temperatures between 350°C and 450°C have been reported in our previous studies.[15] An additional four polyimide samples (i.e., HAB-6FDA-SS, HAB-6FDA, APAF-ODPA, APAF-6FDA) are considered here, and the corresponding TR polymers for these samples were converted at 450°C for 30 min to match the temperature profile of the most highly converted HAB-6FDA-C sample. The TR polymer formed from the polyamide in this study (i.e., APAF-6fCl) was converted at 350°C for 60 min to match work previously reported in the literature.[35]

HAB-6FDA-C	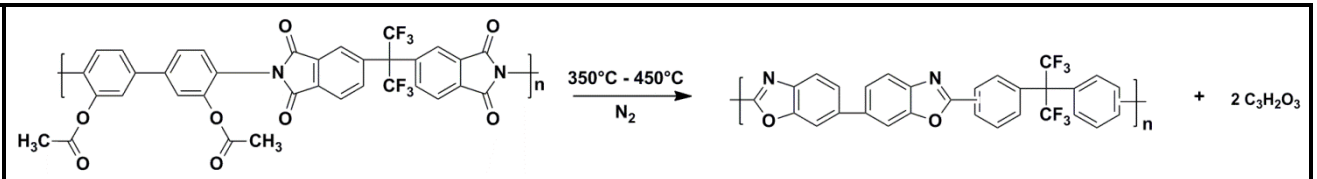
HAB-6FDA-SS HAB-6FDA	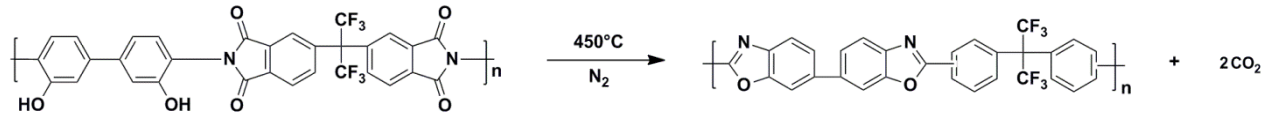
APAF-ODPA	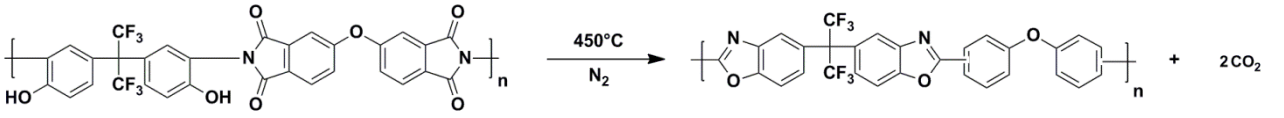
APAF-6FDA	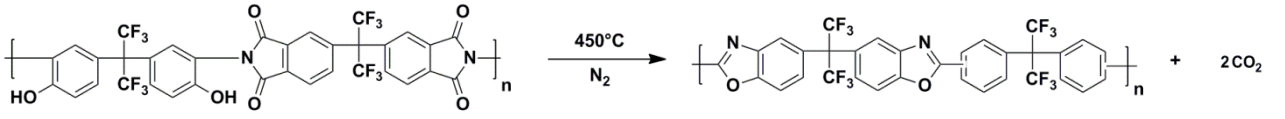
APAF-6fCl	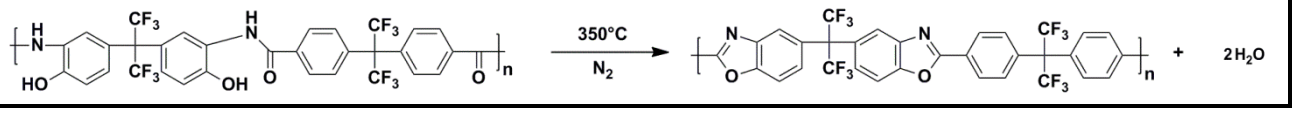

Table 8.1: List of polyimides, a polyamide, and TR polymers considered in this work. Reaction temperatures and reaction products are included in the table. HAB-6FDA-C was thermally treated at 350°C for 1 h, 400°C for 1 h, or 450°C for 30min according to our previous work.[15,16] The HAB-6FDA-SS, HAB-6FDA, APAF-ODPA, and APAF-6FDA samples were treated at 450°C for 30min, and the APAF-6fCl sample was treated at 350°C for 1h. These thermal rearrangement protocols are shown to yield linear polymers, which would be observed if all thermal rearrangement processes were intramolecular. However, intermolecular processes cannot be ruled out, which would lead to some crosslinking.

8.2.2 Thermal reactivity of polyimides and the polyamide

Table 8.2 presents the glass transition temperatures (T_g), theoretical mass loss, and actual mass loss of samples considered in this study. At the thermal treatment conditions used in this study, all of these samples have near-quantitative or slightly above quantitative conversion to their TR polymer structure. The uncertainty in these experiments is approximately ± 0.1%; thus, mass loss beyond that expected from stoichiometric conversion is likely associated with some thermal degradation of the samples.

For the thermally imidized poly(*hydroxy*-imides), the glass transition temperature increases in the following order: APAF-ODPA < APAF-6FDA < HAB-6FDA. These changes in T_g track with the difference between the actual mass loss and the theoretical mass loss. For example, the sample with the highest T_g (i.e., HAB-6FDA), loses 0.4% more mass than theoretically expected, and the sample with the lowest T_g (i.e., APAF-ODPA), loses 0.9% more mass than theoretically expected. Calle *et al.* and Guo *et al.* have correlated the onset of thermal rearrangement with T_g for a variety of polyimides,[5,6] and the trend in mass loss observed in this study is consistent with these earlier findings. Table 8.2 also presents a comparison between the mass loss of chemically, solid-state, or thermally imidized HAB-6FDA with T_g. HAB-6FDA-SS had a similar mass loss to HAB-6FDA (i.e., the sample thermally imidized in solution). However, upon thermal rearrangement, HAB-6FDA-SS had permeabilities that were approximately twice as high as those of its thermally imidized counterpart, results which will be described later. Changes in the synthesis route of the TR polymer precursor likely contribute to these differences in transport properties. The chemically imidized sample (i.e., HAB-6FDA-C) had the lowest T_g of all HAB-6FDA polyimides. Correspondingly, the onset of mass loss for HAB-6FDA-C occurs at a much lower temperature than that of the *hydroxyl*-

functional polyimides. Differences in the onset of mass loss between HAB-6FDA-C and the *hydroxyl*-functional samples likely occurs from two potential mechanisms: (1) the *acetate* group may leave the polyimide to re-form *hydroxyl* groups at temperatures below 350°C, and (2) thermal rearrangement may begin at a lower temperature.[9] Despite the lower temperature required for mass loss, quantitative theoretical conversion for HAB-6FDA-C cannot be achieved using the temperature protocols reported in this study. For the sample treated at 450°C for 30min, the 18.5% mass loss corresponds to 76% conversion using the conversion estimation method shown in Equation (8.1).[15] Theoretical mass loss in the mass loss expected to form a polybenzoxazole structure.

$$\%\,\text{Conversion} = \frac{\text{Actual Mass Loss}}{\text{Theoretical Mass Loss}} \times 100 \qquad (8.1)$$

The polyamide (i.e., APAF-6fCl), which has a similar T_g to that of HAB-6FDA-C, undergoes its thermal rearrangement reaction at a much lower temperature than the poly(*hydroxy*-imide)s, and near-quantitative thermal rearrangement can be achieved by heating at 350°C for 60 min.

Sample	T_g (°C)	Rearrangement Temperature (°C)	Rearrangement Time (min)	Theoretical Mass Loss (%)	Actual Mass Loss (%)†	Theoretical Mass Loss Minus Actual Mass Loss (%)	Reference
HAB-6FDA-C	255[16]	350, 400, 450	60, 60, 30	24.3	9.5, 14.6, 18.5	NA	[16]
HAB-6FDA-SS	--	450	30	14.1	14.6	0.5	This Study
HAB-6FDA	314[6]	450	30	14.1	14.5	0.4	[6]
APAF-ODPA	266[6]	450	30	13.7	14.6	0.9	[6]
APAF-6FDA	303[6]	450	30	11.4	12.2	0.8	[6]
APAF-6fCl	258[35]	350	60	5.0	5.3	0.3	[35]

†All temperature ramps were set at 5°C/min, except for the downward temperature ramp, which was set not to exceed 10°C/min. Polyimides (i.e., all samples except APAF-6fCl) had isothermal holds at 300°C for 1 h.

Table 8.2: Glass transition temperatures for polyimide and polyamide precursors considered in this study, and theoretical mass loss, actual mass loss, and the difference between the theoretical and actual mass loss of samples upon thermal rearrangement. The glass transition temperature of HAB-6FDA-SS could not be determined.

Figure 8.1 presents thermograms for the samples considered in this study. These thermograms were measured by heating samples at 5°C/min between ambient temperatures and 800°C. The derivative weight loss is shown on the secondary ordinate to provide information on the reactivity of the thermal rearrangement reaction, the onset of polymer degradation, and the rate of degradation at elevated temperatures. Additionally, the theoretical mass loss, as calculated based on stoichiometric condensation of the *ortho*-position functional groups, is also labeled on these plots.

Two distinct regions of mass loss can be observed for the samples in Figure 8.1. Such results are common for thermally rearranged polymers, where the first stage of mass loss is attributed to thermal rearrangement, and the second stage of mass loss is attributed to thermal degradation.[2,5-8,16,21,24,35-42] By comparing these regions, the range of

temperatures predominately governed by thermal rearrangement and those governed by thermal degradation can be identified. By analyzing the derivative mass loss results in the thermal rearrangement region, relative rates of reactions can be examined between polymers.

The first row in Figure 8.1 compares TGA thermograms for HAB-6FDA-C (Figure 8.1A), HAB-6FDA (Figure 8.1B), and HAB-6FDA-SS (Figure 8.1C). For the chemically imidized sample, the onset of thermal rearrangement begins shortly before 300°C. However, the *hydroxyl*-functional samples are more thermally stable and do not lose mass until approximately 350°C. Moreover, the higher derivative mass loss in the thermal rearrangement regime suggests faster thermal rearrangement reaction kinetics for the *hydroxyl*-functional HAB-6FDA polyimide than the *acetate*-functional polyimide. For HAB-6FDA, the maximum in the derivative weight loss curve for the thermal rearrangement region is approximately three times that of the maximum for HAB-6FDA-C. Additionally, the temperature range for thermal rearrangement of the thermally imidized sample is narrower than that of the chemically imidized sample. Similar thermograms result for the thermally imidized and solid-state imidized HAB-6FDA polymers; however, the solid-state sample has a slightly lower peak intensity than that of the thermally imidized sample.

Modifying the polyimide diamine can also influence the thermal rearrangement reactivity of these samples. The center column of Figure 8.1 (i.e., Figure 8.1B and Figure 8.1E) compares the thermograms between 6FDA-containing polyimides. The polymers differ in their diamine structures: Figure 8.1B is the thermogram for HAB-6FDA, and Figure 8.1E is the thermogram for APAF-6FDA. The maximum derivative mass loss for the thermal rearrangement regime of HAB-6FDA is nearly three times that of APAF-6FDA, which indicates that HAB is more reactive than APAF. The

hexafluoroisopropylidene groups that bridge the APAF diamine are strongly electron withdrawing, which is known to reduce the reactivity for polyimides containing APAF.[43] Therefore, the reactivity of the *ortho*-functional polyimides to form TR polymers may also be reduced because of this hexafluoroisopropylidene functional group. For APAF-containing polyimides, changing the 6FDA dianhydride to a more flexible ODPA dianhydride increases the reactivity of the thermal rearrangement reaction.[5,37] Figure 8.1D shows the thermogram for APAF-ODPA. For the thermal rearrangement region of this plot, the peak height for the derivative mass loss is almost twice that of the APAF-6FDA polyimide in Figure 8.1E, which is consistent with a higher reactivity of ODPA-containing polyimides compared to 6FDA-containing polyimides.

A final comparison can be made between the reaction of the APAF-6FDA polyimide and the APAF-6fCl polyamide. These results have been reported in Chapter 4. While the degradation regimes for both of these polymers occurs predominately above 450°C, the thermal rearrangement regime is quite different. The onset of thermal rearrangement for the polyimide begins at approximately 350°C; however, the polyamide begins to undergo thermal rearrangement around 250°C. This lower temperature window for conversion allows us to achieve nearly quantitative conversion by heating the sample at only 350°C for 60 min, which may reduce slight polymer degradation that can occur with the polyimides at higher temperatures.

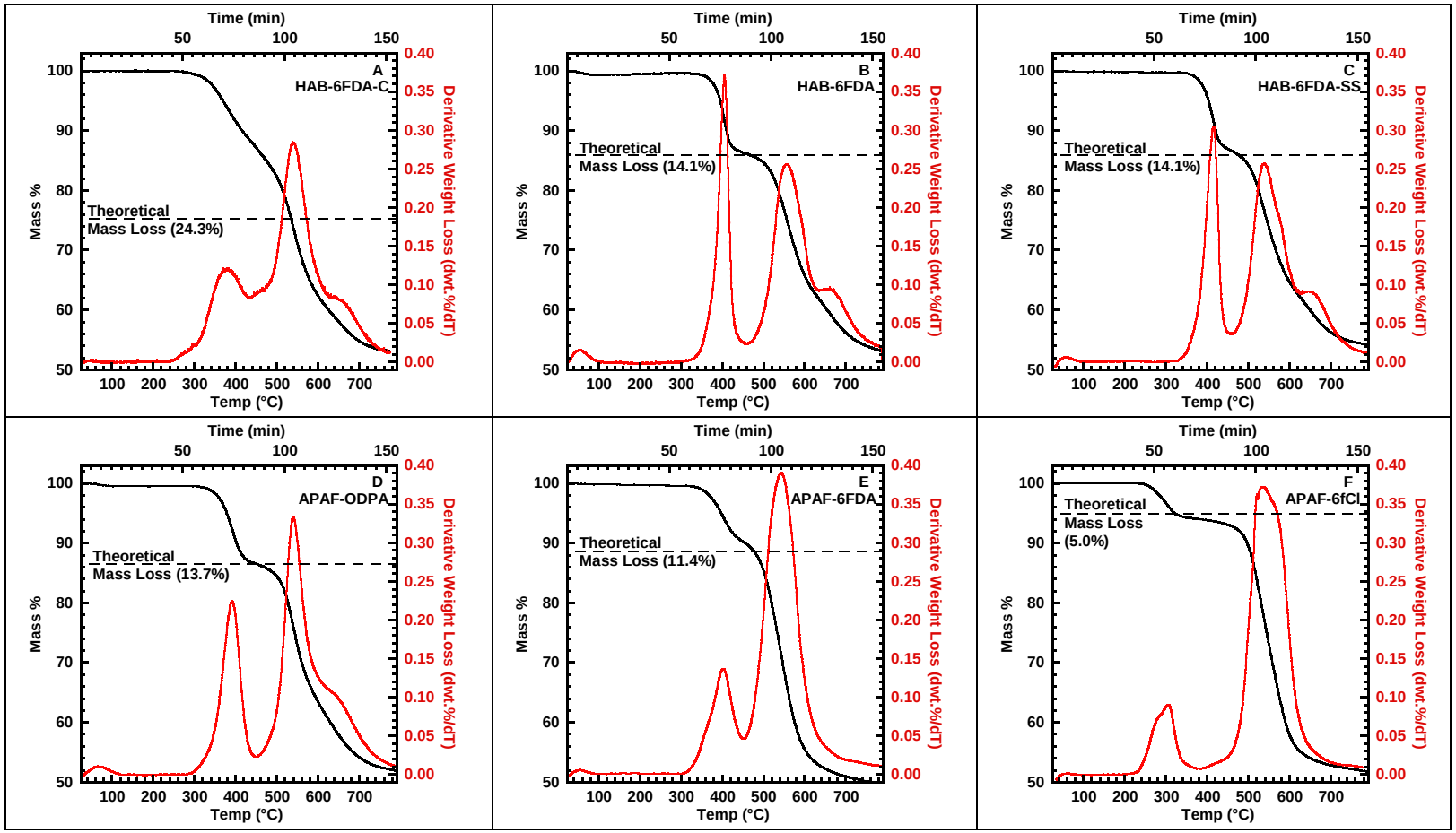

Figure 8.1: TGA scans of (A) HAB-6FDA-C, (B) HAB-6FDA, (C) HAB-6FDA-SS, (D) APAF-ODPA, (E) APAF-6FDA, and (F) APAF-6fCl. Figures (E) and (F) are taken from Chapter 4. Theoretical mass loss was calculated as the mass loss expected for samples to thermally rearrange from their polyimide or polyamide precursors into polybenzoxazoles.

8.2.3 Pure gas permeabilities for the *hydroxyl*-functional polyimides, polyamide, and corresponding TR polymers as a function of pressure

The pure gas permeabilities of H_2, CH_4, N_2, O_2, and CO_2 were determined for the *hydroxyl*-functional polyimides, polyamide and TR polymers at 35°C and pressures between 1 bar and 50 bar. The permeation properties at 35°C and pressures up to approximately 15 bar have been reported for HAB-6FDA-C previously.[15] Furthermore, the H_2, CH_4, and CO_2 permeation properties for APAF-6FDA, APAF-6fCl and their corresponding TR polymers are reported in Chapter 4.

The permeabilities and five selected permselectivities for the precursors and TR polymers are shown in Table 8.3. More complete data, including plots of permeability as a function of pressure for all gases and polymers, are recorded in the Appendix C. To more clearly show comparisons between transport properties for different gas separations, upper bound plots for several gas pairs are shown in Figure 8.2 through Figure 8.6. All TR polymer precursors are shown as open circles, and TR polymers are shown as open squares. Each sample is color-coded, and the effect of pressure on the permeation properties of each sample is shown by plotting individual permeability and selectivity data for each upstream pressure investigated. The 2008 Robeson upper[44] bound is shown on each figure, and, where available, transport properties for relevant polymers, such as tetrabromo polycarbonate (TBPC), cellulose acetate (CA), polysulfone (PSF), Matrimid®, and poly(2,6-dimethyl-1,4-phenylene oxide) (PPO) are also shown.[1]

	HAB-6FDA PI	HAB-6FDA-SS PI	APAF-ODPA PI	APAF-6FDA PI	APAF-6fCl PA
H_2	41 ± 1	43 ± 1	15 ± 1	60 ± 4	36.6 ± 0.9
CO_2	12.3 ± 0.4	11.0 ± 0.4	1.7 ± 0.1	13.3 ± 0.4	10.5 ± 0.3
O_2	2.89 ± 0.08	2.73 ± 0.09	0.60 ± 0.03	4.2 ± 0.2	3.24 ± 0.09
N_2	0.42 ± 0.01	0.42 ± 0.01	0.071 ± 0.003	0.70 ± 0.02	0.59 ± 0.02
CH_4	0.136 ± 0.006	0.135 ± 0.004	0.020 ± 0.001	0.171 ± 0.005	0.23 ± 0.01
N_2/CH_4	3.1 ± 0.2	3.2 ± 0.1	3.5 ± 0.2	4.1 ± 0.2	2.57 ± 0.09
CO_2/CH_4	91 ± 5	82 ± 4	87 ± 6	78 ± 3	46 ± 2
CO_2/N_2	28.9 ± 0.8	26.0 ± 0.9	25 ± 1	19.0 ± 0.6	17.8 ± 0.5
H_2/CH_4	304 ± 8	318 ± 9	740 ± 50	350 ± 30	160 ± 4
O_2/N_2	6.8 ± 0.3	6.4 ± 0.3	8.4 ± 0.6	5.9 ± 0.3	5.5 ± 0.2
	HAB-6FDA TR	HAB-6FDA-SS TR	APAF-ODPA TR	APAF-6FDA TR	APAF-6fCl TR
H_2	111 ± 3	218 ± 6	56 ± 2	592 ± 28	238 ± 6
CO_2	50 ± 1	108 ± 3	7.1 ± 0.6	446 ± 35	127 ± 3
O_2	13.5 ± 0.4	28.9 ± 0.8	4.9 ± 0.2	121 ± 7	38.2 ± 0.9
N_2	2.7 ± 0.1	6.4 ± 0.2	0.82 ± 0.03	32 ± 2	9.2 ± 0.2
CH_4	1.67 ± 0.05	3.9 ± 0.1	0.42 ± 0.01	20 ± 1	5.5 ± 0.1
N_2/CH_4	1.64 ± 0.06	1.64 ± 0.07	2.0 ± 0.1	1.6 ± 0.1	1.67 ± 0.06
CO_2/CH_4	30 ± 1	28 ± 1	41 ± 2	22 ± 2	23.2 ± 0.8
CO_2/N_2	18.3 ± 0.6	16.9 ± 0.6	20.7 ± 0.8	14 ± 2	13.8 ± 0.4
H_2/CH_4	66 ± 2	56 ± 2	135 ± 5	29 ± 2	43 ± 1
O_2/N_2	4.9 ± 0.2	4.5 ± 0.2	5.9 ± 0.3	3.8 ± 0.3	4.2 ± 0.1

Table 8.3: Permeability of H_2, CO_2, O_2, N_2, and CH_4 for the polyimides (PI), polyamide (PA), and TR polymers considered in this study. Additional results are shown for the N_2/CH_4, CO_2/CH_4, CO_2/N_2, H_2/CH_4, and O_2/N_2 pure gas permselectivity of each sample. Data are reported for 35°C and 10 atm.

Figure 8.2 presents data for the CO_2/CH_4 gas pair. As pressure decreases, CO_2 solubility increases more than that of CH_4.[45] Therefore, in the absence of plasticization, CO_2/CH_4 permselectivity is higher at lower pressures. Thus, the highest values of CO_2 permeability are observed at low pressures. As pressure increases, CO_2 permeability and CO_2/CH_4 selectivity generally decrease. Plasticization pressure points, which are defined as the pressure at which permeability first begins to show an increasing trend with increasing pressure, were observed for the two HAB-6FDA samples (i.e., HAB-6FDA

and HAB-6FDA-SS). To avoid reporting selectivities that are strongly influenced by plasticization, data for the HAB-6FDA polymers are not reported in this figure beyond their plasticization pressure points.

Thermal treatment of the polyimides and the polyamide to form TR polymers increases permeability and decreases selectivity for all samples considered. As a given precursor is converted to its corresponding TR polymer, the data move approximately parallel to the upper bound. Park *et al.* observed that conversion of an APAF-6FDA-SS polyimide to its corresponding TR polymer improved gas permeability and selectivity relative to the CO_2/CH_4 upper bound.[2] Furthermore, Guo *et al.* and Sanders *et al.* have observed improvements, relative to the upper bound, in gas permeabilities and selectivities for *hydroxyl*-functional HAB-6FDA samples when converted at intermediate temperatures such as 350°C or 400°C.[8,10] Upon treatment at 450°C, however, the transport properties for these samples move further from the upper bound.[10] The results presented here did not show intermediate states for the samples, so it is unknown if partial conversion of these samples would result in beneficial changes in transport properties relative to the upper bound. Differences in transport properties reported for APAF-6FDA TR polymer in this study and APAF-6FDA-SS TR polymer reported by Park *et al.*,[2] may be related to the difference in synthesis route (i.e., thermal imidization in solution or thermal imidization in the solid-state) and conversion. Park *et al.* investigated thermal rearrangement conditions of 350°C, 400°C, and 450°C for 1 h.[2]

Han *et al.* reported transport properties for TR polymers formed from solid-state imidized polyimides and observed combinations of permeabilities and selectivities closer to the upper bound than those for TR polymers formed from solution-imidized polyimides.[4] For our comparison between a solid-state imidized polyimide and its corresponding TR polymer (i.e., HAB-6FDA-SS) and a solution-imidized polyimide and

its corresponding TR polymer (i.e., HAB-6FDA), higher permeabilities but slightly lower selectivities were obtained for the TR polymer formed from the solid-state imidized polyimide precursor. From an upper bound perspective, TR polymers formed from the solid-state imidized sample were slightly closer to the upper bound for all separations considered.

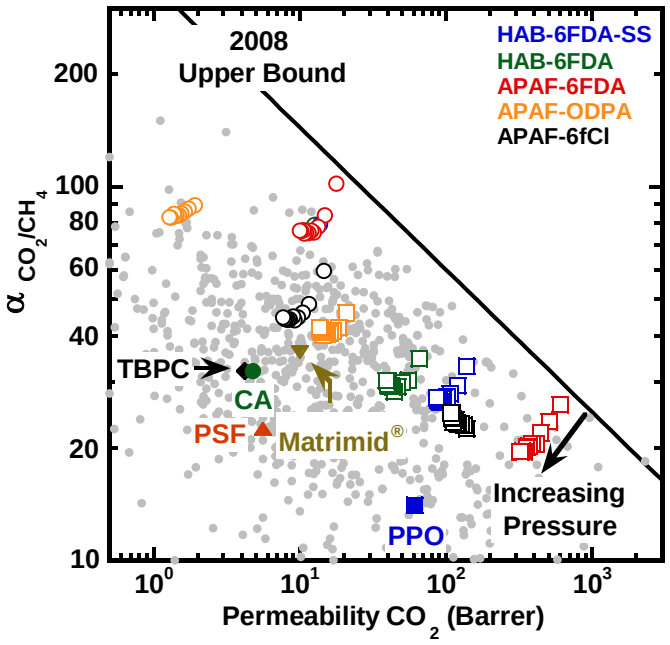

Figure 8.2: Upper bound comparison for the CO_2/CH_4 gas pair. Polyimide and polyamide precursors are shown as open circles, and TR polymers are shown as open squares. TR polymers formed from polyimide precursors were treated at 450°C for 30 min, and TR polymers formed from polyamide precursors were treated at 350°C for 60 min. Literature data are shown as gray circles from Robeson's database,[44] and additional industrially relevant data points (tetrabromo polycarbonate (TBPC), cellulose acetate (CA), polysulfone (PSF), Matrimid®, and poly(2,6-dimethyl-1,4-phenylene oxide) (PPO)) are highlighted from the review by Sanders *et al.*[1] Data points are plotted for pure gas permeability determined between approximately 1 bar and 50 bar with the exception of the HAB-6FDA and HAB-6FDA-SS polyimides, which are only plotted for pressures below their CO_2 plasticization pressure point. The change of permeability and selectivity with increasing pressure is indicated for the APAF-6FDA TR polymer. APAF-6fCl TR polymer shows increasing selectivity with increasing CO_2 pressure, which likely indicates some CO_2 plasticization. This figure includes data for certain samples reported in Chapter 4.

Figure 8.3 shows permeability and selectivity data for the CO_2/N_2 gas pair. Similar to the CO_2/CH_4 case, CO_2 permeability and CO_2/N_2 selectivity data are closest to the upper bound at low pressure. At 35°C, both CA and Matrimid® have comparable transport properties to those of several of the polyimides considered in this study.

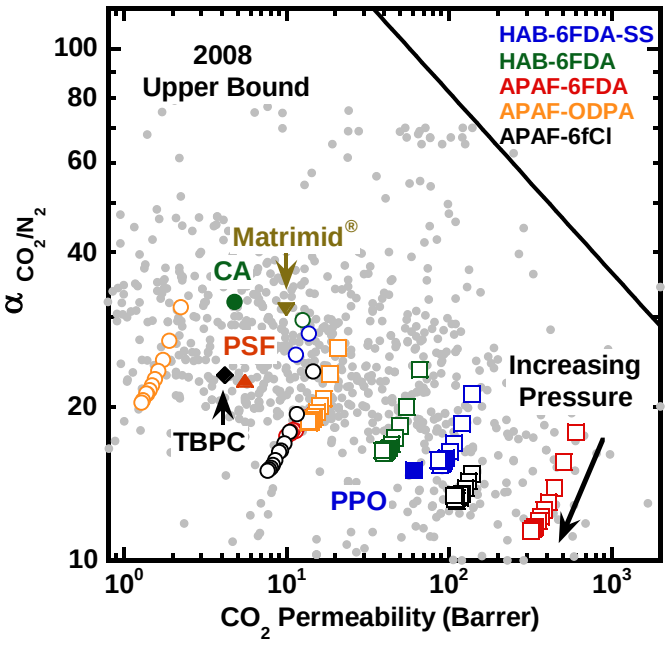

Figure 8.3: Upper bound comparison for the CO_2/N_2 gas pair. Polyimide and polyamide precursors are shown as open circles, and TR polymers are shown as open squares. TR polymers formed from polyimide precursors were treated at 450°C for 30 min, and TR polymers formed from polyamide precursors were treated at 350°C for 60 min. Literature data are shown as gray circles from Robeson's database,[44] and additional industrially relevant data points (tetrabromo polycarbonate (TBPC), cellulose acetate (CA), polysulfone (PSF), Matrimid®, and poly(2,6-dimethyl-1,4-phenylene oxide) (PPO)) are highlighted from the review by Sanders *et al.*[1] Data points are plotted for pure gas permeability determined between approximately 1 bar and 50 bar with the exception of the HAB-6FDA and HAB-6FDA-SS polyimides, which are only plotted for pressures below their CO_2 plasticization pressure point. The change of permeability and selectivity with increasing pressure is indicated for the APAF-6FDA TR polymer.

Figure 8.4 presents data for the N_2/CH_4 gas pair. This separation is particularly difficult for membranes. From the solution-diffusion model, the permselectivity is given by:

$$\frac{P_{N_2}}{P_{CH_4}} = \frac{\left[\overline{D}\right]_{N_2}}{\left[\overline{D}\right]_{CH_4}} \frac{\left[\overline{S}\right]_{N_2}}{\left[\overline{S}\right]_{CH_4}} \tag{8. 2}$$

Because N_2 is smaller than CH_4,[46] $\frac{\left[\overline{D}\right]_{N_2}}{\left[\overline{D}\right]_{CH_4}}$ will be greater than 1. However, because N_2 is less condensable than CH_4, $\frac{\left[\overline{S}\right]_{N_2}}{\left[\overline{S}\right]_{CH_4}}$ will be less than 1. This tradeoff in diffusivity-selectivity and solubility-selectivity results in permselectivity values that are typically not far from unity. However, for the samples in this study, permselectivities over 3 are observed for all of the poly(*hydroxy*-imides) considered (i.e., HAB-6FDA-SS, HAB-6FDA, APAF-ODPA, and APAF-6FDA). The separation performance moves closer to the upper bound with increasing pressure. However, these are pure gas data, and mixed gas data would be needed to confirm this trend from a practical viewpoint. With the exception of the TR polymer formed from APAF-ODPA, none of the TR polymers have permselectivities over 2.

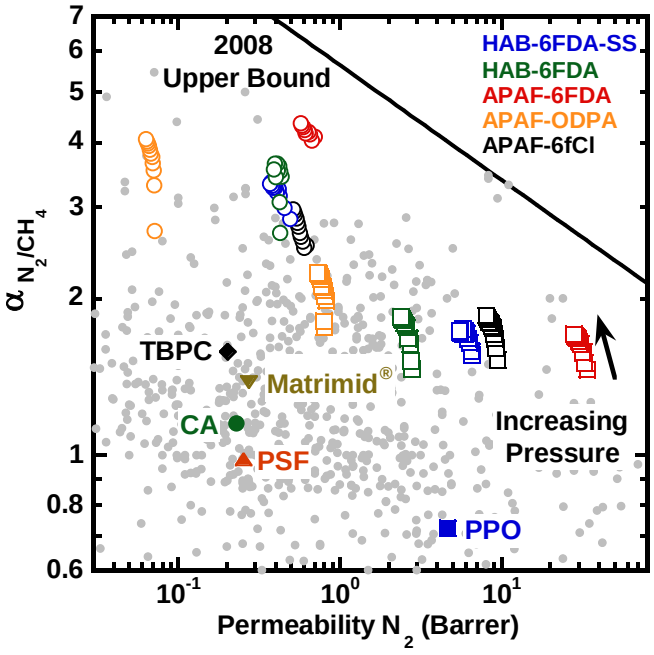

Figure 8.4: Upper bound comparison for the N_2/CH_4 gas pair. Polyimide and polyamide precursors are shown as open circles, and TR polymers are shown as open squares. TR polymers formed from polyimide precursors were treated at 450°C for 30 min, and TR polymers formed from polyamide precursors were treated at 350°C for 60 min. Literature data are shown as gray circles from Robeson's database,[44] and additional industrially relevant data points (tetrabromo polycarbonate (TBPC), cellulose acetate (CA), polysulfone (PSF), Matrimid®, and poly(2,6-dimethyl-1,4-phenylene oxide) (PPO)) are highlighted from the review by Sanders *et al.*[1] Data points are plotted for pure gas permeability determined between approximately 1 bar and 50 bar with the exception of the HAB-6FDA and HAB-6FDA-SS polyimides, which are only plotted for pressures below their CO_2 plasticization pressure point. The change of permeability and selectivity with increasing pressure is indicated for the APAF-6FDA TR polymer.

Several polymers reached or exceeded the 2008 Robeson upper bound for the H_2/CH_4 gas pair, as shown in Figure 8.5. These samples included the HAB-6FDA-SS and APAF-6FDA polyimides and the APAF-6FDA TR polymer. Similar to the N_2/CH_4 gas pair, pure gas H_2/CH_4 selectivity also increased with increasing pressures. Membranes were originally targeted for this separation with selectivities between 15 and 25.[47] All of the TR polymers are near or slightly above this range of selectivity.

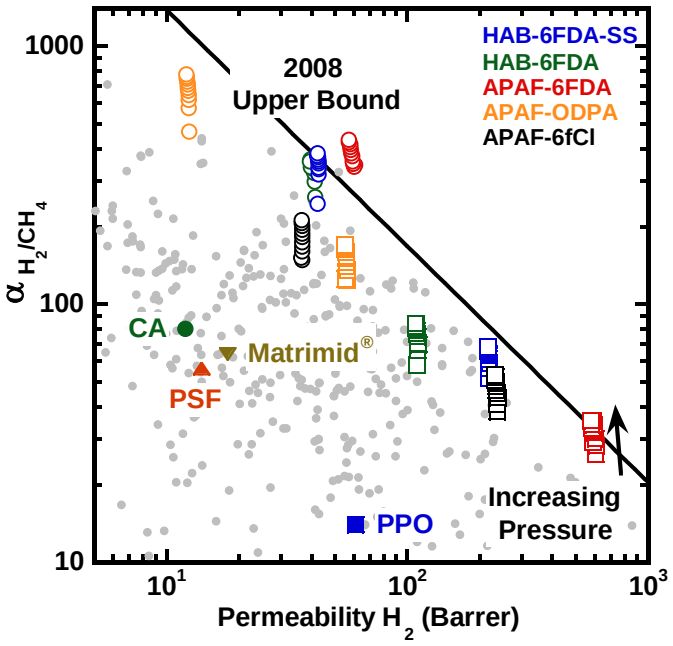

Figure 8.5: Upper bound comparison for the H_2/CH_4 gas pair. Polyimide and polyamide precursors are shown as open circles, and TR polymers are shown as open squares. TR polymers formed from polyimide precursors were treated at 450°C for 30 min, and TR polymers formed from polyamide precursors were treated at 350°C for 60 min. Literature data are shown as gray circles from Robeson's database,[44] and additional industrially relevant data points (cellulose acetate (CA), polysulfone (PSF), Matrimid®, and poly(2,6-dimethyl-1,4-phenylene oxide) (PPO)) are highlighted from the review by Sanders *et al.*[1] Data points are plotted for pure gas permeability determined between approximately 1 bar and 50 bar with the exception of the HAB-6FDA and HAB-6FDA-SS polyimides, which are only plotted for pressures below their CO_2 plasticization pressure point. The change of permeability and selectivity with increasing pressure is indicated for the APAF-6FDA TR polymer. This figure includes data for certain samples reported in Chapter 4.

Figure 8.6 presents data for the O_2/N_2 gas pair. While promising transport properties have been reported for this separation for several synthesis routes involving APAF-6FDA-based TR polymers, our results show a trade-off between permeability and selectivity with thermal treatment that is essentially parallel to the upper bound.[4] For the

APAF-6FDA TR polymer, similar transport properties are reported here and in the study by Han *et al.* despite differences in thermal treatment time.[4] For example, our sample has an O_2 permeability of 121 ± 7 Barrer and an O_2/N_2 permselectivity of 3.8 ± 0.3, while Han *et al.* report an O_2 permeability of approximately 80 Barrer and an O_2/N_2 selectivity of approximately 4.3.[4]

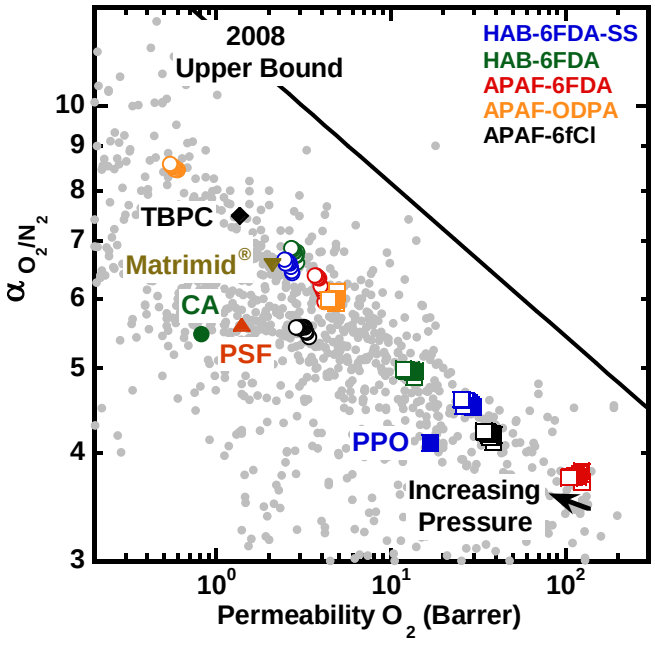

Figure 8.6: Upper bound comparison for the O_2/N_2 gas pair. Polyimide and polyamide precursors are shown as open circles, and TR polymers are shown as open squares. TR polymers formed from polyimide precursors were treated at 450°C for 30 min, and TR polymers formed from polyamide precursors were treated at 350°C for 60 min. Literature data are shown as gray circles from Robeson's database,[44] and additional industrially relevant data points (tetrabromo polycarbonate (TBPC), cellulose acetate (CA), polysulfone (PSF), Matrimid®, and poly(2,6-dimethyl-1,4-phenylene oxide) (PPO)) are highlighted from the review by Sanders *et al.*[1] Data points are plotted for pure gas permeability determined between approximately 1 bar and 50 bar with the exception of the HAB-6FDA and HAB-6FDA-SS polyimides, which are only plotted for pressures below their CO_2 plasticization pressure point. The change of permeability and selectivity with increasing pressure is indicated for the APAF-6FDA TR polymer.

There are several common trends among the data reported in Figure 8.2 through Figure 8.6. First, replacement of the hexafluoroisopropylidene-containing dianhydride with an *ether*-containing dianhydride has the strongest effect on gas permeability. Among the polyimide precursors, the APAF-ODPA had permeabilities that were consistently lower than that of APAF-6FDA; for N_2 and CH_4, these permeabilities were nearly an order of magnitude lower. Similar decreases in permeability have been reported for *ether* versus hexafluoroisopropylidene-functional polyimides for propylene/propane separation. In a study by Shimazu *et al.*, replacing a hexafluoroisopropylidene-functional group with an *ether*-functional group reduced propylene permeability by nearly an order of magnitude, and this decrease in permeability was almost exclusively associated with a decrease in gas diffusivity.[48]

Modification of the biphenyl group in HAB to an aromatic hexafluoroisopropylidene-functional group (i.e., APAF) had a weaker effect on permeability. CH_4 permeability increased by approximately 25% from HAB-6FDA to APAF-6FDA, and H_2 permeability increased by nearly 50%. Interestingly, for the polyimide samples, this modification resulted in increased permselectivity for all separations except O_2/N_2 and CO_2/N_2, where slight decreases in selectivity were observed. Hexafluoroisopropylidene-functional groups often increase the energy required for aromatic ring rotation in polyamides, which, in turn, results in favorable permeability-selectivity.[18] Similar relationships could likely be expected for the polyimide samples considered in this study.

In general, the APAF-6FDA polyimide had transport properties that were closer to the upper bound than the APAF-6fCl polyamide. This relative comparison in upper bound behavior is supported by results reported by Park *et al.*[2] and Han *et al.*[21] for APAF-6FDA-SS and APAF-6fCl, respectively.

Upon conversion of the precursors to their TR polymers, permeability increases for all samples considered. However, this increase in permeability was accompanied by a loss in selectivity that, in general, paralleled the upper bound. In contrast to these results, Park *et al.* showed that incrementally higher thermal treatment temperatures of APAF-6FDA-SS resulted in TR polymers with transport properties that exceeded the upper bound.[2] Interestingly, Han *et al.* later showed that precursor TR polymers prepared from different synthesis routes did not exhibit such high combinations of permeability and selectivity. Polyimides synthesized via thermal imidization in solution resulted in TR polymers with permeability and selectivity values that were further from the upper bound than TR polymers prepared from polyimides synthesized via solid-state imidization.[4] Thus, the TR polymers considered in this study may trade permeability and selectivity due to their synthesis route. Sanders *et al.* show a similar tradeoff with gas permeability and selectivity for a *hydroxyl*-functional HAB-6FDA polyimide and TR polymer that was thermally treated at 450°C for 30min.[10]

To investigate the effect of synthesis route on TR polymer transport properties, a comparison was made between HAB-6FDA and HAB-6FDA-SS polyimides and TR polymers. Table 8.3 shows the similarity in gas permeability between these samples. For the precursor polyimides, within experimental uncertainties, almost all permeabilities are identical - regardless of the synthesis route. However, upon thermal treatment, a divergence in permeabilities becomes apparent. The HAB-6FDA-SS TR polymer has permeabilities that are approximately twice as high as those of the HAB-6FDA TR polymer. Han *et al.* has reported higher gas permeabilities for APAF-6FDA-SS TR polymers relative to APAF-6FDA TR polymers, and our results corroborate this trend.[4] However, Han *et al.* showed permeabilities that were approximately 10 times higher for TR polymers prepared from solid-state imidized precursors.[4] These differences between

our HAB-6FDA results and Han *et al.*'s APAF-6FDA results likely relate to the difference in polymer structures and the difference in thermal treatments protocols (i.e., 450°C for 30 min for the samples in this study and 450°C for 60 min for the samples in Han *et al.*'s study). Finally, we did observe slightly higher combinations of permeability and selectivity for the TR polymers from HAB-6FDA-SS compared to those from HAB-6FDA; however, these differences were minor compared to the changes in permeability and selectivity based on changing polymer backbone chemistry.

Despite the APAF-6FDA and APAF-6fCl TR polymers having nearly identical structures, these polymers showed differences in transport properties for all gases considered. These differences are presumably related to the non-equilibrium nature of these materials, meta/para versus strictly para configuration for the two samples, and differences in crosslinking (cf., Chapter 4).

8.2.4 Study of conditioning and plasticization effects with hysteresis loops

In the presence of high concentrations of condensable gases such as CO_2, polymer membranes can undergo plasticization and conditioning.[25,49-51] Plasticization is often observed when polymer undergo penetrant-induced swelling, which often increases gas diffusion. Conditioning of polymer upon exposure to condensable gases also influences polymer swelling; however, this term is used to describe relatively long-lived changes in transport properties that result after removing a condensable penetrant. To separate the effects of plasticization and conditioning, permeability hysteresis curves were recorded to document the effect of CO_2 exposure on transport properties. In these experiments, CO_2 permeability is measured at increasing feed pressure followed by measurements at decreasing feed pressure. Then, the sample was repressurized with CO_2, and permeability was measured during this second pressurization step. To standardize

experiments for multiple samples of different structures, the time-lag of CO_2 was first estimated at a feed pressure of approximately 1 bar. Next, samples were held for six times this time lag for each pressurization-depressurization point and pseudo steady state permeability was determined at each pressure before proceeding to the next pressure point.

The first set of samples considered are the poly(*hydroxy*-imide)s formed from thermal imidization in solution and their corresponding TR polymers. The hysteresis loops for HAB-6FDA and APAF-6FDA are shown in Figure 8.7 and Figure 8.8, respectively. APAF-ODPA showed no plasticization pressure point and little hysteresis, similar to APAF-6FDA, whose data is included in Appendix C. For the HAB-6FDA polyimide, a plasticization pressure is observed for the first pressurization step between approximately 10 and 15 atm. Such plasticization pressures are common for polyimides, such as untreated Matrimid® (DAPI-BTDA),[52] MDA-6FDA polyimide,[53] 6FpDA-6FDA,[28] and uncrosslinked DAM:DABA-6FDA,[54] among others. One strategy explored to control plasticization is via crosslinking of the polymer, which often results in decreasing CO_2 permeability and increasing permselectivity. Conversion of the HAB-6FDA polyimide to its TR polymer results in the opposite trend. CO_2 permeability increases and permselectivity decreases. Figure 8.7B shows higher CO_2 permeability than HAB-6FDA polyimide and no plasticization pressure for the HAB-6FDA TR polymer. At the lowest pressure considered, the permeability of CO_2 has increased by over 400% for the HAB-6FDA TR polymer relative to its polyimide precursor.

Moreover, the hysteresis results show a strong conditioning effect for the polyimide, but more limited conditioning in the TR polymer. At 10 atm, CO_2 permeability is over 200% higher for HAB-6FDA polyimide upon depressurization; however, CO_2 permeability is only 20% higher for the HAB-6FDA TR polymer. Upon

re-pressurization, the polyimide has higher permeability, but the TR polymer has almost completely recovered. Within the uncertainty of the measurements, the first and second pressurization steps overlap for the TR polymer for almost every pressurization point. In contrast, permeability is consistently higher for the second pressurization step compared to the first for the precursor polyimide.

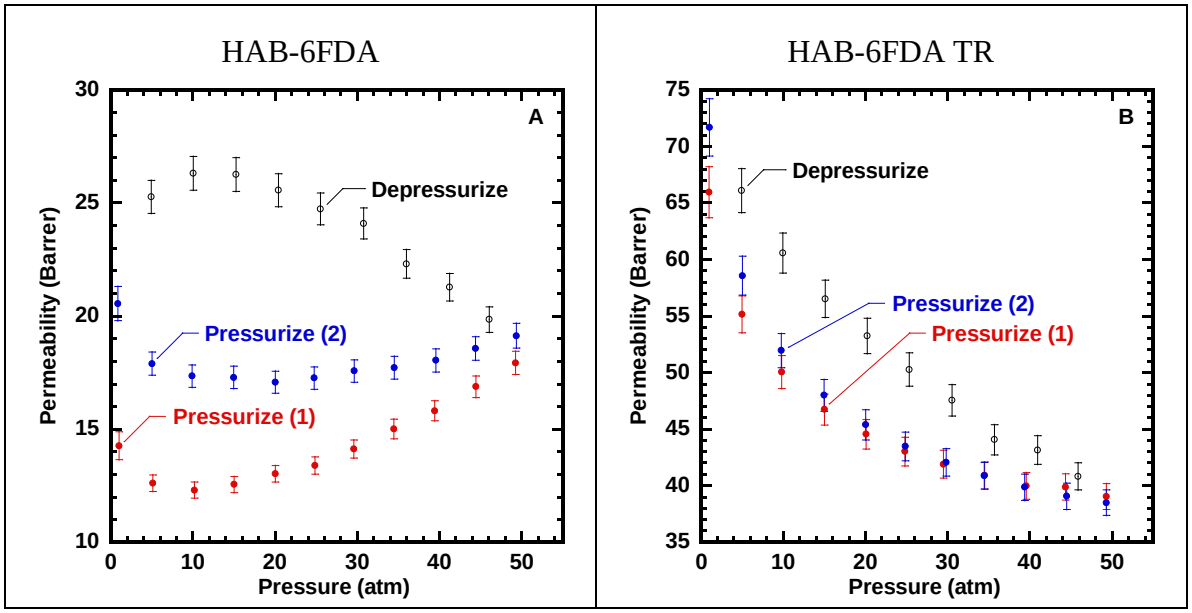

Figure 8.7: CO_2 hysteresis loops for: (A) HAB-6FDA polyimide and (B) HAB-6FDA TR polymer.

No plasticization pressure and little conditioning at feed pressures up to 50 bar are observed for TR polymers prepared from poly(*hydroxy*-imide)s. Interestingly, the APAF-6FDA and APAF-ODPA polyimides (cf., Appendix C) showed no plasticization pressure point and little hysteresis. For the APAF-ODPA polyimide, the difference in plasticization pressure response may relate to crosslinking occurring during solvent removal. The HAB-6FDA polymer had a 0% gel fraction after a three day exposure test in DMAc with a Soxhlet extractor, but the APAF-ODPA sample had a gel fraction of

49.8%. Solvent was removed from all of the poly(*hydroxy*-imide)s at 270°C, which is slightly above the T_g of APAF-ODPA (266°C) but below the T_g of the other poly(*hydroxy*-imide)s. The solvent removal temperature being above the T_g may allow sufficient chain flexibility in APAF-ODPA to induce crosslinking. Interestingly, the APAF-6FDA polyimide, which did not show a plasticization pressure, also had a 0% gel fraction like HAB-6FDA.

Nearly identical hysteresis curves were observed for the solution and solid-state thermally imidized HAB-6FDA samples. The HAB-6FDA-SS polyimide also had a 0% gel fraction, dissolving after a three day exposure test to DMAc, so it is presumably not crosslinked. The hysteresis curve for HAB-6FDA-SS is included in Appendix C.

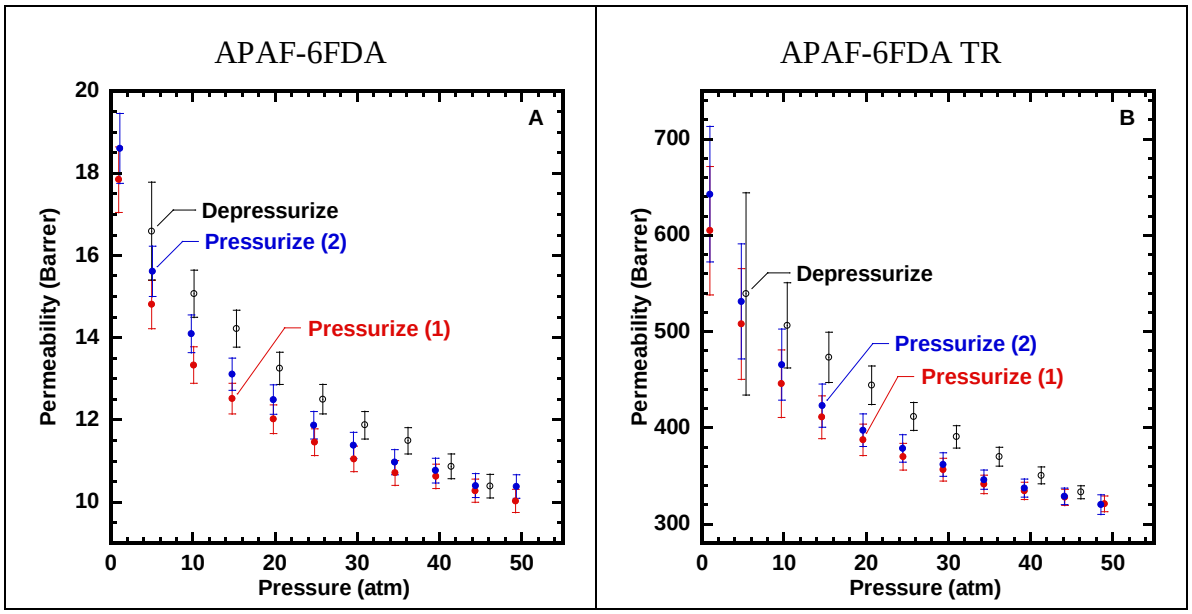

Figure 8.8: CO_2 hysteresis loops for: (A) APAF-6FDA polyimide and (B) APAF-6FDA TR polymer.

Similar to the APAF-6FDA polyimide, the APAF-6fCl polyamide hysteresis loop in Figure 8.9A shows no indication of plasticization pressure based on the lack of an

increase in permeability with increasing pressure even at the highest pressure considered. The APAF-6fCl TR hysteresis loop in Figure 8.9B did not show a plasticization pressure either, but there was a stronger hysteresis effect for this sample compared to that of its polyamide precursor. Moreover, at lower pressures, differences in permeabilities are observed between the first and second pressurization steps suggesting some plasticization. The APAF-6fCl TR polymer appears to show slight increases in CO_2/CH_4 selectivity with increasing pressure (cf., Figure 8.2), so although no plasticization pressure is observed, this sample may be undergoing some plasticization during experiments.

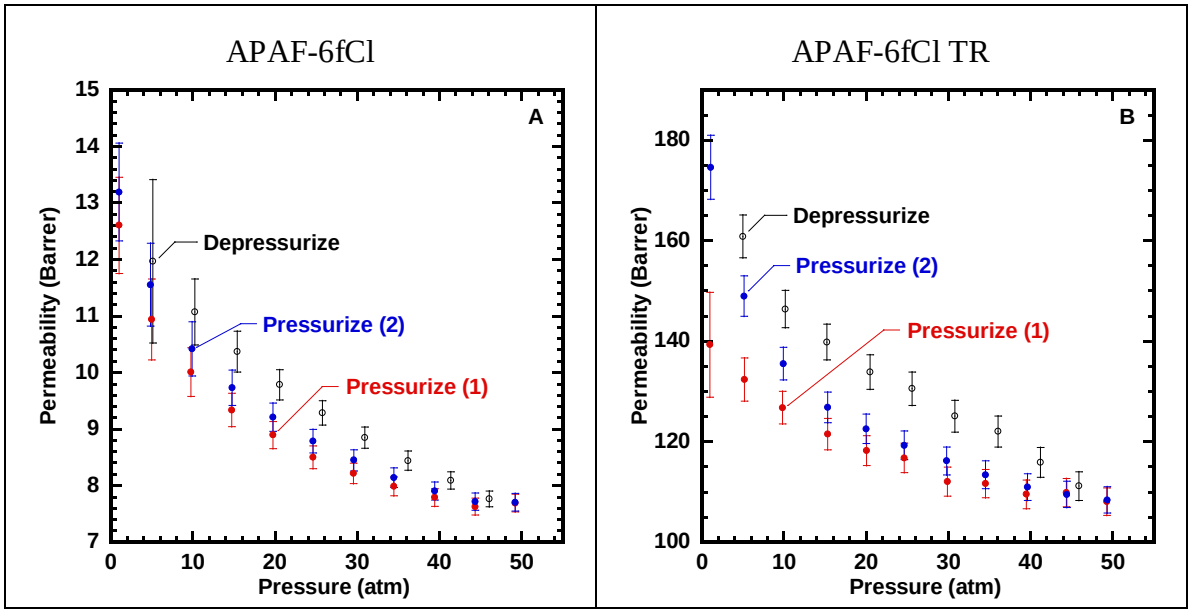

Figure 8.9: CO_2 hysteresis loops for (A) the APAF-6fCl polyamide and (B) the APAF-6fCl TR polymer.

8.2.5 Olefin-paraffin permeation properties with the APAF-6FDA TR polymer

The TR polymer with permeabilities and selectivities closest to the upper bound for light gas and CO_2 separations was also tested for light olefin and paraffin pure gas permeation properties. Permeability was determined for ethylene, ethane, propylene, and propane. To keep the history of exposure to one gas from influencing the permeation properties of the polymer to other gases, a fresh polymer film was used for each gas. To ensure samples were free of pinhole defects, prior to exposure, oxygen and nitrogen permeability coefficients were determined on each film, and measurements were undertaken with olefins and paraffins only on samples that had expected values of O_2 and N_2 permeabilities. Each gas was tested in increments of gas activity between 0.05 and the maximum activity that could be reached with our experimental setup. Each pressurization step was held for approximately 6 time lags to achieve a pseudo-steady-state permeation rate.

The ethylene and ethane permeation results are presented in Figure 8.10A and the propylene and propane results are presented in Figure 8.10B. Dual-mode behavior is observed at low activities since permeability decreases with increasing pressure. No plasticization pressure point is observed for ethylene or ethane, despite these gases having activities of approximately 0.90 and 0.95, respectively, at the highest pressures considered. At the experimental temperature considered (i.e., 35°C), ethylene and ethane are both supercritical gases, which necessitated an extrapolation of their saturation pressures to the temperature of interest to determine their gas phase activities.[55] Propylene and propane show plasticization pressure points between 3 and 4 atm. These points correspond to activity values of approximately 0.25 for propylene and 0.35 for propane. At 35°C, propylene and propane are below their critical temperature, so their saturation pressure was determined from the Wagner equation.[55]

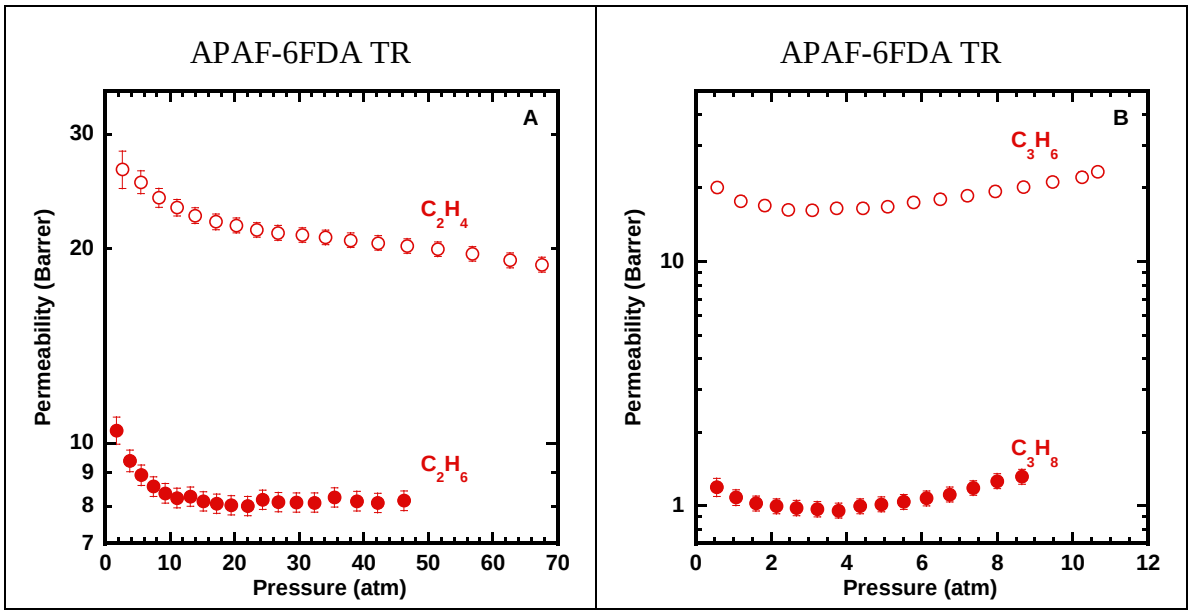

Figure 8.10: Permeability of ethylene, ethane, propylene, and propane as a function of feed pressure in APAF-6FDA TR at 35°C. Olefins are shown as open circles, and paraffins are shown as filled circles. Uncertainties were estimated as one standard deviation based on the propagation of error technique described by Bevington and Robinson.[56]

Upper bound data is presented for ethylene/ethane in Figure 8.11 and for propylene/propane in Figure 8.12. Pure gas selectivities were calculated by fitting a smooth fit to the data in Figure 8.10 and determining the ratio of permeabilities over the range of pressure considered. Therefore, the ethylene/ethane data points represent permeabilities and selectivities up to approximately 46 atm, and the propylene/propane data points represent permeabilities and selectivities up to approximately 8.5 atm. For ethylene/ethane separation, the selectivity of the APAF-6FDA TR polymer is < 3, and this data lies below the upper bound. However, for propylene/propane, the APAF-6FDA TR polymer falls above the current upper bound.

The polymer upper bound for ethylene/ethane and propylene/propane are defined by a limited number of polymers, and the polymers closest to the upper bound are 6FDA-containing polyimides.[32,57] For the ethylene/ethane gas pair, 6FDA-NDA polyimide defines the upper bound,[57] and for the propylene/propane gas pair, 6FDA-DDBT and 6FDA-TrMPD polymers define the upper bound.[32] Therefore, certain chemical structures that have upper bound separation performance for the ethylene/ethane gas pair may not have upper bound separation performance for the propylene/propane gas pair, and *vice versa*. Because olefin/paraffin selectivities are predominantly diffusion controlled, the size-sieving nature of the APAF-6FDA TR polymer may account for differences in upper bound behavior for the C_2H_4/C_2H_6 and C_3H_6/C_3H_8 gas pairs.[33]

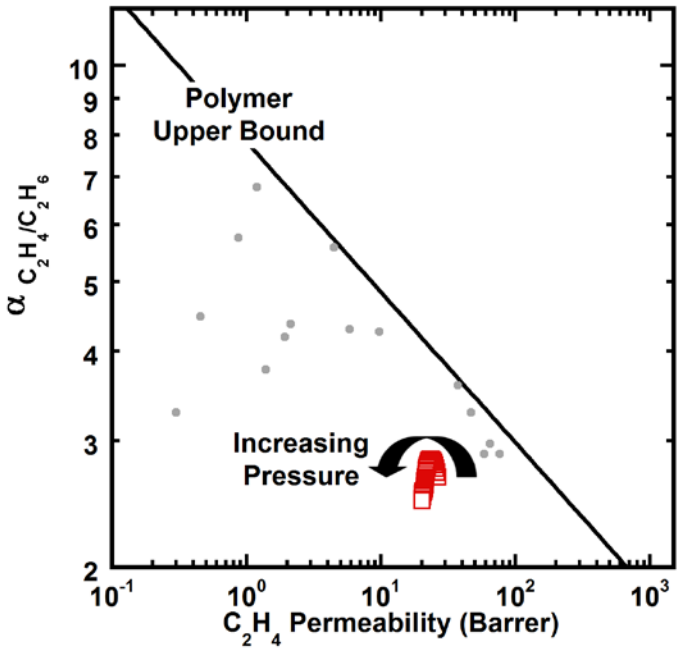

Figure 8.11: Upper bound comparison for C_2H_4/C_2H_6.[57] The APAF-6FDA TR polymer data is presented up to pressures of approximately 46 atm.

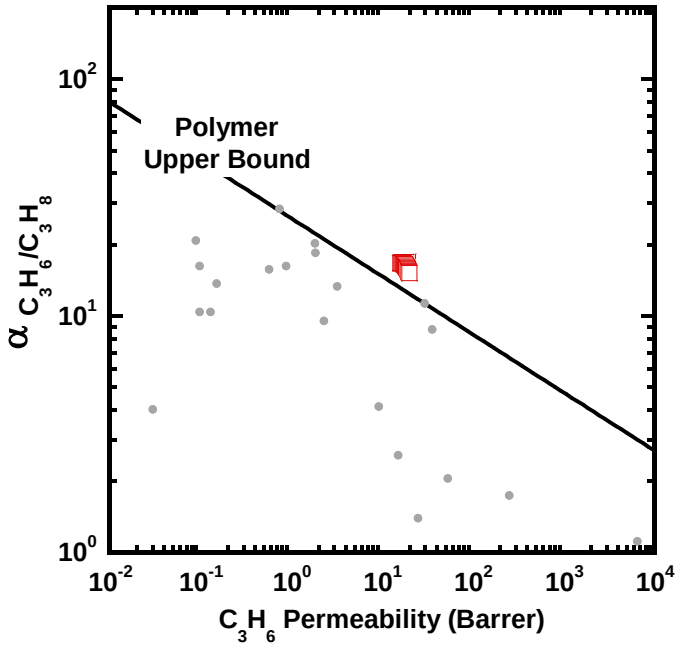

Figure 8.12: Upper bound comparison for C_3H_6/C_3H_8.[32] The APAF-6FDA TR polymer data is presented up to pressures of approximately 8.5 atm.

8.3 CONCLUSIONS

Several polyimides and a polyamide containing reactive functional groups suitable for forming thermally rearranged polymers were synthesized. These polymers include three polyimides (i.e., HAB-6FDA, APAF-6FDA, APAF-ODPA) and a polyamide (i.e., APAF-6fCl). Thermogravimetric analysis shows that the HAB-containing polymers are more reactive than those containing APAF moieties. Furthermore, the flexible ether linkage in ODPA increases the reactivity of the thermal rearrangement reaction relative to 6FDA-containing polyimides. Higher combinations of gas permeability and selectivity are observed for polyimides compared to polyamides and for polyimides containing hexafluoroisopropylidene linkages. Additionally, TR polymers formed from better performing precursors are typically closer to the upper bound, indicating that transport properties for TR polymer precursors can be used to predict the

relative performance of TR polymers. One exception to this correlation is for TR polymer precursors formed from different synthesis routes. For HAB-6FDA, TR polymers synthesized from a solid-state imidized polyimide were slightly closer to the upper bound than the sample synthesized via thermal imidization in solution. Differences in transport properties between these samples likely relates to slight differences in chemical or physical structure of the polyimide casting/imidization procedures. Plasticization and conditioning of all samples were analyzed from CO_2 permeability hysteresis curves. HAB-6FDA samples (thermally imidized in solution and in the solid-state) were the only samples to show evidence of plasticization in permeability pressures curves. Conversion of HAB-6FDA to its corresponding TR polymer resulted in increased permeability and no plasticization pressure. None of the other samples showed CO_2 plasticization pressures up to 50 bar, which may indicate plasticization resistance for several TR polymer precursors. The TR polymer formed from APAF-6FDA was tested for C_2H_4, C_2H_6, C_3H_6, and C_3H_8 permeability, and this sample showed separation performance above the polymer upper bound for propylene/propane separation. These transport results may indicate that APAF-6FDA TR polymer may have a favorable diffusion selectivity for C_3H_6/ C_3H_8, similar to other highly selective glassy polymers for this separation.

8.4 REFERENCES

1. Sanders, D.F., Z.P. Smith, R. Guo, L.M. Robeson, J.E. McGrath, D.R. Paul, and B.D. Freeman, *Energy-efficient polymeric gas separation membranes for a sustainable future: A review.* Polymer, **2013**. 54(18), 4729-4761.

2. Park, H.B., C.H. Jung, Y.M. Lee, A.J. Hill, S.J. Pas, S.T. Mudie, E. Van Wagner, B.D. Freeman, and D.J. Cookson, *Polymers with cavities tuned for fast selective transport of small molecules and ions.* Science, **2007**. 318(5848), 254-258.

3. Park, H.B., S.H. Han, C.H. Jung, Y.M. Lee, and A.J. Hill, *Thermally rearranged (TR) polymer membranes for CO_2 separation.* Journal of Membrane Science, **2010**. 359(1-2), 11-24.

4. Han, S.H., N. Misdan, S. Kim, C.M. Doherty, A.J. Hill, and Y.M. Lee, *Thermally rearranged (TR) polybenzoxazole: Effects of diverse imidization routes on physical properties and gas transport behaviors.* Macromolecules, **2010**. 43(18), 7657-7667.

5. Calle, M., Y. Chan, H.J. Jo, and Y.M. Lee, *The relationship between the chemical structure and thermal conversion temperatures of thermally rearranged (TR) polymers.* Polymer, **2012**. 53(13), 2783-2791.

6. Guo, R., D.F. Sanders, Z.P. Smith, B.D. Freeman, D.R. Paul, and J.E. McGrath, *Synthesis and characterization of thermally rearranged (TR) polymers: Effect of glass transition temperature of aromatic poly(hydroxyimide) precursors on TR process and gas permeation properties.* Journal of Materials Chemistry A, **2013**. 1(19), 6063-6072.

7. Calle, M. and Y.M. Lee, *Thermally rearranged (TR) poly(etherbenzoxazole) membranes for gas separation.* Macromolecules, **2011**. 44(5), 1156-1165.

8. Guo, R., D.F. Sanders, Z.P. Smith, B.D. Freeman, D.R. Paul, and J.E. McGrath, *Synthesis and characterization of thermally rearranged (TR) polymers: Influence of ortho-positioned functional groups of polyimide precursors on TR process and gas transport properties.* Journal of Materials Chemistry A, **2013**. 1(2), 262-272.

9. Sanders, D.F., R. Guo, Z.P. Smith, Q. Liu, K.A. Stevens, J.E. McGrath, D.R. Paul, and B.D. Freeman, *Influence of polyimide precursor synthesis route and ortho-position functional group on thermally rearranged (TR) polymer properties: Conversion and free volume.* Polymer, **2014**. 55(7), 1636-1647.

10. Sanders, D.F., R. Guo, Z.P. Smith, K.A. Stevens, Q. Liu, J.E. McGrath, D.R. Paul, and B.D. Freeman, *Influence of polyimide precursor synthesis route and ortho-position functional group on thermally rearranged (TR) polymer properties: Pure gas permeability and selectivity (in press).* Journal of Membrane Science, **2014**.

11. Tanaka, K., H. Kita, M. Okano, and K.-i. Okamoto, *Permeability and permselectivity of gases in fluorinated and non-fluorinated polyimides.* Polymer, **1992**. 33(3), 585-592.

12. Kim, T.H., W.J. Koros, G.R. Husk, and K.C. Obrien, *Relationship between gas separation properties and chemical-structure in a series of aromatic polyimides.* Journal of Membrane Science, **1988**. 37(1), 45-62.

13. Stern, S.A., Y. Mi, H. Yamamoto, and A.K.S. Clair, *Structure/permeability relationships of polyimide membranes. Applications to the separation of gas mixtures.* Journal of Polymer Science Part B: Polymer Physics, **1989**. 27(9), 1887-1909.

14. Kim, S., H.J. Jo, and Y.M. Lee, *Sorption and transport of small gas molecules in thermally rearranged (TR) polybenzoxazole membranes based on 2,2-bis(3-amino-4-hydroxyphenyl)-hexafluoropropane (bisAPAF) and 4,4'-hexafluoroisopropylidene diphthalic anhydride (6FDA).* Journal of Membrane Science, **2013**. 441, 1-8.

15. Sanders, D.F., Z.P. Smith, C.P. Ribeiro, R.L. Guo, J.E. McGrath, D.R. Paul, and B.D. Freeman, *Gas permeability, diffusivity, and free volume of thermally rearranged polymers based on 3,3 '-dihydroxy-4,4 '-diamino-biphenyl (HAB) and 2,2 '-bis-(3,4-dicarboxyphenyl) hexafluoropropane dianhydride (6FDA).* Journal of Membrane Science, **2012**. 409, 232-241.

16. Smith, Z.P., D.F. Sanders, C.P. Ribeiro Jr, R. Guo, B.D. Freeman, D.R. Paul, J.E. McGrath, and S. Swinnea, *Gas sorption and characterization of thermally rearranged polyimides based on 3,3'-dihydroxy-4,4'-diamino-biphenyl (HAB) and 2,2'-bis-(3,4-dicarboxyphenyl) hexafluoropropane dianhydride (6FDA).* Journal of Membrane Science, **2012**. 416, 558-567.

17. Aitken, C.L., J.S. McHattie, and D.R. Paul, *Dynamic mechanical-behavior of polysulfones.* Macromolecules, **1992**. 25(11), 2910-2922.

18. Espeso, J., A.E. Lozano, J.G. de la Campa, and J. de Abajo, *Effect of substituents on the permeation properties of polyamide membranes.* Journal of Membrane Science, **2006**. 280(1–2), 659-665.

19. Comer, A.C., C.P. Ribeiro, B.D. Freeman, S. Kalakkunnath, and D.S. Kalika, *Dynamic relaxation characteristics of thermally rearranged aromatic polyimides.* Polymer, **2013**. 54(2), 891-900.

20. Ribeiro, C.P., B.D. Freeman, D.S. Kalika, and S. Kalakkunnath, *Aromatic polyimide and polybenzoxazole membranes for the fractionation of aromatic/aliphatic hydrocarbons by pervaporation.* Journal of Membrane Science, **2012**. 390–391(0), 182-193.

21. Han, S., H. Kwon, K. Kim, J. Seong, C. Park, S. Kim, C.M. Doherty, A. Thornton, A.J. Hill, A. Lozano, K. Berchtold, and Y. Lee, *Tuning microcavities in thermally rearranged polymer membranes for CO_2 capture.* Physical Chemistry Chemical Physics, **2012**. 14(13), 4365-4373.

22. Kim, S. and Y. Lee, *Thermally rearranged (TR) polymer membranes with nanoengineered cavities tuned for CO_2 separation.* Journal of Nanoparticle Research, **2012**. 14(7), 1-11.

23. Wang, H., T.-S. Chung, and D.R. Paul, *Physical aging and plasticization of thick and thin films of the thermally rearranged ortho-functional polyimide 6FDA–HAB.* Journal of Membrane Science, **2014**. 458(0), 27-35.

24. Wang, H., T.-S. Chung, and D.R. Paul, *Thickness dependent thermal rearrangement of an ortho-functional polyimide.* Journal of Membrane Science, **2014**. 450(0), 308-312.

25. Bos, A., I.G.M. Punt, M. Wessling, and H. Strathmann, *CO_2-induced plasticization phenomena in glassy polymers.* Journal of Membrane Science, **1999**. 155(1), 67-78.

26. Staudt-Bickel, C. and W.J. Koros, *Olefin/paraffin gas separations with 6FDA-based polyimide membranes.* Journal of Membrane Science, **2000**. 170(2), 205-214.

27. Staudt-Bickel, C. and W.J. Koros, *Improvement of CO_2/CH_4 separation characteristics of polyimides by chemical crosslinking.* Journal of Membrane Science, **1999**. 155(1), 145–154.

28. Wind, J.D., C. Staudt-Bickel, D.R. Paul, and W.J. Koros, *The effects of crosslinking chemistry on CO_2 plasticization of polyimide gas separation membranes.* Industrial & Engineering Chemistry Research, **2002**. 41(24), 6139-6148.

29. Wind, J.D., D.R. Paul, and W.J. Koros, *Natural gas permeation in polyimide membranes.* Journal of Membrane Science, **2004**. 228(2), 227-236.

30. Kita, H., T. Inada, K. Tanaka, and K.-i. Okamoto, *Effect of photocrosslinking on permeability and permselectivity of gases through benzophenone-containing polyimide.* Journal of Membrane Science, **1994**. 87(1–2), 139-147.

31. McCaig, M.S. and D.R. Paul, *Effect of UV crosslinking and physical aging on the gas permeability of thin glassy polyarylate films.* Polymer, **1999**. 40(26), 7209-7225.

32. Burns, R.L. and W.J. Koros, *Defining the challenges for C_3H_6/C_3H_8 separation using polymeric membranes.* Journal of Membrane Science, **2003**. 211(2), 299-309.

33. Tanaka, K., A. Taguchi, J. Hao, H. Kita, and K. Okamoto, *Permeation and separation properties of polyimide membranes to olefins and paraffins.* Journal of Membrane Science, **1996**. 121(2), 197-207.

34. Smith, Z.P., R.R. Tiwari, T.M. Murphy, D.F. Sanders, K.L. Gleason, D.R. Paul, and B.D. Freeman, *Hydrogen sorption in polymers for membrane applications.* Polymer, **2013**. 54(12), 3026–3037.

35. Calle, M., A.E. Lozano, and Y.M. Lee, *Formation of thermally rearranged (TR) polybenzoxazoles: Effect of synthesis routes and polymer form.* European Polymer Journal, **2012**. 48(7), 1313-1322.

36. Tullos, G. and L. Mathias, *Unexpected thermal conversion of hydroxy-containing polyimides to polybenzoxazoles.* Polymer, **1999**. 40(12), 3463-3468.

37. Tullos, G.L., J.M. Powers, S.J. Jeskey, and L.J. Mathias, *Thermal conversion of hydroxy-containing imides to benzoxazoles: Polymer and model compound study.* Macromolecules, **1999**. 32(11), 3598-3612.

38. Choi, J.I., C.H. Jung, S.H. Han, H.B. Park, and Y.M. Lee, *Thermally rearranged (TR) poly(benzoxazole-co-pyrrolone) membranes tuned for high gas permeability and selectivity.* Journal of Membrane Science, **2010**. 349(1-2), 358-368.

39. Han, S.H., J.E. Lee, K.-J. Lee, H.B. Park, and Y.M. Lee, *Highly gas permeable and microporous polybenzimidazole membrane by thermal rearrangement.* Journal of Membrane Science, **2010**. 357(1-2), 143-151.

40. Jung, C.H., J.E. Lee, S.H. Han, H.B. Park, and Y.M. Lee, *Highly permeable and selective poly(benzoxazole-co-imide) membranes for gas separation.* Journal of Membrane Science, **2010**. 350(1-2), 301-309.

41. Li, S., H.J. Jo, S.H. Han, C.H. Park, S. Kim, P.M. Budd, and Y.M. Lee, *Mechanically robust thermally rearranged (TR) polymer membranes with spirobisindane for gas separation.* Journal of Membrane Science, **2013**. 434, 137-147.

42. Wang, H., D.R. Paul, and T.-S. Chung, *The effect of purge environment on thermal rearrangement of ortho-functional polyamide and polyimide.* Polymer, **2013**. 54(9), 2324-2334.

43. Muñoz, D.M., M. Calle, J.G. de la Campa, J. de Abajo, and A.E. Lozano, *An improved method for preparing very high molecular weight polyimides.* Macromolecules, **2009**. 42(15), 5892-5894.

44. Robeson, L.M., *The upper bound revisited.* Journal of Membrane Science, **2008**. 320(1-2), 390-400.

45. Matteucci, S.T., Y.P. Yampolskii, B.D. Freeman, and I. Pinnau, *Transport of gases and vapors in glassy and rubbery polymers,* in *Materials science of membranes for gas and vapor separation*, Y. Yampolskii, I. Pinnau, and B.D. Freeman, Editors. **2006**, John Wiley & Sons: Chichester. 1-47.

46. Robeson, L.M., Z.P. Smith, B.D. Freeman, and D.R. Paul, *Contributions of diffusion and solubility selectivity to the upper bound analysis for glassy gas separation membranes.* Journal of Membrane Science, **2014**. 453, 71-83.

47. Posey, L.G. *Processes*, **1983**, US 4367135.

48. Shimazu, A., T. Miyazaki, M. Maeda, and K. Ikeda, *Relationships between the chemical structures and the solubility, diffusivity, and permselectivity of propylene and propane in 6FDA-based polyimides.* Journal of Polymer Science Part B: Polymer Physics, **2000**. 38(19), 2525-2536.

49. Puleo, A.C., D.R. Paul, and S.S. Kelley, *The effect of degree of acetylation on gas sorption and transport behavior in cellulose acetate.* Journal of Membrane Science, **1989**. 47(3), 301-332.

50. Ismail, A.F. and W. Lorna, *Penetrant-induced plasticization phenomenon in glassy polymers for gas separation membrane.* Separation and Purification Technology, **2002**. 27(3), 173-194.

51. Wonders, A.G. and D.R. Paul, *Effect of CO_2 exposure history on sorption and transport in polycarbonate.* Journal of Membrane Science, **1979**. 5(0), 63-75.

52. Bos, A., I.G.M. Pünt, M. Wessling, and H. Strathmann, *Plasticization-resistant glassy polyimide membranes for CO_2/CO_4 separations.* Separation and Purification Technology, **1998**. 14(1–3), 27-39.

53. Wessling, M., I. Huisman, T.v.d. Boomgaard, and C.A. Smolders, *Time-dependent permeation of carbon dioxide through a polyimide membrane above the plasticization pressure.* Journal of Applied Polymer Science, **1995**. 58(11), 1959-1966.

54. Wind, J.D., C. Staudt-Bickel, D.R. Paul, and W.J. Koros, *Solid-state covalent cross-linking of polyimide membranes for carbon dioxide plasticization reduction.* Macromolecules, **2003**. 36(6), 1882-1888.

55. Poling, B.E., J.M. Prausnitz, and J.P. O'Connell, *The properties of gases and liquids*. **2001**, McGraw Hill Book Co., New York, NY. A.5-A.19.

56. Bevington, P.R. and K.D. Robinson, *Data reduction and error analysis for the physical sciences: Third edition*. **2003**, Boston, McGraw Hill.

57. Rungta, M., C. Zhang, W.J. Koros, and L. Xu, *Membrane-based ethylene/ethane separation: The upper bound and beyond.* AIChE Journal, **2013**. 59(9), 3475-3489.

Chapter 9: Contributions of Diffusion and Solubility Selectivity to the Upper Bound Analysis for Glassy Gas Separation Membranes

Prior analyses of the upper bound of permselectivity versus permeability, both theoretical and empirical, have assumed that this relationship is a consequence of the dependence of gas diffusion coefficients on the molecular diameter of the gases of interest. The solubility selectivity has been assumed to be invariant with permeability (and free volume). However, a few literature sources note that the solubility coefficient for specific families of glassy polymers correlate with free volume. A large database of permeability, diffusivity and solubility data for glassy polymers was compiled to investigate this hypothesis. A critical analysis of the data demonstrates a modest solubility selectivity contribution to permselectivity as a function of free volume and, thus, permeability. The solubility selectivity (S_i/S_j) generally decreases with increasing permeability (and free volume) when the diameter of gas j is larger than that of gas i. This empirical trend is likely a consequence of larger gas molecules having less access than smaller molecules to sorption sites as the polymer packing density increases and free volume decreases. The diffusion data permit the determination of a diffusivity upper bound, which is modestly different from the permeability-based upper bound relationship. The diffusion data analysis allows a determination of a new set of gas diameters more appropriate to gas diffusion in polymers than prior correlations.

9.1 INTRODUCTION

The separation of gases by polymeric membranes has been an active area of research and industrial use for several decades.[1] In 1979, Monsanto (now Permea, owned

---

This chapter has been adapted with permission from: Robeson, L.M., Z.P. Smith, B.D. Freeman, and D.R. Paul, *Contributions of diffusion and solubility selectivity to the upper bound analysis for glassy gas separation membranes.* Journal of Membrane Science, **2014**. 453, 71-83.

by Air Products and Chemicals, Inc.) developed the first commercial asymmetric hollow fiber membrane module for gas separation; the fiber was based on polysulfone, and the first application was for hydrogen recovery (H_2/N_2) in the ammonia synthesis process.[2-6] Polymer membranes have since been commercialized for separating a number of other common gas pairs such as O_2/N_2, CO_2/CH_4, H_2/CH_4, He/air, and for the dehydration of air and natural gas.[2] In general, polymer membrane research focuses on identifying materials with high combinations of permeability and permselectivity. Permselectivity is defined as the ratio of the permeability coefficient of the faster permeating gas, i, to that of the slower permeating gas, j (i.e., P_i/P_j). However, there is a trade-off between P_i/P_j and P_i.[7-11] A large body of experimental evidence empirically suggests an upper bound to this trade-off relationship having the following mathematical form[12]

$$P_i = k_{up}\alpha_{ij(u)}^{n_{up}} \text{ where } \alpha_{ij(u)} = P_i / P_j \tag{9.1}$$

On a log-log plot of $\alpha_{ij(u)}$ versus P_i, polymers with the highest separation efficiency and highest gas throughput are bounded by a linear relationship given by Equation (9.1) that is commonly referred to as the "upper bound". There are virtually no data above this line. This empirical upper bound has been predicted from fundamental principles as will be discussed later.[13] Between 1991 and 2008, as more permeability data became available, modest shifts in the empirical upper bound became apparent for several gas pairs.[14] Correlating permeability data of P_i versus P_j allowed a refinement in the estimation of the kinetic diameters of He, H_2, O_2, N_2, CO_2, and CH_4.[15] Correlations of P_i versus P_j with free volume[16,17] and activation energies of permeation and diffusion[18] have been noted in the literature. Furthermore, the effect of temperature on the upper bound was recently predicted and showed good agreement with the limited data

available.[19] Group contribution approaches have also been employed for predicting gas permeability and permselectivity from information on polymer structure.[20-22]

As noted, two different fundamental approaches have been employed to describe permeability and permselectivity behavior. The approach of Freeman[13] combined fundamental principles involving transition state theory for diffusion and thermodynamic relationships for solubility to predict the upper bound values of n_{up} and k_{up}. The approach by Alentiev and Yampolskii[16,17] involved free volume models applied to diffusion and permeability for gas/polymer systems. The connection between the activated state and free volume theories of diffusion was provided by Prabhakar *et al.*[23] It is well established that diffusion coefficients are related to free volume, and to a lesser extent solubility coefficients are affected by free volume; as a result, permeability coefficients are often strongly correlated with free volume.[20,24-31] Consequently, although the derived parameters from these two approaches have different physical meanings, the general form of the equations is equivalent.

Correlations showing the separate effects of diffusion and solubility coefficients on the relationship between permselectivity and permeability are more limited. A significant amount of data from the literature have been summarized by Yampolskii and Alentiev,[16,17] who employed an extensive database of P, D, and S data on various polymers for the gases of interest.

In the expression

$$\frac{P_i}{P_j} = \frac{D_i}{D_j}\frac{S_i}{S_j} \tag{9.2}$$

for a specific gas pair, the permselectivity (i.e., P_i/P_j) has diffusion (i.e., D_i/D_j) and solubility (i.e., S_i/S_j) selectivity components. It is generally assumed that as P_i (and free volume) decreases, the increase in permselectivity is due to increases in diffusion selectivity, and solubility selectivity remains invariant with P_i (and free volume); thus, the permeability upper bound relationship is controlled by diffusion selectivity.[12-14] This assumption is inherent in the upper bound theory, which embodies solubility coefficients in the constant k_{up} in Equation (9.1). The determination of gas kinetic diameters from upper bound data[32] and from permeability data[15] assumed no changes in the solubility selectivity as P_i varied.

The assumption that solubility is independent of free volume in the upper bound analysis needs to be critically addressed. In most cases, literature data show the diffusion coefficient of CO_2 to be lower than that of O_2 even though the kinetic diameter of CO_2 and O_2 are quite similar from the upper bound[32] and the permeability correlations.[15] Additionally, kinetic diameters determined from zeolites[33] show CO_2 to have a smaller diameter than O_2. If the solubility coefficient is a function of free volume, which is consistent with several correlations noted in the literature,[28,34-36] an accurate description of k_{up} must include this dependency. This chapter demonstrates that solubility selectivity (i.e., S_i/S_j) and the solubility coefficients (i.e., S_i) both vary with permeability (and, thus, free volume), leading to a solubility selectivity contribution to permselectivity. The extent of this contribution changes for each gas pair considered. Correlations in the literature for permeability, diffusivity and solubility often employ fractional free volume. In this paper, we treat free volume and fractional free volume trends as qualitatively equivalent.

9.2 CORRELATIONS OF DIFFUSION COEFFICIENTS

The database for diffusion coefficients employed in this analysis only includes glassy polymers and comprises many of the literature references employed for prior permeability[15] and permselectivity[14] correlations as well as including more recent references. The selection of data follows a similar protocol previously employed; namely, data were selected in the range of 25-35°C from polymers tested in the same laboratory and for gases tested on the same film. The database also included solubility coefficients along with permeability coefficients. Perfluorinated glassy polymers were not included due to their unique gas solubility versus other polymers. The vast majority of the data from the literature determined D from time-lag measurements and calculated S from the relationship P = DS. In a few cases, S was determined directly from sorption measurements, and D was calculated from P = DS. For a given pressure, the effective diffusion coefficients for glassy polymers will have slightly different values depending on whether they were determined from time-lag measurements or from D = P/S.[37] A detailed discussion of these differences for polysulfone and a polymer of intrinsic microporosity (PIM-1) is included in the Appendix D to illustrate the range of possibilities. The database includes over 800 different polymers from over 200 references. The database is not as large as previously noted for the permeability correlations since many papers only report permeability results. Data were compiled for 15 gas pairs involving He, H_2, O_2, N_2, CO_2 and CH_4.

The data are analyzed using the following basic equation

$$D_j = k_d D_i^{n_d} \tag{9.3}$$

where i and j are chosen such that $n_d > 1$. The data are presented on log-log plots where D_i(y-axis) and D_j(x-axis) yield the following equation

$$\log D_i = -\frac{\log k_d}{n_d} + \frac{\log D_j}{n_d} \tag{9.4}$$

When plotted as D_i(x-axis) and D_j(y-axis), the relevant equation is

$$\log D_j = \log k_d + n_d \log D_i \tag{9.5}$$

Standard least squares fits to both Equation (9.4) and Equation (9.5) were made. If there is limited scatter in the data, similar results would be obtained from both equations; however, these results will differ more significantly when there is more scatter in the data. The previously published permeability correlation[15] had limited scatter in the data, and a visual fit was employed. A review of the visual fit to the permeability data showed that the average of the log k and n values from Equation (9.4) and Equation (9.5) gave virtually the same results as the reported visual fit to the data. Since there is significantly more scatter in the diffusion data for some gas pairs, a visual fit was not realistic; thus, the analysis protocol employed the average of the values obtained by the two methods.

Glassy polymers exhibit dual-mode sorption behavior, which is characterized by sorption isotherms that are concave to the pressure axis; this curvature is more pronounced for gases with high condensability.[38,39] Therefore, a pressure dependency on the values of D and S arises when the sorption and permeation behavior exhibits this dual-mode behavior. The literature values of D and S in our database involve some variation in the pressures used for measurement of P, D or S. While these variations will

be expected to yield quantitative differences in our analysis, the qualitative trends are not believed to be significantly affected by dual-mode effects. However, to illustrate the magnitude of the possible effects, an analysis of the pressure dependency on gas sorption and diffusion for polysulfone and PIM-1 is included in Appendix D.

Examples of plots of diffusion coefficient data for several gas pairs are illustrated in Figure 9.1 through Figure 9.3. For gas pairs involving He or H_2, the data show considerable scatter. This is partly due to limited data relative to the other gas pairs but primarily due to the larger experimental error involved with accurately determining very short time-lag values.[40] Table 9.1 includes values of n_d from Equation (9.4) and Equation (9.5), the average n_d values, the n_p values from the permeability correlation using this database, which employs P instead of D (i.e., $P_j = k_p P_i^{n_p}$), and the n_p values from the previously employed database.[15] The correlation of n_p values from this database agree well with the much larger database used previously. Figure 9.4 presents the correlation between the values of n_d from diffusion data and the values of n_p from permeability data. The correlation for gas pairs not containing CO_2 is quite good except that the correlation line shows values of n_d from diffusion data to be uniformly higher than that of the permeability data, which is not expected. Note that the permeability database[15] primarily consisted of glassy polymers although it did include several crystalline polymers, liquid crystalline polymers, and some rubbery polymers as well as perfluorinated polymers. Interestingly, where CO_2 is the j gas in the D_i/D_j pair, the n_d values are all above the n_p data. Conversely, where CO_2 is the i gas in the D_i/D_j pair, the n_d values are all below the n_p data.

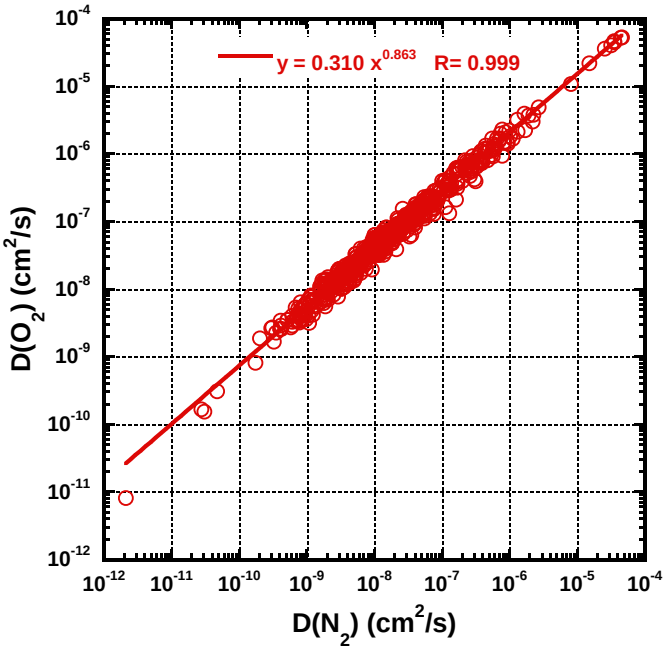

Figure 9.1: Correlation of O_2 and N_2 diffusion coefficient data. Line shown is the least squares fit to Equation (9.4).

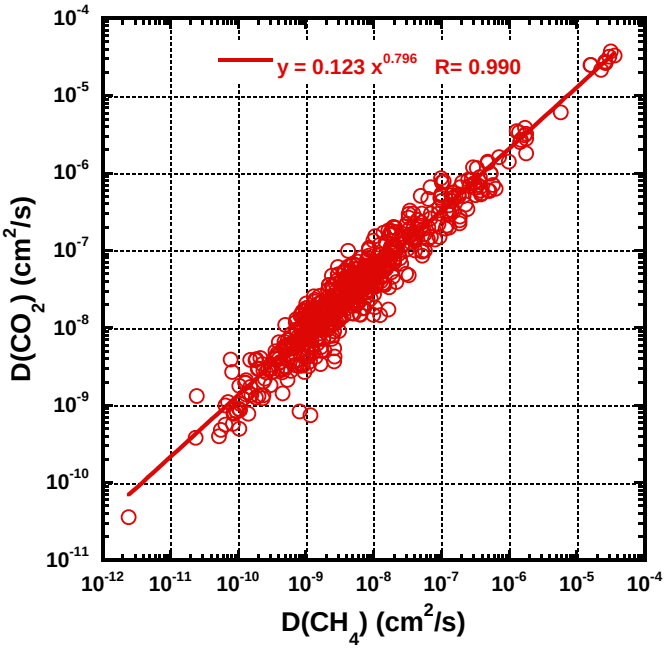

Figure 9.2: Correlation of CO_2 and CH_4 diffusion coefficient data. Line shown is the least squares fit to Equation (9.4).

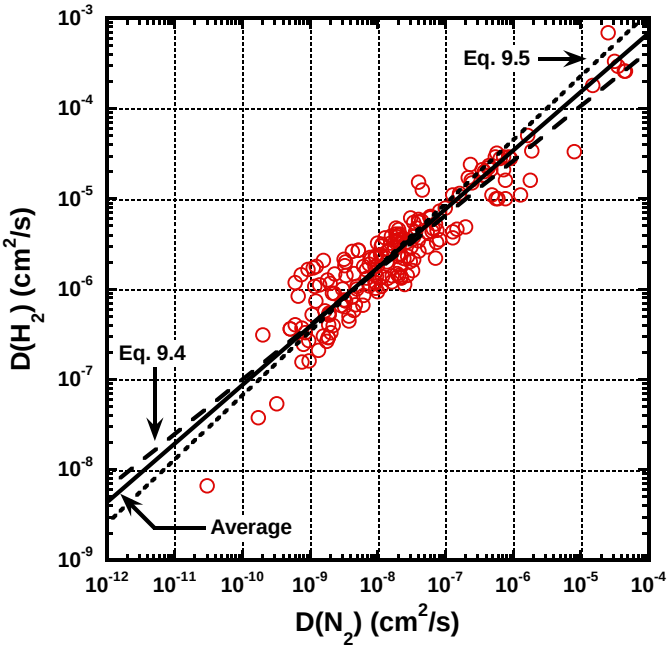

Figure 9.3: Correlation of H_2 and N_2 diffusion coefficient data.

Gas Pair	n_d from Equation (9.4)	n_d from Equation (9.5)	Average n_d	Permeability Correlation, n_p (Previous Database)[a, b]	Permeability Correlation, n_p (This Database)[b]
O_2/N_2	1.16	1.14	1.15	1.16	1.12
H_2/N_2	1.66	1.41	1.55	1.52	1.48
He/N_2	2.09	1.64	1.87	1.83	1.77
H_2/CH_4	2.01	1.71	1.86	1.75	1.68
He/H_2	1.21	1.10	1.16	1.16	1.19
He/CH_4	2.83	1.83	2.33	2.13	2.03
N_2/CH_4	1.18	1.14	1.16	1.14	1.12
He/O_2	1.71	1.43	1.57	1.59	1.62
H_2/O_2	1.41	1.24	1.33	1.33	1.29
O_2/CH_4	1.39	1.31	1.35	1.31	1.26
CO_2/CH_4	1.26	1.17	1.21	1.30	1.23
CO_2/N_2	1.09	1.02	1.05	1.12	1.10
He/CO_2	2.08	1.48	1.78	1.60	1.71
H_2/CO_2	1.76	1.48	1.62	1.35	1.37
O_2/CO_2	1.14	1.07	1.10	0.983	1.03

(a) reference [15]; (b) permeability correlation from $P_j = k_p P_i^{n_p}$

Table 9.1: Values of n_d and n_p determined from the permeability and diffusion coefficient databases.

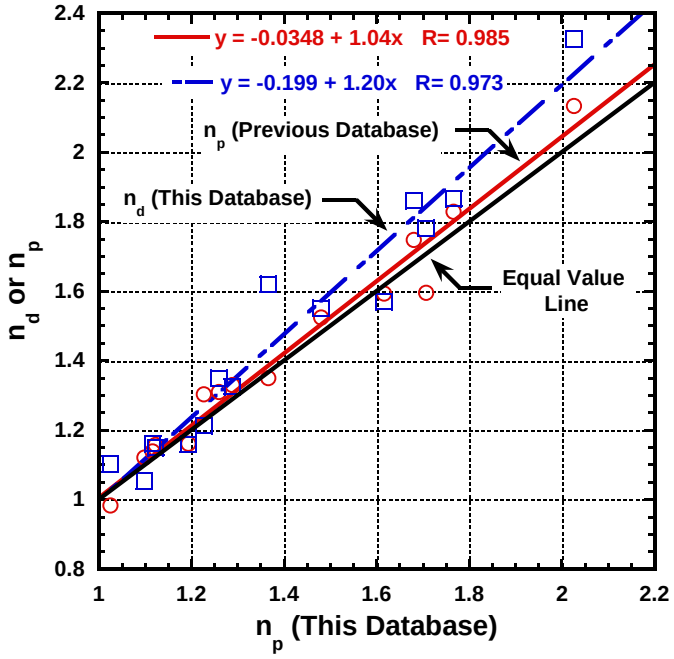

Figure 9.4: Data from Table 9.1 comparing n_d and n_p values. See Equation (9.3) and Table 9.1 for definitions of these terms. The coefficients labeled n_p (Previous Database), which were taken from the permeability database in Ref. 15, are based primarily on glassy polymers, but the database also contains several crystalline polymers, liquid crystalline polymers, some rubbery polymers, and perfluoropolymers. As shown by the equal value line, the coefficients labeled n_p (Previous Database) match closely with the n_p coefficients from this study. The coefficients labeled n_d (This Database) are consistently higher than the coefficients labeled n_p.

The theory and experimental data indicate a relationship between diffusion coefficients and the square of the gas diameters. The kinetic diameter, σ_k, determined from zeolite measurements[33] and the Lennard-Jones collision diameter, σ_c,[41] are often employed in this correlation. Shieh and Chung[41] noted that CO_2 showed poor correlation with these values and proposed an effective gas diameter defined as $\sigma_{eff} = \sqrt{\sigma_k \sigma_c}$, which yielded an excellent correlation for all gases including CO_2. More recently, Dal-Cin *et al.* calculated gas diameters based on upper bound data, σ_{DC},[32] and Robeson *et al.* calculated gas diameters based on permeability correlations using a large permeability

database, σ_{PC}.[15] Analogous to our previous permeability correlation,[15] gas diameters have also been determined from the diffusion database for this study, σ_D, and a discussion of these calculations will follow. The values for these diameters are listed in Table 9.2.

Gas	σ_k, Å	σ_c, Å	σ_{eff}, Å	σ_{DC}, Å	σ_{PC}, Å	σ_D, Å
He	2.60	2.58	2.59	2.555	2.644	2.55 ± 0.10
H_2	2.89	2.92	2.90	2.854	2.875	2.77 ± 0.08
O_2	3.46	3.43	3.44	3.374	3.347	3.23 ± 0.02
N_2	3.64	3.68	3.66	3.588	3.568	3.49 ± 0.02
CO_2	3.30	4.00	3.63	3.427	3.325	3.44 ± 0.06
CH_4	3.80	3.82	3.81	3.882	3.817	3.817

σ_k = kinetic diameter [33], σ_c = collision diameter [41], σ_{eff} = effective diameter [41],
σ_{DC} = Dal-Cin *et al.* correlation diameter [32], σ_{PC} = permeability correlation diameter [15], σ_D = diffusion correlation diameter

Table 9.2: Gas diameters determined from various techniques.

Using the data in Table 9.2, values of $\left(\frac{d_j}{d_i}\right)^2 - 1$ were calculated and compared with values of $(n_d - 1)$ in σk = kinetic diameter [33,] σc = collision diameter [41,] σeff = effective diameter [41,]
σDC = Dal-Cin *et al.* correlation diameter [32,] σPC = permeability correlation diameter [15,] σD = diffusion correlation diameter

Table 9.3. These terms are predicted to be equivalent according to the Freeman theory.[13] The results are shown in Figure 9.5 for the three best correlations. Both the Dal-Cin and effective diameter predictions yield slopes close to unity although there is considerable scatter in the data. Diameters from the permeability correlation give a value for the slope that is less than unity, as expected from the results shown in Figure 9.4.

Gas Pair	σ_k	σ_c	σ_{eff}	σ_{DC}	σ_{PC}	σ_D	$(n_d - 1)$
O_2/N_2	0.107	0.151	0.132	0.131	0.136	0.167	0.151
H_2/N_2	0.586	0.588	0.593	0.581	0.540	0.587	0.551
He/N_2	0.960	1.03	0.997	0.972	0.821	0.873	0.866
H_2/CH_4	0.729	0.711	0.726	0.850	0.763	0.899	0.861
He/H_2	0.236	0.281	0.254	0.245	0.182	0.180	0.158
He/CH_4	1.14	1.19	1.16	1.31	1.08	1.24	1.33
N_2/CH_4	0.0898	0.0775	0.0836	0.171	0.144	0.196	0.162
He/O_2	0.771	0.768	0.764	0.744	0.603	0.604	0.570
H_2/O_2	0.433	0.378	0.407	0.398	0.355	0.360	0.326
O_2/CH_4	0.206	0.240	0.227	0.324	0.301	0.396	0.349
CO_2/CH_4	0.326	-0.0880	0.102	0.283	0.318	0.231	0.214
CO_2/N_2	0.217	-0.154	0.0166	0.0962	0.152	0.0293	0.0531
He/CO_2	0.611	1.40	0.964	0.799	0.582	0.820	0.781
H_2/CO_2	0.304	0.877	0.567	0.442	0.338	0.542	0.621
O_2/CO_2	-0.0903	0.360	0.114	0.0317	-0.0131	0.134	0.102

σ_k = kinetic diameter [33], σ_c = collision diameter [41], σ_{eff} = effective diameter [41], σ_{DC} = Dal-Cin *et al.* correlation diameter [32], σ_{PC} = permeability correlation diameter [15], σ_D = diffusion correlation diameter

Table 9.3: Values of $\left(\frac{d_j}{d_i}\right)^2 - 1$ from Table 9.2 compared with values of $(n_d - 1)$.

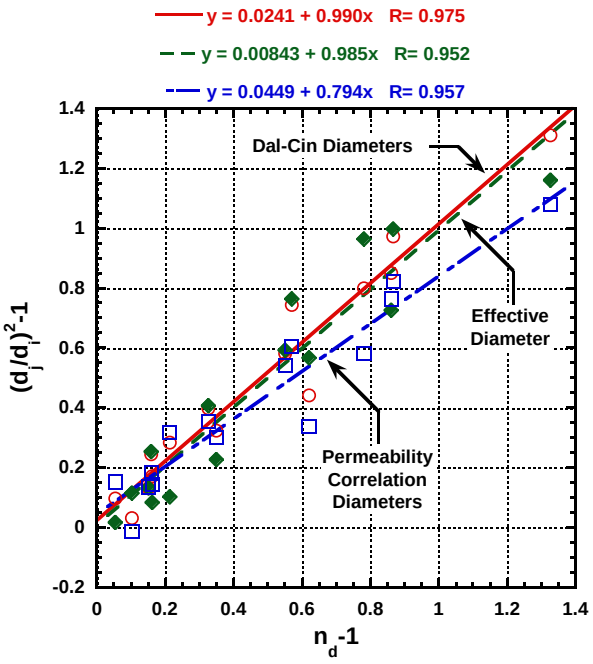

Figure 9.5: Correlation of n_d-1 with the values of $\left(\frac{d_j}{d_i}\right)^2 - 1$ from Table 9.3.

The values of the gas diameters of CO_2 in Table 9.2 appear to be inconsistent with diffusion data except in the case of the effective gas diameter, σ_{eff}, the Dal-Cin diameter, σ_{DC}, and the diffusion database for this study, σ_D. The comparison of $D(O_2)$ versus $D(CO_2)$ shown in Figure 9.6 illustrates that virtually all the diffusion coefficients for O_2 are higher than those for CO_2. Thus, the effective CO_2 gas diameter is clearly larger than that of O_2. The permeability correlations from this paper and the previous correlation[15] show the gas diameter values to be virtually the same. This result is a consequence of a modest solubility selectivity contribution to permeability as free volume changes from one polymer to another.

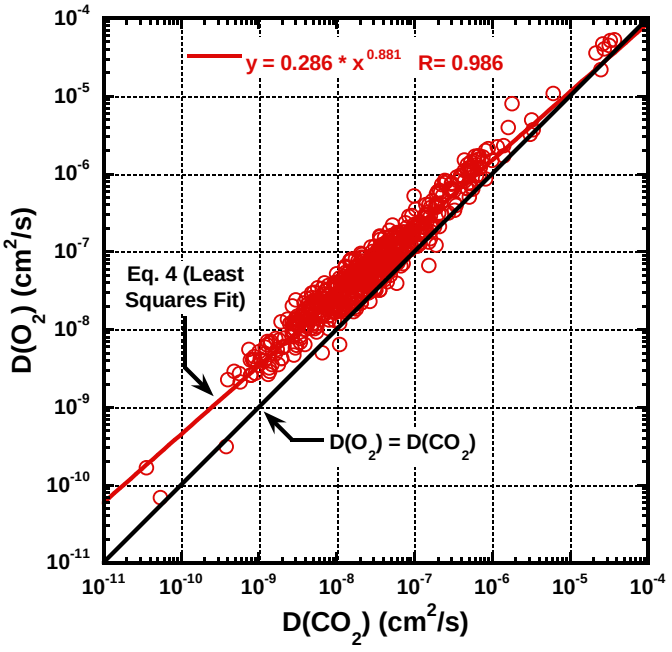

Figure 9.6: Correlation of O_2 and CO_2 diffusion coefficient data. Line noted is least squares fit of Equation (9.4).

Gas diameters were determined from diffusion correlations analogous to the method used for permeability correlations.[15] An average value of n_d was determined by fitting Equation (9.4) and Equation (9.5) to the database of diffusion coefficients. By assuming that one gas diameter is known, the diameters of the other gases can be determined from Equation (9.6) using a least squares minimization technique.

$$\left(n_d - 1\right) = \left(\frac{d_j}{d_i}\right)^2 - 1 \tag{9.6}$$

For this analysis, the diameter of CH_4 was fixed at 3.817Å, and the diameters of He, H_2, O_2, CO_2, and N_2 were calculated. Our reason for fixing the diameter of CH_4 is

that this molecule is nearly spherical, and there is little variation in reported diameters for CH_4 in the literature.[15]

Figure 9.7 shows the correlation between $(n_d - 1)$ and $\left(\frac{d_j}{d_i}\right)^2 - 1$. The line of best fit, which was forced through the origin, is $(n_d - 1) = 0.997\left[\left(\frac{d_j}{d_i}\right)^2 - 1\right]$. Single prediction error bands, which are shown in gray, are used to visually demonstrate the goodness of fit. The bands shown by the long, dashed lines represent a confidence interval of 68%, and bands shown by the short dashes indicate a confidence interval of 95%.

A list of calculated gas diameters is presented in Table 9.2. These diameters represent the best fit to d_j and d_i as calculated from Equation (9.6). Uncertainties were determined by varying chi squared values near their minimum for each gas diameter.[42] Each uncertainty listed in Table 9.2 represents one standard deviation.

The largest uncertainties in gas diameter are for He and H_2. These gases have higher diffusion coefficients and lower gas solubility coefficients compared to the other gases listed in Table 9.2; therefore, it is reasonable to expect that there is more inherent error associated with determining diffusion coefficients for these gases. The larger error for He and H_2 gas diameters can be observed in Figure 9.7, where the largest error bars are always associated with gas pairs containing He, H_2, or both gases.

Additionally, the relative size of gas diameters can be compared to those reported from other correlations. For this analysis, gas diameters increase in the following order: He < H_2 < O_2 < CO_2 < N_2 < CH_4. This order is identical to that reported for Dal-Cin and effective gas diameters,[32,41] but differs slightly from the order reported for collision, kinetic, and permeability correlation diameters.[15,33,41] Breck diameters and permeability

correlated diameters report O_2 to have a slightly larger gas diameter than CO_2. For this analysis, the diameter of CO_2 was found to be between that of O_2 and N_2.

It should be noted that the "effective" gas diameters calculated in this study represent the average molecular cross-section for gases in glassy polymers. For non-spherical molecules (e.g., H_2, O_2, N_2, CO_2, etc.), effective gas diameters would likely be influenced by the free volume distribution of their polymer media; as this distribution narrows, the smallest cross-section of a non-spherical molecule becomes the dominant dimension that relates to gas transport. The extreme case for this effect would come from molecular sieves such as zeolites where the smallest cross-section of the molecule is dominant in transport correlations.

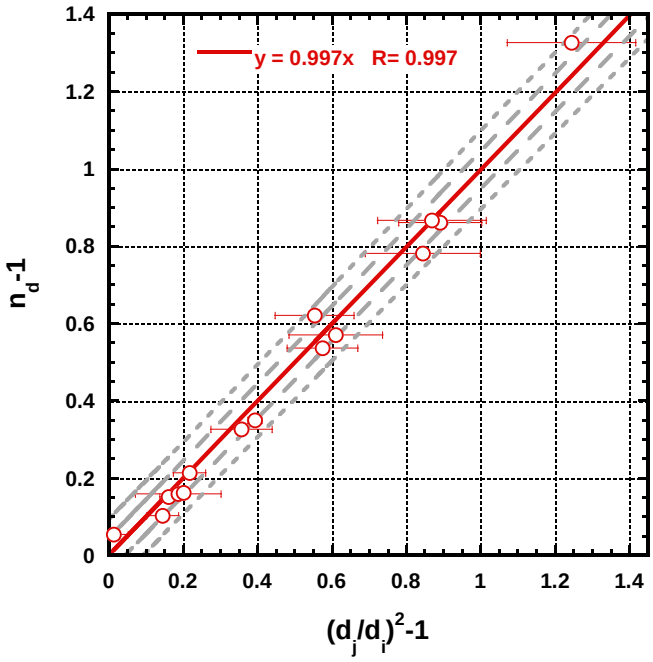

Figure 9.7: Determining gas diameters by minimizing error in Equation (9.6). Data for $n_d - 1$ are from Table 9.3, d_{CH_4} is fixed at 3.817Å, and values of d_i and d_j are allowed to vary to minimize the sum of squares. The solid, red line shows the best fit to the data (y = 0.997x), the long, dashed, gray lines show a single prediction band with confidence intervals of 68%, and the short, dashed, gray lines show the single prediction band with confidence intervals of 95%. Uncertainties represent one standard deviation.

9.3 CORRELATIONS OF THE PARAMETER K_D

The values of the parameter k_d, defined by Equation (9.3) were determined using the averaged values from Equation (9.4) and Equation (9.5) that are listed in Table 9.1. The Freeman theory[13] allows for a prediction of k_d from the following relationship:

$$\ln \alpha_{ij} = \ln \frac{D_i}{D_j} + \ln \frac{S_i}{S_j} = -\lambda_{ij} \ln D_i + \left[\ln \frac{S_i}{S_j} - \lambda_{ij} \left(b - f \frac{1-a}{RT} \right) \right] \tag{9.7}$$

where b = 11.5 cm^2/s for glassy polymers, a has a universal value of 0.64, T is chosen to be 308 K and f is considered an adjustable parameter. Values of f from the upper bound theory and the permeability correlation study were both found to be 12,600 cal/mol. Furthermore, $\lambda_{ij} = \left(\frac{d_j}{d_i}\right)^2 - 1$, where d is the gas diameter of gas i or gas j. Rearranging Equation (9.7) in terms of ln D_j yields

$$\ln D_j = (1+\lambda_{ij}) \ln D_i + \lambda_{ij}(b - f\frac{1-a}{RT}) \tag{9.8}$$

This equation can be recast in the form of Equation (9.3) to obtain

$$D_j = \exp(\lambda_{ij}(b - f\frac{1-a}{RT}))D_i^{1+\lambda_{ij}} \tag{9.9}$$

where the coefficients from Equation (9.3), n_d and k_d, are written as follows

$$n_d = 1+\lambda_{ij} \text{ and } k_d = \exp\left[(n_d - 1)\left(b - f\frac{1-a}{RT}\right)\right] \tag{9.10}$$

Although current theory predicts that $n_d = n_p$, empirical evidence suggests that this equality is not completely valid (i.e., $n_d \neq n_p$). Comparisons of predicted values and experimental values are listed in Table 9.4 and shown in Figure 9.8. The predicted values were calculated from Equation (9.10) using parameters from Freeman,[13] and experimental values of n_d and n_p were determined from the database used in this study. Although there is scatter in the data, the correlation of n_d is quite good judging from the R

value, and the correlation slope is less than one. Using a lower value of *f* would allow for a correlation slope of unity.

Gas Pair	k_d (experimental)	k_d (predicted) using n_d	k_d (predicted) using n_p
O_2/N_2	2.84	1.85	1.65
H_2/N_2	8.76	9.50	7.11
He/N_2	114	34.5	22.9
H_2/CH_4	138	33.7	16.1
He/H_2	3.05	1.91	2.20
He/CH_4	7100	226	66.2
N_2/CH_4	4.93	1.94	1.61
He/O_2	12.0	10.3	12.4
H_2/O_2	1.81	3.79	3.25
O_2/CH_4	24.8	4.17	2.88
CO_2/CH_4	6.73	2.39	2.52
CO_2/N_2	2.52	1.24	1.50
He/CO_2	61.2	24.3	18.0
H_2/CO_2	29.8	12.6	4.46
O_2/CO_2	2.39	1.52	1.11

Table 9.4: Comparison of the front factor k_d: theory versus experiment. For the predicted values, f was held at a value of 12,600 cal/mol.

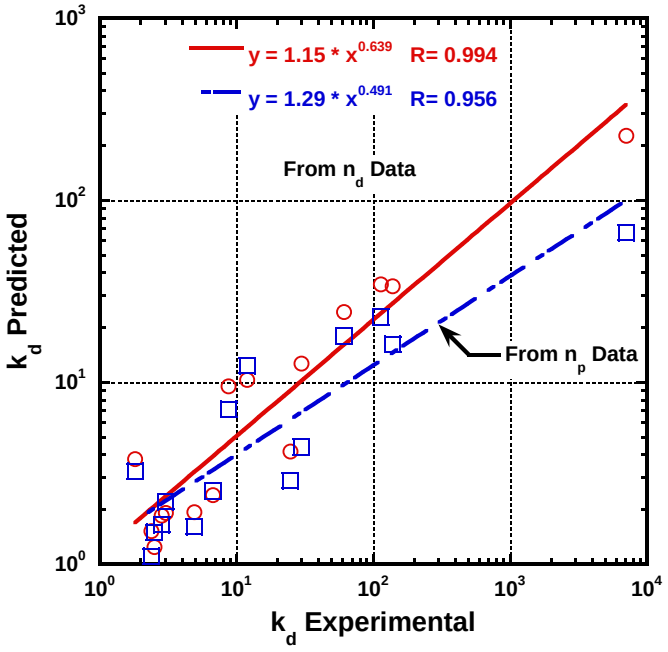

Figure 9.8: Comparison between predicted values of k_d from n_d and n_p data with experimental values of k_d.

9.4 UPPER BOUND FOR DIFFUSIVITY SELECTIVITY

The permeability upper bound data discussed in prior papers[12,14] used the following equation

$$P_i = k_{up}\alpha_{ij(u)}^{n_{up}} \tag{9.11}$$

An analogous equation can be written for diffusion coefficients

$$D_i = k_{ud}\alpha_{ij(u)}^{n_{ud}} \tag{9.12}$$

Plotting α_{ij} (y-axis) versus D_i (x-axis) on a log-log plot yields the following relationship

$$\log \alpha_{ij(u)} = -\frac{\log k_{ud}}{n_{ud}} + \frac{\log D_i}{n_{ud}} \tag{9.13}$$

The slope of the upper bound tradeoff relationship is defined by either n_{up} or n_{ud}. The term n_{up} defines the slope of the upper bound when plotted as the log of the permselectivity versus the log of the permeability, and the term n_{ud} defines the slope of the upper bound when plotted as the log of the diffusion selectivity versus the log of the diffusion coefficient. Therefore, if solubility is independent of permeability, n_{up} and n_{ud} should be identical. However, for some gas pairs, there is considerable difference between these terms. To illustrate this difference, Figure 9.9 and Figure 9.10 show plots in the form of Equation (9.13) both in terms of n_{ud} and n_{up}. For the case of n_{up}, the term n_{ud} in Equation (9.13) is replaced by the term n_{up}. For these figures, n_{up} is taken from reference [14].

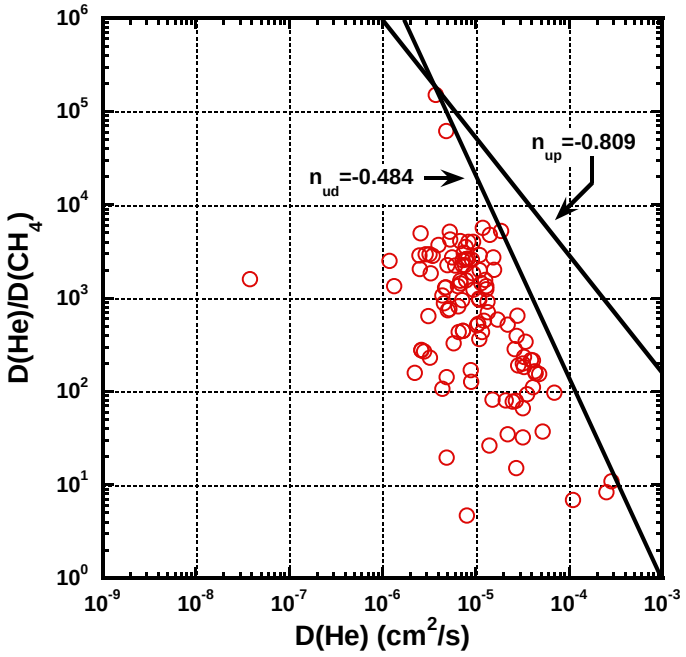

Figure 9.9: Diffusivity upper bound correlation for He/CH_4.

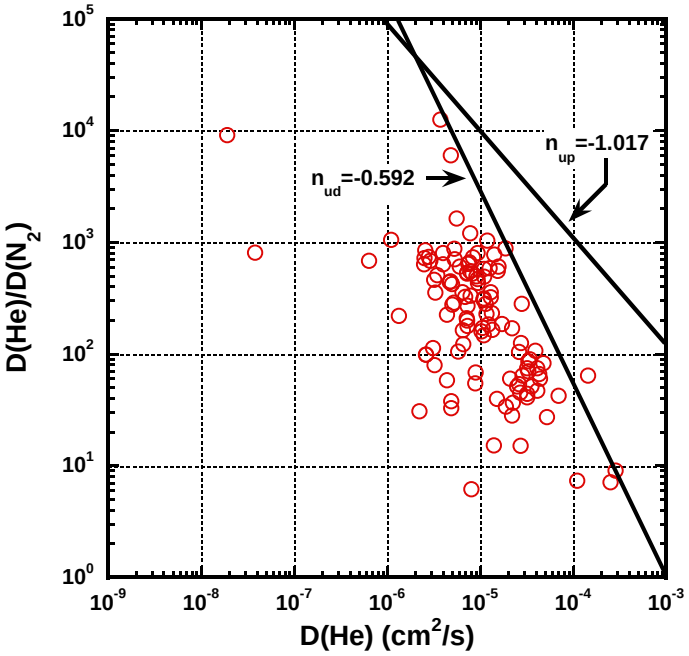

Figure 9.10: Diffusivity upper bound correlation for He/N_2.

9.5 CORRELATIONS OF SOLUBILITY SELECTIVITY

A database of solubility coefficients was compiled from the same references as the database of diffusion coefficients. As with the database of diffusion coefficients, there are significantly fewer values for He and H_2 than for the other gases, but there are still sufficient data to permit a reasonable analysis. Solubility coefficients vary significantly between different polymeric structures. In general, polyimides have higher sorption coefficients than polycarbonates, polysulfones, and poly(aryl ethers) for all gases. As the polymer type is varied, the sorption coefficients for a given gas span a range of one to two orders of magnitude.

The sorption coefficients in the database used here can be correlated with boiling point (T_b), critical temperature (T_c), or the Lennard-Jones parameters (ε/k) according to Equation (9.14)[43,44]

$$\ln S_i = M + N(T_x) \tag{9.14}$$

where T_x is T_b, T_c, or ε/k in units of K.

Gas solubility coefficients and associated metrics of condensability are listed in Table 9.5, and the average and median values for the parameters in Equation (9.14) are presented in Table 9.6. The gas solubility coefficients and parameters from Table 9.5 and Table 9.6 represent the average and median values for each gas in the database. The correlations for Lennard-Jones potential well depth and critical temperature are shown in Figure 9.11 and Figure 9.12, respectively. For a given polymer, the sorption isotherms of the more condensable gases show stronger dual-mode curvature in their isotherms. Therefore, the solubility coefficients and the parameters in Equation (9.14) are strongly affected by the pressure used in the experiment. To illustrate the effect of pressure on gas

solubility, an analysis is shown for polysulfone and PIM-1 in Appendix D. In general, secant sorption coefficients decrease with pressure, and this effect is greater for more condensable gases. For example, the sorption coefficient for N_2 in polysulfone is approximately 0.0035 in the limit of zero pressure but is approximately 0.0028 at 10 atm in units of cm^3(STP)/(cc cmHg). For CO_2 in polysulfone, the secant sorption coefficient is approximately 0.077 in the limit of zero pressure but is approximately 0.028 at 10 atm again in units of cm^3(STP)/(cc cmHg). While the summary of data shown in Table 9.5 and Table 9.6 provides general trends based on multiple sets of data found in the literature, in reality, the parameters in Equation (9.14) are susceptible to variations between polymers that exhibit strong pressure dependence on gas sorption.

Gas	Number of Data Entries	Solubility Coefficient* (average) x 10^3	Solubility Coefficient* (median) x 10^3	$T_{\varepsilon/k}$† (K)	T_b†† (K)	T_c† (K)
He	125	0.883	0.697	10.22	4.222	5.19
H_2	206	2.17	1.60	59.7	20.39	32.98
N_2	722	6.63	4.70	71.4	73.36	126.20
O_2	693	8.60	6.44	106.7	90.20	154.58
CH_4	670	22.1	14.1	148.6	111.67	190.56
CO_2	766	101	57.0	195.2		304.12

*units are cm^3(STP)/(cc cmHg)
†Data taken from Ref. [45]
††Data taken from Ref. [46]

Table 9.5: Solubility data and condensability correlation parameters.

	M*	N	R
Lennard-Jones (average)	-7.30	0.0249	0.994
Lennard-Jones (median)	-7.49	0.0232	0.994
Boiling point (average)	-6.96	0.0269	0.981
Boiling point (median)	-7.21	0.0255	0.990
Critical temperature (average)	-6.91	0.0153	0.999
Critical temperature (median)	-7.14	0.0142	0.999

*units are cm^3(STP)/(cc cmHg)

Table 9.6: Average and median coefficients from Equation (9.14).

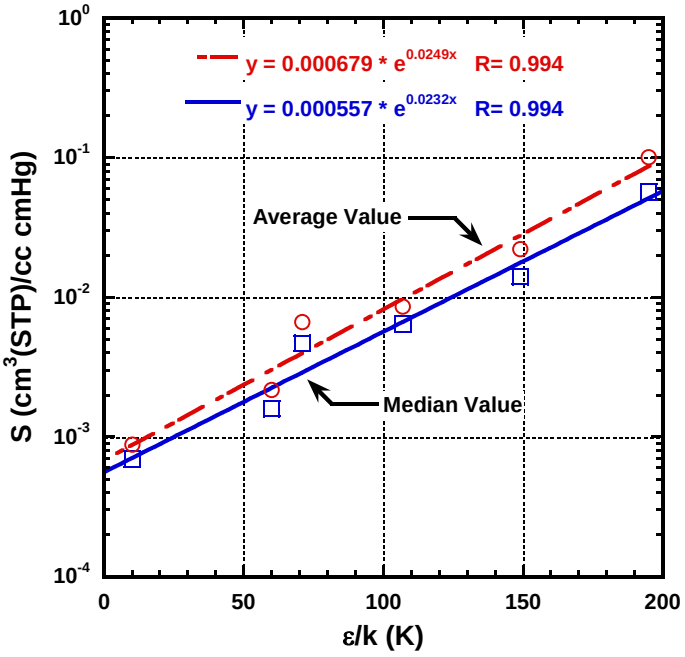

Figure 9.11: Solubility coefficient correlation with Lennard-Jones potential well depth.

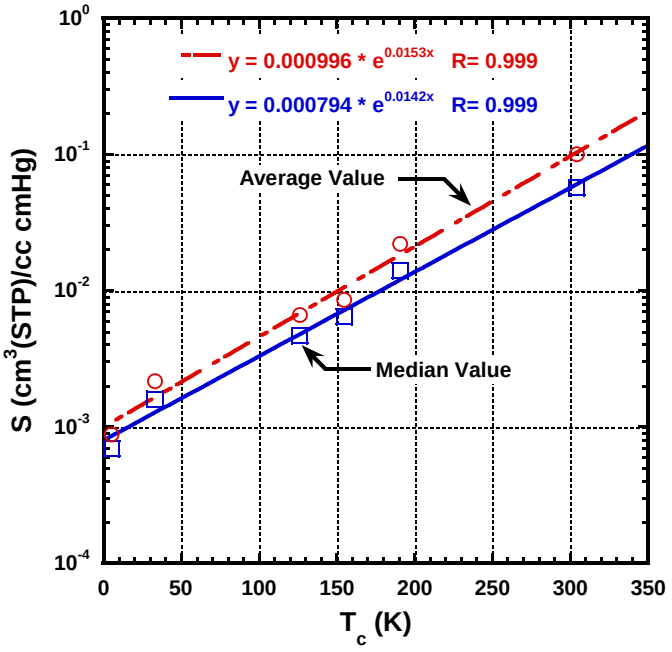

Figure 9.12: Solubility coefficient correlation with critical temperature.

The solubility selectivity can be assessed several different ways in this analysis. For example, Figure 9.13 shows S_i/S_j plotted versus S_j for S(He)/S(CO_2) versus S(CO_2). For the purpose of this paper, a plot of S_i/S_j versus P_i correlates more directly with free volume and is shown in Figure 9.14 for S(He)/S(CO_2) versus P(He). Alternatively, absolute values of S(He) and S(CO_2) are plotted versus P(He) in Figure 9.15. Figure 9.13 shows that the S(He)/S(CO_2) ratio decreases with increasing S(CO_2). Figure 9.14 demonstrates that the S(He)/S(CO_2) ratio decreases with increasing P(He). Figure 9.15 illustrates that both S(He) and S(CO_2) increase with increasing P(He). As the permeability of He (as well as the permeability of other gases) increase with increasing free volume; it is apparent from Figure 9.15 that the solubility coefficient is a function of free volume as noted in various literature references.[28,34-36] Interestingly, when compared to increasing helium permeability (and thus increasing free volume), the solubility of CO_2

increases faster than that of helium. Data for H_2/N_2 solubility selectivity versus H_2 permeability (Figure 9.16) and H_2 and N_2 solubility versus H_2 permeability (Figure 9.17) show similar trends as the He and CO_2 gas pair. From this data and the other gas pair data, there is a modest effect of free volume (or permeability) on solubility selectivity. There is considerable scatter in the data for the solubility correlations in Figure 9.13 through Figure 9.17, and the least squares fit will depend upon the choice of which gas is plotted on the x-axis and which gas is plotted on the y-axis. However, the trends noted with the gas pairs shown are consistent with the other gas pairs regardless of plotting convention.

The solubility selectivity, S_i/S_j, generally decreases with increasing permeability, P_i, when the diameter of gas j is larger than that of gas i. Larger gases generally become more soluble as free volume increases than is the case for smaller gases. This trend suggests that sorption sites become less available for the larger gas molecules as free volume decreases.

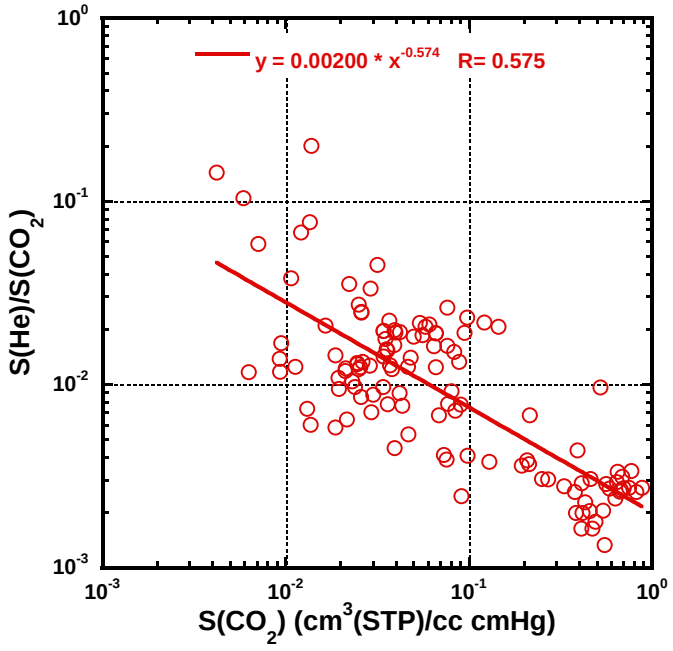

Figure 9.13: He/CO_2 solubility selectivity versus CO_2 solubility.

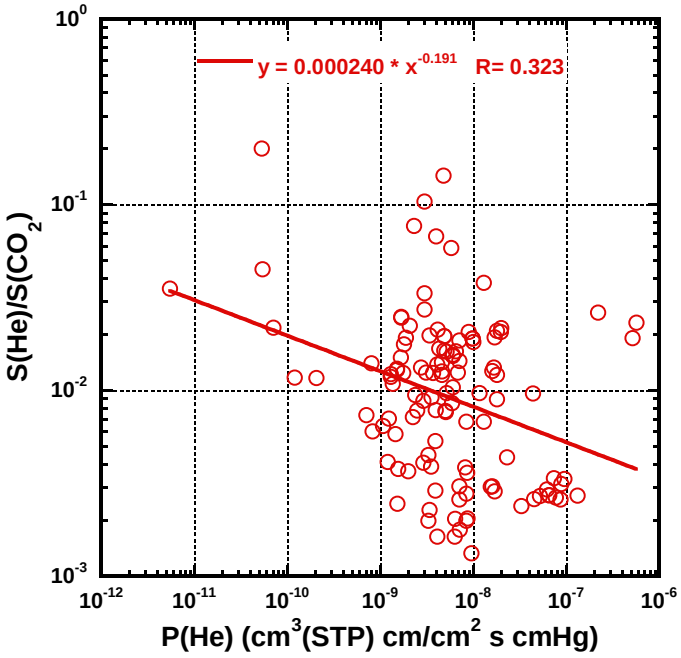

Figure 9.14: He/CO_2 solubility selectivity versus helium permeability.

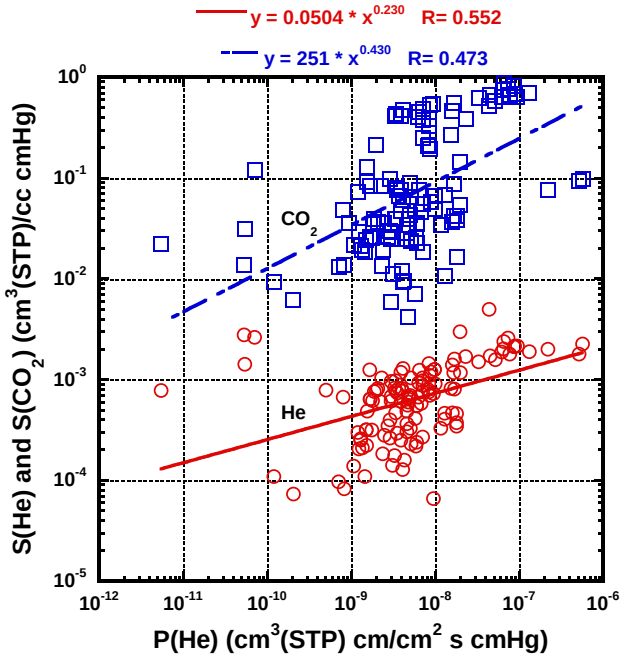

Figure 9.15: He and CO_2 solubility versus helium permeability.

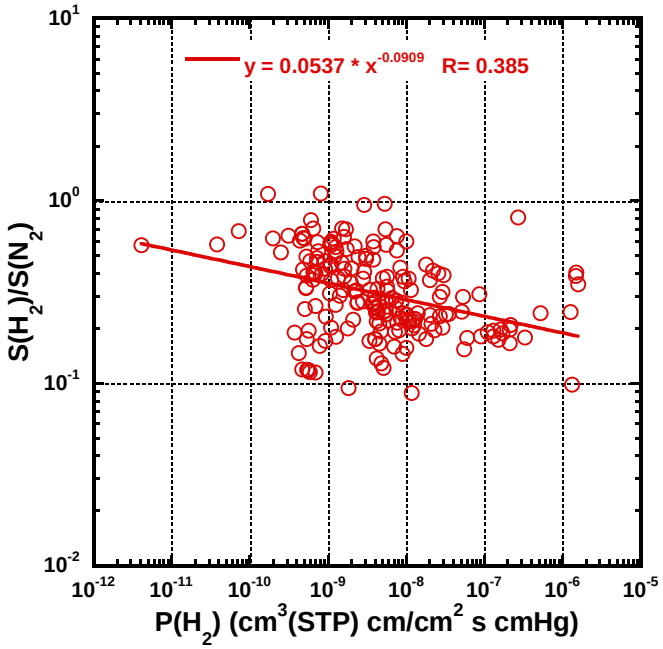

Figure 9.16: H_2/N_2 solubility selectivity versus hydrogen permeability.

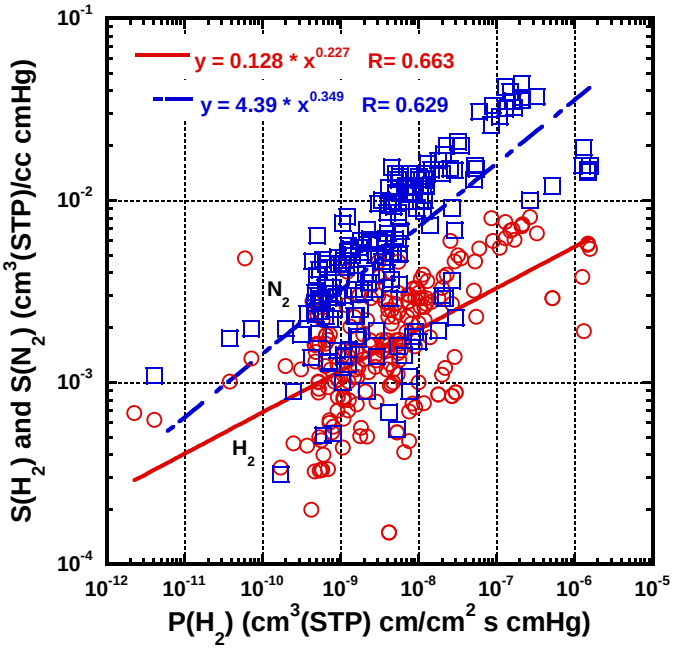

Figure 9.17: H_2 and N_2 solubility as a function of hydrogen permeability.

The effect of free volume on gas solubility has implications for the Freeman theory, which describes the fundamental basis for the upper bound tradeoff empirically described by Robeson.[12-14] According to this theory, sorption coefficients are assumed to be invariant with free volume. The tradeoff relationships employed in this work for permeability and diffusion coefficients are described by the following equations

$$P_j = k_p P_i^{n_p} \quad D_j = k_d D_i^{n_d} \text{ then } \frac{P_j}{D_j} = \frac{k_p P_i^{n_p}}{k_d D_i^{n_d}} \tag{9.15}$$

The Freeman theory defines k_p and k_d by the following equations

$$k_p = \frac{S_j}{S_i} S_i^{(1-n_p)} \exp\left[(n_p - 1)(b - f\frac{1-a}{RT})\right]; k_d = \exp\left[(n_d - 1)(b - f\frac{1-a}{RT})\right] \tag{9.16}$$

If n_d = n_p, as is generally assumed, then Equation (9.15) and (9.16) can be rewritten as follows

$$\frac{P_j}{D_j} = \frac{S_j}{S_i} S_i^{(1-n_p)} \frac{P_i^{n_p}}{D_i^{n_d}};\ \frac{P_j}{P_i^{n_p}} = \frac{S_j}{S_i^{n_p}} \frac{D_j}{D_i^{n_d}} \text{ and } \frac{P_j}{P_i^{n_p}} = \frac{D_j S_j}{(D_i S_i)^{n_p}} \tag{9.17}$$

Traditionally, the term $\frac{S_j}{S_i} S_i^{(1-n_p)}$ is assumed to be constant and, therefore, independent of permeability (or free volume) for different gas pairs. However, our analysis from the solubility coefficient database shows a slight dependency on permeability. The absolute values of S_i increase slightly (for all gases) with increasing permeability (free volume), and S_i/S_j decreases modestly for gases where the diameter of gas i is less than that of gas j.

Comparisons of $D(CO_2)$ and $S(CO_2)$ versus $P(CO_2)$ are shown in Figure 9.18, and the least squares fit to these data are given by the following equations

$$S(CO_2) = 2.40 P(CO_2)^{0.182};\ \text{R} = 0.441 \tag{9.18}$$

$$D(CO_2) = 0.416 P(CO_2)^{0.818};\ \text{R} = 0.946 \tag{9.19}$$

The bold solid line in Figure 9.18 is $P(CO_2)$ plotted versus itself as a parity line. Because P = DS from the solution-diffusion model, the product of the prefactors and the sum of the exponents in Equation (9.18) and Equation (9.19) should equal unity, which is indeed the case. This comparison confirms the expected self-consistency of the solution-

diffusion model and shows the effect of free volume on diffusion and solubility coefficients.

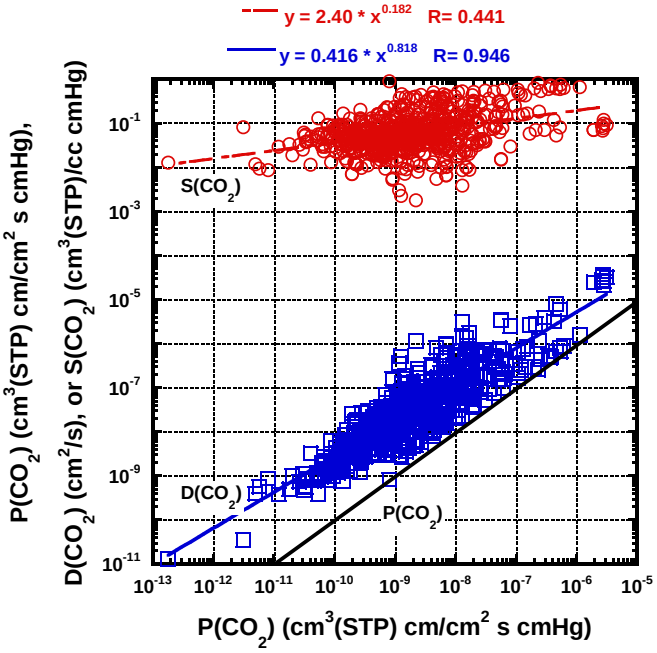

Figure 9.18: Comparison of $D(CO_2)$ and $S(CO_2)$ with changes in $P(CO_2)$.

The permeability selectivity, diffusivity selectivity, and solubility selectivity for H_2/N_2 are plotted versus hydrogen permeability in Figure 9.19, and the least squares fit of the data are noted. When comparing correlations of P = DS, the fitted parameters from the standard least squares regression correspond to the equations noted below with excellent agreement:

$$\frac{P_i}{P_j} = x_p P_i^{y_p} \qquad \frac{D_i}{D_j} = x_d P_i^{y_d} \qquad \frac{S_i}{S_j} = x_s P_i^{y_s} \tag{9.20}$$

(From Equation (9.2), $x_p = (x_d)(x_s)$ (x_p = 0.00747 and $(x_d)(x_s)$ = 0.00740); $y_p = y_d + y_s$ y_p = -0.446 and $y_d + y_s$ = -0.446). Similar agreement is observed when O_2/N_2 selectivity values are plotted versus $P(O_2)$ as shown in Figure 9.20.

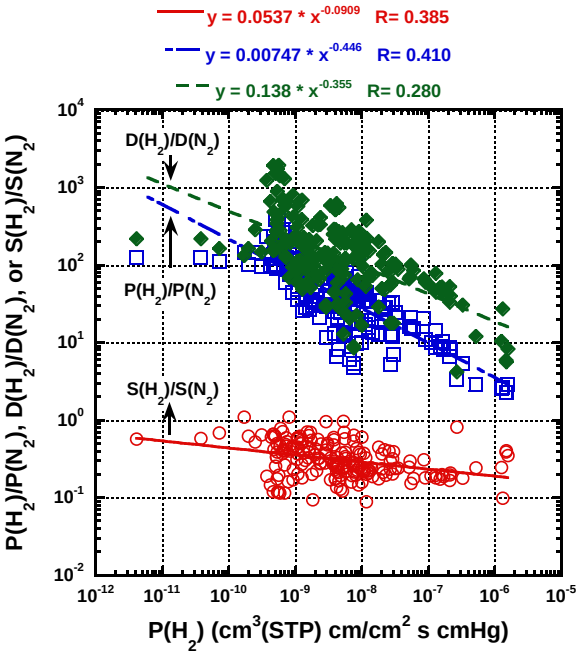

Figure 9.19: Comparison of permeability selectivity, diffusivity selectivity, and solubility selectivity as a function of the more permeable gas in the H_2/N_2 gas pair.

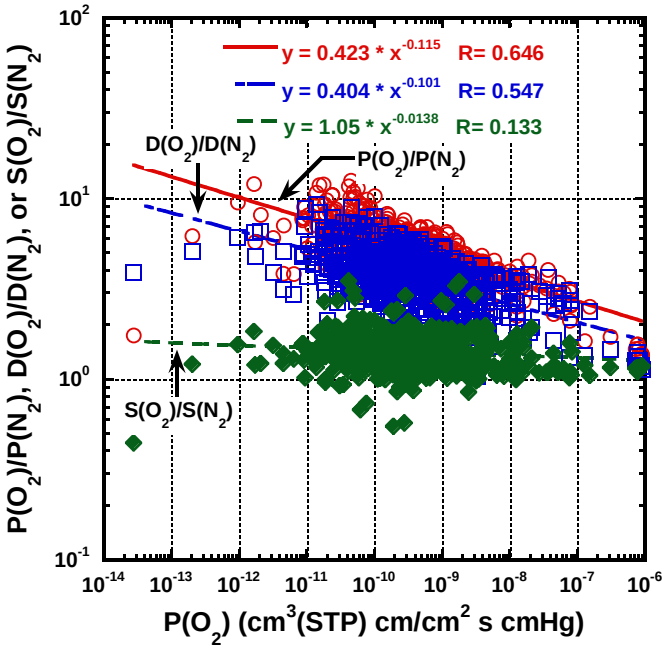

Figure 9.20: Permeability, diffusivity and solubility selectivities for O_2/N_2 versus O_2 permeability.

9.6 CONCLUSIONS

The role of solubility in the tradeoff between permselectivity and permeability in polymer films has been evaluated. The large database compiled for this analysis, which was limited to glassy polymers, shows the existence of a modest contribution of solubility selectivity to changes in permeability (and thus free volume). All gases chosen for this analysis (He, H_2, N_2, O_2, CO_2, and CH_4) show an increase in solubility with increasing permeability or free volume. For specific classes of polymers, there is support in the literature for this trend; however, we have more broadly extended the correlation between increasing solubility and free volume for many classes of polymers here. The solubility selectivity (S_i/S_j) for the ij gas pair is also observed to be a function of permeability and free volume. When the j gas is larger in size than the i gas, the value of S_i/S_j generally decreases with increasing permeability of the i gas (P_i). This trend suggests that the

solubility sites in the polymer are less available to the larger gas as the polymer packing density increases and free volume decreases. An upper bound relationship also exists for D_i/D_j versus D_i similar to that noted for permeability. The slope of the diffusivity upper bound can be different than that observed for the permeability upper bound due to a contribution from the effect of free volume on solubility selectivity.

The solubility database was used to determine the relationship of the equation employed for relating solubility coefficients with critical temperature, boiling point or Lennard-Jones parameters, i.e., $\ln S_i = M + N(T_x)$. Correlations of the average and the median S values were observed with M and N values in the range of those typically noted in the literature.

The data show that the effective diffusing gas diameter for CO_2 is larger than that of O_2 and slightly less than that of N_2. These results differ from zeolite data, which show that CO_2 has a smaller kinetic diameter than O_2 and N_2. The permeability correlation, which inherently assumed the solubility selectivity was invariant with permeability, yielded CO_2 and O_2 diameters that were approximately the same. This analysis allowed for a calculation of a new set of gas diameters with improved prediction, relative to prior determinations, for diffusion in glassy polymers.

9.7 REFERENCES

1. Sanders, D.F., Z.P. Smith, R. Guo, L.M. Robeson, J.E. McGrath, D.R. Paul, and B.D. Freeman, *Energy-efficient polymeric gas separation membranes for a sustainable future: A review.* Polymer, **2013**. 54(18), 4729-4761.

2. Henis, J.M.S., *Commercial and practical aspects of gas separation membranes*, in *Polymeric Gas Separation Membranes*, D.R. Paul and Y.P. Yampolskii, Editors. **1994**, CRC Press: Boca Raton. 441-512.

3. Bernardo, P., E. Drioli, and G. Golemme, *Membrane gas separation: A review/state of the art.* Industrial & Engineering Chemistry Research, **2009**. 48(10), 4638-4663.

4. Yampolskii, Y., *Polymeric gas separation membranes.* Macromolecules, **2012**. 45(8), 3298-3311.

5. Baker, R.W., *Future directions of membrane gas separation technology.* Industrial & Engineering Chemistry Research, **2002**. 41(6), 1393-1411.

6. Spillman, R., *Economics of gas separation membrane processes,* in *Membrane Separation Technology, Principles and Applications,* R.D. Noble and S.A. Stern, Editors. **1995**, Elsevier Science B. V.: Amsterdam. 589 - 663.

7. Kim, T.-H., W.J. Koros, and G.R. Husk, *Advanced gas separation membrane materials: Rigid aromatic polyimides.* Separation Science and Technology, **1988**. 23(12-13), 1611-1626.

8. Barbari, T.A., W.J. Koros, and D.R. Paul, *Polymeric membranes based on bisphenol-A for gas separations.* Journal of Membrane Science, **1989**. 42(1-2), 69-86.

9. Stern, S.A., Y. Mi, H. Yamamoto, and A.K.S. Clair, *Structure/permeability relationships of polyimide membranes. Applications to the separation of gas mixtures.* Journal of Polymer Science Part B: Polymer Physics, **1989**. 27(9), 1887-1909.

10. Stannett, V.T., W.J. Koros, D.R. Paul, H.K. Lonsdale, and R.W. Baker, *Recent advances in membrane science and technology*, in *Advances in Polymer Science*. **1979**, Springer Berlin Heidelberg. 69-121.

11. Muruganandam, N. and D.R. Paul, *Evaluation of substituted polycarbonates and a blend with polystyrene as gas separation membranes.* Journal of Membrane Science, **1987**. 34(2), 185-198.

12. Robeson, L.M., *Correlation of separation factor versus permeability for polymeric membranes.* Journal of Membrane Science, **1991**. 62(2), 165-185.

13. Freeman, B.D., *Basis of permeability/selectivity tradeoff relations in polymeric gas separation membranes.* Macromolecules, **1999**. 32(2), 375-380.

14. Robeson, L.M., *The upper bound revisited.* Journal of Membrane Science, **2008**. 320(1-2), 390-400.

15. Robeson, L.M., B.D. Freeman, D.R. Paul, and B.W. Rowe, *An empirical correlation of gas permeability and permselectivity in polymers and its theoretical basis.* Journal of Membrane Science, **2009**. 341(1-2), 178-178.

16. Alentiev, A.Y. and Y.P. Yampolskii, *Free volume model and tradeoff relations of gas permeability and selectivity in glassy polymers.* Journal of Membrane Science, **2000**. 165(2), 201-216.

17. Alentiev, A. and Y. Yampolskii, *Correlation of gas permeability and diffusivity with selectivity: Orientations of the clouds of the data points and the effects of temperature.* Industrial & Engineering Chemistry Research, **2013**. 52(26), 8864-8874.

18. Yampolskii, Y., *Correlations with and prediction of activation energies of gas permeation and diffusion in glassy polymers.* Journal of Membrane Science, **1998**. 148(1), 59-69.

19. Rowe, B.W., L.M. Robeson, B.D. Freeman, and D.R. Paul, *Influence of temperature on the upper bound: Theoretical considerations and comparison with experimental results.* Journal of Membrane Science, **2010**. 360(1-2), 58-69.

20. Park, J.Y. and D.R. Paul, *Correlation and prediction of gas permeability in glassy polymer membrane materials via a modified free volume based group contribution method.* Journal of Membrane Science, **1997**. 125(1), 23-39.

21. Robeson, L.M., C.D. Smith, and M. Langsam, *A group contribution approach to predict permeability and permselectivity of aromatic polymers.* Journal of Membrane Science, **1997**. 132(1), 33-54.

22. Laciak, D.V., L.M. Robeson, and C.D. Smith, *Group contribution modeling of gas transport in polymeric membranes*, in *Polymer Membranes for Gas and Vapor Separation*, B.D. Freeman and I. Pinnau, Editors. **1999**, American Chemical Society Symposium Series, 733: Washington, DC. 151–177.

23. Prabhakar, R.S., R. Raharjo, L.G. Toy, H. Lin, and B.D. Freeman, *Self-consistent model of concentration and temperature dependence of permeability in rubbery polymers.* Industrial & Engineering Chemistry Research, **2005**. 44(5), 1547-1556.

24. Mohr, J.M., D.R. Paul, G.L. Tullos, and P.E. Cassidy, *Gas transport properties of a series of poly(ether ketone) polymers.* Polymer, **1991**. 32(13), 2387–2394.

25. Ruiz-Treviño, F.A. and D.R. Paul, *Gas permselectivity properties of high free volume polymers modified by a low molecular weight additive.* Journal of Applied Polymer Science, **1998**. 68(3), 403-415.

26. Liu, S.L., R. Wang, T.S. Chung, M.L. Chng, Y. Liu, and R.H. Vora, *Effect of diamine composition on the gas transport properties in 6FDA-durene/3,3'-diaminodiphenyl sulfone copolyimides.* Journal of Membrane Science, **2002**. 202(1-2), 165-176.

27. Assogna, A., G. Perego, A. Roggero, R. Sisto, and C. Valentini, *Structure and gas permeability of silylated polyphenylene oxide.* Journal of Membrane Science, **1992**. 71(1-2), 97–103.

28. Miyata, S., S. Sato, K. Nagai, T. Nakagawa, and K. Kudo, *Relationship between gas transport properties and fractional free volume determined from dielectric constant in polyimide films containing the hexafluoroisopropylidene group.* Journal of Applied Polymer Science, **2008**. 107(6), 3933-3944.

29. Okamoto, K.-i., K. Tanaka, H. Kita, M. Ishida, M. Kakimoto, and Y. Imai, *Gas permeability and permselectivity of polyimides prepared from 4,4'-diaminotriphenylamine.* Polymer Journal, **1992**. 24(5), 451-457.

30. Tanaka, K., M. Okano, H. Toshino, H. Kita, and K.-i. Okamoto, *Effect of methyl substituents on permeability and permselectivity of gases in polyimides prepared from methyl-substituted phenylenediamines.* Journal of Polymer Science Part B: Polymer Physics, **1992**. 30(8), 907-914.

31. Muruganandam, N., W.J. Koros, and D.R. Paul, *Gas sorption and transport in substituted polycarbonates.* Journal of Polymer Science Part B: Polymer Physics, **1987**. 25, 1999-2026.

32. Dal-Cin, M.M., A. Kumar, and L. Layton, *Revisiting the experimental and theoretical upper bounds of light pure gas selectivity–permeability for polymeric membranes.* Journal of Membrane Science, **2008**. 323(2), 299-308.

33. Breck, D.W., *Zeolite molecular sieves: structure, chemistry, and use*. **1973**, John Wiley & Sons: New York, NY. 636.

34. Aitken, C.L., W.J. Koros, and D.R. Paul, *Effect of structural symmetry on gas transport properties of polysulfones.* Macromolecules, **1992**. 25(13), 3424-3434.

35. Pixton, M.R. and D.R. Paul, *Gas transport properties of polyarylates part II: Tetrabromination of the bisphenol.* Journal of Polymer Science Part B: Polymer Physics, **1995**. 33(9), 1353-1364.

36. Wright, C.T. and D.R. Paul, *Gas sorption and transport in poly(tertiary-butyl methacrylate).* Polymer, **1997**. 38(8), 1871-1878.

37. Paul, D.R. and W.J. Koros, *Effect of partially immobilizing sorption on permeability and the diffusion time lag.* Journal of Polymer Science: Polymer Physics Edition, **1976**. 14(4), 675-685.

38. Okamoto, K., K. Noborio, J. Hao, K. Tanaka, and K. Hidetoshi, *Permeation and separation properties of polyimide membranes to 1, 3-butadiene and n-butane.* Journal of Membrane Science, **1997**. 134(2), 171-179.

39. Vieth, W.R., J.M. Howell, and J.H. Hsieh, *Dual sorption theory.* Journal of Membrane Science, **1976**. 1, 177-220.

40. Smith, Z.P., R.R. Tiwari, T.M. Murphy, D.F. Sanders, K.L. Gleason, D.R. Paul, and B.D. Freeman, *Hydrogen sorption in polymers for membrane applications.* Polymer, **2013**. 54(12), 3026–3037.

41. Shieh, J.-J. and T.S. Chung, *Gas permeability, diffusivity, and solubility of poly(4-vinylpyridine) film.* Journal of Polymer Science Part B: Polymer Physics, **1999**. 37(20), 2851-2861.

42. Bevington, P.R. and K.D. Robinson, *Data reduction and error analysis for the physical sciences: Third edition*. **2003**, Boston, McGraw Hill.

43. van Amerongen, G.J., *Diffusion in elastomers.* Rubber Chemistry and Technology, **1964**. 37(5), 1065-1152.

44. Stannett, V., *Simple gases,* in *Diffusion in polymers*, J. Crank and G.S. Park, Editors. **1968**, Academic Press: New York, NY.

45. Poling, B.E., J.M. Prausnitz, and J.P. O'Connell, *The properties of gases and liquids*. **2001**, McGraw Hill Book Co., New York, NY. A.5-A.19.

46. Haynes, W.M., D.R. Lide, and T.J. Bruno, *CRC Handbook of Chemistry and Physics 2012-2013*. **2012**, CRC Press.

Chapter 10: Conclusions and Recommendations

Thermally rearranged (TR) polymers are an emerging platform of materials for membrane-based separations. This dissertation has evaluated the chemical structure of these polymers (Chapters 4 and 5), evaluated their permeability and solubility for light gases (Chapter 5) and sparingly soluble gases (Chapter 6 and 7). In addition, their separation performance has been investigated for different polymer backbone architectures and different polymer synthesis routes (Chapter 8). This dissertation has also evaluated helium and hydrogen permeability, solubility, and diffusivity for a series of polymers, including polyimides, TR polymers, perfluoropolymers, highly fluorinated polymers, and a silicon-based polymer, PDMS (Chapters 6 and 7). Finally, the effect of solubility selectivity on permeability and permselectivity has been investigated from an upper bound perspective using Robeson's database, and this analysis has permitted a more unifying evaluation of effective gas diameters for polymer membrane applications. This chapter summarizes the studies from chapters 4 through 9 and offers recommendations for future research.

10.1 CONCLUSIONS

Several potential chemical structures for TR polymers have been proposed in the literature.[1-5] Our efforts described in Chapter 4 focus on identifying the chemical structure of these materials and determining if variations in synthesis procedures affect TR polymer transport properties. Traditionally, TR polymers formed from polyimide (PI) precursors are insoluble in common solvents, which prevents complete structural characterization by solution-based techniques such as nuclear magnetic resonance (NMR). Our work in Chapter 4 described the synthesis and characterization of a partially soluble TR polymer formed from a polyamide (PA) precursor. Solution-state proton and

carbon NMR experiments, coupled with 2-D NMR analysis, suggest that this PA-TR polymer has a polybenzoxazole structure. To compare the structure of this PA-TR polymer with a PI-TR polymer, a PI-TR polymer of nearly identical chemical structure to that of the PA-TR polymer was synthesized. Using solid-state NMR, this work suggests that both of these structures contain polybenzoxazole functionality. In addition to this characterization work, transport properties for these polymer are reported in Chapter 4 and Chapter 8, and these results indicate that the PI-TR polymer exhibits more beneficial separation characteristics than the PA-TR polymer for separations involving H_2, CH_4, N_2, O_2, and CO_2. Differences in transport properties relate to morphological differences between the PA-TR and PI-TR polymer. $T_{1\rho}$ NMR experiments indicate that the PI-TR polymer has a less ordered packing structure than the PA-TR polymer, and these results are attributed to either crosslinking or the meta/para isomeric nature of the PI-TR compared to the exclusively para nature of the PA-TR. Additionally, positron annihilation lifetime spectroscopy indicates that there are differences in free volume and free volume distribution between these samples.

The mechanism behind the beneficial transport properties of TR polymers was addressed from a solution-diffusion standpoint in Chapter 5. To investigate the role of solubility and diffusivity in TR polymers as a function of conversion, four samples were prepared from a polyimide based on 3,3'-dihydroxy-4,4'-diamino-biphenyl (HAB) and 2,2'-bis-(3,4-dicarboxyphenyl) hexafluoropropane dianhydride (6FDA). The HAB-6FDA sample was thermally treated at 350°C for 60 min, 400°C for 60 min, or 450°C for 30 min, and a comparison was made between these three partially converted samples and the unreacted polyimide. Based on the stoichiometric mass loss expected from thermally converting this HAB-6FDA polyimide to a polybenzoxazole, the samples were converted to the following percentages: 0%, 39%, 60%, and 76%. As a function of conversion,

permeability increased from the polyimide to the most highly converted TR polymer (i.e., TR 450°C 30 min) by approximately 1 order of magnitude, while solubility only increased by a factor of approximately 1.8 - 2.6. Therefore, changes in diffusivity are the dominant contribution to increases in permeability upon conversion of the polyimide precursor to its TR polymer analog. Additional work in Chapter 5 focuses on characterization of the HAB-6FDA polyimides and TR polymers.

Chapter 6 and Chapter 7 focused on determining the sorption of sparingly soluble gases, hydrogen and helium, in a series of polymer, including HAB-6FDA and its corresponding TR polymers. These measurements are often inaccessible using the common pressure-decay sorption techniques, so a more sensitive magnetic suspension balance was employed for determining these isotherms. Chapter 6 also investigated the effect of temperature on H_2 sorption. As temperature increases, solubility decreases as might be expected. For the HAB-6FDA polyimide and corresponding TR polymers, the enthalpy of sorption of each sample was practically invariant, falling in the range from -5.8 ± 0.6 kJ/mol to -7.3 ± 0.5 kJ/mol. For the glassy samples considered in this work, dual-mode curvature was observed at the lowest temperatures. Chapter 7 extended the hydrogen sorption work to include that of helium, and sorption selectivities were compared between polyimides, highly fluorinated polymers, perfluoropolymers, and poly(dimethylsiloxane). Interestingly, the sorption selectivity was much weaker for the highly fluorinated and perfluorinated polymers, and this distinction helped explain the above-upper bound behavior of these materials for He/H_2 separations.

An in-depth structure/property study was reported in Chapter 8 to compare the transport properties of polyimides, a polyamide, and TR polymers containing various backbone chemistries and prepared from different synthesis routes. This work explored the effect of backbone chemistry on the rate of thermal rearrangement by using

thermogravimetric analysis. HAB is a more reactive diamine for thermal rearrangement than 2,2-bis (3-amino-4-hydroxyphenyl)-hexafluoropropane (APAF), and a flexible dianhydride, 4,4'-oxydiphthalic anhydride (ODPA), can be used to increase the reactivity of the thermal rearrangement reaction compared to 2,2'-bis-(3,4-dicarboxyphenyl) hexafluoropropane dianhydride (6FDA). Increasing the thermal rearrangement reactivity does not necessarily lead to more beneficial transport properties. For example, the least reactive poly(*hydroxy*-imide) considered, APAF-6FDA, produced a TR polymer with the highest gas permeabilities of all samples. Additional work was performed in this chapter to study the effect of CO_2 plasticization, and only polyimides based on HAB-6FDA showed a plasticization pressure point. Upon thermal rearrangement, none of the TR polymers showed a plasticization pressure point. For the TR polymer with the best performance (i.e., APAF-6FDA TR polymer), olefin/paraffin separations were considered. The APAF-6FDA TR polymer operates above the upper bound for propylene/propane separation, but below the upper bound for ethylene/ethane separation.

Chapter 9 discusses the effect of solubility and solubility selectivity on the Robeson upper bound.[6,7] This work was completed using a large database of permeability, solubility, and diffusivity data from Robeson.[8] Free volume affects gas solubility, whereby smaller molecules have lower sorption values in more tightly packed polymer networks (i.e., polymers with lower fractional free volume). This analysis also permitted the calculation of diffusion-based upper bounds, and from these results, effective gas diameters related solely to diffusion in polymers were calculated. These effective diffusion diameters increased in the following order: $He < H_2 < O_2 < CO_2 < N_2 < CH_4$.

The appendices provide supplemental information for several of the chapters in this dissertation. Appendix A provides additional characterization information for the

polyimide, polyamide, and TR polymers discussed in Chapter 4. Appendix B provides supplemental information for the permeability, diffusivity, and solubility data from Chapter 7, and Appendix C provides additional characterization and transport results from the work discussed in Chapter 8. Finally, Appendix D provides a comparison between solubility selectivity and diffusivity selectivity when calculated by sorption or time-lag measurements.

10.2 RECOMMENDATIONS FOR FUTURE WORK

10.2.1 Compare experimental sorption results for hydrogen and helium with the Sanchez-Lacombe equation and NELF model

The helium and hydrogen sorption results presented in Chapters 6 and 7 are the first complete data sets of their kind. Therefore, it would be useful to compare these sorption isotherms with those calculated from Lattice Fluid Theory. For the rubbery polymer, PDMS, the Sanchez-Lacombe equation of state can be used to predict sorption isotherms.[9] For several of the glassy polymers, parameters needed to fit data to the Non-Equilibrium Lattice Fluid (NELF) model are also available.[10-13] Lattice fluid theory also permits fitting data over a range of temperatures, and for the H_2 data presented in Chapter 6, sorption isotherms have been determined between -20 and 70°C. Therefore, enthalpies of sorption calculated from the Sanchez-Lacombe equation and NELF model could be evaluated and compared to those determined experimentally. Finally, the difference in solubility selectivities between perfluoropolymers and the hydrocarbon-based polymers could be compared to determine if theoretical models predict the behavior observed experimentally.

10.2.2 Determine light gas and CO_2 sorption for a structure/property study

Detailed permeation results for a structure/property study are reported in Chapter 8. However, detailed sorption and diffusion data are needed to address these results from a more fundamental level. Work from Chapter 5 reports an increase in gas sorption for HAB-6FDA-C[14] as a function of conversion, and similar results have been noted for other TR polymer structures.[15] Increases in diffusion, however, contribute the most to the increases in permeability for TR polymers.[16] To determine structure/property data for sorption and diffusion in TR polymers, sorption isotherms should be determined at temperatures identical to those used in the permeability studies in Chapter 8. Additionally, the role of hysteresis and plasticization can be investigated by determining the change in diffusion coefficients at the same pressurization/depressurization hysteresis loops reported in Chapter 8.

10.2.3 Investigate additional TR polymers for olefin/paraffin separation performance

Work presented in this dissertation has only investigated the APAF-6FDA TR polymer for olefin/paraffin separations, so fundamental and comprehensive structure/property relationships cannot be evaluated for the TR family of polymers. Therefore, a structure/property study for olefin/paraffin separation is proposed.

Tanaka *et al.* have reported detailed structure/property results for polyimides, including polyimides containing 6FDA-based dianhydrides.[17] Additional work on olefin/paraffin separation with 6FDA-based polyimides has also been described by Staudt-Bickel *et al.*,[18] Burns *et al.*,[19] and Das *et al.*[20] These papers do not include results for polyimides containing *hydroxyl*-functional diamines, so structure/property work for this sub-family of polyimides is also needed. Light gas and CO_2 permeation has been reported in Chapter 8 for HAB-6FDA, APAF-6FDA, and APAF-ODPA polyimides and

TR polymers, so the work proposed in this section will likely focus on these structures. A basic synthesis sketch of the polyimide precursors proposed for this work is shown Figure 8.1.

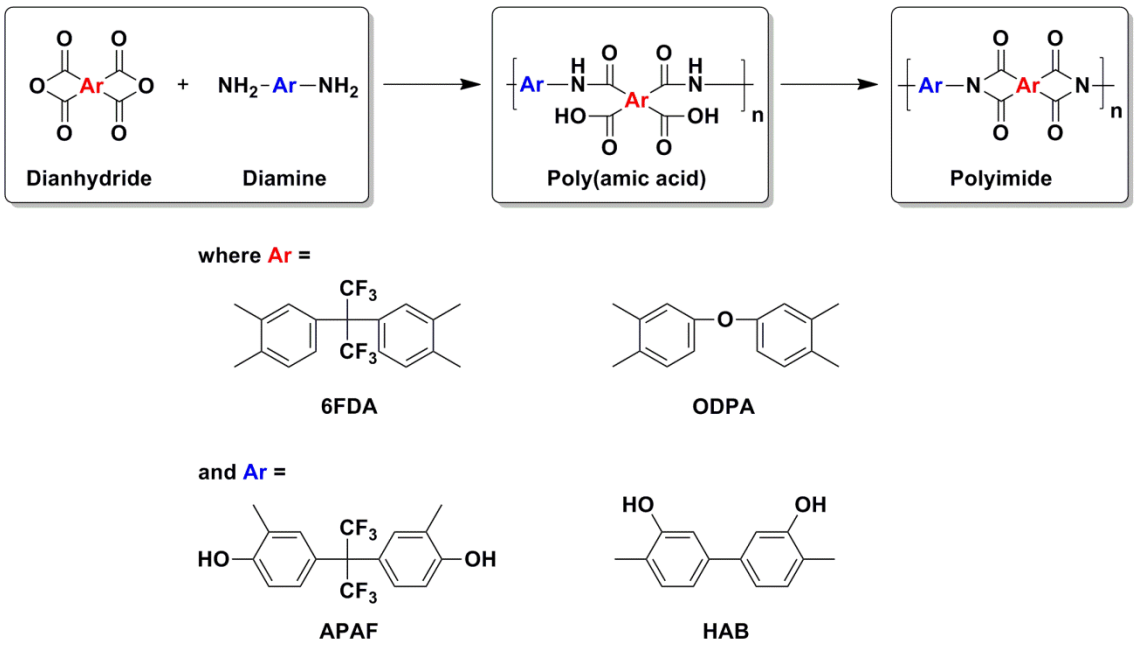

Figure 10.1: Proposed polyimide precursor structures for olefin/paraffin separations.

The olefin/paraffin work is proposed in four phases. First, pure-gas C_2H_4, C_2H_6, C_3H_6, and C_3H_8 permeability should be determined for the *hydroxyl*-functional polyimides and their corresponding TR polymers. This work is envisioned to first take place with polyimides thermally imidized in solution and with TR polymers prepared from these polyimides (i.e., polymers thermally treated at 450°C for 30 min). Additional research should focus on determining sorption isotherms for these samples so the solubility and diffusivity contributions to permeability can be separated. Second, mixed-gas permeability should be compared for the best performing samples from this study. Many polyimides show depressed selectivity when tested in the presence of

olefin/paraffin gas mixtures,[17,20] so this effect should be tracked for the TR polymer family of materials as well. Third, the permeability and selectivity of olefins and paraffins in TR polymers should be determined over a range of temperatures. In certain cases, ethylene/ethane separations are performed at -30°C and propylene/propane separations are performed at 48°C.[21] Finally, the reactive leaving group of polyimide precursors has an effect on transport properties of TR polymers.[22-24] The effect of incorporating bulkier leaving groups on TR polymers should be investigated for the best performing polymers used for olefin/paraffin separation.

10.3 REFERENCES

1. Park, H.B., C.H. Jung, Y.M. Lee, A.J. Hill, S.J. Pas, S.T. Mudie, E. Van Wagner, B.D. Freeman, and D.J. Cookson, *Polymers with cavities tuned for fast selective transport of small molecules and ions.* Science, **2007**. 318(5848), 254-258.

2. Hodgkin, J.H. and B.N. Dao, *Thermal conversion of hydroxy-containing polyimides to polybenzoxazoles. Does this reaction really occur?* European Polymer Journal, **2009**. 45(11), 3081-3092.

3. Hodgkin, J.H., M.S. Liu, B.N. Dao, J. Mardel, and A.J. Hill, *Reaction mechanism and products of the thermal conversion of hydroxy-containing polyimides.* European Polymer Journal, **2011**. 47(3), 394-400.

4. Kostina, J., O. Rusakova, G. Bondarenko, A. Alentiev, T. Meleshko, N. Kukarkina, A. Yakimanskii, and Y. Yampolskii, *Thermal rearrangement of functionalized polyimides: IR-spectral, quantum chemical studies, and gas permeability of TR polymers.* Industrial & Engineering Chemistry Research, **2013**. 52(31), 10476-10483.

5. Kardash, I. and A.N. Pravednikov, *Aromatic polyimides containing hydroxy- and methoxy-groups.* Vysokomol Soyed, **1967**. 9(12), 873-876.

6. Robeson, L.M., *Correlation of separation factor versus permeability for polymeric membranes.* Journal of Membrane Science, **1991**. 62(2), 165-185.

7. Robeson, L.M., *The upper bound revisited.* Journal of Membrane Science, **2008**. 320(1-2), 390-400.

8. Robeson, L.M., Z.P. Smith, B.D. Freeman, and D.R. Paul, *Contributions of diffusion and solubility selectivity to the upper bound analysis for glassy gas separation membranes.* Journal of Membrane Science, **2014**. 453, 71-83.

9. Sanchez, I.C. and R.H. Lacombe, *Statistical thermodynamics of polymer solutions.* Macromolecules, **1978**. 11(6), 1145-1156.

10. Ferrari, M.C., M. Galizia, M.G. De Angelis, and G.C. Sarti, *Gas and vapor transport in mixed matrix membranes based on amorphous Teflon AF1600 and AF2400 and fumed silica.* Industrial & Engineering Chemistry Research, **2010**. 49(23), 11920-11935.

11. Hariharan, R., B.D. Freeman, R.G. Carbonell, and G.C. Sarti, *Equation of state predictions of sorption isotherms in polymeric materials.* Journal of Applied Polymer Science, **1993**. 50(10), 1781-1795.

12. Minelli, M., G. Cocchi, L. Ansaloni, M.G. Baschetti, M.G. De Angelis, and F. Doghieri, *Vapor and liquid sorption in matrimid polyimide: Experimental characterization and modeling.* Industrial & Engineering Chemistry Research, **2013**. 52(26), 8936-8945.

13. De Angelis, M.G., G.C. Sarti, and F. Doghieri, *NELF model prediction of the infinite dilution gas solubility in glassy polymers.* Journal of Membrane Science, **2007**. 289(1–2), 106-122.

14. Smith, Z.P., D.F. Sanders, C.P. Ribeiro Jr, R. Guo, B.D. Freeman, D.R. Paul, J.E. McGrath, and S. Swinnea, *Gas sorption and characterization of thermally rearranged polyimides based on 3,3'-dihydroxy-4,4'-diamino-biphenyl (HAB) and*

2,2'-bis-(3,4-dicarboxyphenyl) hexafluoropropane dianhydride (6FDA). Journal of Membrane Science, **2012**. 416, 558-567.

15. Kim, S., H.J. Jo, and Y.M. Lee, *Sorption and transport of small gas molecules in thermally rearranged (TR) polybenzoxazole membranes based on 2,2-bis(3-amino-4-hydroxyphenyl)-hexafluoropropane (bisAPAF) and 4,4'-hexafluoroisopropylidene diphthalic anhydride (6FDA).* Journal of Membrane Science, **2013**. 441, 1-8.

16. Sanders, D.F., Z.P. Smith, C.P. Ribeiro, R.L. Guo, J.E. McGrath, D.R. Paul, and B.D. Freeman, *Gas permeability, diffusivity, and free volume of thermally rearranged polymers based on 3,3 '-dihydroxy-4,4 '-diamino-biphenyl (HAB) and 2,2 '-bis-(3,4-dicarboxyphenyl) hexafluoropropane dianhydride (6FDA).* Journal of Membrane Science, **2012**. 409, 232-241.

17. Tanaka, K., A. Taguchi, J. Hao, H. Kita, and K. Okamoto, *Permeation and separation properties of polyimide membranes to olefins and paraffins.* Journal of Membrane Science, **1996**. 121(2), 197-207.

18. Staudt-Bickel, C. and W.J. Koros, *Olefin/paraffin gas separations with 6FDA-based polyimide membranes.* Journal of Membrane Science, **2000**. 170(2), 205-214.

19. Burns, R.L. and W.J. Koros, *Defining the challenges for C_3H_6/C_3H_8 separation using polymeric membranes.* Journal of Membrane Science, **2003**. 211(2), 299-309.

20. Das, M. and W.J. Koros, *Performance of 6FDA–6FpDA polyimide for propylene/propane separations.* Journal of Membrane Science, **2010**. 365(1-2), 399-408.

21. Eldridge, R.B., *Olefin/paraffin separation technology: A review.* Industrial & Engineering Chemistry Research, **1993**. 32(10), 2208-2212.

22. Han, S.H., N. Misdan, S. Kim, C.M. Doherty, A.J. Hill, and Y.M. Lee, *Thermally rearranged (TR) polybenzoxazole: Effects of diverse imidization routes on*

physical properties and gas transport behaviors. Macromolecules, **2010**. 43(18), 7657-7667.

23. Guo, R., D.F. Sanders, Z.P. Smith, B.D. Freeman, D.R. Paul, and J.E. McGrath, *Synthesis and characterization of thermally rearranged (TR) polymers: Influence of ortho-positioned functional groups of polyimide precursors on TR process and gas transport properties.* Journal of Materials Chemistry A, **2013**. 1(2), 262-272.

24. Sanders, D.F., R. Guo, Z.P. Smith, Q. Liu, K.A. Stevens, J.E. McGrath, D.R. Paul, and B.D. Freeman, *Influence of polyimide precursor synthesis route and ortho-position functional group on thermally rearranged (TR) polymer properties: conversion and free volume.* Polymer, **2014**. In Press.

Appendix A: Supporting Information for Chapter 4

A.1 Analysis of reaction conversion by TGA

The mass loss for each sample during thermal rearrangement was determined using thermogravimetric analysis (TGA). To convert the PI to the PI-TR, a decarboxylation reaction would result in a theoretical mass loss of 11.4%, and to convert the PA to the PA-TR, a condensation reaction would result in a theoretical mass loss of 5.0%. The conversion times and temperatures were chosen to achieve mass losses very close to these theoretical predicted values. For the PI sample, the actual mass loss was 12.2% and for the PA sample, the actual mass loss was 5.3%. From the proposed reaction mechanism in Scheme 1, these experimental results support the hypothesis that samples considered in this study are nearly quantitatively converted to PBOs. Slight differences between the theoretical and experimental mass loss may be a result of several factors including balance sensitivity in the TGA and low levels of sample degradation.

A.2 Soxhlet extraction of PA-TR

A Soxhlet extractor was used to determine the gel fraction of the PA-TR. The sample was refluxed in chloroform in the extractor for approximately 12 h, and this experiment resulted in the sample losing 25.1% mass, which corresponds to a gel fraction of 74.9%. Solution NMR was performed on the soluble fraction of the PA-TR, and these results indicated that a partially soluble PBO was formed through the reaction described in this study. Furthermore, the PI-TR polymer was completely insoluble in chloroform, which may indicate that the sample formed from a PI is more highly crosslinked than that

---

This appendix has been adapted from: Smith, Z.P., K. Czenkusch, K.L. Gleason, G.H.G.C. Alvarez, A.E. Lozano, D.R. Paul, and B.D. Freeman, *Effect of polymer structure on gas transport properties of polyimides, polyamides and TR polymers (in preparation).*

formed from a PA. However, differences in molecule weights could also contribute to these differences in solubility. The PA was insoluble in chloroform but completely soluble in dimethylsulfoxide (DMSO). The PA-TR was partially soluble in chloroform but completely insoluble in DMSO.

A.3 FULLY ASSIGNED ^{1}H AND ^{13}C SPECTRA FOR THE PA AND PI

The PI and PA were completely soluble in d-DMSO. ^{1}H and ^{13}C peak assignments for these polymers were determined using the 2-D experiments COSY, HSQC, and HMBC. We have included the labeled ^{1}H and ^{13}C spectra for these polymers in Figure A.1 and Figure A.2, respectively. For clarity, we have excluded the quarternary carbons in the ^{13}C spectra (i.e., peaks **g** and **n**). For the PI sample, peak **n** is centered at 64.6 ppm and peak **g** is centered at 62.7 ppm. For the PA sample, peak **n** is centered at 64.7 ppm and peak **g** is centered at 63.9.

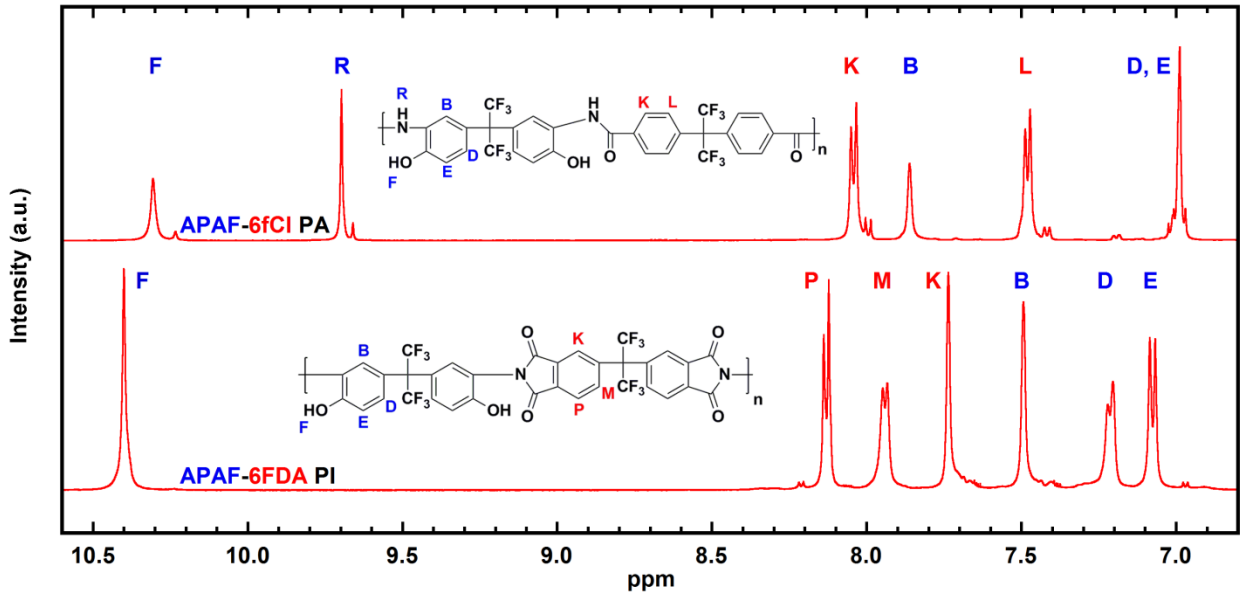

Figure A.1: ^{1}H peak assignment for the APAF-6fCl poly(*hydroxy*-amide) (PA) and APAF-6FDA poly(*hydroxy*-imide) (PI). Peak intensities have been normalized to that of the peak of highest intensity.

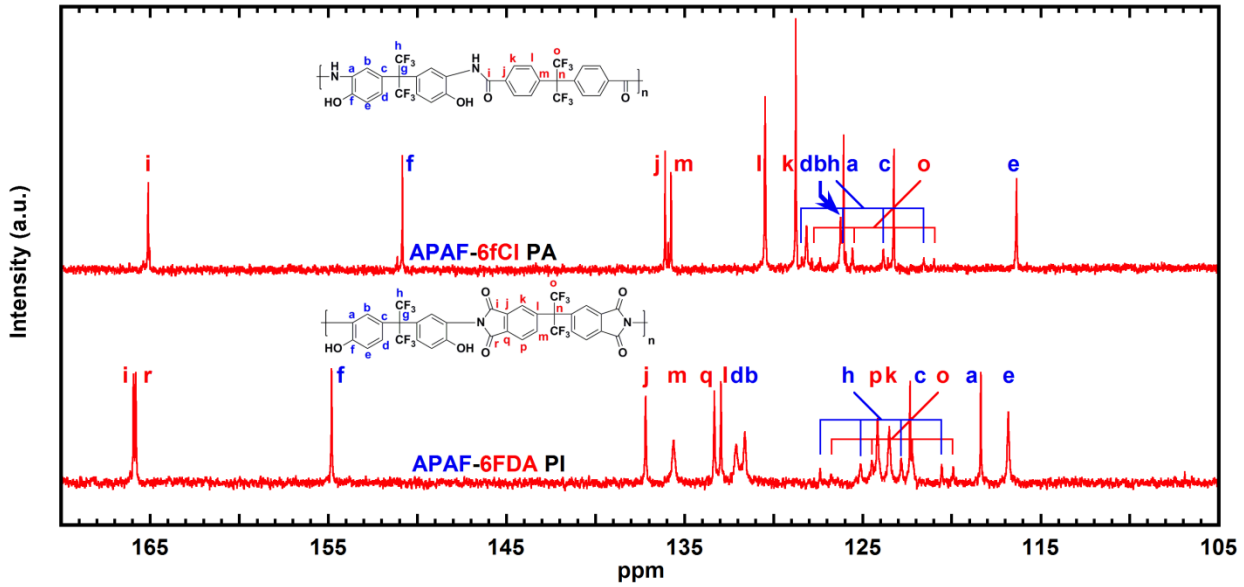

Figure A.2: ^{13}C peak assignments for the APAF-6fCl poly(*hydroxy*-amide) (PA) and APAF-6FDA poly(*hydroxy*-imide) (PI). Maximum peak intensity normalized by peak **f**. Peaks **g** and **n**, which are observed outside the aromatic region, are not included on this plot for clarity.

A.4 FULLY ASSIGNED ^{1}H AND ^{13}C SPECTRA FOR THE PA-TR

The chemical structure of the soluble fraction of the PA-TR sample was identified using 1-D and 2-D NMR. The fully assigned aromatic region of the ^{1}H spectra is shown in Figure A.3. For brevity, Figure A.3 only lists the peaks identified by both solution and solid-state NMR. Figure A.4 shows the chemical structure and peak labels for each carbon in the PA-TR structure. The carbons attached to the F_3 groups, peaks **h** and **o**, appear as 1:3:3:1 quartets centered near 124 to 125 ppm with peaks equally spaced in intervals slightly over 2 ppm. Matsuura *et al.* have reported similar ^{13}C NMR assignments for monomers containing CF_3 groups, and the reason that these quartets appear is because fluorine is NMR active.[1] Because peaks **h** and **o** are 4-bonds removed from the aromaticity of the PA-TR, their relative assignments in Figure A.2 and Figure A.4 were determined by analogy to NMR spectra of soluble APAF and 6FDA containing polyimides.

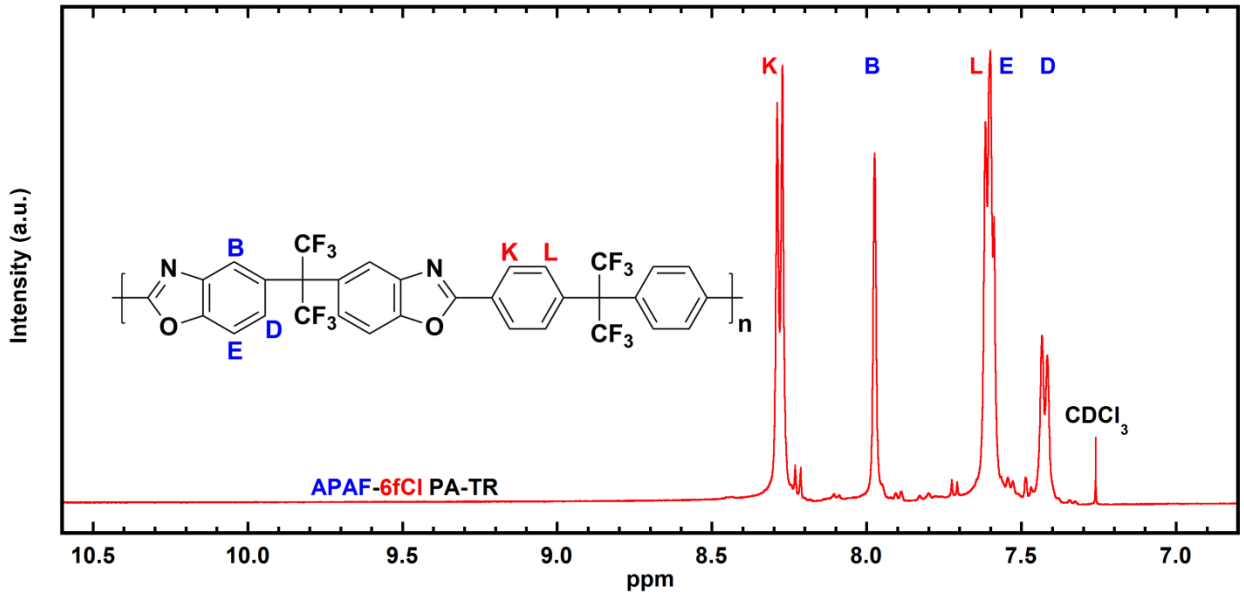

Figure A.3: ^{1}H peak assignments for the protons in the APAF-6fCl TR polymer (PA-TR).

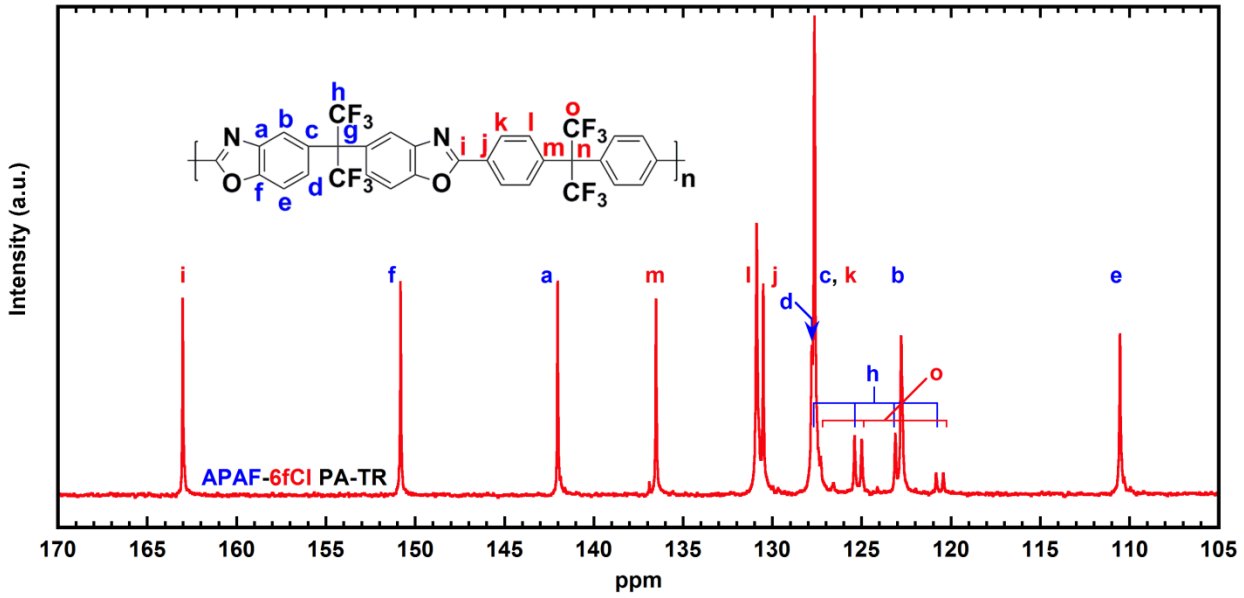

Figure A.4: ^{13}C peak assignments for the APAF-6fCl TR polymer (PA-TR). To provide the clearest peak assignments possible, peaks g and n, which are observed at a shift of 64.9 ppm, are not included in this plot.

A.5 ^{1}H $T_{1\rho}$ MEASUREMENTS

The ^{1}H $T_{1\rho}$ relaxation times of the PI-TR and PA-TR polymers would be determined by ^{1}H–^{1}H homonuclear dipolar interactions because the contribution of protons' small chemical shift anisotropies (CSAs) can be neglected. Furthermore, the contribution of the directly bonded ^{1}H–^{13}C dipolar interactions is also negligible because of the low natural abundance of ^{13}C (~ 1%). If the on-resonance spin-lock pulse irradiation rf pulse amplitude is ν_1 (ν_1 values are 44 and 63 kHz in our experiments), the measured relaxation rate, $1/T_{1\rho}$, can be expressed by the following relaxation equation[2,3]

$$\frac{1}{T_{1\rho}} = \frac{1}{2}\left(\delta_{H,H}\right)^2\left[\frac{3\tau_c}{1+4\nu_1^2\tau_c^2}+\frac{5\tau_c}{1+\nu_H^2\tau_c^2}+\frac{2\tau_c}{1+4\nu_H^2\tau_c^2}\right] \qquad \text{(A.1)}$$

where $\delta_{H,H}, \nu_H$, and τ_c are the effective ^{1}H–^{1}H dipolar coupling strength experienced by the protons at the measurement site, the ^{1}H's Larmor frequency ($\nu_H = 300$ MHz at 7.05 T), and the correlation time of the segmental motions in the polymer chain responsible for the $T_{1\rho}$ relaxation, respectively. Because the segmental motions in the polymer chains that move in the frequency range of a few tenths of a kHz are responsible for the $T_{1\rho}$ relaxation in our experiments, the scale of τ_c in Eq. (1) would be in a few tenths microseconds regime.[4] Then, Eq. (2) can be simplified to

$$\frac{1}{T_{1\rho}} \approx \frac{1}{2}\left(\delta_{H,H}\right)^2\left[\frac{3\tau_c}{1+4\nu_1^2\tau_c^2}\right] \qquad \text{(A.2)}$$

because the second and third terms in Eq. (2) can be neglected ($\nu_H\tau_c \gg 1$).

The observed differences in the $T_{1\rho}$ relaxation times can be attributed to the difference in the thermally rearranged (TR) structures of the PA-TR and PI-TR polymers. The PI-TR polymer possesses a more cross-linked structure than the PA-TR polymer, resulting in an insoluble polymer matrix. Additionally, it contains some *meta* configuration in its thermally rearranged polymer structure because it was formed from a polyimide, APAF-6FDA, resulting in kinked, nonlinear polymer chain segments as confirmed by the solid-state ^{1}H-^{13}C CP-MAS spectrum. However, the thermally rearranged polymer structure of the PA-TR polymer contains only *para* connected aromatic rings because it was formed from the polyamide, APAF-6fCl. Thus, the PI-TR polymer may form a more rigid polymer matrix due to the presence of the cross-linked chains, resulting in slower segmental rotations and/or translations of polymer chains with a longer τ_c. Additionally, the combination of *para* and *meta* configurations in the PI-TR polymer produces a less densely packed polymer matrix, resulting in weaker effective ^{1}H-^{1}H dipolar interactions, $\delta_{H,H}$.[5] Then, the measured $T_{1\rho}$ of the PI-TR polymer would be longer than that of the PA-TR polymer as can be predicted from Equation (A.2). The time scale of the segmental motion responsible for the $T_{1\rho}$ relaxation mechanism will be $\tau_c \approx 1/\nu_1$.

The τ_c values obtained by solving Equation (A.2) based on the $T_{1\rho}$ and ν_1 values are 10. μs for the PI-TR polymer and 7.7 μs for the PA-TR polymer. The τ_c values obtained from these experiments were comparable to the $1/\nu_1$ values (22.7 μs for ν_1 = 44 kHz and 15.9 μs for ν_1 = 63 kHz) employed in both cases. The longer τ_c value of the PI-TR polymer can be attributed to the presence of cross-linked polymer chains in the polymer matrix. The $\delta_{H,H}$ values obtained were 4.56 and 4.82 kHz for the PI-TR and PA-TR polymers, respectively. Indeed, the density of the polymer matrix of the PI-TR polymer that possesses *meta* configuration is slightly higher than that of the PA-TR

polymer, consistent with the relative magnitudes of $\delta_{H,H}$. The PI-TR polymer had a density of 1.45 ± 0.03 g/cm^3 and the PA-TR polymer had a density of 1.43 ± 0.02 g/cm^3. We employed the two-dimensional (2D) ^{1}H-^{13}C wideline separation (WISE) experiment[6] for solid-state NMR spectroscopy under MAS (spinning speed = 7.7 kHz) to measure the strength of $\delta_{H,H}$ of both polymers. Because the strength of $\delta_{H,H}$ was similar for both samples, the ^{1}H spectra of the two samples were almost identical in peak intensity and peak width when overlaid for comparison (Figure A.5).

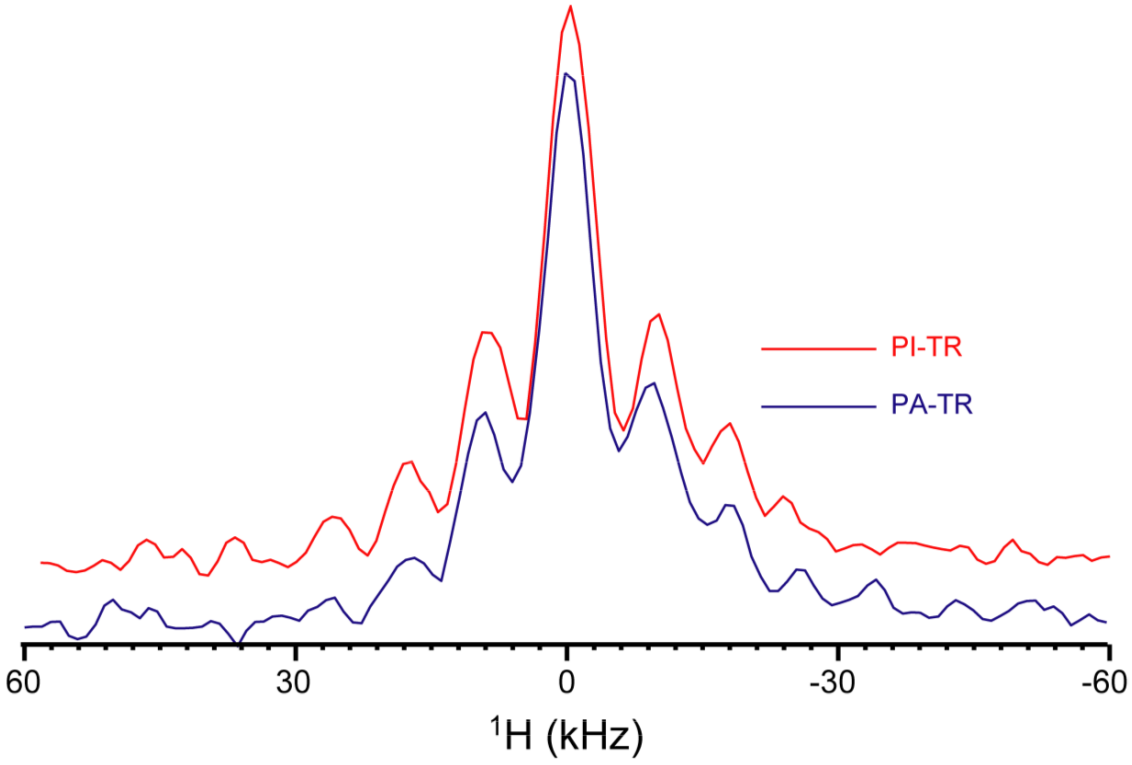

Figure A.5: The proton MAS spectra of the PI-TR and PA-TR polymers obtained along the indirect frequency domain of the 2D ^{1}H-^{13}C wideline separation (WISE) spectra.

A.6 SUPPORT FOR OXAZOLE FUNCTIONALITY BY FTIR

Fourier transform infrared spectroscopy (FTIR) was used to characterize oxazole bands present in the PI-TR polymer and the PA-TR polymer. Figure A.6 shows the FTIR spectra for the PI, PA, PI-TR, and PA-TR. Each of these spectra have been normalized to their maximum peak height and have been offset for easier viewing. Oxazole stretching, which is observed at 1058 cm^{-1} and 1480 cm^{-1}, is not observed in the PI and PA samples; however, these bands do appear for both the PI-TR polymer and PA-TR polymer [7,8].

Bands observed for the PI-TR and PA-TR polymers have nearly identical FTIR spectra, further confirming their highly similar structures. The PI-TR polymer does contain a small peak near 1734 cm^{-1}, and this peak may be an indication of some unreacted imide functionality creating some carbonyl stretching.

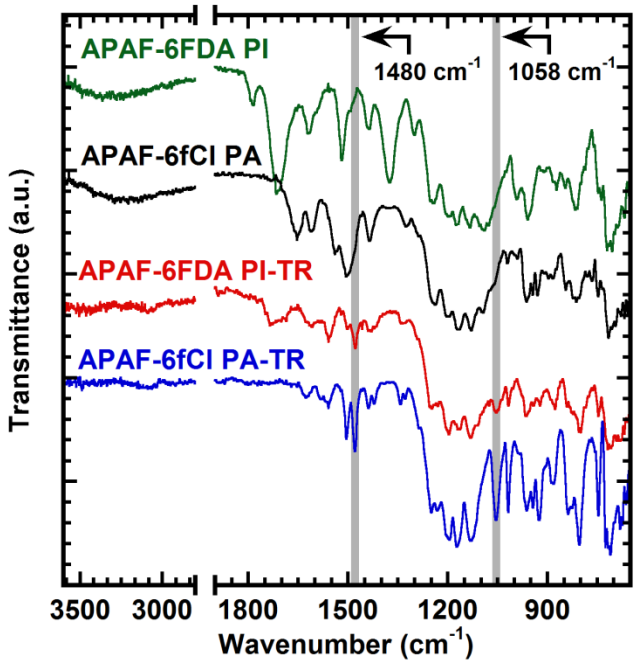

Figure A.6: FTIR spectra for the APAF-6FDA poly(*hydroxy*-imide) (PI), APAF-6fCl poly(*hydroxy*-amide) (PA), polyimide TR (PI-TR), and polyamide TR (PA-TR). Two bands often associated with benzoxazole ring stretching are highlighted in light gray.

A.7 MOLECULAR WEIGHT OF PRECURSORS BY SEC

Table A.1 presents molecular weight data for poly(*hydroxy*-imide) (PI) and poly(*hydroxy*-amide) precursors used in this study. The polydispersity of the PA sample was approximately 1.8, and the polydispersity for the PI sample was approximately 2.7. For samples with polydispersities below 2.0, low molecular weight oligomers in the molecular weight distribution could have been dissolved in the precipitating solvent, thereby removing them from the sample before the SEC experiment was performed. Table A.1 also includes values of intrinsic viscosity (IV), refractive index (dn/dc), and

Mark-Houwink parameters. The PA-TR was not soluble in the SEC solvent, so its molecular weight could not be determined.

Samples	Mn (Daltons)	Mw (Daltons)	PDI	IV (dL/g)[†]	dn/dc (mL/g)	Mark -Houwink Parameters	
						a	Log K
APAF-6FDA PI	22,000	59,000	2.7	0.36	0.121	0.768	-4.067
APAF-6fCl PA	143,000	256,000	1.8	0.67	0.108	0.768	-4.284

Table A.1: Molecular weight characterization for samples considered in this study. Polydispersity (PDI), intrinsic viscosity (IV), refractive index (dn/dc), and Mark-Houwink parameters are also listed.

A.8 EFFECT OF PRESSURE ON GAS PERMEABILITY

To illustrate the effect of pressure on these experiments, pure gas permeation experiments for H_2, CH_4, and CO_2 were conducted between pressures of approximately 1 and 50 atm. Robeson upper bound plots for H_2/CH_4 and CO_2/CH_4 separation, similar to those shown Chapter 4, are shown in Figure A.7 and Figure A.8. These plots present pure-gas transport data as a function of pressure.

For H_2/CH_4 separation, increasing pressure results in higher pure-gas selectivities, a result due to the stronger decrease in solubility for CH_4 than H_2 as pressure increases.[9,10] Interestingly, the PI sample has separation characteristics above the upper bound for all pressures considered. Furthermore, the PI-TR slightly surpasses the upper bound at pressures of approximately 50 atm. The PA and PA-TR samples exceed the 1991 upper bound at higher experimental pressures.

For CO_2/CH_4 separation, pure gas CO_2/CH_4 selectivity decreases with increasing CO_2 pressure for all samples except the PA-TR polymer. These trends typically result from stronger dual-mode sorption effects for CO_2 than for CH_4.[9] However, CO_2/CH_4 selectivity increases slightly with increasing CO_2 permeability for the PA-TR polymer.

While no plasticization pressure point was observed for CO_2 pressure curves for this sample, this polymer may undergo slow structural relaxation in the presence of CO_2.[11,12] Wind *et al.* have shown that crosslinking polyimides can improve plasticization resistance.[13] Our observation that the PI-TR polymer is insoluble and the PA-TR polymer is slightly soluble in chloroform is consistent with our conclusion that the PI-TR is more highly crosslinking than the PA-TR polymer, which may make it more resistant to plasticization and, therefore, affect the pure gas selectivity results presented in Figure A.8.

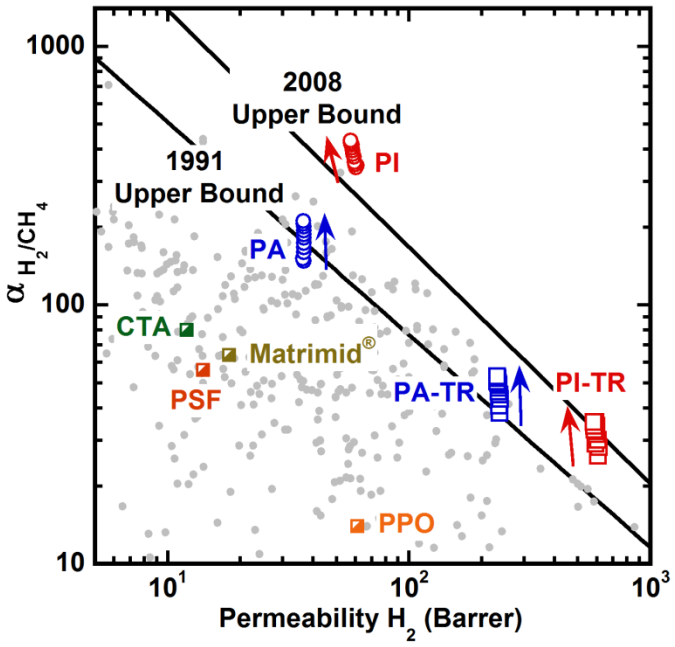

Figure A.7: H_2/CH_4 trade-off plot for the APAF-6FDA PI (PI), APAF-6FDA TR polymer (PI-TR), APAF-6fCl PA (PA), and APAF-6fCl TR polymer (PA-TR). Selectivity of H_2 to CH_4 is labeled as α_{H_2/CH_4}. Literature data is highlighted in light gray,[14] and industrially relevant polymers (i.e., cellulose triacetate (CTA), polysulfone (PSF), Matrimid®, and poly(phenylene oxide) (PPO))[15] are shown for comparison. Gas pressure increasses in the direction given by the arrows drawn next to the samples considered in this study.

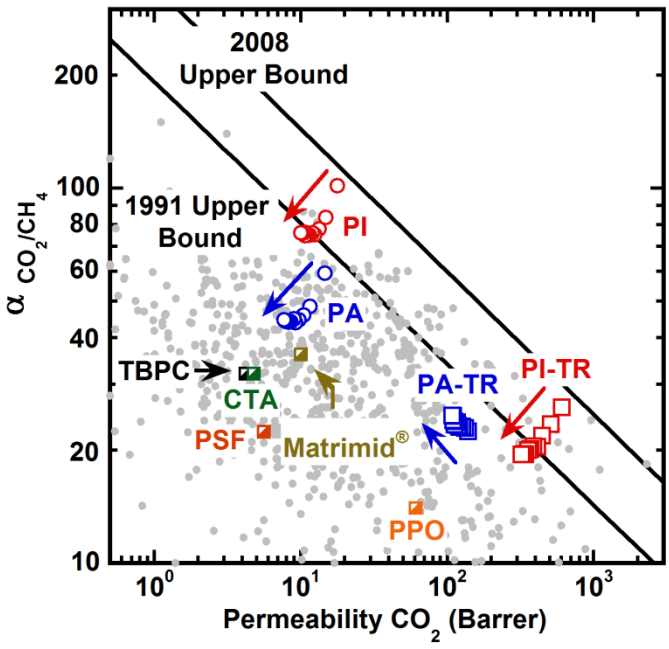

Figure A.8: CO_2/CH_4 Robeson trade-off plot for the APAF-6FDA PI (PI), APAF-6FDA TR polymer (PI-TR), APAF-6fCl PA (PA), and APAF-6fCl TR polymer (PA-TR). Selectivity of CO_2 to CH_4 is labeled as α_{CO_2/CH_4}. Literature data is highlighted in light gray[14], and industrially relevant polymers (i.e., tetrabromo polycarbonate (TBPC), cellulose triacetate (CTA), polysulfone (PSF), Matrimid®, and poly(phenylene oxide) (PPO))[15] are highlighted for comparison. Gas pressure increasses in the direction given by the arrows drawn next to the samples considered in this study.

A.9 PALS RESULTS FOR DETERMINING FREE VOLUME AND FREE VOLUME DISTRIBUTION

The free volume and free volume distribution for samples considered in this study, as determined by positron annihilation lifetime spectroscopy (PALS), are shown in Figure A.9. The diameter of free volume elements increases in the following order: APAF-6fCl PA < APAF-6FDA PI < APAF-6fCl PA-TR (PA-TR) < APAF-6FDA PI-TR (PI-TR). This order of increasing free volume correlates with increases in gas

permeability. Conversion of the PI to the PI-TR and the PA to the PA-TR also increased the intensity of formation of *ortho*-positronium (i.e., parameter I_3); however, the PI has a relatively low I_3 value. Shantarovich *et al.* have reported that positrons can be inhibited by carbonyl groups of imides[16], so these positron inhibition effects may result in artificially low PI I_3 values. Han *et al.* have reported bimodal free volume distributions for APAF-6FDA PI-based TR polymers and APAF PA-based PBOs[17]. Bimodal distributions could also be fit to the PALS data for the PI-TR and PA-TR polymers in this study. However, despite adding additional fitting parameters (i.e., τ_4 and I_4), similar parameter uncertainties were observed. Additionally, the precursor PI and PA could not be reliably fitted with a bimodal distribution. For example, when fitting parameters for the PA, there was an uncertainty of 1% for I_3 when fitting a unimodal distribution, but an uncertainty of 22% for I_3 when fitting a bimodal distribution. Therefore, to draw the most generalized correlation between changes in free volume between different samples, we have only used unimodal fitting for our PALS experiments.

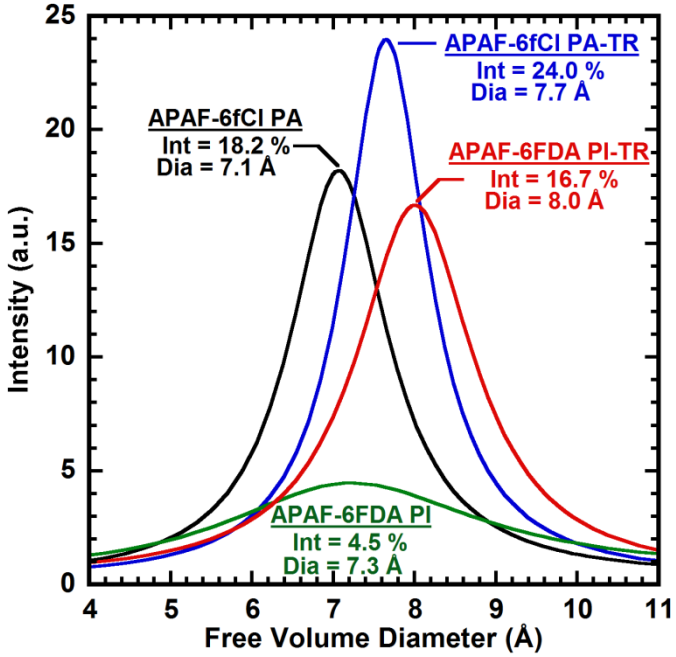

Figure A.9: Positron annihilation lifetime spectroscopy for the APAF-6FDA polyimide (PI), APAF-6fCl polyamide (PA), APAF-6FDA TR polymer (PI-TR), and the APAF-6fCl TR polymer (PA-TR)

A.10 REFERENCES

1. Matsuura, T., M. Ishizawa, Y. Hasuda, and S. Nishi, Polyimides derived from 2, 2'-bis (trifluoromethyl)-4, 4'-diaminobiphenyl. 2. Synthesis and characterization of polyimides prepared from fluorinated benzenetetracarboxylic dianhydrides. Macromolecules, **1992**. 25(13), 3540-3545.

2. Kimmich, R., NMR: tomography, diffusometry, relaxometry. Vol. 432. **1997**, Springer Berlin etc.

3. Look, D.C., I.J. Lowe, and J.A. Northby, Nuclear magnetic resonance study of molecular motions in solid hydrogen sulfide. The Journal of Chemical Physics, **1966**. 44(9), 3441-3452.

4. Fung, B.M., A.K. Khitrin, and K. Ermolaev, An improved broadband decoupling sequence for liquid crystals and solids. Journal of Magnetic Resonance, **2000**. 142(1), 97-101.

5. Zhang, B., J. Spano, Y. Chen, R. Turner, and S. Wi, Crystallinity and motional dynamics study of a series of poly(arylene ether sulfone) segmented copolymer analogues. The Journal of Physical Chemistry B, **2012**. 116(27), 7970-7980.

6. Schmidt-Rohr, K. and H.W. Spiess, Multidimensional solid-state NMR and polymers. **1994**, Elsevier.

7. Park, H.B., C.H. Jung, Y.M. Lee, A.J. Hill, S.J. Pas, S.T. Mudie, E. Van Wagner, B.D. Freeman, and D.J. Cookson, Polymers with cavities tuned for fast selective transport of small molecules and ions. Science, **2007**. 318(5848), 254-258.

8. Smith, Z.P., D.F. Sanders, C.P. Ribeiro Jr, R. Guo, B.D. Freeman, D.R. Paul, J.E. McGrath, and S. Swinnea, Gas sorption and characterization of thermally rearranged polyimides based on 3,3'-dihydroxy-4,4'-diamino-biphenyl (HAB) and 2,2'-bis-(3,4-dicarboxyphenyl) hexafluoropropane dianhydride (6FDA). Journal of Membrane Science, **2012**. 416, 558-567.

9. Paul, D.R. and W.J. Koros, Effect of partially immobilizing sorption on permeability and the diffusion time lag. Journal of Polymer Science: Polymer Physics Edition, **1976**. 14(4), 675-685.

10. Smith, Z.P., R.R. Tiwari, T.M. Murphy, D.F. Sanders, K.L. Gleason, D.R. Paul, and B.D. Freeman, Hydrogen sorption in polymers for membrane applications. Polymer, **2013**. 54(12), 3026–3037.

11. Bos, A., I.G.M. Punt, M. Wessling, and H. Strathmann, CO_2-induced plasticization phenomena in glassy polymers. Journal of Membrane Science, **1999**. 155(1), 67-78.

12. Visser, T. and M. Wessling, When do sorption-induced relaxations in glassy polymers set in? Macromolecules, **2007**. 40(14), 4992-5000.

13. Wind, J.W., C. Staudt-Bickel, D.R. Paul, and W.J. Koros, The effects of crosslinking chemistry on CO_2 plasticization of polyimide gas separation membranes. Industrial & Engineering Chemistry Research, **2002**. 41, 6139-6148.

14. Robeson, L.M., The upper bound revisited. Journal of Membrane Science, **2008**. 320(1-2), 390-400.

15. Sanders, D.F., Z.P. Smith, R. Guo, L.M. Robeson, J.E. McGrath, D.R. Paul, and B.D. Freeman, Energy-efficient polymeric gas separation membranes for a sustainable future: A review. Polymer, **2013**. 54(18), 4729-4761.

16. Shantarovich, V.P., T. Suzuki, C. He, and V.W. Gustov, Inhibition of positronium formation by polar groups in polymers—relation with TSL experiments. Radiation Physics and Chemistry, **2003**. 67(1), 15-23.

17. Han, S., H. Kwon, K. Kim, J. Seong, C. Park, S. Kim, C.M. Doherty, A. Thornton, A.J. Hill, A. Lozano, K. Berchtold, and Y. Lee, Tuning microcavities in thermally rearranged polymer membranes for CO_2 capture. Physical Chemistry Chemical Physics, **2012**. 14(13), 4365-4373.

Appendix B: Supporting Information for Chapter 7

B.1 TABULATED PERMEABILITY, DIFFUSIVITY, AND SORPTION COEFFICIENTS FOR HYDROGEN

Table B.1 presents the tabulated data for hydrogen permeability, diffusivity, and sorption coefficients shown in Figure 7.1, Figure 7.6A, and Figure 7.6B.

This appendix has been adapted from: Smith, Z.P., R.R. Tiwari, M.E. Dose, K.L. Gleason, T.M. Murphy, D.F. Sanders, G. Gunawan, L.M. Robeson, D.R. Paul, and B.D. Freeman, *The influence of diffusivity and sorption on helium and hydrogen separations in hydrocarbon, silicon, and fluorocarbon-based polymers (Submitted).*

Sample	Permeability (Barrer)	Diffusivity $\times 10^5$ (cm^2/s) from $P = [\overline{D}][\overline{S}]$	Sorption (cm^3(STP)/(cm^3 atm))
HAB-6FDA Polyimide	31 ± 2	0.21 ± 0.01	0.1135 ± 0.0006
HAB-6FDA TR 450 30min	420 ± 20	1.14 ± 0.06	0.279 ± 0.002
Matrimid®	28 ± 1	0.181 ± 0.009	0.1177 ± 0.0003
PSF	14 ± 1	0.14 ± 0.01	0.0757 ± 0.0006
PDMS	930 ± 90	6.3 ± 0.6	0.1130 ± 0.0001
Hyflon® AD 60	240 ± 20	1.4 ± 0.1	0.1338 ± 0.0008
Teflon® AF 1600	700 ± 60	3.0 ± 0.2	0.1382 ± 0.0006
Teflon® AF 2400	2500 ± 200	8.9 ± 0.8	0.2137 ± 0.0002
Nafion® N117	9.8 ± 0.5	0.116 ± 0.006	0.0641 ± 0.0006
Tecnoflon® PL 455	18 ± 1	0.17 ± 0.01	0.0814 ± 0.0008
Tecnoflon® P 457	14 ± 1	0.13 ± 0.01	0.078 ± 0.0008
Tecnoflon® P 459	23 ± 3	0.24 ± 0.03	0.072 ± 0.001

NOTES:
All values are reported at 35 ± 1°C. Permeability and permeability uncertainty values are shown for 10 atm. Sorption is taken as the linear fit to sorption isotherms between 0 and 60 bar, and diffusivity is reported as the ratio of permeability to sorption.
There are slight differences in permeability between data in this table and literature data for the HAB-6FDA polyimide,[1] HAB-6FDA TR 450 30min,[1] Matrimid®,[2] AF 1600,[3] AF 2400,[3] and Nafion® N117.[4] Results are within the uncertainty of the measurements for PDMS.[5] Possible reasons for differences in permeation may result from synthesis of different batches of polymers, differences in polymer or monomer supplier, slight variations in thermal treatment, and slight variations in sample casting procedures.
Permeability data for PSF and sorption data for the HAB-6FDA polyimide, HAB-6FDA TR 450 30min, Matrimid®, PSF, PDMS, and AF 2400 are taken from reference.[6]
Uncertainty for permeability was estimated by propagation of error techniques.[7]
Uncertainty for sorption was estimated by taking the standard error of the slope of the sorption isotherms when fit with a linear fit.
Uncertainty for diffusivity was estimated from the solution diffusion model using the uncertainty for permeability and sorption.

Table B.1: Permeability, diffusivity, and sorption data for hydrogen

B.2 TABULATED PERMEABILITY, DIFFUSIVITY, AND SORPTION COEFFICIENTS FOR HELIUM

Table B.2 presents the tabulated data for helium permeability, diffusivity, and sorption coefficients shown in Figure 7.1, Figure 7.6A, and Figure 7.6B.

Sample	Permeability (Barrer)	Diffusivity $\times 10^5$ (cm^2/s) from $P = [\overline{D}][\overline{S}]$	Sorption (cm^3(STP)/(cm^3 atm)
HAB-6FDA Polyimide	39 ± 2	0.96 ± 0.05	0.0310 ± 0.0009
HAB-6FDA TR 450 30min	280 ± 10	2.8 ± 0.2	0.077 ± 0.002
Matrimid®	27 ± 2	0.63 ± 0.04	0.0327 ± 0.0003
PSF	12.5 ± 0.5	0.39 ± 0.02	0.0243 ± 0.0009
PDMS	510 ± 30	5.7 ± 0.3	0.0678 ± 0.0003
Hyflon® AD 60	570 ± 50	5.5 ± 0.5	0.0788 ± 0.0004
Teflon® AF 1600	1100 ± 100	6.6 ± 0.6	0.0874 ± 0.001
Teflon® AF 2400	2800 ± 200	15 ± 1	0.143 ± 0.004
Nafion® N117	48 ± 3	0.99 ± 0.06	0.0369 ± 0.0002
Tecnoflon® PL 455	44 ± 3	0.49 ± 0.04	0.0686 ± 0.0009
Tecnoflon® P 457	39 ± 4	0.49 ± 0.05	0.0604 ± 0.0007
Tecnoflon® P 459	67 ± 9	0.8 ± 0.1	0.064 ± 0.001

NOTES:
All values are reported at 35 ± 1°C. Permeability and permeability uncertainty values are shown for 10 atm. Sorption is taken as the linear fit to sorption isotherms between 0 and 60 bar, and diffusivity is reported as the ratio of permeability to sorption.
There are slight differences in permeability between data in this table and literature data for Matrimid®,[2] and Nafion® N117.[4] Results are within the uncertainty of the measurements for PDMS.[5] Possible reasons for differences in permeation may result from synthesis of different batches of polymers, differences in polymer or monomer supplier, slight variations in thermal treatment, and slight variations in sample casting procedures.
Uncertainty for permeability was estimated by propagation of error techniques.[7]
Uncertainty for sorption was estimated by taking the standard error of the slope of the sorption isotherms when fit with a linear fit.
Uncertainty for diffusivity was estimated from the solution diffusion model using the uncertainty for permeability and sorption.

Table B.2: Permeability, diffusivity, and sorption data for helium

B.3 TABULATED He/H_2 DIFFUSIVITY SELECTIVITY

Table B.3 presents the tabulated data for He/H_2 diffusivity selectivity for the samples considered in this study.

Sample	He/H_2 Diffusivity Selectivity
HAB-6FDA Polyimide	4.6 ± 0.3
HAB-6FDA TR 450 30min	2.5 ± 0.2
Matrimid®	3.5 ± 0.3
PSF	2.8 ± 0.2
PDMS	0.9 ± 0.1
Hyflon® AD 60	4.0 ± 0.5
Teflon® AF 1600	2.5 ± 0.3
Teflon® AF 2400	1.7 ± 0.2
Nafion® N117	8.5 ± 0.7
Tecnoflon® PL 455	2.9 ± 0.3
Tecnoflon® P 457	3.6 ± 0.5
Tecnoflon® P 459	3.3 ± 0.6

Table B.3: He/H_2 diffusivity selectivity for all samples considered in this study. Uncertainty is reported as one standard deviation determined by propagation of error techniques.[7]

B.4 REFERENCES

1. Sanders, D.F., Z.P. Smith, C.P. Ribeiro, R.L. Guo, J.E. McGrath, D.R. Paul, and B.D. Freeman, Gas permeability, diffusivity, and free volume of thermally rearranged polymers based on 3,3 '-dihydroxy-4,4 '-diamino-biphenyl (HAB) and 2,2 '-bis-(3,4-dicarboxyphenyl) hexafluoropropane dianhydride (6FDA). Journal of Membrane Science, **2012**. 409, 232-241.

2. Zhang, Y., I.H. Musselman, J.P. Ferraris, and K.J. Balkus, Gas permeability properties of Matrimid® membranes containing the metal-organic framework Cu–BPY–HFS. Journal of Membrane Science, **2008**. 313(1-2), 170-181.

3. Merkel, T.C., I. Pinnau, R. Prabhakar, and B.D. Freeman, Gas and vapor transport properties of perfluoropolymers, in Materials science of membranes for gas and vapor separations, Y. Yampolskii, P., I. Pinnau, and B.D. Freeman, Editors. **2006**, John Wiley & Sons, Ltd: Chichester. 251 - 270.

4. Chiou, J.S. and D.R. Paul, Gas permeation in a dry Nafion membrane. Industrial & Engineering Chemistry Research, **1988**. 27(11), 2161-2164.

5. Merkel, T.C., V.I. Bondar, K. Nagai, B.D. Freeman, and I. Pinnau, Gas sorption, diffusion, and permeation in poly(dimethylsiloxane). Journal of Polymer Science Part B: Polymer Physics, **2000**. 38(3), 415-434.

6. Smith, Z.P., R.R. Tiwari, T.M. Murphy, D.F. Sanders, K.L. Gleason, D.R. Paul, and B.D. Freeman, Hydrogen sorption in polymers for membrane applications. Polymer, **2013**. 54(12), 3026–3037.

7. Bevington, P.R. and K.D. Robinson, Data reduction and error analysis for the physical sciences: Third edition. **2003**, Boston, McGraw Hill.

Appendix C: Supporting Information for Chapter 8

C.1 MOLECULAR WEIGHT, VISCOSITY, AND LIGHT SCATTERING RESULTS FOR POLYIMIDES AND THE POLYAMIDE

Table C.1 presents molecular weight values for the poly(*hydroxy*-imide)s synthesized in solution and the polyamide considered in this work. For the poly(*hydroxy*-imide)s, the number average molecular weight increases in the following order: APAF-6FDA < APAF-ODPA < HAB-6FDA. The lowest molecular weight sample (i.e., APAF-6FDA), had the least nucleophilic diamine and the most rigid dianhydride.[1,2] By replacing the rigid dianhydride with ODPA, a more flexible dianhydride, the sample reacts more readily, which may account for the higher molecular weight polyimide.[2,3] Finally, HAB-6FDA, which contains a more nucleophilic diamine (i.e., HAB) and the rigid, less reactive dianhydride (i.e., 6FDA), had a number average molecular weight that was the highest of all *ortho*-functional polyimides.

The chemically imidized sample of HAB-6FDA-C had a lower molecular weight than the thermally imidized sample of HAB-6FDA, and the molecular weight of the APAF-6fCl polyamide was significantly higher than that of the APAF-6FDA polyimide. The polydispersity index (PDI) was lowest for the HAB-6FDA-C polyimide and APAF-6fCl polyamide. PDI values below 2 may result from low molecular weight components in these samples partially dissolving in the extraction solvent. The PDI for all of the poly(*hydroxy*-imide)s was greater than 2, which is the theoretically limiting value for the most probable distribution for linear polycondensation reactions.[4] Husk *et al.* have proposed that deviations in PDI from values that are theoretically expected are related to

---

This appendix has been adapted from: Smith, Z.P., K. Czenkusch, K.L. Gleason, G.H.G.C. Alvarez, A.E. Lozano, D.R. Paul, and B.D. Freeman, *Effect of polymer structure on gas transport properties of polyimides, polyamides and TR polymers (in preparation).*

cross-linking, interchain association, or branching, which can occur while the sample is in its poly(amic acid) state.[5]

In addition to molecular weight and PDI, Table C.1 also presents the intrinsic viscosity, [η], refractive index increment, dn/dc, and the empirically determined Mark-Houwink parameters, α and Log K, for samples considered in this study.

Samples	Mn (Daltons)	Mw (Daltons)	PDI	[η] (dL/g)[a]	dn/dc (mL/g)	Mark -Houwink parameters	
						α	Log K
HAB-6FDA-C	44,000	79,000	1.8	1.1	0.153	0.692	-3.333
HAB-6FDA	67,000	163,000	2.4	1.5	0.174	0.541	-2.579
APAF-6FDA	22,000	59,000	2.7	0.36	0.121	0.768	-4.067
APAF-ODPA	59,000	197,000	3.3	0.95	0.159	0.693	-3.621
APAF-6fCl PA	143,000	256,000	1.8	0.67	0.108	0.768	-4.284

Table C.1: Comparison of molecular weight characteristics for TR polymer precursors considered in this study. Data for the APAF-6FDA and APAF-6fCl samples were taken from Appendix A, [a] average value

C.2 NUCLEAR MAGNETIC RESONANCE CHARACTERIZATION OF *HYDROXYL*-FUNCTIONAL POLYIMIDES

^{1}H and ^{13}C nuclear magnetic resonance (NMR) spectra were obtained for the solution imidized polyimides and solution amadized polyamide. To help identify peak locations, several 2-D solution NMR experiments were considered. These experiments included correlation spectroscopy (COSY), heteronuclear single quantum correlation (HSQC) spectroscopy, and heteronuclear multiple bond correlation (HMBC) spectroscopy. From these experiments, all of the protons and carbons could be assigned.

The ^{1}H assignments are shown in Table C.2, and the ^{1}H spectra are shown in Figure C.1. To help clarify peak assignments, a color-coding scheme has been employed: **dark yellow** represents nuclei attached to HAB, **blue** represents nuclei attached to APAF, **red** represents nuclei attached to 6FDA, and **green** represents nuclei attached to ODPA. The *hydroxyl* proton for every sample is shifted furthest downfield, appearing between approximately 10.1 and 10.5 ppm. The dianhydride protons for 6FDA and ODPA are located at chemical shifts between 7.5 and 8.3 ppm, and the diamine protons for APAF and HAB are located the furthest upfield, at chemical shifts between 7.0 and 7.5 ppm.

Polymer	Labels
HAB-6FDA	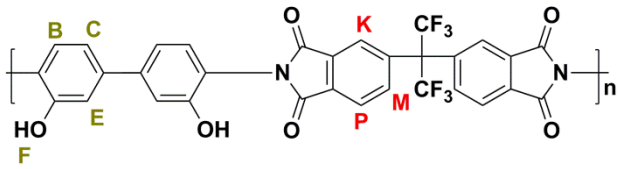
APAF-6FDA	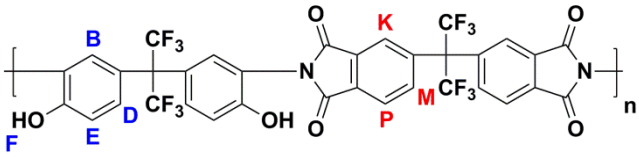
APAF-ODPA	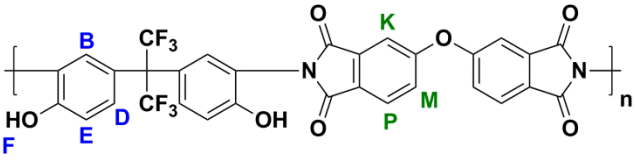

Table C.2: Proton assignments for NMR characterization. Proton assignments are color-coded. **Dark yellow** represents protons attached to HAB, **blue** represents protons attached to APAF, **red** represents protons attached to 6FDA, and **green** represents protons attached to ODPA.

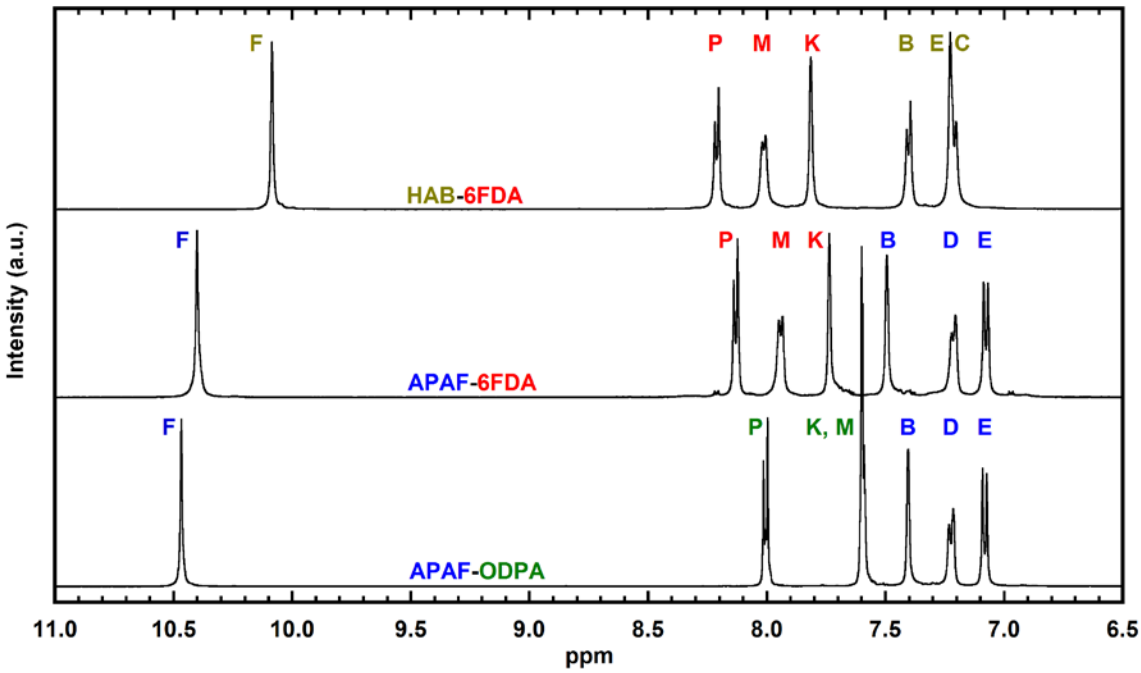

Figure C.1: ^{1}H spectra for HAB-6FDA, APAF-6FDA, and APAF-ODPA. Peaks are labeled according to Table C.2. Spectra have been normalized to peak **F** and offset for easier viewing.

Table C.3 and Figure C.2 presents the ^{13}C NMR peak assignments and ^{13}C NMR spectra for the *hydroxyl*-functional polyimides. Because 16 carbons peaks can be identified from these spectra, the plots have been split into three regions to more clearly show the locations of the labeled peaks. The full-scale spectra, presented in Figure C.2A, shows the peak assignments for only the quaternary carbons on the fluorinated monomers (i.e., peaks **g** and **n**). The only additional non-aromatic peaks (i.e., peaks **h** and **o**), have 1:3:3:1 quartets between 120 and 128 ppm, and these peaks are identified in Figure C.2B. Matsuura *et al.* have reported similar splitting patterns for carbons directly attached to fluorines on molecules containing hexafluoroisopropylidene functional groups,[6] and Cornelius *et al.* have reported these splitting patterns for a 6FDA-6FpDA polyimide.[7]

Figure C.2B and Figure C.2C present the aromatic region of the ^{13}C spectra and peak assignments for the *hydroxyl*-functional polyimides. Regardless of the co-monomer used in synthesis, each monomer maintains a nearly identical chemical shift for each carbon spectra. For example, the chemical shifts for the 6FDA segments in HAB-6FDA and APAF-6FDA are nearly identical. Similarly, the chemical shifts for the APAF segments in APAF-ODPA and APAF-6FDA are nearly identical. For the monomers considered in this work, differences in the polyimide backbone molecular structure result in changes in the chemical shift for the ^{13}C NMR spectra. Carbons adjacent to strongly electron-donating groups, such as the *hydroxyl* groups in the polyimides, and the *carbonyl* and *ether* groups in the ODPA monomer, are shifted furthest downfield. These peaks, labeled **i**, **r**, **l**, and **f**, are all found downfield of 155 ppm. Within the resolution of the NMR experiments, it is possible to differentiate between each carbon attached to the carbonyl groups. For the 6FDA-containing polyimides, peak **i** has a slightly higher chemical shift than peak **r**. However, the relative order of peak locations switch for the ODPA-containing polyimide (i.e., peak **r** has a slightly higher chemical shift than peak **i**). The reason for this shift in peak location relates to the electronic nature of the dianhydride-linking groups. For the 6FDA-containing polyimides, peak **i** is 3-bonds removed from the hexafluoroisopropylidene-linking group and peak **r** is 4-bonds removed. This very slight difference in the separation of chemical bonds results in these carbons having small differences in chemical shifts. In contrast with the strongly electron-withdrawing hexafluoroisopropylidene functional group in 6FDA, the ODPA-containing polyimide has an electron-donating *ether* linkage. Peak **i**, which is 3-bonds removed from this linkage is, therefore, shifted slightly upfield from peak **r**.

Carbons directly connected to moieties that bridge the aromatic units are strongly affected in their chemical shift. Peak **l**, which is directly connected to the *ether* linkage,

has a chemical shift of approximately 161 ppm for ODPA, and peak **l**, which is directly connected to the hexafluoroisopropylidene group, has a chemical shift of approximately 133 ppm for 6FDA. These shifts differ by approximately 28 ppm. For carbons that are one bond removed from the dianhydride linking group (i.e., peaks **k** and **m**), the shift is less. Peak **k** is located at a chemical shift of approximately 114 ppm for ODPA and approximately 124 ppm for 6FDA. Peak **m** is located at a chemical shift of approximately 125 ppm for ODPA and 136 ppm for 6FDA.

Polymer	Labels
HAB-6FDA	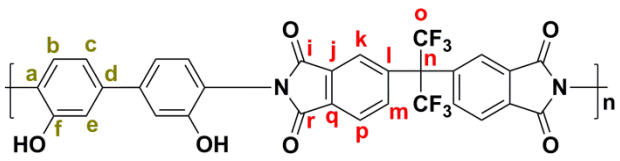
APAF-6FDA	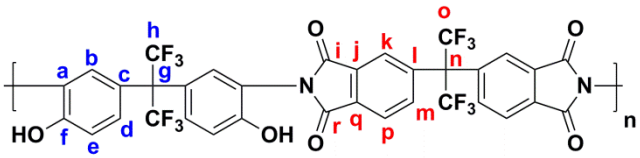
APAF-ODPA	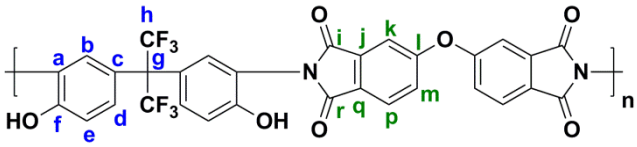

Table C.3: Carbon assignments for NMR characterization. Carbon assignments are color-coded based on their monomer location. **Dark yellow** represents protons attached to HAB, **blue** represents protons attached to APAF, **red** represents protons attached to 6FDA, and **green** represents protons attached ODPA.

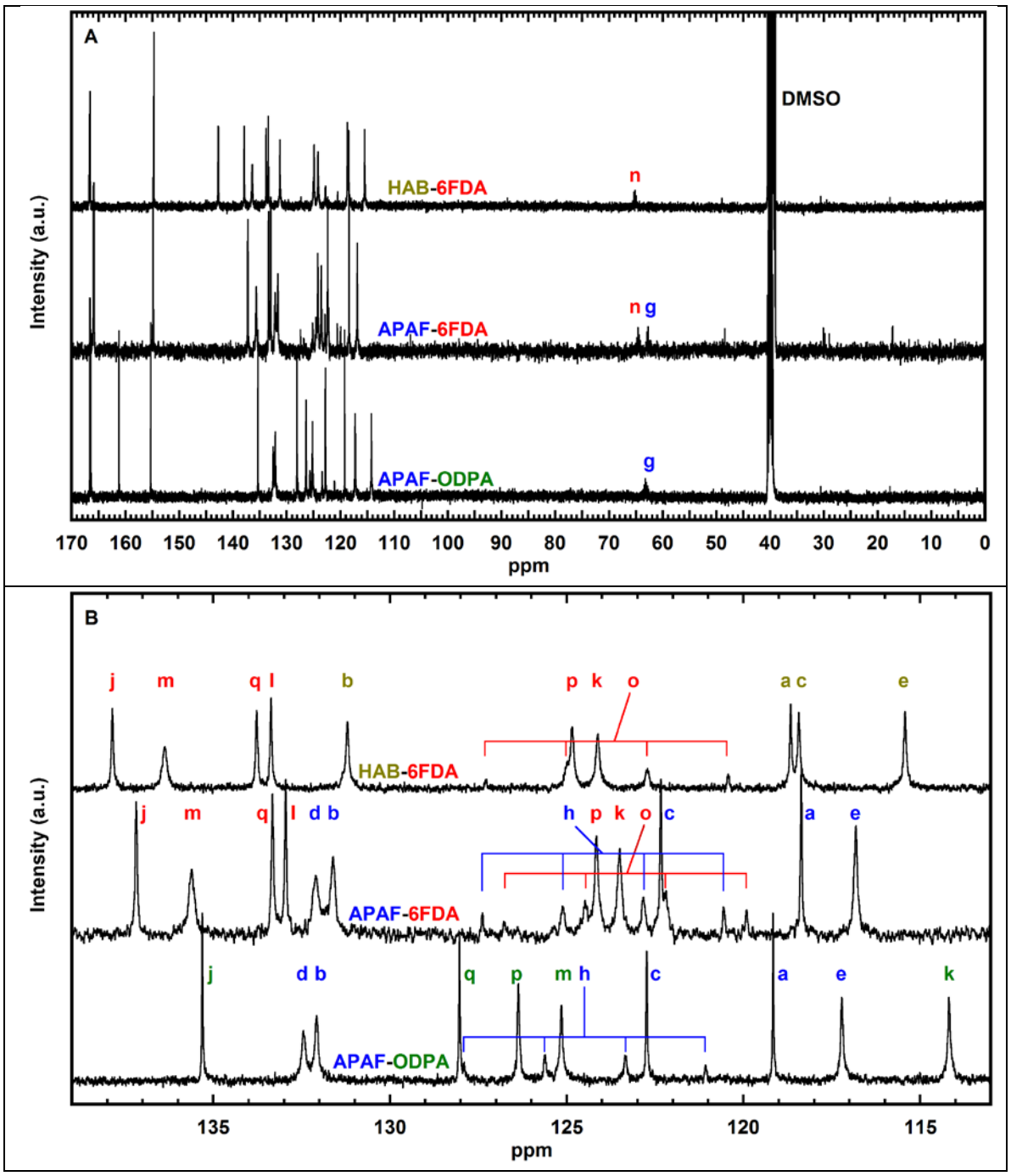
A
DMSO
HAB-6FDA
n
APAF-6FDA
n g
APAF-ODPA
g
Intensity (a.u.)
170 160 150 140 130 120 110 100 90 80 70 60 50 40 30 20 10 0
ppm
B
j m q l b p k o a c e
HAB-6FDA
j m q l d b h p k o c a e
APAF-6FDA
j d b q p m h c a e k
APAF-ODPA
Intensity (a.u.)
135 130 125 120 115
ppm

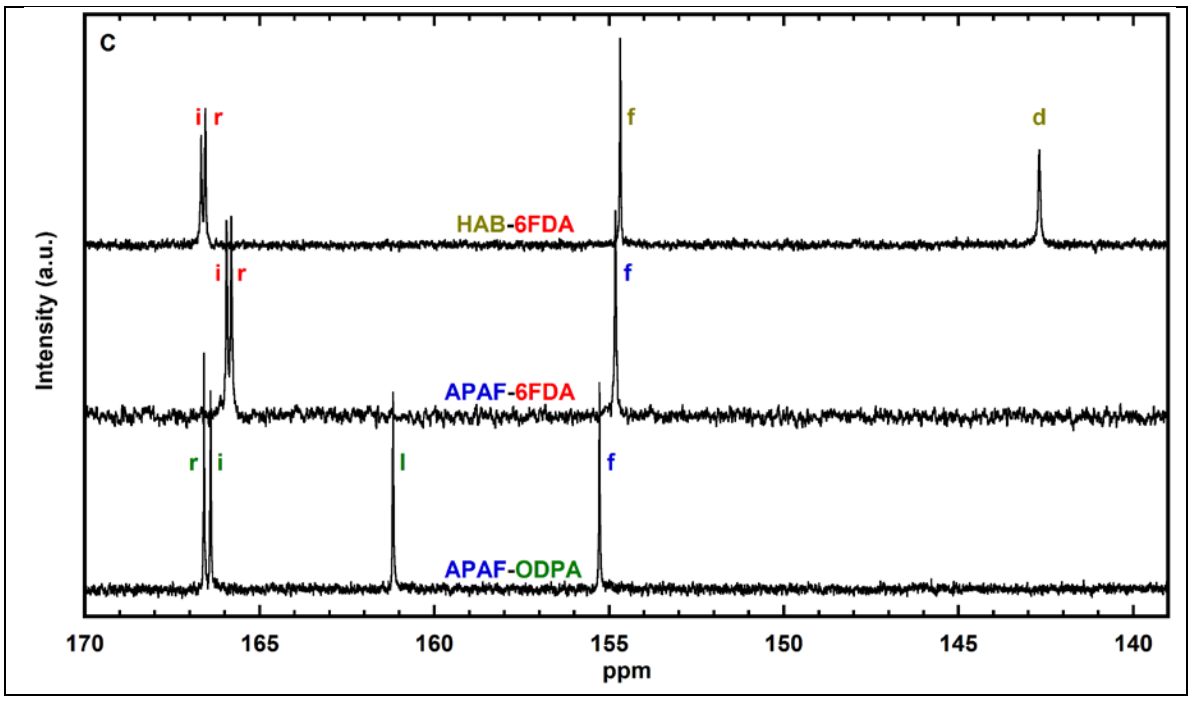

Figure C.2: ^{13}C spectra for HAB-6FDA, APAF-6FDA, and APAF-ODPA. Peaks are labeled as shown in Table C.3. Spectra have been normalized to peak **f** and offset for easier viewing. Figure (A) shows the full-scale spectra, figure (B) shows the spectra between 113 and 139 ppm, and figure (C) shows the spectra between 139 and 170 ppm.

C.3 NUCLEAR MAGNETIC RESONANCE CHARACTERIZATION OF *HYDROXYL* VERSUS *ACETATE*-FUNCTIONAL HAB-6FDA

^{1}H and ^{13}C NMR was also used to identify differences in chemical shifts for the *hydroxyl*- and *acetate*-functional HAB-6FDA polyimides. Table C.4 presents the proton and carbon assignments for HAB-6FDA-C. In addition to the assignments labeled in Table C.2 and Table C.3, the *acetate*-functional HAB-6FDA-C sample has three additional and identical protons (i.e., protons **H**) and two additional carbons (i.e., carbons **g** and **h**). Figure C.3A shows the full-scale ^{1}H spectrum for HAB-6FDA-C. The aromatic protons are shifted downfield of the *methyl* protons, which are located at a chemical shift of approximately 2.2 ppm, and the only major additional peaks detected

are for H_2O, which adventitiously sorbs into these samples due to their contact with ambient air, and d-DMSO, the solvent used in these experiments.

Figure C.3B presents the ^1H NMR spectra for the aromatic protons. From these spectra, there is almost no difference between the dianhydride protons in HAB-6FDA and HAB-6FDA-C. However, the diamine has dramatically different peak locations depending on the *ortho*-functional group. The proton attached to the *hydroxyl*-functional group (i.e., peak **F**) is only observed for HAB-6FDA and not for HAB-6FDA-C. A few trace peaks between 10 and 11 ppm are observed for the HAB-6FDA-C sample, and these peaks are possibly associated with a low level of *hydroxyl* groups that did not fully undergo the esterification reaction during chemical imidization.[8] These peaks may also result from some unreacted poly(amic acid), which would have carboxylic acids, typically detected around 11 ppm.[9]

Figure C.4A shows the entire ^{13}C NMR spectra for HAB-6FDA and HAB-6FDA-C. Only the carbons far outside the aromatic region are labeled. These carbons include the quaternary carbon attached to the hexafluoroisopropylidene functional group, **n**, and the methyl carbon, **h**, that is attached to the *acetate*-functional group on HAB-6FDA-C. No additional peaks were detected below a chemical shift of 115 ppm.

The aromatic carbons and the carbons attached to the CF_3 groups are shown in Figure C.4B and Figure C.4C. The carbon nuclei attached to the carbonyl groups on HAB-6FDA and HAB-6FDA-C are shifted further downfield than any other carbons considered. Similar to the analysis with the *hydroxyl*-functional polyimides, all of these peaks can be identified. Carbon **f** is shifted upfield of the carbonyl carbons. The stronger electron-donating nature of the *hydroxyl*-functional HAB-6FDA results in carbon **f** for this sample having a chemical shift of approximately 155 ppm, whereas carbon **f** in the *acetate*-functional HAB-6FDA-C has a chemical shift of approximately 147 ppm. Other

carbons are affected by the *acetate* functionality as well. For example, peak **e** shifts from 115 ppm for HAB-6FDA to 122 ppm for HAB-6FDA-C. At least minor differences in chemical shifts are also observed for the other carbons attached to the diamine. For the peaks associated with the 6FDA dianhydride, which is identical in HAB-6FDA and HAB-6FDA-C, very little difference in chemical shift is observed between these polymers. Chemical shifts differ by no more than 2 ppm between the *acetate* and *hydroxyl*-functional samples for the dianhydride carbons.

	Labels
Proton Assignments	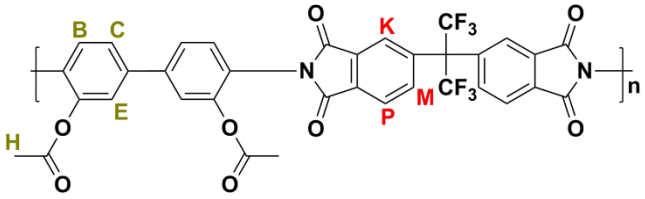
Carbon Assignments	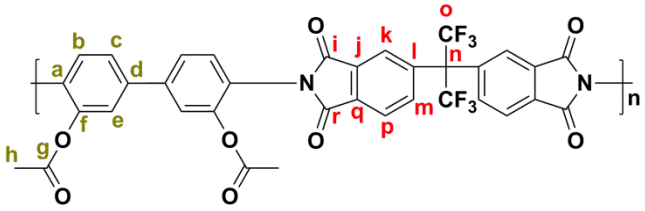

Table C.4: Proton and carbon assignments for NMR characterization of HAB-6FDA-C. Assignments are color-coded based on their monomer location. **Dark yellow** represents nuclei attached to HAB, and **red** represents nuclei attached to 6FDA.

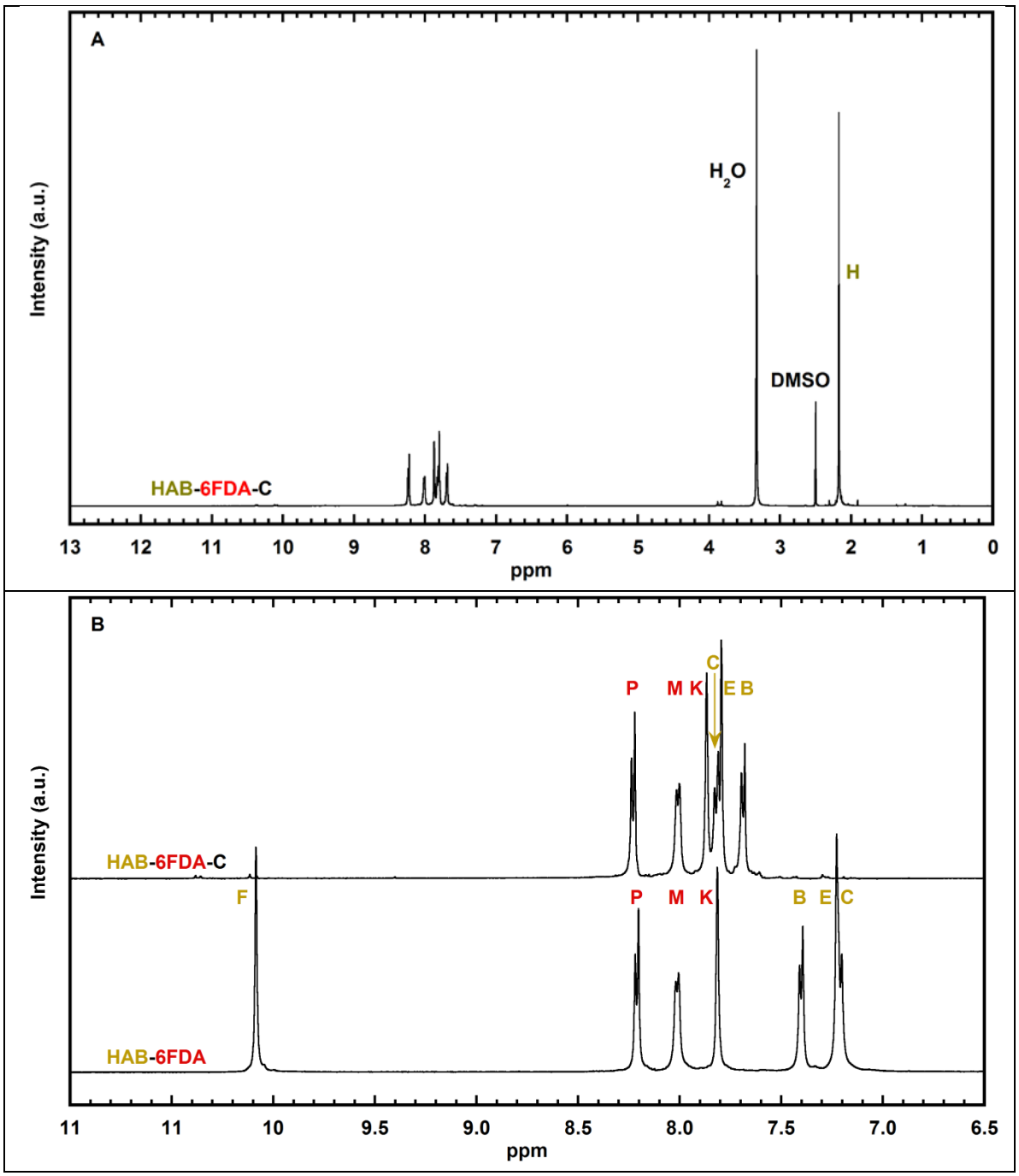

Figure C.3: (A) Full scale ^{1}H NMR spectra for HAB-6FDA-C, and (B) a comparison of the aromatic ^{1}H NMR spectra for the HAB-6FDA-C and HAB-6FDA samples. Peaks have been normalized to the maximum peak height of peak **P**.

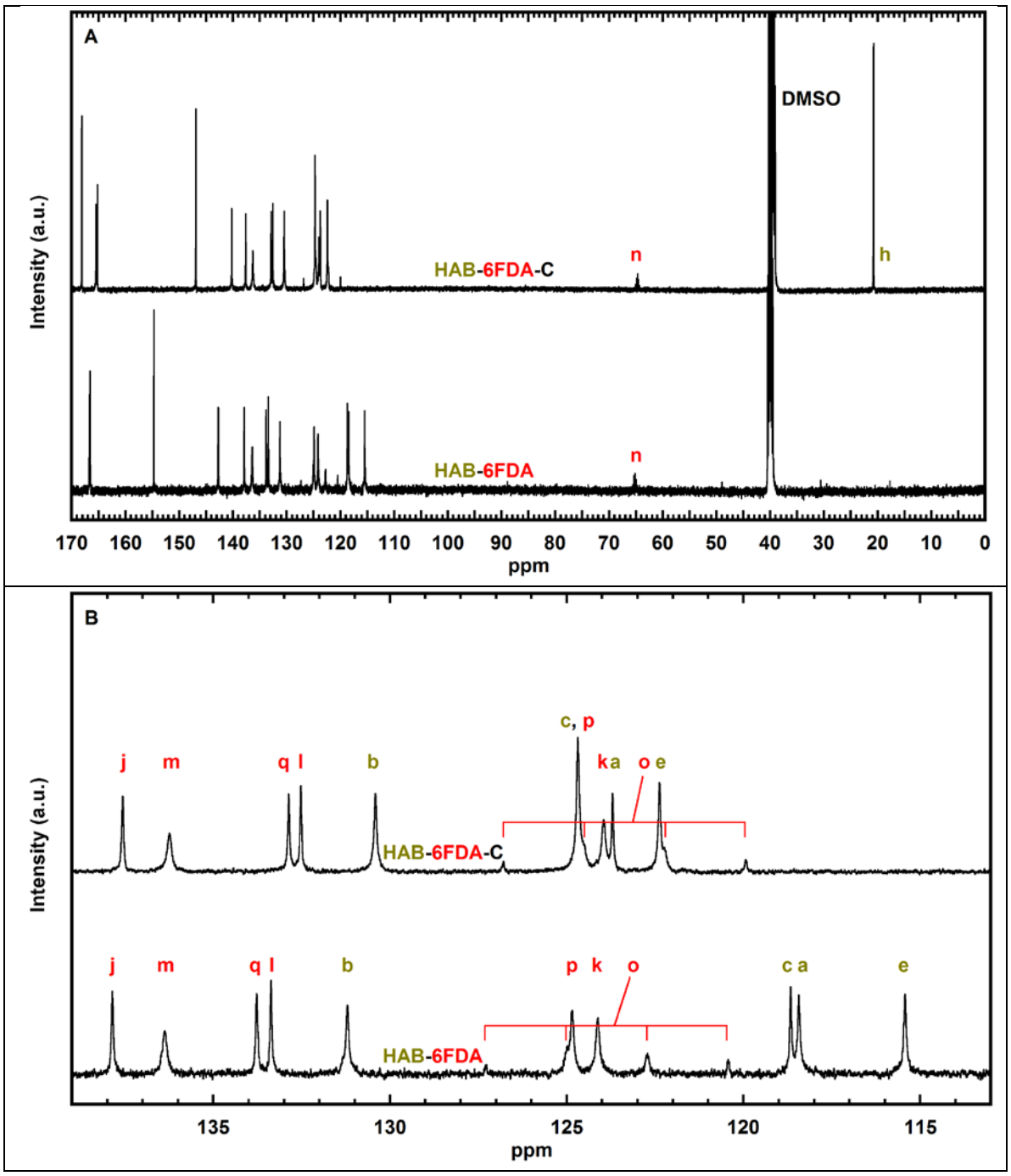
A
DMSO
Intensity (a.u.)
HAB-6FDA-C
n
h
HAB-6FDA
n
170 160 150 140 130 120 110 100 90 80 70 60 50 40 30 20 10 0
ppm
B
Intensity (a.u.)
j m q l b c, p k a o e
HAB-6FDA-C
j m q l b p k o c a e
HAB-6FDA
135 130 125 120 115
ppm

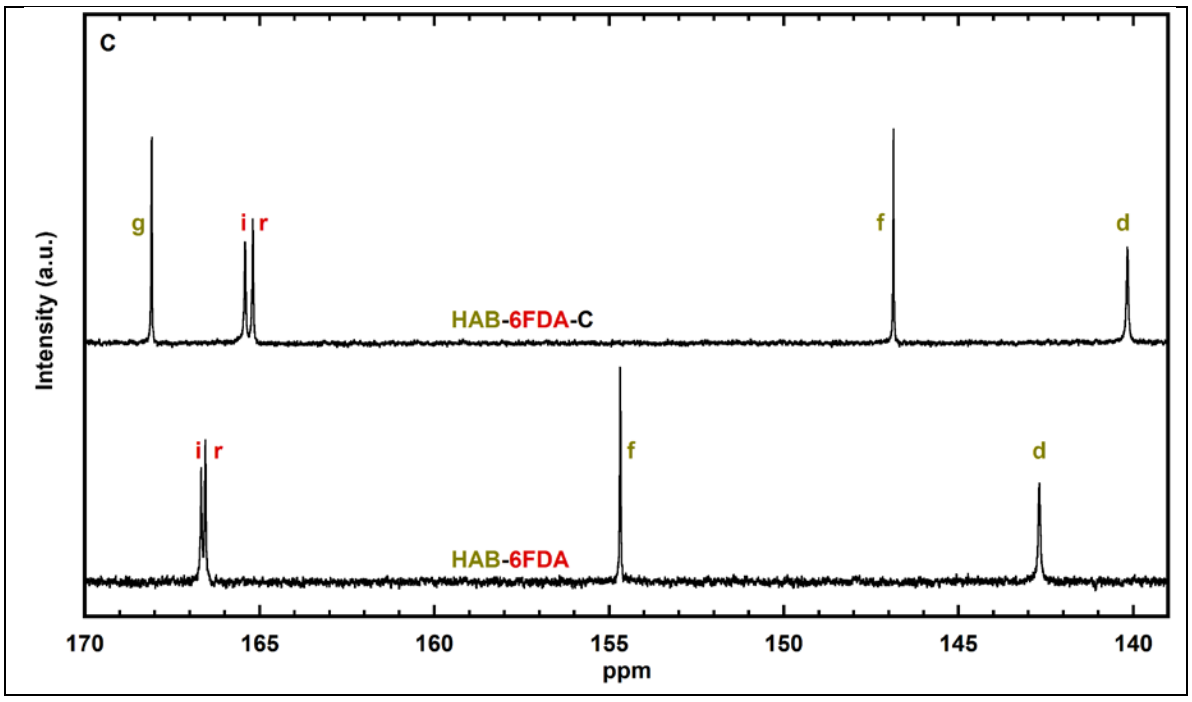

Figure C.4: ^{13}C spectra for HAB-6FDA and HAB-6FDA-C. Peaks are labeled according to Table C.4. Spectra have been normalized to peak **f** and offset for easier viewing. Figure (A) shows the full-scale spectra, figure (B) shows the spectra between 113 and 139 ppm, and figure (C) shows the spectra between 139 and 170 ppm.

C.4 PRESSURE DEPENDENCE OF GAS PERMEABILITY FOR *HYDROXYL*-FUNCTIONAL POLYIMIDES AND CORRESPONDING TR POLYMERS

Pure gas permeabilities of H_2, CH_4, N_2, O_2, and CO_2 were determined for the *hydroxyl*-functional polyimides and their corresponding TR polymers at 35°C and pressures between 1 bar and 50 bar. The permeation properties of HAB-6FDA-C at 35°C and pressures up to approximately 15 bar have been reported in our previously.[10]

The permeabilities for HAB-6FDA, APAF-6FDA, and APAF-ODPA polyimides and their corresponding TR polymers are shown in Figure C.5, Figure C.6, and Figure C.7, respectively. For all of these samples, gas permeability increases in the following order: $CH_4 < N_2 < O_2 < CO_2 < H_2$. This order of increasing gas permeabilities correlates with decreasing kinetic diameter of each penetrant.[11] Such trends are typical for glassy,

diffusion-selective polymers such as polysulfone.[12] Furthermore, for each sample and each gas, permeability decreases with increasing pressure, which is typically observed in glassy polymer films.[12] In addition to the change in permeability with pressure, changes in permeability are correlated with changes in conversion. The TR polymers all have higher gas permeabilities than their precursor polyimides.

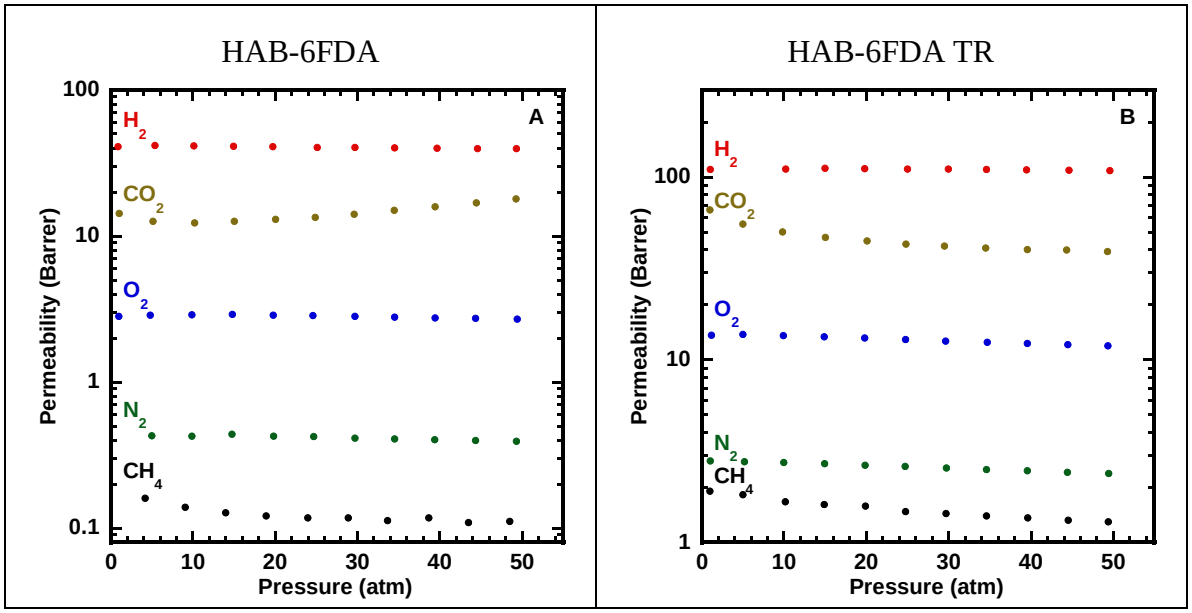

Figure C.5: Permeability of H_2, CO_2, O_2, N_2, and CH_4 in (A) HAB-6FDA and (B) HAB-6FDA TR polymer.

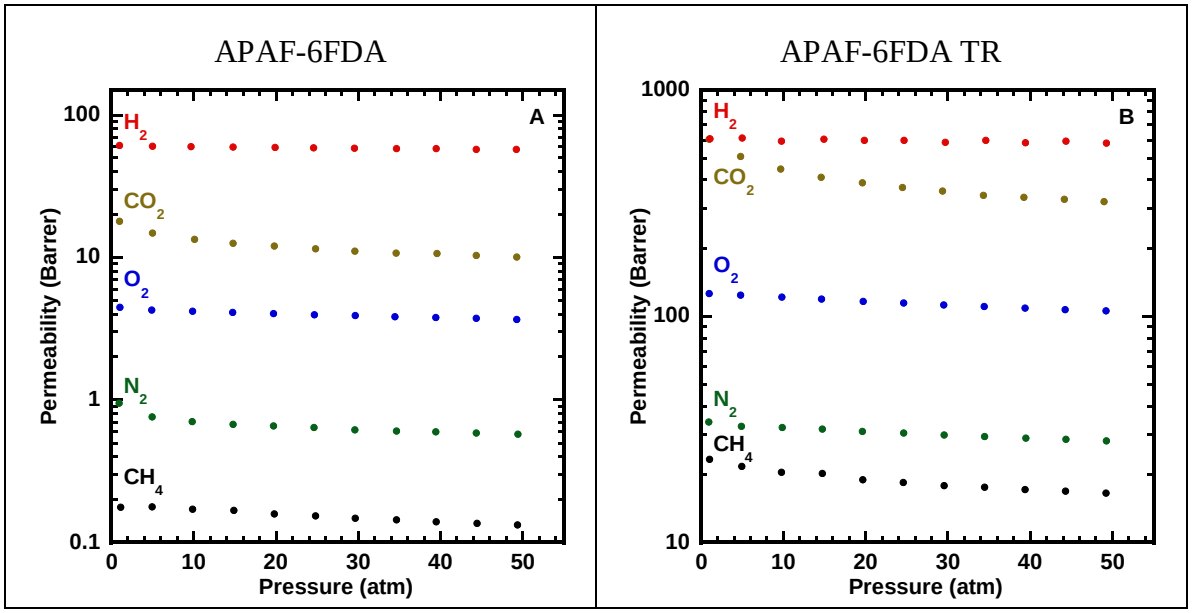

Figure C.6: Permeability of H_2, CO_2, O_2, N_2, and CH_4 in (A) APAF-6FDA and (B) APAF-6FDA TR polymer.

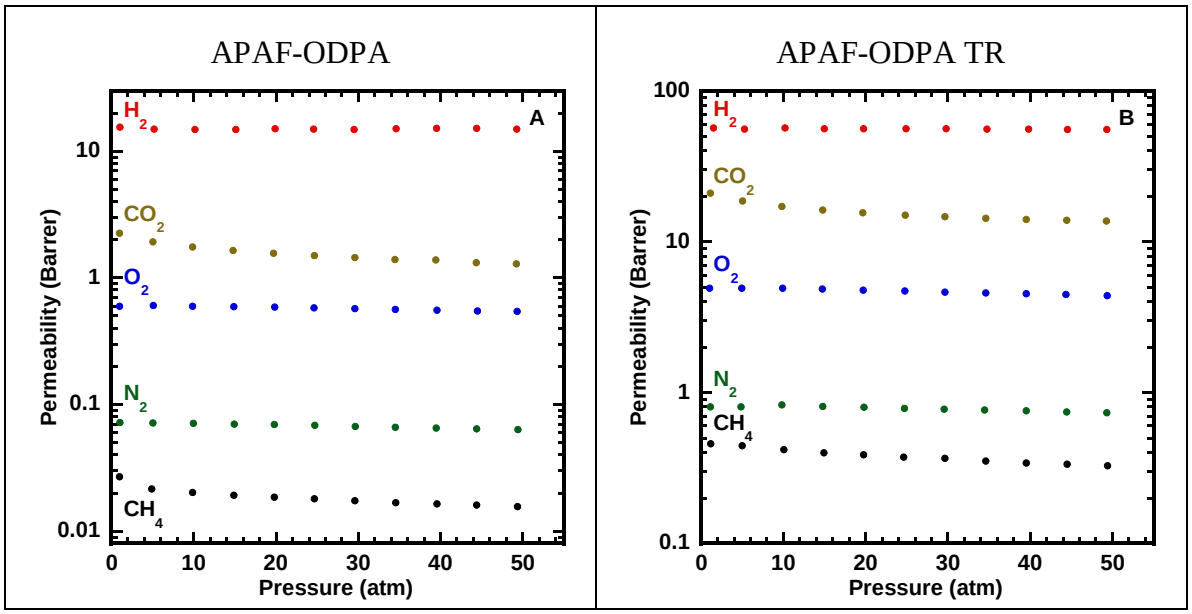

Figure C.7: Permeability of H_2, CO_2, O_2, N_2, and CH_4 in (A) APAF-ODPA and (B) APAF-ODPA TR polymer.

C.5 PERMEABILITY PLOTS AS A FUNCTION OF PRESSURE FOR HAB-6FDA-SS POLYIMIDES AND THEIR CORRESPONDING HAB-6FDA-SS TR POLYMERS

To compare the differences in permeability for polyimides and TR polymers synthesized from thermal imidization in the solid-state and in solution, the transport properties of HAB-6FDA prepared from these synthesis routes, along with the transport properties of their corresponding TR polymers, were investigated. The pure-gas permeabilities for H_2, CH_4, N_2, O_2, and CO_2 for the HAB-6FDA-SS polyimide and its TR polymer are presented in Figure C.8. For the polyimide, the permeabilities of all gases in Figure C.8A are nearly identical to those presented in Figure C.5A. These samples should have nearly identical chemical structures, and therefore, similar transport properties are expected. However, when these polymers are thermally rearranged, the HAB-6FDA-SS TR polymer has consistently higher gas permeabilities than the HAB-6FDA TR polymer. The reason for these differences in transport properties may relate to slight chemical and morphological differences in the polyimide precursors. From thermogravimetric results in Chapter 8, the thermal profiles for HAB-6FDA-SS and HAB-6FDA are nearly identical, and the mass loss during their thermal rearrangement steps are nearly identical as well. For HAB-6FDA-SS, variations in casting procedures with the solid-state sample may endow its corresponding TR polymer with more beneficial transport properties. Specifically, the solid-state sample was simultaneously imidized and formed into a film using a vacuum oven, whereas the solution-imidized sample was imidized in solvent and then cast. The solid-state sample was also imidized in NMP, whereas the solution-imidized sample was imidized in NMP and then cast from DMAc. The differences in these casting procedures may influence the physical and chemical structure of the polyimides, which could affect the physical and chemical structure of their corresponding TR polymers.

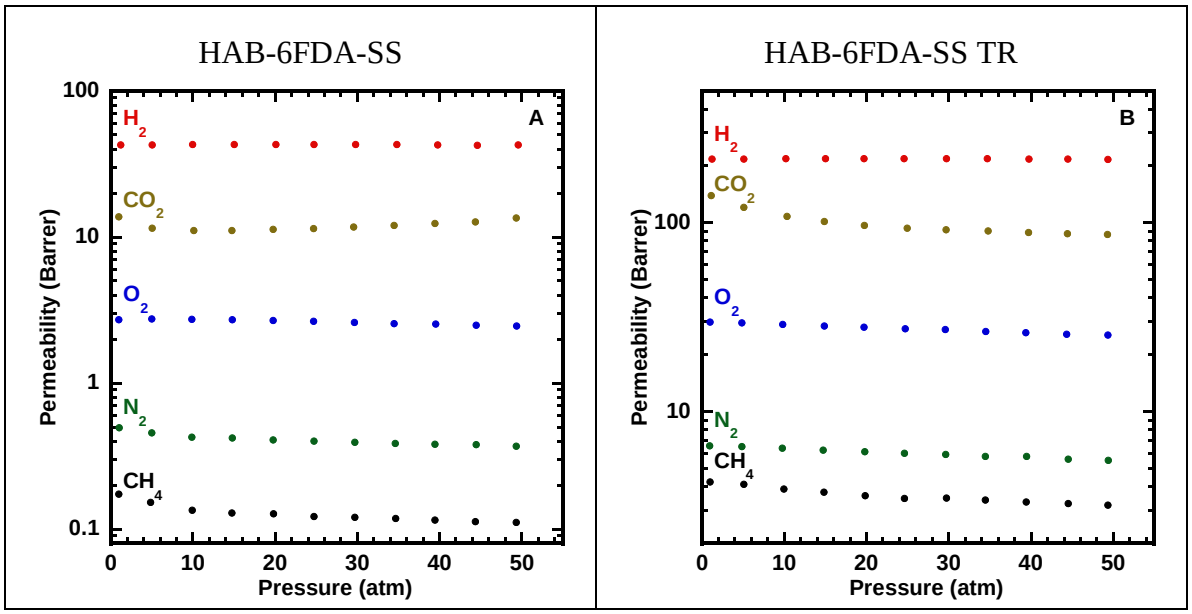

Figure C.8: Permeability of H_2, CO_2, O_2, N_2, and CH_4 in (A) HAB-6FDA-SS and (B) HAB-6FDA-SS TR polymer.

C.6 INFLUENCE OF PRECURSOR GAS PERMEABILITY IN APAF-6FCL AND APAF-6FCL TR POLYMER

The permeability of H_2, CH_4, and CO_2 in the APAF-6fCl polyamide and corresponding TR polymer have been reported in Chapter 4. Figure C.9 presents this permeability data and the permeation data for O_2 and N_2 up to approximately 50 bar. The APAF-6fCl polyamide has lower permeabilities than the APAF-6FDA polyimide (cf., Figure C.6 and Figure C.9), and the polyamide-TR has lower permeabilities than the polyimide-TR. Park *et al.* and Han *et al.* reported transport properties for CO_2/CH_4 for the APAF-6FDA-SS polyimide and transport properties for CO_2/CH_4 and O_2/N_2 for the TR polymers derived from APAF-6FDA-SS.[8,13] Additionally, Han *et al.* reported transport properties for H_2/CO_2 for the TR polymer derived from APAF-6fCl.[14] Similar to the findings by Park *et al.*,[13] we observed a strong increase in permeability with

thermal rearrangement of APAF-6FDA; however, CO_2 and CH_4 permeabilities and CO_2/CH_4 selectivities for our samples differ from those reported by Park *et al.* For example, the CO_2 permeability for our APAF-6FDA TR polymer is 450 ± 40 Barrer, and the APAF-6FDA-SS TR polymer reported by Park *et al.* is approximately 1610 Barrer. Furthermore, the CO_2/CH_4 selectivity for our sample at 10 atm was 41 ± 2 and that reported by Park *et al.* was approximately 45. The differences in these transport properties likely relate to two differences in sample preparation. First, our sample was produced by thermal imidization in solution and was converted to its thermally rearranged analog at 450°C for 30min. The sample reported by Park *et al.* was prepared by thermal imidization in the solid-state and was converted to its thermally rearranged analog at 450°C for 60min. TR polymers formed from solid-state imidized polyimides produce samples with higher permeabilities than TR polymers formed from solution imidized polyimides for HAB-6FDA. Han *et al.* have reported similar transport results to those in this study for a TR polymer prepared from an APAF-6FDA polyimide that was thermally imidized in solution.[8] Therefore, our results are qualitatively consistent with this previously reported trend.

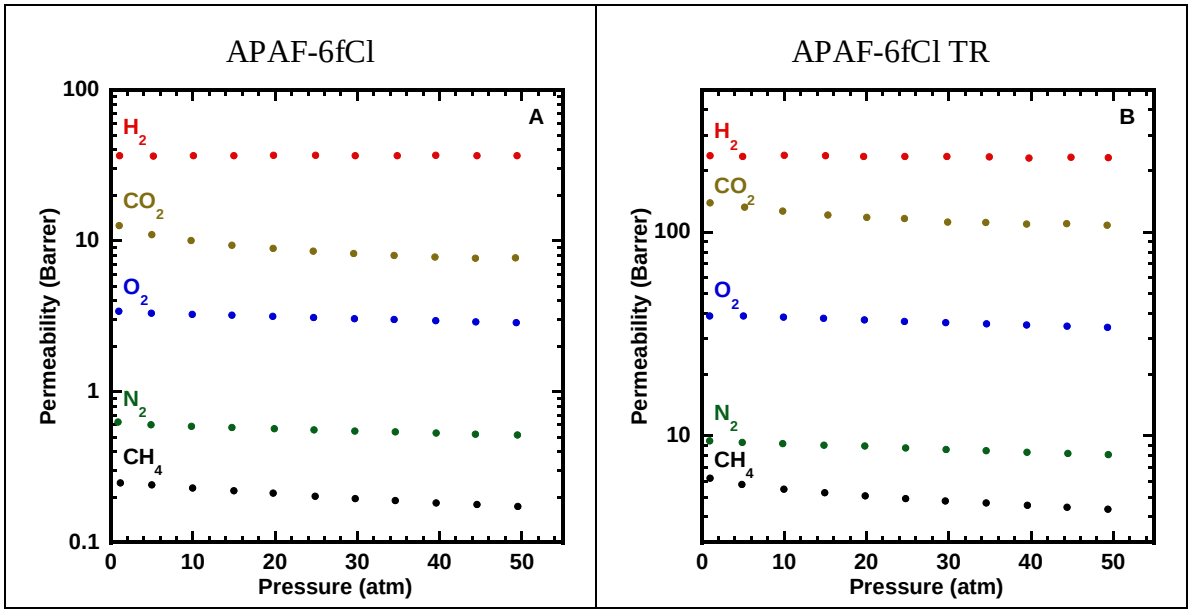

Figure C.9: Permeability of H_2, CO_2, O_2, N_2, and CH_4 in (A) APAF-6fCl and (B) APAF-6fCl TR polymer.

C.7 CONDITIONING AND PLASTICIZATION EFFECTS FOR ADDITIONAL SAMPLES THROUGH HYSTERESIS LOOPS

Hysteresis loops for two additional polyimides and TR polymers are presented in Figure C.10 and Figure C.11. The APAF-ODPA sample showed minimal conditioning and almost identical permeation pressure curves between the first and second pressurization steps, which was similar to that reported earlier for APAF-6FDA (cf., TGA experiments in Chapter 8). The APAF-ODPA TR polymer had a more noticeable difference in permeation properties during depressurization than for its precursor polyimide; however, the first and second pressurization steps are nearly the same. The HAB-6FDA-SS polyimide and TR polymer presented in Figure C.11 showed the same trend as the HAB-6FDA polyimide and TR polymer presented earlier. Both of these samples have the same chemical structure and have very similar responses to CO_2 exposure.

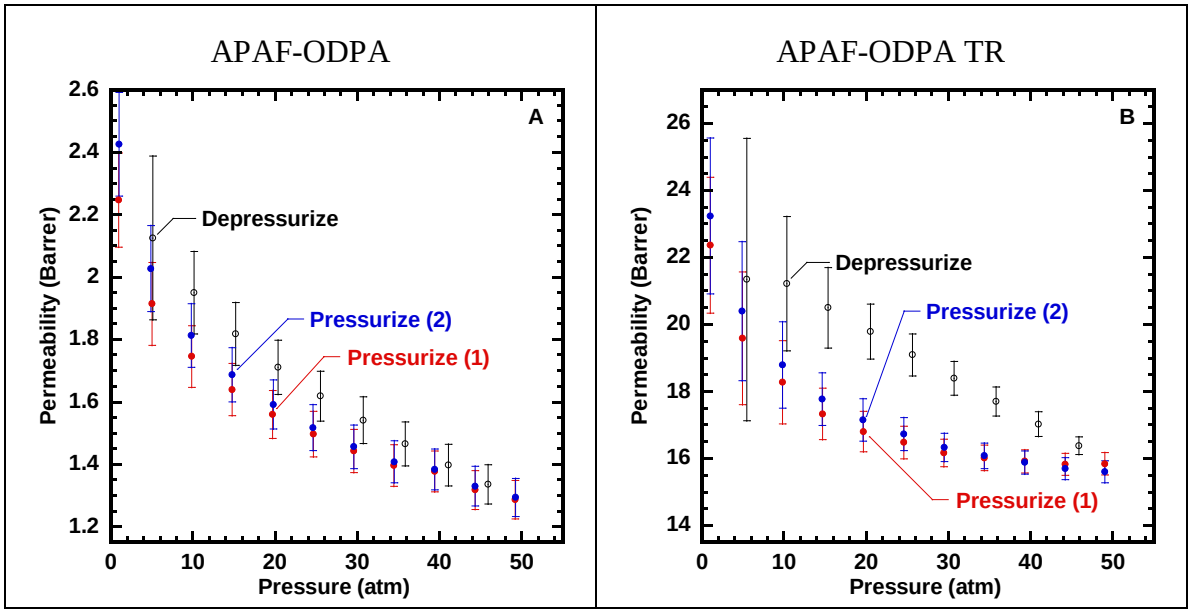

Figure C.10: CO_2 hysteresis loops for (A) APAF-ODPA and (B) APAF-ODPA TR polymer.

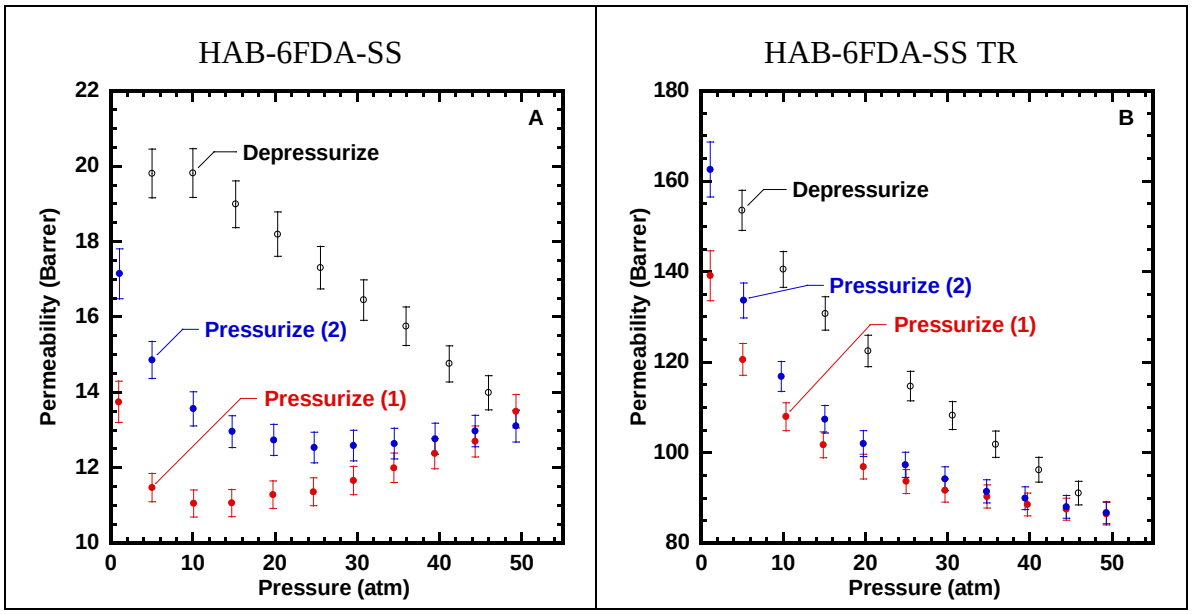

Figure C.11: CO_2 hysteresis loops for (A) HAB-6FDA-SS and (B) HAB-6FDA-SS TR polymer.

To determine the effect of hold-time on CO_2 permeability, a fresh HAB-6FDA-SS TR polymer was held for approximately 60 time lags, and these results are compared to the results from the pressurization-depressurization experiment presented in Figure C.11B. Within the uncertainty of these experiments, Figure C.12 shows that almost no difference for the permeation response of the TR polymer held for 6 times the time lag between each pressure change and the TR polymer held for 60 times the time lag between each pressure change. Therefore, for this TR polymer, there is no change to our interpretation of hysteresis and conditioning effects within the range of time lags considered in Figure C.12.

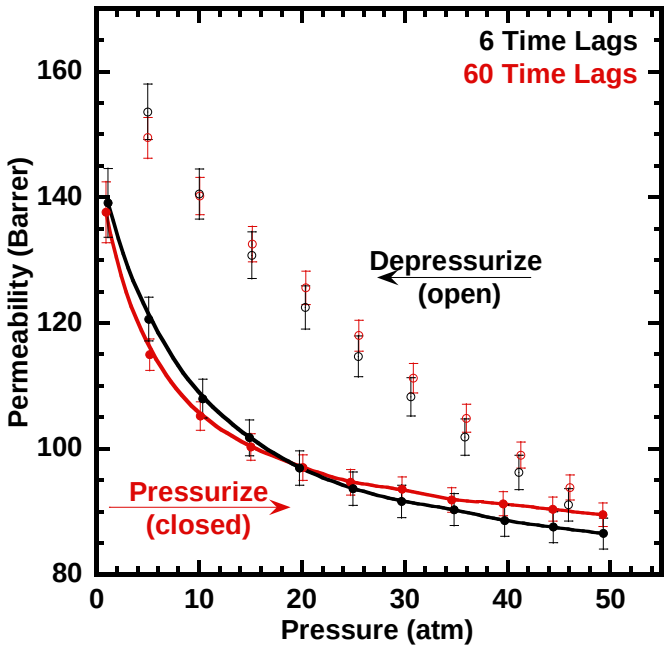

Figure C.12: Comparison of CO_2 hysteresis loops for HAB-6FDA-SS using different hold times at each pressure.

C.8 REFERENCES

1. Muñoz, D.M., M. Calle, J.G. de la Campa, J. de Abajo, and A.E. Lozano, *An improved method for preparing very high molecular weight polyimides.* Macromolecules, **2009**. 42(15), 5892-5894.

2. Tullos, G.L., J.M. Powers, S.J. Jeskey, and L.J. Mathias, *Thermal conversion of hydroxy-containing imides to benzoxazoles: Polymer and model compound study.* Macromolecules, **1999**. 32(11), 3598-3612.

3. Calle, M., Y. Chan, H.J. Jo, and Y.M. Lee, *The relationship between the chemical structure and thermal conversion temperatures of thermally rearranged (TR) polymers.* Polymer, **2012**. 53(13), 2783-2791.

4. Ohya, H., V.V. Kudryavtsev, and S.I. Semenova, *Polyimide membranes: Applications, fabrications, and properties.* **1996**, Amsterdam, Gordon and Breach Publishers.

5. Husk, G.R., P.E. Cassidy, and K.L. Gebert, *Synthesis and characterization of a series of polyimides derived from 4,4'-[2,2,2-trifluoro-1-(trifluoromethyl)ethylidene]bis[1,3-isobenzofurandione].* Macromolecules, **1988**. 21(5), 1234-1238.

6. Matsuura, T., M. Ishizawa, Y. Hasuda, and S. Nishi, *Polyimides derived from 2, 2'-bis (trifluoromethyl)-4, 4'-diaminobiphenyl. 2. Synthesis and characterization of polyimides prepared from fluorinated benzenetetracarboxylic dianhydrides.* Macromolecules, **1992**. 25(13), 3540-3545.

7. Cornelius, C.J. and E. Marand, *Hybrid inorganic–organic materials based on a 6FDA–6FpDA–DABA polyimide and silica: physical characterization studies.* Polymer, **2002**. 43(8), 2385-2400.

8. Han, S.H., N. Misdan, S. Kim, C.M. Doherty, A.J. Hill, and Y.M. Lee, *Thermally rearranged (TR) polybenzoxazole: Effects of diverse imidization routes on physical properties and gas transport behaviors.* Macromolecules, **2010**. 43(18), 7657-7667.

9. Matsuura, T., Y. Hasuda, S. Nishi, and N. Yamada, *Polyimide derived from 2, 2'-bis (trifluoromethyl)-4, 4'-diaminobiphenyl. 1. Synthesis and characterization of polyimides prepared with 2, 2'-bis (3, 4-dicarboxyphenyl) hexafluoropropane dianhydride or pyromellitic dianhydride.* Macromolecules, **1991**. 24(18), 5001-5005.

10. Sanders, D.F., Z.P. Smith, C.P. Ribeiro, R.L. Guo, J.E. McGrath, D.R. Paul, and B.D. Freeman, *Gas permeability, diffusivity, and free volume of thermally rearranged polymers based on 3,3 '-dihydroxy-4,4 '-diamino-biphenyl (HAB) and 2,2 '-bis-(3,4-dicarboxyphenyl) hexafluoropropane dianhydride (6FDA).* Journal of Membrane Science, **2012**. 409, 232-241.

11. Robeson, L.M., Z.P. Smith, B.D. Freeman, and D.R. Paul, *Contributions of diffusion and solubility selectivity to the upper bound analysis for glassy gas separation membranes.* Journal of Membrane Science, **2014**. 453, 71-83.

12. Matteucci, S.T., Y.P. Yampolskii, B.D. Freeman, and I. Pinnau, *Transport of gases and vapors in glassy and rubbery polymers*, in *Materials science of membranes for gas and vapor separation*, Y. Yampolskii, I. Pinnau, and B.D. Freeman, Editors. **2006**, John Wiley & Sons: Chichester. 1-47.

13. Park, H.B., C.H. Jung, Y.M. Lee, A.J. Hill, S.J. Pas, S.T. Mudie, E. Van Wagner, B.D. Freeman, and D.J. Cookson, *Polymers with cavities tuned for fast selective transport of small molecules and ions.* Science, **2007**. 318(5848), 254-258.

14. Han, S., H. Kwon, K. Kim, J. Seong, C. Park, S. Kim, C.M. Doherty, A. Thornton, A.J. Hill, A. Lozano, K. Berchtold, and Y. Lee, *Tuning microcavities in thermally rearranged polymer membranes for CO_2 capture.* Physical Chemistry Chemical Physics, **2012**. 14(13), 4365-4373.

Appendix D: Supporting Information to Chapter 9

D.1 Effect of Pressure and Experimental Measurement Method on Experimentally Determined Diffusion and Solubility Coefficients[12]

The solution-diffusion model relates gas permeability, P, to the sorption, S, and the diffusion, D, coefficients[1]

$$P = DS \tag{D.1}$$

The parameter P can be determined by finding the steady-state flux normalized by the film thickness and pressure driving force.[2] The parameters D and S can be determined by transient permeation or equilibrium sorption experiments.[2] With transient permeation experiments, diffusion coefficients are determined from time-lag measurements, and sorption coefficients are calculated by dividing permeability coefficients by these time-lag diffusion coefficients. Alternatively, equilibrium sorption experiments can be used to directly determine a secant sorption coefficient (S = C/p where C = concentration of gas in the polymer at pressure p), and the diffusion coefficient can be calculated by dividing the permeability coefficient by the equilibrium secant sorption coefficient. The relationship between permeability, diffusion, and sorption coefficients determined from these two methods is given by

$$P = DS = D_\theta S_\theta = D_{\text{sec}} S_{\text{sec}} \tag{D.2}$$

This appendix has been adapted with permission from: Robeson, L.M., Z.P. Smith, B.D. Freeman, and D.R. Paul, *Contributions of diffusion and solubility selectivity to the upper bound analysis for glassy gas separation membranes.* Journal of Membrane Science, **2014.** 453, 71-83.

where D_θ is the diffusion coefficient calculated from time-lag experiments, S_θ is the sorption coefficient determined from P and D_θ, S_{sec} is the secant sorption coefficient determined from equilibrium sorption experiments, and D_{sec} is the diffusion coefficient determined from P and S_{sec}. The dual sorption-mobility model well describes sorption and permeation in glassy polymers; this model predicts that $D_\theta \neq D_{\text{sec}}$ and $S_\theta \neq S_{\text{sec}}$.[3] To evaluate the differences in these sorption and diffusion coefficients, we consider N_2, CH_4, and CO_2 for polysulfone and PIM-1.

The diffusion coefficient, as determined by transient permeation experiments, can be written as follows[4,5]

$$D_\theta = \frac{l^2}{6\theta} \tag{D.3}$$

where θ is the time-lag of gas diffusing through a polymer of thickness, l. The term θ can be written in terms of the Henry's law diffusion coefficient, D_D, and dual-mode parameters

$$\theta = \frac{l^2}{6D_D}\left[f\left(F, K, bp_2\right)\right] \tag{D.4}$$

where p_2 is the gas pressure upstream of the polymer film, and the function in the brackets has been tabulated by Paul and Koros.[3] The terms K and F are defined as follows

$$K = \frac{C_H' b}{k_D} \tag{D.5}$$

$$F = \frac{D_H}{D_D} \tag{D.6}$$

where the terms $C_H^{'}$, b, and k_D are dual-mode sorption parameters, and D_H and D_D are diffusion coefficients of gas associated with the Langmuir (H for “holes”) and Henry’s law (D for "dissolved") modes of sorption.

Permeability can be described in terms of dual-mode parameters as follows

$$P = k_D D_D \left(1 + \frac{FK}{1 + bp_2}\right) \tag{D.7}$$

Therefore, we can define S_θ in terms of Equation (D.3) to Equation (D.7)

$$S_\theta = \frac{P}{D_\theta} = k_D \left(1 + \frac{FK}{1 + bp_2}\right)\left[f\left(F, K, bp_2\right)\right] \tag{D.8}$$

Equilibrium sorption isotherms can be described by the dual-mode sorption model

$$S_{\text{sec}} = k_D + \frac{C_H^{'} b}{1 + bp_2} \tag{D.9}$$

The diffusion coefficient calculated from Equation (D.7) and Equation (D.9) is defined as follows

$$D_{\text{sec}} = \frac{P}{S_{\text{sec}}} = \frac{k_D D_D \left(1 + \frac{FK}{1 + bp_2}\right)}{k_D + \frac{C_H^{'} b}{1 + bp_2}} \tag{D.10}$$

Therefore, after some basic algebraic simplification, we can describe a ratio of diffusion coefficients and solubility coefficients according to Equation (D.11) and Equation (D.12); Equation (D.11) is the inverse of Equation (D.12).

$$\frac{D_{\text{sec}}}{D_\theta} = \frac{\left[f\left(F,K,bp_2\right)\right]k_D\left(1+FK+bp_2\right)}{k_D+b\left(C_H^{'}+k_Dp_2\right)} \tag{D.11}$$

$$\frac{S_{\text{sec}}}{S_\theta} = \frac{k_D+b\left(C_H^{'}+k_Dp_2\right)}{\left[f\left(F,K,bp_2\right)\right]k_D\left(1+FK+bp_2\right)} \tag{D.12}$$

The relationship between D_{sec} and D_θ for polysulfone and PIM-1can be described using the dual-mode parameters for N_2, CH_4, and CO_2 listed in Table D.1.[6,7]

Polymer	Gas	$k_D\left(\frac{cm^3(STP)}{cm^3(Polymer)\,atm}\right)$	$C_H^{'}\left(\frac{cm^3(STP)}{cm^3(Polymer)}\right)$	$b\left(atm^{-1}\right)$	Ref
Polysulfone*	N_2	0.166	0.957	0.104	7
	CH_4	0.257	6.58	0.0901	
	CO_2	0.728	19.6	0.26	
PIM-1**	N_2	0.493	31.012	0.076	6
	CH_4	0.592	64.966	0.15	
	CO_2	2.351	106.796	0.421	

* Data taken at 35°C
** Data taken at 25°C

Table D.1: Dual-mode parameters for diffusion correlation calculations.

To employ Equation (D.11) and Equation (D.12) in this analysis, the parameter F was determined by fitting permeability data from McHattie, Koros, and Paul,[8] and Li, Chung, and Paul[6] to Equation (D.7) assuming that D_D is constant. The parameters F and K for polysulfone and PIM-1 are presented in Table D.2. The value of K increases with increasing penetrant condensability, as is found for other polymers such as

polycarbonate.[9] However, there is some scatter in the data for the parameter F, which typically increases with decreasing penetrant condensability.[9] The scatter in F may be an indication of the difficulty in determining the permeability dependence on pressure for N_2, CH_4, and CO_2 in these polymers.

Polymer	Gas	F	K
Polysulfone*	N_2	0.14	0.60
	CH_4	0.21	2.31
	CO_2	0.12	7.00
PIM-1**	N_2	0.026	4.8
	CH_4	0.009	16.5
	CO_2	0.026	19.1

* Data taken at 35°C
** Data taken at 25°C

Table D.2: Parameters F and K for polysulfone and PIM-1.

As shown in Figure D.1, the ratio of $\frac{D_{\text{sec}}}{D_\theta}$ from Equation (D.11) can be plotted as a function of pressure for each gas. Permeation data fit for this analysis was taken at pressures up to approximately 10 atm for PIM-1 and 20 atm for polysulfone. Sorption data were taken at pressures up to approximately 28 atm for PIM-1 and 20 atm for polysulfone. To clearly show the correlation between Equation (D.11) and pressure, we have extrapolated the fitted parameters to permeability and sorption data (i.e., F, K, k_D, C_H', b) to 50 atm. For polymers that are far from their glass transition temperature, the difference in D_{sec} and D_θ is more pronounced. For example, D_{sec} for CO_2 is approximately 1.4 times higher than D_θ for polysulfone at about 20 atm (cf., Figure D.1A), whereas D_{sec} for CO_2 diffusion is approximately 1.7 times higher than D_θ for

PIM-1 at the same pressure (cf., Figure D.1B). The T_g of polysulfone is 186°C,[7] and the T_g of PIM-1 is undetectable before the onset of polymer degradation around 350°C.[10]

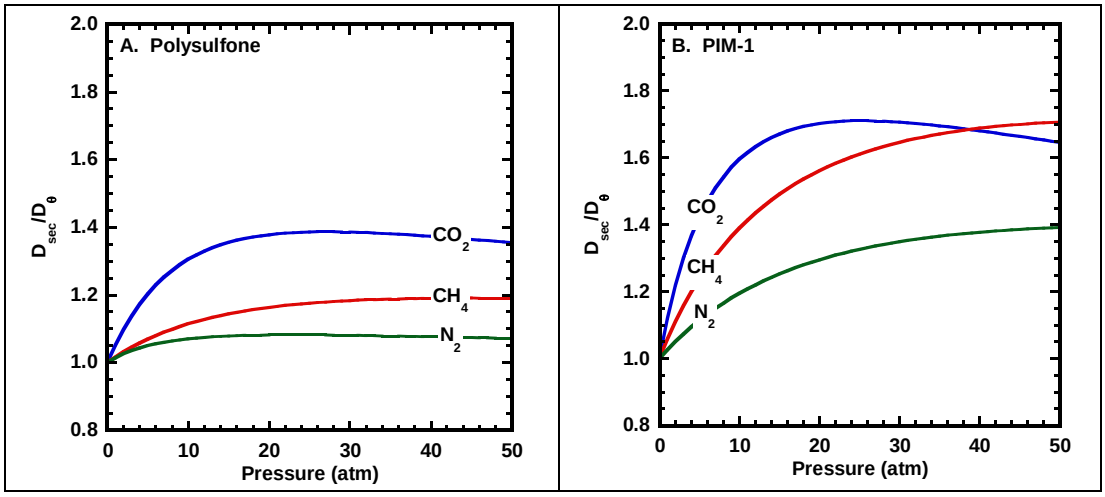

Figure D.1: Comparison of $\frac{D_{sec}}{D_\theta}$ for CO_2, CH_4, and N_2 as a function of pressure for (A) polysulfone and (B) PIM-1.

Using the data from Figure D.1, diffusion selectivity ratios between D_{sec} and D_θ (i.e., $\alpha_{D_{sec}} / \alpha_{D_\theta}$) can be determined for different gas pairs. This comparison is shown for polysulfone and PIM-1 in Figure D.2. Because more highly sorbing gases show more pronounced dual-mode effects at lower pressures, a maximum in $\alpha_{D_{sec}} / \alpha_{D_\theta}$ results for each gas pair, and the pressure location of this maximum will vary from gas to gas. For polysulfone, the largest value of $\alpha_{D_{sec}} / \alpha_{D_\theta}$ is almost 1.3 for CO_2/N_2 at around 30 atm. For PIM-1 and CH_4/N_2, $\alpha_{D_{sec}} / \alpha_{D_\theta}$ varies between approximately 0.9 and 1.5 between vacuum and 50 atm. Therefore, for the samples considered here, diffusion selectivities calculated from equilibrium sorption experiments could differ by as much as a factor of 1.5 when compared to calculating diffusion selectivities from time-lag techniques.

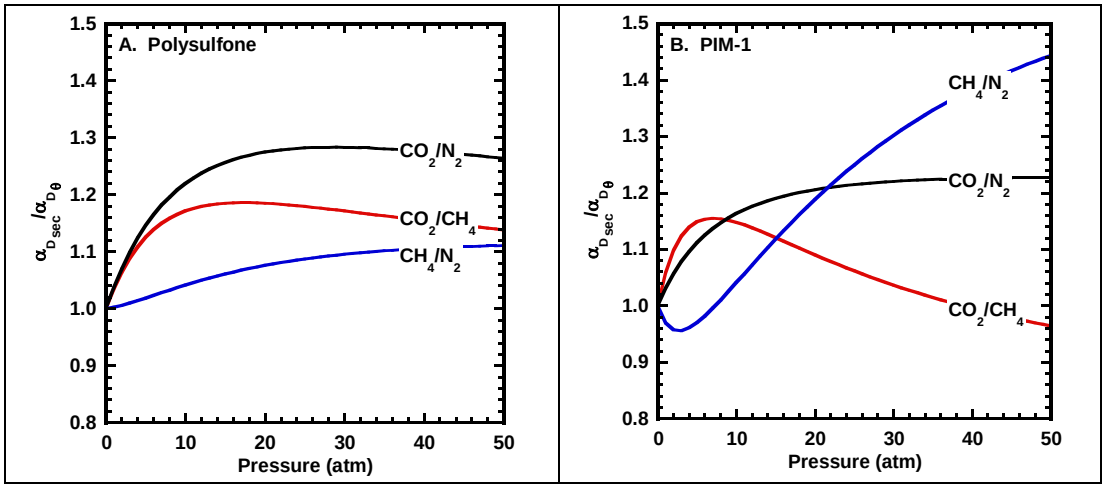

Figure D.2: Comparison of $\alpha_{D_{sec}} / \alpha_{D_\theta}$ for CO_2/N_2, CO_2/CH_4, and CH_4/N_2 for (A) polysulfone and (B) PIM-1.

Analogous to the diffusion analysis in Figure D.1 and Figure D.2, comparisons can be made between sorption coefficients calculated directly from equilibrium sorption experiments (i.e., S_{sec}), sorption coefficients calculated from permeability coefficients and D_θ (i.e., S_θ), and the sorption selectivities from each measurement (i.e., $\alpha_{S_{sec}} / \alpha_{S_\theta}$). The relationship between S_{sec}, S_θ, and $\alpha_{S_{sec}} / \alpha_{S_\theta}$ can be determined by taking the inverse of the plots in Figure D.1 and Figure D.2, and these plots are shown in Figure D.3 and Figure D.4. Similar to the findings for diffusion coefficients, solubility coefficients and solubility selectivities will differ if calculated from sorption isotherms or if derived from time-lag experiments. Furthermore, solubility will vary depending on experimental pressure.

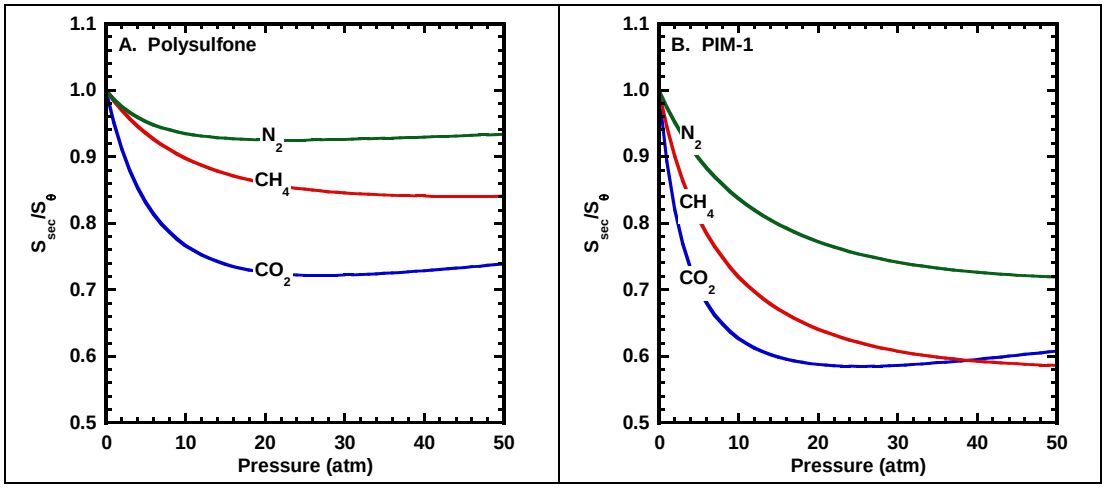

Figure D.3: Comparison of $\frac{S_{sec}}{S_\theta}$ for CO_2, CH_4, and N_2 as a function of pressure for (A) polysulfone and (B) PIM-1.

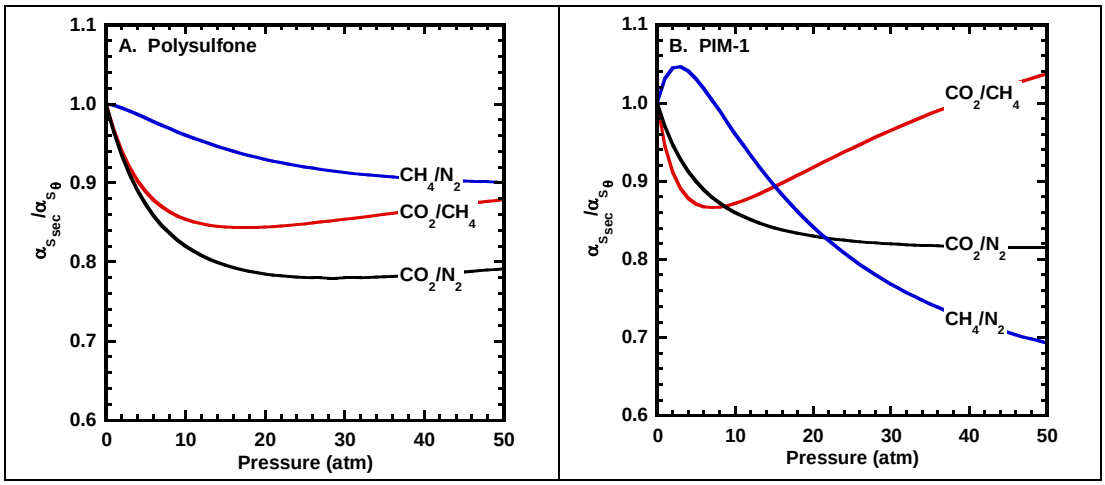

Figure D.4: Comparison of $\alpha_{S_{sec}} / \alpha_{S_\theta}$ for CO_2/N_2, CO_2/CH_4, and CH_4/N_2 for (A) polysulfone and (B) PIM-1.

D.2 REFERENCES

1. Wijmans, J.G. and R.W. Baker, *The solution-diffusion model: A review.* Journal of Membrane Science, **1995**. 107(1-2), 1-21.

2. Lin, H. and B.D. Freeman, *Springer handbook: Permeation and diffusion*, H. Czichos, T. Saito, and L. Smith, Editors. **2006**, Springer: New York. 371-387.

3. Paul, D.R. and W.J. Koros, *Effect of partially immobilizing sorption on permeability and the diffusion time lag.* Journal of Polymer Science: Polymer Physics Edition, **1976**. 14(4), 675-685.

4. Vieth, W.R., J.M. Howell, and J.H. Hsieh, *Dual sorption theory.* Journal of Membrane Science, **1976**. 1, 177-220.

5. Meares, P., *The diffusion of gases through polyvinyl acetate.* Journal of the American Chemical Society, **1954**. 76, 3415-3422.

6. Li, P., T.S. Chung, and D.R. Paul, *Gas sorption and permeation in PIM-1.* Journal of Membrane Science, **2013**. 432, 50-57.

7. Aitken, C.L., W.J. Koros, and D.R. Paul, *Effect of structural symmetry on gas transport properties of polysulfones.* Macromolecules, **1992**. 25(13), 3424-3434.

8. McHattie, J.S., W.J. Koros, and D.R. Paul, *Gas transport properties of polysulphones: 1. Role of symmetry of methyl group placement on bisphenol rings.* Polymer, **1991**. 32(5), 840-850.

9. Koros, W.J., D.R. Paul, and A.A. Rocha, *Carbon dioxide sorption and transport in polycarbonate.* Journal of Polymer Science: Polymer Physics Edition, **1976**. 14(4), 687-702.

10. Du, N., G.P. Robertson, J. Song, I. Pinnau, S. Thomas, and M.D. Guiver, *Polymers of intrinsic microporosity containing trifluoromethyl and phenylsulfone*

groups as materials for membrane gas separation. Macromolecules, **2008**. 41(24), 9656-9662.

Bibliography

Advanced Prism® membrane systems for cost effective gas separations. Available from: http://www.airproducts.com/products/Gases/supply-options/~/media/Downloads/Brochure/advanced-prism-membrane-system-brochure.ashx.

Basic research needs for carbon capture: Beyond 2020, US Department of Energy Basic Energy Sciences Workshop for Carbon Capture. 2010 March 4-5; Available from: http://science.energy.gov/~/media/bes/pdf/reports/files/ CCB2020_rpt.pdf.

Facts & figures: Output declines in U.S., Europe. Chemical & Engineering News, **2010**. 88(27), 54-62.

The future of coal: An interdisciplinary MIT study. 2007; Available from: http://web.mit.edu/coal/The_Future_of_Coal.pdf.

Hydrogen Separations in Syngas. 2009; Available from: http://www.mtrinc.com/pdf_print/refinery_and_syngas/MTR_Brochure_Hydrogen_Separations.pdf.

Membrane Technology. 2012; Available from: http://www.sulzerchemtech.com /de/portaldata/11/Resources//brochures/pt/Membrane_Technology.pdf.

Recovery..., hydrogen... made simple. Chemical & Engineering News, **1979**. 57(48), 26-27.

Region VIII pretreatment guidance on the analysis of BTEX. 1999; Available from: http://www.epa.gov/region8/water/pretreatment/pdf/BTEXGuidance.pdf.

Spectral Database for Organic Compounds (SDBS): ^{13}C NMR SDBS No. 670CDS-05-479. Available from: http://sdbs.riodb.aist.go.jp/sdbs/cgi-bin/direct_frame_top.cgi.

US Department of Energy Report. Materials for separation technology: Energy and emission reduction opportunities. **2004**, BCS, Incorportated, Oak Ridge National Laboratory.

Aitken, C.L., W.J. Koros, and D.R. Paul, *Effect of structural symmetry on gas transport properties of polysulfones.* Macromolecules, **1992**. 25(13), 3424-3434.

Aitken, C.L., J.S. McHattie, and D.R. Paul, *Dynamic mechanical-behavior of polysulfones.* Macromolecules, **1992**. 25(11), 2910-2922.

Alentiev, A. and Y. Yampolskii, *Correlation of gas permeability and diffusivity with selectivity: Orientations of the clouds of the data points and the effects of temperature.* Industrial & Engineering Chemistry Research, **2013**. 52(26), 8864-8874.

Alentiev, A.Y., V.P. Shantarovich, T.C. Merkel, V.I. Bondar, B.D. Freeman, and Y.P. Yampolskii, *Gas and vapor sorption, permeation, and diffusion in glassy amorphous Teflon AF1600.* Macromolecules, **2002**. 35(25), 9513-9522.

Alentiev, A.Y. and Y.P. Yampolskii, *Free volume model and tradeoff relations of gas permeability and selectivity in glassy polymers.* Journal of Membrane Science, **2000**. 165(2), 201-216.

Alentiev, A.Y., Y.P. Yampolskii, V.P. Shantarovich, S.M. Nemser, and N.A. Platé, *High transport parameters and free volume of perfluorodioxole copolymers.* Journal of Membrane Science, **1997**. 126(1), 123-132.

Ameduri, B., *From vinylidene fluoride (VDF) to the applications of VDF-containing polymers and copolymers: recent developments and future trends.* Chem. Rev, **2009**. 109(12), 6632-6686.

Asensio, J.A., E.M. Sánchez, and P. Gómez-Romero, *Proton-conducting membranes based on benzimidazole polymers for high-temperature PEM fuel cells. A chemical quest.* Chemical Society Reviews, **2010**. 39(8), 3210-3239.

Ash, R., R. Barrer, and D. Palmer, *Solubility and transport of gases in nylon and polyethylene.* Polymer, **1970**. 11(8), 421-435.

Assogna, A., G. Perego, A. Roggero, R. Sisto, and C. Valentini, *Structure and gas permeability of silylated polyphenylene oxide.* Journal of Membrane Science, **1992**. 71(1-2), 97–103.

Auvil, S.R., J.S. Choe, and L.J. Kellogg, Jr. *Use of membrane separation to dry gas streams containing water vapor*, **1993**, US 5259869.

Baker, R.W., *Future directions of membrane gas separation technology.* Industrial & Engineering Chemistry Research, **2002**. 41(6), 1393-1411.

Baker, R.W., *Membrane technology and applications.* **2004**, Chichester, John Wiley & Sons, Ltd.

Baker, R.W. and K. Lokhandwala, *Natural gas processing with membranes: An overview.* Industrial & Engineering Chemistry Research, **2008**. 47(7), 2109-2121.

Baker, R.W., I. Pinnau, Z. He, K.D. Amo, A.R. Da Costa, and R. Daniels. *Hydrogen gas separation using organic-vapor-resistant membranes*, **2003**, US 6544316 B2.

Barbari, T.A., W.J. Koros, and D.R. Paul, *Polymeric membranes based on bisphenol-A for gas separations.* Journal of Membrane Science, **1989**. 42(1-2), 69-86.

Barrer, R., J. Barrie, and N. Raman, *Solution and diffusion in silicone rubber I—A comparison with natural rubber.* Polymer, **1962**. 3(3), 595-603.

Barrer, R. and H. Chio, *Solution and diffusion of gases and vapors in silicone rubber membranes.* Journal of Polymer Science: Part C, **1965**. 138(10), 111-138.

Bax, A. and M.F. Summers, *Proton and carbon-13 assignments from sensitivity-enhanced detection of heteronuclear multiple-bond connectivity by 2D multiple quantum NMR.* Journal of the American Chemical Society, **1986**. 108(8), 2093-2094.

Belov, N.A., A.A. Zharov, A.V. Shashkin, M.Q. Shaikh, K. Raetzke, and Y.P. Yampolskii, *Gas transport and free volume in hexafluoropropylene polymers.* Journal of Membrane Science, **2011**. 383(1–2), 70-77.

Berens, A.R. and H.B. Hopfenberg, *Diffusion of organic vapors at low concentrations in glassy PVC, polystyrene, and PMMA.* Journal of Membrane Science, **1982**. 10(2–3), 283-303.

Bernardo, P., E. Drioli, and G. Golemme, *Membrane gas separation: A review/state of the art.* Industrial & Engineering Chemistry Research, **2009**. 48(10), 4638-4663.

Bernardo, P., E. Drioli, and G. Golemme, *Membrane gas separation: A review/state of the art.* Industrial & Engineering Chemistry Research, **2009**. 48, 4638-4663.

Bevington, P.R. and K.D. Robinson, *Data reduction and error analysis for the physical sciences: Third edition*. **2003**, Boston, McGraw Hill.

Bondar, V., B. Freeman, and Y. Yampolskii, *Sorption of gases and vapors in an amorphous glassy perfluorodioxole copolymer.* Macromolecules, **1999**. 32, 6163-6171.

Bondi, A., *Physical Properties of Molecular Crystals, Liquids and Glasses*. **1968**, John Wiley & Sons, Inc.

Bondi, A., *van der Waals volumes and radii.* The Journal of Physical Chemistry, **1964**. 68(3), 441-451.

Bos, A., I.G.M. Punt, M. Wessling, and H. Strathmann, *CO_2-induced plasticization phenomena in glassy polymers.* Journal of Membrane Science, **1999**. 155(1), 67-78.

Bos, A., I.G.M. Pünt, M. Wessling, and H. Strathmann, *Plasticization-resistant glassy polyimide membranes for CO_2/CO_4 separations.* Separation and Purification Technology, **1998**. 14(1–3), 27-39.

Bottoms, R.R. *Process for separating acidic gases*, **1931**, US 1834016.

Bounaceur, R., N. Lape, D. Roizard, C. Vallieres, and E. Favre, *Membrane processes for post-combustion carbon dioxide capture: A parametric study.* Energy, **2006**. 31, 2556-2570.

Breck, D.W., *Zeolite molecular sieves: structure, chemistry, and use*. **1973**, John Wiley & Sons: New York, NY. 636.

Broom, D.P., *Hydrogen storage materials*. **2011**, London, Springer.

Brunetti, A., F. Scura, G. Barbieri, and E. Drioli, *Membrane technologies for CO_2 separation.* Journal of Membrane Science, **2010**. 359(1-2), 115-125.

Bunce, N.J., S.J. Sondheimer, and C.A. Fyfe, *Proton NMR method for the quantitative determination of the water content of the polymeric fluorosulfonic acid Nafion-H.* Macromolecules, **1986**. 19(2), 333-339.

Burnett, E.S., *Compressibility determinations without volume measurements.* Journal of Applied Mechanics, **1936**. 3, 136-140.

Burns, R.L. and W.J. Koros, *Defining the challenges for C_3H_6/C_3H_8 separation using polymeric membranes.* Journal of Membrane Science, **2003**. 211(2), 299-309.

Cai, Z., R.H. Clarke, and W.J. Nuttall, *Helium demand*, in *The Future of Helium As a Natural Resource*, W.J. Nuttall, R.H. Clarke, and B.A. Glowacki, Editors. **2012**, Routledge: New York. 134-156.

Calle, M., Y. Chan, H.J. Jo, and Y.M. Lee, *The relationship between the chemical structure and thermal conversion temperatures of thermally rearranged (TR) polymers.* Polymer, **2012**. 53(13), 2783-2791.

Calle, M. and Y.M. Lee, *Thermally rearranged (TR) poly(ether-benzoxazole) membranes for gas separation.* Macromolecules, **2011**. 44(5), 1156-1165.

Calle, M., A.E. Lozano, and Y.M. Lee, *Formation of thermally rearranged (TR) polybenzoxazoles: Effect of synthesis routes and polymer form.* European Polymer Journal, **2012**. 48(7), 1313-1322.

Carroll, J. *Chevron Phillips studying ethylene cracker amid gas glut*. 2012; Available from: http://www.bloomberg.com/news/2012-02-23/chevron-phillips-may-build-ethylene-cracker-amid-shale-gas-glut.html.

Chapman, P.D., T. Oliveira, A.G. Livingston, and K. Li, *Membranes for the dehydration of solvents by pervaporation.* Journal of Membrane Science, **2008**. 318(1-2), 5-37.

Chiou, J.S. and D.R. Paul, *Gas permeation in a dry Nafion membrane.* Industrial & Engineering Chemistry Research, **1988**. 27(11), 2161-2164.

Choe, E.W. and S.N. Kim, *Synthesis, spinning, and fiber mechanical properties of poly (p-phenylenebenzobisoxazole).* Macromolecules, **1981**. 14(4), 920-924.

Choi, D.W., *How to buy glycol dehydrators.* Hydrocarbon Processing **2006**. 85(7), 69-76.

Choi, J.I., C.H. Jung, S.H. Han, H.B. Park, and Y.M. Lee, *Thermally rearranged (TR) poly(benzoxazole-co-pyrrolone) membranes tuned for high gas permeability and selectivity.* Journal of Membrane Science, **2010**. 349(1-2), 358-368.

Clever, H.L., R. Battino, J.H. Saylor, and P.M. Gross, *The solubility of helium, neon, argon and krypton in some hydrocarbon solvents.* Journal of Physical Chemistry, **1957**. 61(8), 1078-1082.

Cohen, M.H. and D. Turnbull, *Molecular transport in liquids and glasses.* The Journal of Chemical Physics, **1959**. 31(5), 1164-1169.

Coleman, M.R. and W.J. Koros, *The transport properties of polyimide isomers containing hexafluoroisopropylidene in the diamine residue.* Journal of Polymer Science Part B: Polymer Physics, **1994**. 32(11), 1915-1926.

Colling, C., J. Huff, GA, and J.V. Bartles. *Processes using solid perm-selective membranes in multiple groups for simultaneous recovery of specified products from a fluid mixture*, **2004**, US 6830691 B2.

Comer, A.C., C.P. Ribeiro, B.D. Freeman, S. Kalakkunnath, and D.S. Kalika, *Dynamic relaxation characteristics of thermally rearranged aromatic polyimides.* Polymer, **2013**. 54(2), 891-900.

Cooley, T.E. and A.B. Coady. *Removal of H_2S and/or CO_2 from a light hydrocarbon stream by use of gas permeable membrane*, **1978**, US 4130403.

Cornelius, C.J. and E. Marand, *Hybrid inorganic–organic materials based on a 6FDA–6FpDA–DABA polyimide and silica: physical characterization studies.* Polymer, **2002**. 43(8), 2385-2400.

Cougard, N., A. Baudot, and V. Coupard. *Process for separating propane and propylene using a distillation column and a membrane separation column*, **2008**, US 2011/0049051 A1.

Dal-Cin, M.M., A. Kumar, and L. Layton, *Revisiting the experimental and theoretical upper bounds of light pure gas selectivity–permeability for polymeric membranes.* Journal of Membrane Science, **2008**. 323(2), 299-308.

Dantzler, E.M. and C.M. Knobler, *Interaction virial coefficients in fluorocarbon mixtures.* The Journal of Physical Chemistry, **1969**. 73(5), 1335-1341.

Dantzler, E.M., C.M. Knobler, and M.L. Windsor, *Interaction virial coefficients in hydrocarbon mixtures.* The Journal of Physical Chemistry, **1968**. 72(2), 676-684.

Das, M. and W.J. Koros, *Performance of 6FDA–6FpDA polyimide for propylene/propane separations.* Journal of Membrane Science, **2010**. 365(1-2), 399-408.

Dawson, R., A.I. Cooper, and D.J. Adams, *Nanoporous organic polymer networks.* Progress in Polymer Science, **2012**. 37(4), 530-563.

De Angelis, M.G., T.C. Merkel, V.I. Bondar, B.D. Freeman, F. Doghieri, and G.C. Sarti, *Gas sorption and dilation in poly(2,2-bistrifluoromethyl-4,5-difluoro-1,3-dioxole-co-tetrafluoroethylene): Comparison of experimental data with predictions of the nonequilibrium lattice fluid model.* Macromolecules, **2002**. 35(4), 1276-1288.

De Angelis, M.G., G.C. Sarti, and F. Doghieri, *NELF model prediction of the infinite dilution gas solubility in glassy polymers.* Journal of Membrane Science, **2007**. 289(1–2), 106-122.

Dreisbach, F., H.W. Lösch, and P. Harting, *Highest pressure adsorption equilibria data: Measurement with magnetic suspension balance and analysis with a new adsorbent/adsorbate-volume.* Adsorption, **2002**. 8(2), 95-109.

Drioli, E. and L. Giorno, *Membrane operations: Innovative separations and transformations*. **2009**, Weinheim, Wiley-VCH.

Du, N., G.P. Robertson, J. Song, I. Pinnau, S. Thomas, and M.D. Guiver, *Polymers of intrinsic microporosity containing trifluoromethyl and phenylsulfone groups as materials for membrane gas separation.* Macromolecules, **2008**. 41(24), 9656-9662.

Dymond, J.H., K.N. Marsh, R.C. Wilhoit, and K.C. Wong, eds. *The virial coefficients of pure gases and mixtures*. ed. M. Frenkel and K.N. Marsh. Vol. Group IV: Physical chemistry vol 21 subvolumes A and B. **2001**, Landolt-Bornstein: Berlin.

Ehlers, G.F.L., K.R. Fisch, and W.R. Powell, *The thermal breakdown mechanism of polybenzoxazoles and polybenzothiazoles.* Journal of Polymer Science: Polymer Symposia, **1973**. 43(1), 55-75.

Ekiner, O.M. and R.A. Hayes. *Phenylindane-containing polyimide gas separation membranes*, **1991**, US 5015270.

Ekiner, O.M., R.A. Hayes, and P. Manos. *Novel multicomponent fluid separation membranes*, **1992**, US 5085676.

El-Hibri, M.J. and D.R. Paul, *Gas transport in poly(vinylidene fluoride): Effects of uniaxial drawing and processing temperature.* Journal of Applied Polymer Science, **1986**. 31(8), 2533-2560.

Eldridge, R.B., *Olefin/paraffin separation technology: A review.* Industrial & Engineering Chemistry Research, **1993**. 32(10), 2208-2212.

Escobar, J.C., E.S. Lora, O.J. Venturini, E.E. Yáñez, E.F. Castillo, and O. Almazan, *Biofuels: Environment, technology and food security.* Renewable and Sustainable Energy Reviews, **2009**. 13(6-7), 1275-1287.

Espeso, J., A.E. Lozano, J.G. de la Campa, and J. de Abajo, *Effect of substituents on the permeation properties of polyamide membranes.* Journal of Membrane Science, **2006**. 280(1–2), 659-665.

Farr, I.V., *Synthesis and characterization of novel polyimide gas separation membrane material systems*, Ph.D. **1999**, Virginia Polytechnic Institute and State University: Blacksburg, VA, USA.

Farr, I.V., D. Kratzner, T.E. Glass, D. Dunson, Q. Ji, and J.E. McGrath, *The synthesis and characterization of polyimide homopolymers based on 5(6)-amino-1-(4-aminophenyl)1,3,3-trimethylindane.* Journal of Polymer Science Part A: Polymer Chemistry, **2000**. 38(15), 2840-2854.

Favre, E., *Carbon dioxide recovery from post-combustion processes: Can gas permeation membranes compete with absorption?* Journal of Membrane Science, **2007**. 294(1-2), 50-59.

Ferrari, M.C., M. Galizia, M.G. De Angelis, and G.C. Sarti, *Gas and vapor transport in mixed matrix membranes based on amorphous Teflon AF1600 and AF2400 and fumed silica.* Industrial & Engineering Chemistry Research, **2010**. 49(23), 11920-11935.

Fitch, M.W., W.J. Koros, R.L. Nolen, and J.R. Carnes, *Permeation of several gases through elastomers, with emphasis on the deuterium/hydrogen pair.* Journal of Applied Polymer Science, **1993**. 47(6), 1033-1046.

Fogg, P.G.T. and W. Gerrard, *Solubility of Gases in Liquids*. **1991**, Chichester, John Wiley & Sons.

Freeman, B.D., *Basis of permeability/selectivity tradeoff relations in polymeric gas separation membranes.* Macromolecules, **1999**. 32(2), 375-380.

Friesen, D.T., R.J. Ray, D.D. Newbold, and S.B. McCray. *Countercurrent dehydration by hollow fibers*, **1992**, US 5108464.

Frisch, H.L., *Sorption and transport in glassy polymers - A review.* Polymer Engineering and Science, **1980**. 20(1), 2-13.

Fukukawa, K.-i., Y. Shibasaki, and M. Ueda, *A Photosensitive Semi-Alicyclic Poly(benzoxazole) with High Transparency and Low Dielectric Constant.* Macromolecules, **2004**. 37(22), 8256-8261.

Fukukawa, K.-i. and M. Ueda, *Recent Development of Photosensitive Polybenzoxazoles.* Polym. J, **2006**. 38(5), 405-418.

Fung, B.M., A.K. Khitrin, and K. Ermolaev, *An improved broadband decoupling sequence for liquid crystals and solids.* Journal of Magnetic Resonance, **2000**. 142(1), 97-101.

Furukawa, H., M.A. Miller, and O.M. Yaghi, *Independent verification of the saturation hydrogen uptake in MOF-177 and establishment of a benchmark for hydrogen adsorption in metal–organic frameworks.* Journal of Materials Chemistry, **2007**. 17(30), 3197-3204.

Gee, R.H., A. Maiti, S. Bastea, and L.E. Fried, *Molecular dynamics investigation of adhesion between TATB surfaces and amorphous fluoropolymers.* Macromolecules, **2007**. 40(9), 3422-3428.

Ghosal, K., R.T. Chern, and B.D. Freeman, *Effect of basic substituents on gas sorption and permeation in polysulfone.* Macromolecules, **1996**. 29(12), 4360-4369.

Ghosal, K. and B.D. Freeman, *Gas separation using polymer membranes: An overview.* Polymers for Advanced Technologies, **1994**. 5(11), 673-697.

Ghosh, M.K. and K.L. Mital, *Polyimides: Fundamentals and applications*. **1996**, New York, Marcel.

Gmehling, J., J. Menke, J. Krafczyk, K. Fischer, J.C. Fontaine, and H.V. Kehiaian, *Azeotropic data for binary mixtures*, in *CRC Handbook of Chemistry and Physics, 92nd Edition (Internet Version 2012)*, W.M. Haynes, Editor. **2012**, CRC Press/Taylor and Francis: Boca Raton, FL.

Gottlieb, H.E., V. Kotlyar, and A. Nudelman, *NMR chemical shifts of common laboratory solvents as trace impurities.* The Journal of Organic Chemistry, **1997**. 62(21), 7512-7515.

Gottschlich, D.E. and D.L. Roberts, *Energy Minimization of Separation Processes Using Conventional/Membrane Hybrid Systems*. **1990**, U.S. Department of Energy: Menlo Park.

Graham, T., *On the absorption and dialytic separation of gases by colloid septa Part I. Action of a septum of caoutchouc.* The London, Edinburgh, and Dublin Philosophical Magazine and Journal of Science, **1866**. 32, 401-420.

Guo, R., D.F. Sanders, Z.P. Smith, B.D. Freeman, D.R. Paul, and J.E. McGrath, *Synthesis and characterization of thermally rearranged (TR) polymers: Effect of glass transition temperature of aromatic poly(hydroxyimide) precursors on TR process*

and gas permeation properties. Journal of Materials Chemistry A, **2013**. 1(19), 6063-6072.

Guo, R., D.F. Sanders, Z.P. Smith, B.D. Freeman, D.R. Paul, and J.E. McGrath, *Synthesis and characterization of thermally rearranged (TR) polymers: Influence of ortho-positioned functional groups of polyimide precursors on TR process and gas transport properties.* Journal of Materials Chemistry A, **2013**. 1(2), 262-272.

Han, S., H. Kwon, K. Kim, J. Seong, C. Park, S. Kim, C.M. Doherty, A. Thornton, A.J. Hill, A. Lozano, K. Berchtold, and Y. Lee, *Tuning microcavities in thermally rearranged polymer membranes for CO_2 capture.* Physical Chemistry Chemical Physics, **2012**. 14(13), 4365-4373.

Han, S.H., J.E. Lee, K.-J. Lee, H.B. Park, and Y.M. Lee, *Highly gas permeable and microporous polybenzimidazole membrane by thermal rearrangement.* Journal of Membrane Science, **2010**. 357(1-2), 143-151.

Han, S.H. and Y.M. Lee, *Recent High Performance Polymer Membranes for CO_2 Separation*, in *Membrane Engineering for the Treatment of Gases: Volume 1: Gas-separation Problems with Membranes*, E. Drioli and G. Barbieri, Editors. **2011**, Royal Society of Chemistry: Cambridge. 84-124.

Han, S.H. and Y.M. Lee, *Recent high performance polymer membranes for CO_2 separation*, in *Membrane engineering for the treatment of gases: Volume 1: Gas-separation problems with membranes*. **2011**, The Royal Society of Chemistry. 84-124.

Han, S.H., N. Misdan, S. Kim, C.M. Doherty, A.J. Hill, and Y.M. Lee, *Thermally rearranged (TR) polybenzoxazole: Effects of diverse imidization routes on physical properties and gas transport behaviors.* Macromolecules, **2010**. 43(18), 7657-7667.

Hansen, J., M. Sato, R. Ruedy, K. Lo, D.W. Lea, and M. Medina-Elizade, *Global temperature change.* Proceedings of the National Academy of Sciences of the United States of America, **2006**. 103(39), 14288-14293.

Hariharan, R., B.D. Freeman, R.G. Carbonell, and G.C. Sarti, *Equation of state predictions of sorption isotherms in polymeric materials.* Journal of Applied Polymer Science, **1993**. 50(10), 1781-1795.

Haynes, W.M., D.R. Lide, and T.J. Bruno, *CRC Handbook of Chemistry and Physics 2012-2013*. **2012**, CRC Press.

Hellums, M.W., W.J. Koros, and J.C. Schmidhauser, *Gas separation properties of spirobiindane polycarbonate.* Journal of Membrane Science, **1992**. 67(1), 75-81.

Henis, J.M.S., *Commercial and practical aspects of gas separation membranes*, in *Polymeric Gas Separation Membranes*, D.R. Paul and Y.P. Yampolskii, Editors. **1994**, CRC Press: Boca Raton. 441-512.

Henis, J.M.S. and M.K. Tripodi, *Composite hollow fiber membranes for gas separation: the resistance model approach.* Journal of Membrane Science, **1981**. 8, 233-246.

Henis, J.M.S. and M.K. Tripodi. *Multicomponent membranes for gas separations*, **1980**, US 4230463.

Henis, J.M.S. and M.K. Tripodi, *A novel approach to gas separations using composite hollow fiber membranes.* Separation Science and Technology, **1980**. 15(4), 1059-1068.

Hesse, P.J., R. Battino, P. Scharlin, and E. Wilhelm, *Solubility of gases in liquids. 20. Solubility of He, Ne, Ar, Kr, N_2, O_2, CH_4, CF_4, and SF_6 in n-alkanes n-C_lH_{2l+2} ($6 \leq l \leq 16$) at 298.15 K.* Journal of Chemical & Engineering Data, **1996**. 41(2), 195-201.

Hickner, M.A., H. Ghassemi, Y.S. Kim, B.R. Einsla, and J.E. McGrath, *Alternative Polymer Systems for Proton Exchange Membranes (PEMs)*. Chemical Reviews, **2004**. 104(10), 4587-4612.

Hildebrand, J.H., B.B. Fisher, and H.A. Benesi, *Solubility of perfluoro-n-heptane with benzene, carbon tetrachloride, chloroform, n-heptane and 2,2,4-trimethylpentane.* Journal of the American Chemical Society, **1950**. 72(10), 4348-4351.

Hildebrand, J.H., J.M. Prausnitz, and R.L. Scott, *Regular and related solutions: The solubility of gases, liquids, and solids*. **1970**, New York, Van Nostrand Reinhold.

Hirayama, Y., T. Yoshinaga, Y. Kusuki, K. Ninomiya, T. Sakakibara, and T. Tamari, *Relation of gas permeability with structure of aromatic polyimides I.* Journal of Membrane Science, **1996**. 111(2), 169-182.

Hirayama, Y., T. Yoshinaga, Y. Kusuki, K. Ninomiya, T. Sakakibara, and T. Tamari, *Relation of gas permeability with structure of aromatic polyimides II.* Journal of Membrane Science, **1996**. 111(2), 183-192.

Hodgkin, J.H. and B.N. Dao, *Thermal conversion of hydroxy-containing polyimides to polybenzoxazoles. Does this reaction really occur?* European Polymer Journal, **2009**. 45(11), 3081-3092.

Hodgkin, J.H., M.S. Liu, B.N. Dao, J. Mardel, and A.J. Hill, *Reaction mechanism and products of the thermal conversion of hydroxy-containing polyimides.* European Polymer Journal, **2011**. 47(3), 394-400.

Hosseini, S.S., M.M. Teoh, and T.S. Chung, *Hydrogen separation and purification in membranes of miscible polymer blends with interpenetration networks.* Polymer, **2008**. 49(6), 1594-1603.

Huang, H.-J., S. Ramaswamy, U.W. Tschirner, and B.V. Ramarao, *A review of separation technologies in current and future biorefineries.* Separation and Purification Technology, **2008**. 62(1), 1-21.

Huang, Y., R.W. Baker, and L.M. Vane, *Low-energy distillation-membrane separation process.* Industrial & Engineering Chemistry Research, **2010**. 49(8), 3760-3768.

Huang, Y., J. Ly, T. Aldajani, and R.W. Baker. *Liquid-phase and vapor-phase dehydration of organic/water solutions*, **2008**, US 8000874 B2.

Huang, Y., J. Ly, D. Nguyen, and R.W. Baker, *Ethanol dehydration using hydrophobic and hydrophilic polymer membranes.* Industrial & Engineering Chemistry Research, **2010**. 49(23), 12067-12073.

Huang, Y. and D.R. Paul, *Physical aging of thin glassy polymer films monitored by gas permeability.* Polymer, **2004**. 45(25), 8377-8393.

Huang, Y., X. Wang, and D. Paul, *Physical aging of thin glassy polymer films: Free volume interpretation.* Journal of Membrane Science, **2006**. 277(1-2), 219-229.

Husk, G.R., P.E. Cassidy, and K.L. Gebert, *Synthesis and characterization of a series of polyimides derived from 4,4'-[2,2,2-trifluoro-1-(trifluoromethyl)ethylidene]bis[1,3-isobenzofurandione]*. Macromolecules, **1988**. 21(5), 1234-1238.

Ismail, A.F. and W. Lorna, *Penetrant-induced plasticization phenomenon in glassy polymers for gas separation membrane.* Separation and Purification Technology, **2002**. 27(3), 173-194.

Jacobsen, N.E., *NMR spectroscopy explained: simplified theory, applications and examples for organic chemistry and structural biology*. **2007**, Wiley.

Jansen, J.C., M. Macchione, and E. Drioli, *On the unusual solvent retention and the effect on the gas transport in perfluorinated Hyflon AD® membranes.* Journal of Membrane Science, **2007**. 287(1), 132-137.

Jean, Y., P. Mallon, and D. Schrader, *Principles and applications of positron & positronium chemistry*. **2003**, Singapore, World Scientific.

Jiang, Y., F.T. Willmore, D. Sanders, Z.P. Smith, C.P. Ribeiro, C.M. Doherty, A. Thornton, A.J. Hill, B.D. Freeman, and I.C. Sanchez, *Cavity size, sorption and transport characteristics of thermally rearranged (TR) polymers.* Polymer, **2011**. 52(10), 2244-2254.

Jordan, S. and W. Koros, *A free volume distribution model of gas sorption and dilation in glassy polymers.* Macromolecules, **1995**. 28(7), 2228-2235.

Jung, C.H., J.E. Lee, S.H. Han, H.B. Park, and Y.M. Lee, *Highly permeable and selective poly(benzoxazole-co-imide) membranes for gas separation.* Journal of Membrane Science, **2010**. 350(1-2), 301-309.

Kansy, J., *Microcomputer program for analysis of positron annihilation lifetime spectra.* Nuclear Instruments and Methods in Physics Research Section A: Accelerators, Spectrometers, Detectors and Associated Equipment, **1996**. 374(2), 235-244.

Kardash, I. and A.N. Pravednikov, *Aromatic polyimides containing hydroxy- and methoxy-groups.* Vysokomol Soyed, **1967**. 9(12), 873-876.

Keith, L.H. and D.B. Walters, eds. *The national toxicology program's chemical data compendium, volume 7*. **1992**, Lewis Publishers, Inc.

Kim, S., H.J. Jo, and Y.M. Lee, *Sorption and transport of small gas molecules in thermally rearranged (TR) polybenzoxazole membranes based on 2,2-bis(3-amino-4-hydroxyphenyl)-hexafluoropropane (bisAPAF) and 4,4'-hexafluoroisopropylidene diphthalic anhydride (6FDA).* Journal of Membrane Science, **2013**. 441, 1-8.

Kim, S. and Y. Lee, *Thermally rearranged (TR) polymer membranes with nanoengineered cavities tuned for CO_2 separation.* Journal of Nanoparticle Research, **2012**. 14(7), 1-11.

Kim, T.-H., W.J. Koros, and G.R. Husk, *Advanced gas separation membrane materials: Rigid aromatic polyimides.* Separation Science and Technology, **1988**. 23(12-13), 1611-1626.

Kim, T.H., W.J. Koros, G.R. Husk, and K.C. Obrien, *Relationship between gas separation properties and chemical-structure in a series of aromatic polyimides.* Journal of Membrane Science, **1988**. 37(1), 45-62.

Kim, T.K., K.Y. Choi, K.S. Lee, D.W. Park, and M.Y. Jin, *Thermal conversion of t-butyloxycarbonyloxy attached polyamides to polybenzoxazoles.* Polymer Bulletin, **2000**. 44, 55-62.

Kimmich, R., *NMR: tomography, diffusometry, relaxometry*. Vol. 432. **1997**, Springer Berlin etc.

Kita, H., T. Inada, K. Tanaka, and K.-i. Okamoto, *Effect of photocrosslinking on permeability and permselectivity of gases through benzophenone-containing polyimide.* Journal of Membrane Science, **1994**. 87(1–2), 139-147.

Kohl, A. and R. Nielsen, *Gas purification: 5th edition*. **1997**, Houston, TX, Gulf Publishing Company.

Koros, W. and R. Mahajan, *Pushing the limits on possibilities for large scale gas separation: which strategies?* Journal of Membrane Science, **2000**. 175(2), 181-196.

Koros, W.J., *Simplified analysis of gas/polymer selective solubility behavior.* Journal of Polymer Science: Polymer Physics Edition, **1985**. 23(8), 1611-1628.

Koros, W.J., *Sorption and transport of gases in glassy polymers*, Ph.D. Dissertation in Chemical Engineering. **1977**, The University of Texas at Austin: Austin, TX, USA. 254.

Koros, W.J., A.H. Chan, and D.R. Paul, *Sorption and transport of various gases in polycarbonate.* Journal of Membrane Science, **1977**. 2, 165-190.

Koros, W.J. and G.K. Fleming, *Membrane-based gas separation.* Journal of Membrane Science, **1993**. 83(1), 1-80.

Koros, W.J. and D.R. Paul, *CO_2 sorption in poly (ethylene terephthalate) above and below the glass transition.* Journal of Polymer Science: Polymer Physics Edition, **1978**. 16(11), 1947-1963.

Koros, W.J. and D.R. Paul, *Design considerations for measurement of gas sorption in polymers by pressure decay.* Journal of Polymer Science: Polymer Physics Edition, **1976**. 14(10), 1903-1907.

Koros, W.J. and D.R. Paul, *Sorption and transport of CO_2 above and below the glass transition of poly (ethylene terephthalate).* Polymer Engineering and Science, **1980**. 20(1), 14-19.

Koros, W.J., D.R. Paul, and A.A. Rocha, *Carbon dioxide sorption and transport in polycarbonate.* Journal of Polymer Science: Polymer Physics Edition, **1976**. 14(4), 687-702.

Kostina, J., O. Rusakova, G. Bondarenko, A. Alentiev, T. Meleshko, N. Kukarkina, A. Yakimanskii, and Y. Yampolskii, *Thermal rearrangement of functionalized polyimides: IR-spectral, quantum chemical studies, and gas permeability of TR polymers.* Industrial & Engineering Chemistry Research, **2013**. 52(31), 10476-10483.

Krishnan, G., D. Steele, K. O'Brien, R. Callahan, K. Berchtold, and J. Figueroa, *Simulation of a process to capture CO_2 from IGCC syngas using a high temperature PBI membrane.* Energy Procedia, **2009**. 1(1), 4079-4088.

Kwiatkowski, J.R., A.J. McAloon, F. Taylor, and D.B. Johnston, *Modeling the process and costs of fuel ethanol production by the corn dry-grind process.* Industrial Crops and Products, **2006**. 23(3), 288-296.

Laciak, D.V., L.M. Robeson, and C.D. Smith, *Group contribution modeling of gas transport in polymeric membranes*, in *Polymer Membranes for Gas and Vapor Separation*, B.D. Freeman and I. Pinnau, Editors. **1999**, American Chemical Society Symposium Series, 733: Washington, DC. 151–177.

Lee, J.S., W. Madden, and W.J. Koros, *Antiplasticization and plasticization of Matrimid® asymmetric hollow fiber membranes - Part A. Experimental.* Journal of Membrane Science, **2010**. 350(1-2), 232-241.

Lee, J.S., W. Madden, and W.J. Koros, *Antiplasticization and plasticization of Matrimid® asymmetric hollow fiber membranes. Part B. Modeling.* Journal of Membrane Science, **2010**. 350(1-2), 242-251.

LePree, J., *Membranes for gas separation.* Chemical Engineering Magazine, **2012**. 119(2), 17 - 20.

Li, P., T.S. Chung, and D.R. Paul, *Gas sorption and permeation in PIM-1.* Journal of Membrane Science, **2013**. 432, 50-57.

Li, Q., J.O. Jensen, R.F. Savinell, and N.J. Bjerrum, *High temperature proton exchange membranes based on polybenzimidazoles for fuel cells.* Progress in Polymer Science, **2009**. 34(5), 449-477.

Li, S., H.J. Jo, S.H. Han, C.H. Park, S. Kim, P.M. Budd, and Y.M. Lee, *Mechanically robust thermally rearranged (TR) polymer membranes with spirobisindane for gas separation.* Journal of Membrane Science, **2013**. 434, 137-147.

Likhatchev, D., C. Gutierrez-Wing, I. Kardash, and R. Vera-Graziano, *Soluble aromatic polyimides based on 2,2-bis(3-amino-4-hydroxyphenyl)hexafluoropropane: Synthesis and properties.* Journal of Applied Polymer Science, **1996**. 59(4), 725-735.

Lin, H. and B. Freeman, *Materials selection guidelines for membranes that remove CO_2 from gas mixtures.* Journal of Molecular Structure, **2005**. 739(1-3), 57-74.

Lin, H. and B.D. Freeman, *Springer handbook of materials measurement methods.* Materials Today, **2006**. 9(7-8), 52-52.

Lin, H. and B.D. Freeman, *Springer handbook: Permeation and diffusion*, H. Czichos, T. Saito, and L. Smith, Editors. **2006**, Springer: New York. 371-387.

Lin, H., E. Van Wagner, B.D. Freeman, L.G. Toy, and R.P. Gupta, *Plasticization-enhanced hydrogen purification using polymeric membranes.* Science, **2006**. 311(5761), 639-642.

Liu, S.L., R. Wang, T.S. Chung, M.L. Chng, Y. Liu, and R.H. Vora, *Effect of diamine composition on the gas transport properties in 6FDA-durene/3,3'-diaminodiphenyl sulfone copolyimides.* Journal of Membrane Science, **2002**. 202(1-2), 165-176.

Lo Nostro, P., *Phase separation properties of fluorocarbons, hydrocarbons and their copolymers.* Advances in Colloid and Interface Science, **1995**. 56(0), 245-287.

Lonsdale, H.K., *The growth of membrane technology.* Journal of Membrane Science, **1982**. 10(2-3), 81-181.

Look, D.C., I.J. Lowe, and J.A. Northby, *Nuclear magnetic resonance study of molecular motions in solid hydrogen sulfide.* The Journal of Chemical Physics, **1966**. 44(9), 3441-3452.

Lozano, A.E., J. de Abajo, and J.G. de la Campa, *Synthesis of aromatic polyisophthalamides by in situ silylation of aromatic diamines.* Macromolecules, **1997**. 30(8), 2507-2508.

Lu, K., C. Song, and V. Subramani, eds. *Hydrogen and syngas production and purification technologies.* **2010**, John Wiley & Sons, Inc.: Hoboken, NJ.

Macchione, M., J.C. Jansen, G. De Luca, E. Tocci, M. Longeri, and E. Drioli, *Experimental analysis and simulation of the gas transport in dense Hyflon® AD60X membranes: Influence of residual solvent.* Polymer, **2007**. 48(9), 2619-2635.

Matsuura, T., Y. Hasuda, S. Nishi, and N. Yamada, *Polyimide derived from 2, 2'-bis (trifluoromethyl)-4, 4'-diaminobiphenyl. 1. Synthesis and characterization of polyimides prepared with 2, 2'-bis (3, 4-dicarboxyphenyl) hexafluoropropane dianhydride or pyromellitic dianhydride.* Macromolecules, **1991**. 24(18), 5001-5005.

Matsuura, T., M. Ishizawa, Y. Hasuda, and S. Nishi, *Polyimides derived from 2, 2'-bis (trifluoromethyl)-4, 4'-diaminobiphenyl. 2. Synthesis and characterization of polyimides prepared from fluorinated benzenetetracarboxylic dianhydrides.* Macromolecules, **1992**. 25(13), 3540-3545.

Matteucci, S.T., Y.P. Yampolskii, B.D. Freeman, and I. Pinnau, *Transport of gases and vapors in glassy and rubbery polymers*, in *Materials science of membranes for gas and vapor separation*, Y. Yampolskii, I. Pinnau, and B.D. Freeman, Editors. **2006**, John Wiley & Sons: Chichester. 1-47.

Mauritz, K.A. and R.B. Moore, *State of understanding of Nafion.* Chemical reviews, **2004**. 104(10), 4535-4585.

McCaig, M.S. and D.R. Paul, *Effect of UV crosslinking and physical aging on the gas permeability of thin glassy polyarylate films.* Polymer, **1999**. 40(26), 7209-7225.

McHattie, J.S., W.J. Koros, and D.R. Paul, *Gas transport properties of polysulphones: 1. Role of symmetry of methyl group placement on bisphenol rings.* Polymer, **1991**. 32(5), 840-850.

McKeown, N.B., B. Gahnem, K.J. Msayib, P.M. Budd, C.E. Tattershall, K. Mahmood, S. Tan, D. Book, H.W. Langmi, and A. Walton, *Towards polymer-based hydrogen storage materials: engineering ultramicroporous cavities within polymers of intrinsic microporosity.* Angewandte Chemie, **2006**. 45(11), 1804-1807.

Meares, P., *The diffusion of gases through polyvinyl acetate.* Journal of the American Chemical Society, **1954**. 76, 3415-3422.

Merkel, T., V. Bondar, K. Nagai, B. Freeman, and Y. Yampolskii, *Gas sorption, diffusion, and permeation in poly (2,2-bis (trifluoromethyl)-4,5-difluoro-1,3-dioxole-co-tetrafluoroethylene).* Macromolecules, **1999**. 32, 8427-8440.

Merkel, T.C. *NETL Report: Membrane process to capture carbon dioxide from coal-fired power plant flue gas*. Available from: http://www.netl.doe.gov/File%20Library/Research/Coal/ewr/co2/5312-43085-MTR-spiral-wound-polymeric-membrane.pdf.

Merkel, T.C., V. Bondar, K. Nagai, and B.D. Freeman, *Hydrocarbon and perfluorocarbon gas sorption in poly(dimethylsiloxane), poly(1-trimethylsilyl-1-propyne), and copolymers of tetrafluoroethylene and 2,2-bis(trifluoromethyl)-4,5-difluoro-1,3-dioxole.* Macromolecules, **1999**. 32(2), 370-374.

Merkel, T.C., V. Bondar, K. Nagai, and B.D. Freeman, *Sorption and transport of hydrocarbon and perfluorocarbon gases in poly(1-trimethylsilyl-1-propyne).* Journal of Polymer Science Part B: Polymer Physics, **2000**. 38(2), 273-296.

Merkel, T.C., V. Bondar, K. Nagai, B.D. Freeman, and Y.P. Yampolskii, *Gas Sorption, Diffusion, and Permeation in Poly(2,2-bis(trifluoromethyl)-4,5-difluoro-1,3-dioxole-co-tetrafluoroethylene).* Macromolecules, **1999**. 32(25), 8427-8440.

Merkel, T.C., V.I. Bondar, K. Nagai, B.D. Freeman, and I. Pinnau, *Gas sorption, diffusion, and permeation in poly(dimethylsiloxane).* Journal of Polymer Science Part B: Polymer Physics, **2000**. 38(3), 415-434.

Merkel, T.C., H.Q. Lin, X.T. Wei, and R.R. Baker, *Power plant post-combustion carbon dioxide capture: An opportunity for membranes.* Journal of Membrane Science, **2010**. 359(1-2), 126-139.

Merkel, T.C., I. Pinnau, R. Prabhakar, and B.D. Freeman, *Gas and vapor transport properties of perfluoropolymers*, in *Materials science of membranes for gas and vapor separations*, Y. Yampolskii, P., I. Pinnau, and B.D. Freeman, Editors. **2006**, John Wiley & Sons, Ltd: Chichester. 251 - 270.

Merkel, T.C., M. Zhou, and R.W. Baker, *Carbon dioxide capture with membranes at an IGCC power plant.* Journal of Membrane Science, **2012**. 389, 441-450.

Merten, U., S. Beach, and P.K. Gantzel. *Method and apparatus for gas separation by diffusion*, **1968**, US 3415038.

Michaels, A.S. and H.J. Bixler, *Solubility of gases in polyethylene.* Journal of Polymer Science, **1961**. 50(154), 393-412.

Minelli, M., G. Cocchi, L. Ansaloni, M.G. Baschetti, M.G. De Angelis, and F. Doghieri, *Vapor and liquid sorption in matrimid polyimide: Experimental characterization and modeling.* Industrial & Engineering Chemistry Research, **2013**. 52(26), 8936-8945.

Miyata, S., S. Sato, K. Nagai, T. Nakagawa, and K. Kudo, *Relationship between gas transport properties and fractional free volume determined from dielectric constant in polyimide films containing the hexafluoroisopropylidene group.* Journal of Applied Polymer Science, **2008**. 107(6), 3933-3944.

Mohr, J.M., D.R. Paul, G.L. Tullos, and P.E. Cassidy, *Gas transport properties of a series of poly(ether ketone) polymers.* Polymer, **1991**. 32(13), 2387–2394.

Moore, T.T. and W.J. Koros, *Gas sorption in polymers, molecular sieves, and mixed matrix membranes.* Journal of Applied Polymer Science, **2007**. 104(6), 4053-4059.

Morisato, A., B.D. Freeman, I. Pinnau, and C.G. Casillas, *Pure hydrocarbon sorption properties of poly(1-trimethylsilyl-1-propyne) (PTMSP), poly(1-phenyl-1-propyne) (PPP), and PTMSP/PPP blends.* Journal of Polymer Science Part B: Polymer Physics, **1996**. 34(11), 1925-1934.

Morisato, A., K. Ghosal, B.D. Freeman, R.T. Chern, J.C. Alvarez, J.G. de la Campa, A.E. Lozano, and J. de Abajo, *Gas separation properties of aromatic polyamides containing hexafluoroisopropylidene groups.* Journal of Membrane Science, **1995**. 104(3), 231-241.

Moss, R.H., J.A. Edmonds, K.A. Hibbard, M.R. Manning, S.K. Rose, D.P.V. Vuuren, T.R. Carter, S. Emori, M. Kainuma, T. Kram, G.A. Meehl, J.F.B. Mitchell, N. Nakicenovic, K. Riahi, S.J. Smith, R.J. Stouffer, A.M. Thomson, J.P. Weyant, and T.J. Wilbanks, *The next generation of scenarios for climate change research and assessment.* Nature, **2010**. 463(7282), 747-756.

Moy, T.M. and J.E. McGrath, *Synthesis of hydroxyl-containing polyimides derived from 4,6-diamino-resorcinol dihydrochloride and aromatic tetracarboxylic dianhydrides.* Journal of Polymer Science Part A: Polymer Chemistry, **1994**. 32(10), 1903-1908.

Muñoz, D.M., M. Calle, J.G. de la Campa, J. de Abajo, and A.E. Lozano, *An improved method for preparing very high molecular weight polyimides.* Macromolecules, **2009**. 42(15), 5892-5894.

Murphy, T.M., D.S. Langhe, M. Ponting, E. Baer, B.D. Freeman, and D.R. Paul, *Physical aging of layered glassy polymer films via gas permeability tracking.* Polymer, **2011**. 52(26), 6117-6125.

Muruganandam, N., W.J. Koros, and D.R. Paul, *Gas sorption and transport in substituted polycarbonates.* Journal of Polymer Science Part B: Polymer Physics, **1987**. 25, 1999-2026.

Muruganandam, N. and D.R. Paul, *Evaluation of substituted polycarbonates and a blend with polystyrene as gas separation membranes.* Journal of Membrane Science, **1987**. 34(2), 185-198.

Nigam, P.S. and A. Singh, *Production of liquid biofuels from renewable resources.* Progress in Energy and Combustion Science, **2011**. 37(1), 52-68.

Nuttall, W.J., R.H. Clarke, and B.A. Glowacki, *Resources: Stop squandering helium.* Nature, **2012**. 485(7400), 573-575.

Ogura, T., T. Higashihara, and M. Ueda, *Pattern formation of polyimide by using photosensitive polybenzoxazole as a top layer.* European Polymer Journal, **2010**. 46(7), 1576-1581.

Ohya, H., V.V. Kudryavtsev, and S.I. Semenova, *Polyimide membranes: Applications, fabrications, and properties*. **1996**, Amsterdam, Gordon and Breach Publishers.

Okamoto, K.-i., K. Tanaka, H. Kita, M. Ishida, M. Kakimoto, and Y. Imai, *Gas permeability and permselectivity of polyimides prepared from 4,4'-diaminotriphenylamine.* Polymer Journal, **1992**. 24(5), 451-457.

Okamoto, K., K. Noborio, J. Hao, K. Tanaka, and K. Hidetoshi, *Permeation and separation properties of polyimide membranes to 1, 3-butadiene and n-butane.* Journal of Membrane Science, **1997**. 134(2), 171-179.

Pandey, P., *Membranes for gas separation.* Progress in Polymer Science, **2001**. 26(6), 853-893.

Park, C.H., E. Tocci, Y.M. Lee, and E. Drioli, *Thermal treatment effect on the structure and property change between hydroxy-containing polyimides (HPIs) and*

thermally rearranged polybenzoxazole (TR-PBO). The Journal of Physical Chemistry B, **2012**. 116(42), 12864-12877.

Park, H. and B. Freeman, *Gas separation properties and their applications of high permeable amorphous perfluoropolymer membranes.* Membrane Journal, **2007**. 17(2), 81.

Park, H.B., S.H. Han, C.H. Jung, Y.M. Lee, and A.J. Hill, *Thermally rearranged (TR) polymer membranes for CO_2 separation.* Journal of Membrane Science, **2010**. 359(1-2), 11-24.

Park, H.B., C.H. Jung, Y.M. Lee, A.J. Hill, S.J. Pas, S.T. Mudie, E. Van Wagner, B.D. Freeman, and D.J. Cookson, *Polymers with cavities tuned for fast selective transport of small molecules and ions.* Science, **2007**. 318(5848), 254-258.

Park, J.Y. and D.R. Paul, *Correlation and prediction of gas permeability in glassy polymer membrane materials via a modified free volume based group contribution method.* Journal of Membrane Science, **1997**. 125(1), 23-39.

Pascual-Izarra, C., A.W. Dong, S.J. Pas, A.J. Hill, B.J. Boyd, and C.J. Drummond, *Advanced fitting algorithms for analysing positron annihilation lifetime spectra.* Nuclear Instruments and Methods in Physics Research Section A: Accelerators, Spectrometers, Detectors and Associated Equipment, **2009**. 603(3), 456-466.

Paul, D.R., *Sorption and transport in glassy polymers.* Berichte der Bunsengesellschaft für Physikalische, **1979**. 83(1), 294-302.

Paul, D.R. and W.J. Koros, *Effect of partially immobilizing sorption on permeability and the diffusion time lag.* Journal of Polymer Science: Polymer Physics Edition, **1976**. 14(4), 675-685.

Paul, D.R. and Y.P. Yampolskii, *Polymeric gas separation membranes*. **1994**, Boca Raton, CRC Press.

Perry, E. *Process for the recovery of hydrogen from ammonia purge gases*, **1979**, US 4172885.

Pethrick, R.A., *Positron annihilation - A probe for nanoscale voids and free volume?* Progress in Polymer Science, **1997**. 22(1), 1-47.

Pinnau, I. and L.G. Toy, *Gas and vapor transport properties of amorphous perfluorinated copolymer membranes based on 2, 2-bistrifluoromethyl-4, 5-*

difluoro-1,3-dioxole/tetrafluoroethylene. Journal of Membrane Science, **1996**. 109, 125-133.

Pinnau, I. and L.G. Toy, *Solid polymer electrolyte composite membranes for olefin/paraffin separation.* Journal of Membrane Science, **2001**. 184(1), 39-48.

Pixton, M.R. and D.R. Paul, *Gas transport properties of adamantane-based polysulfones.* Polymer, **1995**. 36(16), 3165-3172.

Pixton, M.R. and D.R. Paul, *Gas transport properties of polyarylates part II: Tetrabromination of the bisphenol.* Journal of Polymer Science Part B: Polymer Physics, **1995**. 33(9), 1353-1364.

Poling, B.E., J.M. Prausnitz, and J.P. O'Connell, *The properties of gases and liquids*. **2001**, McGraw Hill Book Co., New York, NY. A.5-A.19.

Posey, L.G. *Processes*, **1983**, US 4367135.

Prabhakar, R.S., B.D. Freeman, and I. Roman, *Gas and vapor sorption and permeation in poly(2,2,4-trifluoro-5-trifluoromethoxy-1,3-dioxole-co-tetrafluoroethylene).* Macromolecules, **2004**. 37(20), 7688-7697.

Prabhakar, R.S., R. Raharjo, L.G. Toy, H. Lin, and B.D. Freeman, *Self-consistent model of concentration and temperature dependence of permeability in rubbery polymers.* Industrial & Engineering Chemistry Research, **2005**. 44(5), 1547-1556.

Prasad, R. *Process and system for the production of dry, high purity nitrogen*, **1990**, US 4931070.

Prasad, R., C.J. Heim, and J.J. Maloney. *Helium recovery process*, **2012**, US 8152898 B2.

Prasad, R., F. Notaro, and D.R. Thompson, *Evolution of membranes in commercial air separation.* Journal of Membrane Science, **1994**. 94, 225-248.

Prasad, R., R.L. Shaner, and K.J. Doshi, *Comparison of membranes with other gas separation technologies*, in *Polymeric gas separation membranes*, D.R. Paul and Y.P. Yampolskii, Editors. **1994**, CRC Press: Boca Raton.

Pryde, C.A., *Polyimide hydrolysis measurement by fourier transform — IR spectroscopy*, in *Polymeric Materials for Electronics Packaging and Interconnection*, J.H. Lupinski and R.S. Moore, Editors. **1989**, American Chemical Society: Washington, DC. 57-66.

Puleo, A.C., D.R. Paul, and S.S. Kelley, *The effect of degree of acetylation on gas sorption and transport behavior in cellulose acetate.* Journal of Membrane Science, **1989**. 47(3), 301-332.

Puri, P.S., *Commercial applications of membranes in gas separations*, in *Membrane engineering for the treatment of gases Vol 1: Gas separation problems with membranes*, E. Drioli and G. Barbieri, Editors. **2011**, Royal Society of Chemistry.

Rabbani, M.G. and H.M. El-Kaderi, *Template-Free Synthesis of a Highly Porous Benzimidazole-Linked Polymer for CO2 Capture and H2 Storage.* Chemistry of Materials, **2011**. 23(7), 1650-1653.

Raharjo, R., B. Freeman, and E. Sanders, *Pure and mixed gas CH_4 and n-C_4H_{10} sorption and dilation in poly(dimethylsiloxane).* Journal of Membrane Science, **2007**. 292(1-2), 45-61.

Rasband, W.S., *ImageJ*. **1997-2012**, U. S. National Institutes of Health: Bethesda, Maryland, USA.

Raymond, P.C. and D.R. Paul, *Sorption and transport of pure gases in random styrene/methyl methacrylate copolymers.* Journal of Polymer Science Part B: Polymer Physics, **1990**. 28(11), 2079-2102.

Ribeiro, C.P., B.D. Freeman, D.S. Kalika, and S. Kalakkunnath, *Aromatic polyimide and polybenzoxazole membranes for the fractionation of aromatic/aliphatic hydrocarbons by pervaporation.* Journal of Membrane Science, **2012**. 390–391(0), 182-193.

Robeson, L.M., *Correlation of separation factor versus permeability for polymeric membranes.* Journal of Membrane Science, **1991**. 62(2), 165-185.

Robeson, L.M., *The upper bound revisited.* Journal of Membrane Science, **2008**. 320(1-2), 390-400.

Robeson, L.M., B.D. Freeman, D.R. Paul, and B.W. Rowe, *An empirical correlation of gas permeability and permselectivity in polymers and its theoretical basis.* Journal of Membrane Science, **2009**. 341(1-2), 178-178.

Robeson, L.M., C.D. Smith, and M. Langsam, *A group contribution approach to predict permeability and permselectivity of aromatic polymers.* Journal of Membrane Science, **1997**. 132(1), 33-54.

Robeson, L.M., Z.P. Smith, B.D. Freeman, and D.R. Paul, *Contributions of diffusion and solubility selectivity to the upper bound analysis for glassy gas separation membranes.* Journal of Membrane Science, **2014**. 453, 71-83.

Rowe, B.W., B.D. Freeman, and D.R. Paul, *Physical aging of ultrathin glassy polymer films tracked by gas permeability.* Polymer, **2009**. 50(23), 5565-5575.

Rowe, B.W., L.M. Robeson, B.D. Freeman, and D.R. Paul, *Influence of temperature on the upper bound: Theoretical considerations and comparison with experimental results.* Journal of Membrane Science, **2010**. 360(1-2), 58-69.

Ruiz-Treviño, F.A. and D.R. Paul, *Gas permselectivity properties of high free volume polymers modified by a low molecular weight additive.* Journal of Applied Polymer Science, **1998**. 68(3), 403-415.

Rungta, M., C. Zhang, W.J. Koros, and L. Xu, *Membrane-based ethylene/ethane separation: The upper bound and beyond.* AIChE Journal, **2013**. 59(9), 3475-3489.

Sada, E., H. Kumazawa, P. Xu, and S.T. Wang, *Permeation of pure carbon dioxide and methane and binary mixtures through cellulose acetate membranes.* Journal of Polymer Science Part B: Polymer Physics, **1990**. 28(1), 113-125.

Sanchez, I.C. and R.H. Lacombe, *Statistical thermodynamics of polymer solutions.* Macromolecules, **1978**. 11(6), 1145-1156.

Sanders, D.F., R. Guo, Z.P. Smith, Q. Liu, K.A. Stevens, J.E. McGrath, D.R. Paul, and B.D. Freeman, *Influence of polyimide precursor synthesis route and ortho-position functional group on thermally rearranged (TR) polymer properties: Conversion and free volume.* Polymer, **2014**. 55(7), 1636-1647.

Sanders, D.F., R. Guo, Z.P. Smith, K.A. Stevens, Q. Liu, J.E. McGrath, D.R. Paul, and B.D. Freeman, *Influence of polyimide precursor synthesis route and ortho-position functional group on thermally rearranged (TR) polymer properties: Pure gas permeability and selectivity (in press).* Journal of Membrane Science, **2014**.

Sanders, D.F., Z.P. Smith, R. Guo, L.M. Robeson, J.E. McGrath, D.R. Paul, and B.D. Freeman, *Energy-efficient polymeric gas separation membranes for a sustainable future: A review.* Polymer, **2013**. 54(18), 4729-4761.

Sanders, D.F., Z.P. Smith, C.P. Ribeiro, R. Guo, J.E. McGrath, D.R. Paul, and B.D. Freeman, *Permeability, diffusivity, and free volume of thermally rearranged polymers based on 3,3'-dihydroxy-4,4'-diamino-biphenyl (HAB) and 2,2'-bis-(3,4-*

dicarboxyphenyl) hexafluoropropane dianhydride (6FDA). Journal of Membrane Science, **2011**. 409-410, 232-241.

Sanders, D.F., Z.P. Smith, C.P. Ribeiro, R.L. Guo, J.E. McGrath, D.R. Paul, and B.D. Freeman, *Gas permeability, diffusivity, and free volume of thermally rearranged polymers based on 3,3 '-dihydroxy-4,4 '-diamino-biphenyl (HAB) and 2,2 '-bis-(3,4-dicarboxyphenyl) hexafluoropropane dianhydride (6FDA).* Journal of Membrane Science, **2012**. 409, 232-241.

Sanders, E.S., *High-pressure sorption of pure and mixed gases in glassy polymers*, Ph.D. Dissertation in Chemical Engineering. **1983**, North Carolina State University: Raleigh, NC, USA.

Sanders Jr, E.S., D.O. Clark, J.A. Jensvold, H.N. Beck, G.G. Lipscomb, and F.L. Coan. *Process for preparing POWADIR membranes from tetrahalobisphenol A polycarbonates*, **1988**, US 4772392.

Schmidt-Rohr, K. and H.W. Spiess, *Multidimensional solid-state NMR and polymers*. **1994**, Elsevier.

Scott, K., *Handbook of Industrial Membranes*. First Edition ed. **1995**, Oxford, UK, Elsevier Science Publishers Ltd.

Scott, R.L., *The anomalous behavior of fluorocarbon solutions.* The Journal of Physical Chemistry, **1958**. 62(2), 136-145.

Senthilkumar, U. and B.S.R. Reddy, *Polysiloxanes with pendent bulky groups having amino-hydroxy functionality: Structure–permeability correlation.* Journal of Membrane Science, **2007**. 292(1–2), 72-79.

Shantarovich, V.P., T. Suzuki, C. He, and V.W. Gustov, *Inhibition of positronium formation by polar groups in polymers—relation with TSL experiments.* Radiation Physics and Chemistry, **2003**. 67(1), 15-23.

Shieh, J.-J. and T.S. Chung, *Gas permeability, diffusivity, and solubility of poly(4-vinylpyridine) film.* Journal of Polymer Science Part B: Polymer Physics, **1999**. 37(20), 2851-2861.

Shimazu, A., T. Miyazaki, M. Maeda, and K. Ikeda, *Relationships between the chemical structures and the solubility, diffusivity, and permselectivity of propylene and propane in 6FDA-based polyimides.* Journal of Polymer Science Part B: Polymer Physics, **2000**. 38(19), 2525-2536.

Siebert, E.D. and C. Knobler, *Interaction virial coefficients in hydrocarbon-fluorocarbon mixtures.* The Journal of Physical Chemistry, **1971**. 75(25), 3863-3870.

Singh, A., B.D. Freeman, and I. Pinnau, *Pure and mixed gas acetone/nitrogen permeation properties of polydimethylsiloxane [PDMS]*. Journal of Polymer Science Part B: Polymer Physics, **1998**. 36, 289-301.

Sircar, S., *Gibbsian surface excess for gas adsorption - revisited.* Industrial & Engineering Chemistry Research, **1999**. 38, 3670-3682.

Smith, J.M., H.C. Van Ness, and M.M. Abbott, *Introduction to chemical engineering thermodynamics*. **2005**, Boston, McGraw-Hill.

Smith, Z.P., D.F. Sanders, C.P. Ribeiro Jr, R. Guo, B.D. Freeman, D.R. Paul, J.E. McGrath, and S. Swinnea, *Gas sorption and characterization of thermally rearranged polyimides based on 3,3'-dihydroxy-4,4'-diamino-biphenyl (HAB) and 2,2'-bis-(3,4-dicarboxyphenyl) hexafluoropropane dianhydride (6FDA).* Journal of Membrane Science, **2012**. 416, 558-567.

Smith, Z.P., R.R. Tiwari, T.M. Murphy, D.F. Sanders, K.L. Gleason, D.R. Paul, and B.D. Freeman, *Hydrogen sorption in polymers for membrane applications.* Polymer, **2013**. 54(12), 3026–3037.

Song, W., P.J. Rossky, and M. Maroncelli, *Modeling alkane + perfluoroalkane interactions using all-atom potentials: Failure of the usual combining rules.* The Journal of Chemical Physics, **2003**. 119(17), 9145-9162.

Spillman, R., *Economics of gas separation membrane processes,* in *Membrane Separation Technology, Principles and Applications*, R.D. Noble and S.A. Stern, Editors. **1995**, Elsevier Science B. V.: Amsterdam. 589 - 663.

Spillman, R.W., *Economics of gas separation membranes.* Chemical Engineering Progress, **1989**. 85(1), 41–62.

Stannett, V., *Simple gases*, in *Diffusion in polymers*, J. Crank and G.S. Park, Editors. **1968**, Academic Press: New York, NY.

Stannett, V.T., W.J. Koros, D.R. Paul, H.K. Lonsdale, and R.W. Baker, *Recent advances in membrane science and technology*, in *Advances in Polymer Science*. **1979**, Springer Berlin Heidelberg. 69-121.

Staudt-Bickel, C. and W.J. Koros, *Improvement of CO_2/CH_4 separation characteristics of polyimides by chemical crosslinking.* Journal of Membrane Science, **1999**. 155, 145-154.

Staudt-Bickel, C. and W.J. Koros, *Improvement of CO_2/CH_4 separation characteristics of polyimides by chemical crosslinking.* Journal of Membrane Science, **1999**. 155(1), 145–154.

Staudt-Bickel, C. and W.J. Koros, *Olefin/paraffin gas separations with 6FDA-based polyimide membranes.* Journal of Membrane Science, **2000**. 170(2), 205-214.

Staudt, R., G. Saller, M. Tomalla, and J.U. Keller, *A note on gravimetric measurements of gas adsorption equilibria.* Berichte der Bunsen-Gesellschaft-Physical Chemistry Chemical Physics, **1993**. 97(1), 98-105.

Stern, S.A., *Polymers for gas separations: the next decade.* Journal of Membrane Science, **1994**. 94(1), 1-65.

Stern, S.A., Y. Mi, H. Yamamoto, and A.K.S. Clair, *Structure/permeability relationships of polyimide membranes. Applications to the separation of gas mixtures.* Journal of Polymer Science Part B: Polymer Physics, **1989**. 27(9), 1887-1909.

Stern, S.A., V.M. Shah, and B.J. Hardy, *Structure-permeability relationships in silicone polymers.* Journal of Polymer Science Part B: Polymer Physics, **1987**. 25(6), 1263-1298.

Stern, S.A., T.F. Sinclair, P.J. Gareis, N.P. Vahldieck, and P.H. Mohr, *Helium recovery by permeation.* Industrial & Engineering Chemistry, **1965**. 57(2), 49-60.

Story, B.J. and W.J. Koros, *Sorption and transport of CO_2 and CH_4 in chemically modified poly (phenylene oxide).* Journal of Membrane Science, **1992**. 67(2-3), 191-210.

Tanaka, K., H. Kita, M. Okano, and K.-i. Okamoto, *Permeability and permselectivity of gases in fluorinated and non-fluorinated polyimides.* Polymer, **1992**. 33(3), 585-592.

Tanaka, K., M. Okano, H. Toshino, H. Kita, and K.-i. Okamoto, *Effect of methyl substituents on permeability and permselectivity of gases in polyimides prepared from methyl-substituted phenylenediamines.* Journal of Polymer Science Part B: Polymer Physics, **1992**. 30(8), 907-914.

Tanaka, K., A. Taguchi, J. Hao, H. Kita, and K. Okamoto, *Permeation and separation properties of polyimide membranes to olefins and paraffins.* Journal of Membrane Science, **1996**. 121(2), 197-207.

Teplyakov, V.V., D.R. Paul, N.B. Bespalova, and E.S. Finkel'shtein, *Gas permeation in a fluorine-containing polynorbornene.* Macromolecules, **1992**. 25(16), 4218-4219.

Tokarev, A., K. Friess, J. Machkova, M. Šipek, and Y.P. Yampolskii, *Sorption and diffusion of organic vapors in amorphous Teflon AF2400.* Journal of Polymer Science Part B: Polymer Physics, **2006**. 44(5), 832-844.

Tsujita, Y., *Gas sorption and permeation of glassy polymers with microvoids.* Progress in Polymer Science, **2003**. 28(9), 1377-1401.

Tullos, G. and L. Mathias, *Unexpected thermal conversion of hydroxy-containing polyimides to polybenzoxazoles.* Polymer, **1999**. 40(12), 3463-3468.

Tullos, G.L. and L.J. Mathias, *Unexpected thermal conversion of hydroxy-containing polyimides to polybenzoxazoles.* Polymer, **1999**. 40, 3463-3468.

Tullos, G.L., J.M. Powers, S.J. Jeskey, and L.J. Mathias, *Thermal conversion of hydroxy-containing imides to benzoxazoles: Polymer and model compound study.* Macromolecules, **1999**. 32, 3598-3612.

Tullos, G.L., J.M. Powers, S.J. Jeskey, and L.J. Mathias, *Thermal conversion of hydroxy-containing imides to benzoxazoles: Polymer and model compound study.* Macromolecules, **1999**. 32(11), 3598-3612.

van Amerongen, G.J., *Diffusion in elastomers.* Rubber Chemistry and Technology, **1964**. 37(5), 1065-1152.

van der Vegt, N., *A molecular dynamics simulation study of solvation thermodynamical quantities of gases in polymeric solvents.* Journal of Membrane Science, **2002**. 205(1-2), 125-139.

Van Krevelen, D.W., *Properties of Polymers: Their Correlation with Chemical Structure, Third Edition.* **1997**, Elsevier.

Vane, L., *Separation technologies for the recovery and dehydration of alcohols from fermentation broths.* Biofuels, Bioproducts and Biorefining, **2008**. 2(6), 553-588.

Vane, L., F. Alvarez, L. Rosenblum, and S. Govindaswamy, *Efficient ethanol recovery from yeast fermentation broth with integrated distillation-membrane process.* Industrial & Engineering Chemistry Research, **2012**. 52(3), 1033–1041.

Vane, L.M., *A review of pervaporation for product recovery from biomass fermentation processes.* Journal of Chemical Technology & Biotechnology, **2005**. 80(6), 603-629.

Vasudevan, V.J. and J.E. McGrath, *Atomistic modeling of amorphous aromatic polybenzoxazoles.* Macromolecules, **1996**. 29(2), 637-645.

Vieth, W.R., J.M. Howell, and J.H. Hsieh, *Dual sorption theory.* Journal of Membrane Science, **1976**. 1, 177-220.

Visser, T. and M. Wessling, *When do sorption-induced relaxations in glassy polymers set in?* Macromolecules, **2007**. 40(14), 4992-5000.

Vos, K.D. and F.O. Burris, *Drying cellulose acetate reverse osmosis membranes.* Industrial & Engineering Chemistry Product Research and Development, **1969**. 8(1), 84-89.

Wang, G., Z. Zhang, S. Chen, and L. Zhang. *Process for producing olefins*, **2010**, US 2010/0274063 A1.

Wang, H., T.-S. Chung, and D.R. Paul, *Physical aging and plasticization of thick and thin films of the thermally rearranged ortho-functional polyimide 6FDA–HAB.* Journal of Membrane Science, **2014**. 458(0), 27-35.

Wang, H., T.-S. Chung, and D.R. Paul, *Thickness dependent thermal rearrangement of an ortho-functional polyimide.* Journal of Membrane Science, **2014**. 450(0), 308-312.

Wang, H., D.R. Paul, and T.-S. Chung, *The effect of purge environment on thermal rearrangement of ortho-functional polyamide and polyimide.* Polymer, **2013**. 54(9), 2324-2334.

Waters, T., R.A.J. O'Hair, and A.G. Wedd, *Catalytic gas phase dehydration of acetic acid to ketene.* International Journal of Mass Spectrometry, **2003**. 228(2-3), 599-611.

Wessling, M., I. Huisman, T.v.d. Boomgaard, and C.A. Smolders, *Time-dependent permeation of carbon dioxide through a polyimide membrane above the*

plasticization pressure. Journal of Applied Polymer Science, **1995**. 58(11), 1959-1966.

White, L.S., I.-f. Wang, and B.S. Minhas. *Polyimide membranes for separation of solvents from lube oil*, **1993**, US 5264166.

Wieneke, J.U. and C. Staudt, *Thermal stability of 6FDA-(co-)polyimides containing carboxylic acid groups.* Polymer Degradation and Stability, **2010**. 95(4), 684-693.

Wijmans, J.G. and R.W. Baker, *The solution-diffusion model: A review.* Journal of Membrane Science, **1995**. 107(1-2), 1-21.

Wijmans, J.G., A. Ng, and A.P. Mairal. *Natural gas dehydration apparatus*, **2004**, US 20040206242 A1.

Wilhelm, E. and R. Battino, *Thermodynamic functions of the solubilities of gases in liquids at 25.deg.* Chemical Reviews, **1973**. 73(1), 1-9.

Wind, J.D., D.R. Paul, and W.J. Koros, *Natural gas permeation in polyimide membranes.* Journal of Membrane Science, **2004**. 228(2), 227-236.

Wind, J.D., C. Staudt-Bickel, D.R. Paul, and W.J. Koros, *The effects of crosslinking chemistry on CO_2 plasticization of polyimide gas separation membranes.* Industrial & Engineering Chemistry Research, **2002**. 41(24), 6139-6148.

Wind, J.D., C. Staudt-Bickel, D.R. Paul, and W.J. Koros, *Solid-state covalent cross-linking of polyimide membranes for carbon dioxide plasticization reduction.* Macromolecules, **2003**. 36(6), 1882-1888.

Wind, J.W., C. Staudt-Bickel, D.R. Paul, and W.J. Koros, *The effects of crosslinking chemistry on CO_2 plasticization of polyimide gas separation membranes.* Industrial & Engineering Chemistry Research, **2002**. 41, 6139-6148.

Wolfe, J.F., *Rigid-rod polymers. 1. Synthesis and thermal properties of para-aromatic polymers with 2,6-benzobisoxazole units in the main chain.* Macromolecules, **1981**. 14(4), 909-915.

Wonders, A.G. and D.R. Paul, *Effect of CO_2 exposure history on sorption and transport in polycarbonate.* Journal of Membrane Science, **1979**. 5(0), 63-75.

Wright, C.T. and D.R. Paul, *Gas sorption and transport in poly(tertiary-butyl methacrylate).* Polymer, **1997**. 38(8), 1871-1878.

Xie, W., H. Ju, G.M. Geise, B.D. Freeman, J.I. Mardel, A.J. Hill, and J.E. McGrath, *Effect of free volume on water and salt transport properties in directly copolymerized disulfonated poly(arylene ether sulfone) random copolymers.* Macromolecules, **2011**. 44(11), 4428-4438.

Yampolskii, Y., *Correlations with and prediction of activation energies of gas permeation and diffusion in glassy polymers.* Journal of Membrane Science, **1998**. 148(1), 59-69.

Yampolskii, Y., *Polymeric gas separation membranes.* Macromolecules, **2012**. 45(8), 3298-3311.

Yampolskii, Y., I. Pinnau, and B.D. Freeman, eds. *Materials science of membranes for gas and vapor separation*. **2006**, John Wiley and Sons: Chichester.

Zhang, B., J. Spano, Y. Chen, R. Turner, and S. Wi, *Crystallinity and motional dynamics study of a series of poly(arylene ether sulfone) segmented copolymer analogues.* The Journal of Physical Chemistry B, **2012**. 116(27), 7970-7980.

Zhang, Y., I.H. Musselman, J.P. Ferraris, and K.J. Balkus, *Gas permeability properties of Matrimid® membranes containing the metal-organic framework Cu–BPY–HFS.* Journal of Membrane Science, **2008**. 313(1-2), 170-181.

Zoller, P., *Specific volume of polysulfone as a function of temperature and pressure*. Journal of Polymer Science: Polymer Physics Edition, **1978**. 16(7), 1261-1275.

Zoller, P. and D.J. Walsh, *Standard pressure-volume-temperature data for polymers*. **1995**, Lancaster, Pennsylvania, Technomic Publishing Company, Inc.

Vita

Zachary Pace Smith earned his bachelor's degree in chemical engineering from the Pennsylvania State University Schreyer Honors College in 2008, and he earned a master of science degree in chemical engineering from the University of Texas at Austin in 2011. During his doctoral research in chemical engineering at the University of Texas at Austin, Zach was awarded a Department of Energy Office of Science Graduate Fellowship. Zach earned his Ph.D. in May of 2014.

Permanent email address: zps5000@gmail.com

This dissertation was typed by the author.